Structural Manipulation of Organoantimony Cations for Tuneable Lewis Acidity and Reactivity of Palladium Organoantimony Complexes

Omar Coughlin

School of Science and Technology

Nottingham Trent University

A thesis submitted in partial fulfilment of the requirements of Nottingham Trent University for the degree of Doctor of Philosophy

April 2021

Parts of this work have been published as:

Omar Coughlin, Tobias Krämer and Sophie L. Benjamin 'Diverse structure and reactivity of pentamethylcyclopentadienyl antimony(III) cations' Dalton Trans., 2020, 49, 1726-1730

Abstract

Recent reports of novel organoantimony cations acting as Lewis acid catalysts as well as unprecedented bonding modes in transition metal complexes with trialkylantimony(III) ligands have yielded a newfound interest in historically neglected fields.

Triarylchlorostibonium salts of the form $[Ar_3SbCl][B(C_6F_5)_4]$ (Ar = Ph, 3-FC_6H_4, 4-FC_6H_4, 3,5-$F_2C_6H_3$, 2,4,6-$F_3C_6H_2$) were synthesised and found to be active catalysts for the Friedel-Crafts dimerization of 1,1-diphenylethylene and Friedel-Crafts alkylation of benzene. This reactivity as well as structural and computational studies yielded a model for the Lewis acidity at the Sb centre which was proportional to the number of fluorine atoms on the aryl ring with a quenching effect from para fluorination.

Pentamethylcyclopentadienyl (Cp*) antimony(III) cations of the form $[Cp^*SbCl][B(C_6F_5)_4]$, $[Cp^*_2Sb][Y]$ (Y = $B(C_6F_5)_4$, OTf) and $Cp^*Sb(OTf)_2$ were prepared and display diversity in both solid state structure and reactivity. The $[Cp^*SbCl]^+$ ion is moderately Lewis acidic. The $[Cp^*_2Sb]^+$ ion shows no reactivity which can be attributed to Lewis acidity. $[Cp^*SbF][B(C_6F_5)_4]$ could not be isolated due to thermal instability but was isolated as an NHC adduct. It was found to undergo chloride/fluoride exchange in chlorinated solvents; computational evidence suggests this occurs *via* a carbocation intermediate.

The potential for a 'frustrated Lewis pair', with both an organoantimony(III) base and an organoantimony(V) acid was explored, leading to the C-Cl bond activation of benzyl chloride (BnCl) with $^tBu_3Sb$ and $[(3,5\text{-}F_2C_6H_3)_4Sb][B(C_6F_5)_4]$. A novel stibinostibonium $[(Bn_2Sb)Bn_3Sb][BF_4]$ was isolated by serendipity when 'one-pot' routes to tetrabenzylstibonium salts ($[Bn_4Sb]^+$) were targeted.

$[Pd_4(Me_3Sb)_8]$ was found to have a range of reactivities with monodentate and bidentate phosphines. A novel Pd_3 cluster, $[Pd_3(Me_3Sb)_3(\mu_2\text{-}(Me_3Sb))_3(\mu_3\text{-}(Me_3Sb))]$, was structurally characterised, representing the first example of a homoleptic palladium(0) complex with terminal, μ_2 and μ_3 pnictine ligands.

A computational study investigated the mechanism by which alkyl/aryl groups exchange with chlorides between homoleptic stibines (Me_3Sb and Ph_3Sb) and $SbCl_3$. This was found to occur *via* an intermediate containing a 3c-2e akyl/aryl bridge.

Table of Contents

Acknowledgments

Several people have contributed to this project whom I would like to thank:

My director of studies, Dr. Sophie Benjamin for conceptualising this work, hiring me for this project and moulding me into the chemist I am today.

Dr. Tobias Krämer for taking me under his wing for a month while undertaking a researcher mobility visit at Maynooth University, teaching me computational chemistry and all his help since.

Prof. Carole Perry for taking on the role of co-supervisor and all the valuable advice over the years.

Dr. Chris Garner for completing all my monitoring forms in a timely fashion.

All the techs: Iain, Tom, Lisa, Barbara, Chris, Dave, Nigel, Mark, Charlotte, Diego, and Hannah for keeping the place running.

The current IST105 crew: Ash, Libby, Mr. Tony James Blundell, Max and Sumaria as well as all the past members, Jonny, Ryan, Ben, and Myles.

All the academics at Nottingham Trent University for their part in creating a welcoming department which they should all be very proud of

List of Abbreviations and Symbols

Ar – Aryl

AN – Acceptor number

BArF – Tetrakis[3,5-bis(trifluoromethyl)phenyl]borate ($(3,5\text{-}(CF_3)_2C_6H_3)_4]^-$)

BCF – tris(pentafluorophenyl)borane ($B(C_6F_5)_3$)

Bn – Benzyl ($-C_7H_7$)

^{t}Bu – tert-butyl ($-C(CH_3)_3$)

Cp- Cyclopentadienyl (C_5H_5)

Cp'- General cyclopentadienyl derivative

Cp* - Pentamethylcyclopentadienyl ($C_5(CH_3)_5$)

DCM – Dichloromethane (CH_2Cl_2)

DFT- Density functional theory

DMF- Dimethylformamide ($(CH_3)_2NCOH$)

EPC – Electrophilic phosphonium cation

Et- Ethyl ($-C_2H_5$)

EWG- Electron withdrawing group

FIA- Fluoride ion affinity

FLP – Frustrated Lewis pair

GEI- Global electrophilic index

GGA- Global gradient approximation

GTO- Gaussian type orbital

HIA – Hydride ion affinity

Lp- Lone pair

LSA – Lewis super acid

Me -Methyl ($-CH_3$)

Mes-Mesityl ($-2,4,6\text{-}(CH_3)_3C_6H_2$)

IHD- Inverse halogen dependence

IIA- Iodide ion affinity

IMes- 1,3-Dimesitylimidazol-2-ylidene

IR- Infrared spectroscopy

IRC – Internal reaction coordinate

KS- Kohn-Sham

LA- Lewis acid

LDA- Local density approximation

NBO- Natural bond orbital

NHC – N-hetrocyclic carbene

NMR – Nuclear magnetic resonance

OTf- Triflate (-$OS(O)_2CF_3$)

PCM - Polarisable continuum model

PES- Potential energy surface

Pn – Pnictogen

ppm – Parts per million

p-Tol- para-tolyl (p-MeC_6H_4)

R – Alkyl group

SCXRD- Single crystal x-ray diffraction

SIMes – Saturated IMes

STO- Slater type orbital

TEP- Tolman electronic parameter

THF – Tetrahydrofuran

TM- Transition metal

TMS – Trimethylsilyl ($(CH_3)_3Si$)

TSC- Through space coupling

WCA – Weakly coordinating anion

X- Halide

Y-Ligand or lone pair

$\sum_{VdW}$ – Sum of Van der Waal's radii

$\sum_{CR}$ - Sum of covalent radii

δ - Chemical Shift

Any other abbreviations or symbols signify their IUPAC meaning and are dependent on the absence of any other specified definitions.

Table of Equations

Table of Figures

Table of Schemes

Table of Tables

1. Introduction

1.1. Antimony in the Periodic Table

In general, the chemistry of the heavier pnictogens is much less explored than their lighter analogues; one notable outlier in certain fields is arsenic, due to assumed toxicity. This is primarily a consequence of more difficult syntheses, weaker element-carbon bonds and a historic assumption that the chemistry of the heavier pnictogens mirrors that of their lighter analogues. Antimony, as the second heaviest naturally occurring group 15 element, has historically suffered this neglect. The recent main group renaissance, after the dominant presence of d-block chemistry in inorganic chemical literature, has begun to overturn this trend. Elemental antimony has six known allotropes: metallic, explosive, black, yellow and two high pressure modification forms.[1] Antimony is commonly encountered in nature as the mineral stibnite (Sb_2S_3).While not particularly abundant, antimony is of significant geological interest and is an important mineral commodity.[2,3] Antimony metal, alloys and minerals are also of historical interest.[4–6]

Antimony is often categorised as a metalloid due to its metallic appearance and semimetal band structure in the elemental form while the chemistry of molecular antimony compounds strongly resembles non-metals; an extensive coordination chemistry with Sb centres acting as the Lewis acid also exists, more closely resembling metals.[7–9] Metalloids have also been defined as elements with a Pauling electronegativity between 1.9 and 2.2,[10] which includes antimony (2.05).[11] Relativistic effects must be considered to appropriately appreciate the chemical properties of heavier elements.[12] While relativistic effects apply to all atoms to some degree, increasing proportionally to the square of the atomic number, they are typically invoked as a rationalisation of features of elements in the 6th period and heavier only. The energetic separation between the s and p orbitals of antimony is larger than for lighter congeners due to a combination of relativistic effects and sterics, yielding less s/p orbital hybridisation. This trend is observed throughout the p-block but is particularly pronounced for row 3 and 6 elements due to the d-block and lanthanide contraction respectively.

A wide range of oxidation state are available to nitrogen; while the same is true for the remaining pnictogens, +3 (with lone pair) and +5 (oxidation of 'lone pair state') are particularly prevalent. The d-block and lanthanide contraction yield a relatively unstable +5 oxidation state for As and Bi respectively; relativistic effects also contribute to this in the

case of Bi. All pnictogen trihalides are known and have an oxidation state of -3; SbH_3 and BiH_3 are extremely unstable and must be handled at low temperatures.[13–16]

Covalent bonds typically get weaker on descending the p-block due to poorer orbital overlap with the more diffuse frontier orbitals of the heavier elements. For P, As, Sb and Bi σ bonds are stronger than π bonds; the opposite is true for N, evident by the extensive organic chemistry containing double bonded nitrogen. This is rationalised by more diffuse p orbitals for 2nd row and heavier elements, and greater lone pair repulsion in 1st row elements.[17]

1.2. The Chemistry of Organoantimony

All antimony compounds reported in this thesis are either Sb(III) or Sb(V), thus only a very brief discussion of organoantimony in other oxidation states is included but this topic has been reviewed elsewhere.[18] Distibines ($R_2Sb\text{-}SbR_2$) contain two Sb(II) centres and are of particular interest due to thermochromism.[19–21] Sb-Sb bonds typically consist of a single σ bond, however distibenes (RSb=SbR) are known (Figure 1.1).[22–25]

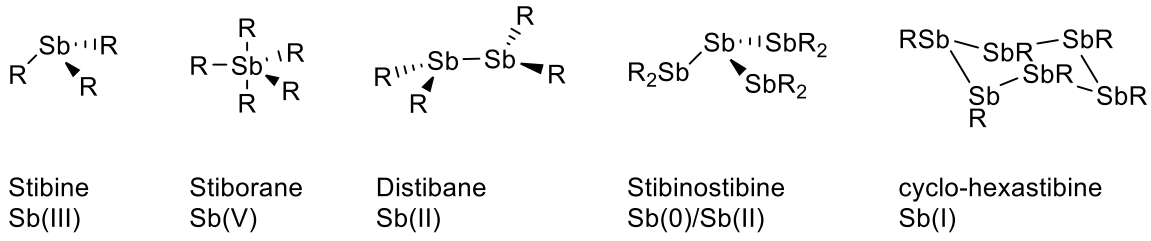

Figure 1.1. Some representative examples of organoantimony compounds in different oxidation states. While the IUPAC name for trivalent organoantimony compounds is stibane, stibine is commonly used.

Antimony centred radicals are relatively rare but have been reported recently. These typically contain highly Lewis basic ligands or electronically rich organic substituents.[26–30]

1.2.1. Organoantimony (III)

Alkyl stibines (R_3Sb) and aryl alkyl stibines ($R_{3-n}Ar_nSb$, n = 1 or 2) are typically prone to oxidation and the low molecular mass alkyl stibines are pyrophoric whereas aryl stibines (Ar_3Sb) are stable in air. This can be rationalised as an effect of the more electronically donating nature of the alkyl group, giving a more electron rich Sb centre and are therefore more easily oxidised. Stibines are typically trigonal pyramidal; because of the greater separation between s and p frontier orbitals in Sb in comparison to lighter pnictogens, the Sb-C bonds in stibines have less s character and have smaller C-Sb-C angles than lighter analogues. Stibines are usually Lewis basic and some coordination chemistry with stibine

ligands has been developed (see 1.3 Transition Metal Complexes), although stibines are much weaker bases than analogous amines or phosphines due to the more inert s pair on Sb. Stibines with highly electron withdrawing organic substituents (e.g. C_6Cl_5, C_6F_5, 3,5-$(CF_3)_2C_6H_3$) show signs of Lewis acidity at the Sb centre in their structure, through close contacts with electron rich atoms, and reactivity.[31,32]

A limited number of stibines are commercially available. There are two overarching strategies for the synthesis of tertiary stibines, from alkali metal derivatives (stibides) or transmetallation of SbX_3 (X typically = Cl) with organolithium/Grignard reagents. The metal stibide (M[R_2Sb], M = Na, K) route, synthetised from R_2SbY (Y = H, R, Ar, H, Cl, Br) and the elemental group 1 metal, is typically employed for the synthesis of asymmetrical stibines.[33,34] Sodium stibides are normally synthesised in liquid ammonia whereas lithium or potassium stibides are usually synthesised in ethereal solvents.[35–37] The metal stibide can then be reacted with the respective organic halide to give a tertiary stibine (Scheme 1.1). As Ph_3Sb is commercially available, it is most typically used as a precursor for the synthesis of diphenylstibide (Ph_2Sb^-), but Ph_2SbCl can also be used.

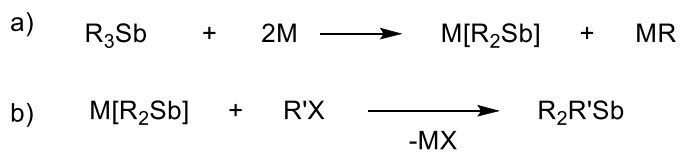

Scheme 1.1. Synthesis of asymmetric tertiary stibines ($R_2R'Sb$). a) synthesis of the metal stibide. MR is typically quenched with ^tBuCl or NH_4Cl. b) Transmetallation with organic halide (X = halide) to yield asymmetric stibine (R ≠ R').

Stibides also react with group 14 nucleophiles such as R_3SiCl,[38] R_3GeCl,[38,39] R_3SnCl[38,40] and Ph_3PbCl[39] to yield Sb-group 14 bonds with the elimination of MCl. Metal antimonides (M_3Sb) are synthons for Sb^{3-} which are generated from Sb^0 and M^0, usually in liquid ammonia.[41–43]

The salt metathesis route is more commonly employed due to more facile experimental demands, e.g., avoiding handling $NH_{3(l)}$ and generally less demanding restrictions on the exclusion of moisture; symmetric stibines (R_3Sb) are almost universally prepared with this method (Scheme 1.2). The exact experimental conditions are typically determined by the organic group to be installed but is usually carried out in ethereal solvents.

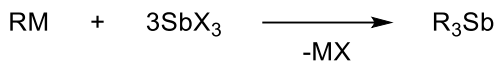

Scheme 1.2. Synthesis of symmetrically tertiary stibines (R_3Sb) by salt metathesis. M = Li, MgX

Alkyl stibines are typically liquids and can be purified by distillation, usually under reduced pressure for higher molecular mass alkyl stibines; Me_3Sb azeotropes with Et_2O, which is typically utilised as a solvent in the synthesis. To circumvent this, Me_3Sb is often oxidised with Br_2 to Me_3SbBr_2, which is an air stable solid, which is then subsequently reduced with Zn.[44] Higher molecular mass alkyl and aryl stibines are often purified by recrystallisation in either aliphatic hydrocarbons or alcohols.[45,46] Aryl stibines with highly electron withdrawing aryl groups (e.g. $(C_6F_5)_3Sb$) can be purified by silica column chromatography;[47] less electronically deficient stibines are typically too basic to be purified in this manner. Sublimation is often used to purify stibines which are solid under ambient conditions.[48]

Arylchlorostibines ($Ar_{3-n}SbCl_n$, n = 1,2) are targeted by redistribution between Ar_3Sb and $SbCl_3$ in the correct stoichiometry, this is typically done without solvent.[31] Alkylchlorostibine ($R_{3-n}SbCl_n$, n = 1,2) cannot be targeted by the same route; alkylchlorostibines are synthesised as per Scheme 1.3. Alternatively, dialkylchlorostibines (R_2SbCl) can be formed by the reductive elimination of RCl from R_3SbCl_2, which occurs when heated *in vacuo*.[49]

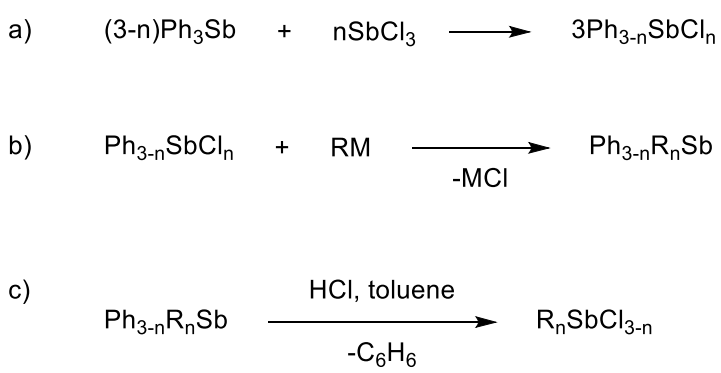

Scheme 1.3. a) redistribution between Ph_3Sb and $SbCl_3$. b)Salt metathesis with organolithium or Grignard (M = Li, MgX) to yield alkylarylstibine. c) Selective bond cleavage of Sb-Ph by bubbling HCl through a toluene solution of the alkylarylstibine.

1.2.2. Organoantimony (V)

There are two routes to stiboranes (organoantimony(V) compounds), oxidation of stibines or alkylation/arylation of Sb(V) halides. Compounds of the form R_3SbX_2 (R = alkyl/aryl group, X = halide), also known as triakylstibine dihalides/triarylstibine dihalides, are typically formed by oxidation of the respective stibine (R_3Sb) with the halogen (X_2). R_3SbF_2 is

typically accessed *via* oxidation by XeF_2,[48] however the cost and difficulty in handling XeF_2 has prompted syntheses with electrophilic N-F reagents.[50,51] Alternatively, R_3SbX_2 ($X \neq F$) may be converted to R_3SbF_2 by KF.[52] A recent report of deoxygenative fluorination of phosphine oxides by $KF/(COCl)_2$ was found to extend to Ph_3SbO to yield Ph_3SbF_2.[51] While Cl_2 gas has been utilised in some of the older reports,[49] SO_2Cl_2 or $PhICl_2$ are more common for the oxidation to R_3SbCl_2.[52,53] R_3SbBr_2 and R_3SbI_2 are typically prepared by direct addition of the halogen.[49,54] Organohalides (RX) can also oxidatively add to stibines (R'_3Sb) to yield tetraorganostiborane halides (RR'_3SbX); this strategy is typically limited to alkylstibines.[55,56] Alkyl bromides and alkyl iodides are typically utilised, which usually yield stibonium salts ($[RR_3'Sb]X$) and thus these reactions are often considered quaternisations. Lewis acid catalysts have been ultilised to oxidise arylstibines with this route.[57] Alkylation/arylation of SbX_5 is typically carried out with a similar salt metathesis strategy as to the synthesis of R_3Sb. This strategy is typically utilised for compounds of the form R_4SbX/R_5Sb.[58,59]

The molecular geometry of organoantimony(V) compounds largely depends on the substituents and in most cases is trigonal bipyramidal, giving a neutral Sb centre (stiborane, Figure 1.2 a);[60,61] large anionic substituents can yield a tetrahedral geometry, giving a cationic Sb centre (stibonium, Figure 1.2 b).[57,62,63] An exception to this is Ph_5Sb, which is a rare example of a square pyramidal main group molecule without a lone pair (Figure 1.2 c).[64,65]

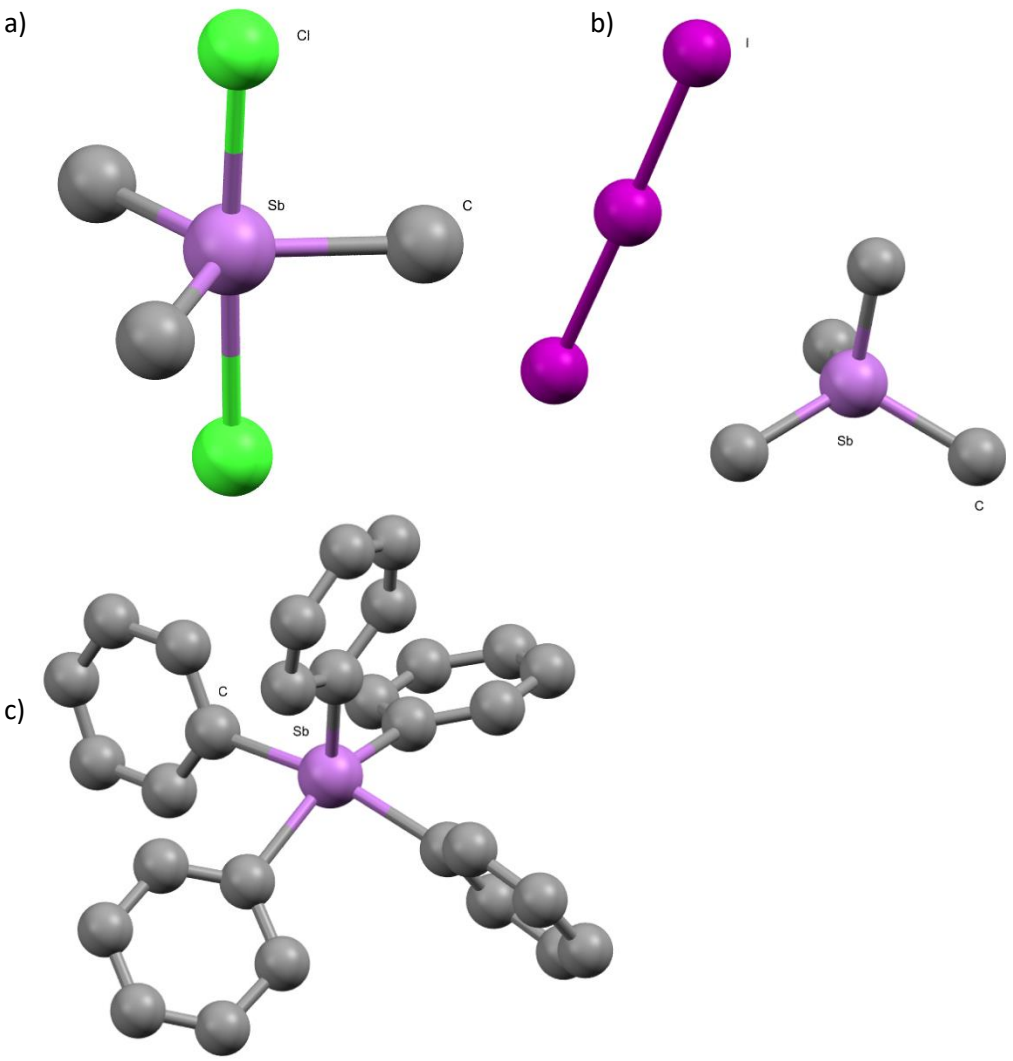

Figure 1.2. a) Solid state structure of Me_3SbCl_2.Co-crystalised $SbCl_3$ has been omitted. Figure redrawn from ref 66. b) Solid state structure of $[Me_4Sb][I_3]$ Figure redrawn from ref 67. c) Solid state structure of Ph_5Sb Figure redrawn from ref 64. Hydrogen atoms have been omitted.

1.2.3 Donor stabilised and Donor free stibeniums Ions

A divalent antimony(III) cation is typically referred to as a stibenium, although the correct IUPAC name is a stibanylium. In contrast to the richly developed chemistry of phosphenium ions, stibenium ions are relatively unexplored. Stibeniums and phosphenium ions are isoelectric to carbenes; phosphenium ions typically have a singlet ground state with a large singlet-triplet separation.[68,69] Akin to carbenes, amino substituents are typically utilised to stabilise phosphenium ions.[70,71] Intra- and intermolecular amine and phosphine substituents have also been used to stabile phosphenium ions. [72,73]

The first donor free stibenium, $[(2,6\text{-}Mes_2C_6H_3)_2Sb][B(C_6F_5)_4]$,was reported by Beckmann in 2018 (Figure 1.3 a).[74] The stability of this species has been attributed to the large steric bulk around the Sb centre. The bismuth analogue was also prepared, however the Phosphorus

and arsenic analogues rapidly decomposed *via* an intramolecular rearrangement.[75] Ph_2Sb^+ was observed quantitatively by the two electron electrochemical oxidation of $[Ph_2Sb]_2$ in THF.[76]

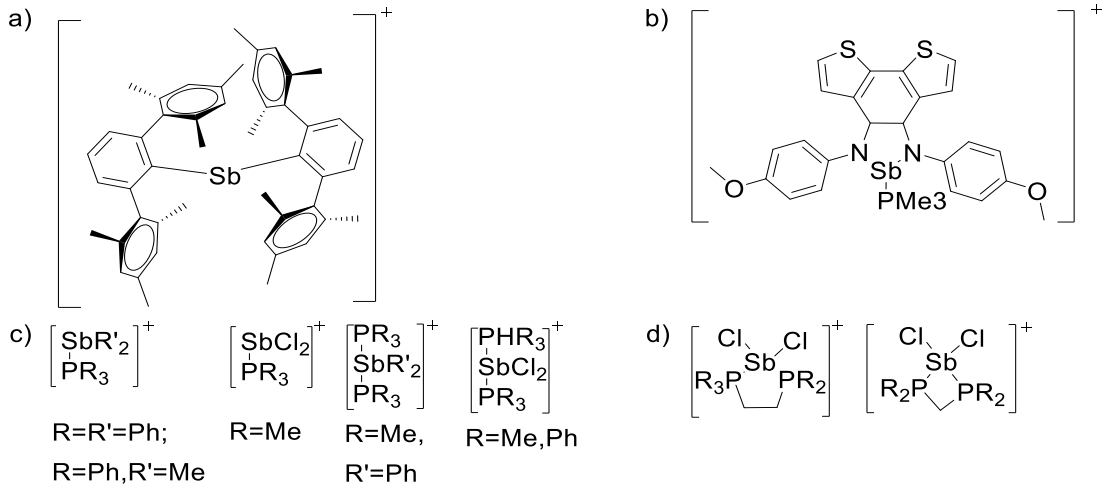

Figure 1.3. a) donor free stibenium, $[(2,6\text{-}Mes_2C_6H_3)_2Sb]^+$, [74] b) phosphine stabilised stibenium with conjugated bithiophene backbone[77]. c) monodentate phosphine stabilised stibeniums. d) bidentate phosphine stabilised stibeniums

Both inter- and intra-molecular stabilised stibeniums have been reported (Figure 1.3 b-d). Some of the first stibeniums reported were stabilised by intermolecular phosphine molecules. Much of the work on phosphine stabilised stibenium ions has been carried out by the Burford group. The prototypical phosphine stabilised stibenium ion, $[Ph_2Sb(Me_2PhP)]Cl$, was reported in 1958.[78] More recent examples of phosphine stabilised stibenium ions typically substitute a weakly coordinating ion for the halide. The addition of 0.75 eq of NH_4PF_6 to an equimolar mixture of Ph_2SbX (X = Cl, Br) and PMe_3 yielded an unusual square planar halide complex $[Ph_2Sb(Me_3P)][PF_6]_3X$.[79] Complexes of the form $[Ph_2Sb(R_3P)_n][X]$ (X = PF_6, R=Ph, n = 1, 2; X = OTf, R = Me, n = 1, 2) and $[SbCl_2(Ph_3P)_n][OTf]$ (n = 1, 2) have been reported.[80,81] The geometry at the Sb centre is typically trigonal pyramidal or see-saw for monophosphine and bisphosphine complexes respectively. In each case the geometry is consistent with a stereochemically active lone pair. Several stibenium ions ($Ph_2Sb^+/SbCl_2^+$) with chelating phosphines ($R_2P(CH_2)_nPR_2$) (n = 1, 2; R = Me, Ph) have been structurally characterised.[82] The electronic structure of these species has been the topic of debate. These species are typically assigned as a phosphine stabilised stibenium (P(III)/Sb(III)), which would be consistent with the cationic charge being localised on the antimony atom. A stibinophosphonium (P(V)/Sb(I)), with the cationic charge on the phosphorus atom, would also be formally possible. The former assignment is consistent

with a dative bond between the two centres while the latter is consistent with a covalent bond between them. Crystallographic data and structural parameters support the former assignment, given the P-Sb bond length is typically slightly greater than the sum of the covalent radii. A computational comparison of $[Ph_2Sb(Ph_3P)_n]^+$ (n=1,2) suggested that the $[Ph_2Sb(Ph_3P)]^+$ is best described as a dative complex with significant ionic contribution whereas $[Ph_2Sb(Ph_3P)_2]^+$ is a ion-ligand complex.[83] There have been no reports on the reactivity of these compounds, which would be insightful. $[Ph_2P(Ph_2PCl)][GaCl_4]$ is reduced to Ph_2PH by two equivalents of Et_3SiH (Scheme 1.4).[84]

$$[Ph_2P(Ph_2PCl)][GaCl_4] \xrightarrow[-Et_3SiCl]{Et_3SiH} [Ph_2P(Ph_2PH)][GaCl_4]$$

$$[Ph_2P(Ph_2PH)][GaCl_4] \xrightarrow[-Et_3SiCl]{Et_3SiH,\Delta} 2Ph_2PH + GaCl_3$$

Scheme 1.4. Reduction of $[PPh_2(PPh_2Cl)][GaCl_4]$ to PPh_2H. Conditions: PhCl, 60°C, overnight. [84]

While $[PPh_2(PPh_2Cl)][OTf]$ is not synthetically accessible, The addition of TMSOTf to Ph_2PCl yields a small thermal population of $[PPh_2(PPh_2Cl)][OTf]$. The addition of Et_3SiH yields Ph_2P-PPh_2 (Scheme 1.5). These salts have been described as phosphine stabilised phosphenium ions.

$$2Ph_2PCl + 2\ Et_3SiH \xrightarrow[-2Et_3SiCl]{TMSOTf,\ \Delta} (Ph_2P)_2 + H_2$$

Scheme 1.5. Reduction of Ph_2PCl to $(Ph_2P)_2$ by Et_3SiH in the presence of TMSOTf. Conditions:PhCl, 100°C.

There are two salts of the same stibine stabilised stibenium/stibinostibonium, $[Me_2Sb(Me_3Sb)][X]$ (X=$GaCl_4$, $Me_2Sb_2Br_6$) reported in the literature.[85,86] Breunig offers both assignments as possible descriptions of the cation while Schulz assigns the cation as a stibinostibonium. Only structural descriptions are reported for these compounds without any further exploration of the reactivity or electronic structure of the cation. In both salts the Sb-Sb bond lengths (2.8205(12) and 2.8273(3) Å) are within the sum of the covalent radii ($\sum_{CR}$=2.78 ± 0.10 Å), suggesting that Schulz's assignment is most accurate.

1.3. Transition Metal Complexes

The soft Lewis basic nature of stibines has mainly confined their coordination chemistry to low oxidation state, soft metals, typically late transition metals of the 2nd and 3rd row. The coordination chemistry of stibines has been thoroughly reviewed up to 2020;[87–89] some

representative examples and noteworthy cases are discussed here rather than a comprehensive review. Particular attention is paid to coordination complexes of group 10, which is included with the introduction of chapter 5. A large amount of the work on transition metal complexes with stibine ligands was carried out before the advent of SCXRD as a routine technique. The chemistry of stibine complexes has been hampered by the tendencies for early reports to utilise Ph_3Sb as the archetypal stibine, which has excluded the isolation of several potential complexes due to its poorer donor abilities than alkylstibines.

Stibine complexes of early transition metals typically have carbonyl coligands and are usually in the 0 oxidation state. Stibine complexes of group 3-5 are extremely rare.[90–95] The chemistry of group 6-8 complexes with stibine ligands is somewhat more developed. Group 6-8 complexes are typically mixed carbonyl complexes, usually in the 0 oxidation state. [96–101] Complexes of the form $[M(CO)_5(L)]$ (M= Cr, Mo, W; L=R_3Sb, PhR_2Sb, Ph_2RSb) have been relatively well studied.[101–107] Mixed group 6 carbonyl stibine complexes with Cp, phosphine, halides and other similar ligands have been reported (Figure 1.4). Several examples of group 9 carbonyl complexes with stibine ligands have been reported.[108–112] Unlike earlier transition metals, the chemistry of group 9 metals in higher oxidation states is relatively well explored. The stibine analogue of Vaska's complex, *trans*-$[RhCl(CO)(Ph_3Sb)_2]$ was found to be in equilibrium with the five-coordinate *trans*-$[RhCl(CO)(Ph_3Sb)_3]$.[113] Complexes of the form $[Ni(CO)_3(Ar_3Sb)]$ were obtained by displacing a carbonyl from $[Ni(CO)_4]$ with Ar_3Sb.[114,115] In contrast to other metals, the Pd(0)/Pt(0) stibine complexes with carbonyl ligands are rare and none have been structurally characterised.

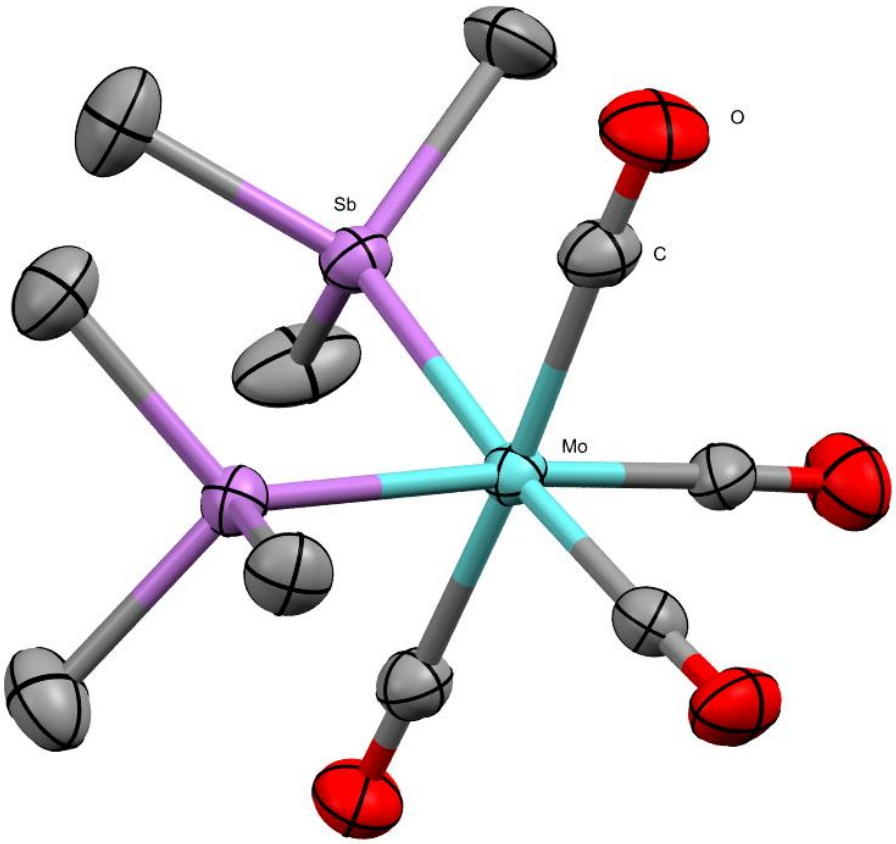

Figure 1.4. Solid state structure of *cis*-[$Mo(CO)_4(Me_3Sb)_2$]. Ellipsoids shown at 50% probability. Hydrogen atoms have been omitted. Redrawn from ref 116.

6 and 7 coordinate Mo(II) or W(II) complexes, typically dihalides, have been reported (Figure 1.5).[117–120] There are also numerous similar Ru complexes with Ph_3Sb ligands,[121] with several of these complexes are active polymerisation catalysts.[122–124]

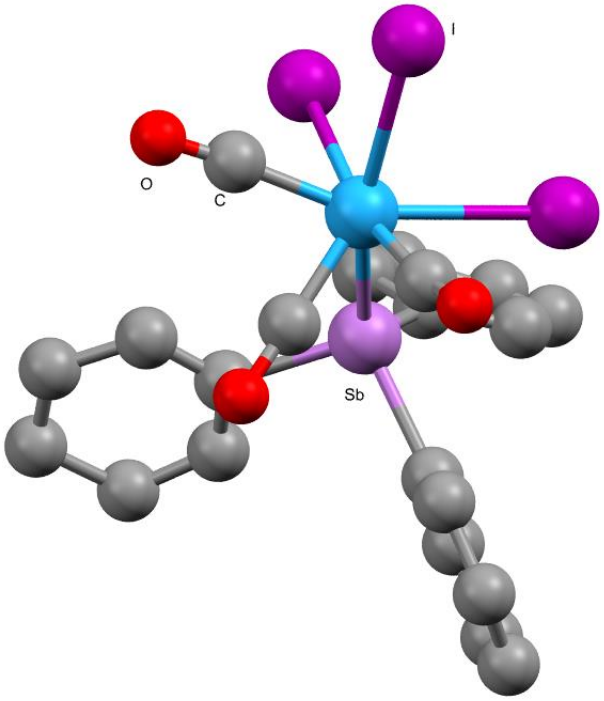

Figure 1.5. Solid state structure of $[WI_3(CO)_3(Ph_3Sb)]^-$. Atoms are shown as spheres and hydrogen atoms are omitted. Cation and co-crystalised solvent have been omitted. Figure redrawn from ref 125.

Several cluster type complexes with stibine ligands have been reported. Numerous substituted Ru and Os clusters with Ph_3Sb ligands and typically carbonyl and/or hydride coligands have been reported;[126–129] $[Ru_6(\mu_5\text{-}Sb)(\mu\text{-}H)_3(CO)_{18}(Ph_3Sb)]$ and $[Os_6(\mu_5\text{-}Sb)(\mu\text{-}H))_2(\mu\text{-}Ph_3)(\mu_3, \eta_2\text{-}C_6H_4)(CO)_{17}]$ are particularly noteworthy examples as they contain an unusual naked μ_5-Sb atom.[130] Clusters of the form $[Cu_4I_4(R_3Sb)_4]$ (R = Cy, ^{i}Pr, ^{t}Bu; R_3 = ^{i}Pr$_2$Ph, ^{t}Bu$_2$Ph; Figure 1.6) are of interest due to thermoluminescence in the solid state; other stibines give iodide bridged dimers $[(Cu(R_3Sb)_2)_2(\mu\text{-}I)_2]$ (R =Ph; R_3 = ^{i}Pr$_2$Ph, Me$_2$Ph).[131,132]

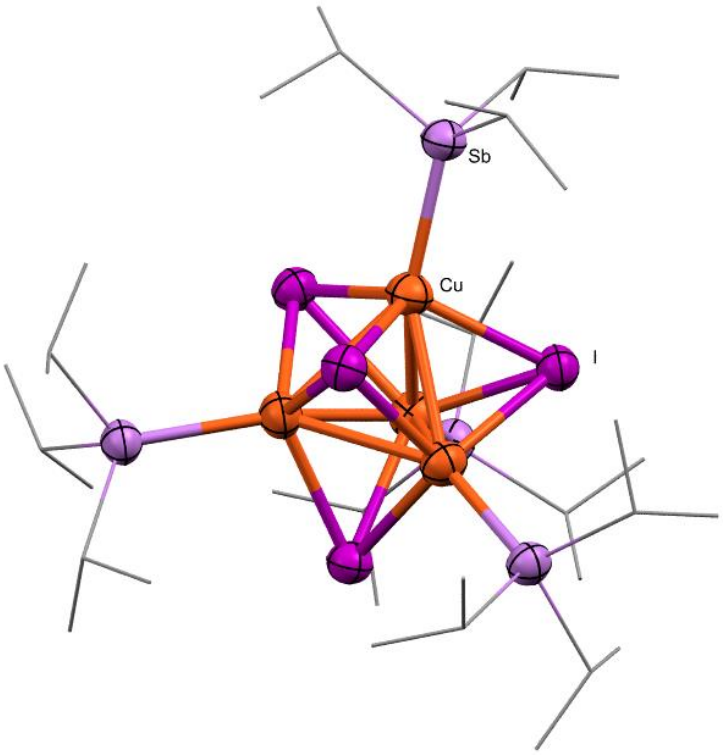

Figure 1.6. Solid state structure of $[Cu_4I_4(^iPr_3Sb)_4]$. Ellipsoids shown at 50% probability. Hydrogen atoms have been omitted.^{i}Pr groups are shown in wireframe.

Stibine complexes of group 11 are almost exclusively limited to the +1 oxidation state and are usually of tetrahedral geometry. Cationic tetrakis(alkylstibine) complexes ($[M(R_3Sb)_4]Y$) (M = Cu, Ag; R = Me, Et, ; Y = BF_4, PF_6) have been reported.[133,134]

A series of multidentate ligands with organoantimony(III) donors have been prepared, some of which can be described a mixed donor ligands due to the presence of other donor atoms. While a tritertiary stibine, $MeC(CH_2SbPh_2)_3$, and several of its complexes have been described,[135,136] polydentate stibines are rare. This can be attributed to weak Sb-C bonds which greatly limits the scope for building polydentate ligands through multistep synthetises. Mixed donor ligands with stibine motifs are much more common. [87–89]

1.4. Lewis Theory of Acidity

The Lewis theory of acidity is extremely useful in rationalising structure and reactivity in a diverse range of chemical species. While the terms Lewis acid and Lewis base are often used interchangeably with electrophile and nucleophile respectively, the former two terms describe the thermodynamic aspect of adduct formation while the latter two terms refer to the kinetic aspect of reactivity.

1.4.1. Experimental Methods of Ranking Lewis Acidity

Unlike Brønsted acids/bases, Lewis acids/base have no universal quantitative definition however several methods to rank relative Lewis acidity/basicity exist. The Gutmann-Beckett method uses triethylphosphine oxide (Et_3PO) as a probe which is combined with a Lewis acid in solution and assessed using ^{31}P NMR spectroscopy.[137] The Et_3PO will coordinate to the Lewis acid at the oxygen atom, which acts as a well-defined site, yielding a reduced electron density at the phosphine oxide probe and an ^{31}P NMR chemical shift perturbed from the free phosphine oxide.[138] From this an acceptor number (AN) can be calculated (Equation 1.1).

$$AN = 2.21(\delta_{Sample}\text{-}41)$$

Equation 1.1. Acceptor number (AN). δ_{Sample} is the ^{31}P NMR shift of the Et_3PO adduct in ppm (*n.b.* the dimensionless quantity is used here).

This method was originally applied to solvents,[138] but has since been adapted to molecular Lewis acids in low acidic solvents.[137,139–141] The AN yields a scale between weakly acidic hexane (AN_{Hexane} = 0) and strongly acidic $SbCl_5$ (AN_{SbCl5} = 100) when applied to solvents but is rarely used for molecular Lewis acids. Et_3PO is highly stable and the ethyl groups impede interactions with the phosphorus atom thus when this method fails to yield a definite result it is typically the result of multiple coordination modes of the Lewis acid rather than divergent reactivity of the phosphine oxide probe.[138,142] The Childs method is a related but much less common NMR method for assessing Lewis acidity where changes in the ^1H NMR chemical shifts of crotonaldehyde (2-butenal) on coordination to Lewis acids are measured.[143] Pyridine-d_5 has also be utilised in a similar way.[144]

Recently fluorescent phosphine oxide probes has been utilised to measure Lewis acidity where the chromaticity of the probe reveals the strength of the Lewis acid (Scheme 1.6).[145,146] While this method is highly applicable, the phosphole probes are not commercially available.[147]

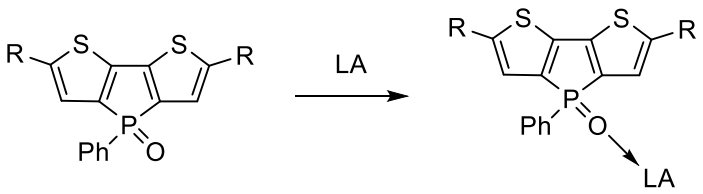

Scheme 1.6. Reaction of fluorescent phosphine probe with Lewis acid (LA).

The ECW model is a semi-quantitative model which describes Lewis acid-base interactions (Equation 1.2); the ECW can be thought of as a quantitative description of Pearson

hard/soft acid and base (HSAB) theory.[148–150] Each acid/base has an E, C, and a W term from which the enthalpy of the formation of an σ adduct without any steric contribution between the acid and base in the gas phase can be calculated. The relation to HSAB theory can be rationalised in that hard acids/base (low polarisability) will have a large value for $E_{A/B}$, conversely soft acids/base (high polarisability) will have a large value for $C_{A/B}$; this can be physically interpretated as hard acid/base pairs being dominated by electrostatic interactions while soft acid/base pairs are dominated by covalent interactions. The ECW equation can be used to calculate the contribution of π bonding to an adduct.[151,152]

$$-\Delta H = E_A E_B + C_A C_B + W$$

Equation 1.2. The ECW equation. E and C are the electrostatic and covalent contribution to the adduct respectively. The subscripts refer to acid and base. W is an additional constant which is typically 0.

1.4.2. Computational Methods of Ranking Lewis Acidity

A range of computational methods are also used to assess Lewis acidity. Fluoride ion affinity (FIA) is the most prevalent (Scheme 1.7 c). This is most commonly calculated using a gas phase *pseudo*isodesmic reaction of the Lewis acid abstracting a F^- from $[COF_3]^-$ to yield a Lewis acid-fluoride adduct (Scheme 1.7 a);[153] an experimentally calculated value for the FIA of carbonyl difluoride (COF_2) is used to avoid directly calculating the enthalpy of a fluoride ion (Scheme 1.7 b).

a) $LA + COF_3^- \longrightarrow COF_2 + LA\text{-}F^-$

b) $COF_2 + F^- \longrightarrow COF_3^-$

c) $LA + F^- \longrightarrow LA\text{-}F^-$

Scheme 1.7. a) pseudoisodesmic reaction of Lewis acid (LA) with COF_3^-. b) Formation of COF_3^-. c) Formation of Lewis acid-fluoride adduct. The enthalpy of reaction c) is equal to the sum of the enthalpy of reaction a) and b).

An alternative is to use a Me_3Si^+/Me_3SiF anchor system with the FIA of Me_3Si^+ calculated at a high level of theory.[154] More recent examples have avoided using a reference system and instead directly calculated the enthalpy of the fluoride ion at a high level of theory.[155] By convention FIAs are reported as a positive value in kJ mol^{-1} and are calculated in the gas phase. This has been the source of criticism and FIAs are occasionally reported as solvent corrected values, although FIA values are only directly comparable if they have been calculated at the same level of theory.[156] The inclusion of a solvent correction typically reduces the FIA by 100-200 kJ mol^{-1}, this reduction is typically inversely proportional to the

size of the Lewis acid. The chloride, hydride and methyl affinities have also been calculated using a similar method.[157]

Fluoride ion affinity (FIA) calculations have been criticised as not a true reflection of Lewis acidity but rather of fluorophilicity. Similar criticisms can also be levelled against the Gutmann-Beckett method and other experimental methods in that they measure a very specific reactivity which is mediated by Lewis acidity rather than a fundamental Lewis acidity. More fundamental computational methods, such as global electrophilic index (GEI) and Fukui function,[158–162] have been proposed as universal measures of Lewis acidity as they are based on the electronic structure of a chemical species rather than any specific reactivity. While the GEI is a measure of the electrophilicity (Equation 1.3), it was found to have a strong correlation with the FIA of a series of hard acids and the iodide ion affinity (IIA) of a series of soft acids.[163,164]

$$\omega = \frac{\mu^2}{2\eta} = \frac{\chi^2}{2\eta}$$

Equation 1.3. Global electrophilic index (ω). μ = chemical potential, η = chemical hardness , χ = electronegativity.

The Fukui function describes the electron density of a frontier orbital and allows for the prediction of the most electrophilic or nucleophilic site in a molecule (Equation 1.4).

$$f(r) = \frac{\partial \rho(r)}{\partial N_{electron}}$$

Equation 1.4. The Fukui function. ρ(r) = electron density.

Several chemical species have historically been called Lewis superacids (LSAs), including: SiF_3^+,[165] a cationic oxazaborinane[166], metal triflates and triflimides (derived from the Brønsted superacids HOTf or $HNTf_2$),[167] and Lewis acids stronger than $AlCl_3$.[168] The most prevalent definition used for LSAs, proposed by Krossing, is a molecular Lewis acid stronger than SbF_5 in the gas phase.[169]

1.4.3. Frustrated Lewis Pairs (FLP) for Small Molecule Activation

Frustrated Lewis pairs (FLPs), compounds or mixtures containing both a Lewis acidic and basic component which for steric reasons can not form an adduct,[170] have become a fruitful avenue in the pursuit of meaningful replacement of transition metal systems with main group systems for catalytic applications. Given the wealth of literature on FLP systems for stoichiometric and catalytic transformations, which has been thoroughly reviewed,[171–176] only a brief description with some prototypical examples is given here. A description of FLPs for the activation of C-X bonds is found in the introduction to chapter 4.

The bond fission and addition of small molecules to metal centres has traditionally been seen to be restricted to transition metals. While some limited exceptions to this are known,[177–183] the paradigm that reversible dihydrogen activation was limited to transition metals was challenged in 2005 with the seminal report that a Lewis amphoteric compound, $B(C_6F_5)_2(4\text{-}(PMes_2)C_6F_4)$, carries out reversible heterolytic bond fission on dihydrogen (Scheme 1.8).[184] A kinetic study suggests that dihydrogen elimination from $BH(C_6F_5)_2(4\text{-}(PHMes_2)C_6F_4)$ is intramolecular.

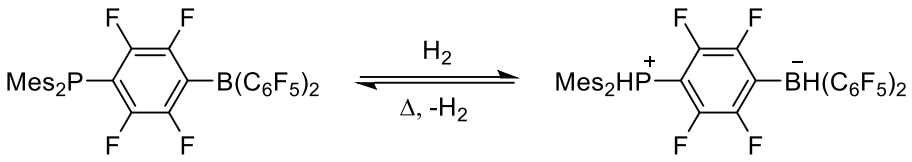

Scheme 1.8. Reversable activation of dihydrogen by $B(C_6F_5)_2(4\text{-}(PMes_2)C_6F_4)$.

This reactivity was further expanded to other intra-/intermolecular system including $PR_3/B(C_6F_5)_3$ (R = ^{t}Bu, Mes) and $(C_6F_5)_2B(CH_2)_2PMes_2$.[185,186] While the aminoborane reported by Piers in 2003, $1\text{-}(NPh_2)\text{-}2\text{-}(B(C_6F_5)_2)C_6H_4$,[187] does not activate dihydrogen, a class of related ansa-aminoboranes do (Figure 1.7).[188,189]

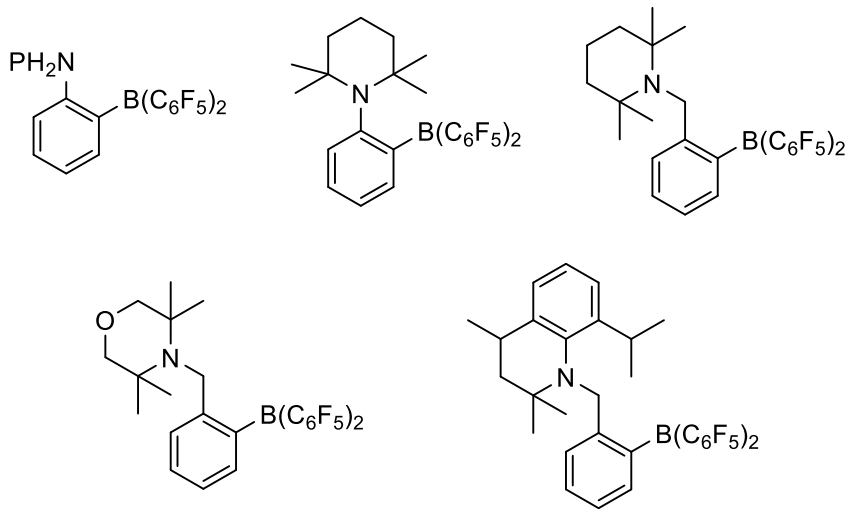

Figure 1.7. Pier's aminoborane (top left) and related aminoboranes which activate dihydrogen.

The mechanism of dihydrogen addition was initially thought to occur *via* a side-on interaction between the Lewis acid and dihydrogen, leading to a polarisation of the H-H bond and allowing protonation of the Lewis base. An alternative explanation invokes the donation of the Lewis base's lone pair into a $\sigma^*_{H\text{-}H}$ orbital. Initial computational studies suggest that the heterolytic cleavage of dihydrogen by P/B FLPs involve an almost linear P···H-H···B transition state dominated by non-covalent interactions and occurs in a

concerted manner.[190–192] Further studies present a model where the dihydrogen molecule is activated in the electric field between the Lewis acid and base.[193]

These systems are also capable of transfer hydrogenation on unsaturated organic compounds such as olefins, silyl enol ethers, imines, aziridines and enamines (Scheme 1.10); this topic has been thoroughly reviewed.[174,194–196] The reduction of protected imines has been proposed to occur *via* hydride attack on the imine carbon followed by protonation of the nitrogen.[197,198]

The reactivity of FLP systems with small molecules was initially attributed to a steric hindrance between the acidic and basic component preventing a quenching of their respective reactivity by adduct formation (*vide supra*). This rudimentary model has been developed with computational studies yielding the encounter complex model.[192,193] Recent literature has highlighted a radical single electron transfer (SET) mechanism in the activation of small molecules by FLP systems. A bulky triarylamine was oxidised to the radical cation by $B(C_6F_5)_3$.[26] Mixing Mes_3P with $E(C_6F_5)_3$ (E = B, Al) gave deeply coloured solution; EPR measurements and reactivity with Ph_3SnH suggested the formation of radical species (Scheme 1.9).[199] This suggests that on mixing Mes_3P with $E(C_6F_5)_3$, an equilibrium between the classical frustrated pair and $[Mes_3P^{\bullet}]^+/[E(C_6F_5)_3^{\bullet}]^-$ forms, favouring the former. $PR_3/E(C_6F_5)_3$ (R = ^{t}Bu, Mes; E = B, Al) activate tetrachloro-1,4-benzoquinone (1,4-$O_2C_6Cl_4$) to yield $[(R_3POC_6Cl_4OE(C_6F_5)_3]$ however $[Mes_3P^{\bullet}]_2[(C_6F_5)_3EOC_6Cl_4OE(C_6F_5)_3]$ was identified as an intermediate for the $Mes_3P/E(C_6F_5)_3$ system, suggesting a SET mechanism in the formation of the adduct.

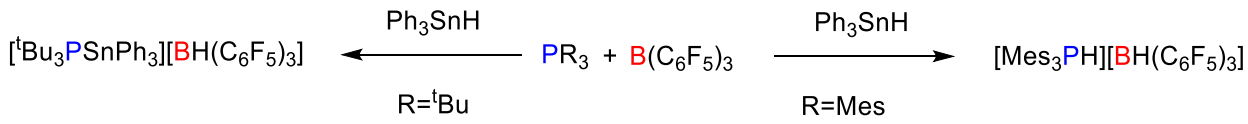

Scheme 1.9. Reaction of $PR_3/B(C_6F_5)_3$ (R=^{t}Bu, Mes) with Ph_3SnH. $P^tBu_3/B(C_6F_5)_3$ heterolytically cleaves the Sn-H bond while $PMes_3/B(C_6F_5)_3$ homolytically cleaves the Sn-H bond.[199]

Similar SET reactions have been observed between both classical and frustrated Lewis pairs of silylium/phosphines and germylene/borane.[200,201] The $PMes_3/B(C_6F_5)_3$ has been deployed to couple diaryl substituted esters with olefins to yield α,β-substituted olefins.[202]

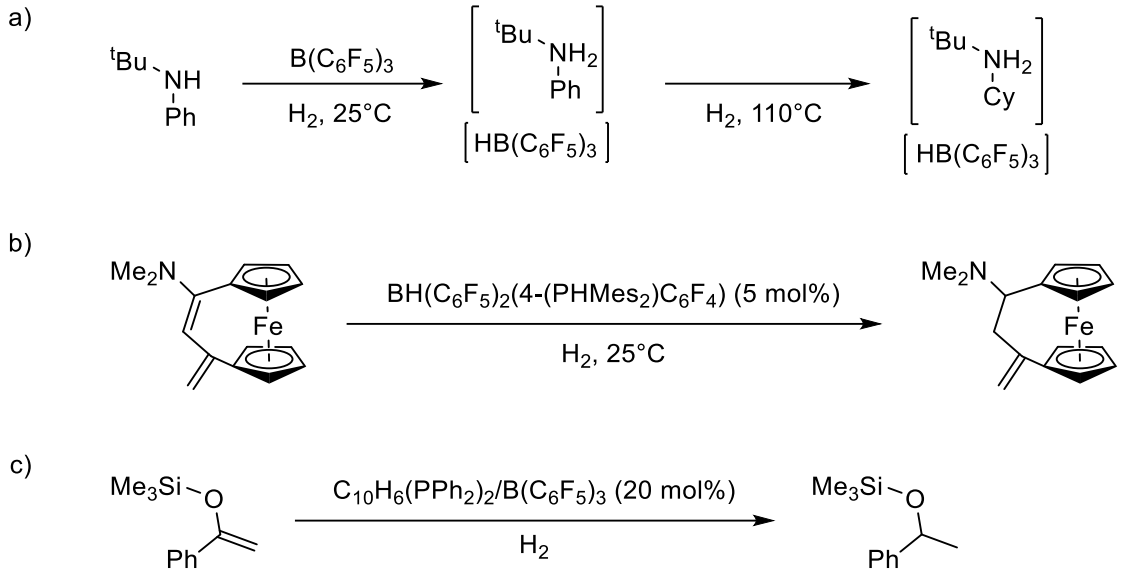

Scheme 1.10. a) reduction of aniline by $B(C_6F_5)_3$. [203] b) Reduction of a conjugated metallocene dienamine.[204] c) Reduction of silyl enol ether.[205]

The current interest in effective carbon capture technology has yielded a wealth of examples of FLP for greenhouse gas capture. Both $(Mes)_2PCH_2CH_2B(C_6F_5)_2$ and $P^tBu_3/B(C_6F_5)_3$ reversibly bind to CO_2 to form a zwitterionic carboxylate species (Scheme 1.11).[206] FLP systems have since been developed to utilise CO_2 as a C1 feedstock; 2,2,6,6-tetramethylpiperidine (TMP)/$B(C_6F_5)_3$ has been deployed to reduce CO_2 to both CH_3OH and CH_4 with H_2 and Et_3SiH as hydride sources respectively.[207,208] SO_2 has been captured by FLP systems in a similar way (Scheme 1.11).[209]

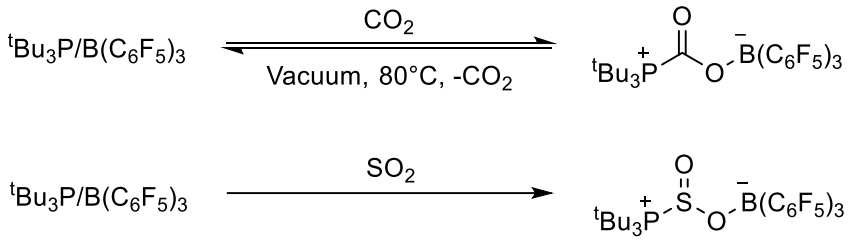

Scheme 1.11. Reversible binding of CO_2 (top) and irreversible binding of SO_2 (bottom) by $P(^tBu_3)/B(C_6F_5)_3$.[206,209]

Traditionally considered to be confined to the realms of transition metal chemistry, some limited examples of C-H activation by FLP systems have recently been reported. In an equivalent mater to the above reaction, $PR_3/Al(C_6F_5)_3$ (R=^{t}Bu, Mes, Nap(naphthyl)) form $(R_2P)N{=}NO(Al(C_6F_5)_3)$ with nitrous oxide. [210] A second equivalent of $Al(C_6F_5)_3$ yields a radical ion pair, $[PR_3^{\bullet}][(\mu\text{-}O)(Al(C_6F_5)_3)_2^{\bullet}]$, with the elimination of N_2. The ^{t}Bu group in $[P(^tBu)_3^{\bullet}][(\mu\text{-}O)(Al(C_6F_5)_3)_2^{\bullet}]$ is activated whereas $[P(Nap)_3^{\bullet}][(\mu\text{-}O)(Al(C_6F_5)_3)_2^{\bullet}]$ actives aromatic solvents

(Scheme 1.12). $(Mes)_2PCH_2CH_2B(C_6F_5)_2$ and the related cyclohexylene-bridged P/B frustrated Lewis pair $(Mes)_2PC_6H_{10}B(C_6F_5)_2$ chelate NO at the N atom to yield an persistent hetrocyclic N-oxyl radical which is capable of H-atom abstraction from a range of olefins.[211,212]

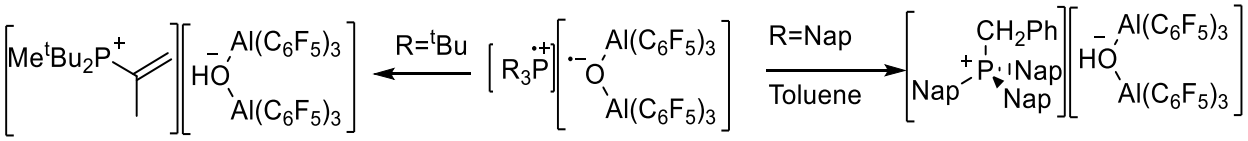

Scheme 1.12. C-H activation by $[PR_3^{\bullet}][(\mu\text{-}O)(Al(C_6F_5)_3)_2^{\bullet}]$ (R=^{t}Bu, Nap).[210]

1.5. Lewis Acid Catalysis

In general, Lewis acid mediated catalysis can be divided into two categories based on mechanism: the Lewis acid abstracting an anionic fragment from the substrate to yield an active cation (heterolytic bond cleavage) or the Lewis acid coordinating to the substrate to yield an activated complex. The former reactivity is typical of cationic catalysts and substrates with halides, such as the Friedel-Crafts reaction (Scheme 1.13 i), whereas the latter is typical of neutral catalysts and organic substrates with electron rich functional groups such as carbonyls; the Mukaiyama aldol reaction (Scheme 1.13 ii) and Diels-Alder reaction (Scheme 1.13 iii) are examples of this reactivity.

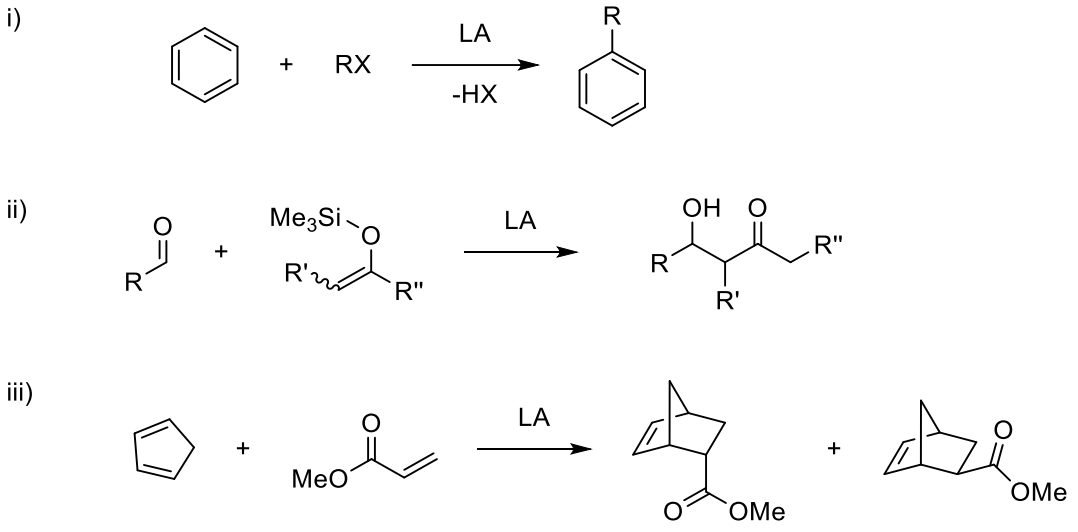

Scheme 1.13. Some examples of Lewis acid catalysed reactions. i) Friedel–Crafts alkylation of benzene by RX; only the monoalkylated product is shown here however a higher degree of alkylation is typically observed.[213] ii) Mukaiyama aldol reaction.[214] iii) Diels-Alder reaction between cyclopentadiene and methyl methacrylate.[215]

As well as stoichiometric reactivity (*vide supra, 1.4.1* Experimental Methods of Ranking Lewis Acidity), several catalytic test reactions are utilised to gauge Lewis acidity. The

Friedel-Crafts dimerisation of 1,1-diphenylethylene (DPE) is typically deployed as a proof-of-concept reaction as it is relatively facile, gives a highly coloured solution and is easy to monitor by NMR spectroscopy (Scheme 1.14).[216–218]

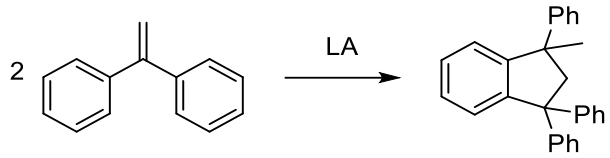

Scheme 1.14. Friedel-Crafts dimerisation of 1,1-diphenylethylene to 1-methyl-1,3,3-triphenyl-2,3-dihydro-1H-indene.

A vast amount of literature concerning Lewis acid catalysis and the ubiquitous nature of Lewis acid catalysis in synthetic chemistry signifies that even a concise review could amount to an entire book.[219,220] Early reports of Lewis acid catalysis typically involved simple neutral main group and transition metal halides, such as $TiCl_4$, $AlCl_3$ and BF_3.[221,222]

A trend of utilising organometallic Lewis acids for catalysis, giving better tunability and the potential for stereospecific catalysis, has recently emerged. $B(C_6F_5)_3$ (BCF) is often considered to be the prototypical organometallic Lewis acid due to its high stability, robustness of B-C bonds in comparison to similar species, solubility in organic solvents and high Lewis acidity.[223] Like boron(III) halides, the Lewis acidity of BCF is derived from a vacant p_z orbital centred on the boron atom. BCF is typically assigned as a stronger Lewis acid than BF_3 but weaker than BCl_3.[141,224,225] As well as a wide variety of reactions catalysed by the Lewis acidity of BCF,[226–229] BCF can also abstract halides from other main group centres to reveal cationic species.[230] BCF is commonly deployed to reveal titanocenium species as active catalyst in Ziegler–Natta chemistry.[231–234] Derivatives of BCF have also been pursed.[231,235–238]

1.6. Analytical Methods and Characterisation

The analytical methods and characterisation of new compounds deployed in this work is typical of modern organometallic and coordination chemistry. Some special consideration is required for the characterisation of organoantimony compounds.

1.6.1. Nuclear Magnetic Resonance Spectroscopy

There are two naturally occurring antimony isotopes, ^{121}Sb (I = 5/2) and ^{123}Sb (I = 7/2) which have a natural abundance of 57.3% and 42.7% respectively.[239] While ^{121}Sb and ^{123}Sb NMR spectroscopy techniques are known, the large quadrupolar spin yields a fast relaxation in non-symmetrical environments and is typically restricted to species with cubic symmetry. Neither ^{121}Sb nor ^{123}Sb NMR has been used as part of this work; there are several examples

of the use of ^{121}Sb and ^{123}Sb NMR in the literature.[240–243] The presence of an antimony atom in organometallic compounds has some characteristic effects on spectra obtained through more routine NMR methods. ^{1}H NMR signals for H atoms which are near the Sb atom are typically broad due to coupling to the quadrupolar Sb, this coupling is typically poorly resolved; ^{13}C NMR signals of C atoms directed bonded to an Sb atom may not be observed due to this broadening. The heavy atom effect has a pronounced impact on NMR spectra of organoantimony compounds, which yields an upfield shift for signals corresponding to atoms directly bonded to heavy atoms. This was initially observed in halogens and termed normal halogen dependence (NHD), the opposite effect was observed in some transition metals in low oxidation states and termed inverse halogen dependence (IHD). [244,245] Several explanations have been given to rationalise this observation; a greater diamagnetic shielding due to the greater number of electrons in heavy atoms,[246,247] a radial dependence of the paramagnetic term affecting shielding,[244,245] and spin-orbit coupling in the heavy atom.[248,249] This spin-orbit coupling has been supported by DFT calculations.[250] ^{19}F NMR shifts of Sb-F species are typically *ca.* -80 ppm for Sb(III)-F and -150 ppm for Sb(V)-F species.

1.6.2. Structure Determination by Single Crystal X-Ray Diffraction

The advent of single crystal x-ray diffraction (SCXRD) has improved the ability of chemists to interrogate inorganic and organometallic compounds to an immeasurable degree. SCXRD gives a route to accurately measure structural parameters of a compound in the solid state and offers confidence in a structural assignment that spectroscopic methods cannot. The relatively structural simplicity of reported organometallic compounds in comparison to typically reported organic compounds restricts the potential for throughout structural analysis based on NMR spectroscopy and highlights the importance of SCXRD. Few specific concerns exist for antimony containing compounds in terms of SCXRD. Given the large atomic mass of Sb, antimony containing crystals are typically strong diffractors and weak diffraction can often be diagnostic of the isolation of an organic side-product rather than the targeted organoantimony compound.

1.6.3. Elemental Analysis

CHN elemental analysis is typically expected as part of the reporting of novel organometallic and coordination compounds as evidence of uniform composition of a sample. CHN analysis is typically performed in duplicate and experimental mass percentages are expected to be within 0.4% of the calculated values. The presence of highly fluorinated groups has been used as an explanation of inaccurate composition results.[251]

1.7. Computational Methods

Developments in computational chemistry software along with a more widespread acceptance among synthetic chemists has made computational chemistry more accessible and has since become more prevalent in reports of synthetic inorganic chemistry. At the most basic level of understanding, computational chemistry seeks to find solutions to the Schrödinger equation (Equation 1.5) to determine properties (energies, bond lengths, reactivity) about a chemical system.

$$\hat{H}\psi(r) = E\psi(r)$$

Equation 1.5. Time independent Schrödinger equation. Ĥ- Hamiltonian operation, ψ-Wavefunction (function of particle position (r)), E=energy

As well as an expansive range of topics, ranging from drug/protein interactions to battery technology, where computational methods may be deployed there is also a range of methods differing in their mathematical underpinning. The many-body problem, affecting any chemical systems with more than one electron precedes exact solutions to the Schrödinger equation and for this system necessitates this varied approach; this can be likened to the wide variety of solution programs in SCXRD with the many-body problem akin to the phase problem. Calculations employed in molecular inorganic chemistry are mostly based on density functional theory (DFT). DFT treats chemical systems as electron density rather than using a many-body wavefunction; this is analogous to treating the electrons as a gas.[252–255] The Kohn-Sham (KS) equation is an one-electron Schrödinger equation of non-interacting electrons which have an equivalent electron density to interacting particles (Equation 1.6).

$$\left(-\frac{\hbar^2}{2m}\nabla^2 + \upsilon_{eff}(r)\right)\varphi(r) = \varepsilon_i\varphi_{i(r)}$$

Equation 1.6. The Kohn-Sham equation. ε_i are the KS eigenvalues and $\varphi_i(r)$ are the KS orbitals. υ_{eff} is the KS potential.

From this energy can be written in terms of its constituent parts: kinetic energy (T_s), Hartree energy (U), potential energy (V) and exchange-correlation energy (E_{XC}) (Equation 1.7).

$$E = T_s + U + V + E_{XC}$$

Equation 1.7. Total energy of a Kohn-Sham system.

Only the exchange-correlation energy cannot be solved exactly. A range of density functionals (functions of functions), both *ab initio* and semi-empirical, have been

developed for different chemical systems. DFT functionals have been qualitatively ranked in terms of chemical accuracy with an inverse dependence on computational cost by Jacob's ladder (Figure.1.8).[256] At the bottom of ladder, local density approximation (LDA) assumes that the exchange-correlation energy at any point is only dependent on the electron density at that point. For molecular systems, LDA typically overestimates bond strengths. The generalised gradient approximation (GGA) is more chemically complex and based on a gradient exchange-correlation energy.[257–260]

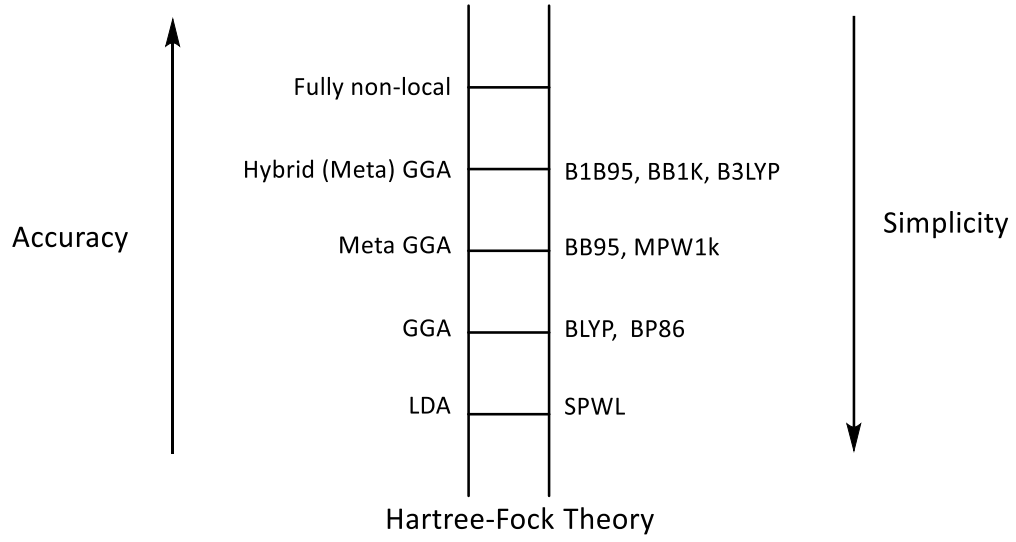

Figure.1.8. Jacob's ladder. Each rung represents a level of increased accuracy and complexity. The category of DFT functional is shown on the left and example functionals on the right. Adapted from ref. [256].

DFT calculations also require a basis sets, which are basis functions that describe the electronic wave function and can be thought of as mathematical descriptions of electrons. Unlike functionals, which have differing suitability to different chemical systems and problems, basis sets typically become more accurate with increased size at the expense of computational efficiency. While DFT functionals typically have relatively arbitrary names (M06 is named as it was developed at the University of Minnesota in 2006),[261] basis sets are usually given more descriptive names but still no absolute naming convention exists. Gaussian type orbitals (GTOs) are commonly deployed. The smallest basis sets, minimal basis set, contain a single basis function for each orbital in the free atom of each atom in the molecule. Split valance basis sets contain additional basis functions to describe valance electrons to reflect distortions in the structure of atoms in molecules from isolated atoms. [262] Polarisation functions can be added to reflect anisotropy in the electronic structure of orbitals in molecules. This is typically done by adding p-type functions to valence s orbitals, f-type functions to valence p orbitals *etc*. Diffuse functions can also be added to account for

electron density far away from the nuclei, they are important for modelling anions and molecules with large Van der Waal interactions.

DFT typically models long range dispersion interactions poorly.[263,264] Two approaches are utilised to counteract this, incorporating dispersion interactions into the DFT functional or as an additional empirical correction.[265–270]

The effects of solvent can be accounted in DFT calculations through computationally demanding explicit models or more efficient implicit models.[271] Implicit models generally treat solvent molecules as a homogenous field.[272,273]

Computational chemistry has been used to interrogate the nature of chemical bonds with a number of bond indices. The Wiberg bond index (WBI) is one of the simplest bond indices and for simple homonuclear diatomic molecules the WBI is often equal to the ideal integral equal to half of the difference between the number of electrons occupying bonding and antibonding orbitals.[274] The Mayer bond index (MBI) is seen as an extension of the WBI which is more able to account for the ionic nature of some bonds as well as delocalisation and multicentre effects.[275] The fuzzy atom bond order (FBO) is based on the fuzzy atom partition, in which there is a 'fuzzy' continuous transition between the electron clouds of atoms in a molecule rather than sharp boundaries.[276] Several metrics for measuring population or partial atomic charges have been developed. The Mulliken population analysis (MPA) is one of the most common but is frequently criticised for failing to give physical meaningful results for complex cases and a high basis set dependence.[277,278] The natural population analysis (NPA), based on the population of natural atomic orbitals (NAOs) has been proposed as an alternative.[279]

1.8. Global Aims

This body of work has two overarching aims, to develop a coherent understanding of the relationship between the structure and Lewis acidity of organoantimony cations, and to explore the chemistry of $[Pd_4(Me_3Sb)_4(\mu_3\text{-}(Me_3Sb)_4)]$, an unprecedented complex previously reported by the group.[280] This work can be placed into the wider context of the ongoing main group renaissance and builds on recent interest on group 15 cationic Lewis acids, in particular that of organoantimony Lewis acids which has been advanced by the groups of Gabbaï, Hudnall, Matile, Chitnis and Burford among others. The state of the art is that a diverse range of Lewis acidic organoantimony cations have been reported although the utility of these compounds is relatively limited. This body of work aims to provide a more complete picture of what structural properties of organoantimony cations affect the Lewis

acidity of these cations and to explore their reactivity with the goal of utilising them as catalytic and/or stoichiometric reagents for organic transformations. The second overarching aim is related to the historic neglect of organoantimony(III) compounds as ligands for transition metals, often being treated as an addendum to work on the more ubiquitous phosphine ligands (see 5.1.1 Stibines as Transition Metal Ligands). $[Pd_4(Me_3Sb)_4(\mu_3\text{-}(Me_3Sb)_4)]$ was the first example of a homoleptic complex with unsupported bridging pnictine ligands and is among a sparing series of complexes with bridging pnictine ligands. The original report thoroughly described the synthesis and electronic structure of $[Pd_4(Me_3Sb)_4(\mu_3\text{-}Me_3Sb)_4]$ but did not delve into its reactivity. Given the historic inattention to stibines as ligands and the unanticipated nature of this complex, a further exploration of its reactivity is timely.

2. Interrelationship between Structure and Lewis Acidity in Triarylchlorostibonium Salts

2.1 Introduction

2.1.1 Electrophilic Phosphonium Cations

Much of the recent work on p-block Lewis acids has focused on boron(III) centred species, which have been well reviewed (see 1.5 Lewis Acid Catalysis).[281] Phosphorus based Lewis acids, while not as well developed as boron based species, have been the subject of an immense amount of work recently. Unlike boron-based Lewis acids, which typically derive their Lewis acidity from a vacant p_z orbital, Phosphorus Lewis acids are typically in the +5 oxidation state and therefore formally saturated. The source of electrophilicity in a Phosphorus(V) based Lewis acid is typically a low lying σ* orbital trans to a strongly electron withdrawing species (Figure 2.1). Literature examples of Phosphorus Lewis acids are useful for structural and design considerations when investigating similar antimony-based Lewis acids as they are isoelectric and typically isolobal. Similar antimony-based species would be expected to be more Lewis acidic due to antimony being a more electropositive element than Phosphorus; due to its larger size antimony species are more amenable to hypervalent interactions and organometallic scrambling, possibly yielding divergent reactivity.

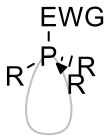

Figure 2.1. σ* orbital of tetrahedral phosphonium salt. EWG = Electron withdrawing group.

Phosphonium salts are ubiquitous synthetic tools in organic chemistry; they are utilised in the Wittig reaction,[282–285] dehydration reactions, [286–288] ionic liquids[289–291] and as phase transfer catalysts.[292–295] Catalytic reactivity of phosphonium salts can be considered a form of organocatalysis although they are commonly compared to organometallic main group catalysts. Catalytic reactions mediated by phosphonium salts acting as Lewis acids reported before 2009 have been reviewed by Werner.[296] A seminal publication by the Stephan group in 2013 on the catalytic applications of the perfluorinated phosphonium salt, $[(C_6F_5)_3PF][B(C_6F_5)_4]$ (**A**), for defluorination of fluoroalkanes has generated a novel field.[142] The cation of this salt and related salts are typically referred to as electrophilic phosphonium cations (EPCs). $[(C_6F_5)_3PF][B(C_6F_5)_4]$ was synthesised *via* a halide abstraction reaction with $[Et_3Si][B(C_6F_5)_4]$ from $(C_6F_5)_3PF_2$; this yielded a tetrahedral phosphonium cation which is able to form a hypervalent adduct with Lewis bases. This is a typical design of previously reported phosphonium catalysts.[296] The perfluorinated aryl rings and fluoride render the Phosphorus centre highly electron

deficient. The orbital rationale for the electrophilicity of **A** is a low lying $\sigma^*_{P\text{-}F}$ orbital which provides a definite site for Lewis base coordination. **A** is capable of catalytic hydrodefluorination of a range of alkyl fluorides in the presence of Et_3SiH. Mechanistic investigations suggest that this reactivity is mediated by a carbocation which is formed after fluoride abstraction by **A** (Scheme 2.1). The carbocation is reduced by Et_3SiH, yielding the respective alkane and $[Et_3Si]^+$, which regenerates the catalyst. The original report found **A** to be unreactive with Et_3SiH, discounting the possibility that $[Et_3Si]^+$ actually acts as the active species, which is established as a hydrodefluorination catalyst.[297]

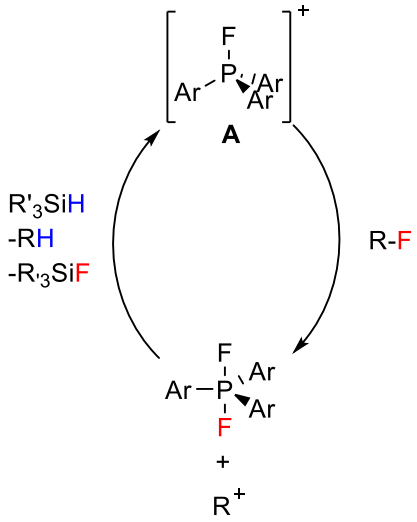

Scheme 2.1. Catalytic cycle for the hydrodefluorination of alkyl fluorides. Ar = C_6F_5

The reactivity of $[(C_6F_5)_3PF][B(C_6F_5)_4]$ (**A**) has been expanded to include a wide variety of other Lewis acid mediated reactions, particularly C-C bond formatting reactions. **A** has been deployed for the Friedel–Crafts alkylation of aromatics with benzyl fluorides in the presence of Et_3SiH, which is proposed to occur *via* a similar mechanism to the hydrodefluorination reaction.[298] Et_3SiH acts to reduce the Wheland intermediate, producing dihydrogen and $[Et_3Si]^+$, which regenerates the catalyst. $[(C_6F_5)_3PF][B(C_6F_5)_4]$ is also a potent catalyst for Diels−Alder reactions and Nazarov cyclisations.[299] These reactions were not probed mechanistically but most rationally involves the EPC coordinating to the ketone; $(C_6F_5)_3PO$ was observed as a side product, supporting this. **A** was also observed to hydrosilylate ketones, imines and nitriles.[300] Computational investigations suggest that this reactivity is mediated by a trimolecular transition state (P···H-Si···O-C), yielding $(C_6F_5)_3PFH$ and a carbocation, which forms the silyl ether and regenerates the catalyst *via* hydride abstraction; hydrodeoxygenation of ketone, yielding the respective alkane and $(Et_3Si)_2O$ was also observed.[301] $[(C_6F_5)_3PF][B(C_6F_5)_4]$ also acts as a catalyst for: the hydroarylation and

hydrothiolation of olefins[302], dehydrocoupling reactions[303] and the reduction of phosphine oxides.[304]

$[(C_6F_5)_3PF][B(C_6F_5)_4]$ (**A**) has been structurally modified to yield improved stability and reactivity. **A** is sensitive to both moisture and protonic solvents due to the P-F bond. $[(C_6F_5)_3P(OAr)][B(C_6F_5)_4]$ (Ar = 4-FC_6H_4, Ph) were stable in a DCM solution exposed to air for 90 minutes whereas $[(C_6F_5)_3P(OAr)][B(C_6F_5)_4]$ (Ar = 2,4-$F_2C_6H_3$, C_6F_5) decomposed in less than 10 minutes.[305] $[(1,8\text{-}(Ph_2P)_2C_{10}H_6)][B(C_6F_5)_4]_2$ is stable in air in the solid state for 24 hours. $[Ph_3(CF_3)P][Y]$ and $[Ph_2(CF_3)MeP][Y]$ (Y = OTf, $B(C_6F_5)_4$) are stable in air, HCl and wet/protonic solvents up to 100°C but do decompose in the presence of a combination of water and base.[306] While more stable than the fluorophosphonium cation, these salts and the aryloxyphosphoniums cations were less catalytically active.

The influence of the identity of the alkyl/aryl group in $[R_3PF][B(C_6F_5)_4]$ on the Lewis acidity of the EPC was probed (Table 2.1).[307] A higher degree of electron withdrawing character of R was found to yield a more Lewis acidic Phosphorus centre. To probe the influence of a sterically hindered phosphonium centre, $[(3,5\text{-}(CF_3)_2C_6H_3)_3PF][B(C_6F_5)_4]$ was synthesised and screened for catalytic activity.[308] Computational and exchange reactions suggest that $[(3,5\text{-}(CF_3)_2C_6H_3)_3PF][B(C_6F_5)_4]$ is slightly less Lewis acidic than $[(C_6F_5)_3PF][B(C_6F_5)_4]$ however the absence of ortho fluorides was hypothesised to yield a more sterically accessible phosphonium centre. While $[(3,5\text{-}(CF_3)_2C_6H_3)_3PF][B(C_6F_5)_4]$ was a less effective catalyst for the dimerisation of 1,1-diphenylethylene and the hydroarylation of Ph_2NH than $[(C_6F_5)_3PF][B(C_6F_5)_4]$ (**A**), it was more active for the double hydroarylation of $(p\text{-Tol})_2NH$, which has been attributed to a kinetic enhancement due to a more sterically accessible phosphonium centre.

Table 2.1. ^{31}P NMR shifts, ^{19}F NMR shifts and FIA of selected phosphonium cations. The ^{19}F NMR shift refers to the phosphonium fluoride. ^{31}P and ^{19}F NMR shifts are shifted downfield with increased cationic character. FIA is based on an *psuedo*isodesmic reaction with COF_3^- . The anion is omitted from calculations for the FIA. Data adapted from ref 307.

Compound	**^{31}P NMR (ppm)**	**^{19}F NMR (ppm)**	**FIA (kJ mol^{-1})**
$[tBu_3PF]^+$	148.5	-171.6	148
$[Mes_3PF]^+$	92.9	-116.7	-
$[o\text{-}Tol_3PF]^+$	104.3	-125.5	-
$[Ph_3PF]^+$	94.7	-128.3	165
$[(4\text{-}FC_6H_4)_3PF]^+$	93.3	-123.8	214
$[Ph(C_6F_5)_2PF]^+$	87.2	-123.4	227
$[(C_6F_5)_2PhPF]^+$	77.7	-121.9	280
$[(2,3,5,6\text{-}F_4C_6H)_3PF]^+$	70.1	-124.4	287
$[(C_6F_5)_3PF]^+$	68.0	-120.7	323

Other more exotic EPCs have also been reported (Figure 2.2). $[Ph_2PF(SIMes)][B(C_6F_5)_4]_2$ (SIMes = 1,3-dimesitylimidazolidin-2-ylidene) is a rare example of an isolatable dicationic phosphonium salt which is more Lewis acidic than $[(C_6F_5)_3PF]^+$ without the use of highly fluorinated organic groups (Figure 2.2).[309] Chiral EPCs with binaphthyl backbones have also been reported.[310]

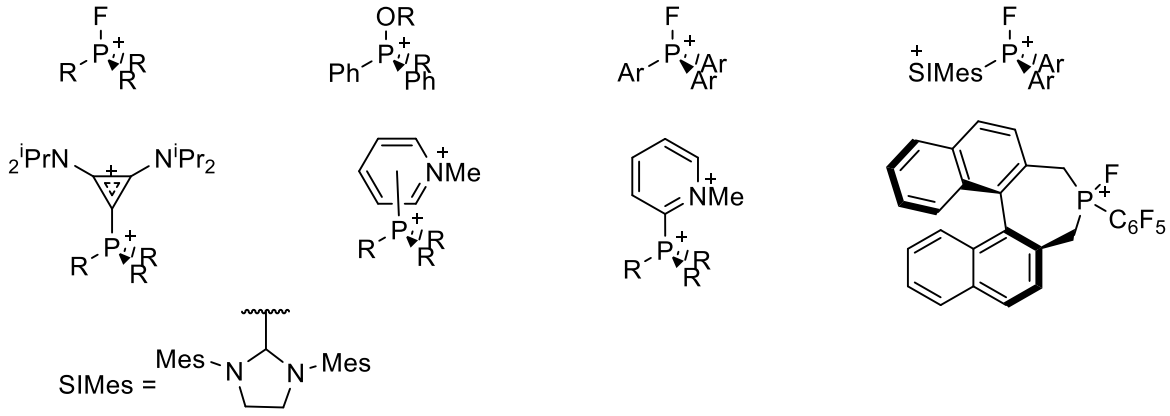

Figure 2.2. Structure of reported EPCs. SIMes = saturated Mes (1,3-Bis(2,4,6-trimethylphenyl)-4,5-dihydroimidazol-2-ylidene).

To mimic the chemistry of transition metals, reversible P^{III}/P^{V} redox cycles have been deployed for catalytic applications.[311] These typically involve phosphines with rigid backbones to stabilise certain oxidation states *via* an orbital engineering approach. Such systems have been deployed for methylamination of arylboronic acids and esters,[312] reductive C–N coupling of nitroaromatics and boronic acids,[313] and the annulation of amines and carboxylic acids.[314]

2.1.2 Organoantimony Lewis Acids

The strongly corrosive nature of simple antimony(III) and antimony (V) halides has limited their deployment as Lewis acid catalysts in both academic and industrial chemistry. Despite this, $SbCl_3$ has been reported as a catalyst for the Mukaiyama Aldol reaction,[315] Michael addition, ring opening of epoxides with anilines,[316] Biginelli reaction,[317] selective cleavage of trityl ethers,[318] fluorination of thiocarbonyl compounds[319], Friedel−Crafts transformations[320] and solvent free acetylation of alcohols, phenols, and amines among other reactions.[321] Antimony(V) chloride and fluoride, which are significantly more corrosive and somewhat volatile, have more limited use.[322–325] To circumvent the difficult nature of antimony halide compounds, organoantimony Lewis acids with highly electron withdrawing organic groups and/or a cationic antimony centre have been pursued as Lewis acid catalysts. The tetraphenylstibonium ion, ($[Ph_4Sb]^+$) has been extensively studied and yielded several insights into the design of organoantimony Lewis acids. A catalyst screen for the synthesis of cyclic carbonates from carbon dioxide and epoxides demonstrated that pentavalent antimony compounds are typically more active than trivalent compounds and that triphenylstibine dihalides (Ph_3SbX_2) are more active than tetraphenylstibine halide (Ph_4SbX); while pentaphenyl stibine (Ph_5Sb) was the least active pentavalent species it was significantly more active than the trivalent species, including $SbCl_3$.[326] The cycloaddition of oxetane and CO_2 is catalysed by Ph_4SbI whereas Ph_4SbBr and Ph_3SbI_2 are inactive.[327] Ph_4SbI is more active in benzene than coordinating solvents and having discounted a free iodide as the catalytically active species, it was concluded that the $[Ph_4Sb]^+$ was the active species. This was further supported by conductivity measurements.[328] The requirement for an open coordination site in Lewis acid catalysis is commonly observed. The cycloaddition of oxiranes with isocyanates to yield disubstituted oxazolidinones is also catalysed by Ph_4SbI; the 3,4-isomer can be nearly selectively obtained with careful selection of conditions (Scheme 2.2).[329]

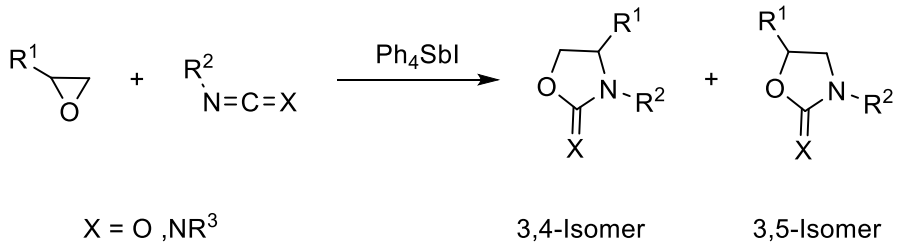

Scheme 2.2. Ph_4SbI catalysed cycloaddition of oxiranes with heterocumulenes

Similarly, Ph_4SbI also catalyses the cycloaddition of oxiranes with carbodiimides, giving the 3,4-isomer exclusively (Scheme 2.2).[330] Similar reactivity with other heterocumulenes and a

mechanistic study suggests that the reaction proceeds *via* ring opening of the oxiranes, insertion of the heterocumulene and finally cyclisations of the antimony carbamate.[331] The selectivity was determined to be dependent of the differences in reactivity of the antimony alkoxide resulting from the ring opening of the oxirane.

This reactivity has recently been revisited with a series of catalysts of the form $[ArPh_3Sb][OTf]$ (Ar = Ph, 1-naphthyl, 9-anthracenyl, Mes, 2-Me_2N-C_6H_4, 2-Me_2NCH_2-C_6H_4); all of the catalysts favour the 3,4-isomer however the $[(Mes)Ph_3Sb][OTf]$ was found to be the most selective catalyst.[332] The ancillary amino donors were found to quench the activity of the catalyst. $[(C_6F_5)_4Sb][B(C_6F_5)_4]$ has been reported as an air stable salt which activates alkyl C-F bonds in the presence of Et_3SiH.[58] Mechanistically, this is distinct from the reaction catalysed by the phosphonium salt, $[(C_6F_5)_3PF][B(C_6F_5)_4]$ (see. 2.1.1 Electrophilic Phosphonium Cations). $[(C_6F_5)_4Sb][B(C_6F_5)_4]$ is reduced by the silane to produce $(C_6F_5)_3Sb$, C_6F_5H and the active species, $[Et_3Si]^+$. The strongly electron withdrawing aryl groups reduce the nucleophilicity of the stibine ($(C_6F_5)_3Sb$) such that it does not coordinate to the silylium cation and quench reactivity. $[(C_6F_5)_4Sb][B(C_6F_5)_4]$ also abstracts a fluoride from $[B(C_6F_5)_3F]^-$ and SbF_6^-, rendering it a Lewis super acid. Similar reactivity was not observed with $(C_6F_5)_4Sb(OTf)$, highlighting the importance of an open coordination site. Both $[Ph_3SbCl][SbCl_6]$ and $[Mes_3SbCl][SbCl_6]$ catalytically polymerise THF, while $Ar_3Sb(OTf)_2$ and $Ar_3SbF(OTf)$ (Ar = Ph, Mes) are inactive; of these only $[Ph_3SbCl][SbCl_6]$ is active in the Friedel−Crafts dimerisation of 1,1-Diphenylethylene (Scheme 2.3), the inactivity of $[Mes_3SbCl][SbCl_6]$ has been attributed to the steric bulk around the antimony centre.[52]

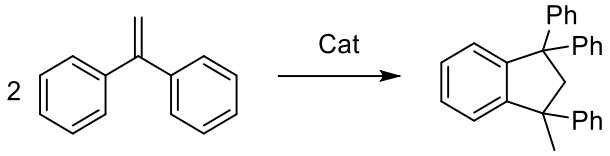

Scheme 2.3. Friedel−Crafts dimerisation of 1,1-Diphenylethylene to 1-methyl-1,3,3-triphenyl-2,3-dihydro-1H-indene

The interaction between an electron deficient pnictogen centre and a Lewis basic species can also be described as a pnictogen bond, analogous to the more well established chalcogen and halogen bonding.[333,334] This terminology asserts an aspect of non-covalent, electrostatic interactions in contrast to the σ* orbital description, which is purely based on orbital interactions. In the pnictogen bonding model, an electron deficient region, known as a σ hole, forms on the pnictogen atom when bonded to a more electronegative element, opposite to the substituent.[335,336] This model has been used to rationalise the reactivity of a series of stibines of the form $(C_6F_5)_nPh_{3-n}Sb$ (n = 0-3), which are active catalysts for the

Reissert-type substitution of isoquinoline and conversion of 1-chloroisochromane to an ester substituted isochromane (Scheme 2.4).[31] The yield and binding constant with a chloride anion was found to increase with higher numbers of pentafluorophenyl substitution. Comparison with the analogous phosphine, arsine, selenoether, telluraether, aryl bromide and aryl iodide found the stibine to the most active catalytically and have the highest experimental chloride anion affinity.

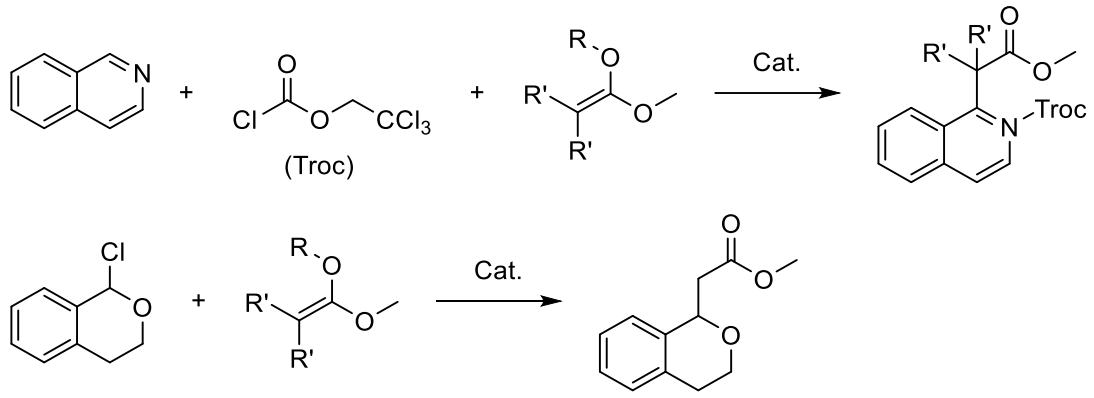

Scheme 2.4. Reissert-type substitution of isoquinoline (top) and conversion of 1-chloroisochromane to an ester substituted isochromane (bottom). R = TMS, R' = Me; R = TBS, R' = H.

The Lewis acidity of a series of stibines, Ar_3Sb (Ar = Ph, C_6F_5, 3,5-$(CF_3)_2C_6H_3$), and their respective triarylantimony(V) tetrachlorocatecholates ($Ar_3Sb(O_2C_6Cl_4)$) have been assessed *via* phosphine oxide binding constants, computational studies and catalytic screening.[155] The Lewis acidity was found to increase with Ar = Ph< C_6F_5 <3,5-$(CF_3)_2C_6H_3$, however oxidation had a more pronounced effect. This was rationalised with a dual pnictogen bonding and lowering the energy of σ* orbital model. The binuclear antimony complexes $[(Ph_3Sb)_2\mu\text{-}O][Y]_2$ (Y = $O_3SC_6F_5$, $O_3SC_8F_{17}$) are active catalysts for Michael addition with indole and the allylation of benzaldehyde with tetraalyltin.[337]

2.1.3 Aims and Objectives

The aim of this body of work is to explore and rationalise a correlation between the substitution pattern of an aryl ring on an antimony(V) Lewis acid and the Lewis acidity on the Sb centre. For this work cations of the form $[Ar_3SbX]^+$ (X = halide) were targeted as they contain several features that would render them strong, tuneable antimony based Lewis acids: the Sb is in the more electron deficient +5 state, the organoantimony fragment is cationic, the Sb-X bond would yield a definite coordination site for Lewis bases *trans* to the bond and the aryl groups allow for tuning the chemical environment of the Sb centre. A range of weaky coordinating anions (WCAs) have been reported and meticulous literature

on their installation and use is available indicating that synthetic strategies from neutral Sb(V) halide precursors are accessible.[338]

The specific objectives of this body of work are:

a) Synthesise and characterise the necessary precursors for the cations of the form $[Ar_3SbX]^+$: Ar_3Sb and Ar_3SbX_2 (Ar = fluorinated aryl, X = halide).
b) Synthesise and characterise salts of the form $[Ar_3SbX][Y]$ (Ar = fluorinated aryl, X = halide, Y = WCA).
c) Assess the Lewis acidity of the $[Ar_3SbX]^+$ cation *via* stoichiometric reactivity including halide abstraction from halocarbons and coordination of Lewis bases.
d) Assess the suitability of the triarylhalostibonium salts $[Ar_3SbX][Y]$ for hydro-dehalogenation of halocarbons.
e) Assess the suitability for the triarylhalostibonium salts $[Ar_3SbX][Y]$ for other Lewis acid mediated catalysis, e.g. the Friedel-Crafts dimerisation of diphenylethylene.
f) Utilise computational methods such as fluoride ion affinities (FIAs) to rank the Lewis acidity of the $[Ar_3SbX]^+$ cations and elucidate an orbital rationale for Lewis acidity.

2.2 Results and Discussions

2.2.1 Synthesis of Neutral Stibines and Stibine dichlorides

The parent organoantimony compounds for the topic of this project, triarylstibines (Ar_3Sb), were synthesised *via* a salt metathesis reaction between $SbCl_3$ and the respective Grignard reagent (ArMgBr) in diethyl ether. A variety of stibines with fluorinated rings were synthesised (Scheme 2.5). These proceeded in moderate yields. Except for $(2,4,6\text{-}F_3C_6H_2)_3Sb$ (**1-4**), ortho fluorides precluded a synthetically viable route to the respective triarylstibine. These reactions produced a large amount of a white solid, which is presumably SbOCl, the hydrolysis product of $SbCl_3$, on aqueous work-up. This suggests that either any Grignard formed decomposed due to the elimination of MgF_2 and the formation of a benzyne-like compound or that the Grignard was not formed initially due to mesomeric donation destabilising the prospective Grignard. This has been observed previously.[339,340] NMR evidence suggests that the Grignard reagent was not formed in any sizeable yields, as the crude mixture primarily consisted of starting aryl bromide along with unknown minor impurities. The structures of triarylstbines and triarylstibine dihalides are well established; the solid-state structures of some previously unknown compounds were analysed by SCXRD and found to be consistent with the expected structure. The solid-state structures of **1-3** and **1-6** do not reveal any noteworthy intermolecular interactions (Figure 2.3, Figure 2.4). In both cases the antimony centre has the expected trigonal pyramidal geometry.

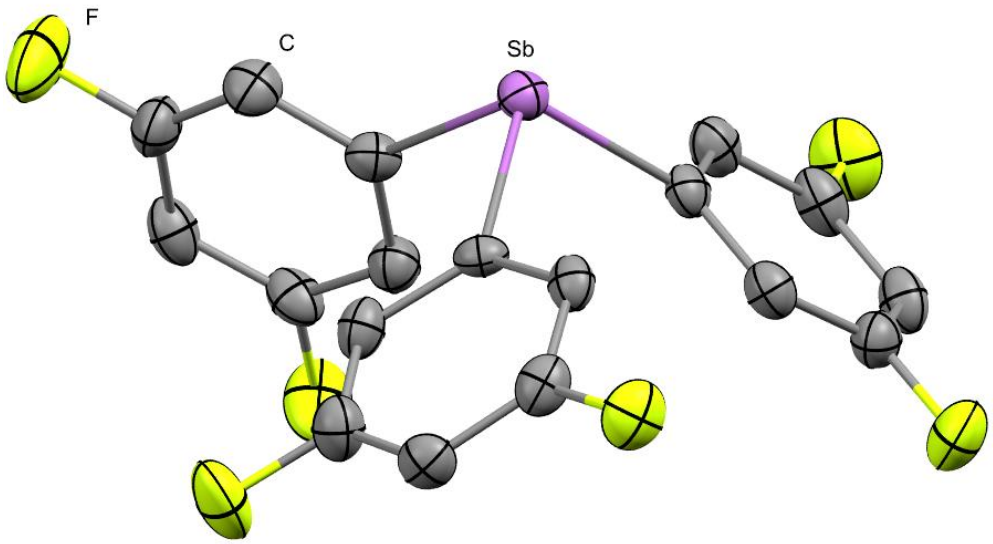

Figure 2.3. Solid state structure of **1-3**. Ellipsoids shown at 50% probability. Hydrogen atoms have been omitted.

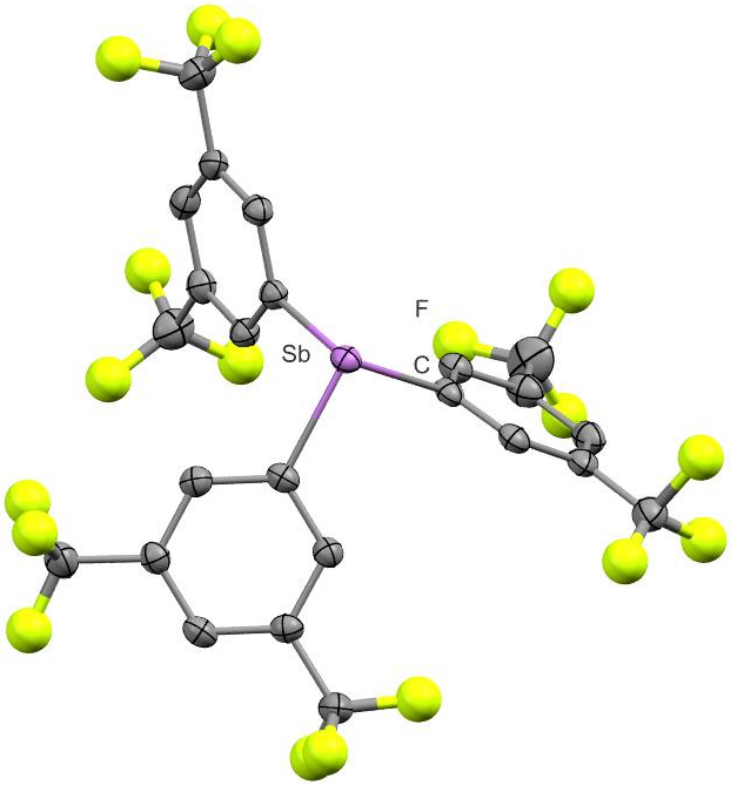

Figure 2.4. Solid state structure of **1-6**. Ellipsoids shown at 50% probability. Hydrogen atoms have been omitted. The trifluoromethyl groups are modelled as disordered over two positions, only one is shown. The fluorides are shown as isotropic.

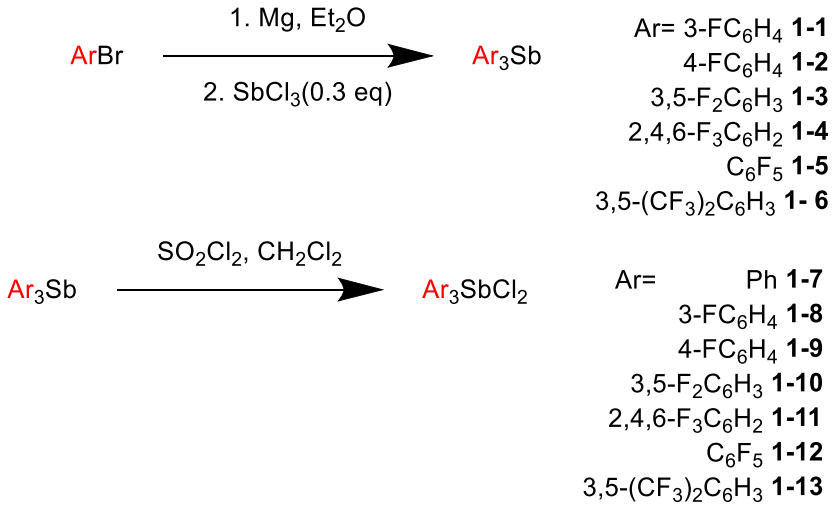

Scheme 2.5. Synthesis of triarylstbines and oxidation to triarylstibine dichlorides.

Triarylstibine dichlorides (Ar_3SbCl_2) were synthesised in moderate to good yields *via* oxidative addition of Cl_2 to Ar_3Sb with SO_2Cl_2 acting as an *in-situ* source of Cl_2.[341] The solid-state structures of **1-10**, **1-11** and **1-13** were determined by SCXRD. In each case the

structure has an expected trigonal bipyramidal Sb centre (Figure 2.5). The stibine dichlorides were used as precursors for the target of this body of work, triarylchlorostibonium salts.

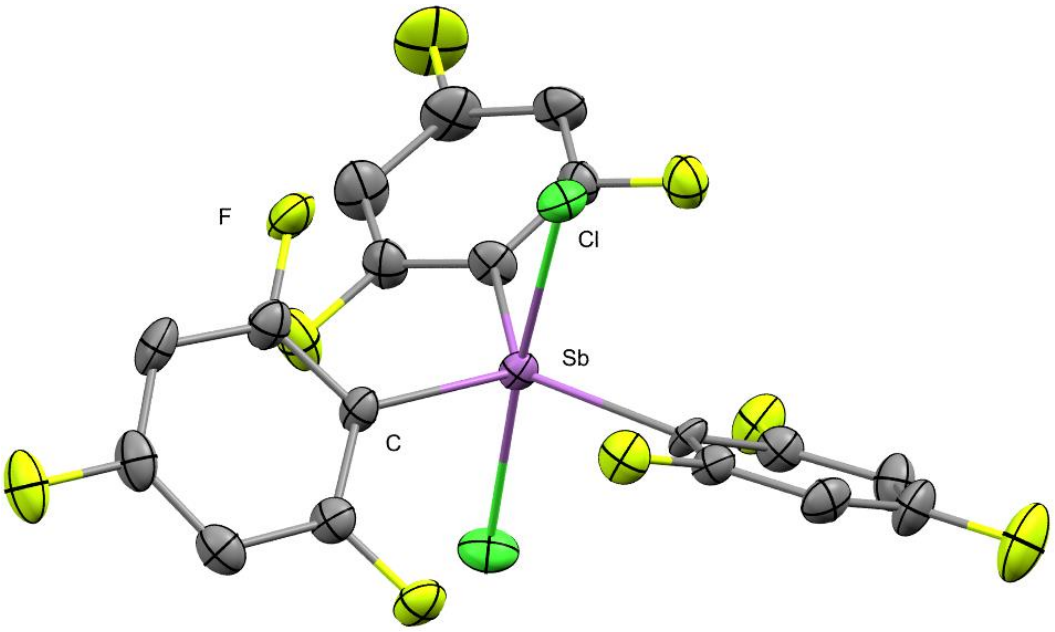

Figure 2.5 Solid state structure of **1-11**. Ellipsoids shown at 50% probability. Hydrogen atoms have been omitted. Two molecules are present in the asymmetric unit, only one is shown.

2.2.2 Synthesis and Structure of Triarylchlorostibonium Salts

The initial targets of this work were salts of the form $[Ar_3SbCl][B(3,5\text{-}(CF_3)_3C_6H_3)_4]$ ($[Ar_3SbCl][BAr^F]$), which were targeted *via* chloride abstraction from Ar_3SbCl_2 with $Ag[BAr^F]$. The products of these reactions were oils that failed to crystallise. NMR spectra obtained on the crude product indicated the presence of a multiple of fluorine containing impurities with signals between -100 and -150 ppm consistent with the formation of Sb-F bonds. One possible explanation is that the resulting cationic antimony centre interacts with the trifluoromethyl groups of the anion, which is supported by the observation that a signal corresponding to the respective stibine difluorides was observed. This precludes use as a catalyst, as the presence of a decomposition pathway would severely limit potential for high turnover. Although this does serve as a proof of concept for the Lewis acidity of similar compounds, difficultly characterising these salts through spectroscopy and SCXRD also restricts the potential for profound examination of their chemistry.

Salts of the form $[Ar_3SbCl][B(C_6F_5)_4]$ were then targeted to exclude the presence of any C_{sp3}-F bonds on the counteranion. $[Et_3Si][B(C_6F_5)_4]$ is a well-established reagent for the abstraction of halides and the installation of the $[B(C_6F_5)_4]^-$ counteranion. $[Et_3Si][B(C_6F_5)_4]$

was synthesised according to modified literature procedure,[342–344] taking extra precautions due to the potentially explosive nature of the $Li[B(C_6F_5)_4]$ intermediate.[344]

Recrystallising the silyl borate ($[Et_3Si]_2(\mu\text{-}H)[B(C_6F_5)_4]$) in toluene yielded off-white crystals of $[Et_3Si(C_7H_8)][B(C_6F_5)_4]$ which was used to synthesise $[Ar_3SbCl][B(C_6F_5)_4]$ (**1-14** to **1-18**) (Scheme 2.6), in each case giving a reddish oil which was recrystallised in DCM/hexane to yield analytically pure salts of $[Ar_3SbCl][B(C_6F_5)_4]$ (**1-14** to **1-18**). $[(4\text{-}FC_6H_4)_4Sb][B(C_6F_5)_4]$ was also isolated as a minor product from the synthesis of $[(4\text{-}FC_6H_4)_3SbCl][B(C_6F_5)_4]$ (**1-16**) (Figure 2.6).

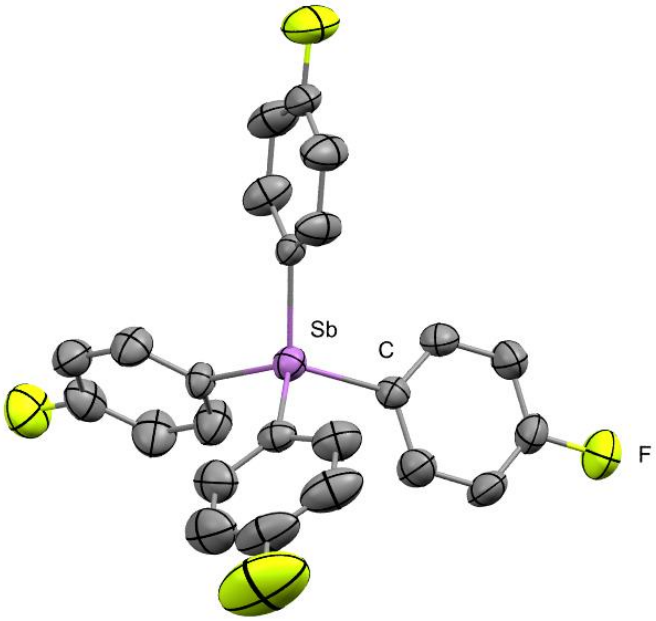

Figure 2.6. Solid state structure of $[(4\text{-}FC_6H_4)_4Sb][B(C_6F_5)_4]$. Ellipsoids shown at 50% probability. Hydrogen atoms and borate counteranion have been omitted.

Initially, these synthetic procedures utilised 1.2 eq of Ph_3SbCl_2 in toluene at room temperature. An excess of Ph_3SbCl_2 was utilised on the assumption that the resulting stibonium salt, $[Ph_3SbCl][B(C_6F_5)_4]$, and any residual $[Et_3Si][B(C_6F_5)_4]$ would have similar solubility profiles and be difficult to separate. This yielded clear colourless crystals which were determined to be $[(Ph_3SbCl)_2(\mu\text{-}Cl)][B(C_6F_5)_4]$ (**1-19**) (Figure 2.7) by SCXRD.

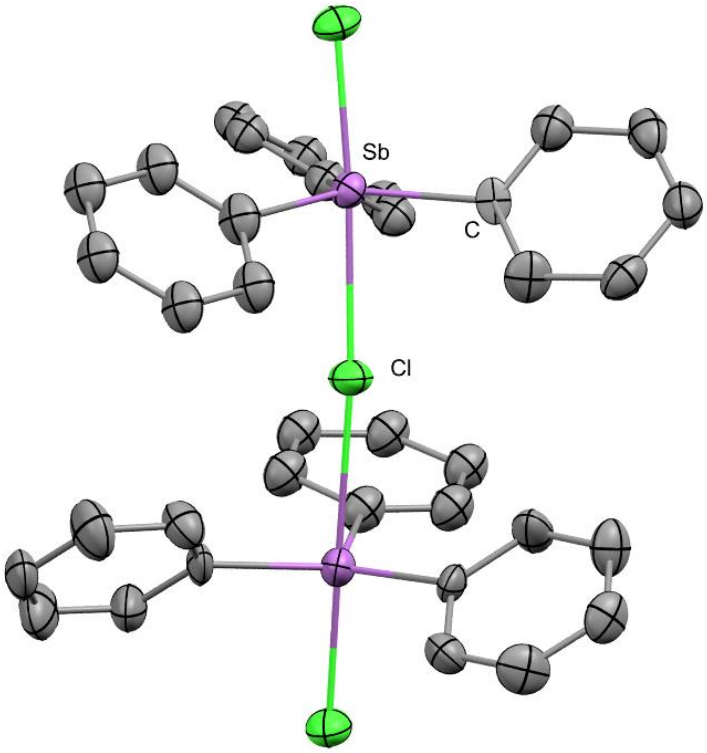

Figure 2.7. Solid state structure of $[(Ph_3SbCl)_2(\mu\text{-}Cl)][B(C_6F_5)_4]$ (**1-19**). Ellipsoids shown at 50% probability. Hydrogen atoms and borate counteranion have been omitted.

The bond lengths of the terminal chlorides (aver: 2.372(3) - 2.388(3) Å) are shorter than in the parent stibine dihalide (2.4709(6) - 2.4925(6) Å),[345] consistent with the formation of a cationic antimony centre. Both Sb centres are trigonal bipyramidal. Repeating the same reaction with 2.4 equivalents of Ph_3SbCl_2 yielded a red oil which on work-up gave $[(Ph_3SbCl)_2(\mu\text{-}Cl)][B(C_6F_5)_4]$ (**1-19**) in 62% yield.

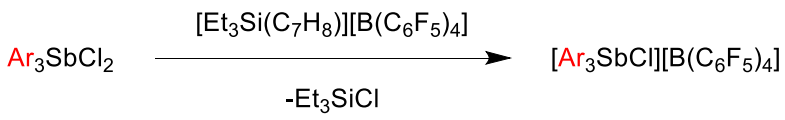

Ar=	
Ph	**1-14**
3-FC_6H_4	**1-15**
4-FC_6H_4	**1-16**
3,5-$F_2C_6H_3$	**1-17**
2,4,6-$F_4C_6H_2$	**1-18**

Scheme 2.6. Synthesis of Triarylchlorostibonium tetrakis(pentafluorophenyl)borates

Earlier synthesises utilised the silyl borate ($[Et_3Si]_2(\mu\text{-}H)[B(C_6F_5)_4]$), without initial recrystallisation. This yielded a red oil which contained the parent stibine (Ph_3Sb) among other products. The parent stibine, despite being soluble in aromatic solvents, was difficult

to wash out with toluene. It is hypothesised here that the stibine and stibonium form a weak adduct which hinders work-up and crystallisation. For this reaction the source of $[Et_3Si][B(C_6F_5)_4]$ was synthesised as per the initial report by Lambert in 1994,[342] which was later revealed to actually be ($[(Et_3Si)_2(\mu\text{-}H)][B(C_6F_5)_4]$), necessitating recrystallisation (*vide supra*).[346,347] $[Ar_3SbCl][B(C_6F_5)_4]$ was reduced to the parent stibine in the presence of Et_3SiH, which likely accounts for the observation of the reduced stibine (see 2.2.3 Stoichiometric Reactivity of Triarylchlorostibonium Salts).

Attempted synthesis of $[Ar_3SbCl][B(C_6F_5)_4]$ (Ar = C_6F_5, 3,5-$(CF_3)_2C_6H_3$) from **1-12** and **1-13** respectively with an equivalent strategy yielded multiple species, predominantly the starting Triarylstibine dichlorides. This suggests that the strongly electron withdrawing nature of the aryl rings precludes the abstraction of a chloride by $[Et_3Si(C_7H_8)][B(C_6F_5)_4]$.

All stibonium salts **1-14** to **1-18** were structurally characterised by SCXRD (Table 2.2,Figure 2.8). Each stibonium salt had a monomeric tetrahedral cation without any significant interactions with the counteranion, in the solid state. The τ4 parameters, a measure of the geometry around a four coordinate centre (τ4 = 1 for a perfect tetrahedral),[348] are between 0.90 and 0.97. In each case the Sb-Cl bond length significantly contracts from the parent stibine dihalide, consistent with the formation of a cationic metal centre.

Table 2.2. Crystallographic parameters of triarylchlorostibonium salts **1-14** to **1-18**. * Average of crystallogrpahically inequivalent Sb-Cl bond length. a) [349] b)[350]

Compound	Sb-Cl bond length	Average Sb-C bond length	Average Sb-Cl bond length (Parent Stibine dichloride)	Average C-Sb-C bond angle	τ4	Sb-B separation
1-14	2.2821(19)	2.086	2.463[a]	114.21	0.90	6.344
1-15	2.2924(11)	2.086	-	113.50	0.92	7.363
1-16	2.2757(9)	2.083	2.458 [b]	111.24	0.96	7.795
1-17	2.260*	2.091	2.455	110.82	0.96	7.484
1-18	2.2532(19)	2.073	2.415	111.64	0.97	7.297

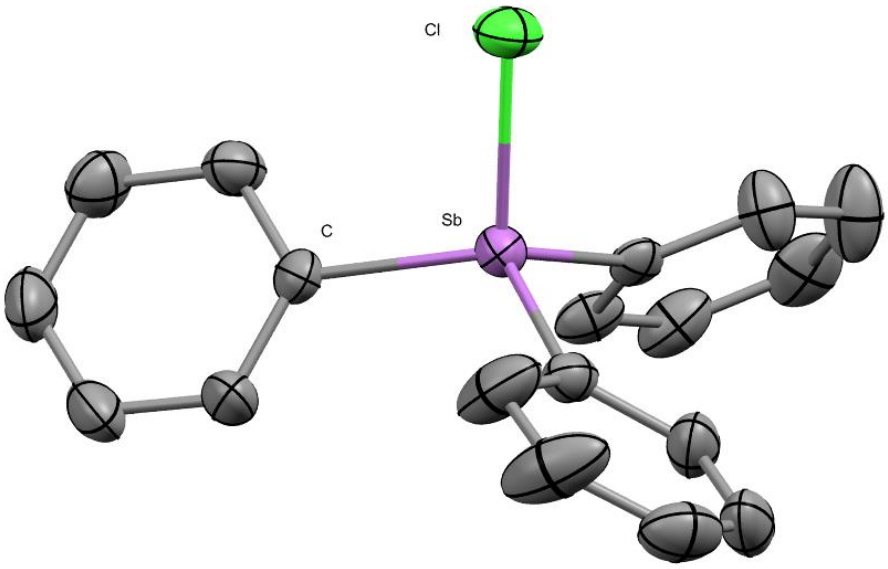

Figure 2.8. Solid state structure of **1-14.** Ellipsoids shown at 50% probability. Hydrogen atoms and borate counteranion have been omitted. One phenyl group is disordered over two positions, only one is shown here.

Computational evidence suggests that the source of Lewis acidity in these stibonium salts is a low lying $\sigma^*_{Sb\text{-}Cl}$ orbital (*vide infra*). A stronger Sb-Cl bond would suggest a more accessible $\sigma^*_{Sb\text{-}Cl}$ orbital/electron deficient Sb centre. Probing the length of the Sb-Cl bond in the solid state *via* SCXRD data would thus allow for a direct measure of the electrophilicity of $\sigma^*_{Sb\text{-}Cl}$ orbital. Based on this, the Lewis acidity of the triarylchlorostibonium salts generally increases with increased fluorination, **1-15** is an exception to this, which has a slightly longer Sb-Cl bond than **1-14** (difference: 0.0103 Å) (Figure 2.9). Fluorine substituents in aryl systems are both inductively withdrawing and weakly mesomerically donating. This suggests that the 4-fluorine mesomerically donates to the Sb centre and thus quenches some of the Lewis acidity. The smaller difference in Sb-Cl bond length between **1-18** and **1-17** (difference 0.007 Å) verses **1-17** and **1-16** (difference: 0.016 Å) further supports this explanation. This observation suggests some degree of π bonding between the C_{ipso} and Sb.

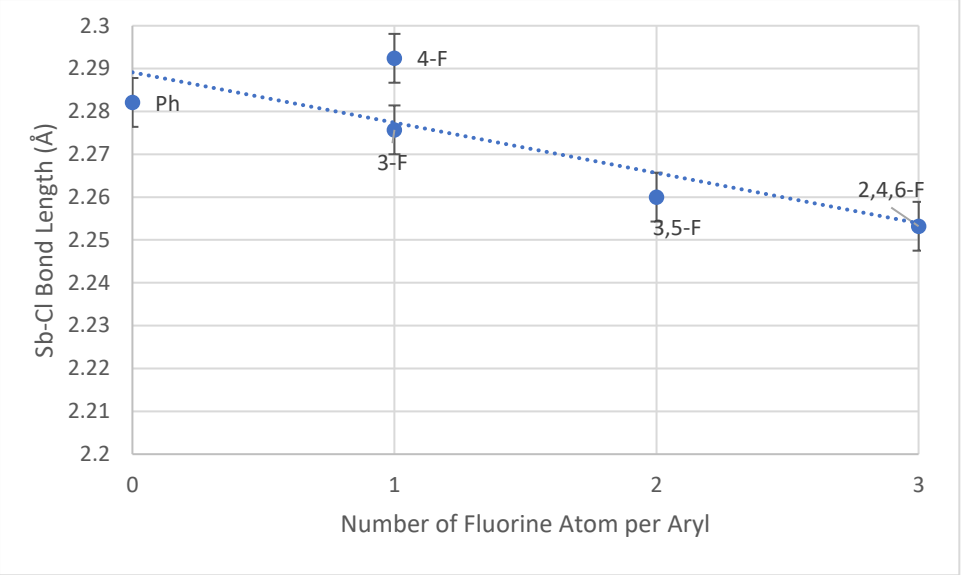

Figure 2.9. Graph showing the linear relation between degree of aryl fluorination and Sb-Cl bond length in **1-14** to **1-18.** Error bars = 3σ

To further probe the Lewis acidity of the triarylchlorostibonium salts **1-14** to **1-18**, the fluoride ion affinity (FIA) and hydride ion affinity (HIA) were calculated for the respective cations along with Et_3Si^+ at the M062x/def2SVP with D3 dispersion correction, in the gas phase (Table 2.3). The computational method was determined by a functional testing procedure where a starting structure, obtained from the solid-state structure was optimised ultilising various DFT functionals (M06, M06-2X, ωB97xD, PBEPBE and B97D) with def2SVP as the basis set. M062x/def2SVP gave the closest agreement between optimised and experimental structural parameters. The FIAs and HIAs were calculated according to a method by Gabbaï, where the affinity is calculated by direct reaction with either a fluoride or hydride ion.[155]

Table 2.3. FIA and HIA of Et_3Si^+ and the respecitve cations of triarylchlorostibonium salts 1-14 to 1-18. The LUMO energy is given relative to the LUMO of Ph_3SbCl^+

Cation	FIA (kJ mol^{-1})	HIA (kJ mol^{-1})	LUMO energy (eV)
$Et3Si^+$	880.8895653	961.086723	-
Ph_3SbCl^+	666.2969745	773.3971057	0.0000
$(3\text{-}FC_6H_4)_3SbCl^+$	700.4647064	808.4630999	-0.0114
$(4\text{-}FC_6H_4)_3SbCl^+$	697.1912855	803.3019182	-0.0067
$(3,5\text{-}F_2C_6H_3)_3SbCl^+$	733.569741	843.3901789	-0.0223
$(2,4,6\text{-}F_3C_6H_2)_3SbCl^+$	689.9734185	806.8709967	-0.0180

While the FIAs and HIAs generally increase with increased fluorination, para and ortho fluorination seem to quench the Lewis acidity at the Sb centre according to this measure.

This is in accordance with the crystallographic evidence (*vide supra*). Each of the adducts is C_{3v} symmetrical and, except for $(2,4,6\text{-}F_3C_6H_2)_3SbClF$ and $(2,4,6\text{-}F_3C_6H_2)_3SbClH$, has aryl groups which are coplanar with the Cl-Sb-F/H angle. Some of these adducts did not fully optimise according to the RMS displacement and maximum displacement criteria, suggesting a flat energy surface. This discounts different isomers as a rationalisation for the varying FIAs/HIAs. The respective LUMO energies follow a similar trend.

The orbital rationale for the observed Lewis acidity was also probed. The Kohn-Sham (KS) HOMO of $[Ph_3SbCl]^+$ consists primarily of the aryl π system (Figure 2.10 a) and the KS LUMO consists primarily of the $\sigma^*_{Sb\text{-}Cl}$ (Figure 2.10 b). The KS LUMO is made up of a combination of the s and p_z orbital on Sb and the p_z orbital on Cl. The other cations have a similar frontier electronic structure.

a)

b)

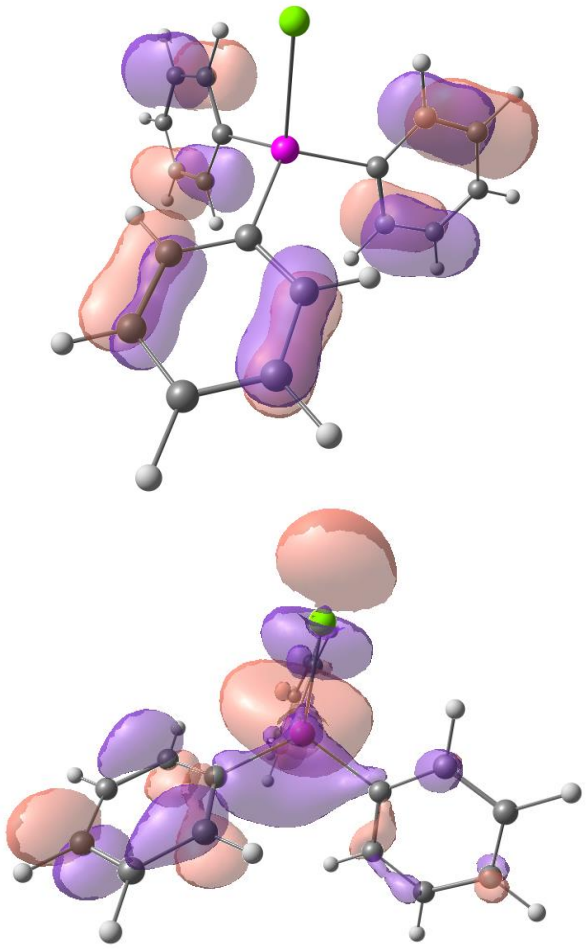

Figure 2.10. a) Kohn-Sham HOMO and b) Kohn-Sham LUMO of $[Ph_3SbCl]^+$

2.2.3 Stoichiometric Reactivity of Triarylchlorostibonium Salts

The Lewis acidity of the stibonium ions was initially established by stoichiometric reactivity with Lewis bases. The reactivity of the stibonium ions with Et_3PO is complex. An equimolar

mixture of **1-18** and Et_3PO yielded crystals which were determined to be a molecule of the parent stibine dichloride ($(2,4,6\text{-}F_3C_6H_2)_3SbCl_2$, **1-11**) co-crystalised with Et_3PO (Figure 2.11). Similar reactivity was observed with $[(C_6F_5)_3PF][B(C_6F_5)_4]$, which formed $(C_6F_5)_3PF_2$ on mixing with DMF, although $[(C_6F_5)_3PF(DMF)]^+$ was observed spectroscopically.[142]

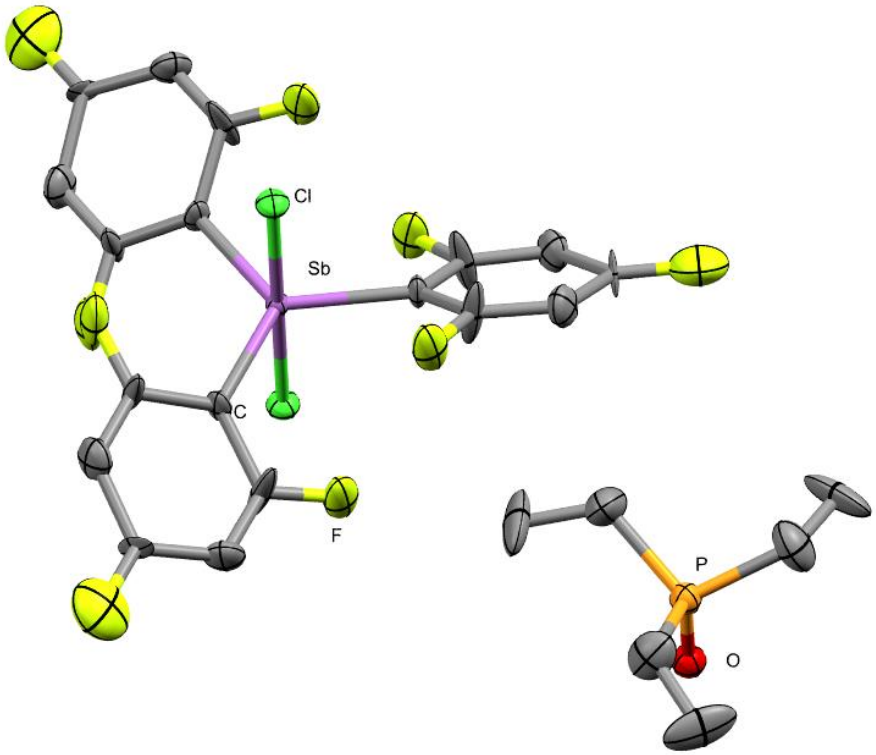

Figure 2.11. Solid state structure of **1-11/**Et_3PO**.** Ellipsoids shown at 30% probability. Hydrogen atoms and triflate counteranions have been omitted.

To further probe this reactivity, equimolar amount of Ph_3SbCl_2 (**1-7**) and AgOTf were mixed and filtered to remove AgCl. An equimolar amount of Et_3PO was added to the filtered solution. The resulting ^{31}P NMR spectrum contained three $^{31}P\{^1H\}$ signals, none of which corresponded to free Et_3PO. The structure of colourless crystals that were obtained from the reaction solution were determined to be $[Ph_3Sb(OPEt_3)_2][OTf]_2$ (**1-20**); the crystallographic data was of poor quality and the triflate counteranions could not be fully modelled due to a large degree of disorder, precluding extensive structural discussion (Figure 2.12). Based on this, it is likely that a Schlenk-type equilibrium exists. (Scheme 2.7). This precludes the use of the Gutmann-Beckett analysis for probing the Lewis acidity of these compounds as a $^{31}P\{^1H\}$ NMR signal cannot be unambiguously assigned as the mono-phosphine oxide adduct (see 1.4.2 Computational Methods of Ranking Lewis Acidity).

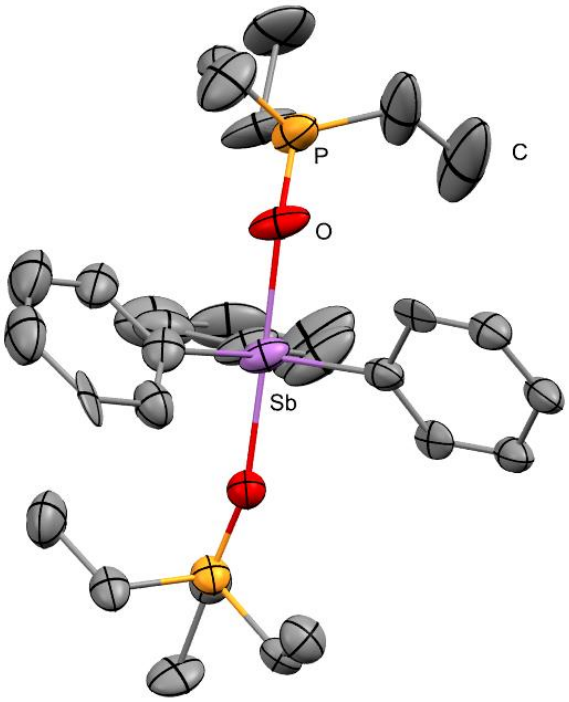

Figure 2.12. Solid state structure of **1-20.** Ellipsoids shown at 30% probability. Hydrogen atoms and triflate counteranions have been omitted.

$$2[Ar_3SbClD]^+ \rightleftharpoons Ar_3SbCl_2 + [Ar_3SbD_2]^{2+}$$

Scheme 2.7. Hypothetical Schlenk-type equilibrium. D = neutral donor

The stibonium salts **1-14, 1-18** and the dimer **1-19** rapidly react with trityl chloride/trityl fluoride (Ph_3CCl/Ph_3CF) in CD_2Cl_2 to form Ar_3SbCl_2/Ar_3SbClF respectively, demonstrating the halophilicity of these cations. As a moderately Lewis acidic stibonium salt, **1-14** was mixed with triflurotoluene ($PhCF_3$) to give an intensely red solution which contained trace amounts of $(4\text{-}FC_6H_4)_3SbClF$ by NMR.

The stibonium salts **1-14, 1-18** and the dimer **1-19** rapidly reduce to the parent stibine (Ar_3Sb) in the presence of Et_3SiH. Sb-H bonds are typically thermally unstable.[351] Similar reactivity is also observed in $[(C_6F_5)_4Sb][B(C_6F_5)_4]$, which reduced to $(C_6F_5)_3Sb$ and C_6F_5H in the presence of Et_3SiH; [58] other less electron deficient stibonium ions are known to be redox stable in the presence of Et_3SiH.[352,353]

The mechanism for the reduction of $[Ph_3SbCl]^+$ in the presence of silane was probed by computational methods, through a series of relaxed potential energy surface (PES) scans and transition state optimisations. The mechanism was determined to occur *via* a three step mechanism (Figure 2.13).

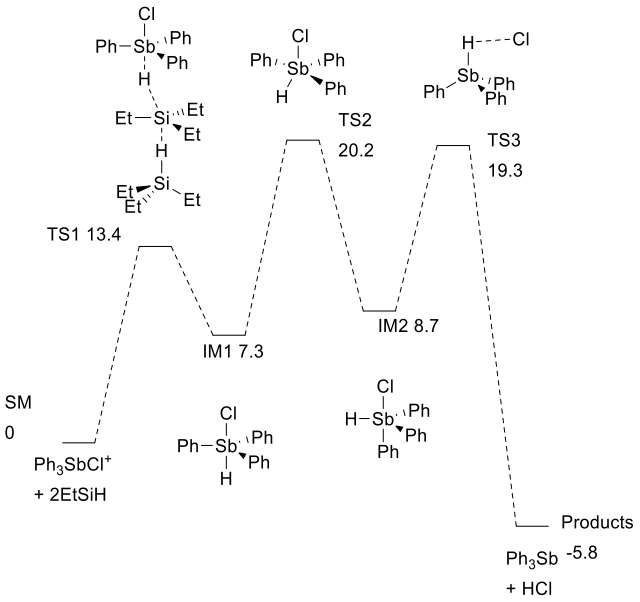

Figure 2.13. Free energy profile for the reduction of $[Ph_3SbCl]^+$ by Et_3SiH. All energies are free energies shown in kcal/mol at calculated at M062X(D3)/def2SVP level of theory in dichloromethane.

The initial step is the nucleophilic attack of Et_3SiH on $[Ph_3SbCl]^+$ *via* a trimolecular transition state (**TS1**, Figure 2.14). A second molecule of Et_3SiH stabilises the hydride donating Et_3SiH, yielding Ph_3SbClH and $[(Et_3Si)_2(\mu\text{-}H)]^+$ (**IM1**).

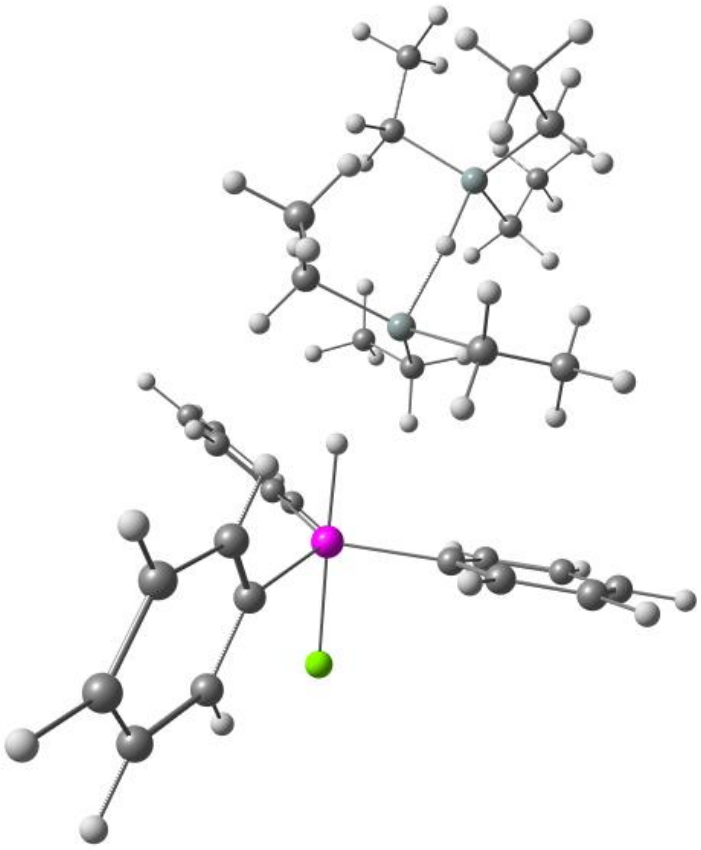

Figure 2.14. **TS1**. Pink-Sb, grey-C, white-H, green-Cl, teal-Si.

This is reminiscent of the reduction of acetophenone by Et_3SiH with catalytic $[(C_6F_5)_3PF]^+$, which was computationally determined to occur *via* a mechanism with the initial silylation of the ketone occurs *via* a similar trimolecular transition state with a P···H-Si···O motif.[354] A $[(C_6F_5)_3PF]^+/Et_3SiH$ adduct was computationally observed however no equivalent adduct was observed here.

The remaining reduction of Ph_3SbClH is unimolecular. In **IM1**, the hydride and chloride are in the axial positions; a berry *pseudo*-rotation type mechanism (**TS2**) yields Ph_3SbClH with an equatorial H (**IM2**). HCl is then reductively eliminated *via* a highly ionic transition state (**TS3**, Figure 2.15). The high barrier to the reverse reaction, the oxidative addition of HCl to Ph_3Sb, renders the reaction kinetically irreversible.

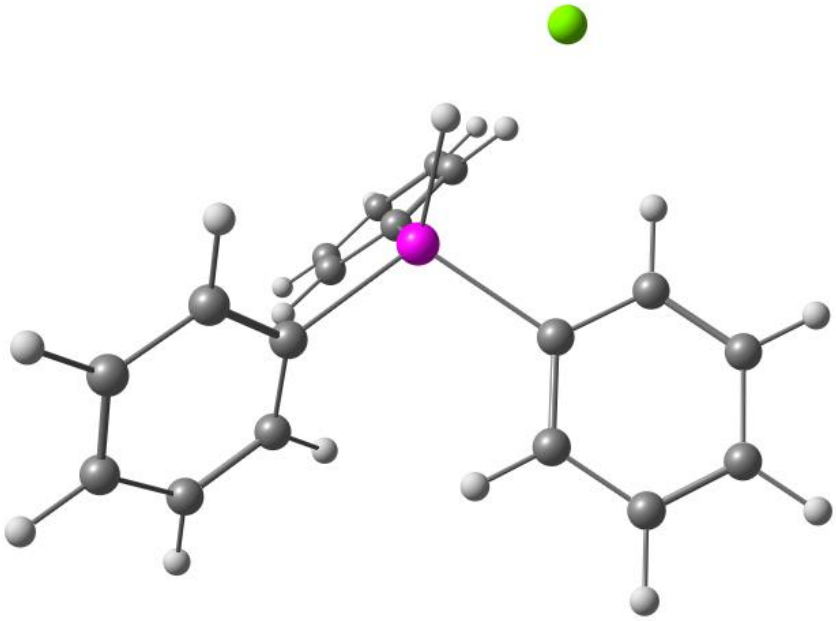

Figure 2.15. TS3. Pink-Sb, grey-C, white-H, green-Cl, teal-Si.

The formation of $[(Et_3Si)_2(\mu\text{-}H)]^+$ is experimentally supported by the multiple products observed in the ^{19}F NMR spectra, one of which was identified as Et_3SiF. Silylium cations are known to be highly unstable in chlorinated solvents.[342] The HCl is not observed, either directly or *via* derived decomposition products; however this is not unduly surprising given HCl has a low solubility in chloroform and is extremely volatile. As silane is frequently utilised in C-X bond activation by main group reagents, deploying these stibonium salts for similar reactivity is largely precluded.

To test the relative chlorophilicity of the stibonium ions, stibonium salt ($[Ar_3SbCl][B(C_6F_5)_4]$) was mixed with a triarylstbine dichloride (Ar'_3SbCl_2) in CD_2Cl_2 where Ar≠Ar'. Thermodynamic rearrangement allows for the formation of ($[Ar'_3SbCl][B(C_6F_5)_4]$) and

(Ar_3SbCl_2) (Scheme 2.8.) Mixing an equimolar solution of **1-8** and **1-17** in CD_2Cl_2 led to the complete formation of **1-10** and **1-15** by NMR which was further supported by isolating crystals of **1-15** by layering the reaction solution with n-hexane. Mixing a solution of **1-7** and **1-16** under the same conditions gave complete formation of **1-9** and **1-14**. These observations support conclusions drawn from crystallographic evidence.

$$Ar_3SbCl_2 + [Ar'_3SbCl][B(C_6F_5)_4] \rightleftharpoons Ar'_3SbCl_2 + [Ar_3SbCl][B(C_6F_5)_4]$$

Scheme 2.8. Halide exchange between a triarylchlorostibonium (Ar'_3SbCl^+, Ar ' = 4-FC_6H_4, 3,5-$F_2C_6H_3$) and triarylstibine dichloride (Ar_3SbCl_2) (Ar = Ph, 3-FC_6H_4). Ar≠Ar'

2.2.4 Catalytic Reactivity of Triarylchlorostibonium Salts

The dimerisation of 1,1 diphenylethylene to 1-methyl-1,3,3-triphenyl-2,3-dihydro-1H-indene is commonly utilised as a test reaction for Lewis acidity (Scheme 2.9 i). $[Ph_3SbCl][SbCl_6]$ is known to catalyse this reaction.[52] To test if a more electrophilic salt would also act as a catalyst for this reaction, both **1-17** and **1-18** were probed and catalysed this dimerisation to completion after 2 hours at room temperature in CD_2Cl_2 with 5% catalyst loading. The dimeric $[(Ph_3SbCl)_2(\mu\text{-}Cl)][B(C_6F_5)_4]$ (**1-19**) only gave traces of 1-methyl-1,3,3-triphenyl-2,3-dihydro-1H-indene in the same reaction, suggesting that the dimeric structure is largely retained in solution.

The potential for the deployment of these salts as Diels-Alder catalysts was probed, the Diels-Alder reaction between 1,3-cyclohexadiene and E-chalcone was considered as it is a relatively facile reaction. Loading an NMR tube with 1,3-cyclohexadiene (1 eq), E-chalcone (1 eq) and $[(3,5\text{-}F_2C_6H_3)_3SbCl][B(C_6F_5)_4]$ (**1-17**) (0.25 eq) in CD_2Cl_2 resulted in the production of a black precipitate and a deep red solution (Scheme 2.9 ii). The resulting NMR was complex and suggests three Ar-F species in solution, none of which could be identified. No Diels-Alder product was formed. No polymerisation of the 1,3-cyclohexadiene was observed.

The potential for the stibonium salts to act as catalysts for the Friedel-Crafts alkylation of benzene was probed (Scheme 2.9 iii). ^{t}BuBr was chosen as an alkylating agent, as it was assumed that the resulting Sb-Br intermediate bond would be weak enough to eliminate HBr on reaction with the Wheland intermediate. ^{t}BuBr was used to impede any carbocation rearrangements. Relative integrations of NMR spectroscopic signals were used to determine the yield after 30 minutes due to the absence of other obvious organic products (Table 2.4).

Table 2.4. Yield for the alkylation of benzene by ^{t}BuBr with triarylchlorostibonium salt as a catalyst.

Catalyst	Catalyst Loading	^{t}Bu-Br bond cleavage
1-14	1%	8%
1-14	5%	37%
1-16	1%	81%
1-18	1%	12%

Interestingly, $[(4\text{-}FC_6H_4)_3SbCl][B(C_6F_5)_4]$ (**1-16**) gives the highest yield despite being a weaker Lewis acid, which can be rationalised as a result of a more labile Sb-Br bond in the dihalide intermediate. An alternative explanation is that small amounts of decomposition product, which were undetectable by NMR are the actual active catalytic species. No major decomposition of the catalyst was observed in any of the tests.

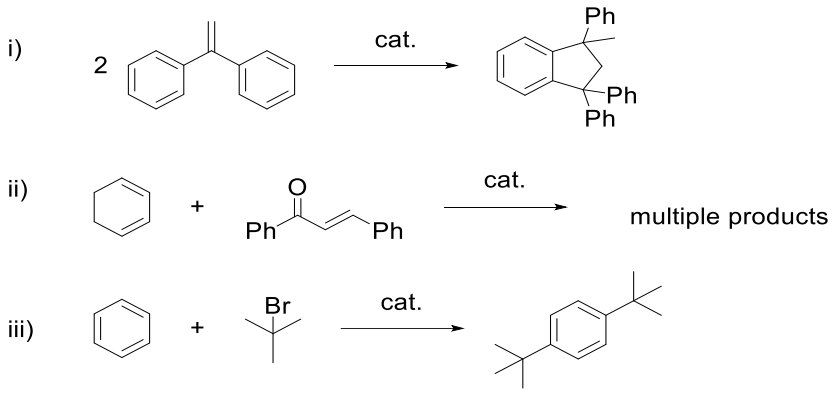

Scheme 2.9. Catalytic reactions reported here. i) Dimerisation of 1,1 diphenylethylene to 1-methyl-1,3,3-triphenyl-2,3-dihydro-1H-indene. ii) Diels-Alder cyclisation of 1,3-cyclohexadiene and E-chalcone . iii) Friedel Crafts alkylation of benzene with ^{t}BuBr.

2.2.5 Attempted Synthesis of Triarylfluorostibonium Salts

Cations of the form $[Ar_3SbF][B(C_6F_5)_4]$ were also targeted to elucidate the impact of the halide on the Lewis acidity of salts of the form $[Ar_3SbX][B(C_6F_5)_4]$. The necessitated the synthesis of Ar_3SbF_2 (Ar = Ph **1-21**, 3,5-$F_2C_6H_3$ **1-22**, 3,5-$(CF_3)_2C_6H_3$ **1-23**) by oxidative addition of F_2 to Ar_3Sb, provided by XeF_2.

$[Ph_3SbF][B(C_6F_5)_4]$ was targeted using an equivalent strategy as the triarylchlorostibonium salts which gave crystals of $[Ph_3(p\text{-}Tol)Sb][B(C_6F_5)_4]$ (Figure 2.16), NMR evidence suggested this was not the bulk product. The antimony atom is co-planar with the p-tolyl group, showing that this is correctly assigned as a covalently bonded p-totyl group as opposed to a coordinating toluene molecule.

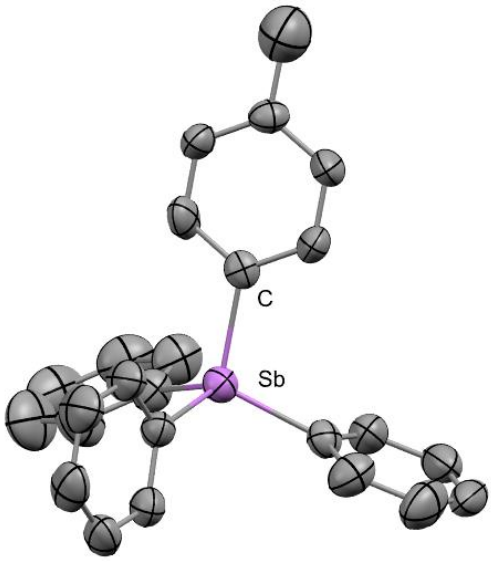

Figure 2.16. Solid sate structure of $[Ph_3(p\text{-}Tol)Sb][B(C_6F_5)_4]$. Ellipsoids shown at 50% probability. Hydrogen atoms and borate counteranion have been omitted.

The only obvious source of p-Tolyl substituent was the toluene solvent, suggesting that this was the product of a transient species reacting with the solvent. It was hypothesised that, due to the stronger thermodynamic driving force of the formation of a Si-F bond over Si-Cl bond, that $[Et_3Si][B(C_6F_5)_4]$ was capable of double defluorinating Ph_3SbF_2 while the equivalent reaction was not observed with Ar_3SbCl_2. This could yield $[Ph_3Sb]^{2+}$ which electrophilically attacks the 4 position of a toluene molecule to give $[Ph_3Sb(C_7H_8)]^{2+}$, similar reactivity was observed with $[Et_3Si][B(C_6F_5)_4]$.[346] To yield the observed product, $[Ph_3(p\text{-}Tol)Sb][B(C_6F_5)_4]$, the hypothesised adduct $[Ph_3Sb(C_7H_8)]^{2+}$ would have to be deprotonated at the 4 position, no obvious sources of base are present. Although Et_3SiH is used in synthesising the halide abstracting agent this is removed in recrystallisation.

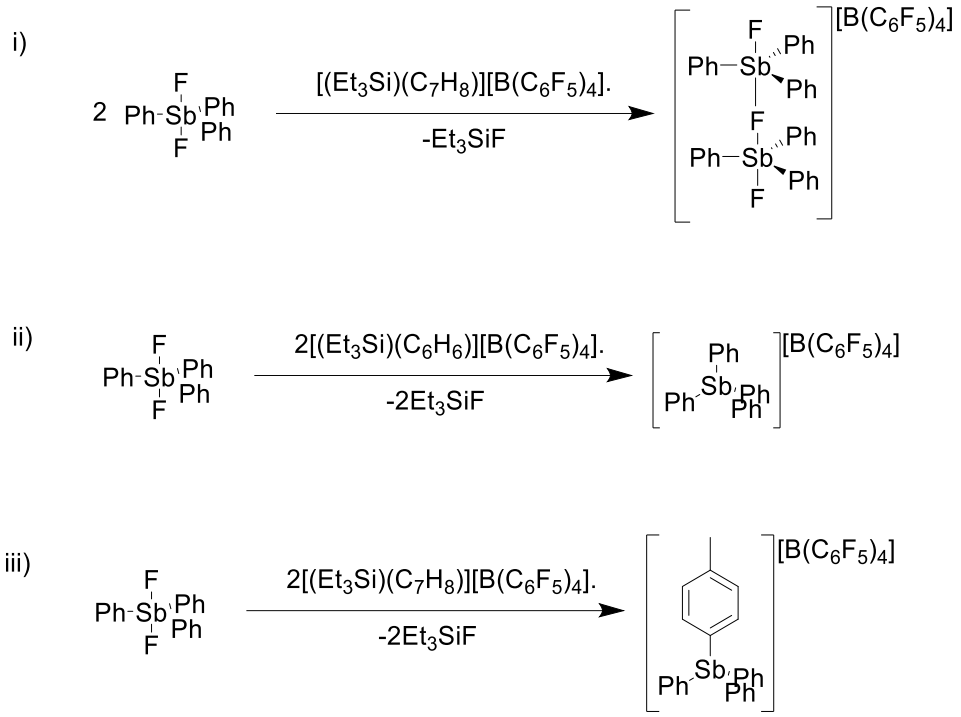

Scheme 2.10. i) Formation of $[(Ph_3SbF)_2(\mu\text{-}F)][B(C_6F_5)_4]$. Ii) Formation of $[Ph_4Sb][B(C_6F_5)_4]$. Iii)Formation of $[Ph_3(p\text{-}Tol)Sb][B(C_6F_5)_4]$

An alternative mechanism that could be proposed would involve the electrophilic attack of $[Ph_3SbF][B(C_6F_5)_4]$ on a toluene molecule to yield $[Ph_3SbF(C_7H_8)][B(C_6F_5)_4]$ followed by either intra- or intermolecular HF elimination. To probe the formerly proposed mechanism two equivalents of $[Et_3Si][B(C_6F_5)_4]$ was added to Ph_3SbF_2 in C_6D_6. NMR evidence suggests that using two equivalents of $[Et_3Si][B(C_6F_5)_4]$ double defluorinates Ph_3SbF_2 by the absence of any ^{19}F signals in the resulting NMR spectrum except for Et_3SiF, supporting the former hypothesis, no crystals suitable for SCXRD were isolated. Using exactly stoichiometric amounts of $[Et_3Si][B(C_6F_5)_4]$ and Ph_3SbF_2 yielded what was identified as $[(Ph_3SbF)_2(\mu\text{-}F)][B(C_6F_5)_4]$ by NMR spectroscopy. Due to the complications in efficient synthesis, triarylfluorostibonium salts were not pursed any further.

2.3 Conclusions

This body of work presents an account of the synthesis, structure and reactivity of salts of the form $[Ar_3SbCl][B(C_6F_5)_4]$ (Ar = Ph, 3-FC_6H_4, 4-FC_6H_4, 3,5-$F_2C_6H_3$, 2,4,6-$F_3C_6H_2$). A rudimentary model for relating the electronic structure of the aryl rings (Ar) in $[Ar_3SbCl]^+$ and the Lewis acidity at the Sb centre can be derived from this body of work from structural studies, catalytic experiments and computational studies. While there are some slight discrepancies between the structural studies and computational investigations, it can be reasonably concluded that in general increased fluorination of Ar increases the Lewis acidity in $[Ar_3SbCl]^+$ and that para fluorination quenches the Lewis acidity but not to a degree that totally negates the effect of the increased fluorination provided by the para-fluorine (Figure 2.17). This is dissimilar to analogous phosphonium cations.[307]

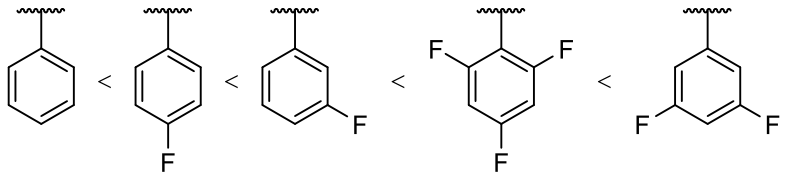

Figure 2.17. Approximate ranking of aryl groups from this body of work in order of increasing ability to render Sb centre Lewis acidic in $[Ar_3SbCl]^+$.

This body of work has also yielded novel information on the reactivity of these compounds; these salts were found to be Lewis acidic, as demonstrated by their activity in the dimerisation of DPE and alkylation of benzene. However, certain features may hinder their deployment as synthetically useful catalysts. The redox instability in the presence of silane greatly limits their usefulness and their reactivity with E-chalcone suggests a restricted usefulness in the activation of carbonyl compounds.

In terms of future work it would be worthwhile to pursue cations of the form $[Ar_3RSb]^+$, where R is a highly fluorinated alkyl group such as CF_3 or C_2F_5. Given that the silane mediated reduction involves the elimination of the chloride from $[Ar_3SbCl]^+$, replacing this with a highly fluorinated alkyl group may hinder this reduction while maintaining the electron deficient Sb centre. However, $[(C_6F_5)_4Sb]^+$ is similarly unstable in the presence of Et_3SiH,[58] suggesting that this may require a highly nuanced approach. An alternative solution would be to change to source of hydride from Et_3SiH to either a more sterically hindered silane or a completely different source. However, to achieve hydrodefluorination with the stibonium cations this way the silane would have to be sterically hindered enough to prevent the reduction of the stibonium but not too sterically hindered that the resulting silylium cation would not be able to dehalogenate the stibine dihalide (Scheme 2.11).

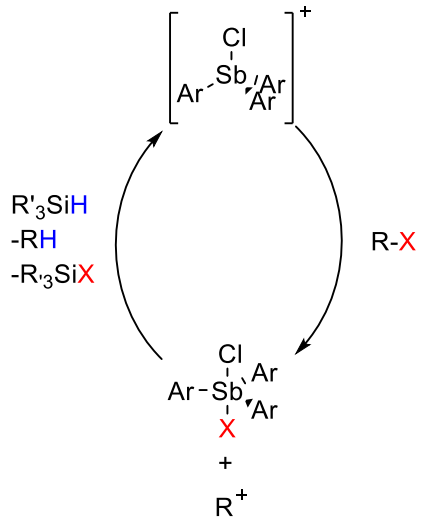

Scheme 2.11. Hypothetical reaction mechanism for the hydrodehalogenation of haloalkanes by $[Ar_3SbCl]^+$ and R_3SiH, where R = sterically demanding organic group.

It would also be useful to establish how general the effects of fluorination of aryl rings on stibonium cations (*vide supra*) are. For this, it would be useful to target, either experimentally or computationally, compounds of the form $[Ar_4Sb]^+$ and assess their Lewis acidity with varying degrees of fluorination of the aryl ring and interrogate their reactivity in a similar way to that described here. It would also be useful to investigate mixed aryl stibonium cations of the form $[Ar_2Ar'SbCl]^+$ (Ar≠Ar').

Overall this suggests that while these cations are certainly of fundamental interest, they are unlikely to be a step towards deployable transition metal free catalysis.

2.4 Experimental

See Appendix I: General Experimental Methods for general experimental information.

$(4\text{-}FC_6H_4)_3Sb$ (**1-2**)

A solution of 4-fluorophenyl bromide (1.7523 g, 1.1 mL, 10 mmol) in diethyl ether (30 mL) was added to freshly activated magnesium turnings (5.00 g, 205 mmol) at such a rate as to maintain a reflux. The was stirred for 3 hours then filtered. Freshly sublimed $SbCl_3$ (0.65 g, 2.84 mmol) was added dropwise over 15 minutes to the filtered solution to form a white precipitate. The solution was stirred at room temperature for 1 hour and at reflux for a further hour. The reaction mixture was exposed to the atmosphere and H_2O was added dropwise until effervescence ceased. The diethyl ether fraction was removed and the aqueous layer was extracted with ether (30 x 3 mL). Combined extractions were dried over $MgSO_4$ and diethyl ether was removed i*n vacuo*. The resulting oily solid was recrystallised in hexane.

Yield: 0.5567 g, 0.80 mmol 28%. ^{1}H-NMR (400MHz, $CDCl_3$,) δ ppm: 7.43-7.31 (m, 6H, o-H), 7.10 – 6.98 (m, 6H, m-H). $^{13}C\{^1H\}$ NMR ($CDCl_3$, 100 MHz) δ ppm:163.5 (d, J 248 Hz, p-C) 137.9 (d, J = 8 Hz, o-C), 132.9 (s, ipso-C) ,116.5 (d, J = 20 Hz, m-C). ^{19}F-NMR ($CDCl_3$, 376 MHz) δ ppm: -111.90 (s). Elemental Analysis, Found (Cal): C: 53.21% (53.11%) H: 3.04% (2.97%)

$(3\text{-}FC_6H_4)_3Sb$ (**1-1**)

Synthesised in an equivalent manner to $(4\text{-}FC_6H_4)_3Sb$ (*vide supra*). Yield: 0.5373 g, 1.32mmol, 46%. Clear oil. Repeated crystallisation attempts failed. ^{1}H NMR (400 MHz, $CDCl_3$) δ ppm: 6.99 - 7.13 (m, 2 H, o-H) 7.20 (d, J = 7.32 Hz, 1 H, p-H) 7.35 (td, J = 7.78, 5.49 Hz, 1 H, m-H) $^{13}C\{^1H\}$ NMR (100 MHz, $CDCl_3$) δ ppm: 116.2 (d, J = 21 Hz) 122.44 (d, J = 19 Hz) 131.14 (dd, J = 118.8, 5 Hz) (ipso carbon not observed). ^{19}F NMR (376 MHz, $CDCl_3$) δ ppm: -111.63 (s, 1 F) Elemental Analysis, Found (Cal): C: 52.89% (52.89%) H: 2.97 % (2.97%)

$(3,5\text{-}F_2C_6H_3)_3Sb$ (**1-3**)

Synthesised in an equivalent manner to $(4\text{-}FC_6H_4)_3Sb$ (*vide supra*). Yield: 0.7330g, 1.59 mmol, 56%. ^{1}H-NMR ($CDCl_3$, 400 MHz) δ ppm: 6.89-6.95 (m, 6H, o-H), 6.88 – 6.81 (tt, J = 8.92 Hz, 2.29 Hz, 3H, p-H). $^{13}C\{^1H\}$ NMR (100 MHz, $CDCl_3$) δ ppm 105.3 (t, J = 25 Hz), 118.3 (dd J = 9 ,6 Hz), 140.4 (s), 163.4 (dd, J = 256, 11 Hz) ^{19}F-NMR ($CDCl_3$, 376 MHz) δ ppm: -107.92 (s). Elemental Analysis, Found (Cal): C: 46.69% (46.89%) H: 1.67% (1.69%) Crystals suitable for SCXRD were removed from the bulk sample.

$(2,4,6\text{-}F_3C_6H_2)_3Sb$ (1-4)

Synthesised in an equivalent manner to $(4\text{-}FC_6H_4)_3Sb$ (*vide supra*). Red oil. Repeated crystallisation attempts failed. ^{1}H NMR (400 MHz, $CDCl_3$) δ ppm: -0.10 - 0.29 (impurity), 6.66 (br dd, J = 8.80, 6.29 Hz, 6 H, m-H). 7.15 (ddd, J = 7.89, 2.29, 1.26 Hz, impurity) ^{19}F NMR (376 MHz, $CDCl_3$) δ ppm: -105.60 (s, 6 F, o-F), -90.57 (s, 3 F, p-F). Due to the presence of impurities yield, elemental analysis and $^{13}C\{^{1}H\}$ NMR are not reported.

$(C_6F_5)_3Sb$ (1-5)

Mg turnings (0.4735 g, 19.7 mmol) in diethyl ether (15 mL) were activated by the addition of a crystal of I_2, which was indicated by a slight effervesce and diminishing of the brown colour. Bromopentafluorobenzene (4.8153 g, 19.4 mmol) was added over 20 minutes at 0°C. The solution turned a brown colour over the course of the addition. This was stirred at 0°C for 30 mins, then warmed to room temperature and stirred for 1h. $SbCl_3$ (1.4258 g, 6.24 mmol) in diethyl ether (5mL) was added dropwise over 15 minutes at -15°C . The solution was slowly warmed to room temperature over 16h. The reaction mixture was exposed to the atmosphere and 0.5M HCl (5 mL) was added dropwise until effervescent ceased. The diethyl ether fraction was removed and the aqueous layer was extracted trice with diethyl ether. Decolourising charcoal was added to combined extractions and the solution was filtered through celite to result in a brown solution. The solution were dried over $MgSO_4$ and diethyl ether was removed i*n vacuo*. The resulting brown oil was dissolved in hexane and filtered through silica to result in an off-white solution, which was reduced to a colourless oil *in vacuo.* The oil solidified to a white solid at to -15°C which was isolated by vacuum filtration to give a white solid (2.920 g, 4.7mmol, 75%). $^{13}C\{^{1}H\}$ NMR (101 MHz, $CDCl_3$) δ ppm 103.97 (br t, J=38.53 Hz), 137.43 (dt, J=258.65, 18.06 Hz), 143.1 (br d, J = 255 Hz), 148.4 (br d, J = 240 Hz). ^{19}F NMR (376 MHz, $CDCl_3$) δ ppm: -158.10 (br t, *J* = 17.34 Hz) -147.67 (s) -121.37 (s). NMR spectrum matched expected values.[47]

$(3,5\text{-}(CF_3)_2C_6H_3)_3Sb$ (1-6)

2.3M nBuLi in hexanes (4.8 mL, 11 mmol) was added dropwise to a solution of $3,5\text{-}(CF_3)_2C_6H_3Br$ (3.2527 g, 11.10 mmol) in Et_2O (20 mL) at -78°C, yielding the instant formation of an off-white precipitate which was stirred at -78°C for 3 hours. $SbCl_3$ (0.767 g, 3.33 mmol) in Et_2O (15 mL) was added dropwise at -78°C affecting the instant formation of a deep red solution which was stirred at -78°C for 1 hour then slowly warmed to room temperature overnight, turning dark yellow and then black over the course of warming and producing a white precipitate. The reaction mixture was exposed to the atmosphere and H_2O was added dropwise until effervescent ceased. The black diethyl ether fraction was

removed and the aqueous layer was extracted with diethyl ether (30 x 3 mL). Combined extractions were dried over $MgSO_4$ and diethyl ether was removed i*n vacuo*. The resulting red oil was recrystallised in hexane.

Yield: 95%. Off white solid. ^{1}H-NMR ($CDCl_3$, 400 MHz) δ ppm: 7.88 (s, 6 H, o-H) 7.96 (s, 3 H, p-H). $^{13}C\{^{1}H\}$ NMR ($CDCl_3$, 100MHz) δ ppm: 121.5 (s) 124.1 (m) 132.6 (q, *J* = 34 Hz) 135.6 (br s) 139.2 (s) ^{19}F-NMR ($CDCl_3$, 376 MHz) δ ppm: -63.65 - -62.53 (m). Elemental Analysis, Found (Cal): C: 37.71% (37.88%) H: 1.09% (1.19%) Crystals suitable for XRD were grown by layering a CH_2Cl_2 solution with hexane and cooling to -18°C.

Attempted Synthesis of $(2\text{-}FC_6H_4)_3Sb$

Synthesised in an equivalent manner to $(4\text{-}FC_6H_4)_3Sb$ (*vide supra*). Intractable red/black solid. NMR data matched starting material.

Attempted Synthesis of $(2,6\text{-}F_2C_6H_3)_3Sb$

Synthesised in an equivalent manner to $(4\text{-}FC_6H_4)_3Sb$ (*vide supra*). Intractable red/black solid.

Attempted Synthesis of $(2,3,5,6\text{-}F_4C_6H)_3Sb$

Synthesised in an equivalent manner to $(4\text{-}FC_6H_4)_3Sb$ (*vide supra*). Intractable red/black solid.

$(4\text{-}FC_6H_4)_3SbCl_2$ (**1-9**)

To a stirring solution of the **1-2** (0.2997 g, 0.75 mmol) in CH_2Cl_2 (12 mL) at -78°C, a 1M solution of SO_2Cl_2 (0.135 g, 1 mmol, 1mL) in CH_2Cl_2 was added dropwise over the course of 15 minutes. The clear solution was stirred for a further hour, when it was allowed to slowly warm to room temperature and stirred overnight. solvent was removed i*n vacuo* on a rotary evaporator. The resulting white solid was recrystallised in hexane/ CH_2Cl_2

Yield: 0.2074 g, 0.36 mmol, 48%. ^{1}H-NMR ($CDCl_3$, 400MHz) δ ppm: 8.20 -8.15 (m, 6H, o-H), 7.23 – 7.17 (m, 6H, m-H). $^{13}C\{^{1}H\}$ NMR ($CDCl_3$, 100 MHz) δ ppm: 116.9 (d, J = 21 Hz) 136.5 (d, J = 9 Hz, 1 C) ^{19}F-NMR ($CDCl_3$, 376 MHz) δ ppm: -106.06 (s). Elemental Analysis, Found (Cal): C: 45.37% (45.23%) H: 2.39% (2.53%) Crystals suitable for XRD were removed from the bulk sample.

$(3\text{-}FC_6H_4)_3SbCl_2$ (**1-8**)

Synthesised from **1-3** in an equivalent manner to $(4\text{-}FC_6H_4)_3SbCl_2$ (*vide supra*). Yield: 0.3585 g, 0.75 mmol,100%. ^{1}H NMR (400 MHz, $CDCl_3$) δ ppm: 7.28 - 7.38 (m, 1 H, m-H) 7.58 (td, J = 8.06, 5.49 Hz, 1 H, p-H) 7.96 - 8.15 (m, 2 H, o-H). ^{19}F NMR (376 MHz, $CDCl_3$) δ ppm: -108.52 (br s). $^{13}C\{^{1}H\}$ NMR (100 MHz, $CDCl_3$) δ ppm: 120.4 (dd, J = 196, 23 Hz) 130.4 (dd, J = 112, 5

Hz, 1 C) 140.5 (s, 1 C) 161.5 (s,) 164.0 (s). Elemental Analysis, Found (Cal): C: 45.43% (45.23%) H: 2.42 % (2.53%)

$(3,5\text{-}F_2C_6H_3)_3SbCl_2$ (**1-10**)

Synthesised from **1-4** in an equivalent manner to $(4\text{-}FC_6H_4)_3SbCl_2$ (*vide supra*). Yield: 0.2007 g, 0.42 mmol,56%. ^{1}H-NMR ($CDCl_3$, 400MHz): δ ppm: .84 (m, 6H, o-H/m-H), 7.08 (tt, 3H, J = 2.29 Hz, 8.46 Hz, p-H). $^{13}C\{^1H\}$ NMR ($CDCl_3$, 100 MHz) δ ppm: 108.0 (t, $J_{C\text{-}F}$ = 25 Hz, p-C), 117.6 (dd, $J_{C\text{-}F}$ = 80 Hz, 8 Hz, m-C) 140.8 (t, $J_{C\text{-}F}$ = 7.2 Hz, ipso-C) 162.9 (dd, $J_{C\text{-}F}$ = 512 Hz, 11 Hz, m-C) ^{19}F-NMR ($CDCl_3$, 376 MHz) δ ppm: -107.92 (s) .Elemental analysis, Found (Cal): C: 40.75% (40.64%) H: 1.52% (1.71%) Single crystals suitable for SCXRD were grown by slow evaporation of a CH_2Cl_2 solution in air.

$(2,4,6\text{-}F_3C_6H_2)_3SbCl_2$ (**1-11**)

Synthesised from crude **1-5** in an equivalent manner to $(4\text{-}FC_6H_4)_3SbCl_2$ (*vide supra*). Yield 6% (based on $SbCl_3$ used in synthesis of **1-5)**. ^{1}H NMR (400 MHz, $CDCl_3$) δ ppm 6.93 (br d, *J* = 7.20 Hz, 6 H, m-H). $^{13}C\{^1H\}$ NMR (100 MHz, $CDCl_3$) δ ppm 101.9 (br t, J = 25.4 Hz) 116.0 (br dd, J = 34, 10 Hz) 162.3 (br dd, J = 251, 12 Hz, 164.7 - 168.4 (m) ^{19}F NMR (376 MHz, $CDCl_3$) δ ppm -98.93 (s) -93.71 (s). Crystals suitable for XRD were removed from the bulk sample. Elemental Analysis, Found (Cal): 37.08% (36.90%) H: 0.95 % (1.03%)

$(C_6F_5)_3SbCl_2$ (**1-12**)

Synthesised from **1-6** in an equivalent manner to $(4\text{-}FC_6H_4)_3SbCl_2$ (*vide supra*). Yield 0.2220 g, 0.32 mmol,43 %. $^{13}C\{^1H\}$ NMR (100 MHz, $CDCl_3$-d) δ ppm 116.7 (br m) 137.8 (dt, J = 260 Hz, 15 Hz) 145.3 (dt, J = 261 Hz, 15 Hz).^{19}F NMR (376 MHz, $CDCl_3$) δ ppm -155.47 (br t, J = 17.34 Hz) -144.30 - -141.94 (m) -126.63 - -124.27 (m). Elemental Analysis, Found (Cal): C: 31.30% (31.16%) H: 0.00 % 0.00%)

$(3,5\text{-}(CF_3)_2C_6H_3)_3SbCl_2$ (**1-13**)

Synthesised from **1-10** in an equivalent manner to $(4\text{-}FC_6H_4)_3SbCl_2$ (*vide supra*) Yield: 0.4659 g ,0.56 mmol,74%. ^{1}H-NMR ($CDCl_3$, 400MHz) δ ppm: 8.17 (s, 3H, p-H), 8.79 (s, 6 H, o-H) $^{13}C\{^1H\}$NMR ($CDCl_3$, 100 MHz) δ ppm: 123.9 (s), 126.9 (br d, J = 4 Hz) ,133.3 (q, J = 34Hz), 134.6 (br s), 140.4 (s) ^{19}F-NMR ($CDCl_3$, 376 MHz) δ ppm: -62.69 (br m) Elemental Analysis, Found (Cal): H: 1.16% (1.09%) C: 34.52% (34.65%) Crystals suitable for SCXRD were removed from the bulk sample.

$[(Ph)_3SbCl][B(C_6F_5)_4]$ (**1-14**)

To a stirring solution of $[(Et_3Si)C_7H_8][B(C_6F_5)_4]$(0.4160 g, 0.47 mmol) in toluene (30 mL) was added a solution of Ph_3SbCl_2 (0.1653 g, 0.39 mmol) in toluene (15 mL) at room temperature. An off white oily suspension formed instantly. This was stirred at room

temperature for 90 min. The oil was allowed to settle and the solution was decanted. The oil was dried *in vacuo* to an oily solid. Crude NMR showed only one phenyl containing species. The oily solid was dissolved in CH_2Cl_2 and layered with hexane (to give white crystals (0.0650 g, 0.06 mmol, 15%). ^{1}H NMR (400 MHz, CD_3CN) δ ppm 7.67 - 7.87 (m, 9 H, o/p-H) 8.06 (br d, *J* = 7.78 Hz, 6 H, m-H). $^{13}C\{^{1}H\}$ NMR (101 MHz, CD_3CN) δ ppm 132.3 (s) 135.2 (s) 135.5 (s). ^{19}F NMR (376 MHz, CD_3CN) δ ppm -168.25 (br d, *J* = 14.45 Hz, B-C_6F_5) -163.81 (br d, *J* = 20.23 Hz, B-C_6F_5) -133.66 (br s, B-C_6F_5). Elemental Analysis, Found (Cal): H: 1.49% (1.42%) C: 47.15% (47.25%) Crystals suitable for XRD were removed from the bulk sample.

$[(3\text{-}FC_6H_4)_3SbCl][B(C_6F_5)_4]$ (**1-15**)

To a stirring solution of $[(Et_3Si)C_7H_8][B(C_6F_5)_4]$(0.4160 g, 0.47 mmol) in toluene (30 mL) was added a solution of $(3\text{-}FC_6H_4)_3SbCl_2$ (0.1860 g, 0.39 mmol) in toluene (15 mL) at room temperature. A red oil formed instantly. This was stirred at room temperature for 90 min. The oil was allowed to settle and the solution was decanted. The oil was dried under vacuum and triturated with hexane to give a white wax. This was dissolved in CH_2Cl_2 (5mL) and layered with hexane (30 mL) to give white crystals (0.120 g, 0.1 mmol, 25%). ^{1}H-NMR (400 MHz, CD_3CN): 7.53 - 7.62 (m, 1 H) 7.79 (td, J = 8.23, 5.49 Hz, 1 H) 7.86 - 7.93 (m, 2 H). ^{13} C-NMR (101 MHz, CD_3CN): 122.4 (dd, J = 23, 11 Hz) 131.4 (s) 133.9 (d, J = 8 Hz) 147.9 (br s) 150.3 (br s) 164.1 (d, J = 252 Hz). ^{19}F NMR (376 MHz, CD_3CN): -168.23 (br t, J = 17.34 Hz, B-C_6F_5) -163.80 (br t, J = 19Hz, B-C_6F_5) -133.67 (br s, B-C_6F_5) -108.90 (br s, m-F). 11B NMR (128 MHz, CD_3CN): -17.73 (s). Crystals suitable for XRD were removed from the bulk sample. Elemental Analysis, Found (Cal): H: 1.15% (1.08%) C: 45.12% (44.98%) Crystals suitable for SCXRD were removed from the bulk sample.

$[(4\text{-}FC_6H_4)_3SbCl][B(C_6F_5)_4]$ (**1-16**)

To a stirring solution of $[(Et_3Si)C_7H_8][B(C_6F_5)_4]$(0.3540 g, 0.40 mmol) in toluene (30 mL) was added a solution of $(4\text{-}FC_6H_4)_3SbCl_2$ (0.1620 g, 0.34 mmol) in toluene (15 mL) at room temperature. An red oil formed instantly. This was stirred at room temperature for 90 min. The oil was allowed to settle and the solution was decanted. The oil was dried under vacuum to give a white foam. The foam was dissolved in CH_2Cl_2 and layered with hexane to give white crystals and black oil. The solution was decanted and re-suspended in DCM, then filtered through celite to gave a clear solution which was layered again with hexane to give clear colourless crystals (0.0563 g, 0.05 mmol, 15%). ^{1}H NMR (400 MHz, CD_3CN) δ ppm 7.49 - 7.54 (t, J = 8.66 Hz , 6 H, m-H) 8.08 - 8.12 (m, 6 H, o-H). $^{13}C\{^{1}H\}$ NMR (101 MHz, CD_3CN) δ

ppm 119.7 (d, *J* = 22 Hz), 138.4 (d, *J* = 10 Hz,) ^{19}F NMR (376 MHz, CD_3CN) δ ppm -168.27 (br t, *J* = 15.89 Hz, B-C_6F_5) -163.83 (br t, *J* = 18.79 Hz-133.71 br s, B-C_6F_5) -104.63 (br s,p-F). Elemental Analysis, Found (Cal): H: 1.01% (1.08%) C: 44.45% (44.98%) Crystals suitable for SCXRD were removed from the bulk sample. Crystals of $[(4\text{-}FC_6H_4)_4Sb][B(C_6F_5)_4]$ were isolated on standing of the mother liquor.

$[(3,5\text{-}F_2C_6H_3)_3SbCl][B(C_6F_5)_4]$ (**1-17**)

Synthesised as per **1-15**. Yielded off white crystals (0.1860 g, 0.16 mmol, 34%).^{1}H-NMR (400 MHz, CD_3CN):7.44 (br t, J = 8.80 Hz, 3 H, p-H) 7.77 (br s, 6 H, o-H). $^{13}C\{^1H\}$ NMR (101 MHz, CD_3CN): 111.5 (m) 138.3 (br d, J = 46 Hz) 148.0 (br s) 150.3 (br s) 163.2 (d, J = 12 Hz) 165.8 (d, J = 12 Hz). ^{19}F-NMR (376 MHz, CD_3CN): -168.28 (s, B-C_6F_5) -163.84 (br t, *J* = 20.23 Hz, B-C_6F_5) -133.72 (s, B-C_6F_5) -105.80 (s, m-F). Elemental Analysis, Found (Cal): H: 0.72% (0.77%) C: 42.75% (42.91%) Crystals suitable for SCXRD were removed from the bulk sample.

$[(2,4,6\text{-}F_3C_6H_2)_3SbCl][B(C_6F_5)_4]$ (**1-18**)

A solution of $[(Et_3Si)_2H][B(C_6F_5)_4]$(0.132 g, 0.15 mol) in toluene was added dropwise to a solution of the $(2,4,6\text{-}F_3C_6H_2)_3SbCl_2$ (0.0879 g, 0.15 mmol) in toluene (2 mL), which resulted in the formation of a red orange oil; which was stirred for 1 hour. Solvent was removed i*n vacuo*, to afford a red oil which was washed with hexane. The oil was dissolved in CH_2Cl_2 (~10 mL) and layered with hexane (~15 mL) to afford green clear crystals (0.078 g, 0.06 mmol, 40 %). ^{1}H NMR (400 MHz, $CDCl_3$) δ ppm 7.19 - 7.37 (m, 6 H).$^{13}C\{^1H\}$ NMR (101 MHz, CD_3CN) δ ppm 103.6 (br t, J=28 Hz), 137.10 (dd, J=261Hz, J = 176. Hz,) 148.1 (d, J=239 Hz), 163.4 (d, J= 252Hz). ^{19}F NMR (376 MHz, $CDCl_3$) δ ppm -166.66 (s, B-C_6F_5) -162.62 (s, B-C_6F_5) -132.75 (s, B-C_6F_5) -91.92 (s) -85.68 (s) Elemental Analysis, Found (Cal): H: 41.15% (41.03%) C: 0.62% (0.49%) . Crystals suitable for SCXRD were removed from the bulk sample.

$[(Ph_3SbCl)_2(\mu\text{-}Cl)][B(C_6F_5)_4]$ (**1-19**)

A solution of Ph_3SbCl_2 (0.254 g, 0.60 mmol) in toluene (15 mL) was added to a suspension of $[Et_3Si][B(C_6F_5)_4]$ in toluene (10 mL), freshly prepared from $[Ph_3C][B(C_6F_5)_4]$ (0.231 g, 0.25 mmol), to yield reddish oily suspension which was stirred at room temperature for 90 minutes then the solution was decanted and stood at room temperature which yielded white crystals which were washed with n-hexane (3x5 mL) and dried *in vacuo* to yield a white crystalline solid (0.022 g, 0.015 mmol). ^{1}H NMR (400 MHz, $CDCl_3$) δ ppm 7.61 - 7.72 (m, 9 H), 7.97 - 8.03 (m, 6 H). $^{13}C\{^1H\}$ NMR (101 MHz, $CDCl_3$) δ ppm 130.9 (s,) 133.8 (s) 134.23 (s). ^{19}F NMR (376 MHz, $CDCl_3$) δ ppm -166.56 (br t, J = 17.34 Hz), -162.85 (br t, J = 20.23 Hz), -132.38 (br d, J = 8.68 Hz). Crystals of $[(Ph_3SbCl)_2(\mu\text{-}Cl)][B(C_6F_5)_4]$, identified by SCXRD, were obtained by layering a DCM solution with n-hexane.

The red oil which dried *in vacuo* then washed with n-hexane (3x5 mL) and dried *in vacuo* to give a light red powder (0.200 g, 0.14 mmol). ^{1}H NMR (400 MHz, $CDCl_3$) δ ppm 7.63 - 7.71 (m, 6 H) 7.71 - 7.77 (m, 3 H) 7.86 - 7.94 (m, 4 H). $^{13}C\{^{1}H\}$ NMR (101 MHz, $CDCl_3$) δ ppm 129.6 (s) 131.4 (s) 134.2 (s) 134.6 (s). 19F NMR (376 MHz, $CDCl_3$) δ ppm -166.56 (br t, J = 17.34 Hz) -162.83 (br t, J = 20.23 Hz) -132.40 (s). Crystals of $[(Ph_3SbCl)_2(\mu\text{-}Cl)][B(C_6F_5)_4]$, identified by SCXRD, were obtained by layering a DCM solution with n-hexane.

Combined yield: 0.222 g, 0.156 mmol, 62%

$[(Ph_3Sb(OPEt_3)Cl][OTf]$ (**1-20**)

A flask was charged with Ph_3SbCl_2 (0.100 g, 0.23 mmol), AgOTf (0.059 g, 0.23 mmol) and DCM (10 mL) and stirred overnight. The resulting white precipitate was removed via celite filtration. Et_3PO (0.310 g, 0.23 mmol) was added and stirred overnight. Solvent removed in vacuo. ^{1}H NMR (400 MHz, CD_2Cl_2) δ ppm 0.76 (dt, *J* = 18.35, 7.69 Hz, 5 H) 1.09 - 1.25 (m, 8 H) 1.57 (dq, *J* = 11.61, 7.68 Hz, 3 H) 1.86 (br d, *J* = 0.80 Hz, 4 H) 3.43 (q, *J* = 7.01 Hz, 1 H) 7.34 - 7.45 (m, 2 H) 7.50 (br t, *J* = 7.55 Hz, 2 H) 7.56 - 7.62 (m, 3 H) 7.62 - 7.70 (m, 1 H) 7.71 - 7.78 (m, 4 H) 7.96 - 8.05 (m, 3 H) 8.16 - 8.26 (m, 2 H). $^{13}C\{^{1}H\}$ NMR (100 MHz, CD_2Cl_2) δ ppm 5.4 (s) 15.6 (s) 18.5 (br dd, *J* = 65, 10 Hz) 66.2 (s) 130.1 (s) 131.1 (s) 131.4 (s) 132.4 (s) 133.3 - 133.5 (m) 133.6 (s) 133.9 (s) 134.5 (s) 136.4 (s) 140.5 (s) ^{19}F NMR (376 MHz, CD_2Cl_2) δ ppm -78.81 (s). ^{31}P NMR (162 MHz, CD_2Cl_2) δ ppm 65.74 - 73.87 (m) 77.62 (s) 85.01 (s, minor). XRD quality crystals of $[(Ph_3Sb(OPEt_3)_2][OTf]_2$ were obtained by vapour diffusion of hexane into a THF solution. Due to multiple products, yield and elemental analysis are not reported.

Ph_3SbF_2 (**1-21**)

A solution of XeF_2 (0.184 g, 1.08 mmol) in CH_2Cl_2 (10 mL) was added dropwise to a stirring solution of Ph_3Sb (0.3553 g, 1.00 mol) in CH_2Cl_2 (10 mL) at -78°C, over the course of 15 minutes. The clear solution was stirred for a further hour, when it was allowed to slowly warm to room temperature and stirred overnight. The solution was removed to the bench and solvent was removed in vacuo, yielding an off white solid (0.3134 g, 0.80 mmol, 80%). ^{1}H NMR (400 MHz, $CDCl_3$) δ ppm 7.48 - 7.72 (m, 9 H), 8.11 - 8.24 (m, 6 H). $^{13}C\{^{1}H\}$ NMR (101 MHz, $CDCl_3$) δ ppm 129.53 (s), 132.14 (s), 134.1 (t, J = 15 Hz, ipso-C), 135.3 (s). ^{19}F NMR (376 MHz, $CDCl_3$) δ ppm -152.32 (br s).

$(3,5\text{-}F_2C_6H_3)_3SbF_2$ (**1-22**)

Synthesised from **1-3** in an equivalent manner to Ph_3SbF_2 (**1-21**) (vide supra). Yield: 41%. 1H-NMR ($CDCl_3$, 400MHz): 6.89-6.95 (m, 6H), 6.88 – 6.81 (tt, J=8.92 Hz, 2.29 Hz, 3H). ^{19}F-

NMR ($CDCl_3$, 376 MHz):-107.92 (s). Elemental Analysis, Found (Cal): C: 43.54% (43.32 %) H: 1.71% (1.81%)

$(3,5\text{-}(CF_3)_2C_6H_3)_3SbF_2$ (1-23)

Synthesised from **1-6** in an equivalent manner to Ph_3SbF_2 (**1-21**). Yield: 45%. ^1H NMR ($CDCl_3$, 400MHz): 8.10 - 8.29 (m, 1 H) 8.14 (s, 2 H) 8.68 (s, 6 H) $^{13}C\{^1H\}$ NMR (CDCl3, 100 MHz): 121.3 (s) 124.0 (s) 127.3 (br s) 133.4 (m) 135.80 (br s) ^{19}F NMR (376 MHz, $CDCl_3$) δ ppm -62.69 (br m) 19F -153.76 (s) Elemental Analysis, Found (Cal): C: 36.07% (35.90%) H: 1.04% (1.13%)

Attempted Synthesis of $[(3,5\text{-}F_2C_6H_3)_3SbCl][B(3,5\text{-}(CF_3)_2C_6H_3)_4]$

To a solution of $(3,5\text{-}F_2C_6H_3)_3SbCl_2$ (**1-10**) (0.0547g, 0.1 mmol) in CH_2Cl_2(10 mL) was added a solution of Ag $B(3,5\text{-}(CF_3)_2C_6H_3)_4$ (0.100g, 0.1 mmol) in CH_2Cl_2(10 mL) in the dark. This caused an immediate white precipitate with a light brown solution. The solution was stirred for 90 minutes in the dark, then filtered through celite. The filtrate was not treated as light sensitive. The solvent was removed from the filtrate under reduced pressure to a yellow oil.^1H NMR (400 MHz, CD_3CN) -0.06 - 0.38 (m, 19 H) 0.75 - 0.93 (m, 3 H) 1.10 - 1.21 (m, 2 H) 1.26 - 1.35 (m, 5 H) 1.38 (s, 2 H) 1.89 - 2.02 (m, 8 H) 2.06 - 2.24 (m, 2 H) 2.41 - 2.81 (m, 24 H) 3.34 - 3.51 (m, 2 H) 3.61 - 3.74 (m, 1 H) 4.20 - 4.39 (m, 2 H) 5.47 (s, 1 H) 5.81 (s, 1 H) 6.08 (s, 2 H) 5.94 (s, 1 H) 7.23 - 7.40 (m, 7 H) 7.60 - 8.43 (m, 47 H) ^{19}F NMR (376 MHz, CD_3CN):-148.01 (s, minor) -132.00(s, minor) -108.19 (s) -107.68 (s,) -66.33 - -60.35 (br m). Despite repeated attempted, no solid was crystallised from the oil.

Attempted Synthesis of $[(3,5\text{-}(CF_3)_2C_6H_3)_3SbCl][B(3,5\text{-}(CF_3)_2C_6H_3)_4]$

As per attempted synthesis of $[(3,5\text{-}F_2C_6H_3)_3SbCl][B(3,5\text{-}(CF_3)_2C_6H_3)_4]$ (*vide supra*) from $(3,5\text{-}(CF_3)_2C_6H_3)_3SbCl_2$ (**1-13**). ^1H NMR (400 MHz, CD_2Cl_2) δ ppm -0.17 - 0.37 (m, 4 H) 0.84 - 1.02 (m, 1 H) 1.26 (s, 1 H) 1.78 - 1.90 (m, 1 H) 3.56 - 3.77 (m, 1 H) 7.42 - 7.65 (m, 1 H) 7.64 - 7.89 (m, 1 H) 8.03 - 8.28 (m, 1 H) 8.82 (d, *J* = 12.12 Hz, 1 H)^{19}F NMR (376 MHz, CD_2Cl_2): -153.68(s, minor), -137.84(s, minor), -130.93(s, minor), -69.83 - -52.55 (br m). Despite repeated attempted, no solid was crystallised from the oil.

Friedel-Crafts Alkylation of Benzene

An NMR tube was loaded with ^{t}BuBr (14 mg, 0.01 mmol), benzene (16.0 mg, 0.2 mmol) and the respective catalyst in $CDCl_3$ (0.7 mL). The tube was stood for 30 mins, then a ^1H spectrum was taken. Yield was determined by relative integration of the ^{t}BuBr (δ_H = 1.81 ppm) and ^{t}Bu-Ph (δ_H = 1.34 ppm) peaks.

Gutmann Beckett Method

The stibonium salt (0.05 mmol) and Et_3PO (0.0012 g, 0.001 mmol) were mixed in CD_2Cl_2 and loaded into a J-Young NMR tube. ^1H, ^{19}F and $^{31}P\{^1H\}$ spectra were obtained.

1-14. ^1H NMR (400 MHz, CD_2Cl_2) δ ppm 0.75 (dt, J=18.24, 7.69 Hz, 9 H), 1.42 (dq, J=11.52, 7.67 Hz, 6 H), 7.62 - 7.79 (m, 9 H), 7.89 - 7.98 (m, 6 H). ^{19}F NMR (376 MHz, CD_2Cl_2) δ ppm -167.52 (s, $B(C_6F_5)_4$), -163.68 (s, $B(C_6F_5)_4$) ,-133.03 (s, $B(C_6F_5)_4$. $^{31}P\{^1H\}$ NMR (162 MHz, CD_2Cl_2) δ ppm 75.89 (s).

1-15. 1H NMR (400 MHz, CD_2Cl_2) δ ppm 0.85 (dt, J=18.52, 7.66 Hz, 7 H), 1.09 - 1.31 (m, 14 H), 1.54 (dq, J=11.52, 7.67 Hz, 5 H), 1.87 (dq, J=11.72, 7.68 Hz, 6 H), 3.43 (q, J=7.09 Hz, 2 H,) 7.46 - 7.54 (m, 2 H), 7.66 - 7.71 (m, 2 H), 7.72 - 7.81 (m, 5 H). ^{19}F NMR (376 MHz, CD_2Cl_2) δ ppm -167.52 (br t, J=17.34 Hz, $B(C_6F_5)_4$), -163.66 (br t, J=20.23 Hz, $B(C_6F_5)_4$), -133.07 (br s, $B(C_6F_5)_4$), -109.62 (br s, Ar-F, minor) -106.22 (s, Ar-F) -105.58 (m, Ar-F, minor) $^{31}P\{^1H\}$ NMR (162 MHz, CD_2Cl_2) δ ppm 78.16 (s).

1-17. ^1H NMR (400 MHz, CD_2Cl_2) δ ppm 0.73 - 1.27 (m, 4 H), 1.52 - 1.98 (m, 3 H), 3.14 - 3.21 (m, 1 H,) 7.20 - 7.27 (m, 1 H), 7.29 - 7.35 (m, 1 H), 7.37 - 7.42 (m, 1 H), 7.48 - 7.56 (m, 1 H), 7.80 - 7.87 (m, 1 H). ^{19}F NMR (376 MHz, CD_2Cl_2) δ ppm -167.52 (s, $B(C_6F_5)_4$), -163.68 (s, $B(C_6F_5)_4$) ,-133.03 (s, $B(C_6F_5)_4$), -109.09 (s, Ar-F, minor) -106.19 (br s,Ar-F, minor) -103.22 (br s, Ar-F, minor) -102.10 (br s,Ar-F). $^{31}P\{^1H\}$ NMR (162 MHz, CD_2Cl_2) δ ppm 72.25 - 73.15 (m), 73.30 - 74.50 (m), 77.32 (s), 78.73 (s), 80.86 (s).

1-18. ^1H NMR (400 MHz, CD_2Cl_2) δ ppm 0.98 - 1.24 (m, 31 H) 1.66 (dq, J=11.61, 7.72 Hz, 18 H) 3.42 (q, J=6.98 Hz, 2 H) 7.28 (t, J=8.63 Hz, 2 H) 8.14 - 8.29 (m, 2 H). ^{19}F NMR (376 MHz, CD_2Cl_2) δ ppm -167.52 (s, $B(C_6F_5)_4$), -163.68 (s, $B(C_6F_5)_4$),-133.03 (s, $B(C_6F_5)_4$), -107.03 (s, Ar-F). $^{31}P\{^1H\}$ NMR (162 MHz, CD_2Cl_2) δ ppm 55.77 (br s).

Stoichiometric Dehalogenation of Trityl Halide

A NMR tube was charged with a sample of $[(2,4,6\text{-}F_3C_6H_2)_3SbCl][B(C_6F_5)_4]$ (**1-18**) (0.002 g, 0.002 mmol) and Ph_3CCl/Ph_3CF (0.0015 g, 0.05 mmol) in $CDCl_3$ (0.5 mL).

1-18/Ph_3CF: Ph_3CF: ^1H NMR (400 MHz, $CDCl_3$) δ ppm 7.04 - 7.33 (br m). ^{19}F NMR (376 MHz, $CDCl_3$) δ ppm -166.71 (br d, J=17.34 Hz, $B(C_6F_5)_4$), -162.91 (br d, J=23.12 Hz, $B(C_6F_5)_4$), -132.50 (br s, $B(C_6F_5)_4$), -125.80 (s, 1 F, Ph_3CF), -98.98 (m, Ar-F), -93.71 (s, Ar-F).

1-18/Ph_3CCl: ^1H NMR (400 MHz, $CDCl_3$) δ ppm 7.21 (br m). ^{19}F NMR (376 MHz, $CDCl_3$) δ 166.71 (br d, J=17.34 Hz, $B(C_6F_5)_4$) -162.91 (br d, J=23.12 Hz, $B(C_6F_5)_4$) -132.50 (br s, $B(C_6F_5)_4$), -98.95 (s, Ar-F), -93.72 (s, Ar-F)

An instant red coloured solution formed on mixing. The equivalent reaction was also performed with $[Ph_3SbCl][B(C_6F_5)_4]$ (**1-14**) and $[(Ph_3SbCl)_2(\mu\text{-}Cl)][B(C_6F_5)_4]$ (**1-19**).

1-14/Ph_3CF: ^1H NMR (400 MHz, $CDCl_3$) δ ppm 7.10 - 7.40 (m, 8 H), 7.47 - 7.67 (m, 2 H), 8.10 - 8.37 (m, 1 H). ^{19}F NMR (376 MHz, $CDCl_3$) δ ppm -166.67 (br t, J=17.34 Hz, $B(C_6F_5)_4$), -162.88 (br t, J=20.23 Hz, $B(C_6F_5)_4$) -136.66 (br s, Sb-F) -132.50 (br s, $B(C_6F_5)_4$), -125.83 (s, Ph_3CF).

1-19/Ph_3CCl: ^1H NMR (400 MHz, $CDCl_3$) δ ppm 7.33 - 7.71 (m, 27 H), 7.85 - 7.96 (m, 3 H), 8.05 - 8.23 (m, 10 H), 8.21 - 8.33 (m, 1 H). ^{19}F NMR (376 MHz, $CDCl_3$) δ 166.71 (br d, J=17.34 Hz, $B(C_6F_5)_4$) -162.91 (br d, J=23.12 Hz, $B(C_6F_5)_4$) -132.50 (br s, $B(C_6F_5)_4$).

Dimerisation of 1,1 -Diphenylethylene

A J-Young NMR tube was loaded with 1,1 -Diphenylethylene (DPE) (0.018 g, 0.1 mmol) and $[(2,4,6\text{-}F_3C_6H_2)_3SbCl][B(C_6F_5)_4]$ (**1-18**) (0.008 g, 0.005 mmol, 5% loading) in CD_2Cl_2 (0.7 mL). The CD_2Cl_2 solution turned yellow instantly on mixing The tubes were stood for 2h then ^1H and ^{19}F NMR spectra were obtained. Conversion was determined by relative integration of DPE (5.46 ppm) to dimerised product (3.14 ppm). The equivalent reaction was also performed with $[(3,5\text{-}F_2C_6H_3)_3SbCl][B(C_6F_5)_4]$ (**1-17**) (0.007 g, 0.005 mmol, 5% loading) and **1-19.**

Decomposition by Silane

Et_3SiH (0.030 g, 0.26 mmol) was added to a solution of $[Ph_3SbCl][B(C_6F_5)_4]$ (**1-14**) (0.002 g, 0.002 mmol) in $CDCl_3$ giving the instant formation of a yellow solution. ^1H and ^{19}F spectra were obtained. 1H NMR (400 MHz, $CDCl_3$) δ ppm 0.59 (qd, J=7.97, 1.72 Hz, 59 H, $CH_2(Et_3SiH)$) 0.86 - 1.14 (m, 123 H, $CH_3(Et_3SiH)$) 7.30 - 7.34 (m, 3 H, Ph_3Sb) 7.40 - 7.45 (m, 2 H, Ph_3Sb). ^{19}F NMR (376 MHz, $CDCl_3$) δ ppm -175.82 (m, Et_3SiF), -166.89 (br s, $B(C_6F_5)_4$), -163.16 (br s, $B(C_6F_5)_4$),-132.45 (br s, $B(C_6F_5)_4$), *N.B*. Several minor peaks between -100 ppm and -150 ppm were observed. The equivalent reaction was performed with $[(2,4,6\text{-}F_3C_6H_2)_3SbCl][B(C_6F_5)_4]$ (**1-18**) and $[(Ph_3SbCl)_2(\mu\text{-}Cl)][B(C_6F_5)_4]$ (**1-19**).

1-18/Et_3SiH: ^1H NMR (400 MHz, $CDCl_3$) δ ppm 0.59 (qd, J=7.93, 3.09 Hz, 6 H, $CH_2(Et_3SiH)$), 0.98 (t, J=8.00 Hz, 9 H, $CH_3(Et_3SiH)$. ^{19}F NMR (376 MHz, $CDCl_3$) δ ppm -175.94 (s, 1 F) -166.75 (s, Et_3SiF) -162.74 (s, $B(C_6F_5)_4$), -132.64 (s, $B(C_6F_5)_4$), -105.76 (s, Ar-F), -90.66 (br s, Ar-F).

1-19/Et_3SiH: ^1H NMR (400 MH $CDCl_3$) δ ppm 0.60 (q, J=8.00 Hz, 125 H, $CH_2(Et_3SiH)$) 0.76 - 1.14 (m, 227 H, $CH_3(Et_3SiH)$) 3.62 (s, 16 H, Si-H(Et_3SiH)) 7.33 - 7.44 (m, 12 H, Ph_3Sb) 7.44 - 7.55 (m, 3 H, Ph_3Sb). ^{19}F NMR (376 MHz, $CDCl_3$) δ ppm -175.82 (m, Et_3SiF), -166.89 (br s, $B(C_6F_5)_4$), -163.16 (br s, $B(C_6F_5)_4$),-132.45 (br s, $B(C_6F_5)_4$), *N.B*. Several minor peaks between -100 ppm and -150 ppm were observed.

Reaction of α,α,α-Trifluorotoluene with 1-16

A J-Young NMR tube was loaded with $[(4\text{-}FC_6H_4)_3SbCl][B(C_6F_5)_4]$ (**1-16**) (0.010 g, 0.009 mmol) and $PhCF_3$ (0.002 g, 0.013 mmol) in $CDCl_3$ (0.7 mL) giving a slightly red solution. ^1H and ^{19}F spectra were obtained initially and after standing at room temperature for 24 hours. Both spectra were identical. 1H NMR (400 MHz, $CDCl_3$) δ ppm 7.36 - 7.46 (m, 3 H, $PhCF_3$) 7.48 - 7.56 (m, 11 H, $PhCF_3$) 7.56 - 7.67 (m, 6 H, **1-16**) 7.71 - 7.81 (m, 7 H, **1-16**). ^{19}F NMR (376 MHz, $CDCl_3$) δ ppm -166.45 (s, $B(C_6F_5)_4$), -162.62 (s, $B(C_6F_5)_4$), -132.45 (s, $B(C_6F_5)_4$) -98.92 (s, Ar-F-**1-16**) -94.71 (s, Ar-F **1-16**) -62.57 (s, $PhCF_3$).

Attempted synthesis of $[Ph_3SbF][B(C_6F_5)_4]$

A solution of Ph_3SbF_2 (0.1500 g, 0.38 mmol) in toluene (30 mL) was added to a suspension of $[Et_3Si(C_7H_8)][B(C_6F_5)_4]$ (0.4610 g, 0.47 mmol) in toluene (20 mL) to yield a white oil which was stirred at room temperature for 1 hour. The solution was decanted and the oil was dried *in vacuo* to yield a white powder which was insoluble in $CDCl_3$. The powder was dissolved in DCM (10 mL) and layered with n-hexane (10 mL) and left overnight to yield white crystals. The solution was decanted and the crystals dried *in vacuo* to yield a white powder (0.1810 g). ^1H NMR (400 MHz, CD_3CN) δ 7.46 - 7.63 (m, 1 H), 7.64 - 7.83 (m, 1 H), 7.92 - 8.15 (m, 1 H). ^{19}F NMR (376 MHz, CD_3CN) δ ppm -168.68 (br s, $B(C_6F_5)_4$) -165.34 (br d, J=5.77 Hz) -163.83 (br t, J=18.78 Hz, $B(C_6F_5)_4$) -148.90 (br d, J=2.89 Hz) -133.73 (br d, J=5.78 Hz, $B(C_6F_5)_4$) Crystals of $[Ph_3(tolyl)Sb][B(C_6F_5)_4]$ were removed from the bulk.

Diel-Alder Reaction of E-Chalcone and Cyclohexa-1,3-diene

An NMR tube was loaded with $[(3,5\text{-}F_2C_6H_3)_3SbCl][B(C_6F_5)_4]$ (**1-17**) (0.0059 g, 0.005 mmol, 20% loading), cyclohexa-1,3-diene (0.0016 g, 0.2 mmol) and E-chalcone (0.0042 g, 0.2 mmol) in CD_2Cl_2 giving an instant red solution and black precipitate. The tube was stood for 2 hours then NMR spectra were obtained. ^1H NMR (400 MHz, CD_2Cl_2) δ ppm 1.16 (br t, J=6.98 Hz, 2 H) 1.85 (t, J = 7.19 Hz, 3 H) 2.13 (s, 2 H) 3.37 - 3.61 (m, 3 H) 6.80 - 6.90 (m, 1 H) 6.95 (ddd, J=4.32, 2.83, 1.77 Hz, 1 H) 7.43 - 7.57 (m, 23 H) 7.62 - 7.72 (m, 10 H) 7.76 (br d, J=15.67 Hz, 5 H) 7.83 - 7.94 (m, 8 H). ^{19}F NMR (376 MHz, CD_2Cl_2) δ ppm –167.44 (br s, $B(C_6F_5)_4$), -163.59 (br t, J=20.23 Hz, $B(C_6F_5)_4$), -133.04 (br s, $B(C_6F_5)_4$), -109.08 (br s), -102.48 (br s), -101.59 (br s).

Exchange Reactions

An NMR tube was loaded with $[(3,5\text{-}F_2C_6H_3)_3SbCl][B(C_6F_5)_4]$ (**1-17**) (0.010 g, 0.008 mmol) and $(3\text{-}FC_6H_4)_3SbCl_2$ (**1-15**) (0.004 g, 0.008 mmol) in CD_2Cl_2 (0.7 mL) and NMR specta were obtained 1H NMR (400 MHz, Solvent) δ p,pm 7.07 - 7.18 (m, 1 H), 7.58 (br dd, J=13.15, 7.20 Hz, 2 H,) 7.66 (br t, J=8.35 Hz, 1 H) 7.75 - 7.84 (m, 2 H) 7.84 - 7.91 (m, 1 H). 19F NMR (376

MHz, Solvent) δ ppm -167.40 (br t, J=17.34 Hz, $B(C_6F_5)_4$)) -163.54 (br t, J=21.68 Hz, $B(C_6F_5)_4$)) -133.03 (br s, $B(C_6F_5)_4$)) -105.85 (br d, J=17.34 Hz). -103.50 (br d, J=8.67 Hz) The solution was layered with n-hexane yielding colorless crystals that were identified as [(3-$FC_6H_4)_3SbCl][B(C_6F_5)_4$] by SCXRD.

The equivalent reaction was also performed with [(4-$FC_6H_4)_3SbCl][B(C_6F_5)_4$] (**1-16**) (0.0089 g, 0.008 mmol) and $PhSbCl_2$ (**1-8**) (0.0034 g, 0.008 mmol). ^{1}H NMR (400 MHz, CD_2Cl_2) δ ppm 7.18 - 7.47 (m, 3 H) 7.74 - 7.82 (m, 4 H) 7.84 - 7.92 (m, 1 H) 8.08 - 8.32 (m, 3 H). ^{19}F NMR (376 MHz, CD_2Cl_2) δ ppm -167.42 (m, $B(C_6F_5)_4$) -163.57 (m, $B(C_6F_5)_4$) -133.03 (br d, J=2.89 Hz, $B(C_6F_5)_4$), -105.60 (br s, (4-$FC_6H_4)_3SbCl_2$), -104.96 (br d, J=2.89 Hz, [(4-$FC_6H_4)_3SbCl]^+$).

Computational Methods

All calculations were performed using Gaussian 09 Revision E0.01.[355] All geometries were optimised in vacuum without imposing symmetry constraints at the M062X/def2-SVP level of theory with the GD3 empirical dispersion correction.[261,356,357] Counteranions were omitted from all calculations. Some of these structures did not fully optimise according to the RMS displacement and maximum displacement criteria, suggesting a flat energy surface. Subsequent analytical IR frequency calculations on optimised geometries were utilised to confirm the nature of stationary points (zero and exactly one imaginary mode for minima and transition states, respectively), some. Moreover, within the ideal gas/rigid rotor/harmonic approximation (RRHO) these calculations also provided thermal and entropic corrections to the Gibbs Free Energy at 1 atm and 298.15 K. Electronic energies were obtained from single-point calculations at the M062X-D3/def2-TZVPP level of theory including a polarisable continuum model (SMD) to account for solvent effects.[358] The Kohn-Sham orbitals were visualised using Chemcraft.[359] FIAs were calculated following a reported procedure from the literature.[155] Single point energies for FIA were calculated in the gas phase using M062X-D3/aug-cc-PTZ-pp (for Sb) and 6-331G** (for C, H, Cl and F). [360,361] The FIA was calculated using the enthalpy of a free fluoride calculated at the same level of theory (-99.840107 E_h (gas phase)).

3. Diversity in the Structure and Reactivity of Pentamethylcyclopentadienyl Antimony(III) Cations

3.1 Introduction

3.1.1 Main group metallocenes

The prototypical metallocene, ferrocene, first prepared unintentionally in the lab of Pauson and Kealy at Duquesne University in 1951,[362] has since become a familiar feature in chemical research; applications of ferrocene and its derivatives include catalysis,[363–367] ligand scaffolds[368–370] and redox reagents.[371–374] Despite the strict IUPAC definition of a metallocene as 'compounds in which one atom of a transition metal'…'bonded to and only to the face of two cyclopentadienyls (η^5-(C_5H_5)) ligands which lie in parallel planes',[375] the literature often extends this term to main group metal-based analogues. Similar compounds containing derivatives of cyclopentadienyl ligands (Cp') are also often grouped under the category of main group metallocenes; pentamethylcyclopentadienyl (Cp*) is frequently utilised, due to the stabilising effects of Cp* ring alkylation on the structure. More varied bonding modes and the absence of d-orbital mediated bonding gives rise to greater diversity in the structure of main group metallocenes in comparison to their transition metal counterparts.

3.1.2 Structure of main group metallocenes

Structural features of main group metallocenes vary in terms of the position of the metal in relation to the Cp' ligands, number of Cp' ligands and involvement of other ligands. Intermolecular interactions habitually play a role, leading to the observation of dimers, oligomers and polymers in the solid state. Most commonly associated with metallocenes is the sandwich structure, which contains two Cp' ligands on opposite sides of the metal centre. For symmetrically substituted Cp based ligands (Cp^x), these may be parallel, and staggered (D_{5d}) or eclipsed (D_{5h}) (Figure 3.1). Cp' ligands may also not be parallel, leading to a bent structure (C_{2V} for structures with Cp^x ligands). This is usually the result of other substituents but may also be due to non-bonding interactions between the Cp' ligands (see 3.1.4 Electronic structure of main group metallocenes). The interactions between the metal and Cp' ligands in sandwich complexes are usually equivalent, with the unusual exception of $(Cp^{5Bz}Li)_2$ ($Cp^{5Bz} = C_5(C_7H_7)_5$), which forms a triple decker structure consisting of a Cp^{5Bz}-Li-Cp^{5Bz}Li-(C_6H_6) in the solid state.[376]

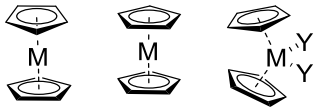

Figure 3.1. Parallel sandwich metallocenes with eclipsed (left), staggered (centre) and bent (right) confirmation

The structural motifs observed in half sandwich compounds, containing one Cp' ligand, are more varied (Figure 3.2).

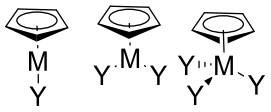

Figure 3.2. Half sandwich metallocenes showing the milking stool (left), three co-ordinate (centre) and piano stool (right) configuration. Y= auxillary ligand or lone pair

Hapticity is another defining characteristic for metallocenes; while hapticities of less than 5 are rare for transition metal metallocenes, main group metallocenes contain a range of hapticities from η^5 and slipped ring η^n (n = 1-4) to σ-bonded Cp'. Energy differences between hapticities are typically small and are rarely telling of the specific electronic structure of the metallocene; the presence of lone pairs and auxiliary ligands as well as the population of through space coupling (TSC) orbitals (see 3.1.4 Electronic structure of main group metallocenes) determine the hapticity of the metallocene. There is no universal method to determining the hapticity of a Cp', M-C bond lengths, patterns in M-C bond lengths and relative position of M from the Cp' centroid are commonly used.[377] There is usually an apparent contradiction between the solid state and solution phase hapticity, spectroscopic evidence usually indicates that the latter is higher than the former by symmetric chemical environments. This is usually the result of fluxional behaviour in solution.[378]

Main group metallocenes often form extended structured in the solid state; once such example is $[Li(12\text{-crown-4})]_2[(C_5H_5)_9Pb_4][(C_5H_5)_5Pb_2]$. A Pb centre interacts with the cyclopentadienyl ligand of a neighbouring Pb in a π fashion, forming a polymeric structure (Figure 3.3). [379]

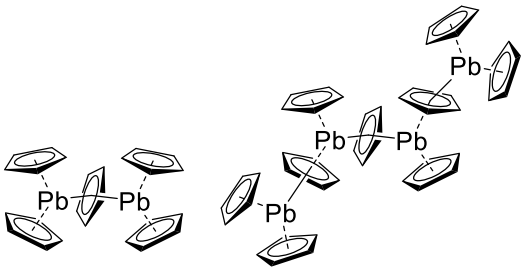

Figure 3.3. $[(C_5H_5)_5Pb_2]$ (left) and $[(C_5H_5)_9Pb_4]$ (right) units in $[Li(12\text{-crown-4})]_2[(C_5H_5)_9Pb_4][(C_5H_5)_5Pb_2]$.

Dimers containing halide bridges are known, $Cp^{3t}BiCl_2$ (Cp^{3t} = 1,2,4-$^tBu_3C_5H_2$) and $Cp^{4i}BiI_2$ (Cp^{4i} = $C_5{}^iPr_4H$) adopt such structures.[380]

3.1.3 Synthetic and characterisation particularities of main group metallocenes

Synthetic strategies employed are typical for organometallic chemistry. Cyclopentadiene is a starting material for simple Cp compounds, which must be freshly prepared by cracking dicyclopentadiene at 160°C and distilling the cyclopentadiene at 38-46°C.[381] For more reactive s-block metals, the relevant metallocenes can be synthesised by direct reaction with cyclopentadiene, eliminating H_2.[382] Salt metathesis reactions are commonplace in synthetic organometallic chemistry and metallocenes are no exception. For a more general method for the synthesis of group 2, 13, 14 and 15, the halide salt can be transmetallated with cyclopentadienyl lithium or bis(cyclopentadienyl) magnesium.[383] Magnesocene (Cp_2Mg) may be prepared by thermal decomposition of the relevant Grignard reagent.[384] Conversely, comproportionation reactions can be used to obtain half sandwich structures, for example CpMeMg can be obtained from a mixture of Cp_2Mg and Me_2Mg.[385] The most common ligand deployed in main group metallocenes, pentamethylcyclopentadienyl (Cp*), is commercially available as Cp*H. Several laboratory scale preparations for Cp*H are known.[386–388] Halides may be abstracted by AlX_3, resulting in a cationic metal centre with $[AlX_4]^-$ acting as a counter anion. Such systems are known for B,[389] Ge,[383] Sn, As, Pb,[390] Sb and Bi. [391]

Main group metallocenes can be characterised by standard synthetic characterisation methods. Metallocenes have characteristic IR/Raman spectra. Heteronuclear NMR is particularly informative for main group metallocenes. Drastic chemical shifts of the metal nucelus observed upfield from the respective alkyl metals can be rationalised as a consequence of ring current of the aromatic Cp ring, in which the metal sits. [385,392,393]

More telling is the observation of $J_{E\text{-}H}$ coupling in these spectra, indicative of the covalent character of the M-Cp bond. Both Sn and Pb have magnetically active nuclei of spin ½. Thus a 31 line peak can be expected for the Cp^*_2Sn and Cp^*_2Pb, which is observed as 16 lines for Sn($^3J_{Sn\text{-}H}$= 3.7Hz) and Pb($^3J_{Pb\text{-}H}$ =11.2 Hz) due to the resolution of spectra obtained.[394] NMR can also yield insights into the symmetry of these compounds; for $[Cp^*_2B][BCl_4]$, ^{11}B NMR measurements gave a long relaxation time, suggesting a highly symmetrical chemical environment.[395]

Trends in the physical properties of these compounds can also be rationalised by interactions in the solid state. Cp^X based compounds have higher melting points than those that have an unsymmetrical substitution pattern around the Cp ligand.[396]

3.1.4 Electronic structure of main group metallocenes

Metallocenes of the s-block contain a predominately ionic interaction between the metal centre and the Cp' ligand. The computational evidence presents an out of plane bending of hydrogens on the Cp ligand in CpLi, consistent with a point charge on the Cp ligand.[397] For p-block metal based metallocenes, covalent interactions between the metal centre and the Cp' ligand dominate. There is a greater tendency for π bonding with heavier group 15 elements, due to more metallic character. This has been shown experimentally by spectroscopic studies; there exists a rapid interconversion between an $8e^-$ σ-bonding structure and $20e^-$ π-bonding structure in Cp_3Sb and Cp_3Bi, whereas in Cp_3As a single $8e^-$ σ-bonding structure exists.[398]

Simple formal electron counting rules, either the 8-electron rule (no d orbital participation) or the 18-electron rule (d orbital participation) cannot be readily applied to main group metallocenes. The 'islands of electronic stability' is an empirical rule which predicts that main group metallocenes with 8, 14 or 20 bonding electrons will be stable,[399] with several exceptions (e.g. CpSnCl). A 3D aromaticity model, based on the 4n+2 interstitial electron rule, has been proposed for CpBeH by counting 5 electrons for the Cp ring and 1 from the Be-H bond.[400]

Main group metallocenes typically contain non-stereoactive lone pairs; Cp^*_2Si contains both a bent and linear molecule in the solid state.[401,402] This can be rationalised as reduced s/p mixing yielding an isotropic lone pair.

Main group metallocenes are a case study for non-bonding (Van der Waals) effects between ligands on a central atom on structural parameters of metal complexes; an orbital treatment of VdW attraction-repulsion is known as through space coupling (TSC). Ligand orbitals are combined to form TSC orbitals (see Figure 3.4 for an example with $Cp'ML_3$) which then interact with the metals AOs.

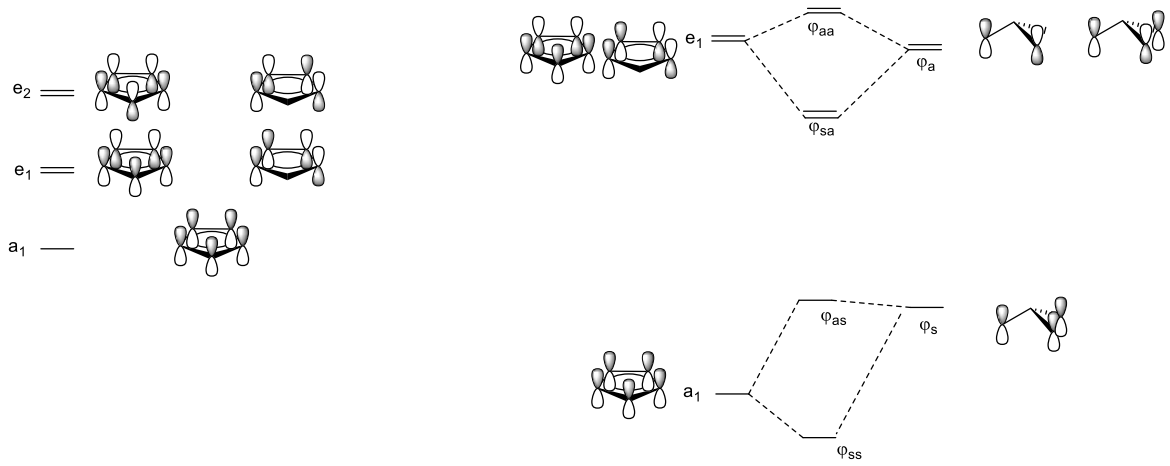

Figure 3.4. Molecular orbitals of Cp (left). TSC orbitals of Cp*ML_3. Initially the p_z orbitals of L_3 combine to form a symmetric TSC orbital(Ψ_s) and asymmetric TSC orbitals (Ψ_a). These orbitals combine with a_1 and e_1 orbitals of the Cp to form combined Cp*L_3 TSCs. For the combined Cp'/L TSC orbital the first letter in the subscript refers to the symmetry of the combination of constituent orbitals and the second letter refers to the symmetry of the constituent orbitals. The bonding orbitals (Ψ_{ss} and Ψ_{sa}) determine vdW attraction while the anti-bonding orbitals (Ψ_{sa} and Ψ_{aa}) determine the vdW repulsion.

The Cp'/L TSC orbitals of Cp'ML_3 (Ψ_{ss}, Ψ_{as} and Ψ_{sa}) combine with the metal AOs to form four bonding MOs. There is a contribution of 6-δ and 2+δ electrons (δ = bonding electrons) from Cp' and L_n respectively. While the formal electron count ranges from 8 to 14 from Cp'ML to Cp'ML_4, in each case there is a total of 8 bonding electrons, fulfilling the octet rule.

TSC allows for an electronic rationalisation for bending and slipping of Cp' ligands; by reducing the hapcitiy from η^5 the vdW repulsion can be reduced. Thus s-block metallocenes provide an idealised example of this as the presence of a lone pair or auxiliary ligands can be precluded when rationalising the geometry of these compounds. While Cp*$_2$Mg in in a linear staggered (D_{5h}) in both the solid and gas phase, Cp*$_2$Ca is bent.[403–405] This has been attributed to VdW attractive forces between the Cp* rings in Cp*$_2$Ca from the results of molecular mechanics calculations.[406,407]

3.1.5 Metallocenes of the p-block

Of the p-block metallocenes, group 14 metallocenes are the most well studied (Figure 3.5). Most of the work on p-block metallocenes have been on the topic of structural concerns and synthetic methods, comparatively little work has been done on reactivity until recently. Cp' ligands have allowed for the isolation of p-block elements in oxidation states/charges that are normally unattainable. For group 13 metals reduced monovalent Cp' based species have been reported for all the elements except boron, the species are usually symmetric η^5 complexes.[408]

Monovalent group 13 metallocenes typically act as Lewis bases towards transition metals and main group Lewis acids. [409–415] Group 13 metallocenes which form a variety of oligomeric and polymeric species have been reported. [408,416–419]

Metallocenes have also been fruitful tools for the pursuit of M(III) cations for group 13 elements.[420–425] [Cp*B(Mes)]OTf has been hailed as a masked Lewis acid.[426] In non-polar solvents the Cp*B bond can best be described as a σ bond and the triflate is strongly coordinated to the B atom; in polar solvents this forms a naked $[\eta^5\text{-Cp*B}]^+$ which is a stronger acid than $B(C_6F_5)_3$ according to the Gutmann-Beckett scale and is a potent catalyst for reduction of ketones with Et_3SiH.

Stannocene (Cp_2Sn) and plumbocene (Cp_2Pb) were among the first p-block metallocenes to be reported.[427,428] Both act as Lewis acids with amine and carbene donors.[429–431] The metal-donor interaction has been attributed to a dispersion interaction in the case of the carbene donor as omission of the dispersion correction yields negligible bonding energy between the two fragments *in silico*. In the case of the amine donors the interaction is primarily $Lp_N \rightarrow Lp^*_{Sn}$. Computational investigations also revealed that the lone pair is highly inert and in the case of the carbene does not partake in back-bonding. The Cp* analogues have also been reported.[432] Cationic mono-Cp' metallocene with group 14 centres have been reported. [433–437]

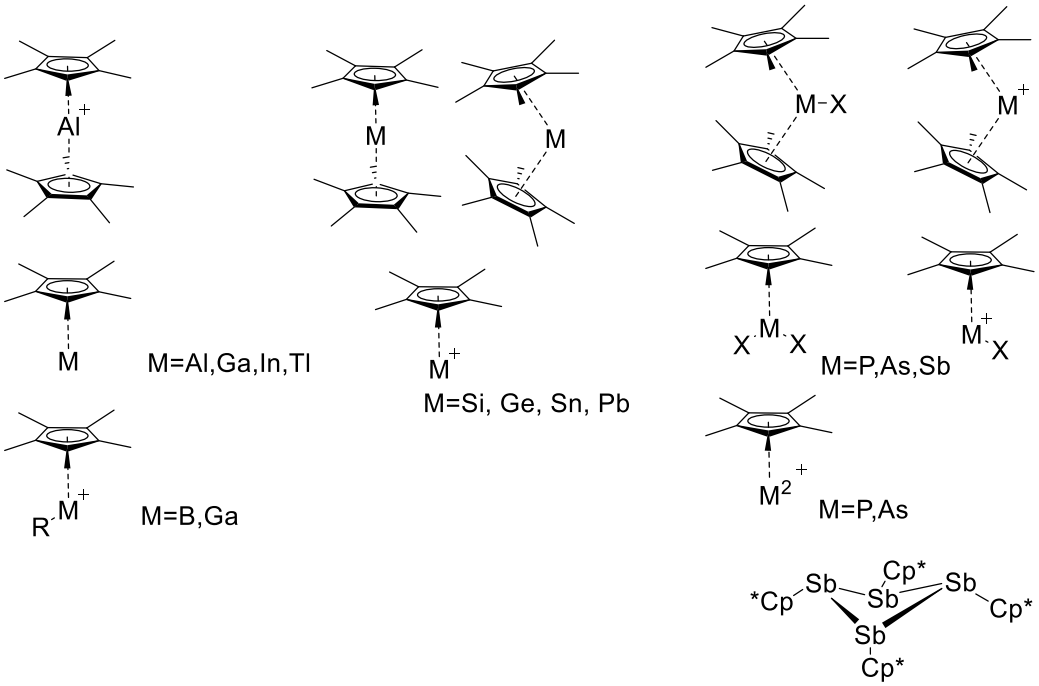

Figure 3.5. Representative examples of p-block Cp* based metallocenes

For metallocenes of group 15 elements, there is a reduced tendency for the formation of π bonds relative to group 14. Pnictogen metallocenes of the form Cp'_3Pn (Pn = Sb, Bi), Cp'_2PnX (Pn = P, As, Sb, Bi) and $Cp'PnX_2$ (Pn = P, As, Sb, Bi) are known. Compounds in this group tend to be highly coloured, ranging from yellow to deep red. Interactions in tris(Cp')pnictogens (Cp'_3Pn) are σ based.[438,439] π interactions can be observed in Cp'_2PnY and $Cp'PnY_2$. Cp^*_2PnCl (Pn=As, Sb, Bi) have been prepared from LiCp* and the respective $PnCl_3$.[440] Cp^*_2BiCl shows both light and thermal sensitivity. ^{1}H and ^{13}C NMR data shows equivalence between methyl groups, suggesting fluxional behaviour in solution. SCXRD data suggests that the hapticities are η^1, η^3, and η^5 in the solid state respectively. Cp^*_2AsCl adopts a non-eclipsed structure, while the Cp^*_2SbCl and Cp^*_2BiCl have a bent sandwich structure. Using Al_2Cl_6, chlorides were abstracted from Cp^*_2PnCl (Pn=As, Sb) to afford $[Cp^*_2Pn][AlCl_4]$ (Pn=As, Sb); however $[Cp^*_2Bi][AlCl_4]$ was too unstable. The asymmetric unit of $[Cp^*_2As][AlCl_4]$ contains four cations distinguished by hapacity, two cations displayed bis-η^3 and the remaining cations displayed η^2/η^3 and η^3/η^4. $[Cp^*_2Sb][AlCl_4]$ shows bis-η^4 hapacity. In $[Cp^*_2Sb][AlI_4]$ a Sb-I interaction can be observed.[441] The rings in $[(({}^tBu)_3C_5H_2)_2Sb][AlCl_4]$ are essentially parallel.[441] Cationic $[Cp^*_2Pn][AlCl_4]$ and dicationic mono(pentamethylcyclopentadienyl) compounds of Phosphorus and arsenic, $[Cp^*PCl][B(C_6F_5)_4]$, $[Cp^*PF][B(C_6F_5)_4]$, $[Cp^*P][B(C_6F_5)_4]_2$, $[Cp^*AsCl][B(C_6F_5)_4]$, $[Cp^*AsF][B(C_6F_5)_4]$ and $[Cp^*As][B(C_6F_5)_4]_2$ have recently been reported.[442,443] The Phosphorus dication, $[Cp^*P][B(C_6F_5)_4]_2$, crystalises with a weak interaction to co-crystallised toluene. The reactivity of $[Cp^*P][B(C_6F_5)_4]_2$ suggests an extremely Lewis acidic Phosphorus centre, even more so than $[Et_3Si]^+$ (Scheme 3.1).

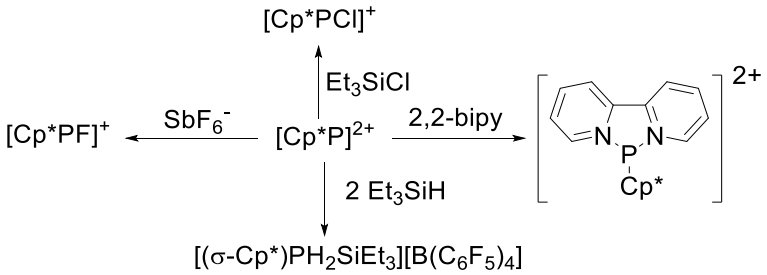

Scheme 3.1. Reactivity of $[Cp^*P][B(C_6F_5)_4]_2$. The dication abstracts a chloride and fluoride from Et_3SiCl and SbF_6^- respectively. 2,2-bipyridine chelates to the dication. $[Cp^*P][B(C_6F_5)_4]_2$ abstracts a hydride from Et_3SiH then a second molecule of Et_3SiH oxidatively adds.

The reactivity of the analogous arsenic dication, $[Cp^*As][B(C_6F_5)_4]_2$, is similar (Scheme 3.2). $[Cp^*As][B(C_6F_5)_4]_2$ reacts with THF to form what can be regarded as the first step of THF polymerisation, catalysed by $[Cp^*As][B(C_6F_5)_4]_2$.

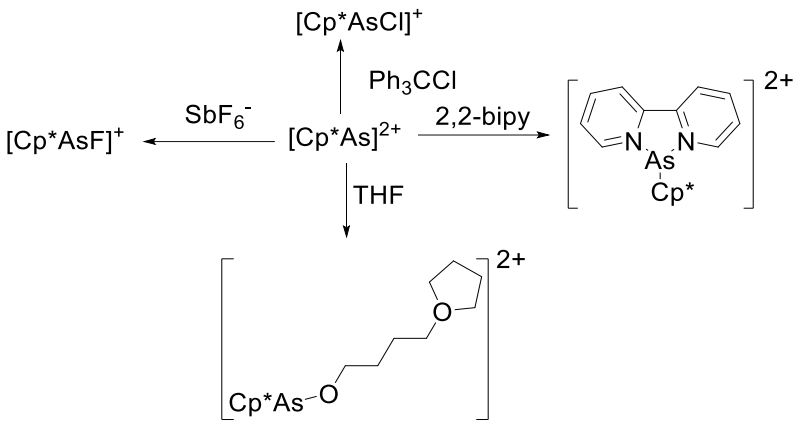

Scheme 3.2. Reactivity of $[Cp^*As][B(C_6F_5)_4]_2$. The dication abstracts a chloride and fluoride from Ph_3CCl and SbF_6^- respectively. 2,2-bipyridine chelates to the dication. THF ring opens on reaction with $[Cp^*As][B(C_6F_5)_4]_2$.

3.1.7 Fluorination of Organic Compounds

The unique nature of organofluorine compounds has led to their prevalence in industry (agrochemical, flame suppression systems) as well as emerging applications as a treatment for ischemic diseases, as organic semiconducting materials, and have become prevalent in medicinal chemistry.[444–447] Procedures for installing organofluorine bonds can broadly be categorised as either electrophilic or nucleophilic fluorination, depending on the source of the fluorine atom (Figure 3.6). Industrial routes to access these compounds typically require corrosive, difficult to handle reagents and demanding conditions. One approach is to use HF for the stepwise replacement of C-Cl bonds, though this route is restricted to allylic and benzylic chlorocarbon substrates.[448] The Swarts reaction uses SbF_3, SbF_5 or SbF_3Cl_2 in catalytic amounts in the presence of anhydrous HF to generalise this reactivity.[449] These processes have generally been attributed to a cyclic transition state and are generally referred to as the Swart process (Scheme 3.3); carbocationic intermediates have also been attributed.

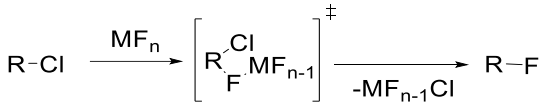

Scheme 3.3. Swarts process.

Other metal fluorides, generally high valent transition metal fluorides, act as a fluorine carrier (Scheme 3.4), these reagents can also add F_2 across a double bond.

Scheme 3.4. Fluorination by high valent metal fluoride.

Electrophilic fluorination agents ultilise N-fluoro or O-fluoro compounds to provide a source of 'F⁺'. [450,451] Direct fluorination with either F_2 or XeF_2 on organic compounds involves the formal exchange of H^+ with F^+, eliminating HF. Direct fluorination typically occurs *via* a radical mechanism.

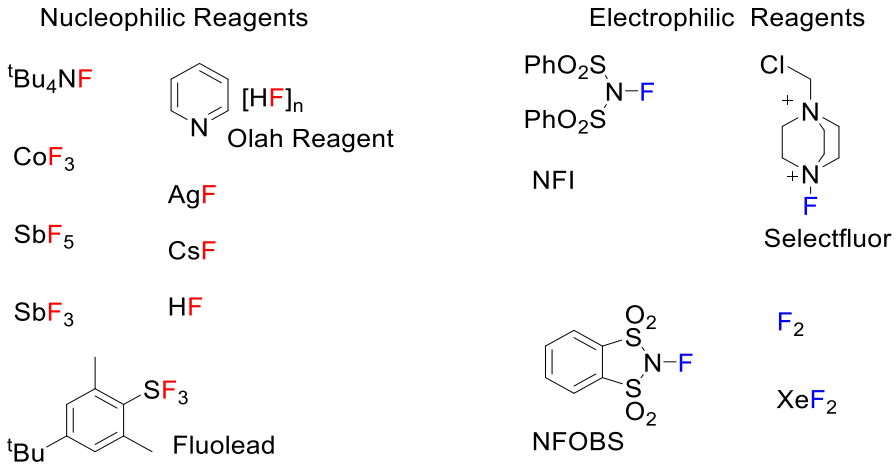

Figure 3.6 Typical nucleophilic and electrophilic fluorination agents.

3.1.8 Aims and Objectives

The aim of this body of work is to determine the scope for deploying cyclopentadienyl and cyclopentadienyl-based ligands for stabilising stibenium ions and investigating the Lewis acidic mediated reactivity. The observation that $[Cp^*_2Sb][AlI_4]$ contains a Sb···I interaction in the solid state suggests that these cations could be electrophilic.[440]

The specific objectives of this body of work are:

a) Synthesise a library of organoantimony(III) species of the form $Cp'_{3-n}SbX_n$ (n=1 or 2) where X is a halide or psuedohalide.
b) Subjecting the compounds described above to halide abstraction to yield cationic species (stibeniums).
c) Investigating the Lewis acidic behaviour of these stibeniums through the formation of adducts and proof of concept catalytic testing against model systems including the dimerisation of 1,1-diphenylethylene, C-X bond activation and aldol type reactivity.
d) Using DFT studies to investigate the electronic structure of these species.

3.2 Results and Discussions

3.2.1 Synthesis and Structure of Neutral Stibocenes

Despite the prevalence of the pentamethylcyclopentadienyl (C_5Me_5/Cp*) ligand in the reported literature of main group metallocenes, the cyclopentadienyl (C_5H_5/Cp) ligand was originally envisioned for this work as it is a weaker donor than Cp*, which would prevent the quenching of Lewis acidity at the Sb centre. The addition of $SbCl_3$ to two equivalents of Cp*Li at 0°C gave a pale-yellow solution which decomposed to a brown oil on warming to room temperature. NMR spectroscopy gave a complex mixture of signals and only $SbCl_3$·THF could be identified by X-ray crystallography. While structural data on $CpSbCl_2$ has been reported, it has been noted that the required synthesis from CpNa and $SbCl_3$ yields poorly and the product undergoes a similar decomposition to a black solid.[452] This decomposition has been attributed to the poor donor ability of Cp.

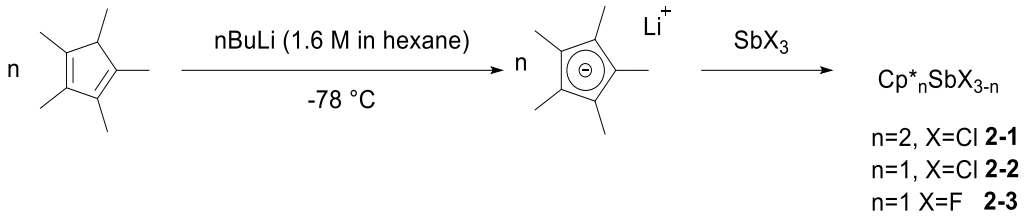

Scheme 3.5. Synthesis of Cyclopentadienyl Lithium from Cp*H and nBuLi and synthesis of neutral stibocene. X=Cl, F.

Cp^*_2SbCl (**2-1**) and Cp^*SbCl_2 (**2-2**) have both been reported and were synthesised as precursors for cationic stibonocenium species (Scheme 3.5).[391,453] In both cases, the appropriate ratio of Cp*Li and $SbCl_3$ were combined at 0°C in THF. Initial experiments used a one-pot approach with the addition of nBuLi to Cp*H, followed by the addition of $SbCl_3$. This led to a mixture of products, presumably due to the incomplete deprotonation of Cp*H. The isolation of Cp*Li before reacting with $SbCl_3$ gave clean conversion. Both **2-1** and **2-2** were highly oxygen sensitive, giving a purple colour on exposure to an aerobic environment. Cationic species containing both Cp* and fluoride were also identified as targets, which necessitated the synthesis of previously unknown Cp^*SbF_2 (**2-3**). Combination of Cp^*SbCl_2 and two equivalents of AgF gave two signals in the resulting ^{19}F NMR spectrum (-150 ppm and -156 ppm + other minor peaks). The observed chemical shifts are typical of F-Sb(V), suggesting an oxidation process, no metallic deposits were observed. Difficulty in separating these species necessitated an alternative synthesis. Mixing a suspension of Cp*Li and SbF_3 instantly yielded a yellow solution and white suspension which yielded Cp^*SbF_2, identified by NMR spectroscopy and SCXRD. The ^{19}F

spectrum of Cp^*SbF_2(**2-3**) contained a singlet at -60.56 ppm, which is typical of a Sb(III)-F. This suggested the combination of Cp^*SbCl_2 and AgF yielded some other unidentified species. Compound **2-3** is also oxygen sensitive, decomposing in an unidentified purple species in a similar fashion to **2-1** and **2-2**, albeit at a slower rate. This could be attributed to the stronger electron withdrawing ability of the fluorides, lowering the energy of the Sb lone pair. Crystals of Cp^*SbF_2 for SCXRD were grown via sublimation; Cp^*SbF_2 was isostructural with Cp^*SbCl_2 (Figure 3.7).[453] **2-3** forms linear chains in the solid state via a intermolecular Sb-Cp* interaction (Figure 3.8). The intramolecular hapticity has been assigned as η^3 according to a literature procedure.[377] The range of intermolecular Sb-Cp* bonds (3.3768(19) - 3.438(3) Å) and very slight displacement of the Sb from the centroid of the intermolecular ring would suggest an η^4 assignment for the intermolecular Sb-Cp* interaction. Bond lengths in **2-3** are typical.

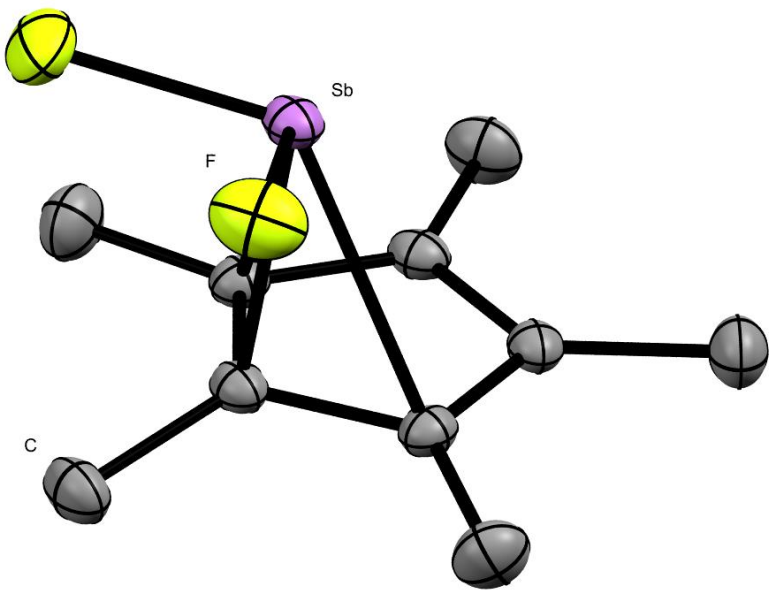

Figure 3.7. Solid state structure of 2-3. Ellipsoids shown at 50% probability. Hydrogen atoms have been omitted.

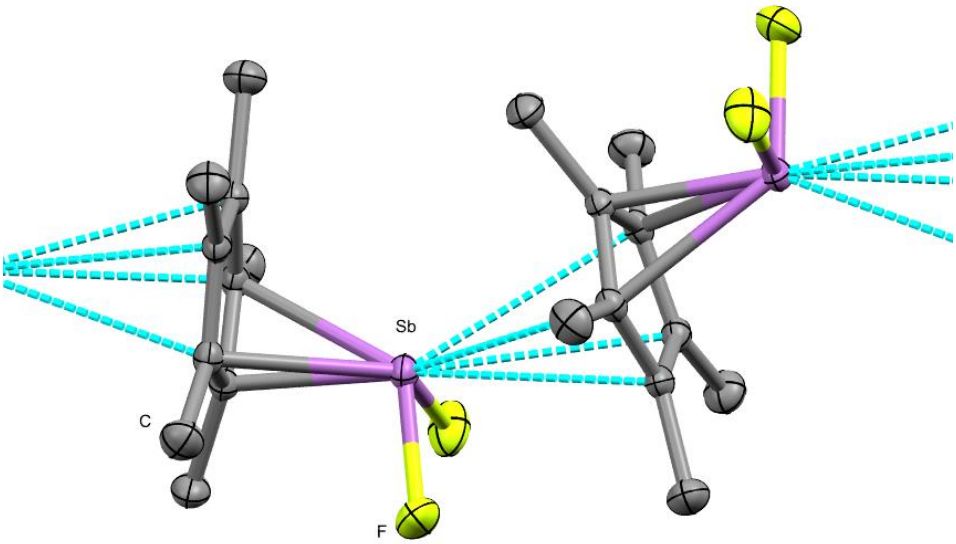

Figure 3.8. Solid state structure of **2-3**. Ellipsoids shown at 50% probability. Hydrogen atoms have been omitted. Intermolecular Cp*-Sb contacts are shown as blue dotted lines.

3.2.2 Synthesis and Structure of Monocationic Stibocenium Salts

Chloride abstraction from Cp^*_2SbCl (**2-1**) with $[Et_3Si(C_7H_8)][B(C_6F_5)_4]$, synthesised as per modified literature procedures,[342–344] in toluene yielded $[Cp^*_2Sb][B(C_6F_5)_4]$ (**2-4**) as a dark red/purple solid in 43% yield.

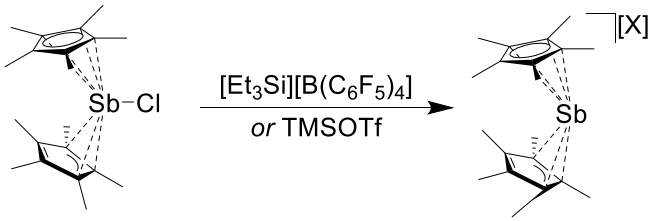

2-4 (X = $[B(C_6F_5)_4]$)
2-5 (X = [OTf])

Scheme 3.6. Synthesis of **2-4** and **2-5**.

The solid state structure consisted of well separated $[Cp^*_2Sb]^+$ and $[B(C_6F_5)_4]^-$ fragments; the ring hapticites are η^3/η^4 . The $\angle Cp^*_{centroid}$-Sb- $Cp^*_{centroid}$ is 162.4866(9)° and the Cp*-Sb bond lengths are 2.29278(9) Å and 2.27595(10) Å for the η^4 and η^3 rings respectively (Figure 3.9), which is consistent with reports from the literature.[441,454] To support the hypothesis that

this deviation from linearity was due to electronic effects as opposed to being the result of crystal packing effects, Cp^*_2SbOTf (**2-5**) was synthesised from **2-1** and AgOTf. The solid state structure of **2-5** also had no cation/anion interactions, allowing for a direct comparison. The structure of the cation in **2-4** and **2-5** was similar, suggesting that the deviation from linearity was primarily an electronic effect (Table 3.1). The $\angle Cp^*_{centroid}$-Sb-$Cp^*_{centroid}$ is 158.8929(5)°/158.7861(5)° and the Cp*-Sb bond lengths are 2.29070(4)/2.30271 Å and 2.28715(4)/2.27935(4) Å for the η^4 and η^3 rings respectively (*N.B.* there are two crystallographically independent molecules per asymmetric unit).

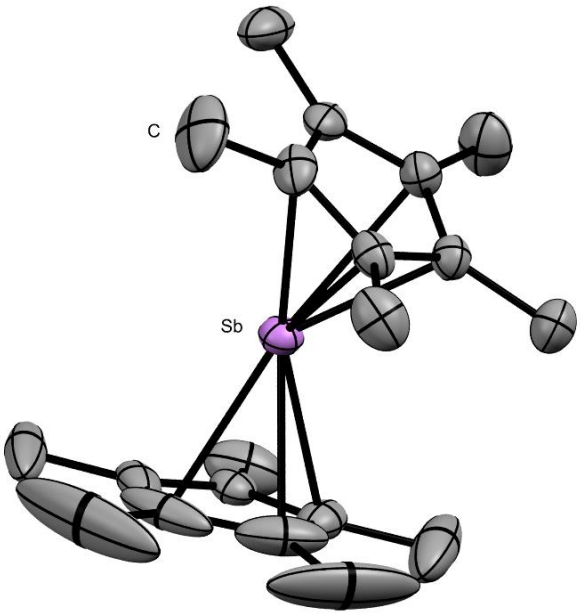

Figure 3.9. Solid state structure of **2-4**. Ellipsoids shown at 50% probability. Hydrogen atoms and borate counteranion have been omitted.

Table 3.1. Selected Structural parameters for Cp^*_2Sb cation. There are two crystallographically inequivalent cations in the asymmetric unit of 1a. Both Cp* rings in $[Cp^*_2Sb][AlCl_4]$ are crystallographically inequivalent (indicated by ~). Figure 8.18 contains a labelled diagram of the $[Cp^*_2Sb]^+$ motif.

Parameter	**2-4**	**2-5**	**$[Cp^*_2Sb][AlCl_4]$**[391]	**$[Cp^*_2Sb][AlI_4]$**[441]
Sb-C1	2.455(5)	2.46(1)/2.44(1)	2.484	2.45(1)
Sb-C2	2.521(4)	2.521(7)/2.518(9)	2.51	2.49(1)
Sb-C3	2.573(6)	2.597(8)/2.556(7)	2.613	2.61(1)
Sb-C4	2.673(2)	2.684(6)/2.692(6)	2.653	2.66(1)
Sb-C5	2.706(3)	2.733(7)/2.727(7)	2.728	2.74(1)
Sb-C6	2.459(3)	2.44(1)/2.45(1)	2.484~	2.48(1)
Sb-C7	2.486(2)	2.520(8)/2.513(7)	2.51~	2.52(1)
Sb-C8	2.601(4)	2.535(8)/2.545(7)	2.613~	2.592(8)
Sb-C9	2.634(2)	2.701(7)/2.690(7)	2.653~	2.67(1)
Sb-C10	2.705(4)	2.703(7)/2.717(7)	2.728~	2.71(1)
Centroid-Sb-Centroid	162.4866(9)°	158.8929(5)°/158.7861(5)°	161.10	157.37
Centroid-Sb	2.29278(9)/ 2.27595(10)	2.29070(4)/2.30271 2.28715(4)/2.27935(4)	2.299	2.291/2.299

Chloride abstraction from Cp^*SbCl_2 (**2-2**) with $[Et_3Si][B(C_6F_5)_4]$ in toluene yielded $[Cp^*SbCl][B(C_6F_5)_4]$ (**2-6**) as a light yellow solid in 38% yield (Scheme 3.7). An initial attempt to synthesise **2-6** from equimolar amounts of **2-2** and $[Et_3Si][B(C_6F_5)_4]$ in C_6D_6 yielded $[Cp^*_2Sb][B(C_6F_5)_4]$ (**2-4**).

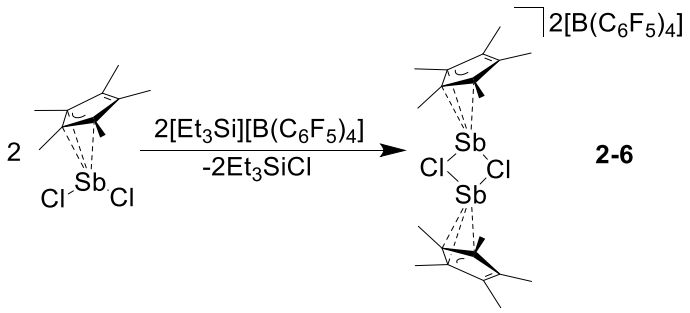

Scheme 3.7. Synthesis of **2-6**

The Cp^*SbCl^+ fragment forms dimers in the solid state via an intermolecular Sb···Cl interaction, suggesting significant Lewis acidity at Sb (Figure 3.10). The Cp*-Sb interaction can be described as η^3; the Sb-centroid distance is 2.14202(15) Å and the $\angle Cp^*_{centroid}$-Sb-Cl_{intra} is 122.230(5)°. There are no cation-anion interactions.

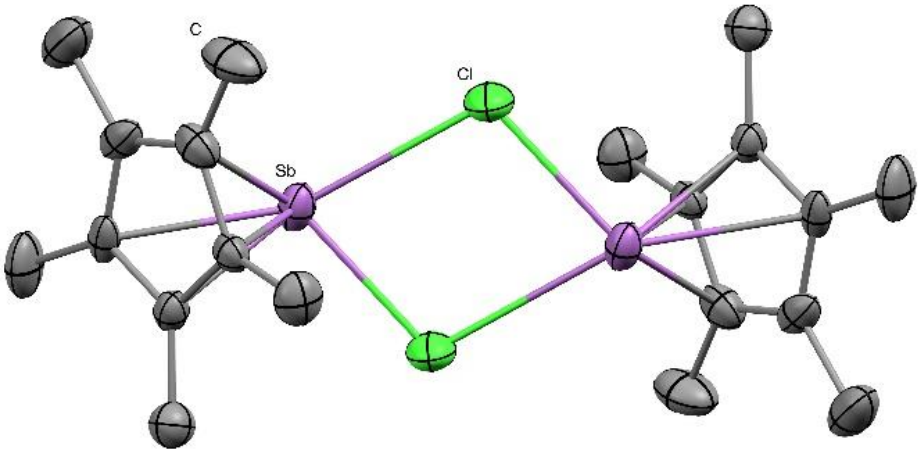

Figure 3.10. Solid state structure of **2-6.** Ellipsoids shown at 50% probability. Hydrogen atoms and borate counteranion have been omitted.

$[Cp^*SbF][B(C_6F_5)_4]$ was targeted with an equivalent strategy from Cp^*SbF_2 (**2-3**) and spectroscopically identified but could not be isolated due to its unstable nature. Recrystallisation of crude $[Cp^*SbF][B(C_6F_5)_4]$ from DCM/hexane gave $[Cp^*SbCl][B(C_6F_5)_4]$ (**2-6**) and $[Cp^*H_2][B(C_6F_5)_4]$ in 95%/5% ratio (by relative ^1H NMR integrals). Similar decomposition has also been observed in $[Cp^*AsF][B(C_6F_5)_4]$,[442] which has been attributed to thermal instability. The $[Cp^*H_2][B(C_6F_5)_4]$ is infamous due to the controversy surrounding its initial synthesis by Lambert from Cp*H and $[Ph_3C][B(C_6F_5)_4]$,[455] in which is it was identified as planar $C_5Me_5^+$. The report of a stable antiaromatic cation was quickly disputed and corrected by Lambert himself.[456,457] In no case was the source of H elucidated. $[Cp^*H_2][B(C_6F_5)_4]$ could potentially be formed by reductive elimination of Cp* from $[Cp^*SbF][B(C_6F_5)_4]$ to yield $[Cp^*]^+$, which, due to its anti-aromatic character, rapidly reduces to $[Cp^*H_2][B(C_6F_5)_4]$, with solvent possibly acting as a source of H. The formation of $[Cp^*SbCl][B(C_6F_5)_4]$ (**2-6**) is likely the result of chloride/fluoride exchange with the solvent (see 3.2.7 Chlorodefluoroination by Chlorinated Solvents). Recrystallisation of crude $[Cp^*SbF][B(C_6F_5)_4]$ in aromatic solvents yielded an intractable black powder and $[Cp^*_2Sb][B(C_6F_5)_4]$ (**2-4**). To ascertain the existence of the highly unstable $[Cp^*SbF]^+$ fragment, an N-heterocyclic carbene (NHC), IMes, was deployed to yield an isolatable adduct. To prevent any decomposition of the $[Cp^*SbF]^+$ fragment, a solution of IMes was added to a solution of Cp^*SbF_2 (**2-3**) before the addition of $[Et_3Si][B(C_6F_5)_4]$. NMR spectroscopy suggested the IMes and Cp^*SbF_2 (**2-3**) formed an adduct, but this was not

isolated. Crystalline [Cp*SbF(IMes)][$B(C_6F_5)_4$] (**2-7**) was isolated by recrystallisation from 1,2-DFB/hexane (Scheme 3.8).

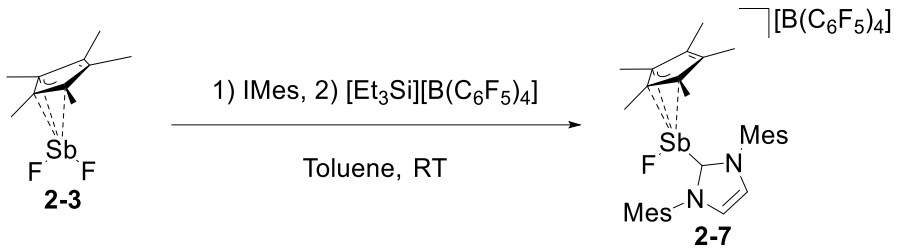

Scheme 3.8. Synthesis of **2-7**.

The hapticity of the Cp*-Sb interaction is η^3 and the Sb-Centroid distance of is 2.3820(5) Å. The Sb-F and Sb-$C_{carbene}$ bond lengths are 1.942(5) Å and 2.294(6) Å respectively, which are typical values (Figure 3.11).[458] Compound **2-7** appeared unstable in CD_2Cl_2.

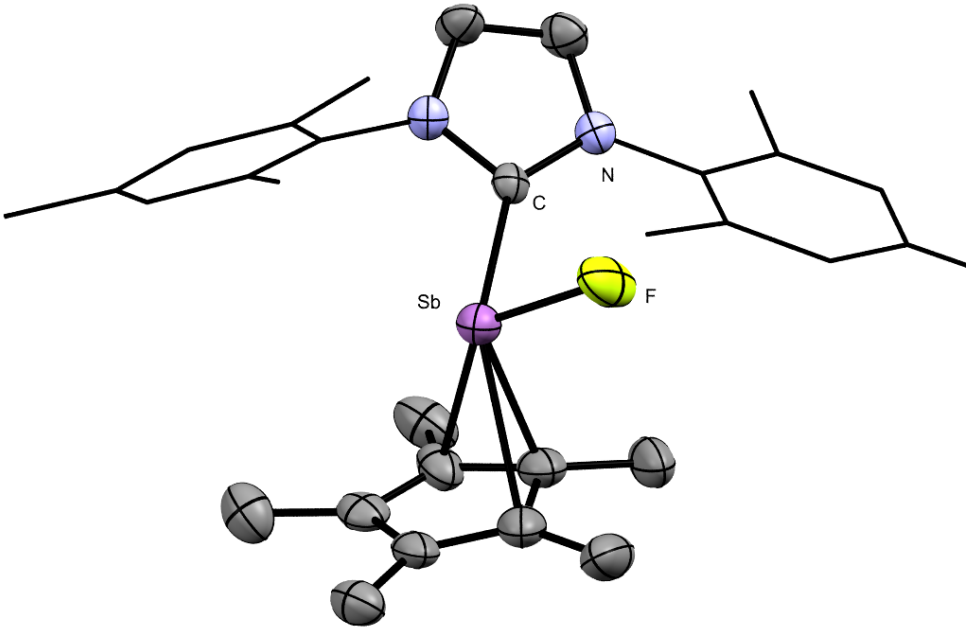

Figure 3.11. Solid state structure of **2-7**. Ellipsoids shown at 50% probability. Hydrogen atoms, borate counteranion and disorder solvent have been omitted. The mesityl groups are shown in wireframe style.

3.2.3 Synthesis and Structure of Dicationic Stibocenium Salts

The addition of two equivalents of [Et_3Si][$B(C_6F_5)_4$] to either Cp*$SbCl_2$ (**2-2**) or Cp*SbF_2 (**2-3**) failed to yield [Cp*Sb][$B(C_6F_5)_4]_2$. Co-crystallised [Cp*SbCl][$B(C_6F_5)_4$]/ [Cp*SbF][$B(C_6F_5)_4$] was obtained from **2-3** and [Et_3Si][$B(C_6F_5)_4$], giving further credence to the existence of Cp^*SbF^+ and the F/Cl exchange with chlorinated solvent.

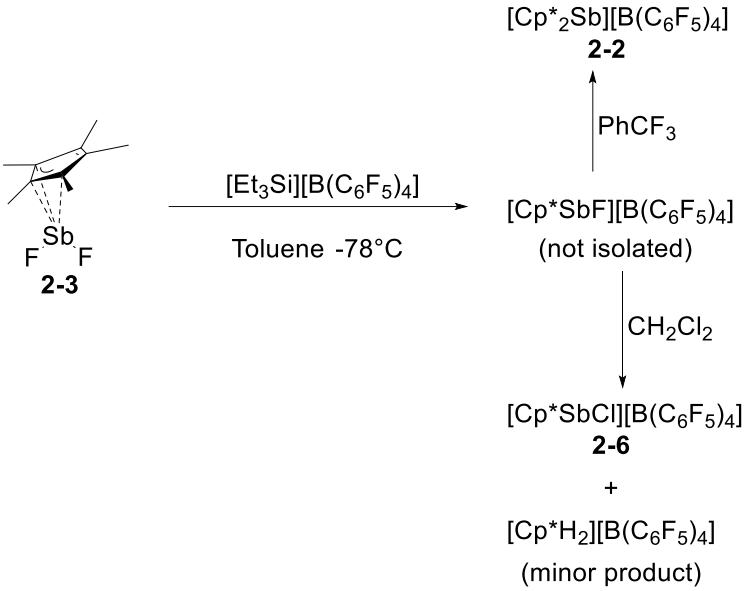

Scheme 3.9. Decomposition pathways of $[Cp^*SbF][B(C_6F_5)_4]$.

$[Ph_3C][B(C_6F_5)_4]$ is typically used to abstract hydride and alkyl groups to form cations in an analogous way to $[Et_3Si][B(C_6F_5)_4]$;[459] it was envisioned that the trityl group could be used to abstract a Cp* group from $[Cp^*_2Sb]^+$ to yield a dication. $[Ph_3C][B(C_6F_5)_4]$ was found to decompose the Cp* anion, as mixing Cp*Li and $[Ph_3C][B(C_6F_5)_4]$ in $CDCl_3$ yielded a black precipitate and Ph_3CH, precluding this strategy.

The addition of two equivalents of TMSOTf to either Cp^*SbCl_2 (**2-2**) or Cp^*SbF_2 (**2-3**) yielded $Cp^*Sb(OTf)_2$ (**2-8**) as a light pink powder in 30% yield (Scheme 3.10, based on synthesis from Cp^*SbF_2).

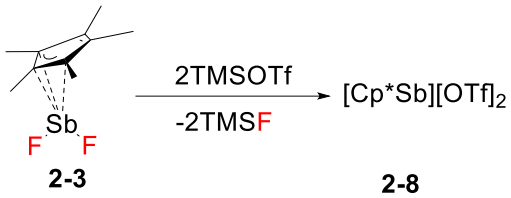

Scheme 3.10. Synthesis of **2-8**.

Compound **2-8** was found to be extremely sensitive to oxygen, which precluded accurate microanalysis. SCXRD revealed strongly co-ordinated triflate anions (Sb-O = 2.40486(10) Å/2.52652(10) Å) ($\sum_{vdW}$=3.58 Å) (Figure 3.12). The Sb atom has two intermolecular $Sb\cdots O_{triflate}$ interactions (2.77468(7) Å/2.79331(11) Å) in the solid state, yielding a dimer with pseudo-square pyramidal Sb centres (τ_5= 0.15).[460] The hapticity of the metallocene is

η^5 with a Sb-Centroid distance of 2.09164(6) Å, which is contracted from **2-4** and **2-6** (*cf.* 2.294 Å and 2.142 Å respectively), suggesting an increased positive charge at Sb.

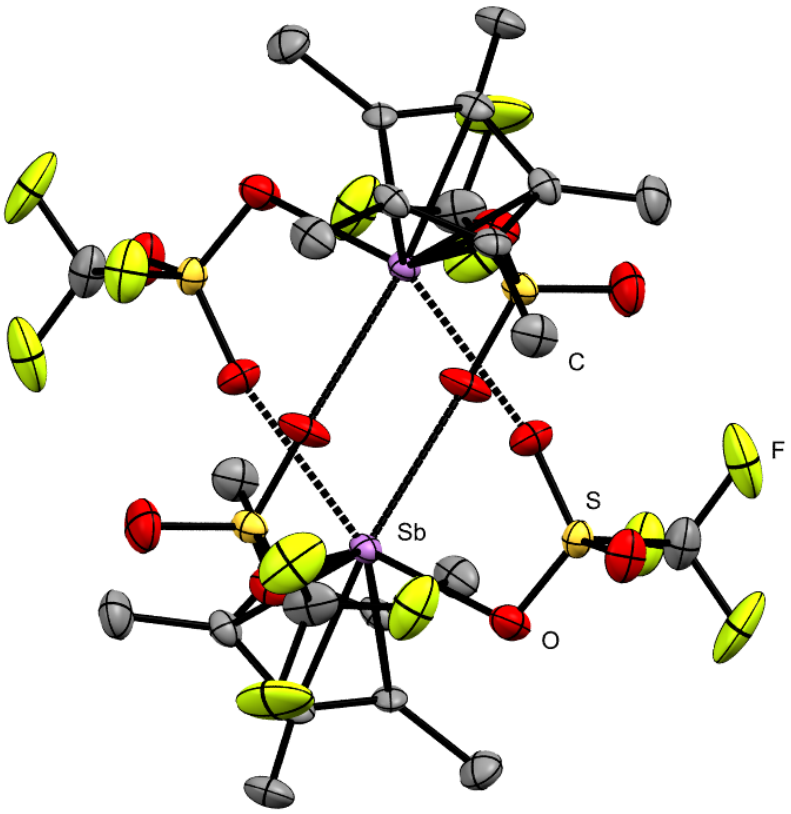

Figure 3.12. Solid state structure of **2-3**. Ellipsoids shown at 50% probability. Hydrogen atoms have been omitted. Intermolecular Sb-O contacts are shown as dotted lines.

$[Cp^*Sb][B((3,5\text{-}CF_3)_2C_6H_3)_4]_2$ ($[Cp^*Sb][BArF]_2$) was targeted by the addition of two equivalents of AgBArF to Cp^*SbCl_2, this yielded orange crystals of $[Cp^*_2Sb][BArF]$.

3.2.3 Coordination of Stibocenium Cations with Lewis Bases

$[Cp^*_2Sb][B(C_6F_5)_4]$ (**2-4**) does not form a Lewis adduct with either Et_3PO or pyridine, as evident by NMR spectra of respective mixtures amounting to the sum of the reagents. Computational evidence (*see* 3.2.6 Computational Investigation of the Electronic Structure) suggests that this is due to steric crowding at the Sb centre as opposed to an electronic effect. Conversely, $[Cp^*SbCl][B(C_6F_5)_4]$ (**2-6**) forms adducts with both Et_3PO and pyridine. Structural characterisation of both adducts was precluded by the absence of suitable single crystals. The $^{31}P\{^1H\}$ NMR chemical shift of **2-6**/Et_3PO shift at 80.65 ppm indicates a similar Lewis acidity to a tris(haloaryl)borane according to the Gutmann-Beckett test.[225] The ^1H

NMR spectrum of **2-6**/pyridine indicates the formation of an adduct as the Cp^*_{Me} protons are shifted downfield.

3.2.4 Reactivity with Silane

Addition of Et_3SiH to **2-6** yielded an intractable black powder, which was hypothesised to be antimony metal. It was initially hypothesised that this was the result of a series of reductive elimination steps after the nucleophilic attack of a hydride onto the Sb cation resulting in the formation of pentamethylcyclopentadiene (Cp*H), HCl and antimony metal. However, the absence of any Cp*H in the resulting ^{1}H NMR spectra suggests that this is not the case. While the exact mechanism of the decomposition remains unknown, the ^{19}F NMR spectrum contains multiple species, including Et_3SiF, suggesting that a transient Et_3Si^+ cation is formed. This reactivity impedes the use of **2-6** in catalysis requiring the use of Et_3SiH.

3.2.5 Catalytic Activity of $[Cp^*SbCl][B(C_6F_5)_4]$

Due to its common use as a test reaction for Lewis acidity, **2-6** was probed for reactivity in the dimerisation of 1,1-diphenylethylene (DPE). Compound **2-6** catalysed the dimerisation of DPE to 1-methyl-1,3,3-triphenyl-2,3-dihydro-1H-indene with 86% conversion after 2 hours at RT with 5mol% catalyst loading in CD_2Cl_2 (Scheme 3.11 i). No catalyst decomposition or side-products were observed. $[Cp^*_2Sb][B(C_6F_5)_4]$ (**2-4**) is unreactive under the same conditions.

Some transition metal metallocenes have been reported as catalysts for the Mukaiyama-aldol addition.[461] Compound **2-6** also shows some catalytic activity in the Mukaiyama-aldol addition of methyl trimethylsilyl dimethylketene acetal to benzaldehyde yielding methyl-2,2-dimethyl-3-phenyl-3-trimethylsilyloxypropionate with 14% conversion after 2 hours at RT with 5 mol% catalyst loading in CD_2Cl_2 (Scheme 3.11 ii). Multiple side products were observed. The solution turned a purple colour over the course of the two hours, suggesting the formation of an oxidised antimony species, by analogy to the colour formed on exposure to oxygen. Repeating this reaction in the absence of **2-6** did not yield any reactivity, discounting the possibility of silyl species catalysing the observed reaction. Compound **2-6** yielded some Diels-Alder reactivity, yielding endo-1-(-3-Phenylbicyclo[2.2.2]oct-5-en-2-yl)ethan-1-one from E-chalone and 1,3-cyclohexadiene in 20% yield after 2 hours at RT in CD_2Cl_2 with 5 mol% catalyst loading (Scheme 3.11 iii). Polymerised diene was also identified by NMR spectroscopy, by broad signals at 5.5 -6.0 ppm and 1.0 – 2.2 ppm. Repeating the same reaction with the omission of E-chalchone

yields similar signals. Mixing E-chalcone and **2-6** causes a shift in the ^{1}H NMR chemical shift of **2-6**. Me signal upfield by 0.1 ppm, suggesting the formation of an adduct.

An attempt to carry out a [2+2] cycloaddition between methyl propiolate and 2-methyl-2-butene in the presence of catalytic amounts of **2-6** yielded polymerised 2-methyl-2-butene (Scheme 3.11 iv).[462]

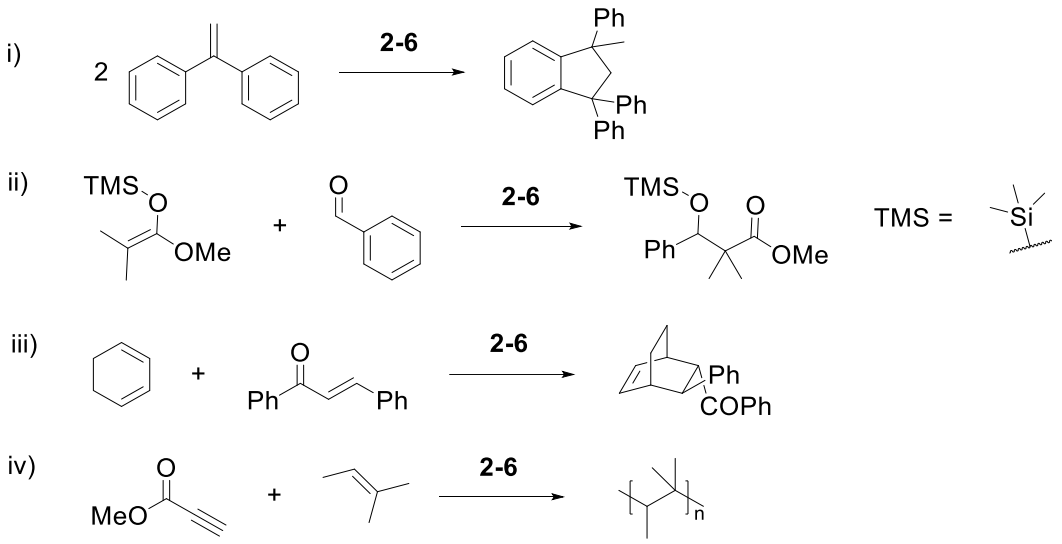

Scheme 3.11 . Catalytic reactions reported here. i) dimerisation of 1,1 diphenylethylene to 1-methyl-1,3,3-triphenyl-2,3-dihydro-1H-indene. ii) Mukaiyama-aldol addition of methyl trimethylsilyl dimethylketene acetal to benzaldehyde yielding methyl-2,2-dimethyl-3-phenyl-3-trimethylsilyloxypropionate iii) Diels-Alder cyclisation of 1,3-cyclohexadiene and E-chalcone . iv) [2+2] cycloaddition between methyl propiolate and 2-methyl-2-butene yielding poly(2-methyl-2-butene)

3.2.6 Computational Investigation of the Electronic Structure

Functional testing was undertaken to elucidate a suitable computational method; which was carried out by comparing structures optimised at various levels of theory to crystallographic parameters. Functional testing suggested that M062X/def2SVP (GJ3) would suitably model the stibocenium system, which was carried out in an analogous way to that for the triarylchlorostibonium salts (see 2.2.3 Stoichiometric Reactivity of Triarylchlorostibonium Salts). The electronic structures of Cp^*SbCl^+, Cp^*SbF^+ and $Cp^*_2Sb^+$ were initially investigated by natural bond orbital (NBO) analysis; this yielded unphysical results such as a localised negative charge on the Cp* ring, suggesting that the constricted Lewis structure foundation of NBO analysis might not be suitable for these highly delocalised species. The Kohn-Sham orbitals , from HOMO -4 to LUMO + 3, were visualise to visualise the electronic structure of these species (Figure 3.13, Figure 3.14 and Figure 3.15). While nucleophilicity was not probed experimentally, the computationally obtained electronic structure suggests that despite the presence of a lone pair, no nucleophilicity

would be observed. The lone pair is pacified to HOMO -2 in each case, where a stibine would typically contain the lone pair in the frontier HOMO. In each case the HOMO consists of the π_{Cp^*} system. In each case the source of the experimentally observed electrophilicity (see 3.2.3 Coordination of Stibocenium Cations with Lewis Bases and 3.2.5 Catalytic Activity of [Cp*SbCl][B(C_6F_5)$_4$]) was determined to be vacant p_{Sb} orbitals. In the case of $Cp^*_2Sb^+$ the p_y and p_z orbital are practically degenerate (-4.37 eV and -4.87 eV) and form the LUMO and LUMO +1. In the case of Cp^*SbCl^+ and Cp^*SbF^+, the P_y orbitals (-6.09 eV and -6.01 eV respectively) are significantly lower in energy than the P_z orbitals (-4.15 eV and -4.12 eV respectively). The major Cp*-Sb bonding interaction in $Cp^*_2Sb^+$ is contained in the HOMO -3, consisting of an s/p_{Sb}- π_{Cp^*} interaction. The primary bonding interaction in Cp^*SbCl^+ and Cp^*SbCl^+ is similar and is contained in the HOMO-1 orbital.

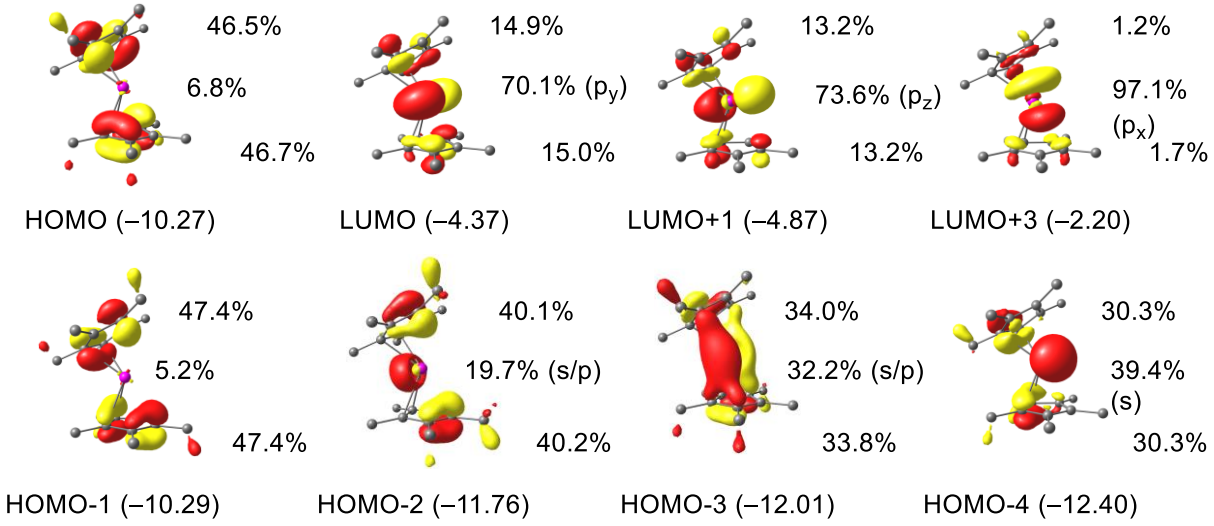

Figure 3.13. Kohn-Sham Orbitals of $Cp^*_2Sb^+$ in eV (Contour value = 0.03, occupancy = 2).

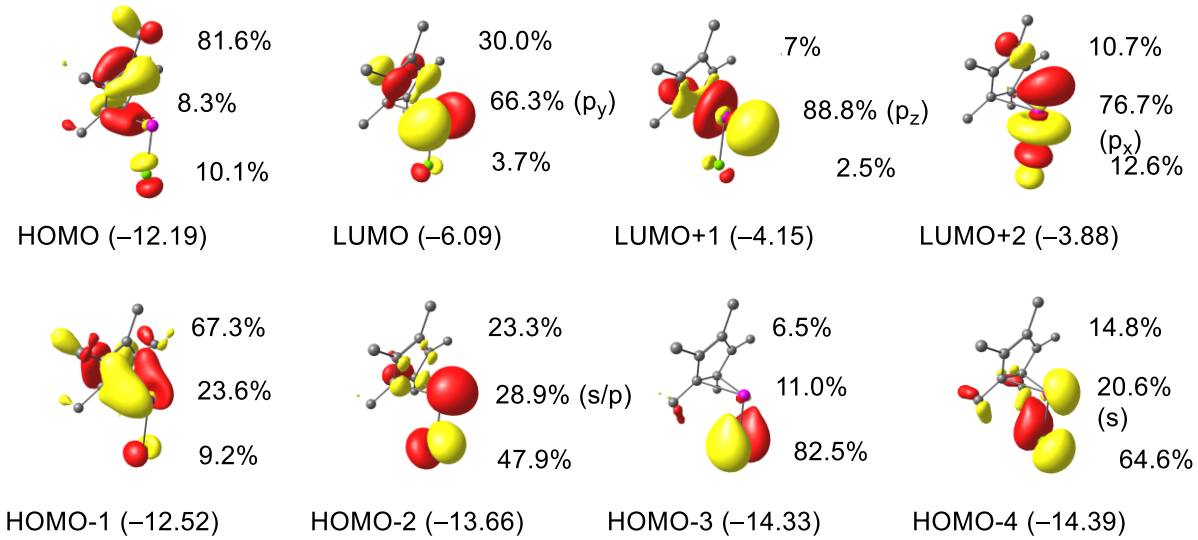

Figure 3.14. Kohn-Sham Orbitals of Cp^*SbCl^+ in eV (Contour value = 0.03, occupancy = 2).

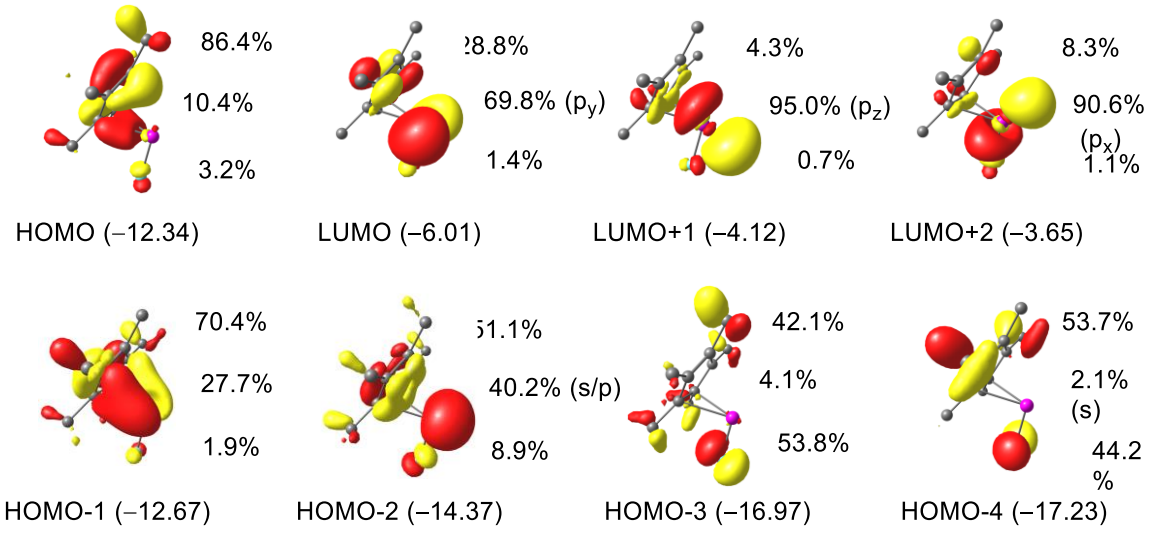

Figure 3.15. Kohn-Sham Orbitals of Cp^*SbF^+ in eV (Contour value = 0.03, occupancy = 2).

Comparison of the relative free energies of both the monomer and dimer for both $[Cp^*SbCl]^+$ (ΔG=2.2 kcal mol^{-1})and $[Cp^*SbF]^+$ (ΔG=1.8 kcal mol^{-1}) in dichloromethane, modelled using a polarisable continuum model (PCM), suggests that the monomer is the major product in solution, which contrasts with the dimeric form in the solid state. While the preference for a hypovalent Sb centre might be counterintuitive, this can be rationalised as a result of the energy penalty for a dication over two separate monocations.

3.2.7 Chlorodefluoroination by Chlorinated Solvents

The recrystallisation of crude $[Cp^*SbF][B(C_6F_5)_4]$ in dichloromethane yielded **2-6** (Scheme 3.9 i) and co-crystallised Cp^*SbCl^+/Cp^*SbF^+ was recovered from an attempted synthesis of $[Cp^*Sb][B(C_6F_5)_4]$ (3.2.2 Synthesis and Structure of Monocationic and 3.2.3 Synthesis and Structure of Dicationic). For the latter reaction, chloride abstraction of dichloromethane by transient Cp^*Sb^{2+} could potentially explain this observed product although no evidence of carbocation species was found. It was hypothesised that this reactivity was the result of Cl/F exchange between the solvent and the transient Cp^*SbF^+ species. No CD_2ClF or CD_2F_2 was observed by NMR spectroscopy when dissolving crude $[Cp^*SbF][B(C_6F_5)_4]$ in CD_2Cl_2.

To further interrogate this reactivity, a series of halocarbons ($CDCl_3$, $PhCCl_3$, BnCl, Ph_3CCl and MeI) were added to a crude sample of $[Cp^*SbF][B(C_6F_5)_4]$ which was then dissolved in C_6D_6 and monitored by NMR spectroscopy. $CDCl_3$ and BnCl yielded no reactivity although this could be attributed to the negligible solubility of the crude Cp^*SbF^+ in these solvents (Scheme 3.9 ii and iii). Ph_3CCl produced Ph_3CF; this could be attributed to nucleophilic addition of the labile Cl^- to the Cp^*SbF^+ to give Cp^*SbClF, followed by abstraction the F^- by the formed trityl cation. Alternatively, the Cl/F exchange could occur in a concerted

manner. To test this $[Ph_3C][B(C_6F_5)_4]$ was added to a sample of Cp^*SbF_2, which yielded a small trace of Ph_3CF. This suggests that the latter mechanism is more likely. This is distinct from the reactivity of **2-6** which forms $[Ph_3C][B(C_6F_5)_4]$ and Cp^*SbCl_2 on reaction with Ph_3CCl. The reaction of **2-6** with $PhCCl_3$ yielded a peak at -48 ppm in the ^{19}F NMR spectrum which was attributed to $PhCCl_2F$ (Scheme 3.12 iv).[463] This supports the hypothesis that the observed reactivity with CH_2Cl_2 can be attributed to chloride/fluoride exchange. Both Cp^*SbF_2 and the black intractable precipitate that are formed in these reactions were screened for the same reactivity and neither yielded any $PhCCl_2F$. The iodomethane yielded a complex mixture, observed by NMR spectroscopy, which was likely the result of methylation of the Cp* ring (Scheme 3.12 v).

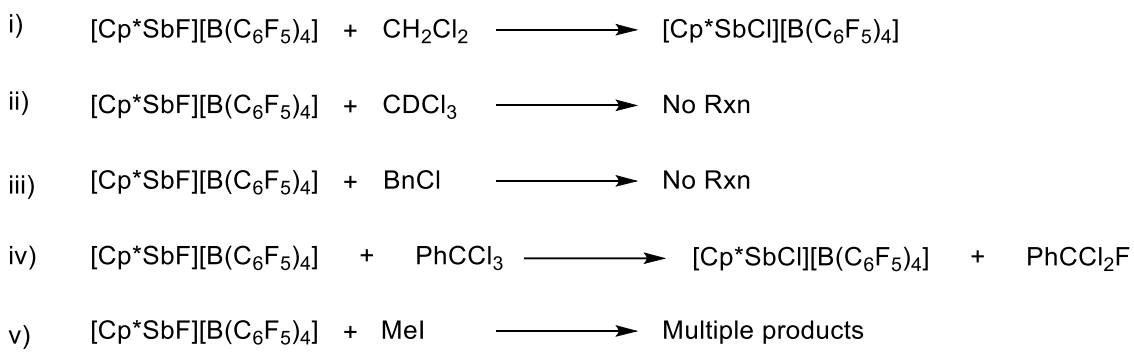

Scheme 3.12 Reaction of $[Cp^*SbF][B(C_6F_5)_4]$ with i) CH_2Cl_2, ii) $CDCl_3$, iii) BnCl, iv) $PhCCl_3$ and v) iodomethane.

3.2.8. Mechanistic Investigation of Fluorodechlorination

Due to the instability of Cp^*SbF^+, limited NMR handles and other reactivity, experimental probing of the mechanism was largely precluded. To gain some insights into the mechanism a computational DFT study of potential mechanistic pathways was undertaken. No kinetically reasonable pathway was found for the fluorodechlorination of CH_2Cl_2 was found, both an S_N2 type mechanism and a cyclic concerted exchange were both found to have too high of an energy barrier at 37.5 and 36.3 kcal mol^{-1} respectively. Investigations of trimolecular transition states, with stabilisation from the $[B(C_6F_5)_4]^-$ or a second CH_2Cl_2 molecule was also attempted but did not yield a suitable pathway; trimolecular transition states are typically rare due to the large entropy barrier and the cost on the preexponential term of the equation.

The fluorodechlorination of $PhCCl_3$ was also computationally investigated, in this case a feasible mechanism was elucidated (Figure 3.16). According to this mechanism the stibocenium initially abstracts a chloride from $PhCCl_3$ to yield a carbocation and Cp*SbClF

with a barrier of 10.6 kcal mol^{-1}. The carbocation then abstracts a fluoride from Cp*SbClF to yield the products with an overall thermodynamic stabilisation of 9 $kcalmol^{-1}$.

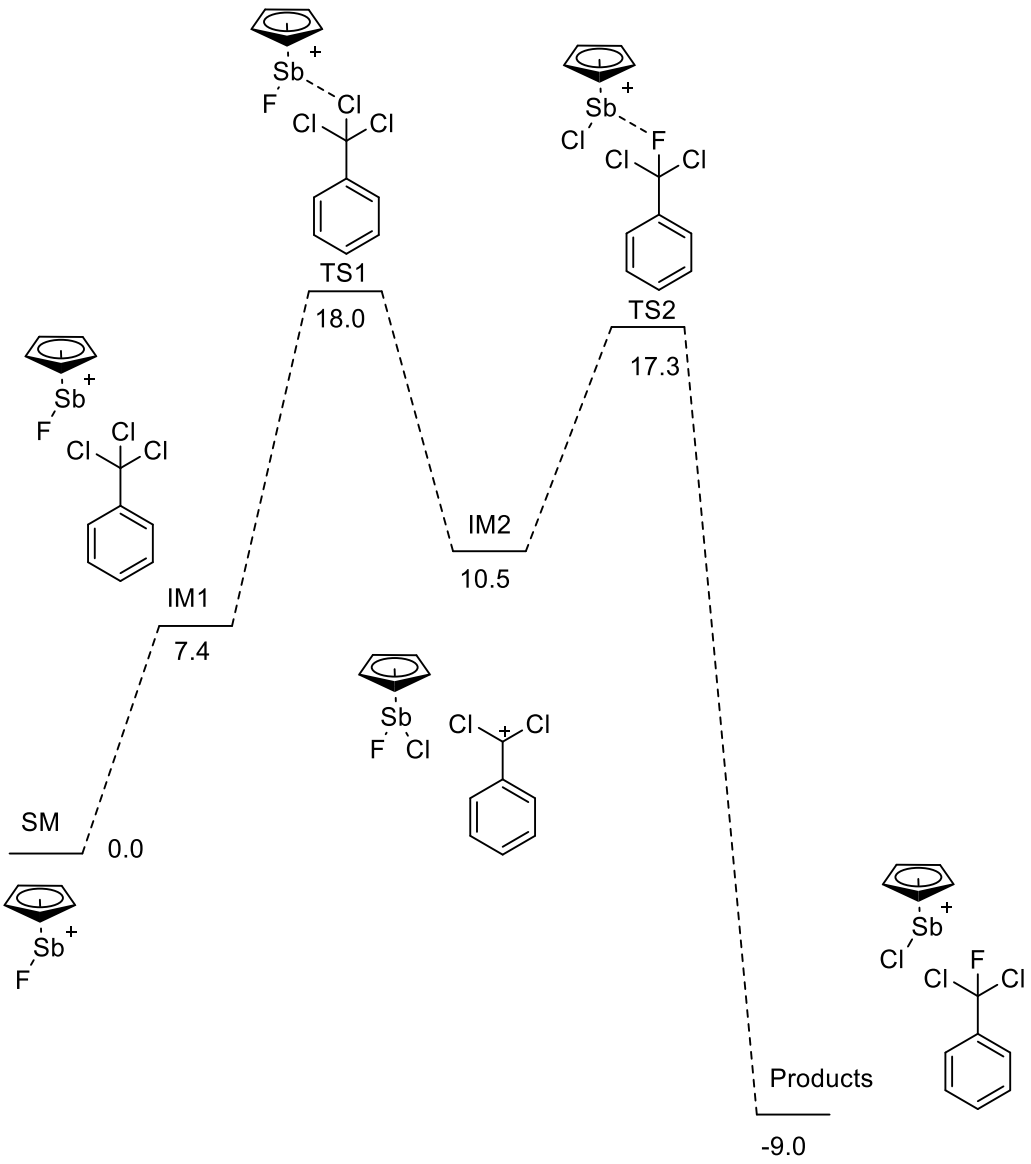

Figure 3.16. Computed reaction profile (M062X-D3/def2-TZVPP) for the fluorination of $BnCl_3$ by $[Cp^*SbF]^+$. Relative Gibbs free energies (1 atm, 298 K, $kcalmol^{-1}$) corrected for benzyl chloride solvent are given.

3.2.9. Attempted Oxidation of Pentamethylcyclopentadienyl Antimony(III)

Main group metallocenes are typically found in the lone pair oxidation state (see 3.1.4 Electronic structure of main group metallocenes); $[Cp^*PH_2(SiEt_3)][B(C_6F_5)_4]$ is the only reported group 15 metallocene in the lone pair +2 oxidation state, although the Cp* is sigma bonded are thus is probably better considered as a vinyl-Phosphorus bond as opposed to a Cp*-P bond.[443] Several attempts to oxidise the stiboncene species Cp^*SbCl_2 and Cp^*_2SbCl with SO_2Cl_2 failed to yield any isolatable Sb(V) stiboncenes, typically yielding a

complex mixture of products. A similar result was obtained when Cp^*SbCl_4 was targeted by the metathesis of equimolar Cp^*Li with $SbCl_5$.

3.2.10. Attempted Installation of an Aryl Group to Pentamethylcyclopentadienyl Antimony(III)

Installing a highly electron withdrawing organic group in place of the halide in Cp^*SbX^+ was hypothesised to yield novel reactivity while retaining the electrophilicity of the Sb centre. $Cp^*SbCl(C_6F_5)$ was targeted as a precursor to $[Cp^*Sb(C_6F_5)]^+$ by the reaction of C_6F_5MgBr with Cp^*SbCl_2. Work-up of the resulting yellow powder gave yellow crystals of Cp^*SbI_2 when sublimed *in vacuo* at 70° C (Figure 3.17). Two potential sources of the iodine could be identified, either residual I_2 or MgI_2 from the activation of magnesium. As addition of a halogen to stibocenes typically yields a transient Sb(V) species followed by decomposition, the latter source of iodide is more probable.

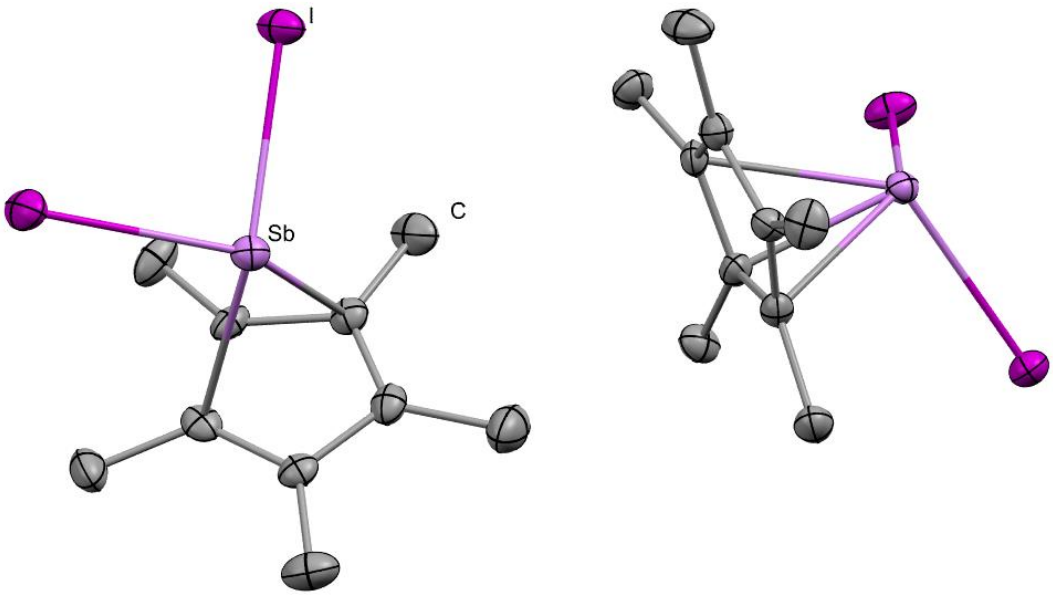

Figure 3.17. Solid state structure of Cp^*SbI_2. Two non-equivalent molecules are present in the asymmetric unit. Ellipsoids shown at 50% probability. Hydrogen atoms have been omitted.

While Cp^*SbI_2 was an unexpected side product, it is of interest for the different antimony coordination environment. There are two crystallographically inequivalent Sb centres in the solid state which are η^3. Rather than the Cp*···Sb coordination to build up 1D chains that is present in Cp^*SbCl_2 and Cp^*SbF_2 (**2-3**), each Sb centre forms 1D chains via Sb-I interactions. Both molecules contain unique coordination spheres about the Sb atom. One Sb has two nearly symmetric intermolecular contacts (3.83208(10) Å) and 3.83835(8) Å) to neighbouring I atoms of the same neighbouring molecule to yield a 1D chain (Figure 3.18).

The other Sb centre forms highly distorted Sb_2I_2 rings via asymmetric Sb···I contacts (3.79325(10) Å and 3.88555(9) Å) to two neighbouring atoms (Figure 3.18). The intramolecular Sb-I bonds (2.84775(8) Å -2.86676 (4) Å) are comparable to the closest related structurally characterised compound reported, $(Me_4C_5H)SbI_2$.[464] $(Me_4C_5H)SbI_2$ also consists of a coordination polymer in the solid state *via* Me···Me and I···I interactions.

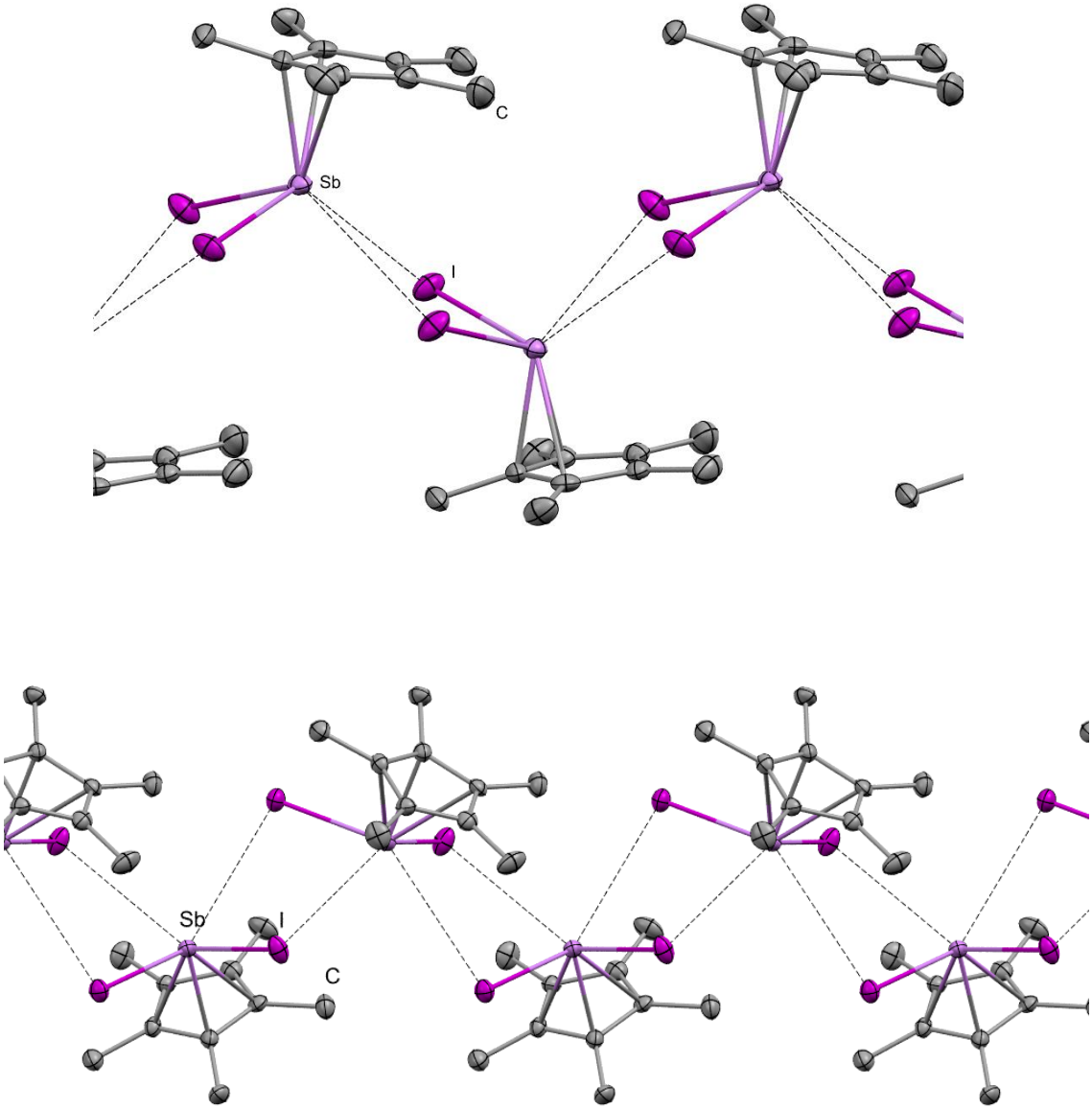

Figure 3.18. Solid state structure of Cp^*SbI_2 showing the 1D chain with symmetric coordination (top) and the 1D chain with asymmetric coordination (bottom). Ellipsoids shown at 50% probability. Hydrogen atoms have been omitted.

3.3 Conclusions

As a result of this work five previously unknown stibenceniums have been synthesised and characterised as well as one new neutral stibocene. A serendipitously observed fluoro/chloro exchange has been mechanistically mapped computationally and the electronic structure of these compounds has also been revealed. Lewis acid mediated reactivity with the $[Cp^*SbCl]^+$ cation was investigated. The overarching conclusion is that while investigating the chemistry of compounds containing a Cp*-Sb organometallic bond was a worthwhile endeavour and yielded novel reactivity and unique structures, several features of these compounds preclude extensive deployment as catalysts. Such features include instability in the presence of Et_3SiH, labile Cp*-Sb bonds, instability of certain species and a high degree of sensitivity to oxygen. While the $[Cp^*_2Sb]^+$ proved the most stable, the high amount of steric bulk shields the electrophilic Sb centre. The relatively small nature of the Cp* ring precludes the possibility to isolate species of the form$[Cp'_2Sb]^+$ species that are still stable while having a sterically accessible Sb centre. This body of work has yielded some novel insights into organoantimony chemistry. One point of interest is that the deployment of Cp* ligands pacifies the lone pair and removes any expected nucleophilicity. The observation of chloride/fluoride exchange as well as the resulting mechanistic investigation demonstrated the unique reactivity of the $[Cp^*SbF]^+$ ion. The existence of $[Cp^*Sb]^{2+}$ was suggested by crystallographic evidence but is likely highly unstable. A similar argument can be made for $[Cp^*SbF]^+$ albeit that the evidence is stronger for the existence of transient $[Cp^*SbF]^+$. Since this work was carried out the dication was reported as the toluene adduct ($[\eta^5\text{-}Cp^*Sb(C_7H_8)][B(C_6F_5)_4]_2$).[465]

Several avenues could still be explored. Rudimentary work on the synthesis of compounds of the form Cp*RSbCl did not lead to any of the targeted compound isolated however there is scope to further optimise this reaction by changing the order of reagents i.e. use $RSbCl_2$ as a precursor to Cp*RSbCl and ensure total removal of any salt by products. As the presence of the fluoride in $[Cp^*SbF]^+$ was essential to its instability in chlorinated solvents, it would be logical to assume that replacing this halide with a highly electron withdrawing group may impede this decomposition while retaining the Lewis acidity of the species. Similar compounds with other Cp' ligands, in particular ansa-metallocenes, would also be another possible avenue for future work.

3.4 Experimental

See Appendix I: General Experimental Methods for general experimental information.

Synthesis of Cp*Li

1.6 M n-BuLi in hexane (9.0 mL, 14 mmol) was added dropwise to a solution of pentamethylcyclopentadiene (1.74 g, 12.77 mmol) in THF (50 mL) at -78 °C. A slightly off white suspension formed on warming to room temperature. The suspension was stirred at room temperature for 2h. The solution was removed by cannula filtration and the resulting powder was washed with hexane (3x20 mL). The solid was dried *in vacuo* to yield a white powder (1.168 g, 8.22 mmol, 64%). The product was suspended in $CDCl_3$ and a ^1H NMR spectrum was obtained to confirm absence of any starting material.

Synthesis of Cp^*_2SbCl (2-1)

A solution of $SbCl_3$ (0.4860 g, 2.13 mmol) in THF (20 mL) was added dropwise to a suspension of Cp*Li (0.6060 g, 4.26 mmol) in THF (30 mL) at 0 °C, a deep red solution formed initially and a white precipitate formed. The suspension was stirred at room temperature overnight. The solvent was removed *in vacuo* and the resulting yellow oil was extracted in n-hexane (100 mL). The solvent was removed *in vacuo.* This yielded a red solid (0.4775 g, 1.12 mmol, 53 %).^1H NMR (400 MHz, CD_2Cl_2): δ ppm 2.03 (s, 30 H, Me-H) $^{13}C\{^1H\}$ NMR (101 MHz, C_6D_6): 11.0 (s, Me-C), 123.8 (s, Cp-C).

Synthesis of Cp^*SbCl_2 (2-2)

A solution of $SbCl_3$ (0.652 g, 2.86 mmol) in THF (20 mL) was added to a suspension of Cp*Li (0.408 g, 2.86 mmol) in THF (30 mL) at 0 °C. A deep red solution formed initially, this turned to a light yellow when the addition of $SbCl_3$ was complete. A white precipitate formed. The suspension was stirred at room temperature overnight. The solvent was removed *in vacuo* and the resulting yellow oil was extracted in CH_2Cl_2 (15 mL). The CH_2Cl_2 was removed *in vacuo.* This yielded a yellow solid (0.405 g, 1.23 mmol, 44 %). ^1H NMR (400 MHz, C_6D_6): δ ppm 1.69 (s, 15 H, Me-H) $^{13}C\{^1H\}$NMR (101 MHz, C_6D_6): δ ppm 10.6 (s, Me-C) 124.0 (s, Cp-C). Screening crystals from the a sample sublimed at 90 °C *in vacuo* yielded a unit cell which confirmed the identity as Cp^*SbCl_2.[466]

Synthesis of Cp^*SbF_2 (2-3)

To a suspension of SbF_3 (0.520 g, 2.90 mmol) in THF (15 mL) was added a suspension of Cp*Li (0.4067 g, 2.81 mmol) in THF (15 mL) at room temperature. On addition, a red solution formed which rapidly dissipated to give a light yellow solution and a white precipitate. The solution was stirred at room temperature overnight. The solvent was removed *in vacuo* and the resulting yellow oil was extracted in CH_2Cl_2 (15 mL). The CH_2Cl_2

was removed *in vacuo.* This yielded a yellow solid (0.362 g, 1.23 mmol, 44 %). ^{1}H NMR (400 MHz, CD_2Cl_2): δ ppm 2.03 (s, 30 H, Me-H) $^{13}C\{^{1}H\}$ NMR (101 MHz, C_6D_6): 10.3 (s, Me-C), 122.8 (s, Cp-C). ^{19}F NMR (376 MHz, CD_2Cl_2): δ ppm -60.56 (br s). Crystals suitable for SCXRD analysis were grown by sublimation at 90°C *in vacuo*. Elemental Analysis Found (Cal): C: 40.60% (40.72%) H: 5.06% (5.13%).

Synthesis of $[Cp^*_2Sb][B(C_6F_5)_4]$ (2-4)

A suspension of $[(Et_3Si)C_7H_8][B(C_6F_5)_4]$ (0.262 g, 0.29 mmol) in toluene (10 mL) was added dropwise to a solution of Cp^*_2SbCl (0.122 g, 0.29 mmol) in toluene (20 mL) at room temperature. A red oil formed immediately from the deep red solution. The oily suspension was stirred for 30 mins and then left to settle. The solution was decanted and hexane (10 mL) was added to precipitate an orange crystalline solid. The resulting solid was dried *in vacuo.* This gave an orange powder (0.1336 g, 0.12 mmol, 43%). ^{1}H NMR (400 MHz, CD_2Cl_2): δ ppm 2.18 (s, 15 H, Me-H). $^{13}C\{^{1}H\}$ NMR (101 MHz, CD_2Cl_2) δ ppm 10.2 (s, Cp-Me) 127.7 (s, Cp-C). ^{19}F NMR (376 MHz, CD_2Cl_2): δ ppm -167.31 (br t, J=17.34 Hz,) -163.46 (br t, J=20.23 Hz) -132.96 (s). Crystals suitable for XRD were grown by layering a CH_2Cl_2 solution with hexane. Elemental Analysis Found (Cal): C: 49.47% (49.33%) H: 2.74% (2.82%).

Synthesis of Cp^*_2SbOTf (2-5)

A suspension of AgOTf (0.027 g, 0.10 mmol) in CH_2Cl_2 (5 mL) was added to a solution of Cp^*_2SbCl (0.043 g, 0.10 mmol) in CH_2Cl_2 (5 mL) in the dark. The resulting suspension was stirred overnight then filtered to yield a red solution. Solvent was removed *in vacuo* to yield a red powder (0.030 g, 0.057 mmol, 57%). ^{1}H NMR (400 MHz, $CDCl_3$): δ ppm 2.21 (s, 30 H, Me-H). $^{13}C\{^{1}H\}$ NMR (101 MHz, $CDCl_3$) δ ppm 10.1 (s, 5 C, Me-C) 126.2 (s, C, Ar-C). The triflate carbon was not observed. ^{19}F NMR (376 MHz, $CDCl_3$): δ ppm -77.58 (s). Crystals suitable for XRD were grown by layering a CH_2Cl_2 solution with hexane. Elemental Analysis Found (Cal): C: 46.48 % (46.60%) H: 5.38% (5.58%).

Synthesis of $[Cp^*SbCl][B(C_6F_5)_4]$ (2-6)

A suspension of $[(Et_3Si)C_7H_8][B(C_6F_5)_4]$ (0.4000 g, 0.45 mmol) in toluene (30 mL) was added dropwise to a solution of Cp^*SbCl_2 (0.1470 g, 0.45 mmol) in toluene (30 mL) at room temperature. A red oil formed immediately. The oily suspension was stirred for 30 mins and then left to settle. The solution was decanted and the resulting oil was dried *in vacuo.* The resulting yellow solid was washed with hexane (3x5 mL) and dried *in vacuo.* This gave a yellow powder (0.1850 g, 0.17 mmol, 38 %). ^{1}H NMR (400 MHz, CD_2Cl_2): δ ppm 2.33 (s, 15 H, Me-H). $^{13}C\{^{1}H\}$ NMR (101 MHz, CD_2Cl_2): δ ppm 10.7 (s, Me-C) 131.3 (s, Cp-C). ^{19}F NMR (376 MHz, CD_2Cl_2): δ ppm -167.51 (br t, J=17.34 Hz) -163.68 (br t, J=20.23 Hz -133.03 (s).

Crystals suitable for XRD were grown by layering a CH_2Cl_2 solution with hexane. Elemental Analysis Found (Cal): C: 42.24 % (42.04%) H: 1.41 % (1.56 %).

Gutmann-Beckett Analysis of 2-6

A NMR tube was loaded with **2-6** (0.010 g, 0.01 mmol), Et_3PO (0.001 mg, 0.01 mmol) and CD_2Cl_2 (0.6 mL)**.** ^1H NMR (400 MHz, CD_2Cl_2) δ ppm 0.99 - 1.44 (m, CH_3-Et_3PO) 1.98 - 2.17 (m, CH_2 + Me-**2**) (Due to overlapping signals, integrals are not reported). ^{19}F NMR (376 MHz, CD_2Cl_2) δ ppm -167.71 (m), -163.63 (br t, *J*=20.23 Hz), -133.06 (br d, *J*=2.89 Hz). ^{31}P NMR (162 MHz, CD_2Cl_2) δ ppm 80.65 (br s). Layering the NMR solution with hexane produced a white powder which was not suitable for SCXRD analysis.

NMR Scale Synthesis of 2-6/Pyridine

A NMR tube was loaded with **2-6** (10 mg, 0.01 mmol), pyridine (2 mg, 0.02 mmol) and CD_2Cl_2 (0.6 mL), forming a clear solution**.** ^1H NMR (400 MHz, CD_2Cl_2) δ ppm 2.04 (s, 15 H, Me-H), 7.84 (br t, J=6.1 Hz, 2 H) 8.26 (br t, J=7.4 Hz, 1 H), 8.63 (br d, J=3.4 Hz, 2 H). ^{19}F NMR (376 MHz, CD_2Cl_2) δ ppm -167.41 (br t, J=17.3 Hz) -163.56 (br t, J=20.2 Hz) -133.01 (s).

Diels-Alder Dimerisation of 1,1-Diphenylethylene by 2-6

An NMR tube was loaded with **2** (5 mg, 0.005 mmol) in CD_2Cl_2 (0.075 mL) to which 1,1-diphenylethylene (16.8 mg, 0.082 mmol) in CD_2Cl_2 (0.075 mL) was added. A red colour formed instantly. The solution was stood for 2h. CD_2Cl_2 (0.5 mL) was added before obtaining NMR spectra. Relative integration of ^1H NMR signals arising from the product (δ_H=3.12 ppm) vs residual starting material (δ_H=4.47 ppm) gave a conversion of 86%.

Mukaiyama Aldol Addition of Methyl Trimethylsilyl Dimethylketene Acetal to Benzaldehyde

A NMR tube was loaded with **2-6** (0.005 g, 0.005 mmol), Methyl trimethylsilyl dimethylketene acetal (0.017 g, 0.1 mmol) and benzaldehyde (0.010 mg, 0.1 mmol) in CD_2Cl_2 (0.7 mL). The reaction solution turned orange after 5 minutes then purple over the course of 2 hours. Mesitylene (2.4 mg, 0.019 mmol) was added as an internal standard and NMR spectra were obtained. Yield by relative integration of mesitylene (2.26 ppm) vs product proton (4.89 ppm): 0.01 mmol, 14%.[467]

The reaction was repeated with the omission of **2-6** which yielded no reactivity.

Synthesis of [Cp*SbF][B(C_6F_5)$_4$]

A solution of Cp^*SbF_2 (0.1216 g, 0.29 mmol) in toluene (15 mL) was added dropwise to a suspension of [(Et_3Si)C_7H_8][B(C_6F_5)$_4$] (0.2620 g, 0.29 mmol) in toluene (15 mL) at -78°C. A deep yellow solution formed instantly. On warming to room temperature the reaction

solution yielded a dark yellow oil (crude $[Cp^*SbF][B(C_6F_5)_4]$) which was stirred at room temperature for 1 hour. ^{19}F NMR (400 MHz, $PhCCl_3/C_6D_6$): δ ppm -166.18 (t), -162.32 (t) and -131.72 (s) ($B(C_6F_5)_4$), 18.08 (s, Sb-F).

Decomposition of $[Cp^*SbF][B(C_6F_5)_4]$ in CD_2Cl_2

Crude $[Cp^*SbF][B(C_6F_5)_4]$ was washed with hexane (15 mL) and dissolved in CH_2Cl_2 (15 mL). The resulting black precipitate was removed by filtration through celite to give a yellow solution which was layered with hexane (15 mL). The resulting yellow crystalline solid was dried *in vacuo.* NMR and SCXRD from a sample from the bulk confirmed the identity as a mixture of **2-6** and $[Cp^*H_2][B(C_6F_5)_4]$**.**

Decomposition of $[Cp^*SbF][B(C_6F_5)_4]$ in $PhCCl_3$

Crude $[Cp^*SbF][B(C_6F_5)_4]$ was synthesised as above from Cp^*SbF_2 (0.028 mmol) and $[(Et_3Si)C_7H_8][B(C_6F_5)_4]$ (0.2620 g, 0.29 mmol) without purification except washing with toluene (3 x 5 mL). The crude oil was dissolved in $PhCCl_3$ (0.3 mL) to give a dark solution and stood for 2 hours. C_6D_6 (0.4 mL) was added. A small sample of this solution was removed and CD_2Cl_2 (0.5 mL) was added. Both solutions were then heated at 40°C for 96 hours with ^{19}F NMR spectra taken intermittently showing a diminishing Sb-F resonance at around 18 ppm and an increasing $PhCFCl_2$ resonance at around -53 ppm over this period. [463]

Decomposition of $[Cp^*SbF][B(C_6F_5)_4]$ in other Halocarbons

A solution of Cp^*SbF_2 (0.0247 g, 0.09 mmol) in C_6D_6 (1 mL) was added dropwise to a suspension of $[(Et_3Si)C_7H_8][B(C_6F_5)_4]$ (0.0755 g, 0.09 mmol) in C_6D_6 (1 mL) at -10°C. This yielded black oil and yellow solution. The solution was decanted and the residual yellow oily solid was divided into 6 parts. To each of these was added a halocarbon and then C_6D_6. NMR specta were obtained.

Ph_3CCl: ^1H NMR (400 MHz, C_6D_6) δ ppm 1.68 (s, 1 H), 6.94 - 7.05 (m, 3 H, Ph_3CCl), 7.33 - 7.43 (m, 2 H, Ph_3CCl). ^{19}F NMR (376 MHz, C_6D_6) δ ppm -166.53 (s, $B(C_6F_5)_4$), -162.29 (br t, J=20.86 Hz, $B(C_6F_5)_4$), -131.75 (br s, $B(C_6F_5)_4$), -125.54 (br s, Ph_3CF).

BnCl: ^{19}F NMR (376 MHz, C_6D_6) δ ppm -165.91 (br s, $B(C_6F_5)_4$), -161.72 (br t, J=20.86 Hz, $B(C_6F_5)_4$), -132.80 (m, $B(C_6F_5)_4$).

MeI: ^1H NMR (400 MHz, C_6D_6) δ ppm 1.20 (s, 1 H), 1.25 (s, 1 H), 1.44 (s, 208 H, MeI), 1.56 (s, 1 H), 1.59 (s, 1 H), 1.63 (s, 1 H), 2.12 (s, 1 H). ^{19}F NMR (376 MHz, C_6D_6) δ ppm -166.06 (br t, J=17.88 Hz, $B(C_6F_5)_4$),) -162.82 (m, $B(C_6F_5)_4$)), -134.70 (br s, minor), -131.88 (br s, $B(C_6F_5)_4$))

CDCl: ^{1}H NMR (400 MHz, C_6D_6) δ ppm 1.32 (s, 1 H), 1.55 (s, 1 H). ^{19}F NMR (376 MHz, C_6D_6) δ ppm -166.22 (s, $B(C_6F_5)_4$)), -162.33 (br t, J=20.86 Hz, $B(C_6F_5)_4$)), -131.95 (s, $B(C_6F_5)_4$)).

Synthesis of [Cp*SbF/IMes][$B(C_6F_5)_4$] (2-7)

Cp^*SbF_2 (0.030 g, 0.033 mmol) and IMes (0.009 g, 0.029 mmol) were mixed in toluene (10 mL) for 5 minutes to give a deep yellow solution. A suspension of [$(Et_3Si)C_7H_8$][$B(C_6F_5)_4$] (0.030 g, 0.33 mmol) in toluene (15 mL) was added to the reaction solution dropwise. A small amount of yellow oil formed. The solution was stirred at room temperature for 1 hour, then hexane (15 mL) was added to precipitate a yellow solid. The yellow solid was washed with hexane (3 x 15 mL), then dissolved in 1,2-DFB (15 mL) and layered with hexane (15 mL) to form yellow crystals which were dried *in vacuo* (0.020 g, 0.016 mmol, 55%). ^{1}H NMR (400 MHz, CD_2Cl_2) δ ppm: 2.12 (m, 33 H, Cp*+Ar-CH_3) 7.56 (d, J=1.37 Hz, 4 H, Ar-H) 8.22 - 8.27 (m, 2 H, IMes H). ^{19}F NMR (376 MHz, CD_2Cl_2) δ ppm -167.52 (br t, J=17.34 Hz) -163.67 (br t, J=20.23 Hz) -133.07 (m), 115.14(s) Elemental Analysis Found (Cal): C: 52.18% (52.45%), H 2.93% (3.12%), N 1.96% (2.22%).

Synthesis of $Cp^*Sb(OTf)_2$ (2-8)

TMSOTf (0.044 g, 0.2 mmol) in CH_2Cl_2 (5 mL) was added to a solution of Cp^*SbF_2 (0.030 g, 0.1 mmol) in CH_2Cl_2 (5 mL) which formed a deep red solution. The solution was stirred for 2 hours at room temperature then hexane (30 mL) was added to precipitate a pink powder. The solution was decanted and the powder was washed with hexane (3 x5 mL) then dried in vacuo to yield a pink powder (0.018 g, 0.03 mmol, 30%). ^{1}H NMR (400 MHz, $CDCl_3$) δ ppm 2.09 (s, 15 H) . ^{13}C{^{1}H} NMR (100 MHz, $CDCl_3$) δ ppm 10.4 (s, Cp*-Me) 124.5 (s, Cp*-C). ^{19}F NMR (376 MHz, $CDCl_3$) δ ppm -77.53 (s, v minor) -76.80 (s, CF_3). Due to the highly sensitive nature of **2-8**, microanalysis could not be obtained.

Attempted Synthesis of [Cp*Sb][$B(C_6F_5)_4]_2$

A solution of Cp^*SbF_2 (0.009 g, 0.03 mmol) in C_6D_6 (0.5 mL) was added dropwise to a suspension of [$(Et_3Si)C_7H_8$][$B(C_6F_5)_4$] (0.053 g, 0.06 mmol) in C_6D_6 (0.5 mL) to give a dark yellow oil and a yellow solution. The solution was decanted and CD_2Cl_2 (0.7mL) was added to the oil which partially solubilised it. 1,2-DFB (1 mL) was added to fully solubilise the oil and the resulting solution was layered with hexane (5 mL) to yield light yellow crystals of **2-2** and **2-2/2-3**.

Attempted Synthesis of Cp_2SbCl

Dicyclopentadiene was heated to 180^{o} C and fractionally distilled to yield monomeric cyclopentadiene (bp: 42^{o} C). 1.6M nBuLi in hexane (0.4 mL, 0.6 mmol) was added dropwise

to a solution of freshly cracked cyclopentadiene (0.03 mL, 0.60 mmol) in THF (40 mL) at -78 ^{o}C. A slight red colour formed on warming to RT. The solution was cooled to -15 ^{o}C and $SbCl_3$ (0.073 g, 0.30 mmol) in THF (10 mL) was added. A yellow solution formed which gradually formed a brown/black intractable oil at room temperature. Crystals of $SbCl_3$·THF were removed and identified by SCRXD.

Attempted Synthesis of [Cp*Sb][B(3,5-$(CF_3)_2C_6H_3)_4$]$_2$

Cp^*SbCl_2 (0.0439 g, 0.10 mmol) in DCM (5 mL) was added to AgBArF.MeCN (0.2086 g, 0.20 mmol) in DCM (5 mL). A white precipitate formed instantly. The reaction solution was stirred for 30 minutes then filtered through celite to give a red solution. This was then overlayered with n-hexane (20 mL) to give orange needle crystals which were identified as [Cp^*_2Sb][BArF] by SCXRD. The crystals were dried *in vacuo* (0.0954 g). ^{1}H NMR (400 MHz, CD_2Cl_2) δ ppm 2.12 (s, 5H), 2.25 (s, 5 H), 7.59 (m, 4 H, BArF) 7.74 (m, 8 H, BArF) ^{19}F NMR (376 MHz, CD_2Cl_2) δ ppm -62.78 (s, BArF)

Attempted Synthesis of Cp*(C_6F_5)SbCl

C_6F_5Br (0.1578 g, 0.60 mmol) was added dropwise to freshly activated Mg (1.000 g, 41.66 mmol) in Et_2O (30 mL) at 0°C which was then warmed to room temperature and stirred for 2 hours. The reaction solution was added through a canula filter to Cp^*SbCl_2 (0.200 g, 0.60 mmol) in Et_2O (10 mL) to 0°C which gave a deep yellow solution was some oil. The reaction solution was stirred overnight then reduced *in vacuo* to a yellow oily solid. NMR spectra were obtained. ^{1}H NMR (400 MHz, C_6D_6) δ ppm 0.97 (t, J=6.98 Hz, 1 H, coordinated Et_2O) 1.16 (s, 1 H) 1.46 (s, 1 H) 1.51 (s, 1 H) 1.57 (s, 1 H) 1.61 (s, 1 H) 1.67 (s, 1 H) 1.77 (s, 1 H) 3.38 (br m, 1 H, coordinated Et_2O).^{19}F NMR (376 MHz, C_6D_6) δ ppm -160.33 (m), -159.39 (dt, J=19.50, 9.03 Hz), -158.51 (br t, J=18.79 Hz), -150.94 (m), -149.97 (br t, J=20.23 Hz), -147.72 (br t, J=20.23 Hz), -121.35 (m), -120.04 (m), -117.63 (br d, J=14.45 Hz), -115.63 (br d, J=23.12 Hz), -115.59 - -114.99 (m).

The oil was extracted into toluene (20 mL), leaving a white residue and golden solution which was layered with n-hexane (20 mL) which formed colourless crystals which were identified as $MgCl_2$·Et_2O by SCXRD and a black intractable powder. The remaining solution was reduced to a yellow oil *in vacuo* and sublimed at 70°C to give yellow crystals of Cp^*SbI_2.

Attempted Synthesis of $Cp^*_2SbCl_3$

SO_2Cl_2 (0.0282 g, 0.21 mmol) was added dropwise to a solution of Cp^*SbCl_2 (0.0698 g, 0.16 mmol) in n-hexane (15 mL) at room temperature. The reaction solution instantly turned a slight blue/green colour and turned deep purple over the course of 30 minutes. The reaction solution was stirred at room temperature overnight then dried *in vacuo* to give a

purple oil. ^{1}H NMR spectroscopy suggested the formation of multiple poorly soluble products with ^{1}H NMR signals between 0.50 ppm and 1.75 ppm.

Attempted Synthesis of Cp*$SbCl_4$ by Oxidation

SO_2Cl_2 (0.0287 g, 0.21 mmol) was added dropwise to a solution of Cp*$SbCl_2$ (0.0510 g, 0.16 mmol) in 4:1 DCM/n-hexane (15 mL) at room temperature. The reaction solution instantly turned a slight green colour and turned deep purple over the course of 15 minutes. The reaction solution was stirred at room temperature overnight then dried *in vacuo* to give a purple oil. ^{1}H NMR spectroscopy suggested the formation of multiple poorly soluble products with ^{1}H NMR signals between 0.05 ppm and 1.90 ppm.

Attempted Synthesis of Cp*$SbCl_4$ by Salt Metathesis

Cp*Li (0.0142 g, 0.10 mmol) suspended in DCM (5 mL) was added dropwise to $SbCl_5$ (0.0338 g, 0.11 mmol) in DCM (5 mL) giving a purple-coloured suspension instantly. The reaction solution was stirred at room temperature overnight then dried *in vacuo* to give a purple oil. ^{1}H NMR spectroscopy suggested the formation of multiple poorly soluble products similar to the above reaction. The oil was extracted into n-hexane (3 mL), filtered through celite and stored at -18°C to yield an intractable black solid (0.010 g).

Computational Methods

All calculations were performed using Gaussian 09 Revision E0.01.[355] All geometries were optimised in vacuum without imposing symmetry constraints at the M062X/def2-SVP level of theory with the GD3 empirical dispersion correction.[261,356,357] Counteranions were omitted from all calculations. Subsequent analytical IR frequency calculations on optimised geometries were utilised to confirm the nature of stationary points (zero and exactly one imaginary mode for minima and transition states, respectively). Moreover, within the ideal gas/rigid rotor/harmonic approximation (RRHO) these calculations also provided thermal and entropic corrections to the Gibbs Free Energy at 1 atm and 298.15 K. Electronic energies were obtained from single-point calculations at the M062X-D3/def2-TZVPP level of theory including a polarisable continuum model (SMD) to account for solvent effects.[358] In the absence of parameters for $PhCCl_3$, the chosen dielectric constant (ε = 6.72) corresponded to α-chlorotoluene. The Kohn-Sham orbitals were visualised using Chemcraft.[359] The analysis of molecular orbitals (MOs) in terms of fragment contributions were carried out using the AOMix program.[468,469] FIAs were calculated following a reported procedure from the literature.[155] Single point energies for FIA were calculated in the gas phase and including a polarisable continuum model (dichloromethane) using M062X-D3/aug-cc-PTZ-pp (for Sb) and 6-331G** (for C, H, Cl and F). [360,361] The FIA was calculated

using the enthalpy of a free fluoride calculated at the same level of theory (-99.840107 E_h (gas phase) or -99.963301 E_h (dichloromethane)).

Assigning Hapticity

Assignment of hapticity was based on ring slippage. The carbon with the shortest Sb-C bond length was assigned as C_α. The ring slippage was considered as the distance from the centroid to intersection of a vector between the Cp* ring and Sb, normal to the centroid-C_α distance, and the centroid-C_α vector (A). Using the fact that the angles of a triangle sum to 180^o, the centroid-Sb-A angle was calculated. The ring slippage was calculated using ring slippage = sin(∠A-Sb-centroid)*Sb-centroid. Hapcticity was then assigned as per ref [377].

4. Deployment of Organoantimony Compounds in Frustrated Lewis Pairs

4.1. Introduction

4.1.1 C-X Bond activation by FLPs

Frustrated Lewis pairs (FLPs) are compounds or mixtures containing both a Lewis acidic and basic component which for steric reasons can not form an adduct.[170] A general description of FLPs in included in the general introduction (1.4.3. Frustrated Lewis Pairs (FLP) for Small Molecule Activation).

The deployment of main group Lewis acids for the activation of C-F bonds has been thoroughly developed since the turn of the century,[470,471] however the use of FLPs for C-F activation is only a relatively recent development. The FLP approach was first used to activate a series of alkyl fluorides with $B(C_6F_5)_3$ and P^tBu_3 to yield a phosphonium salt counterbalanced by $[FB(C_6F_5)_3]^-$ (Scheme 4.1).[472] Divergent reactivity occurred with fluorocyclohexane which gave dehydrofluorination reactivity, yielding cyclohexene. Utilising the hydridoborate salt, $[P^tBu_3H][HB(C_6F_5)_3]$, in place of P^tBu_3 yielded the alkane. The mechanism of this C-F bond activation was not investigated however the fact that these alkyl fluorides were reduced by Et_3SiH with catalytic amounts of $B(C_6F_5)_3$ without any base suggests that the borane abstracts the fluoride before the nucleophilic attack of the phosphine as opposed to a synchronous mechanism.

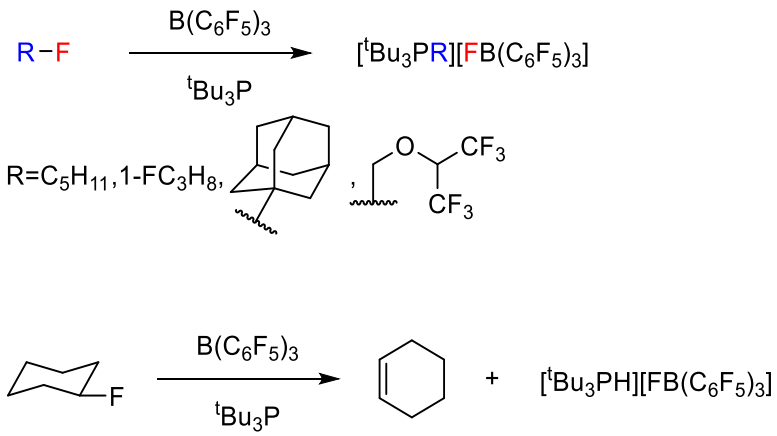

Scheme 4.1. Activation of alkyl fluorides by $^tBu_3P/B(C_6F_5)_3$.[472]

FLPs are typically used when selective activation of $-CF_3$ groups is required; this is often synthetically challenging,[473–476] due to the fact that any substituents other than fluorine will be more activating.[477] The FLP approach was envisioned to circumvent this by acting through a base stabilised cationic intermediate which would not be amenable to further C-F activation.[478] This approach was utilised to selectively convert gem-difluoromethyl groups to fluoroalkenes *via* the Wittig reaction of the intermediate phosphonium salt (Scheme 4.2).[478]

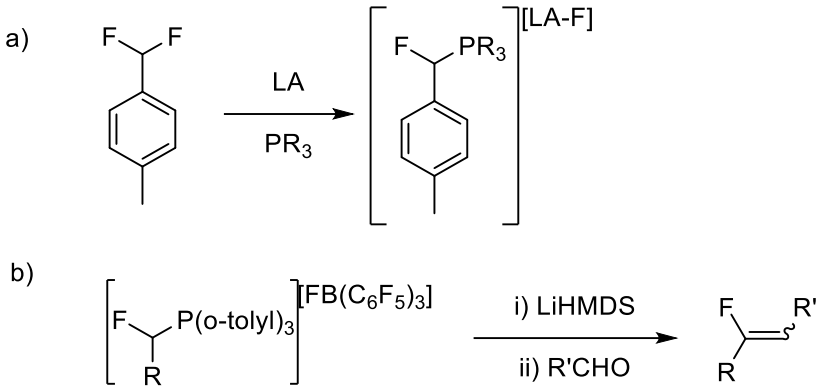

Scheme 4.2. a) formation of phosphonium salt from gem-difluoromethylarene. LA = Lewis acid. b) Wittig reaction of phosphonium salt to form fluoroalkenes. LiHMDS = Lithium bis(trimethylsilyl)amide

This phosphonium intermediate has also been used for more diverse reactivity; di- and tri-fluoromethylbenzene have both been mono-selectively substituted with a range of nucleophiles.[479,480] Two tri(imine) phosphorus dications, ([(R=N)P][X]) (X = $B(C_6F_5)_4$, BAr^F), activate *a,a,a*-trifluorotoluene derivatives both inter- and intra-molecularly depending on the presence of an external base (Scheme 4.3).[481]

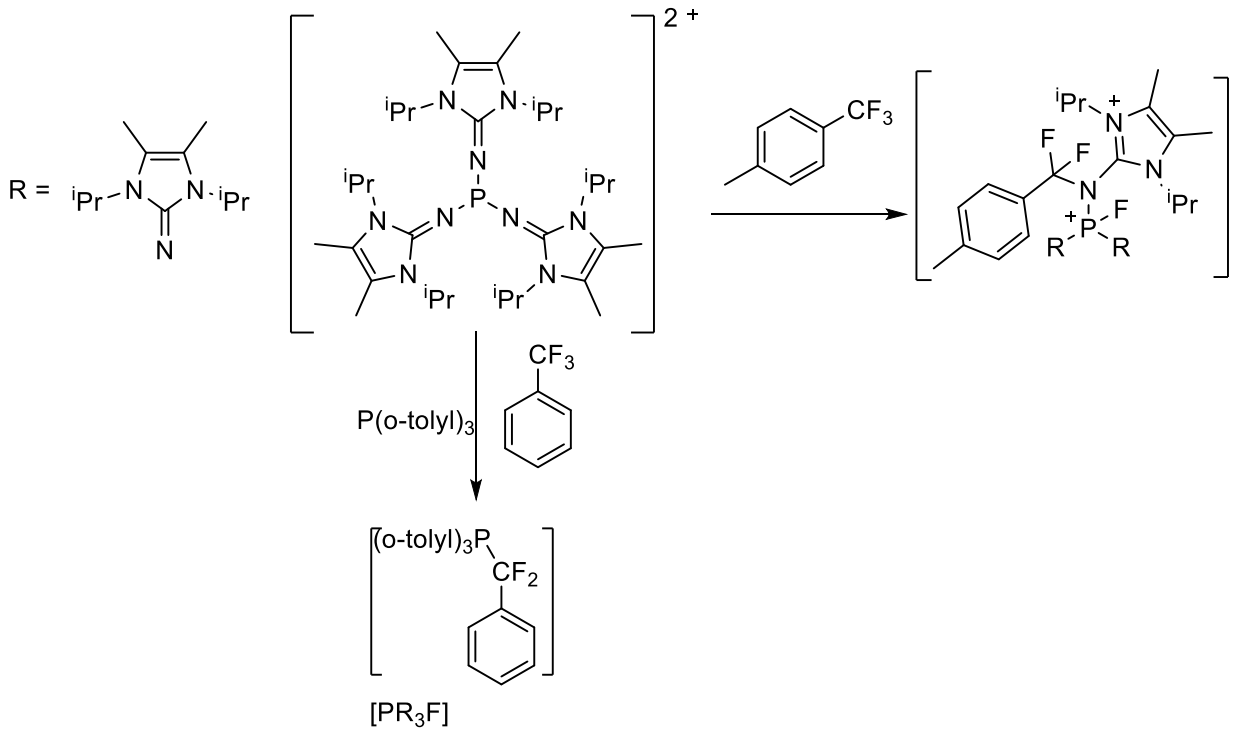

Scheme 4.3. Activation of trifluorotoluene by a tri(imine) phosphorus dication which is intermolecular in the presence of phosphine and intramolecular without any external base, with an imine nitrogen acting as a base.

The salt $[C_6H_4(1\text{-}PPh_2)(2\text{-}SiPh_2)][B(C_6F_5)_4]$, contains both an acidic silylium and basic phosphine which do interact but are frustrated by the virtue of forming a strained four membered ring, is able to mono-hydrodefluorinate $PhCF_3$, $PhCF_2H$ and Ph_2CF_2 (Scheme 4.4).[482] DFT calculations suggest that the acidic silylium initially abstracts the fluoride from Ph_3CF_3 yielding a carbocation which rapidly reacts with the basic phosphine.

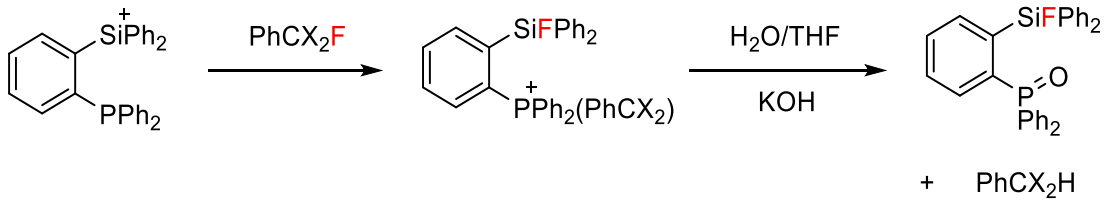

Scheme 4.4. Hydrodefluorination of benzyl fluoride derivatives. X= H or F.[482]

A thorough computational investigation elucidated a cooperative mechanism for the activation of 4-Me(C_6H_4R) (R = CF_3, CF_2H, CFH_2) by $B(C_6F_5)_3$/2,4,6-triphenylpyridine (Scheme 4.5).[483] The elucidated mechanism is not concerted; initially the borane abstracts the fluoride with significant stabilising non-covalent interactions from the base. The reaction proceeds through an intermediate F-C···N 3c-2e bond, which is a rare example of a hypervalent pentacoordinate carbon.

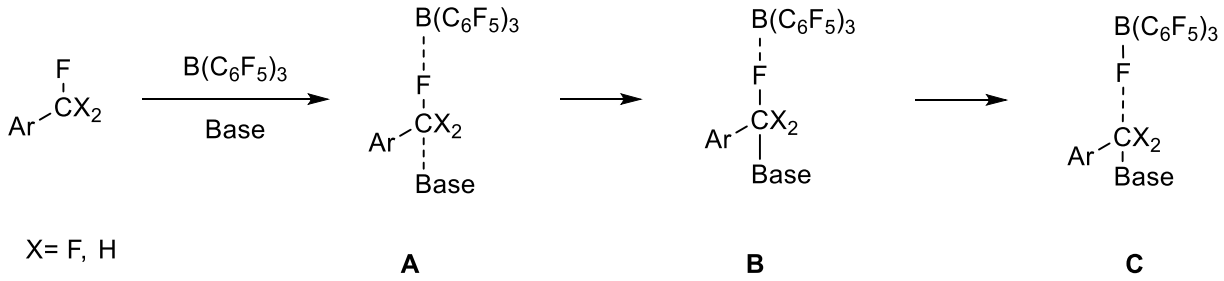

Scheme 4.5. Mechanism for the activation of 4-Me(C_6H_4R) (R = CF_3, CF_2H, CFH_2) by $B(C_6F_5)_3$/2,4,6-triphenylpyridine. Initially, a reactive complex (**A**) form, which then affords the neutral intermediate **B** which has a hypervalent pentacoordinate carbon as it is simultaneously bonded to the releasing fluoride and base. An intramolecular S_N2 yields the observed product (**C**).

While much of the focus has been on the activation of C-F bonds, due to a stronger bond enthalpy and the prevalence of organofluorines in pharmaceuticals and compounds of environmental concern, there have been some reports of the activation of C-X bonds (X = Cl, Br) by FLP systems. The geminal FLP $^tBu_2PCH_2BAr^F_2$ (Ar^F = 3,5-$(CF_3)_2C_6H_3$) activates a range of substrates, including CX_4 (X = Cl, Br).[484] In Et_2O the product from heterolytic C-X bond cleavage, a zwitterionic geminal phosphonium borate was obtained (Scheme 4.6). In

less polar solvents the formal addition of X_2 occurs; interestingly the addition of X_2 to $^tBu_2PCH_2BAr^F{}_2$ does not yield any reactivity.

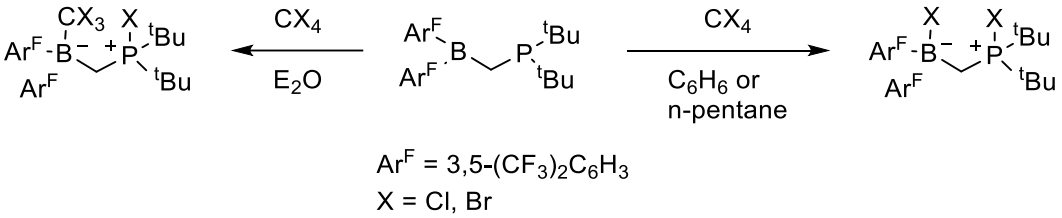

Scheme 4.6. Reaction of $^tBu_2PCH_2BAr^F{}_2$ with CX_4 in E_2O (left) or C_6H_6/n-pentane (right). [484]

4.1.2 Aims and Objectives

The aim of this body of work is to apply the design principles of frustrated Lewis pairs to organoantimony compounds to yield an 'all antimony' FLP or a FLP with an antimony based acid or base component due to the potential for different reactivity. Given the larger size of Sb and its higher metallic character, Sb is likely to have a higher halide affinity than Phosphorus analogues, making it a useful target for FLP chemistry. This will involve screening a series of stibonium salts/stibine pairs to determine if these display frustrated reactivity, this may involve establishing new synthetic protocols. These FLPs will be screened for useful reactivity, in particular haloalkane bond activation given the higher fluoride affinity of antimony compounds in comparison to those of known FLPs. To date, antimony compounds have not been used in FLPs and there is even a report of a failed project to utilise antimony(V) cations for FLP type activation of C-F bonds.[485]

The specific objectives of this body of work are:

a) Screening a series of stibonium/stibine pairs to establish frustration between them and ideally elucidate a set of design principles to yield this frustration. The stibonium salts of the form $[Ar_3SbCl][B(C_6F_5)_4]$ (**1-14** to **1-18,** 2. Interrelationship between Structure and Lewis Acidity in Triarylchlorostibonium Salts) and trialkylstibines will be screened.
b) Novel stibonium salts of the form $[Ar_4Sb][B(C_6F_5)_4]$ will be targeted and screened for reactivity with stibines.
c) Establishing synthetic protocols for the components of these FLPs if not already known.
d) Establishing Lewis acidity of any novel stibonium salts by coordination of Lewis bases and activity in the dimerisation of 1,1-diphenylethylene.

e) Exploring the potential for C-X bond activation by these FLPs, benzyl chloride will be used initially as it is a relatively labile C-Cl bond.

4.2. Results and Discussion

4.2.1. Frustrated and Non-Frustrated Sb(V)/Sb(III) Pairs

As part of this work, an intermolecular frustrated Lewis pair consisting of a Sb(V) Lewis acid and Sb(III) Lewis base was targeted. Combining $^{t}Bu_3Sb$ and $B(C_6F_5)_3$ in $CDCl_3$ yielded a complex mixture of products, none of which could be identified. This could potentially be attributed to substituent scrambling, which has been observed between BBr_3 and Ph_3Sb.[486]

$^{t}Bu_3Sb$ and $[(3,5\text{-}F_2C_6H_3)_3SbCl][B(C_6F_5)_4]$ (**1-17**), selected as it was a moderately Lewis acidic triarylchlorostibonium salt, yielded the formation of a black precipitate and a yellow solution on mixing of these two compounds in CD_2Cl_2. Multiple products formed, one of which was identified as $(3,5\text{-}F_2C_6H_3)_3Sb$ by NMR; no components were identified by SCXRD. This suggests that the main reaction was the reduction of the triarylchlorostibonium salt by $^{t}Bu_3Sb$, yielding $[^{t}Bu_3SbCl][B(C_6F_5)_4]$; thermodynamically this can be expected given the greater electron donating power of the ^{t}Bu groups which would be more readily able to stabilise the Sb(V) cation. This is reminiscent of the reactivity of $Ph_3Sb(OTf)_2$ with two equivalents of PMe_3, which yields the reduced Ph_3Sb.[487]

To circumvent this, $[(3,5\text{-}F_2C_6H_3)_4Sb][B(C_6F_5)_4]$ was targeted with anticipation that the tetraarylstibonium centre would be more sterically hindered and the lack of a chloride would create a sufficient kinetic barrier to reduction with trialkylstibines. Based on a reported synthetic procedure for $[(C_6F_5)_4Sb][B(C_6F_5)_4]$,[58] $[(3,5\text{-}F_2C_6H_3)_4Sb][B(C_6F_5)_4]$ (**3-2**) was synthesised by halide abstraction from $(3,5\text{-}F_2C_6H_3)_4SbCl$ (**3-1**), which itself was synthesised from $SbCl_5$ with 4 equivalents of $3,5\text{-}F_2C_6H_3Li$ (Scheme 4.7). The former reaction gave **3-2** in 70% yield and the latter gave **3-1** in 18% yield, which is consistent with similar reactions reported in the literature.[58,59] One important point of the synthesis of **3-1** is that the highly exothermic addition of the solution of $SbCl_5$ to ethereal $3,5\text{-}F_2C_6H_3Li$ must be done is a highly controlled and dropwise manner, otherwise $(3,5\text{-}F_2C_6H_3)_3SbCl_2$ is obtained instead.

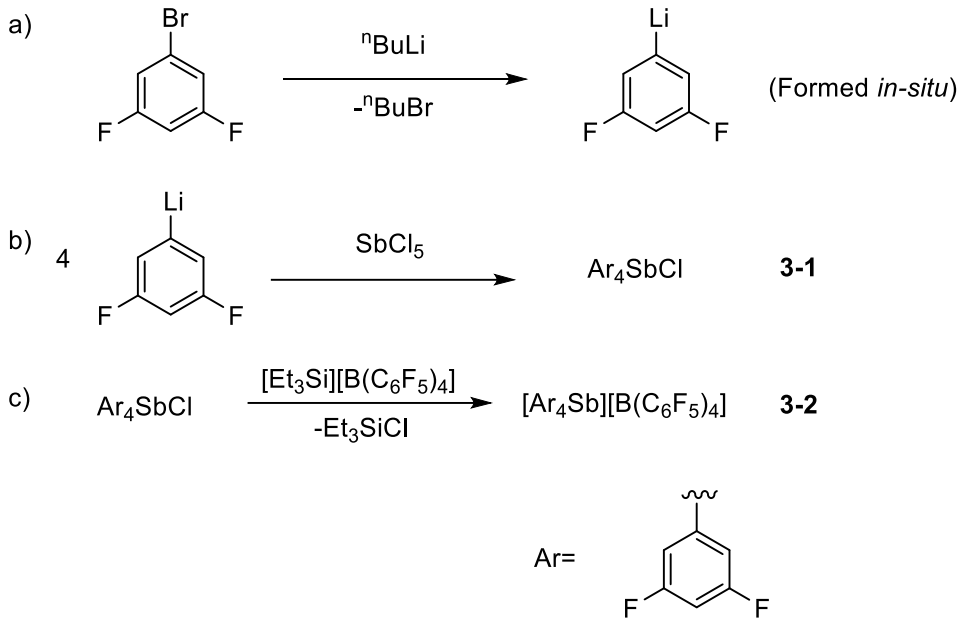

Scheme 4.7. a) Synthesis of ArLi. Conditions: Et_2O, -78°C, 1 hour. ArLi was not isolated. b) Synthesis of Ar_4SbCl. Conditions: Et_2O, -78°C→ RT, 16 hour. c) Synthesis of $[Ar_4Sb][B(C_6F_5)_4]$. Conditions: toluene, 1 hour.

Both **3-1** and **3-2** were structurally characterised by SCXRD and have the expected structures (Figure 4.1, Figure 4.2). The solid state structure of **3-1** has a trigonal bipyramidal geometry with an apical chloride. The ^{1}H, $^{13}C\{^{1}H\}$ and ^{19}F NMR spectra of **3-1** suggest a single aryl environment in the solution. The Sb-Cl bond length (2.5777(7) Å) is somewhat longer than that in $(3,5\text{-}F_2C_6H_3)_3SbCl_2$ (**1-10**) (2.4555(4) Å). The Sb-C bond lengths in **3-1** (2.115(2) -2.136(2) Å for C_{eq} and 2.169(2) Å for C_{ax}) are comparable to that in **1-10** (2.1089(18) - 2.128(3) Å). Compound **3-2** has a tetrahedral Sb centre (τ_4=0.96) in the solid state.[348] The Sb-C bond lengths in **3-2** (2.088(7) - 2.096(7) Å) are comparable to that in $[(3,5\text{-}F_2C_6H_3)_3SbCl][B(C_6F_5)_4]$ (**1-17**) (2.086(6) – 2.107(6) Å).

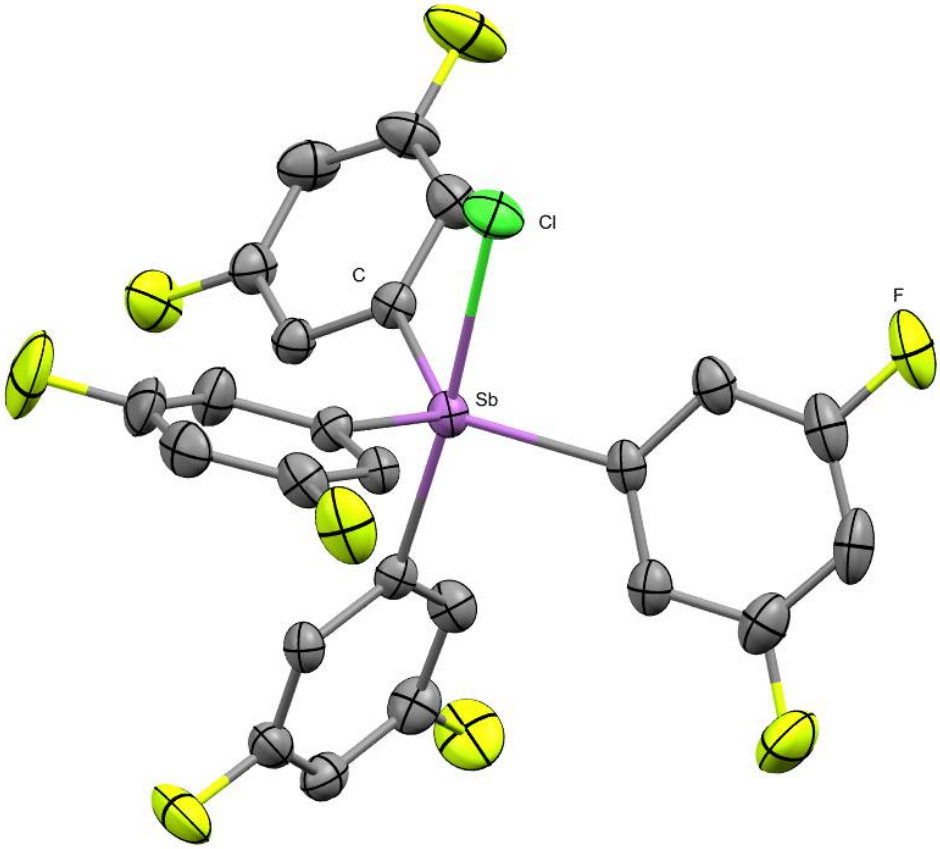

Figure 4.1 Solid state structure of $(3,5\text{-}F_2C_6H_3)_4SbCl$ (**3-1**). Ellipsoids shown at 50% probability. Hydrogen atoms have been omitted.

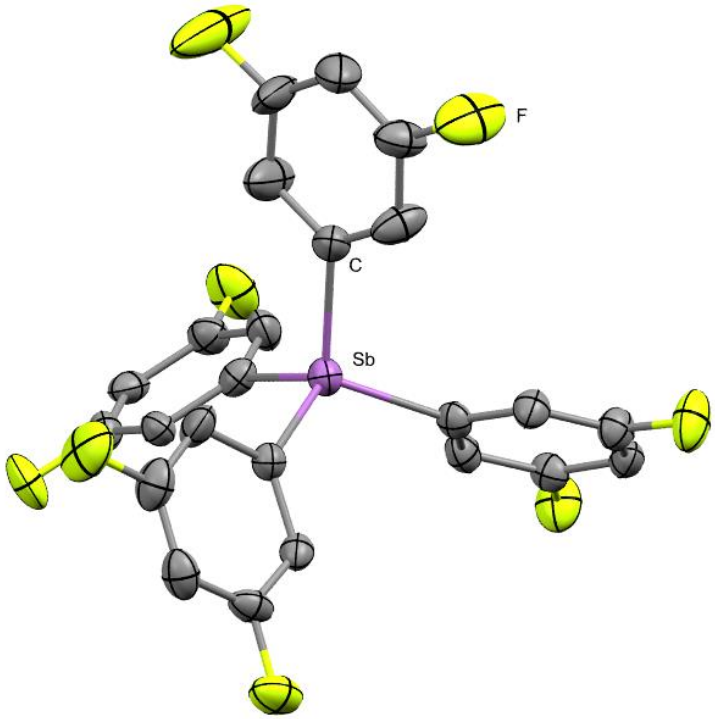

Figure 4.2. Solid state structure of $[(3,5\text{-}F_2C_6H_3)_4Sb][B(C_6F_5)_4]$ (**3-2**). Ellipsoids shown at 50% probability. Hydrogen atoms and borate counteranion have been omitted.

The Lewis acidic properties of $[(3,5\text{-}F_2C_6H_3)_4Sb][B(C_6F_5)_4]$ (**3-2**) were experimentally assessed. Compound **3-2** was assessed *via* the Gutmann-Beckett method which gave a single Phosphorus environment in the $^{31}P\{H\}$ NMR spectrum at 67.3 ppm (Scheme 4.8 a). In comparison, free Et_3PO and $B(C_6F_5)_3{\cdot}OPEt_3$ gave $^{31}P\{^1H\}$ NMR spectroscopy signals at 42 ppm and approximately 77 ppm respectively.[225] The Lewis acidity was also assessed *via* their catalytic activity for the dimerisation of 1,1-diphenylethylene, yielding 9% and 0% of the dimerised product (1-methyl-1,3,3-triphenyl-2,3-dihydro-1H-indene) after 2 hours with 5% catalyst loading in CD_2Cl_2 and CD_3CN respectively (Scheme 4.8 c). The ^{19}F NMR shift of **3-2** in CD_3CN is similar to **3-1**, suggesting coordination of CD_3CN to the Sb centre which would give a similar chemical environment to **3-1**. Given the low activity of **3-2** in the dimerisation of 1,1-diphenylethylene, even in CD_2Cl_2, and the relatively small acceptor number, according to the Gutmann-Beckett method (see 1.4.1 Experimental Methods of Ranking Lewis Acidity),[58,141,488,489] **3-2** can be considered to be a comparatively poor Lewis acid. However, mixing **3-2** with Ph_3CCl in CD_2Cl_2 does yield **3-1** (Scheme 4.8 b).

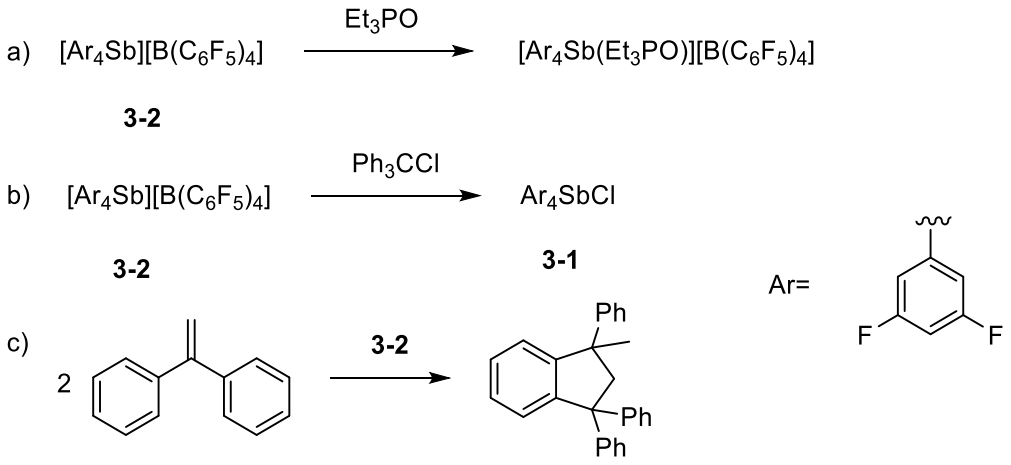

Scheme 4.8. Reactivity of **3-2**. a) Gutmann-Beckett method. b) Formation of **3-1** on reaction of labile chloride anions. c) Friedel-Crafts dimerisation of 1,1-diphenylethylene to 1-methyl-1,3,3-triphenyl-2,3-dihydro-1H-indene.

Mixing a solution of **3-2** with either Et_3Sb, $^tBu_3Sb$, Bn_3Sb or Mes_3Sb in CD_2Cl_2 yielded NMR spectra which were equivalent to the sum of the two components, revealing no reactivity between the stibines and **3-2** (Scheme 4.9). However, the addition of Et_3PO to a mixture of $^tBu_3Sb$ and **3-2** in CD_2Cl_2 did give a single $^{31}P\{^1H\}$ NMR spectroscopy signal at 64.9 ppm, which was slightly downfield from the equivalent signal obtained with a mixture of **3-2** and Et_3PO (67.33 ppm) (see 1.4.1 Experimental Methods of Ranking Lewis Acidity). This suggests that the addition of $^tBu_3Sb$ might slightly reduce the Lewis acidity of **3-2**,

potentially *via* the formation of an encounter complex, however the difference is relatively minor.

Scheme 4.9. **3-2** and R_3Sb do not form a Lewis acid/base adduct.

It is prudent to be cautious when using the term frustrated Lewis pair (FLP) to describe these mixtures; no stibine/stibonium Lewis adducts have either been observed as part of this work or previously in the literature. The observation that Et_3Sb does not form an adduct with PF_5, whereas PPh_3, PMe_3 and $AsEt_3$ do, gives credence the rationale that the absence of reactivity between **3-2** and these stibines is at least somewhat due to electronic effects instead of steric effects which most FLP systems are attributed to.[490] However, given that both **3-2** and the trialkylstibines have experimentally observed Lewis acidity and basicity respectively, the use of the term frustrated Lewis pairs can still be justified.[486] A mixture of **3-2** and Et_3Sb formed $[(3,5\text{-}F_2C_6H_3)_4SbOSbEt_3][B(C_6F_5)_4]$, as identified by SCXRD, on exposure to oxygen (Figure 4.3).

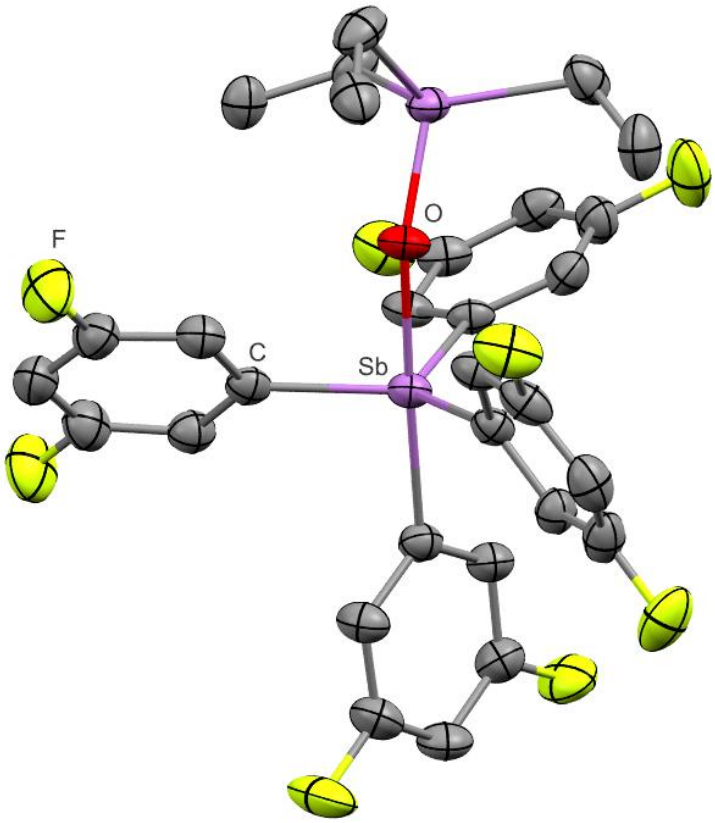

Figure 4.3. Solid state structure of $[(3,5\text{-}F_2C_6H_3)_4SbOSbEt_3][B(C_6F_5)_4]$. Ellipsoids shown at 50% probability. Hydrogen atoms and borate counteranion have been omitted.

The Et_3Sb-O and Ar_4Sb-O bond lengths are 1.871(1) and 2.123(3) respectively, suggesting that this can be assigned as a stibonium with coordinated stibine oxide ($Et_3Sb{=}O{\rightarrow}Sb(3,5\text{-}F_2C_6H_3)_4$). Monomeric stibine oxides are extremely rare;[491] two similar complexes have been reported in the literature, $Ph_3SbO\text{-}B(C_6F_5)_3$ and 1-(Ph_3SbO),8-($Ph_3Sb(O_2C_6Cl_4)$)$C_{12}H_6$ (Figure 4.4).[492,493]

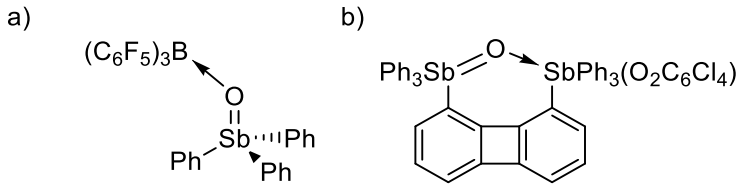

Figure 4.4. Structure of a) $Ph_3SbO\text{-}B(C_6F_5)_3$ and b) 1-(Ph_3SbO),8-($Ph_3Sb(O_2C_6Cl_4)$)$C_{12}H_6$.

4.2.2. Activation of C-Cl Bonds by Frustrated Sb(V)/Sb(III) Pairs

With several Sb(III)/Sb(V) 'FLP' systems in hand, their potential C-Cl bond activation was probed. $[(3,5\text{-}F_2C_6H_3)_4Sb][B(C_6F_5)_4]$ (**3-2** ,1 eq), $^tBu_3Sb$ (2eq) and benzyl chloride (6 eq) were mixed and heated at 40°C for 4 hours, yielding a new ^{t}Bu environment in the ^{1}H NMR spectrum and a single Ar-F environment in the ^{19}F NMR spectrum with matched neither **3-1**

or **3-2**. The tube was stood at room temperature for a further 92 hours, at which point (3,5-$F_2C_6H_3)_4SbCl$ (**3-1**) has formed and **3-2** was completely consumed. Crystals of $[^tBu_3BnSb][B(C_6F_5)_4]$ were obtained by slowly evaporating the reaction solution (Figure 4.5, Scheme 4.10).

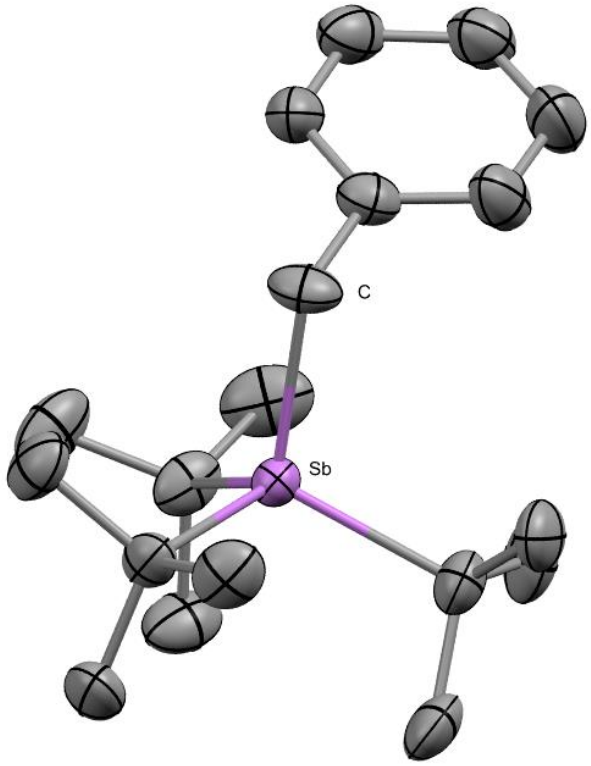

Figure 4.5. Solid state structure of $[^tBu_3BnSb][B(C_6F_5)_4]$. Ellipsoids shown at 50% probability. Hydrogen atoms and borate counteranions have been omitted. Two molecules are present in the asymmetric unit, only one is shown.

The Sb-C_{Bn} bond lengths are 2.150(4)/ 2.154(5) Å which is comparable to the same parameter in $[Bn_4Sb][[B(3,5\text{-}(CF_3)_2C_6H_3)_4]$ (2.130(4)-2.141(4) Å).[494] This reactivity was not observed under the same conditions in the absence of **3-2**, discounting the possibility that $^tBu_3Sb$ is initially oxidised by the BnCl to form $^tBu_3BnSbCl$. Reactivity is not observed in the absence of $^tBu_3Sb$, discounting a route where BnCl forms a benzyl cation which then oxidises the $^tBu_3Sb$ to $[^tBu_3BnSb]^+$. This suggests that this reactivity is mediated by a cooperative mechanism, which is consistent with other similar systems (see 4.1.1 C-X Bond activation by FLPs).[483] $^tBu_3Sb$ is thermally unstable and extensive decomposition was noted under the reaction conditions by the formation of multiple products in the ^1H NMR spectrum of a CD_2Cl_2 solution of $^tBu_3Sb$; the thermal instability of $^tBu_3Sb$ has been noted in the literature.[107] While **3-2** does not react with $^tBu_3Sb$, it does react with the unidentified

decomposition products as adding **3-2** to a solution of $^{t}Bu_3Sb$ which has been heated instantly yields reactivity by NMR spectroscopy. This renders it impossible to attribute this reactivity to just **3-2**, $^{t}Bu_3Sb$ and BnCl without invoking the possibility of decomposition products being involved in the formation of $[^{t}Bu_3BnSb][B(C_6F_5)_4]$ and $(3,5\text{-}F_2C_6H_3)_4SbCl_2$ (**3-1**). To circumvent this, this reactivity was probed with the more stable Et_3Sb and Mes_3Sb in the place of $^{t}Bu_3Sb$, however this yielded no reactivity. $^{t}Bu_3Sb$/**3-2** did not activate $PhCF_3$ under the same conditions according to NMR spectroscopy.

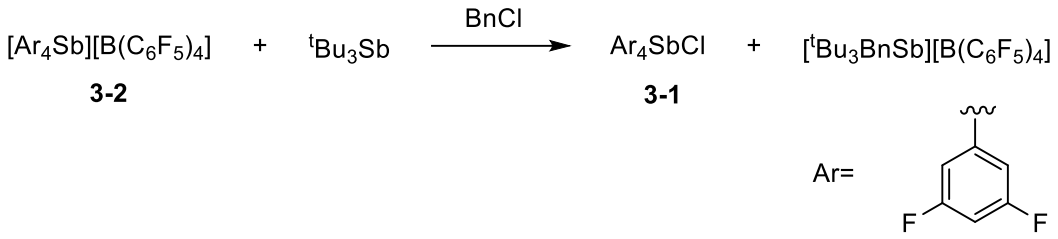

Scheme 4.10. **3-2** activate the C-Cl bond in benzyl chloride. Conditions: DCM, 4 hours, 40°C

4.2.3. 'One pot' Oxidation of Tribenzylstibine to Tetrabenzylstibonium Salts

As part of this work, a method for the direct formation of a tetraalkylstibonium salt ($[R_4Sb]^+$) from the respective stibine (R_3Sb) was targeted. A tetraalkylstibonium salt was targeted as opposed to a tetraarylstibonium salt as the oxidation of trialkylstibines is more facile. For this work, tetrabenzylstibonium salts ($[Bn_4Sb]^+$) were targeted as the tetrakis(3,5-bis(trifluoromethyl)phenyl)borate (BArF) salt has already been characterised as part of previous work in the group and the starting stibine, trisbenzylstibine (Bn_3Sb) is relatively easy to handle in comparison to other trialkylstibines.[495]

$[Bn_4Sb][BClF_3]$ was targeted by heating Bn_3Sb with BnCl and $BF_3{\cdot}OEt_2$ at 90°C, these reaction conditions were based on the Friedel -Crafts alkylation by BnCl.[496] Ph_4SbBr has been synthesised from Ph_3Sb and PhBr with catalytic amounts of $AlCl_3$.[57] This yielded a small amount of white powder which was determined to consist mainly of $[Bn_4Sb][BF_4]$ (**3-3**) but also traces of $[Bn_2Sb(Bn_3Sb)][BF_4]$ which was structurally characterised (Figure 4.6). $[Bn_4Sb][BF_4]$ (**3-3**) was not isolated from the reaction mixture but spectroscopically identified and compared to an independently synthesised sample. $[Bn_2Sb(Bn_3Sb)][BF_4]$ could be assigned as either a stibinostibonium salt (Sb(I) substituted Sb(V) cation) or stibine coordinated stibenium (neutral Sb(III) coordinating to Sb(III) cation). A related compound, $[Me_2Sb(Me_3Sb)]^+$, has been reported as both a $[GaCl_4]^-$ and $[(Me_3SbBr)_2]^-$ salt; the former is described as a stibinostibonium salt.[85,86] The Sb-Sb bond length (2.855(1) Å) is within the range expected for covalent Sb-Sb single bonds ($\sum_{CR}$=2.78(10) Å). While the organometallic

bonds are consistent for a Sb(V) cation for the Bn_3Sb fragment (2.135-2.162 Å) and for a neutral Sb(III) species for the Bn_2Sb fragment (2.177-2.183 Å), no comparisons for a Bn_3Sb fragment acting as a Lewis donor exist. There is a short contact between the stibenium fragment and a borate fluoride (2.9019(3) Å).

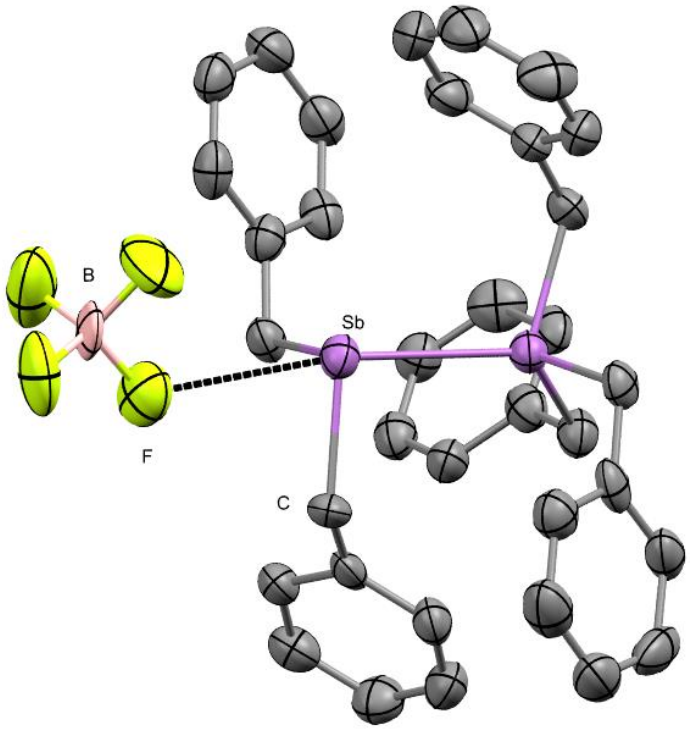

Figure 4.6. Solid state structure of $[Bn_2Sb(Bn_3Sb)][BF_4]$. Ellipsoids shown at 50% probability. Hydrogen atoms have been omitted. Sb-F short contact is shown as a black dotted bond.

A natural population analysis (NPA) yielded a natural charge of 1.50 and 0.970 for Sb_{Bn3Sb} and Sb_{Bn2Sb} respectively. The Wiberg bond index (WBI) for the Sb-Sb bond is 0.8129. Similarly, the Mayer bond index (MBI) is 0.80297. The Mayer valence is 4.06813 and 2.97519 for Sb_{Bn3Sb} and Sb_{Bn2Sb} respectively. The fuzzy atom bond order (FBO) is 1.07211. Natural bond orbital (NBO) analysis shows that the primary bonding interaction consists of a polarised covalent bond with 64% contribution from $Sb_{Bn3Sb.}$ The bond consists of an overlapping $sp_{2.6}$ orbital on Sb_{Bn3Sb} and a p orbital on Sb_{Bn2Sb}. Taken together, this suggests that the stibinostibonuim is the most appropriate description.

The mechanism by which $[Bn_2Sb(Bn_3Sb)][BF_4]$ formed was interrogated. To probe if this was mediated by the Lewis acidity of $BF_3{\cdot}OEt_2$, Bn_3Sb was reacted with trityl tetrafluoroborate ($[Ph_3C][BF_4]$) to check if it would yield $[Bn_2Sb(Bn_3Sb)][BF_4]$. $BF_3{\cdot}OEt_2$ is known to abstract a phenyl group from Ph_4MeSb to yield $[Ph_3MeSb][BF_4]$.[497] This yielded $[Bn_3(Ph_3C)Sb][BF_4]$ (**3-4**), suggesting that the formation of $[Bn_2Sb(Bn_3Sb)][BF_4]$ is not mediated by this pathway

(Figure 4.7, Scheme 1.12). There are no intermolecular interactions between the Sb atom and the BF_4^- anion. This compound is of interest itself due to the question of whether this should be described as a stibonium ion with a trityl group as a substituent or as a trityl adduct of tribenzylstibine *i.e.* is the positive charge located on the Sb atom or trityl carbon. The Sb-C_{trityl} bond length (2.238(3) Å) is longer than the Sb-C_{Bn} bonds (2.146(3) - 2.155(3) Å), suggesting the latter assignment.

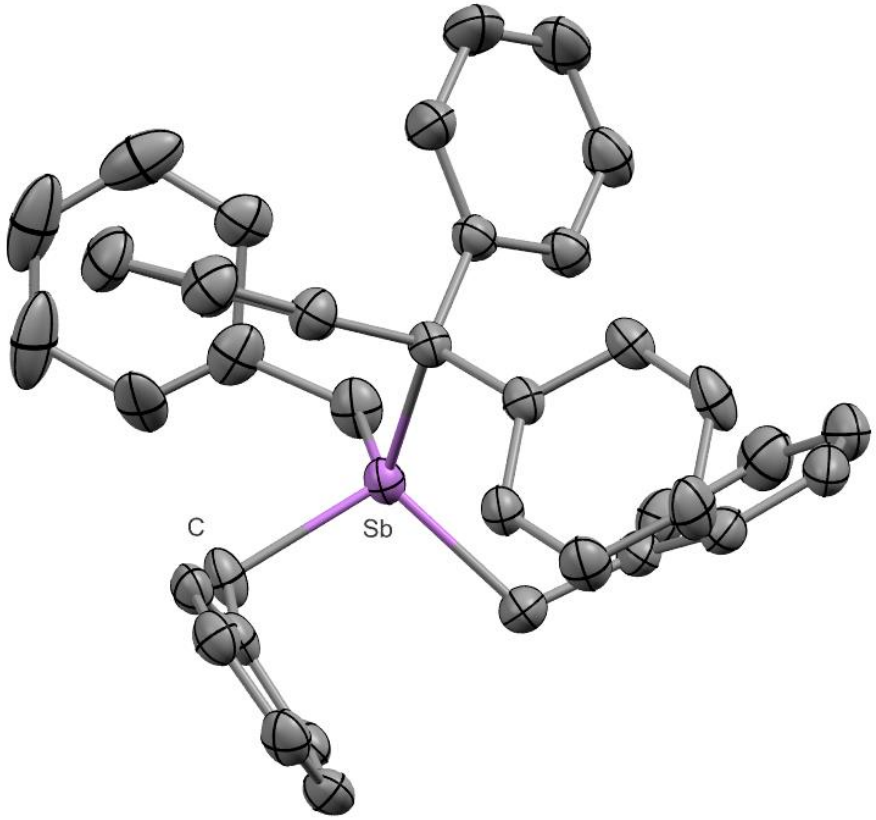

Figure 4.7. Solid state structure of $[Bn_3(Ph_3C)Sb][BF_4]$ (**3-4**). Ellipsoids shown at 50% probability. Hydrogen atoms, BF_4^- and disordered solvent have been omitted. One phenyl ring is disordered over two positions, only one is shown.

3-4 is unstable and forms $[Bn_4Sb][BF_4]$ (**3-3**) along with other minor impurities over the course of 3 days storing neat at room temperature (Scheme 4.11). $[Bn_3(Ph_3C)Sb][B(C_6F_5)_4]$ (**3-5**) was also synthesised by an equivalent strategy and found be similarly unstable, discounting the involvement of the $[BF_4]^-$ counteranion in the decomposition.

$$Bn_3Sb + [Ph_3C][BF_4] \longrightarrow \underset{\textbf{3-4}}{[Bn_3Sb(Ph_3C)][BF_4]} \xrightarrow{3\ \text{days}} \underset{\textbf{3-3}}{[Bn_4Sb][BF_4]}$$

Scheme 4.11. Synthesis of **3-4**, Conditions: room temperature, DCM, and decomposition to $[Bn_4Sb][BF_4]$ (**3-3**).

To further investigate the potential for the formation of $[Bn_2Sb(Bn_3Sb)][BF_4]$ to be mediated by just the Lewis acid, Bn_3Sb and $BF_3{\cdot}OEt_2$ were combined without BnCl under the conditions that lead to the formation of $[Bn_2Sb(Bn_3Sb)][BF_4]$, this yielded a white powder which was not structurally characterised by SCXRD but NMR spectra suggested that $BF_3{\cdot}Bn_3Sb$ was formed. This powder was highly unstable and formed a white intractable powder on standing neat at room temperature.

The possibility of *in-situ* formed $[Bn_4Sb]^+$ reacting with Bn_3Sb to yield $[Bn_2Sb(Bn_3Sb)][BF_4]$ and Bn_2 was also investigated; no reactivity between either $[Bn_4Sb][B(C_6F_5)_4]$ or $[Bn_4Sb][BF_4]$ (**3-3**) with Bn_3Sb was observed. Traces of HF are commonly found in commercial supplies of $BF_3{\cdot}OEt_2$;[498] to interrogate the possibility that $[Bn_2Sb(Bn_3Sb)][BF_4]$ had formed by the reaction of HF with Bn_3Sb, $[H(OEt_2)][BF_4]$ was reacted with Bn_3Sb. This yielded, among other products, clear colourless crystals of $[Bn_4Sb][B_2F_7]$ (**3-6,** Scheme 4.12).

$$Bn_3Sb \quad + \quad [H(OEt_2)][BF_4] \longrightarrow \quad \underset{\textbf{3-6}}{[Bn_4Sb][B_2F_7]}$$

Scheme 4.12. Isolation of **3-6**.

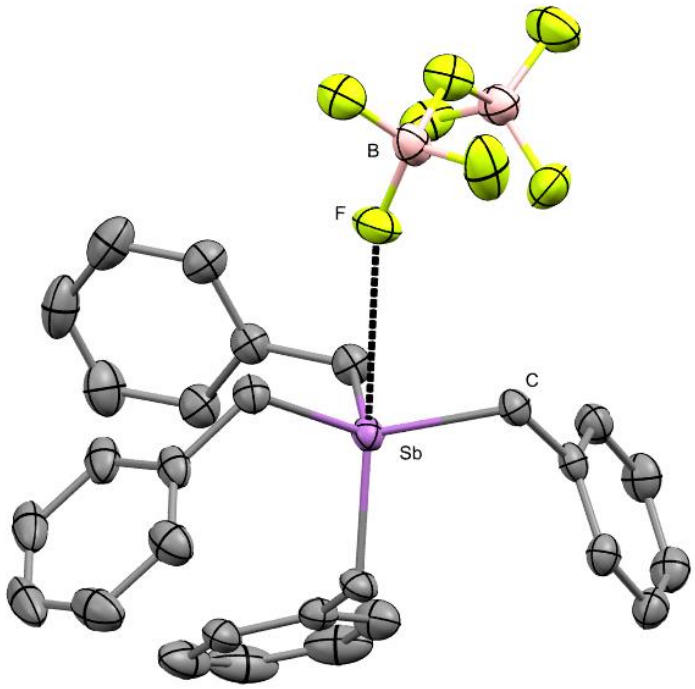

Figure 4.8. Solid state structure of $[Bn_4Sb][B_2F_7]$. Ellipsoids shown at 50% probability. Hydrogen atoms have been omitted. Sb-F short contact is shown as a black dotted bond.

While the presence of the heptafluorodiborate anion is unexpected here it is not without precedent. The heptafluorodiborate anion ($[B_2F_7]^-$) has been observed before but is relatively rare; there are 10 structurally characterised examples in the literature, in each case the heptafluorodiborate anion was formed unexpectedly.[499,500,509,501–508] The formal oxidation of Bn_3Sb^{III} to $[Bn_4Sb^V][B_2F_7]$ is surprising especially given the lack of obvious oxidising agents. One potential explanation is that the HBF_4 reacts with Bn_3Sb to yield a Bn^+ cation, which then oxidises another molecule of Bn_3Sb to yield $[Bn_4Sb]^+$.

The potential for the sample of Bn_3Sb used to be contaminated with Bn_2SbCl, from the incomplete alkylation of $SbCl_3$, as a factor in the formation of $[Bn_2Sb(Bn_3Sb)][BF_4]$ was also investigated. This necessitated the independent synthesis of Bn_2SbCl. Heteroleptic stibines are typically challenging synthetic targets due to substituent scrambling (see 1.2.1 Organoantimony (III)). Heteroleptic alkylchlorostibines are typically targeted by first synthesising the respective alkylphenylstibine and using $HCl_{(g)}$ to protonate the phenyl groups, yielding the alkylchlorostibine and benzene.[510] Initially, mixing Bn_3Sb and $SbCl_3$ both neat and in ethereal solution in a 2:1 ratio was attempted. In solution, this yielded a complex mixture of compounds which is typically observed.[511] The neat mixture did produce Bn_2SbCl along with a large amount of intractable black powder, assumably Sb^0, which precluded this as a viable route to Bn_2SbCl. A sample of Bn_3SbCl_2 was heated to melt *in vacuo*, as trialkylstibine dihalides (R_3SbX_2) are known to reductively eliminate alkyl halides (RX) to yield the respectively dialkylhalostibine (R_2SbX) under such conditions.[49] In this case no such reactivity was observed. Thus, the more established route for targeting heteroleptic alkylchlorostibines was employed; $PhSbCl_2$ was synthesised by combining neat Ph_3Sb and $SbCl_3$ in a 1:2 molar ratio respectively; the $PhSbCl_2$ is not isolated due to poor solubility and is therefore difficult to purify by recrystallisation. Two equivalents of BnMgCl were added to $PhSbCl_2$ in Et_2O (Scheme 4.13 a). This yielded an oil which contained a mixture of compounds including Bn_3Sb. Distillation failed to purify this oil. To identify the components of the mixture, a solution of SO_2Cl_2 was added to a solution of the oil to oxidise any stibines present to the respective stibine dichloride. While low molecular weight alkyl stibines are typically oils, their respective stibine dichlorides are usually crystalline solids. This yielded a white solid containing a mixture including Bn_3SbCl_2 and what was identified by SCXRD as $Bn_2PhSbCl_2$ (**3-7**,Figure 4.9, Scheme 4.13 b). The Sb-Cl bond length (2.4731(16)/ 2.4732(16) Å) is typical *c.f.* Sb-Cl bond length in Bn_3SbCl_2 (2.4608(6) - 2.4992(6) Å).[495]

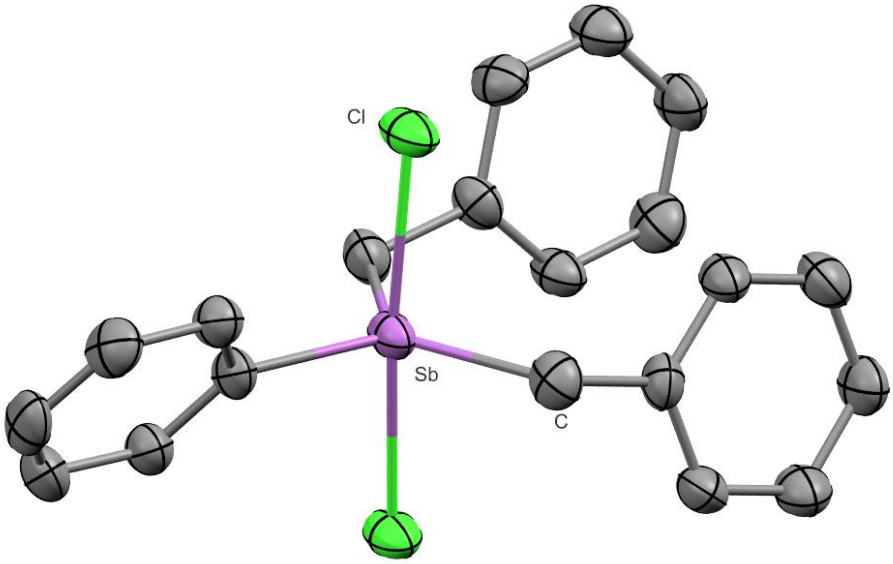

Figure 4.9. Solid state structure of $Bn_2PhSbCl_2$ (**3-7**). Ellipsoids shown at 50% probability. Hydrogen atoms have been omitted.

It was possible to separate **3-7** from the impurities by recrystallisation in hexanes. Compound **3-7** could then be reduced to Bn_2PhSb (**3-8**) with zinc dust in MeOH (Scheme 4.13 c). The benzylic protons in **3-8** are chemically inequivalent, yielding two doublets (δ^{1H} = 2.97 and 3.07 ppm, J = 11.6 Hz) in the ^{1}H NMR spectrum. Given that only one signal is observed in the $^{13}C\{^{1}H\}$ NMR spectrum and the coupling constant is typical of a geminal $^{2}J_{HH}$ coupling constant, it has been attributed to a chemical inequivalence between geminal hydrogen atoms which can not be resolved due to the high barrier of inversion in stibines. This is not observed for the analogous phosphine.[512]

Bubbling $HCl_{(g)}$ through a solution of **3-8** in toluene yielded Bn_2SbCl among several other impurities (Scheme 4.13 d). This suggests that the Sb-C_{benzyl} are unstable in acidic conditions, this is consistent with the finding that Bn_3Sb forms $[Bn_4Sb][B_2F_7]$ (**3-6**) on reaction with HBF_4. This precluded reacting an equimolar mixture of Bn_2SbCl and Bn_3Sb with $BF_3{\cdot}OEt_2$ but did allow for spectroscopic identification of Bn_2SbCl and careful examination of the sample of Bn_3Sb used in the formation of $[Bn_2Sb(Bn_3Sb)][BF_4]$ suggested that Bn_2SbCl was not present.

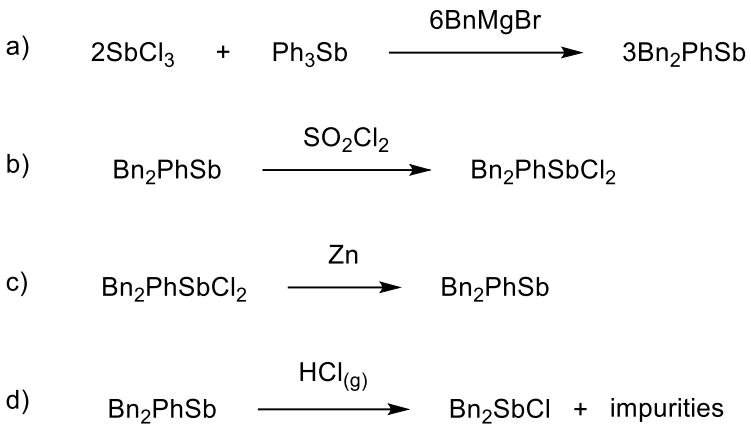

Scheme 4.13. a) -c) synthesis and purification of Bn_2PhSb via $Bn_2PhSbCl_2$ and d) attempted synthesis of Bn_2SbCl.

^{t}BuBr, Bn_3Sb and $BF_3{\cdot}OEt_2$ were reacted under similar conditions to that which yielded $[Bn_2Sb(Bn_3Sb)][BF_4]$, this yielded $SbBr_3$ primarily. This raises the possibility of *in situ* formation of R_2SbCl as a mechanism for the formation of $[Bn_2Sb(Bn_3Sb)][BF_4]$.

4.3 Conclusions

This body of work has revealed some novel insights into the reactivity of stibines, stibonium salts and the applicability to 'frustrated Lewis pair' chemistry. The synthesis of a previously unknown tetraarylstibonium salt ([(3,5-$F_2C_6H_3)_4Sb][B(C_6F_5)_4$], **3-2**), while not unprecedented, is only the second example of such a salt.[58] This body of work also acts as an initial point for the exploration of stibonium salts in 'FLP' systems; it has been revealed that while stibonium salts of the form $[Ar_3SbCl][B(C_6F_5)_4]$ will reduce in the presence of stibines (R_3Sb), the tetraarylstibonium salt ([(3,5-$F_2C_6H_3)_4Sb][B(C_6F_5)_4$], (**3-2**) will not.

This body of work also included the first example of a C-Cl bond activation by a stibonium/stibine system ([(3,5-$F_2C_6H_3)_4Sb]^+$/$^tBu_3Sb$), with experimental evidence and literature precedent suggesting this is mediated by a cooperative mechanism.[483] While this is useful for the objective of expanding variety in strategies for bond activation by main group systems, it is unlikely to be a competitor for existing catalytic systems. This is primarily because the only stibine found to be useful for this reactivity, $^tBu_3Sb$, is thermally unstable; this thermal instability limits opportunities for a thorough examination of this reactivity and would strictly limit catalytic turnover. While not observed here, the tendency for heteroleptic antimony compounds to scramble would also likely hinder the potential for such a system to be deployable under a wide variety of conditions.

In terms of future work, it would be pragmatic to target alternative stibines for the stibonium/stibine system to circumvent the decomposition of $^tBu_3Sb$. The failure of Mes_3Sb to activate benzyl chloride in place of $^tBu_3Sb$ would suggest that a triakylstibine is required; Cy_3Sb (Cy = cyclohexyl) or $^iPr_3Sb$ would potentially be fruitful given that they are both stibines with secondary alkyl groups, which have not been assessed here and would be an intermediate between the stibines with primary and tertiary alkyl groups investigated here. Previous work has ultilised phosphine FLP systems to functionalise C-F bonds with Wittig-type reactivity (see 4.1.1 C-X Bond activation by FLPs).[478] Given that the intermediate of these reactions are phosphonium cations, similar to the stibonium cation, $[^tBu_3BnSb][B(C_6F_5)_4]$, it is possible that similar chemistry could be deployed with this system. Antimony ylides are expected to have different reactivity to Phosphorus ylides,[513] suggesting the possibility of complementary not competing reactivity to the phosphine FLP systems.

A novel compound containing a Sb-Sb bond, $[Bn_2Sb(Bn_3Sb)][BF_4]$, was found by serendipity during the course of this work. This is the second example of such a compound.[85,86] This

nature of this compound (a stibinostibonium (Sb^{I}/Sb^{V}) or stibne stibenium(Sb^{III}/Sb^{III})) has previously been debated,[85] structural and computational evidence suggests that the former description is most accurate. A higher yielding synthetic pathway to this compound, to allow for a greater exploration of its chemistry would be useful.

4.4 Experimental

See Appendix I: General Experimental Methods for general experimental information.

$(3,5\text{-}F_2C_6H_3)_4SbCl$ (3-1)

2.3 M nBuLi in hexanes (8.50 mL, 19.8 mmol) was added dropwise to a solution of 3,5-$F_2C_6H_3Br$ (3.8107 g, 19.75 mmol) in Et_2O (50 mL) at -78°C, yielding a white precipitate which was stirred at -78°C for 80 minutes. $SbCl_5$ (1.709 g, 5.71 mmol) in n-hexane (15 mL) was added dropwise to the aryl lithium at -78°C yielding a yellow solution which was stirred at -78°C for 3 hours then warmed to -15°C and left to slowly warm overnight, then stirred for a further 2 hours. The resulting colourless solution was filtered through celite to remove a white precipitate which had formed overnight. The solution was reduced *in vacuo* to an off-white solid, which was dissolved in DCM (5 mL) and layered with n-hexane (30 mL) to yield clear colourless crystals (0.070 g, 0.11 mmol). Further crystalisation occurred in the mother liquor, yielding clear colourless crystals (0.220 g, 0.36 mmol). The decanted solution was placed in the frezzer, yielding colourless crystals (0.360 g, 0.58 mmol).

Total yield: 0.650 g, 1.05 mmol, 18%. ^{1}H NMR (400 MHz, $CDCl_3$) δ ppm 6.98 - 7.10 (m, 4 H, p-H), 7.23 (br s, 8 H, o-H). $^{13}C\{^{1}H\}$ NMR (101 MHz, $CDCl_3$) δ ppm 107.8 (t, J=25 Hz, p-C), 117.9 (dd, 257 Hz, J= 18, J=7 , o-C), 139.7 (s, ipso-C), 163.1 (dd, J=257, 11 Hz, m-C). ^{19}F NMR (376 MHz, $CDCl_3$) δ ppm -104.93 (s). Elemental Analysis Found (Cal): C: 47.07 (47.29) H: 2.11 (1.98). Crystals suitable for SCXRD were removed from the bulk sample.

$[(3,5\text{-}F_2C_6H_3)_4Sb][B(C_6F_5)_4]$ (3-2)

A suspension of $(3,5\text{-}F_2C_6H_3)_4SbCl$ (0.183 g, 0.30 mmol) in toluene (10 mL) was added dropwise to a suspension of $[Et_3Si(C_7H_8)][B(C_6F_5)_4]$ (freshly synthesised from $[Ph_3C][B(C_6F_5)_4]$ (0.306 g, 0.34 mmol)) to give an instant white crystalline suspension. The reaction mixture was stirred for a further 1 hour and n-hexane (15 mL) was added, and the solution was decanted. The resulting crystalline solid was washed with n-hexane (3x10 mL) then dried in vacuo to yield a white microcrystalline solid (0.300 g, 0.24 mmol, 70%). ^{1}H NMR (400 MHz, CD_2Cl_2) δ ppm 7.21 (br s, 8 H, o-H), 7.44 (tt, J=8.49, 2.26 Hz, 4 H, p-H). $^{13}C\{^{1}H\}$ NMR (101 MHz, CD_2Cl_2) δ ppm 111.4 (br t, J=24 Hz) 117.4 (br d, J=27 Hz) 147.0 (br d, J= 256 Hz) 163.6 (br d, J= 242 Hz). ^{19}F NMR (376 MHz, CD_2Cl_2) δ ppm -167.53 (br t, J=17.34 Hz, B $B(C_6F_5)_4$), -163.99 (m, B $B(C_6F_5)_4$), -133.31 (m, $B(C_6F_5)_4$), -99.52 (s, Ar-F). Elemental Analysis, Found (Cal): C: 45.91 (46.00) H: 1.05 (0.98). Crystals suitable for SCXRD were removed from the bulk sample.

Gutmann-Beckett Method on $[(3,5\text{-}F_2C_6H_3)_4Sb][B(C_6F_5)_4]$

$[(3,5\text{-}F_2C_6H_3)_4Sb][B(C_6F_5)_4]$ (0.0069 g, 0.006 mmol) and Et_3PO (0.0007 g,0.005 mmol) were mixed in CD_2Cl_2 (0.7 mL) and NMR spectra were obtained. ^1H NMR (400 MHz, $CDCl_2$) δ ppm 0.82 (dt, J=17.61, 7.78 Hz, 4 H), 1.38 (dq, J=11.64, 7.63 Hz, 2 H), 7.19 (br s, 8 H) ,7.38 (br t, J=8.46 Hz, 4 H). ^{19}F NMR (376 MHz, $CDCl_2$) δ ppm -167.54 (br t, J=17.34 Hz,), -163.69 (br t, J=20.23 Hz), -133.10 (br s), -102.45 - -97.27 (br s). ^{31}P NMR (162 MHz, CD_2Cl_2) δ ppm 67.33 (s).

Friedel Crafts Dimerisation of 1,1-diphenylethylene by $[(3,5\text{-}F_2C_6H_3)_4Sb][B(C_6F_5)_4]$

A J-Young NMR tube was loaded with DPE (0.018 g, 0.1 mmol) and $[(3,5\text{-}F_2C_6H_3)_4Sb][B(C_6F_5)_4]$ (0.008 g, 0.005 mmol, 5% loading) in either CD_2Cl_2 (0.7 mL) or CD_3CN (0.7 mL). The CD_2Cl_2 solution turned yellow instantly on addition whereas the CD_3CN solution remained colourless. The tubes were stood for 2h then ^1H and ^1F NMR spectra were obtained. Conversion was determined by relative integration of DPE to dimerised product.

Reaction of **3-2** and Ph_3CCl

A J-young NMR tube was loaded with $[(3,5\text{-}F_2C_6H_3)_4Sb][B(C_6F_5)_4]$ (**3-2**) (0.010 g, 0.007 mmol), Ph_3CCl (0.002 g, 0.007 mmol and CD_2Cl_2 (0.7 mL), giving a deep yellow solution instantly. NMR spectra were obtained. 1H NMR (400 MHz, CD_2Cl_2) δ ppm 7.13 (br t, J=8.58 Hz, 3 H, p-H), 7.23 (br s, 6 H, o-H). ^{19}F NMR (376 MHz, CD_2Cl_2) δ ppm -167.47 (s, $B(C_6F_5)_4$), -163.62 (br t, J=20.23 Hz, $B(C_6F_5)_4$), -133.05 (s, $B(C_6F_5)_4$), -104.69 (s, Ar-F).

$(2,4,6\text{-}Me_3C_6H_2)_3Sb$ (Mes_3Sb)

This procedure was adapted from ref [203]. $2,4,6\text{-}Me_3C_6H_2Br$ (4.5119 g, 22.61 mmol) was added dropwise to activated magnesium turnings (2.000 g, 90.40 mmol) in THF (25 mL) over 20 mins to maintain a gentle reflux without external heating, giving a dark suspension. This was heated to reflux for 1 h and then filtered , giving a dark yellow solution. $SbCl_3$ (1.725 g, 7.56 mmol) in Et_2O (10 mL) was added dropwise to this solution, causing the formation of a yellow precipitate and a highly exothermic reaction. The solution was heated to reflux for 1h, at which point the precipitate redissolved. The solution was cooled back to room temperature and stirred for another hour. The work-up was carried out in ambient, aerobic conditions. H_2O (25 mL) was added dropwise to affect effervesce and the formation of a yellow ethereal layer and cloudy aqueous layer. The layers were separated, and the aqueous layer was extracted with $CHCl_3$ (3 x 30 mL). The combined organic layers were dried over $MgSO_4$ and dried *in vacuo,* firstly to a viscous yellow oil, then in a stronger vacuum (1 x 10^{-1} mbar) to form a light yellow solid which was washed with cold ethanol (3 x

10 mL) and dried *in vacuo* to give an off white solid (2.8797g, 6.00 mmol, 79%).1^{H} NMR (400 MHz, $CDCl_3$) δ ppm 2.27 (s, 9 H, p-Me) 2.29 (s, 18 H, o-Me) 6.83 (s, 6 H, Ar-H). $^{13}C\{^1H\}$ NMR (101 MHz, $CDCl_3$) δ ppm 20.9 (s), 25.3 (s), 128.8 (s), 136.6 (s), 137.8 (s), 144.7(s). The ^{13}C NMR data closely matches Ref [514]. The ^1H NMR spectrum is not a complete match with Ref [514], however it does not match other potential side-products: Mes_2SbCl, $MesSbCl_2$, MesH or MesBr.[514,515] There is some variation of reported ^1H NMR spectra of Mes_3Sb in the literature.[514,515]

Et_3Sb

EtBr (1.8850 g, 17.30 mmol) was added dropwise to activated magnesium turnings (5.000 g, 207 mmol) in Et_2O (50 mL) over 20 mins. The resulting suspension was stirred at room temperature for 3 h, then filtered to give a yellow solution. $SbCl_3$ (1.1480 g, 5.03 mmol) in Et_2O (30 mL) was added at 0°C, yielding a white precipitate and yellow solution. The reaction mixture was warmed to room temperature and stirred overnight. Degassed H_2O (10 mL) was added dropwise, effecting a vigorous effervesce and yielding a white ethereal layer and dark aqueous layer. The ethereal layer was transferred onto $MgSO_4$ and the Et_2O was removed by distillation. The product was removed by distillation (1 mbar, 60°C), yielding a clear colourless oil (0.731 g, 3.50 mmol, 70%). ^1H NMR (400 MHz, $CDCl_3$) δ ppm 1.24 (q, J=7.6 Hz, 9 H), 1.35 (t, J=7.5 Hz, 6 H).

$^tBu_3Sb$

1.7M ^{t}BuLi in pentane (10.2 mL, 17.3 mmol) was added dropwise to $SbCl_3$ in Et_2o (40 mL) at -78°C, giving a red/brown solution. The reaction mixture was warmed to room temperature, yielding a white precipitate and an orange solution. The reaction mixture was stirred at room temperature overnight. Degassed H_2O (10 mL) was added dropwise, effecting a vigorous effervesce and yielding a brown ethereal layer and dark aqueous layer. The ethereal layer was transferred onto $MgSO_4$ and then filtered to give a light brown solution which darkened over the course of an hour. The solution was reduced *in vacuo* to a dark oil, which darkened on standing. (0.803 g, 2.74 mmol, 56 %). ^1H NMR (400 MHz, $CDCl_3$) δ ppm 1.33 (s, 27 H). $^{13}C\{^1H\}$ NMR (101 MHz, $CDCl_3$) δ ppm 31.1 (s, v. minor) 32.2 (s). NMR data matches ref [132]. The thermal decomposition of $^tBu_3Sb$ has been previously noted.[107]

Reaction of $^tBu_3Sb$ and $B(C_6F_5)_3$

A J-Young NMR tube was loaded with $B(C_6F_5)_3$ (0.008 g, 0.015 mmol), $^tBu_3Sb$ (0.005 g, 0.017 mmol) and $CDCl_3$ (0.7 mL) to yield a very light yellow solution. NMR spectra were obtained, revealing multiple products. ^1H NMR (400 MHz, $CDCl_3$) δ ppm 0.77 - 0.95 (m, 1 H), 1.18 -

1.27 (m, 1 H), 1.31 - 1.45 (m, 1 H), 1.31 - 1.41 (m, 1 H), 1.35 - 1.38 (br s, 18 H), 1.51 (s, 1 H), 1.63 (s, 1 H) ,1.76 - 1.84 (m, 1 H), 1.80 (s, 1 H), 3.87 - 4.06 (m, 1 H). ^{19}F NMR (376 MHz, $CDCl_3$) δ ppm -168.61 - -166.76 (m, minor) -166.21 (br t, J=18.79 Hz, minor) -164.84 (br t, J=18.79 Hz, minor) -159.90 (br s, $B(C_6F_5)_3$) -157.80 - -157.51 (m, minor) -157.23 - -155.38 (m, minor) -146.57 - -139.74 (m, minor) -143.09 (s, $B(C_6F_5)_3$) -139.17 - -135.76 (m, minor) -134.04 (br d, J=20.23 Hz, minor) -133.20 - -131.78 (m, minor) -127.85 (br s, $B(C_6F_5)_3$). ^{11}B NMR contained no signals not attributable to borosilicate glass.

The solution was stood at room temperature for 2 hours and further NMR spectra were obtained.^{1}H NMR (400 MHz, $CDCl_3$) δ ppm 0.72 - 0.99 (m, 1 H), 1.17 - 1.18 (m, 1 H), 1.29 - 1.32 (m, 1 H), 1.38 (s, 2 H), 1.40 - 1.44 (m, 2 H), 1.63 (s, 1 H), 1.68 - 1.79 (m, 2 H). ^{19}F NMR (376 MHz, $CDCl_3$) δ ppm -167.99 (br t, J=21.68 Hz), -165.34 - -164.77 (m), -163.31 (br d, J=23.12 Hz), -162.35 - -161.78 (m), -161.01 (td, J=20.95, 10.11 Hz), -159.08 - -156.95 (m), -158.79 - -157.94 (m), -156.80 - -154.24 (m),-155.80 (br t, J=20.23 Hz), -150.45 (br t, J=20.23 Hz), -150.12 - -148.41 (m), -137.59 (s), -136.49 (br s), -135.62 - -135.33 (m), -133.34 - -133.06 (m), -132.91 - -131.35 (m). Crystallisation by layering with n-hexane and cooling failed to yield any SCRXD quality crystals.

Bn_3Sb

BnCl (2.3314 g, 18.4 mmol) was added dropwise to activated Mg turnings (2.0000 g, 82.2 mmol) in Et_2O (40 mL) over 15 min at such a rate as to maintain a gentle reflux without external heating. A white precipitate formed over the course of the addition was stirred for 90 mins then filtered into a solution of $SbCl_3$ (1.113 g, 4.87 mmol) in Et_2O (20 mL). The addition yielded a grey precipitate and a yellow solution; the yellow colour subsisted on complete addition. The reaction mixture was stirred at room temperature overnight then filtered to yield a colourless solution. The solution was reduced *in vacuo* to the point where a small white crystalline precipitate formed which was redissolved with gentle heating then the solution was placed at -18°C to affect the formation of white crystals which were separated by filtratation and dried *in vacuo* to yield white crystals (1.307 g, 3.31 mmol). ^{1}H NMR (400 MHz, $CDCl_3$) δ ppm 2.76 - 2.86 (br d, 6 H) 7.00 (dd, 6 H, J=7.1 Hz J=1.1 Hz), 7.09 (tt, 3 H, J=7.4, J=1.1 Hz), 7.26 (br t, 6 H, J = 7.7 Hz).

The mother liquor was reduced *in vacuo* to the point where a small white crystalline precipitate formed which was redissolved with gentle heating then the solution was placed at -18°C to affect the formation of white crystals which were separated by filtratation and dried *in vacuo* to yield white crystals (0.220 g, 0.56 mmol). ^{1}H NMR (400 MHz, $CDCl_3$) δ ppm

2.78 (s, 6 H) 6.99 (br d, J=7.55 Hz, 6 H) 7.04 - 7.13 (t, 3 H, J=7.3 Hz) 7.18 - 7.28 (t, 6 H, J=7.6 Hz).

Combined yield: 1.527 g, 3.86 mmol, 80%. NMR data matches data previously obtained in the group.[495]

Screening for Reactivity Between $^{t}Bu_3Sb$ and $[(3,5\text{-}F_2C_6H_3)_3SbCl][B(C_6F_5)_4]$ (1-16)

A J-young NMR tube was loaded with $[(3,5\text{-}F_2C_6H_3)_3SbCl][B(C_6F_5)_4]$ (**1-6**) (0.0134 g, 0.011 mmol), $^{t}Bu_3Sb$ (0.0059 g, 0.020 mmol) and CD_2Cl_2 (0.7 mL), affecting the instant formation of a black precipitate and a dark yellow solution. NMR spectra were obtained. ^{1}H NMR (400 MHz, CD_2Cl_2) δ ppm 0.86 - 0.91 (m, 11 H) 0.94 - 1.03 (m, 5 H) 1.10 (s, 2 H) 1.37 (s, 5 H, $^{t}Bu_3Sb$) 1.47 (s, 3 H) 1.77 (s, 7 H) 1.80 (s, 13 H) 1.84 (d, J=5.26 Hz, 10 H) 6.79 - 6.91 (m, 3 H, p-H ($[(3,5\text{-}F_2C_6H_3)_3Sb]$) 6.94 - 6.99 (m, 6 H, o-H ($[(3,5\text{-}F_2C_6H_3)_3Sb]$). ^{19}F NMR (376 MHz, CD_2Cl_2) δ ppm -167.42 (br t, J=17.34 Hz, $B(C_6F_5)_4$) -163.60 (br t, J=20.23 Hz, $B(C_6F_5)_4$) -133.00 (br s, $B(C_6F_5)_4$) -109.07 (br s, Ar-F ($[(3,5\text{-}F_2C_6H_3)_3Sb]$). *N.B.* several other minor signals were present in the ^{19}F NMR spectrum between -100 and -180 ppm.

Screening for Reactivity Between 3-2 and Stibines (R_3Sb)

A J-young NMR tube was loaded with $[(3,5\text{-}F_2C_6H_3)_4Sb][B(C_6F_5)_4]$ (**3-2**) (0.0061 g, 0.005 mmol), $^{t}Bu_3Sb$ (0.0027 g, 0.009 mmol) and CD_2Cl_2 (0.7 mL). NMR spectra were obtained, which were the equivalent to the sum of the individual components. Et_3PO (0.0007 g, 0.005 mmol) was added and NMR spectra were obtained. ^{1}H NMR (400 MHz, CD_2Cl_2) δ ppm 0.79 - 0.90 (m, 15 H), 1.20 (s, 3 H), 1.30 (s, 47 H), 1.35 - 1.49 (m, 9 H), 7.06 - 7.15 (m, 9 H), 7.20 - 7.26 (m, 3 H). ^{19}F NMR (376 MHz, CD_2Cl_2) δ ppm -167.57 (br t, J=17.34 Hz, $B(C_6F_5)_4$) -163.74 (br t, J=20.23 Hz, $B(C_6F_5)_4$) -133.10 (br s, $B(C_6F_5)_4$) -102.97 (br s, Ar-F) $^{31}P\{^{1}H\}$ NMR (162 MHz, CD_2Cl_2) δ ppm 64.89 (br s).

A J-young NMR tube was loaded with $[(3,5\text{-}F_2C_6H_3)_4Sb][B(C_6F_5)_4]$ (**3-2**) (0.006 g, 0.005 mmol), Et_3Sb (0.005 g, 0.025 mmol) and CD_2Cl_2 (0.7 mL). NMR spectra were obtained, which were the equivalent to the sum of the individual components. The sample was inadvertently exposed to ambient atmosphere and yielded crystals of $[(3,5\text{-}F_2C_6H_3)_4Sb(OSbEt_3)][B(C_6F_5)_4]$ on layering with n-hexane.

A J-young NMR tube was loaded with $[(3,5\text{-}F_2C_6H_3)_4Sb][B(C_6F_5)_4]$ (**3-2**) (0.006 g, 0.005 mmol), Mes_3Sb (0.005 g, 0.001 mmol) and CD_2Cl_2 (0.7 mL). NMR spectra were obtained, which were the equivalent to the sum of the individual components. The sample was deliberately exposed to ambient atmosphere and stood overnight then additional NMR spectra were obtained. ^{1}H NMR (400 MHz, CD_2Cl_2) δ ppm 2.17 - 2.28 (m, 44 H, o-Me) 2.31 -

2.42 (m, 17 H, p-Me) 6.77 - 6.85 (m, 10 H, Ar-H (Mes)) 7.13 (s, 3 H, p-H (3,5-$F_2C_6H_3$)) 7.16 - 7.24 (m, 8 H, o-H (3,5-$F_2C_6H_3$))) ^{19}F NMR (376 MHz, CD_2Cl_2) δ ppm -167.51 (br t, J=17.34 Hz, $B(C_6F_5)_4$) -163.68 (br t, J=21.67 Hz, $B(C_6F_5)_4$) -133.06 (br d, J=5.78 Hz, $B(C_6F_5)_4$), -103.79 (s, Ar-F). *N.B.* several other minor signals -110 to -100 were present.

Activation of Benzyl Chloride (BnCl) with **3-2** and ^{t}Bu$_3$Sb

A J-young NMR tube was loaded with [(3,5-$F_2C_6H_3)_4$Sb][$B(C_6F_5)_4$] (**3-2**) (0.006 g, 0.005 mmol), ^{t}Bu$_3$Sb (0.003 g, 0.01 mmol), BnCl (0.03 mmol) and CD_2Cl_2 (0.7 mL). Initial NMR spectra were obtained, which were the equivalent to the sum of the individual components. The tube was heated to 40°C for 4 hours and NMR spectra were obtained. ^{1}H NMR (400 MHz, CD_2Cl_2) δ ppm 1.32 (s, 22 H, ^{t}Bu$_3$Sb) 1.62 (s, 3 H), 4.60 (s, 4H, Bn-H (BnCl)), 6.92 - 6.93 (m, 1 H), 7.17 - 7.23 (m, 3 H), 7.28 - 7.34 (m, 3 H), 7.34 - 7.44 (m, 7 H). ^{19}F NMR (376 MHz, CD_2Cl_2) δ ppm -167.51 (m, $B(C_6F_5)_4$), -163.66 (br t, J=20.23 Hz, $B(C_6F_5)_4$), -133.07 (br d, J=2.89 Hz, $B(C_6F_5)_4$), -101.44 (br d, J=5.78 Hz, Ar-F).

The tube was stood at room temperature for 96 hours and NMR spectra were obtained. 1H NMR (400 MHz, CD_2Cl_2) δ ppm 1.32 (s, 32 H), 1.62 (s, 22 H), 3.68 (s, 1 H), 4.60 (s, 9 H), 7.04 - 7.14 (m, 3 H), 7.22 - 7.27 (m, 7 H), 7.30 - 7.35 (m, 6 H), 7.36 - 7.43 (m, 8 H). ^{19}F NMR (376 MHz, CD_2Cl_2) δ ppm -167.46 (br t, J=17.34 Hz, $B(C_6F_5)_4$), -163.64 (br t, J=21.67 Hz, $B(C_6F_5)_4$), -133.05 (br s, $B(C_6F_5)_4$), -105.42 (s, Ar-F). The reaction solution was layered with n-hexane which failed to produce any crystallisation. The solution was slowly evaporated to yield crystals of [^{t}Bu$_3$BnSb][$B(C_6F_5)_4$].

Decomposition of ^{t}Bu$_3$Sb

A sample of ^{t}Bu$_3$Sb (0.008 g, 0.03 mmol) in $CDCl_2$ (0.7 mL) was heated to 40°C for 4 hours. A ^{1}H NMR spectrum was taken. ^{1}H NMR (400 MHz, CD_2Cl_2) δ ppm 0.80 - 0.91 (m, 1 H), 1.08 - 1.17 (m, 1 H), 1.20 (s, 1 H) 1.22 - 1.31 (m, 1 H), 1.33 (s, 1 H), 1.40 - 1.58 (m, 4 H).

A sample of **3-2** (0.004 g, 0.03 mmol) was added and NMR spectra were obtained.^{1}H NMR (400 MHz, CD_2Cl_2) δ ppm 0.73 - 0.95 (m, 1 H), 1.11 - 1.27 (m, 1 H), 1.33 - 1.75 (m, 1 H). ^{19}F NMR (376 MHz, CD_2Cl_2) δ ppm -167.55 (br t, J=15.90 Hz, $B(C_6F_5)_4$), -163.74 (br t, J=20.23 Hz, $B(C_6F_5)_4$), -133.10 (s, $B(C_6F_5)_4$), -108.53 (br s, Ar-F).

Screening for Reactivity Between ^{t}Bu$_3$Sb and BnCl

A J-young NMR tube was loaded with [(3,5-$F_2C_6H_3)_4$Sb][$B(C_6F_5)_4$] (**3-2**) (0.006 g, 0.005 mmol), ^{t}Bu$_3$Sb (0.003 g, 0.01 mmol)and CD_2Cl_2 (0.7 mL). Initial NMR spectra were obtained, which were the equivalent to the sum of the individual components. The tube was heated to 40°C for 4 hours and NMR spectra were obtained. 1H NMR (400 MHz, CD_2Cl_2) δ ppm 1.20

- 1.26 (m, 4 H), 1.29 (d, J=5.72 Hz, 1 H) 1.31 - 1.34 (m, 5 H) 1.35 - 1.37 (m, 2 H, $^{t}Bu_3Sb$) 1.47 - 1.59 (m, 9 H) 4.58 (s, 2 H, Bn-H (BnCl)), 7.22 - 7.44 (m, 3 H, Ar-H (BnCl)).

Bn_4SbBr

The synthetic procedure was based on previous work in the group.[495] BnBr (2.0 mL, 17 mmol) was added neat to Bn_3Sb (0.212 g, 0.54 mmol). The suspension was heated at 80°C overnight and then to 110° for 2 hours. n-hexane (20 mL) was added to the cooled suspension yielding a white precipitate. The suspension was exposed to the ambient atmosphere and filtered in air then washed with petroleum ether 40-60°C (2 x30 mL) then dried *in vacuo* to yield a white powder (0.1332 g, 0.23 mmol, 43%). ^{1}H NMR (400 MHz, DMSO-d6) δ ppm 3.50 (s, 8 H, Bn-H) 6.53 - 6.74 (m, 4 H, p-H) 7.18 - 7.30 (m, 12 H, o-H, m-H). NMR spectrum matches data previously obtained in the group.[495]

$[Bn_4Sb][BF_4]$ (3-3)

$NaBF_4$ (0.11g, 0.1 mmol) in DCM (10 mL) was added to Bn_4SbBr (0.059 g, 0.010 mmol) was suspended in DCM (10 mL) to give a white suspension. The suspension was dried *in vacuo* to yield a white powder which was extracted into Et_2O (20 mL) through a cannula filter to give a white residue and colourless solution. Both were dried *in vacuo* to yield a white powder. ^{1}H NMR of both solids matched Bn_4SbBr. The residue was suspended in toluene (20 mL) and $BF_3.OEt_2$ (0.070 g, 0.50 mmol) was added dropwise at 0°C then warmed to room temperature and stirred overnight. The suspension was dried *in vacuo* and extracted into DCM (20 mL) to give a colourless solution to which n-hexane (30 mL) was added to give a white precipitate. The solution was reduced *in vacuo* to ~20 mL and decanted off. The residue was dried under vacuum to give a white powder (0.010 g, 0.02 mmol, 20%). ^{1}H NMR (400 MHz, $CDCl_3$) δ ppm 3.60 (s, 6 H, Bn-H) 6.72 (br d, J=5.49 Hz, 6 H, m-H) 7.24 (br s, 12 H, o-H, p-H). $^{13}C\{^{1}H\}$ NMR (101 MHz, $CDCl_3$) δ ppm 25.7 (s, Bn-C) 127.8 (s) 129.4 (s) 129.7 (s) 132.1 (s). ^{19}F NMR (376 MHz, $CDCl_3$) δ ppm -146.52 (br s). Crystals for SCXRD were grown by layering a DCM solution with n-hexane.

$[Ph_3C][BF_4]$

Synthesis was adapted from literature method.[516] $BF_3{\cdot}Et_2O$ (3.0 mL, 2.44 mmol) was added dropwise to a solution of Ph_3CF (0.525 g, 2.00 mmol) in toluene (20 mL) in the dark, affecting an instant yellow precipitate which was stirred for 15 minutes then left to settle. The solution was decanted and the remaining powder washed with toluene (15 mL) and n-hexane (3 x 20 mL) to give a light yellow powder which was dried *in vacuo* (0.200 g, 0.60 mmol, 30%). ^{1}H NMR (400 MHz, CD_2Cl_2) δ ppm 7.69 (dd, J=8.46, 1.37 Hz, 6 H) 7.81 - 7.99 (t, J=7.55Hz, 6 H) 8.29 (tt, J=7.49, 1.20 Hz, 3 H). $^{13}C\{^{1}H\}$ NMR (101 MHz, CD_2Cl_2) δ ppm 130.7

(s), 140.0 (s), 142.7 (s), 143.6 (s), 211.0 (s). ^{19}F NMR (376 MHz, CD_2Cl_2) δ ppm -153.02 (s), -150.27 (s, minor).

$[Bn_3(Ph_3C)Sb][BF_4]$ (3-4)

$[Ph_3C][BF_4]$ (0.066 g, 0.20 mmol) in DCM (10 mL) was added to Bn_3Sb (0.080 g, 0.20 mmol) in DCM (10 mL) to give a light yellow solution which was stirred at room temperature then reduced *in vacuo* to a light yellow powder. The powder was washed with n-hexane (3 x 5 mL) and dried *in vacuo* to yield a light yellow powder (0.100 g, 0.14 mmol, 70%). ^{1}H NMR (400 MHz, CD_2Cl_2) δ ppm 3.66 - 3.92 (v br s, 6 H, benzyl H) 6.50 (br d, J=7.09 Hz, 7 H, aryl H) 7.17 - 7.33 (m, 13 H, aryl H). ^{13}C{^{1}H} NMR (101 MHz, CD_2Cl_2) δ ppm 30.0 (br s, benzyl C), 127.8 (m, aryl H) 128.2 (s, aryl H) 129.7 (s, aryl H) 130.0 (s, aryl H). ^{19}F NMR (376 MHz, CD_2Cl_2) δ ppm -149.20 (s). This powder was sensitive to air, rapidly turning red on exposure. Crystals for SCXRD were grown by layering a saturated DCM solution with n-hexane.

$[Bn_3(Ph_3C)Sb][B(C_6F_5)_4]$ (3-5)

$[Ph_3C][B(C_6F_5)_4]$ (0.189 g, 0.20 mmol) in DCM (10 mL) was added to Bn_3Sb (0.080 g, 0.20 mmol) in DCM (10 mL) which remained a deep red solution. The reaction was stirred at room temperature for 90 minutes then the solvent was removed *in vacuo* to give a dark yellow foam which was washed with n-hexane (3 x 5 mL) then dried *in vacuo* to five a golden powder (0.176 g, 0.13 mmol, 65%). ^{1}H NMR (400 MHz, $CDCl_3$) δ ppm 3.09 (s, 3 H) 6.16 - 6.49 (m, 1 H) 6.65 (br d, J=6.40 Hz, 3 H) 6.94 (br d, J=7.09 Hz, 1 H) 7.11 (br d, J=7.32 Hz, 1 H) 7.20 - 7.31 (m, 6 H) 7.33 - 7.41 (m, 1 H). ^{13}C{^{1}H} NMR (101 MHz, $CDCl_3$) δ ppm 14.2 (s), 22.8 (s), 31.7 (s), 126.4 (s), 127.4 (br s), 128.4 (s), 128.6 (s), 128.8 (s), 129.5 (s), 129.7 (s), 130.5 (m). ^{19}F NMR (376 MHz, $CDCl_3$) δ ppm -166.52 (s), -162.71 (br t, J=20.23 Hz), -132.45 (s). Attempted crystallisation for SCXRD only yielded red oil.

$[Bn_4Sb][B_2F_7]$ (3-6)

$[H(OEt_2)_2][BF_4]$ (0.008 g, 0.05 mmol) was added dropwise to a solution of Bn_3Sb (0.040 g, 0.10 mmol) in toluene (10 mL) at 0°C, yielding the instant formation of a white precipitate. The reaction mixture was warmed to room temperature and stirred for 1 hour. The solution was decanted into air, affecting the formation of an instant white precipitate. The remaining powder was dried *in vacuo*. The powder was sparingly soluble in CD_2Cl_2, it was washed with CD_2Cl_2 (0.7 mL) and NMR spectra were obtained. 1H NMR (400 MHz, CD_2Cl_2) δ ppm 1.54 - 1.73 (m, 4 H) 3.62 - 3.64 (m, minor) 4.73 - 4.88 (m, 3 H), 6.67 - 6.87 (m, minor) 6.96 (br d, J=5.49 Hz, minor) 7.03 - 7.21 (m, 2 H), 7.37 (br s, 2 H). ^{11}B NMR (128 MHz, CD_2Cl_2) δ ppm -1.98 (br s). ^{19}F NMR (376 MHz, CD_2Cl_2) δ ppm -149.59 (s, BF_4).

The remaining powder was dissolved in CD_3CN (0.7 mL) and NMR spectra were obtained. 1H NMR (400 MHz, CD_3CN) δ ppm 0.93 - 1.21 (m, 6 H, CH_2 (Et_2O)) 1.38 - 1.64 (m, 21 H, CH_3 (Et_2O-coordinated)) 1.81 - 2.05 (m, 17 H, CH_2 (Et_2O-coordinated)) 3.24 - 3.55 (m, 4 H, CH_3 (Et_2O)) 4.34 - 4.82 (m, 17 H) 8.97 - 9.56 (m, 2 H). ^{11}B NMR (128 MHz, CD_3CN)) δ ppm -2.19 (br s, BF_4). ^{19}F NMR (376 MHz, CD_3CN) δ ppm -151.92 (br s) -150.35 (br s, minor) -149.12 (br m, minor). Colourless crystals of $[Bn_4Sb][B_2F_7]$ (**3-6**) were obtained by layering the CD_2Cl_2 solution with n-hexane.

Reaction of $BF_3{\cdot}Et_2O$, BnCl and Bn_3Sb

$BF_3{\cdot}Et_2O$ (0.143 g, 1.00 mmol) was added dropwise to a solution of Bn_3Sb (0.200 g, 0.51 mmol) and BnCl (0.076 g, 0.60 mmol) in toluene (15 mL) at 0°C. The reaction solution was heated to 90°C overnight then cooled to room temperature to give a light-yellow solution and white precipitate. The solution was decanted and the residue dried *in vacuo* then dissolved in DCM (10 mL) to give a yellow solution and layered with n-hexane to give block crystals, needles and a small amount of powder. The solution was decanted into air, which instantly give a white precipitate. The residue was dried *in vacuo* to yield a white powder (0.020 g). ^1H NMR (400 MHz, CD_2Cl_2) δ ppm 2.34 (s, 1 H, resid C_7H_8), 3.08 (s, 5 H), 3.13 (br s, 2 H), 3.57 (s, 4 H, Bn-H (Bn_4Sb^+)), 6.72 - 6.79 (m, 3 H, Bn-H (Bn_4Sb^+)), 6.87 (d, J=7.09 Hz, 5 H), 7.02 (br d, J=7.32 Hz, 2 H), 7.16 - 7.24 (m, 5 H), 7.24 - 7.38 (m, 14 H, Bn-H (Bn_4Sb^+)). ^{11}B NMR (128 MHz, CD_2Cl_2) δ ppm -1.81 (br s). ^{19}F NMR (376 MHz, CD_2Cl_2) δ ppm -148.28 (br s), -147.75 - -146.90 (m). NMR The powder has decomposed within 21 days had become intractable into DCM or MeCN. Crystals of $[Bn_2Sb(Bn_3Sb)][BF_4]$ were identified from the bulk sample by SCXRD.

Reaction of $BF_3{\cdot}Et_2O$ and BnCl

$BF_3{\cdot}Et_2O$ (0.1662 g, 1.16 mmol) was added dropwise to a solution of BnCl (0.086 g, 0.67 mmol) in toluene (15 mL) at 0°C. The reaction solution was heated to 90°C overnight then cooled to room temperature and the solvent was removed *in vacuo* to yield a clear oil. 1H NMR (400 MHz, $CDCl_2$) δ ppm 2.23 (s, 2 H) 2.29 (s, 4 H) 3.91 (s, 3 H) 3.97 (s, 2 H) 4.13 (s, minor) 4.47 - 4.71 (m, minor) 6.94 - 7.39 (m, 22 H). ^{19}F NMR spectrum contained no signals.

Reaction of $BF_3{\cdot}Et_2O$ and Bn_3Sb

$BF_3{\cdot}Et_2O$ (0.1159 g, 0.81 mmol) was added dropwise to a solution of Bn_3Sb (0.200 g, 0.51 mmol) in toluene (15 mL) at 0°C. The reaction solution was heated to 90°C overnight then cooled to room temperature and the solvent was removed *in vacuo* to yield a white powder (0.167 g). ^1H NMR (400 MHz, CD_2Cl_2) δ ppm 2.77 (s, 6 H, Bn-H) 6.96 (br d, J=7.55 Hz,

6 H) 7.04 (br t, J=7.32 Hz, 6 H) 7.15 - 7.23 (m, 6 H). ^{11}B NMR (128 MHz, CD_2Cl_2) δ ppm -1.07 (br s). ^{19}F NMR (376 MHz, CD_2Cl_2) δ ppm -153.12 (br s).

Attempted Reductive elimination of BnCl from Bn_3SbCl_2

Bn_3SbCl_2 (0.0063 g, 0.01 mmol) was heated to melt (100°C) *in vacuo* (2.16 x 10^{-2} mbar) for 1 hour then cooled back to room temperature, forming white crystals on cooling. ^{1}H NMR spectroscopy showed no reaction.

$Bn_2PhSbCl_2$ (3-7)

A mixture of $SbCl_3$ (1.114 g, 5.02 mmol) and Ph_3Sb (0.082 2.49 mmol) were stirred for 3 days to give a yellow oil. of $PhSbCl_2$. Separately, BnCl (2.0768 g, 16.41 mmol) was added dropwise to activated Mg turnings (4.3307 g,16.40 mmol) in Et_2O (30 mL) over 15 minutes to maintain a gentle reflux without external heating. The reaction solution was stirred at room temperature for 90 minutes. The Grignard solution was then added dropwise to the $PhSbCl_2$ (*vide supra*) in Et_2O (30 mL) at 0°C to give a clear solution and white precipitate which was stirred overnight. Degassed H_2O (3 mL) was added dropwise until the resulting effervesce was not observed on any further addition. The ethereal layer dried over degassed $MgSO_4$ to give a colourless solution; the solvent was removed *in vacuo* to yield a yellow oil. The oil was distilled *in vacuo*, a single fraction was collected at 165°C/3.36 x 10^{-2} mbar which consisted of a yellow oil. A darkening of the residue was noted at 180°C. The resulting oil was dissolved in DCM (20 mL) and degassed SO_2Cl_2 (1.0368 g, 7.68 mmol) was added dropwise at -60°C to give a red solution. The reaction solution was stirred at -60°C for 1 hour then warmed to room temperature, at which point it became colourless, and stirred for a further 3 hours. The reaction solution was then exposed to ambient atmosphere and reduced *in vacuo* to a light yellow oil. The oil was recrystallised in DCM/hexanes to yield white crystals (0.1648 g, 0.36 mmol, 17%). ^{1}H NMR (400 MHz, $CDCl_3$) δ ppm 4.14 (s, 4 H, Bn-H) 7.27 - 7.34 (m, 7 H, Ar-H) 7.37 (d, J=7.32 Hz, 1 H, Ar-H) 7.42 - 7.49 (m, 5 H, Ar-H) 7.66 (d, J=7.32 Hz, 2 H, Ar-H) 7.89 - 7.98 (m, 1 H, p-H (Ph)). ^{13}C{^{1}H} NMR (101 MHz, $CDCl_3$) δ ppm 51.7 (s), 128.1 (s), 128.9 (s), 129.1 (s), 130.0 (s), 131.5 (s), 134.6 (s,) 135.1 (s).

Bn_2PhSb (3-8)

$Bn_2PhSbCl_2$ (0.4619 g, 1.02 mmol) was suspended in degassed MeOH (10 mL) and Zn dust (0.1968 g,3.00 mmol). The suspension was heated to 70°C for 2 hours then cooled to room temperature to give a yellow solution with a black and white powder suspended. The solvent was removed *in vacuo* to yield a black oil which was extracted through a filter into Et_2O (30 mL) and then reduced *in vacuo* to a yellow oil (0.381 g, 1.00 mmol, 98%). ^{1}H NMR

(400 MHz, $CDCl_3$) δ ppm 2.97 (d, 2 H, J = 11.6 Hz, Bn-H), 3.07 (d, 2 H, J = 11.6 Hz), 6.90 - 6.98 (m, 4 H), 6.99 - 7.08 (m, 2 H), 7.11 - 7.18 (m, 4 H), 7.28 - 7.34 (m, 4 H), 7.39 - 7.48 (m, 3 H). $^{13}C\{^1H\}$ NMR (101 MHz, $CDCl_3$) δ ppm 26.4 (s, Bn-C), 128.1 (s), 128.5 (s), 128.7 (s), 128.1 (s), 135.6 (s), 135.9 (s), 140.5 (s).

Attempted Synthesis of Bn_2SbCl From Bn_3Sb and $SbCl_3$

$SbCl_3$ (0.023 g, 0.10 mmol) and Bn_3Sb (0.079 g, 0.20 mmol) were mixed neat to give an instant yellow oil. This was stirred for 24 hours at room temperature giving some black precipitate, then dissolved in $CDCl_3$ (0.7 mL) and an NMR spectrum was obtained. Neat: ^1H NMR (400 MHz, $CDCl_3$) δ ppm 2.63 - 2.79 (br s, Bn-H, (Bn_3Sb)), 3.24 (s), 6.93 - 7.00 (m, Ar-H, (Bn_3Sb)), 7.05 - 7.10 (m, Ar-H, (Bn_3Sb)), 7.18 - 7.24 (m, Ar-H, (Bn_3Sb)), 7.24 - 7.31 (m). Similar results were obtained when stirred at 90°C. (*N.B.* Due to multiple impurities, integrations are not reported).

$SbCl_3$ (0.023 g, 0.10 mmol) in Et_2O (3 mL) was added to Bn_3Sb (0.079 g, 0.20 mmol) in Et_2O (5 mL) at room temperature and stirred for 4 hours. The solution was reduced *in vacuo* to 2 mL and cooled to -18°C which yielded clear colourless crystals. These crystals were separated by filtration and dried *in vacuo* to yield a white crystalline solid (0.015 g). ^1H NMR (400 MHz, $CDCl_3$) δ ppm 2.75 (s, Bn-H, (Bn_3Sb)), 3.47 (q, J=7.01 Hz), 3.60 (s), 3.71 (s), 6.85 - 7.03 (m, Ar-H, (Bn_3Sb)), 7.04 - 7.15 (m, Ar-H, (Bn_3Sb)) ,7.17 - 7.23 (m), 7.32 - 7.38 (m) (*N.B.* Due to multiple impurities, integrations are not reported).

Attempted Synthesis of Bn_2SbCl from Bn_2PhSb

Bn_2PhSb (0.353 g, 1.00 mmol) was dissolved in toluene (40 mL) and $HCl_{(g)}$ in a stream of dry N_2 was bubbled through the solution, generated from concentrated H_2SO_4 (30 mL) and concentrated HCl (20 mL),for 1 hour. Dry N_2 was bubbled through for a further 1 hour, then the solution was reduced *in vacuo* to a yellow oil.^1H NMR (400 MHz, $CDCl_3$) δ ppm 2.77 (s, 1 H, Bn-H, (Bn_3Sb)), 3.56 (s, 1 H), 4.09 (s, 1 H), 6.85 – 7.04 (m, 1 H, Ar-H, (Bn_3Sb)), 7.14 - 7.21 (m, 1 H, Ar-H, (Bn_3Sb)), 7.21 - 7.35 (m, 1 H, Ar-H, (Bn_3Sb)), 7.30 - 7.36 (m, 1 H).

Computational Methods

All calculations were performed using Gaussian 09 Revision E0.01.[355] All geometries were optimised in vacuum without imposing symmetry constraints at the M062X/def2-SVP level of theory with the GD3 empirical dispersion correction.[261,356,357] Subsequent analytical IR frequency calculations on optimised geometries were utilised to confirm the nature of stationary points (zero and exactly one imaginary mode for minima and transition states, respectively). Moreover, within the ideal gas/rigid rotor/harmonic approximation (RRHO)

these calculations also provided thermal and entropic corrections to the Gibbs Free Energy at 1 atm and 298.15 K. The Kohn-Sham orbitals were visualised using Chemcraft.[359]

5. Synthesis and Reactivity of $[Pd_4(Me_3Sb)_8]$

5.1 Introduction

5.1.1 Stibines as Transition Metal Ligands

While the paradigm that the chemistry of the p-block is less diverse in comparison to the d-block has been called into question by the immense novel chemistry that has been reported recently,[173,517] particularly in the last two decades, the chemistry of the d-block is nonetheless extremely diverse. Given the importance of d-block chemistry to both pure and applied chemistry, it has been thoroughly described in a number of undergraduate and graduate textbooks.[518–520]

Transition metal complexes with phosphine ligands (PR_3) have become ubiquitous due to their place in one of the most impactful discoveries from the d-block, C-C coupling reactions for synthetic organic chemistry.[521–525] The chemistry of transition metal complexes with heavier phosphine analogues are much less developed than their phosphine counterparts, in part due to the assumption that their chemistry would mirror that of the phosphine complexes and would prove to be fruitless due to poorer donor abilities. A description of the bonding of stibine ligands (R_3Sb) to transition metals can be discussed in relation to phosphine ligands. Phosphine ligands act as σ donors *via* donation of the LP_P to a vacant metal d-orbital and π acceptors by accepting electron density from a d-orbital of π symmetry to a phosphine vacant orbital (Figure 5.1). Due to the difficulties in rationalising hypervalent molecules with p-block centres, this π acceptance was originally thought to involve donation into vacant d-orbitals on the P atom,[526,527] however this has since been discredited.[528] A thorough review of metal phosphine and metal phosphite complexes has revealed that oxidation of the metal, yielding a reduction in degree of π bonding, increases the M-P bond length and decreases the P-R bond length.[529] This led to the conclusion that $\sigma^*_{P\text{-}R}$ orbitals act as the π acceptor orbital. Due to the inert pair effect, the σ donor orbital of a stibine has more s character and therefore is of lower energy and less directional. This portends that stibines are typically poorer donors than phosphines; the same rationale can be applied to arsine and bismuthine ligands. The heavier pnictogen analogues are also weaker π acceptors due to lower electronegativities and more diffuse orbitals.[87]

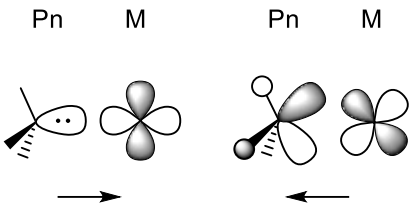

Figure 5.1. σ donation from a pnictine (Pn) lone pair to transition metal centre (M) (left) and π backbonding from a transition metal to a pnictine $\sigma^*_{Pn\text{-}R}$ orbital (right). The arrows show the direction of electron density donation.

Along with electronic parameters, steric properties of pnictine ligands must also be considered to appreciate their impact on transition metal complexes. This is predominantly parameterised with the ligand cone angle, the most common example being the Tolman cone angle, which is defined as the apex angle of a cone with the transition metal at the vertex and the outmost edge of the Van der Waals radii of the ligand as the perimeter of the cone (Figure 5.2).[530–532] The cone angle has important implications for the steric crowding around the transition metal complex and rates of dissociation. While Tolman cone angles are experimentally determined from tetrahedral nickel(0) complexes, computational methods for determining cone angles have become commonplace.[533,534] The Tolman cone angle has been criticised as the simplistic symmetric cone model fails to account for unsymmetrical coordination of phosphines and intermeshing in crowded complexes.[535] The solid angle approach has been proposed as a solution.[535–537] The cone angles of pnictines typically decreases on descending the group due to a greater degree of pyramidalisation (see 1.2.1 Organoantimony (III)).

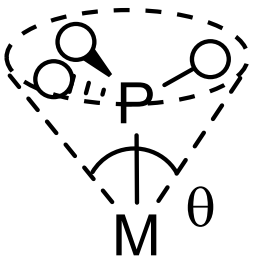

Figure 5.2. Tolman's Cone angle (θ) of a phosphine. M=Transition metals. The white spheres represent the Van der Waal radii of the phosphine substituents.

Unlike phosphines, the C-Sb-C bond angles in stibines typically expand on coordination and a slight elongation of the Sb-C bond lengths is also observed.[538–540] DFT investigations of the bonding of certain systems revealed that the change is due to an increase of the relative amount of 5s character of the Sb-C bonds and p character of the lone pair on coordination.[116,486,541,542]

Like phosphines, the steric and electronic properties of stibines can be tuned by careful selection of the substituents. Trialkylstibines are typically stronger donors than triarylstibines due to the stronger electron donor abilities of alkyl groups in comparison to aryl groups.[543] Unlike phosphine(III) halides, antimony(III) halides as transition metal ligands are extremely rare, with the exception of a pendent $SbCl_3$ on an Au(I) complex,[544] which acts as a Z-ligand, only one example has been structurally characterised, a nickel(II) dithiocarbamate with coordinated SbI_3.[545] Akin to the cone angles, electronic properties of phosphines has been parameterised *via* the Tolman electronic parameters (TEPs).[530] Similarly to cone angles, computational methods and other alternatives have been proposed.[546–548] TEPs have been calculated for a small number of homoleptic and heteroleptic stibines.[549]

A relatively recent trend of identifying organoantimony(III) ligands acting as acceptors *via* secondary interactions, giving formally Lewis amphoteric Sb centres when considered with the Sb→ TM interaction, has emerged.[550] Such Sb centres may be termed hypervalent atoms in reference to the presence of 3 organic substituents, 1 coordinating lone pair and secondary interaction giving an apparent contradiction to the 8 electron rule. This is one point of divergent behaviour between stibines and their lighter analogues, in which such interactions are much rarer. There are two classes of organoantimony(III) ligands which typically display hypervalance in the coordination sphere of a transition metal complex, stibines (R_3Sb) where R typically contains a pendant donor atom and halostibines ($R_{3-n}SbX_n$). Hypervalence is typically observed in uncoordinated ligand for those species with pendant donor atoms (Figure 5.3 a).[551] Alternatively, halides coordinated to the transition metal may also form a Lewis donor/acceptor interaction with coordinated stibines (Figure 5.3 b). This type of hypervalence is commonly observed in coordinated halostibines, which can be attributed to the halogen giving a low lying $\sigma^*_{Sb\text{-}X}$ orbital.[552]

a) b)

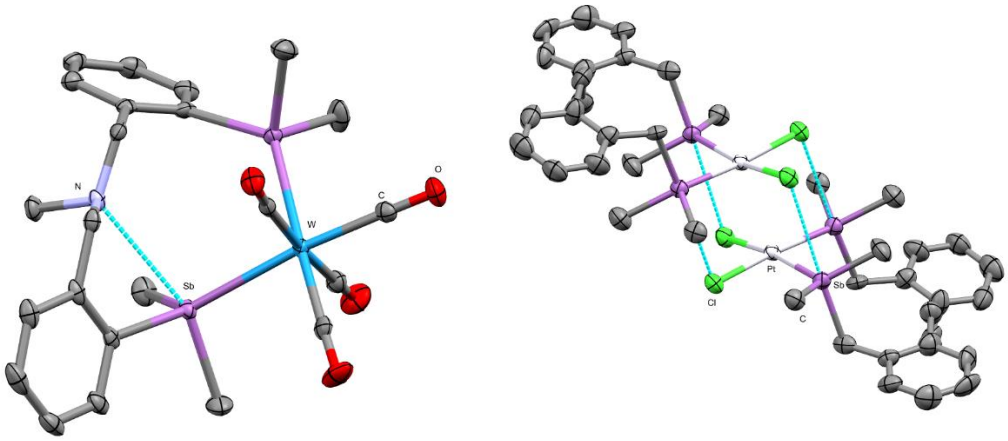

Figure 5.3. a) Solid state structure of $[W(CO)_4\{MeN(CH_2\text{-}2\text{-}C_6H_4SbMe_2)_2\}]$. Redrawn from ref 553. Intramolecular Sb···N interactions shown as blue dotted lines. b) Solid state structure of -$[PtCl_2(\{CH_2(2\text{-}C_6H_4CH_2SbMe_2)\}_2)]$. Redrawn from ref 554. Intermolecular Sb···Cl interactions shown as blue dotted lines.

5.1.2. Group 10 Complexes with Stibine Ligands

Ni(II) stibine complexes are rare. $[Ni(\eta^3\text{-}CH_2C(R)CH_2)(Ph_3Sb)_3][BAr^F]$ (R = CH_3, H) and other similar complexes are active catalysts for oligomerisation of styrenes.[555–563] A series of heteroleptic and homoleptic stibines were investigated as series to elucidate their impact on the geometry of complexes; yielding square planar complexes of the form $[NiI_2(R_2R'Sb)_2]$ (R= R'= ^{i}Pr; R= ^{i}Pr, R'= Ph) and trigonal pyramidal $[NiI_2(R_2R'Sb)_3]$ (R= Me, R'= Ph; R= Ph, R'= Me); these complexes were utilised as precursors for NiCu alloys.[549] A series of five-coordinate complexes with trimethylstibine, $[NiX_2(Me_3Sb)_3]$ (X = Cl, Br, I, Me_3Sb) and $[Ni(Me_3Sb)_5][BF_4]_4$, have been prepared.[564,565] $[Ni((2\text{-}(Ph_2P)C_6H_4)_3Sb)(PPh_3)]$ serves as a particular noteworthy example of a Ni(II) stibine; the stibine can best be described as a L-ligand although oxidation by $PhICl_2$ to yields $[NiCl((2\text{-}(Ph_2P)C_6H_4)_3SbCl)]$, were the stibine is a X-ligand (Scheme 5.1).[566] Reaction with catechol gives a cationic Ni complex, $[Ni((2\text{-}(Ph_2P)C_6H_4)_3Sb(1,2\text{-}C_6H_4O_2))(CyCN)]$; here the stibine acts as a Z-ligand.

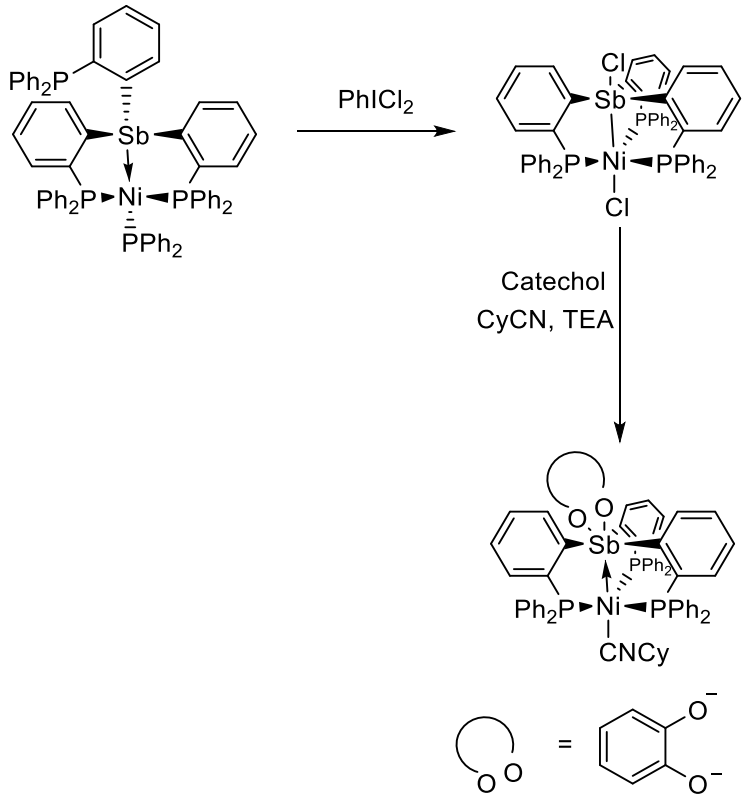

Scheme 5.1. Oxidation of [Ni((2-(Ph_2P)C_6H_4)$_3$Sb)(PPh_3)] to yield [NiCl((2-(Ph_2P)C_6H_4)$_3$SbCl)] and reaction with catechol (1,2-$C_6H_4O_2$) to yield [Ni((2-(Ph_2P)C_6H_4)$_3$Sb(1,2-$C_6H_4O_2$))(CyCN)]. TEA=triethylamine.[566]

Most reported palladium/platinum stibine complexes contain a group 10 metal centre in the +2 oxidation state. [$MX_2(R_3Sb)_2$] (M = Pd, Pt; R = Me, Et, ^{n}Pr, ^{n}Bu, Ph, 2-MeC_6H_4, 3-MeC_6H_4, 4-MeC_6H_4; X =Cl, Br, I, NO_2) are typically red/yellow solids which are prepared from either MX_2 or $[MCl_4]^{2-}$ (with a source of X if X ≠ Cl).[567,568,577–581,569–576] For the series of complexes [$MCl_2(R_3Sb)_2$] (M= Pd, R = Ph, Me, ^{n}Pr; M = Pt, R = Me, Et, ^{n}Pr, ^{n}Bu) typically the *cis* isomer is isolated as a solid.[571–574] Both isomers are present in solution, typically favouring the *trans* isomer; for the platinum complexes in benzene, replacing the chloride with iodide or phenyl with alkyl pushes the equilibrium between the *cis* and *trans* isomer to the *trans* side; the antimony complexes contain a higher proportional of *cis* isomer than the Phosphorus or arsenic analogues. A series of mixed NHC/stibine complexes, [$PdCl_2$NHC(Ph_3Sb)] (NHC = IMes, IPr, SIMes, SIPr), are active catalysts in Hiyama cross-coupling reactions and Buchwald–Hartwig aminations.[582]

Tetrastibine Pd(0) [$Pd(Ar_3Sb)_4$] (Ar = Ph, 4-MeC_6H_4, 4-$(MeO)C_6H_4$) complexes have been prepared *via* reduction of [$Pd(acac)_2$] (acac = acetylacetonate) in the presence of the respective stibine.[583] [$Pt(R_3Sb)_4$] has not been reported although the mixed phosphine/stibine complex [$Pt(PPh_3)(Ph_3Sb)_2$] has been prepared.[583] [$M(Ph_3Sb)_n$] (M = Pd,

Pt; n = 2-3) and [{Pt(Ph_3Sb)}$_3N_2$] have been reported although the characterisation of the platinum complexes is incomplete.[88,584,585] Air stable [Pt($^nBu_3Sb$)$_4$] was prepared from [Pd(cod)$_2$] (cod = 1,5-Cyclooctadiene).[586]

5.1.3. Bridging Stibine Ligands

Bridging pnictine ligands are extremely rare; the first example was reported in 1994 by Werner and consists of a μ_2-$^iPr_3Sb$ ligand linking two RhCl fragments alongside two bridging carbenes (Scheme 5.2).[587] Several acetylacetonato derivatives of this complex have been prepared and well as derivatives, including the first examples of μ_2-bridging phosphines and arsines, where the $^iPr_3Sb$ ligand has been displaced by other bases (R_3Sb, ^{t}BuCN, R_3P, R_3As, CO); in each case the bridging motif is retained.[588–590]

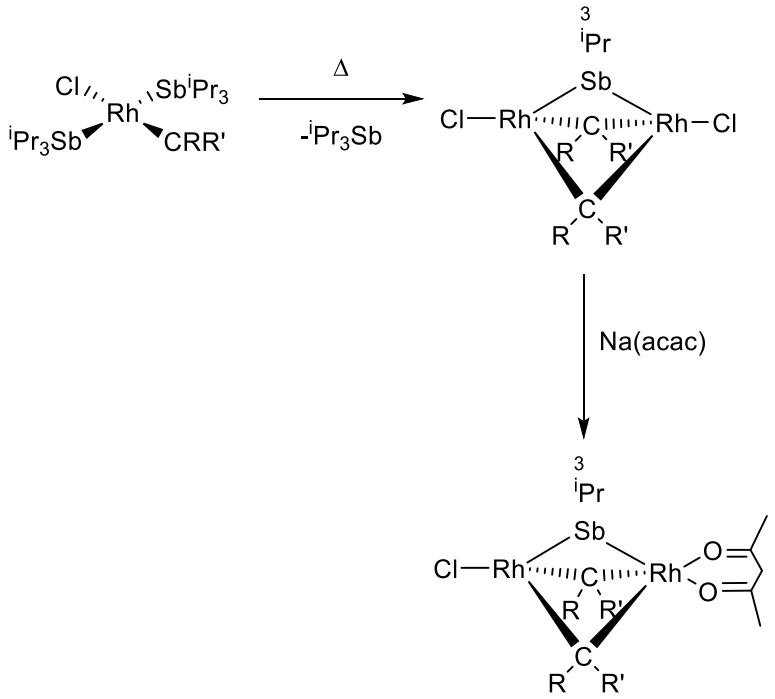

Scheme 5.2. Synthesis of [(RhCl)$_2$(μ_2-$^iPr_3Sb$)(μ_2-CRR')$_2$] by heating [RhCl(($^iPr_3Sb$)$_2$(CRR')] in benzene (R = p-Tol, Ph). Addition of Na(acac) yields [(RhCl)(Ph(ACAC))(μ_2-$^iPr_3Sb$)(μ_2-CRR')$_2$] (acac = acetylacetonato).[587]

One of the most unexpected stibine complex reported recently and the topic of further study in this body of work is [Pd_4(μ_3-Me_3Sb)$_4$(Me_3Sb)$_4$],[280] a rare example of a homopletic complex with bridging pnictine ligands. [587,588,591] The complex contains a Pd_4 tetrahedron core with a terminal Me_3Sb on each Pd atom and a μ_3-Me_3Sb capped each face of the tetrahedron core (Figure 5.4). [Pd(Me_3Sb)$_8$] was obtained from [Pd_2Cl_4(Me_2SbCl)$_4$] and eight equivalents of MeLi (Scheme 5.3, *vide infra*). Spectroscopic evidence suggests the solid-state structure is retained in solution.

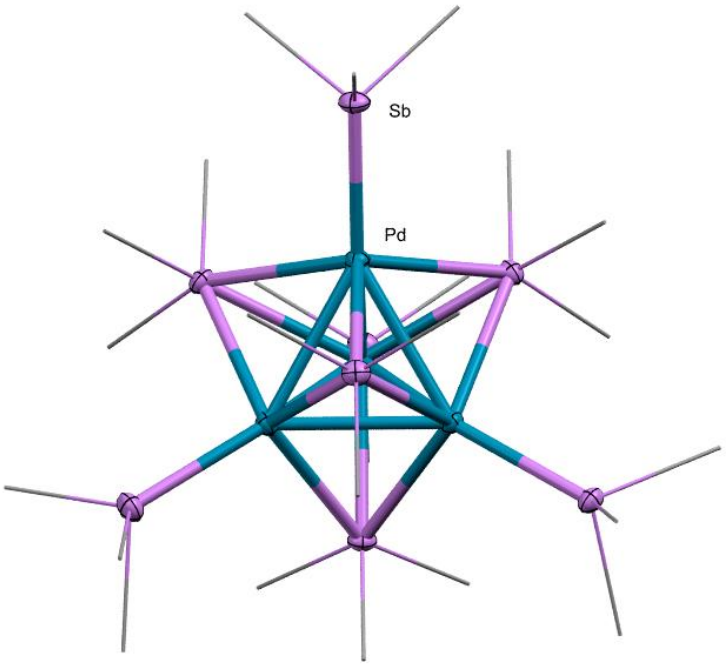

Figure 5.4. Solid state structure of $[Pd_4(\mu_3\text{-}Me_3Sb)_4(Me_3Sb)_4]$. Ellipsoids shown at 50% probability and hydrogen atoms omitted. Methyl groups are shown in wireframe. One stibine ligand is disordered, only one position is shown. Figure redrawn from ref 280.

The formal electron count is 56, which is below the predicted 60 for a tetrahedron with localised bonding; electron deficient Pd/Pt tetrahedrons are known.[592–595] Energy decomposition analysis (EDA) suggests that the bonding interaction for both types of ligand is primarily electrostatic (70 – 75%).[280] Of the orbital contribution, both σ-donation (Sb → Pd) and π-back bonding (Pd → Sb) are significant. Dispersion interaction also significantly contributes to the stability of the complex.

5.1.4. Aims and Objectives

The aims of this body of work are to further understand the formation of $[Pd_4(Me_3Sb)_8]$ and develop a more extensive understanding of its reactivity. This body of work will aim to improve current synthetic routes to $[Pd_4(Me_3Sb)_8]$ and will seek to further understand its reactivity with Lewis basic molecules. Previous work in the group gave preliminary validation of a 'one-pot strategy' to $[Pd_4(Me_3Sb)_8]$ from 1 equivalent of $[PdCl_2(MeCN)_2]$, 2 equivalents of $SbCl_3$ and 8 equivalents of MeLi and investigated the reactivity on $[Pd_4(Me_3Sb)_8]$ with phosphines.

The specific objectives of this body of work are:

a) Develop a higher yielding and more facile route to $[Pd_4(Me_3Sb)_8]$ than current routes.

b) Experimentally investigate the mechanism of the formation of $[Pd_4(Me_3Sb)_8]$ from the current and any new 'one-pot' routes.

c) Probe the reactivity of $[Pd_4(Me_3Sb)_8]$ with a range of phosphines to elucidate a rationale for the varying reactivities.

d) Explore the reactivity of $[Pd_4(Me_3Sb)_8]$ with other Lewis basic ligands.

e) Probe oxidative addition of organic halides to $[Pd_4(Me_3Sb)_8]$.

5.2. Results and Discussion

5.2.1. Synthesis of $[Pd_4(Me_3Sb)_8]$

A thorough investigation of the reactivity of $[Pd_4(Me_3Sb)_8]$ (**4-1**) has previously been precluded by a poorly yielding (overall yield from $PdCl_2(MeCN)_2$ = 28%) and multistep synthesis (Scheme 5.3).[280]

a) $2SbCl_3 + Ph_3Sb \longrightarrow 3PhSbCl_2$

$PhSbCl_2 \xrightarrow[M=MgBr,\ Li]{MeM} PhMe_2Sb$

$PhMe_2Sb \xrightarrow{HCl_{(g)}} Me_2SbCl$

b) $PdCl_2(MeCN)_2 + 2Me_2SbCl \longrightarrow$

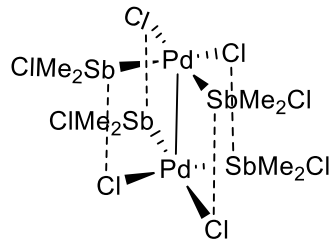

8MeLi

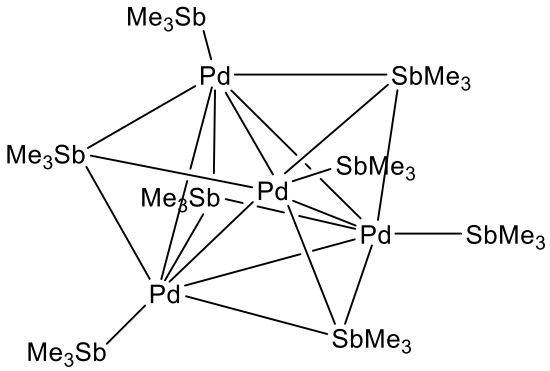

4-1

Scheme 5.3. a) Synthesis of Me_2SbCl.[510] and b) Synthesis of dimeric $[PdCl_2(Me_2SbCl)_2]_2$ conditions: benzene, 20 mins (top) and synthesis of $[Pd_4(Me_3Sb)_8]$ conditions: THF, -89°C → room temperature, 30 mins (bottom).[280]

To circumvent this, a more facile synthetic route to **4-1** was targeted. Previous work in the group has investigated the addition of 2 equivalents of MeLi to $[PdCl_2(Me_3Sb)_2]$ and a 'one-pot' approach to yield **4-1**, however no higher yielding synthetic strategies were

elucidated.[596] The 'one-pot' approach previously utilised involved the addition of 8 equivalents of MeLi to a suspension of $SbCl_3$ and $PdCl_2$ in a 2:1 molar ratio in Et_2O and either dried *in vacuo*, extracted into n-hexane and briefly refluxed, or briefly refluxed before removing the Et_2O *in vacuo* and extracting into n-hexane.[596] These procedures yielded **4-1** in 18% and 9% yield respectively. In both cases metallic deposits were observed. Mechanistically these procedures were hypothesised to occur *via* the *in-situ* formation of Me_3Sb, coordination of the stibine to the Pd centre, methylation of Pd followed by reductive elimination of ethane (Scheme 5.4). Similar mechanisms are known for palladium phosphine complexes.[597]

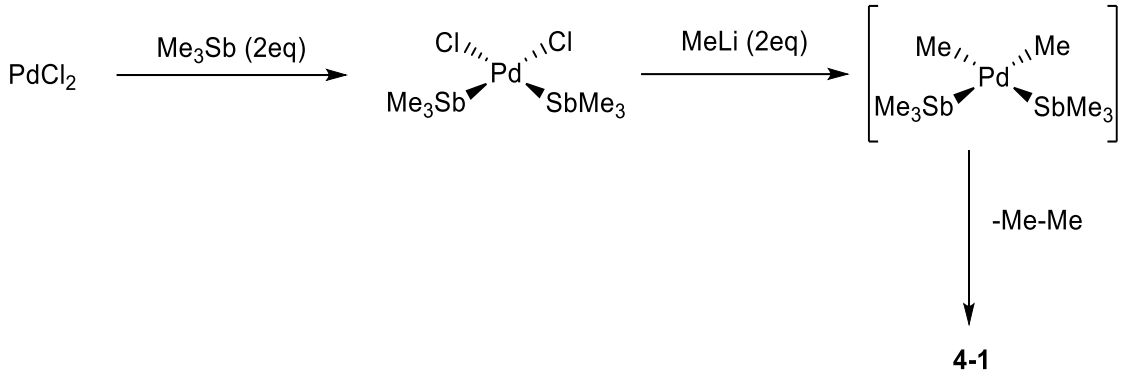

Scheme 5.4. Hypothesised mechanism for the formation of $[Pd_4(Me_3Sb)_8]$ (**4-1**) via the 'one-pot' method.

Based on this hypothesised mechanism it was rationalised that the poor yield in previously reported 'one pot' reactions was based on a simultaneous side reaction where the Pd centre is methylated before either the formation of Me_3Sb or the coordination of the stibine, yielding transient Me_2Pd which rapidly reductively eliminates ethane and forms metallic Pd^0. To circumvent this, it was hypothesised that by utilising a base stabilised and more soluble source of Pd^{II}, $[PdCl_2(MeCN)_2]$, this 'early' reduction could be avoided. This strategy increased the isolated yield of **4-1** to 40% and did not yield any observable metallic deposits. As an alternative strategy, the reduction of $[PdCl_2(Me_3Sb)_2]$ was targeted; adding potassium yielded the formation of a metallic precipitate and the addition of NaH to $[PdCl_2(Me_3Sb)_2]$ did not yield any reactivity.

In comparison, the same synthetic procedure, utilising $PdCl_2$ instead of $[PdCl_2(MeCN)_2]$ yielded **4-1** in much lower yield. An additional impurity was observed *via* ^1H NMR spectroscopy and visually as a brown solid which co-crystallised, with **4-1**, as an amber block crystals which were identified as $[Pd_3(Me_3Sb)_7]$ (**4-2**) by SCXRD. The complex can be described as cluster with a trigonal planer Pd_3 core with a capping μ^3-(Me_3Sb), 3 terminal

Me_3Sb ligands and 3 μ^2-(Me_3Sb) ligands (Figure 5.5). Compound **4-2** is the only known example of a transition metal complex with terminal, μ^2- and μ^3- pnictine ligands. The mean Pd-(μ^2-$SbMe_3$) bond distances in **4-2** (2.6934(10) Å) are comparable to that in the [$Rh_2Cl_2\mu^2$-($^iPr_3Sb$)μ^2-(CPh_2)$_2$] (2.6782(5) Å).[587] The $Pd(0)_3$ triangle motif has been reported, typically with terminal phosphine, isocyanide or carbene ligand and μ^2- halides, carbonyl, thiolate or phosphido ligands.[598–602] The Pd-Sb bond distances are comparable to **4-2** (Table 5.1). Compound **4-2** was not isolated in bulk as it was present in minor quantities. The ratio of Pd/Me_3Sb in 1:2 in **4-1** whereas it is 3:7 in **4-2**, thus some reduction of $PdCl_2$ to Pd^0 would potentially bring the ratio of Pd/Me_3Sb closer to 3:7 and allow for the formation of **4-2**. However, a targeted synthesis of **4-2**, with a 3:7 molar ratio of [$PdCl_2(MeCN)_2$]:$SbCl_3$ did not yield **4-2** but rather **4-1.**

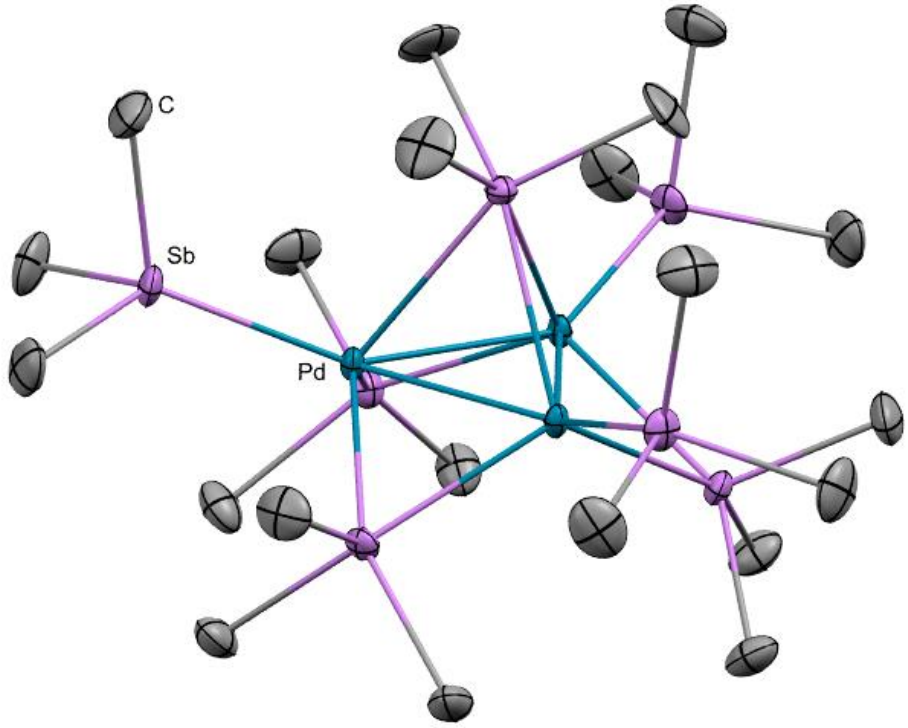

Figure 5.5. Solid state structure of [$Pd_3(Me_3Sb)_7$] (**4-2**). Ellipsoids shown at 50% probability. Hydrogen atoms have been omitted.

Table 5.1. Structural parameters of **4-1** and **4-2**. *The value is a mean of crystallographically inequivalent parameters. ^ Bonds with disordered atoms were omitted.

Structural Parameter	**$[Pd_4(Me_3Sb)_8]$ (4-1)**	**$[Pd_3(Me_3Sb)_7]$ (4-2)**
Pd-Pd distance	2.805 Å *	2.7534(17) Å
terminal-(Me_3Sb)-Pd Distance	2.520 Å *	2.5255(14) Å
μ^2-(Me_3Sb)-Pd Distance	N/A	2.6934(10) Å *
μ^3-(Me_3Sb)-Pd Distance	2.773 Å *	2.7729(17) Å
Terminal-Sb-C	2.16 (1) *^	2.14(2) Å *
μ^2-Sb-C	N/A	2.16(2) Å *
μ^3-Sb-C	2.16(1) *	2.159(19) Å

The mechanism of the formation of $[Pd_4(Me_3Sb)_8]$ (**4-1**) in this 'one-pot' synthesis was further investigated. performing an approximately equivalent reaction with the phosphine analogue by the addition of two equivalents of MeLi to one equivalent of $[PdCl_2(MeCN)_2]$ and two equivalents of PMe_3 and heating in an equivalent way to the 'one-pot' strategy yielded a white crystalline solid which was spectroscopically identified as *cis*-$[PdMe_2(PMe_3)_2]$ (**4-3**). While spectroscopic details for this complex are known[517], the solid state structure was previously unknown. Cooling a concentrated hexane solution of crude $[PdMe_2(PMe_3)_2]$ to -18°C yielded colourless crystals which were identified as *cis*-$[PdMe_2(PMe_3)_2]$ by SCXRD however the data quality was poor precluding an extensive structural analysis. The isolation of **4-3** gives greater credence to the mechanism proposed in Scheme 5.4. The fact that the hypothesised $[PdMe_2(Me_3Sb)_2]$ reduces to the Pd^0 species **4-1** whereas the phosphine analogue remains as $[PdMe_2(PMe_3)_2]$ (**4-3**) can be rationalised in terms of the phosphine ligands being better donors are thus more readily able to stabilise the more electron deficient Pd(II) state.

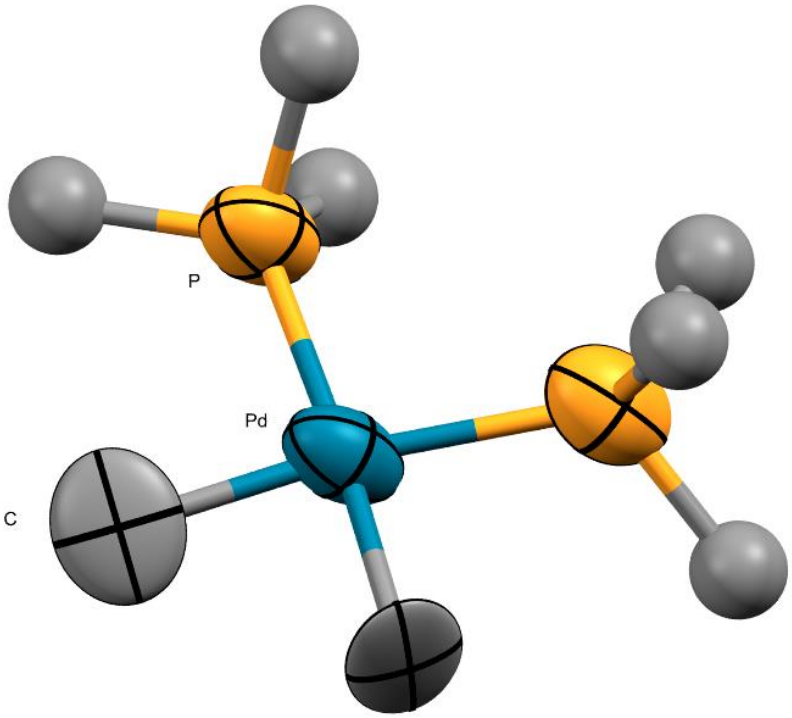

Figure 5.6. Solid state structure of cis-[$PdMe_2(PMe_3)_2$] (**4-3**). Ellipsoids shown at 50% probability, phosphine carbons are shown in ball and stick. Hydrogen atoms have been omitted.

An NMR monitoring of the formation of [$Pd_4(Me_3Sb)_8$] (**4-1**) was carried out in an endeavour to observe transient [$PdMe_2(Me_3Sb)_2$]. Unsolvated MeLi was synthesised according to modified literature procedures.[603,604] Combining [$PdCl_2(MeCN)_2$] (1 eq.), $SbCl_3$ (2 eq.) and MeLi (8 eq.) in THF-d8 under the same conditions as the bulk synthesis (*vide supra*) did not yield **4-1.** Initially, this was hypothesised to be due to inaccuracies in weighing small amounts; to interrogate this possibility, a bulk synthesis of **4-1** was carried out using the unsolvated MeLi which was synthesised in house instead of commercially purchased solutions of MeLi in Et_2O. This did not yield **4-1** but rather multiple products by NMR, crystals of *cis*-[$PdCl_2(Me_3Sb)]\cdot SbCl_3$ (Figure 5.7) were isolated from a DCM solution of the reaction mixture.

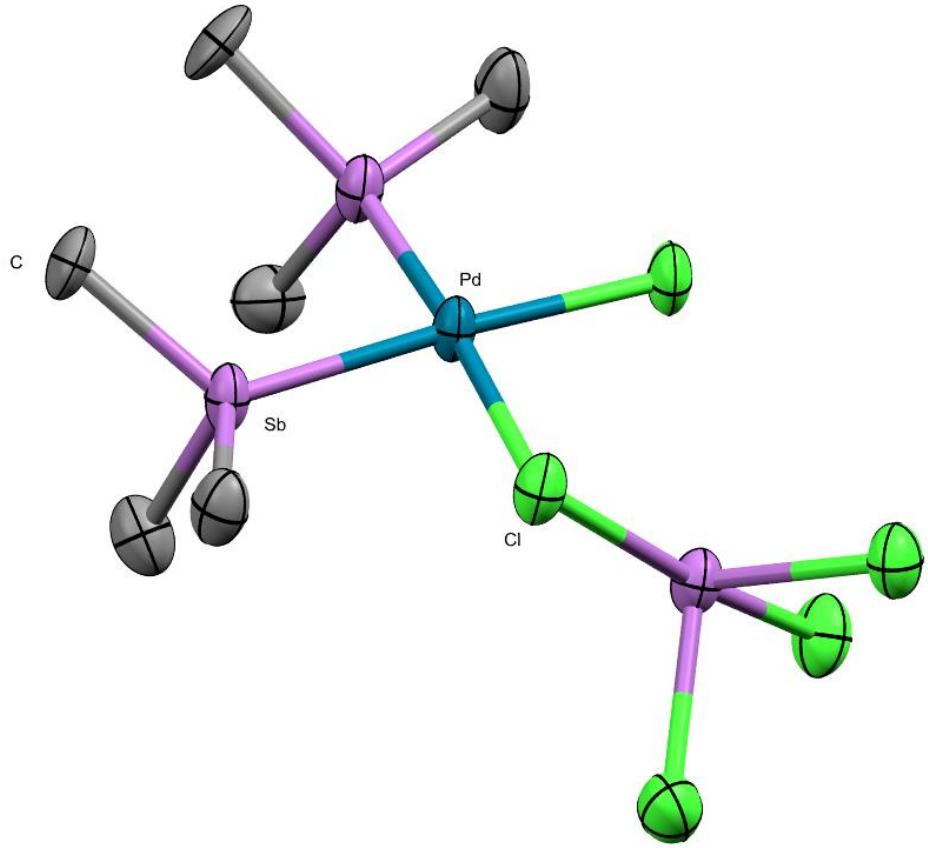

Figure 5.7. Solid state structure of $[PdCl_2(Me_3Sb)]\cdot SbCl_3$, only the asymmetric unit is shown. Ellipsoids shown at 50% probability. Hydrogen atoms and co-crystalised solvent have been omitted.

The structure of *cis*-$[PdCl_2(Me_3Sb)]\cdot SbCl_3$ has some noteworthy features; the solid state structure consists of 1D chains which are build up through two hypervalent motifs (Figure 5.8).

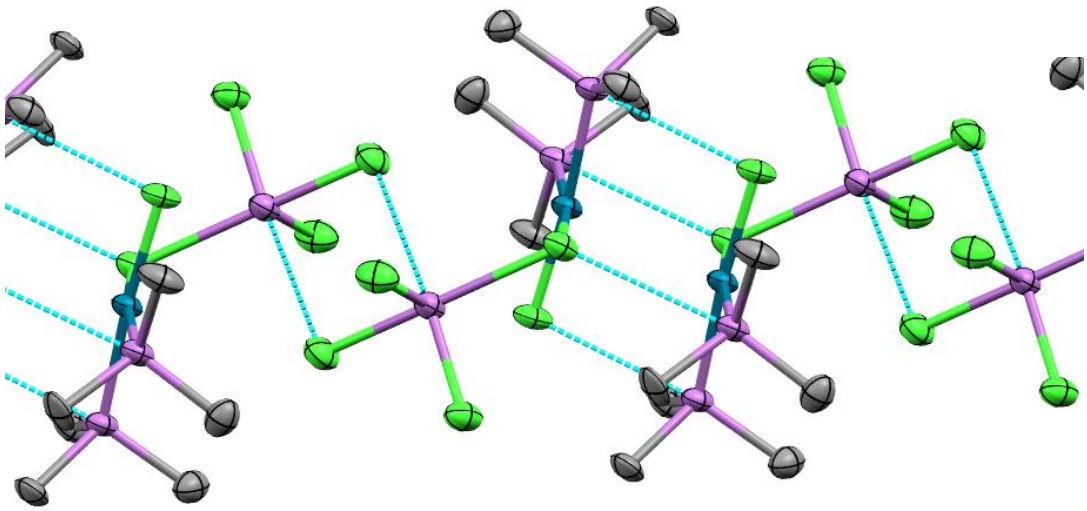

Figure 5.8. Solid state structure of $[PdCl_2(Me_3Sb)]\cdot SbCl3$, showing the 1D supramolecular chain. Ellipsoids shown at 50% probability. Hydrogen atoms and co-crystalised solvent have been omitted.

The $SbCl_3$ unit coordinates to one of the palladous chlorides and forms two Sb···Cl interactions (3.256(3) Å) to a neighbouring $SbCl_3$ unit, giving a square pyramidal Sb centre (Figure 5.9).

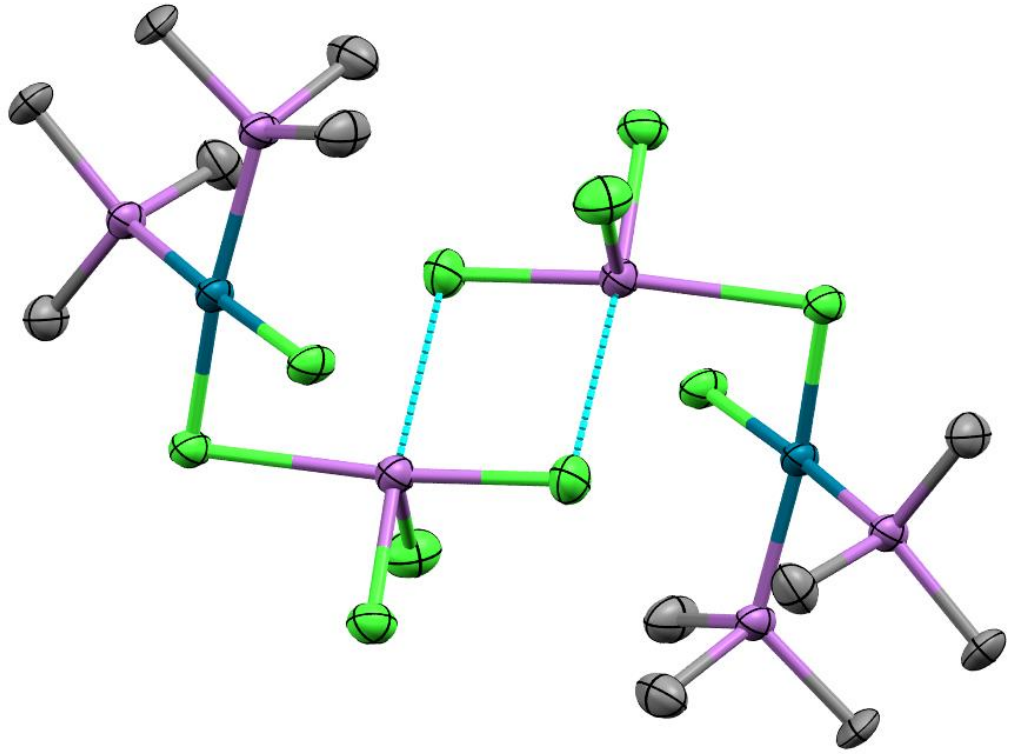

Figure 5.9. Solid state structure of $[PdCl_2(Me_3Sb)]\cdot SbCl_3$, showing the Sb···Cl interactions between neighbouring $SbCl_3$ units. Ellipsoids shown at 50% probability. Hydrogen atoms and co-crystalised solvent have been omitted.

Secondly, the coordinated Me_3Sb ligands form a close contact with the palladous chlorides of a neighbouring $[PdCl_2(Me_3Sb)_2]$ unit (Figure 5.10). The Sb···Cl distance is elongated for the chloride which coordinated to $SbCl_3$ (3.584(3) Å vs 3.725(2) Å). This is reminiscent of the structure of *cis*-$[Pd_2Cl_4(Me_2SbCl)_4]$, which forms dimers in the solid state through a similar hypervalent interaction (Scheme 5.3).[280,552] the Cl···Sb-Me bond angles deviate from linear (169.8 (3)° and 168.0 (4)°) whereas the Cl···Sb-Cl bond angles in *cis*-$[Pd_2Cl_4(Me_2SbCl)_4]$ are nearly linear. This suggests the Sb···Cl interaction may be more electrostatic rather than evoking the orbital rationale ($LP_{Cl}\rightarrow\sigma^*_{Sb\text{-}Cl}$) explanation used to rationalise the hypervalence in *cis*-$[Pd_2Cl_4(Me_2SbCl)_4]$.[280,552] *cis*/*trans*-$[PdCl_2(Me_3Sb)_2]$ does not have such interactions in the solid state.[596] This is an usual example of a triorganostibine with hypervalent interactions in the coordination sphere of a transition metal complex without any pendant donor atoms. Combining $[PdCl_2(Me_3Sb)_2]$ with $SbCl_3$ in yielded a large amount of black precipitate, assumably metallic palladium; crystals of a different polymorph of *cis*-

$[PdCl_2(Me_3Sb)]\cdot SbCl_3$ (**4-4**) were isolated, which was similar except there is a Pd···Pd interaction (3.129(1) Å) and there is no co-crystalised DCM.

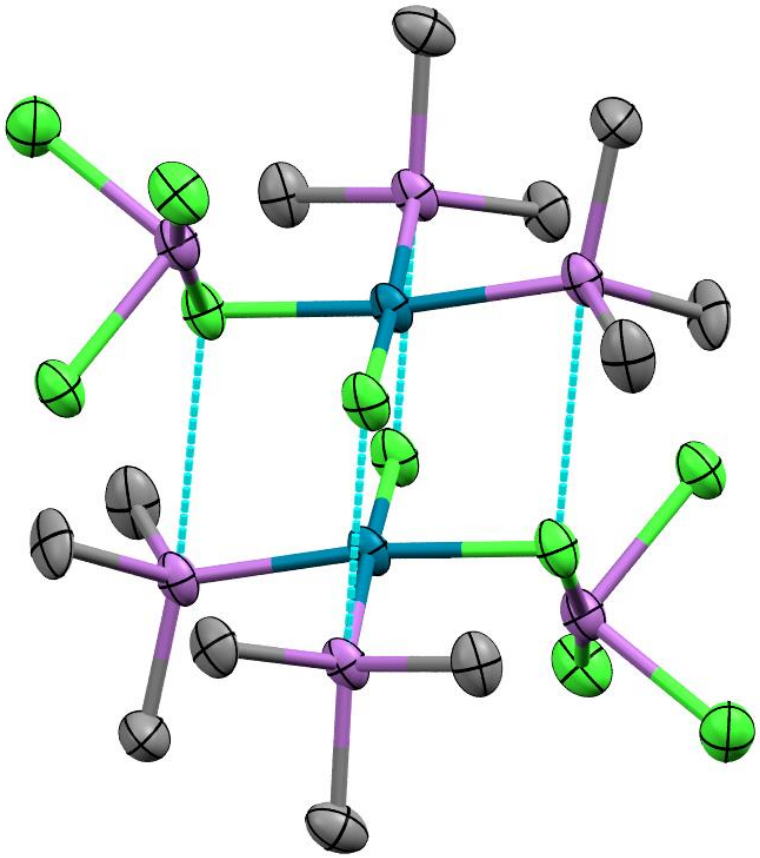

Figure 5.10. Solid state structure of $[PdCl_2(Me_3Sb)]\cdot SbCl_3$ (**4-4**), showing the Sb···Cl interactions between neighbouring $[PdCl_2(Me_3Sb)_2]$ units. Ellipsoids shown at 50% probability. Hydrogen atoms have been omitted.

The isolation of $[PdCl_2(Me_3Sb)]\cdot SbCl_3$ suggests that the MeLi contained a significant amount of inorganic impurities; titration with N-benzylbenzamide found that the powder was only 44% (w/w) pure, which is consistent with literature synthesis of MeLi.[603] Repeating the NMR scale reaction while accounting for the substoichiometric amounts of MeLi in the sample did not give **4-1**, suggesting that the unidentified impurity hindered the formation of **4-1**. Finally, **4-1** was synthesised as per the 'one-pot' (*vide supra*) and reduced *in vacuo* on reaching room temperature to give a reddish oil which was identified as **4-1** by NMR. Exposure to vacuum seemed to promote the formation of **4-1** and precluded the identification of any intermediates.

5.2.2. Reactivity of $[Pd_4(Me_3Sb)_8]$ with Stibines

As part of this work, complexes of the form $[Pd_4(R_3Sb)_8]$ (R≠Me) were targeted. $[Pd_4(Et_3Sb)_8]$ was targeted by the addition of 2 equivalents of MeLi to a mixture of 1 equivalent of $[PdCl_2(MeCN)_2]$ and 2 equivalents of Et_3Sb. This yielded a black/yellow oil

which formed a black precipitate in C_6D_6 and the resulting solution devoid of any non-solvent signals by NMR spectroscopy. The black precipitate can likely be assigned as metallic palladium. Et_3Sb is likely to be electronically similar to Me_3Sb and this absence of any Pd(0) complexes is more likely a steric consequence. As an alternative route to a Pd(0) cluster with Et_3Sb ligands, an exchange of the Me_3Sb ligands in **4-1** with Et_3Sb was targeted. An NMR scale mixture of **4-1** with 4 equivalents of Et_3Sb in C_6D_6 yielded the formation of free Me_3Sb. In contrast to the 2 broad singlets at 0.89 and 1.11 ppm, characteristic of **4-1**, the ^1H NMR spectrum of the mixture contained a signal at 0.89 ppm which remained a singlet, a broad triplet at 1.11 ppm and a complex multiplet at 1.19 ppm. The observation that one signal was unperturbed by the addition of Et_3Sb suggested that Me_3Sb was exchanged at only type of position. From this reaction mixture purple crystals of $[Pd_4(Me_3Sb)_7(Et_3Sb)]$ (**4-5**) were obtained. Compound **4-5** has the same Pd_4 core structure as **4-1** is equivalent to **4-1** except one terminal Me_3Sb ligand has been exchanged for Et_3Sb (Figure 5.11). The Pd-$SbEt_3$ bond length (2.516(2) Å) is comparable to the Pd-(terminal-$SbMe_3$) bond lengths in **4-1** (see Table 5.1).

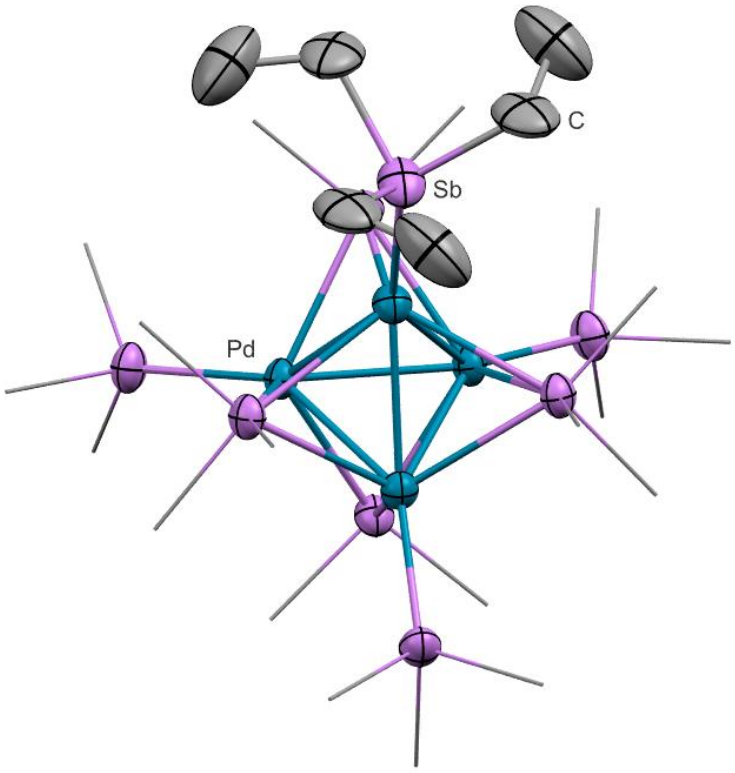

Figure 5.11. Solid state structure of $[Pd_4(Me_3Sb)_7(Et_3Sb)]$ (**4-5**). Ellipsoids shown at 50% probability. Methyl groups are shown in wireframe. The ethyl groups are disordered over two positions, only one is shown. Hydrogen atoms have been omitted.

In contrast, the same reaction with $^{t}Bu_3Sb$ produces no reactivity, most evident by the absence of any free Me_3Sb. This contrasts with $P^{t}Bu_3$ (see 5.2.3. Reactivity of $[Pd_4(Me_3Sb)_8]$ with Phosphines).

5.2.3. Reactivity of $[Pd_4(Me_3Sb)_8]$ with Phosphines

Some exploration of the reactivity of $[Pd_4(Me_3Sb)_8]$ (**4-1**) with phosphines has previously been untaken within the group. *trans*-$[PdClMe(PMe_3)_2]$ was isolated from the reaction of 14 equivalents of PMe_3 with $[Pd_4(Me_3Sb)_8]$, which was synthesised from $[Pd_2Cl_4(Me_2SbCl)_4]$ (Scheme 5.3).[596] Given the absence of chlorides in **4-1** and lack of obvious oxidising agent, it is likely that this is the result of the reactivity of PMe_3 with minor impurities with chloride substituents.[596] Repetition of this reaction with 17 equivalents of PMe_3 yielded a yellow/brown solid with spectroscopically identified coordinated PMe_3 but no obvious signals from coordinated Me_3Sb.[596] As part of this work, of 8 equivalents of PMe_3 were mixed with $[Pd_4(Me_3Sb)_8]$ (**4-1**), yielding a similar yellow/brown solid which was spectroscopically similar to that powder previously isolated within the group. From this, colourless plate crystals were isolated which were preliminarily assigned as the unusual $[PdMe(PMe_3)_3]$ (**4-6**) (Figure 5.12, Scheme 5.5). The Pd—C bond is relatively long (2.315(18) Å), whereas P_3Pd-C are typically between 1.99 and 2.18 Å.[509] The spectroscopic evidence suggests that only one Phosphorus containing species is formed in this reaction, however the palladium methyl has not been observed in either ^{1}H or $^{13}C\{^{1}H\}$ NMR specta, typically giving a ^{1}H NMR signal between 0.5 and 1.1 ppm in ^{1}H NMR specta,[605] suggesting this might be a minor product.

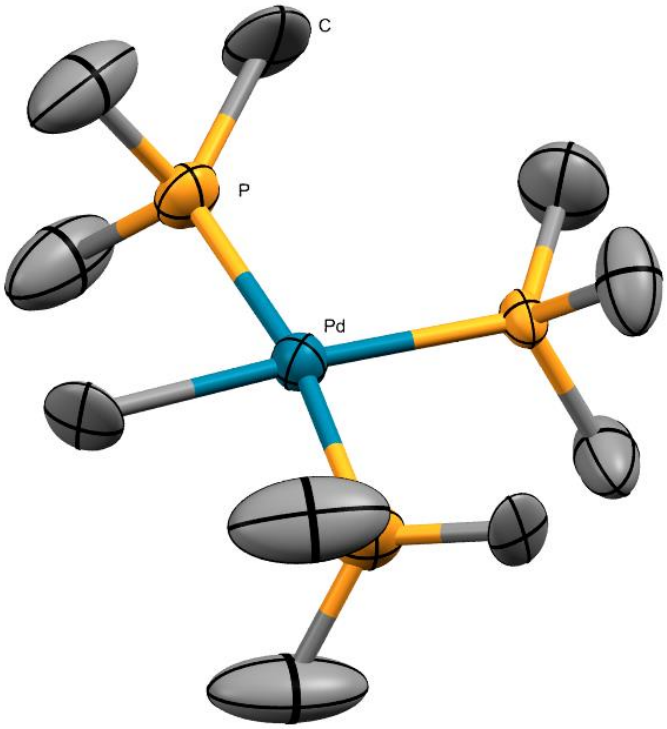

Figure 5.12. Solid state structure of [PdMe(PMe_3)$_3$] (**4-6**). Ellipsoids shown at 50% probability. Hydrogen atoms have been omitted. Two PMe3 ligands are disordered, only one position is shown.

Previous work in the group demonstrated that [Pd(PPh_3)$_2$(Me_3Sb)$_2$] could be obtained by reacting 8 equivalents of PPh_3 with **4-1,** giving [Pd(PPh_3)$_4$] as a side product.[596] As part of this work, it was established that mixing equimolar amounts of **4-1** with [Pd(PPh_3)$_4$] also yielded [Pd(PPh_3)$_2$(Me_3Sb)$_2$] (Scheme 5.5 g). This is consistent with the fact that PPh_3 ligands on [Pd(PPh_3)$_4$] are labile.[606]

An NMR monitoring of a mixture of 8 equivalents of P^{t}Bu$_3$ with an equivalent of **4-1** in C_6D_6 showed the slow formation of [Pd(P^{t}Bu$_3$)$_2$] (Scheme 5.5).[607] This is in contrast to ^{t}Bu$_3$Sb, which does not react with **4-1**. P^{t}Bu$_3$ and ^{t}Bu$_3$Sb have Tolman cone angles of 187° and 175° respectively;[531,608] suggesting that this divergent reactivity can not just be rationalised by steric considerations. Using a slight excess of the cluster gave the same reactivity, suggesting that this can not be attributed just to the use of excess of P^{t}Bu$_3$.

Other phosphines were also screened for reactivity. Bis(diphenylphosphino)methane (dppm) was mixed with **4-1** to yield a red/yellow solid. This solid was found to consist of residual **4-1** mainly (Scheme 5.5 e). Analysis of the solid by $^{31}P\{^1H\}$ NMR spectroscopy contained a single signal (δ_P = 22.44 ppm), which is consistent with a palladium(0) coordinated phosphine however it was not identified by ^{1}H NMR, suggesting that it is either present in minor quanties or is poorly soluble in C_6D_6 and CD_2Cl_2.[606] The equivalent reaction

with 1,4-bis(diphenylphosphino)butane (dppb) gave a similar result (Scheme 5.5 f). The equivalent reaction with XantPhos produced [Pd(XantPhos)$_2$] (Scheme 5.5 d).

While a number of P/Sb mixed donor ligands are known, heteroleptic Pd/Pt complexes with monodentate stibines and phosphines are rare; no such Pd(0)/Pt(0) complexes have been structurally characterised by SCXRD except for [Pd(PPh$_3$)$_2$(Me$_3$Sb)$_2$] (*vide supra*).[596] Complexes of the form [Pd(PPh$_3$)$_2$(Ar$_3$Sb)$_2$] (Ar = Ph, p-Tolyl) and [Pt(PAr$_3$)$_2$(Ar'$_3$Sb)$_2$] [Pt(PPh$_3$)$_2$(Ar$_3$Sb)$_2$] (Ar = Ph, p-Tolyl, SPh) have been prepared by addition of the respective stibine to the zerovalent palladium/platinum phosphine complex.[583]

Trimethylphosphite (P(OMe)$_3$) reacts with **4-1** to yield a white powder which did not contain any signals on analysis by NMR spectroscopy, suggesting decomposition to inorganic compounds (Scheme 5.5 b).

a) $[Pd_4(Me_3Sb)_8] + 8PMe_3 \longrightarrow [PdMe(PMe)_3]$

b) $[Pd_4(Me_3Sb)_8] + exP(OMe)_3 \longrightarrow$ Decomposed

c) $[Pd_4(Me_3Sb)_8] + 8P^tBu_3 \longrightarrow [Pd(P^tBu_3)_2]$

d) $[Pd_4(Me_3Sb)_8] + 4XantPhos \longrightarrow [Pd(XantPhos)_2]$

e) $[Pd_4(Me_3Sb)_8] + 4dppm \longrightarrow$ Residual $[Pd_4(Me_3Sb)_8]$ + Unidentifed minor products

f) $[Pd_4(Me_3Sb)_8] + 4dppb \longrightarrow$ Residual $[Pd_4(Me_3Sb)_8]$ + Unidentifed minor products

g) $[Pd_4(Me_3Sb)_8] + [Pd(PPh_3)_4] \longrightarrow [Pd(PPh_3)_2(Me_3Sb)_2]$

f) $[Pd_4(Me_3Sb)_8] + 8PPh_3 \longrightarrow [Pd(PPh_3)_2(Me_3Sb)_2]$

XantPhos = 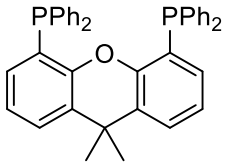

dppm =

dppb = 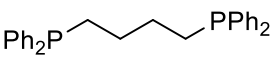

Scheme 5.5. Reactivity of [Pd$_4$(Me$_3$Sb)$_8$] (**4-1**) with a variety of phosphines. N.B. f) represents previous work in the group.[596]

5.2.4. Other Reactivity of [Pd$_4$(Me$_3$Sb)$_8$]

Reacting [Pd$_4$(Me$_3$Sb)$_8$] (**4-1**) with two equivalents of IMes (1,3-Dimesitylimidazol-2-ylidene) yielded [Pd(IMes)$_2$] with the liberation of Me$_3$Sb by NMR without the observation of any Pd-Me$_3$Sb containing intermediates.

Attempted oxidation of **4-1** with 4 equivalents of bromobenzene in C_6D_6 instantly gave a deep red solution. NMR spectroscopy showed the formation of a broad singlet (δ^{1H} = 0.64 ppm) and an additional set of phenyl signals. The broad singlet would be consistent with either free Me_3Sb or labile Me_3Sb ligands. The formation of free Me_3Sb would not be consistent with the oxidative addition of PhBr to **4-1** to yield [$PdPhBr(Me_3Sb)_2$]**.** No organopalladium(II) complexes with alkylstibine ligands have been reported to allow for spectroscopic comparison and the lack of SCXRD characterisation of the products of this reaction preclude definite assignment of this reactivity.

5.3. Conclusions

This body of work has presented an advancement in the knowledge of the chemistry of $[Pd_4\mu_3\text{-}(Me_3Sb)_4(Me_3Sb)_4]$ (**4-1**), a rare palladium(0) stibine complex first reported in 2015.[280] The reported synthesis involves the addition of 8 eq of MeLi to *cis*-$[Pd_2Cl_4(Me_2SbCl)_4]$ and previous work in the group elucidated a poorly yielding 'one-pot' synthesis from the methylation of a mixture of $PdCl_2$ and $SbCl_3$. This 'one-pot' synthesis has been optimised as part of this work, allowing for a more thorough analysis of the reactivity of **4-1**. Experimental evidence suggests that this occurs *via* an *in-situ* methylation of $SbCl_3$ to give Me_3Sb as well as a methylation of the formed $[PdCl_2(Me_3Sb)_2]$ to give $[PdMe_2(Me_3Sb)_2]$ which rapidly eliminates ethane to give a Pd(0) species which formed the tetrameric **4-1**; $[PdMe_2(Me_3Sb)_2]$ has not been observed previously or as part of this work. In the course of this work, a side product, $[Pd_3\mu_3\text{-}(Me_3Sb)\mu_2\text{-}(Me_3Sb)_3(Me_3Sb)_3]$ (**4-2**) was observed, this is the first example of a transition metal complex with terminal, μ2- and μ3- pnictine ligands. Similarly, *cis*-$[PdCl_2(Me_3Sb)]\cdot SbCl_3$ was serendipitously isolated and is a rare example of triorganostibine ligands displaying hypervalence in the coordination sphere of a transition metal complex without any pendent donor atoms.

A diverse range of **4-1**'s reactivity with phosphines and other Lewis bases was observed including that which breaks up **4-1** Pd_4 core yielding PdP_2, PdP_2Sb_2 and PdP_3C coordination sphere as well as a limited ligand exchange with Et_3Sb.

While there is likely scope for **4-1** as part of palladium catalyzed reactivity, this field has been thoroughly interrogated, although this has not been investigated for complexes with bridging stibine ligands. A more fruitful approach to future work would be an investigation of the fundamental coordination chemistry at play for complexes with bridging stibine ligands and the development of a predictive framework for the conditions that yield bridging stibine ligands. Given that **4-1,** which was the first example of a bridging pnictine in a homoleptic stibine complex, was reported in 2015, it is reasonable to consider complexes bridging pnictines as a chemical oddity rather than a feature that can be predictably targeted. It is important to consider this in light of the historic neglect of the coordination of heavier group 15 elements and it is possible that more will come to light with a more complete exploration of the coordination chemistry of trialkylstibine complexes.

5.4. Experimental

See Appendix I: General Experimental Methods for general experimental information.

$[Pd_4(Me_3Sb)_8]$ (**4-1**)

A 1.6 M solution of MeLi in Et_2O (5.0 mL, 8.00 mmol) was added dropwise to an orange suspension of $[PdCl_2(MeCN)_2]$ (0.259 g, 1.00 mmol) and $SbCl_3$ (0.457 g, 2.00 mmol) in THF (50 mL) at -78°C, affecting the instant formation of a light yellow solution. The solution was stirred for a further 15 minutes at -78°C then warmed to room temperature, yielding a light red/yellow solution. The reaction solution was stirred at room temperature for 1 hour then warmed to 60°C, causing the development of a dark red colour. The characteristic dark purple colour started to develop after 10 minutes at 60°C. The solution was stirred for a total of 30 minutes at 60°C, then cooled to room temperature and stirred at room temperature overnight. The solvent was removed *in vacuo* to yield a purple/yellow solid which was extracted into n-hexane (20 mL) and washed with additional n-hexane (3x5 mL), yielding a deep purple solution which was then reduced to ~5 mL and placed in the freezer overnight. A white precipitate formed in the vacuum trap. A crop of purple crystals formed which were separated from the mother liquor by filtrated and dried to a purple crystalline solid (0.180 g, 0.115 mmol, 40%). ^{1}H NMR (400 MHz, C_6D_6): δ ppm 0.89 (s, 36 H) 1.11 (s, 36 H). $^{13}C\{^1H\}$ NMR (101 MHz, C_6D_6) δ ppm 0.6 (s) 8.2 (s) NMR spectra matches literature data.[280]

$[Pd_4(Me_3Sb)_8]$ (**4-1**) Stability *in vacuo*

A solid sample of $[Pd_4(Me_3Sb)_8]$ (~ 5 mg) was exposure to dynamic vacuum ($4x10^{-2}$ mbar) for 1 hour. No visual change occurred. The sample was dissolved in C_6D_6 (0.7 mL) and NMR spectra were measured, which matched the spectra before exposure to vacuum.

$[Pd_4(Me_3Sb)_8]$ (**4-1**) and $[Pd_3(Me_3Sb)_7]$ (**4-2**)

A 1.6 M solution of MeLi in Et_2O (5.0 mL, 8.00 mmol) was added dropwise to an orange suspension of $PdCl_2$ (0.177 g, 1.00 mmol) and $SbCl_3$ (0.457 g, 2.00 mmol) in THF (50 mL) at -78°C, affecting the instant formation of a light yellow solution. The solution was stirred for a further 15 minutes at -78°C then warmed to room temperature, yielding a light red/yellow solution. The reaction solution was stirred at room temperature for 1 hour then warmed to 60°C, causing the development of a dark red colour along with a grey precipitate. The characteristic dark purple colour started to develop after 10 minutes at 60°C. The solution was stirred for a total of 30 minutes at 60°C, then cooled to room temperature and stirred at room temperature overnight. The solvent was removed *in vacuo* to yield a brown/black solid which was extracted into n-hexane (20 mL) and washed

with additional n-hexane (3x5 mL), yielding a deep purple solution which was then reduced to ~5 mL and placed in the freezer overnight. A white precipitate formed in the vacuum trap. A crop of purple crystals and a few of amber crystals formed which were separated from the mother liquor by filtrated and dried to a purple crystalline solid contaminated with traces of amber crystals (0.010 g). ^{1}H NMR (400 MHz, C_6D_6) δ ppm 0.89 (s, 36 H, [$Pd_4(Me_3Sb)_8$]), 0.97 (br s, 27 H), 1.11 (s, 36 H, [$Pd_4(Me_3Sb)_8$]). The purple crystals were identified as [$Pd_4(Me_3Sb)_8$] and the amber crystals were identified as [$Pd_3(Me_3Sb)_7$] by SCXRD. The mother liquour was reduced by ~75% and replaced in the fridge to yield another crop of purple crystals which were dried *in vacuo* (0.015 g). ^{1}H NMR (400 MHz, C_6D_6) δ ppm 0.89 (s, 36 H, [$Pd_4(Me_3Sb)_8$]), 0.97 (br s, 21 H), 1.11 (s, 36 H, [$Pd_4(Me_3Sb)_8$]). $^{13}C\{^{1}H\}$ NMR (101 MHz, C_6D_6) δ ppm 0.6 (s, [$Pd_4(Me_3Sb)_8$]), 1.8 (s), 8.2 (s, [$Pd_4(Me_3Sb)_8$]). The remaining solution was dried to yield a greasy red/yellow solid (0.045 g). ^{1}H NMR (400 MHz, C_6D_6) δ ppm 0.30 (s, 183 H), 0.89 - 0.96 (m, 95 H), 1.11 (s, 36 H). $^{13}C\{^{1}H\}$ NMR (101 MHz, C_6D_6) δ ppm 0.6 (s, [$Pd_4(Me_3Sb)_8$]), 1.8 (s), 8.2 (s, [$Pd_4(Me_3Sb)_8$]). This sample was heavily contaminated with silicone grease.

$PdMe_2(PMe_3)$] (4-3)

PMe_3 (0.0213 g, 0.27 mmol) was added dropwise to a suspension of [$PdCl_2(MeCN)_2$] (0.026 g, 0.10 mmol) in THF (5 mL) at -78°C, yielding a yellow precipitate instantly. 1.6 M MeLi in Et_2O (0.125 mL, 0.2 mmol) was added dropwise to give a yellow solution. The reaction solution was stirred at -78°C for 15 minutes then warmed to room temperature, which gave a colourless solution. The reaction solution was stirred at room temperature for 1 hour then warmed to 60°C. The solution was stirred for a total of 30 minutes at 60°C, then cooled to room temperature and stirred at room temperature overnight. The solvent was removedMe*n vacuo* to yield a white oily solid. ^{1}H NMR (400 MHz, C_6D_6) δ ppm 0.70 (d, J=7.78 Hz, 6 H, [$PdMe_2(PMe_3)_2$]*Pd-Me*), 0.83 (d, J=2.97 Hz, 20 H), 0.91 (d, J=5.95 Hz, 88 H, *trans*-[$PdMe_2(PMe_3)_2$]-*PMe*), 0.94 (s, 55 H). $^{31}P\{^{1}H\}$ NMR (162 MHz, C_6D_6) δ ppm -22.19 (s, *trans* [$PdMe_2(PMe_3)_2$]-*PMe*), -14.13 (s). Cooling a saturated n-hexane solution to -18°C yielded colourless crystals of *cis*-[$PdMe_2(PMe_3)_2$]. *trans* [$PdMe_2(PMe_3)_2$] was identified spectroscopically by comparison to ref [605].

[$Pd_4(Me_3Sb)_7(Et_3Sb)$] (4-5)

A J-young NMR tube was loaded with [$Pd_4(Me_3Sb)_8$] (0.009 g, 0.005 mmol), Et_3Sb (0.005 g, 0.023 mmol) and C_6D_6 (0.7 mL) which gave a dark pink solution. A ^{1}H NMR spectrum were measured. ^{1}H NMR (400 MHz, C_6D_6) δ ppm 0.60 (br s, 1 H, Me_3Sb) 0.89 (s, 3 H) 1.11 (br t, 2 H) 1.14 - 1.28 (br m, 10 H). The solution was removed *in vacuo* to give a pink oil, which was

dissolved in n-hexane (1 mL) and placed in the freezer. No solid formed, which necessitated the further reduction of solvent *in vacuo* to ~0.5 mL and the solution was replaced in the freezer which yielded traces of purple crystals which were determined to be $[Pd_4(Me_3Sb)_7(Et_3Sb)]$ by SCXRD.

$[PdCl_2(Me_3Sb)_2]$

A 1.6 M solution of MeLi in Et_2O (2.5 mL, 4.0 mmol) was added dropwise to a suspension of $SbCl_3$ (0.303 g, 1.33 mmol) in n-hexane (30 mL) at -78°C. The solution was stirred for a further 10 minutes at -78°C then warmed to room temperature, yielding a white precipitate. The reaction solution was stirred at room temperature for 90 mins then filtered through celite into a suspension of $[PdCl_2(MeCN)_2]$ (0.133 g, 0.51 mmol) in hexane (30 mL) at -78°C causing the instant formation of a light yellow powder; stirring at -78°C was continued for 15 mins at which point the reaction solution was warmed to room temperature where stirring was continued for 2 days. The clear solution was filtered from the light yellow precipitate into air, affecting an instant formation of white precipitate. The residue was dried *in vacuo* to give a yellow powder (0.106 g, 0.2 mmol, 48%). ^{1}H NMR (400 MHz, $CDCl_3$) δ ppm 1.22 - 1.25 (m, 2 H, minor unidentified impurity), 1.42 (s, 18 H, $[PdCl_2(Me_3Sb)_2]$), 2.03 (s, 2 H, residual $[PdCl_2(MeCN)_2]$). $^{13}C\{^1H\}$ NMR (101 MHz, C_6D_6) δ ppm 0.2 (s). Major peak at 1.42 ppm in ^{1}H NMR was previously identified as $[PdCl_2(Me_3Sb)_2]$, similar impurities were also observed.[596]

$[PdCl_2(Me_3Sb)_2]$ Stability *in vacuo*

A solid sample of $[PdCl_2(Me_3Sb)_2]$ (~ 5 mg) was exposure to dynamic vacuum ($4x10^{-2}$ mbar) for 1 hour. No visual change occurred. The sample was dissolved in CD_2Cl_2 (0.7 mL) and NMR spectra were measured, which matched the spectra before exposure to vacuum.

Attempted Reduction of $[PdCl_2(Me_3Sb)_2]$ by K

Potassium (≈0.010 g, 0.3 mmol) was added to $[PdCl_2(Me_3Sb)_2]$ (0.010 g, 0.02 mmol) in THF (10 mL) at -78°C, no visual change was observed. The reaction suspension was warmed to room temperature and stirred for 90 mins, over which time the solution darkened, and a precipitate formed. The reaction suspension was heated to 65°C for 20 minutes, which gave a black precipitate. The reaction suspension was cooled to room temperature and stirred overnight then filtered to give a colourless suspension. The suspension was reduced *in vacuo* to traces of a colourless oil, ^{1}H NMR spectroscopy suggested that this oil was residual mineral oil.

Attempted Reduction of $[PdCl_2(Me3Sb)_2]$ by NaH

NaH (0.002 g, 0.08 mmol) in THF (5 mL) was added to $[PdCl_2(Me_3Sb)_2]$ (0.010 g, 0.02 mmol) in THF (10 mL) at room temperature, no visual change observed. The reaction solution was heated to 60°C for 6 hours which gave very little change visually, except for the slight formation of a black precipitate. The reaction solution was reduced *in vacuo* to give a green/yellow solution and black solid. The entire sample was suspended in CD_2Cl_2 (0.7 mL) to give a yellow solution and black solid. The solution was decanted and NMR spectra were obtained. ^{1}H NMR (400 MHz, CD_2Cl_2) δ ppm 1.35 (br s, 20 H), 1.70 (s, 1 H).

$[Pd_4(Me_3Sb)_8]$ (**4-1**) with IMes

A portion of a 0.22 M solution of IMes in C_6D_6 (0.05 mL, 0.012 mmol) was added to a solution of $[Pd_4(Me_3Sb)_8]$ (0.010 g, $5.68x10^{-3}$ mmol) in C_6D_6 (0.6 mL), no obvious charge from the purple solution was observed. A ^{1}H NMR spectrum was measured. ^{1}H NMR (400 MHz, C_6D_6) δ ppm 0.89 (s, 21 H, $[Pd_4(Me_3Sb)_8]$), 1.11 (s, 21 H, $[Pd_4(Me_3Sb)_8]$), 2.16 (s, 18 H, IMes-Me), 6.47 (s, 2 H, IMes-backbone), 6.81 (s, 4 H, Imes-Ar). The solution was then heated to 60°C in a sealed J-Young NMR tube for 30 minutes and another ^{1}H NMR spectrum was measured. 1H NMR (400 MHz, C_6D_6) δ ppm 0.60 (s, 6 H, Me_3Sb), 0.89 (s, 43 H, $[Pd_4(Me_3Sb)_8]$), 1.11 (s, 42 H, $[Pd_4(Me_3Sb)_8]$), 2.05 (s, 8 H, $[Pd(IMes)_2]$-o-Me), 2.16 (s, 25 H, IMes-Me), 2.34 (s, 4 H, $[Pd(IMes)_2]$-p-Me), 6.13 (s, 1 H, $[Pd(IMes)_2]$-backdone), 6.47 (s, 3 H, IMes-backbone), 6.81 (s, 8 H, $[Pd(IMes)_2]$-Ar-H). The solution was heated for a further 2 hours and another ^{1}H NMR spectrum was obtained. ^{1}H NMR (400 MHz, C_6D_6) δ ppm 0.60 (s, 8 H, Me_3Sb), 0.89 (s, 42 H, $[Pd_4(Me_3Sb)_8]$), 1.11 (s, 40 H, $[Pd_4(Me_3Sb)_8]$), 2.05 (s, 13 H, $[Pd(IMes)_2]$-o-Me), 2.16 (s, 19 H, IMes-Me), 2.34 (s, 6 H, $[Pd(IMes)_2]$-p-Me), 6.13 (s, 2 H, $[Pd(IMes)_2]$-backdone), 6.47 (s, 2H, IMes-backbone), 6.81 (s, 8 H, $[Pd(IMes)_2]$-Ar-H).

Attempted Synthesis of $[Pd_4(Et_3Sb)_8]$

Et_3Sb (0.042 g, 0.20 mmol) in THF (5 mL) was added to $PdCl_2(MeCN)_2$ (0.026 g, 0.10 mmol) in THF (5 mL) at -78°C to afford a light-yellow solution which was stirred for 5 minutes. 1.6 M MeLi in Et_2O (0.128 mL, 0.20 mmol) was added dropwise. The reaction solution was stirred at -78°C for a further 15 minutes then warmed to room temperature which caused the reaction solution to darken. The reaction solution was heated to 60°C for 30 minutes then cooled to room temperature and reduced *in vacuo* to a very dark yellow oil. The oil was extracted into n-hexane (10 mL) to yield a dark yellow solution and a black solid.

Synthesis of MeLi

Synthesis was based on modified literature procedure.[603,604] A solution of ^{n}BuLi (11.5 mmol) in hexanes (11 mL) was made by the addition of 2.3 M ^{n}BuLi in hexanes (5 mL, 11.5 mmol)

to n-hexane (6 mL). Iodomethane (1.6498 g, 11.62 mmol) in n-hexane (10 mL) was added to this solution at -25°C. The reaction was stirred at 25°C for 75 mins then warmed to room temperature which affected the formation of a white precipitate. The solution was decanted and the remaining precipitate was washed with n-hexane (3 x 10 mL) and then dried *in vacuo* to give a white powder (0.342 g). Titration of this powder in THF against N-benzylbenzamide gave a purity of 44% (w/w, performed in duplicate). Actual yield: 0.150 g, 6.82 mmol, 59%. ^{1}H NMR (400 MHz, THF-d4) δ ppm -2.04 (br s, 3 H). ^{13}C{^{1}H} NMR (101 MHz, THF-d4) δ ppm -15.2 (br s). NMR spectra consistent with literature values.[609]

NMR Scale Synthesis of of $[Pd_4(Me_3Sb)_8]$ (4-1)

MeLi (0.002 g, 0.009 mmol) in THF-d8 (0.5 mL) was added to $[PdCl_2(MeCN)_2]$ (0.003 g, 0.01 mmol) and $SbCl_3$ (0.005 g, 0.002 mmol) in THF-d4 (0.5 mL) at -78°C, giving a light-yellow solution and a small amount of black precipitate. The reaction solution was warmed to room temperature and transferred to a J-Young NMR tube. An initial ^{1}H NMR spectrum was taken. 1H NMR (400 MHz, THF-d4) δ ppm 0.11 (br s, 1 H), 1.23 (br s, 5 H), 1.91 (br s, 8 H), 3.89 (s, 1 H).

The reaction solution was heated to 60°C for 100 minutes, with an NMR spectrum taken at 10 mins (1H NMR (400 MHz, THF-d4) δ ppm 0.11 (br s, 1 H), 1.23 (br s, 5 H), 1.91 (br s, 8 H), 3.93 (br s, 1 H)), 40 mins (1H NMR (400 MHz, THF-d4) δ ppm 0.11 (br s, 1 H), 1. 1.23 (br s, 7 H), 1.91 (br s, 9 H), 3.27 (br s, 1 H), 3.93 (br s, 1 H)) and 100 mins (1H NMR (400 MHz, THF-d4) δ ppm 0.11 (br s, 1 H), 1.23 (br s, 5 H), 1.91 (br s, 9 H), 3.22 (br s, 1 H), 3.89 (br s, 1 H)). No change in visual appearance occurred over the course of the heating. The tube was stood at room temperature overnight and a ^{1}H NMR spectrum was obtained. 1H NMR (400 MHz, THF-d4) δ ppm 0.11 (br s, 1 H), 1.23 (br s, 5 H), 1.91 (br s, 9 H), 3.89 (br s, 1 H).

Cis-$[PdCl_2(Me_3Sb)_2]\cdot SbCl_3$

MeLi (0.088 g, 4.0 mmol) in THF (10 mL) was added dropwise to an orange suspension of $[PdCl_2(MeCN)_2]$ (0.130 g, 0.50 mmol) and $SbCl_3$ (0.228 g, 1.00 mmol) in THF (50 mL) at -78°C, affecting the instant formation of a dark brown/red suspension. The reaction suspension was stirred for a further 15 minutes at -78°C then warmed to room temperature, giving no change in visual appearance. The reaction solution was stirred at room temperature for 1 hour then warmed to 60°C and was stirred for a total of 1 hour at 60°C, then cooled to room temperature and stirred at room temperature overnight. The solvent was removed *in vacuo* to yield a red oily solid. An NMR was taken in both $CDCl_3$ and C_6D_6. ^{1}H NMR (400 MHz, $CDCl_3$) δ ppm 1.33 - 1.42 (m, 1 H) 1.42 - 1.51 (m, 2 H) 1.57 (br s, 2 H) 1.84 - 1.96 (m, 2 H) 2.20 (s, 1 H) 2.37 (d, J=0.69 Hz, 1 H) 3.67 - 3.85 (m, 2 H). ^{1}H NMR (400

MHz, C_6D_6) δ ppm 0.92 - 1.06 (m, 2 H) 1.34 - 1.48 (m, 6 H) 1.66 (dd, J=1.94, 1.03 Hz, 2 H) 2.04 (br s, 1 H) 3.55 - 3.60 (m, 4 H)

The oil was washed with Et_2O (5 mL) to give an orange solution which was stood at -18°C but did not yield any crystalline solid. The residue from the washing was dissolved to give a deep red solution which was was stood at -18°C to yield deep red crystals of *cis*-$[PdCl_2(Me_3Sb)_2]\cdot SbCl_3$.

A targeted synthesis of $[PdCl_2(Me_3Sb)_2]\cdot SbCl_3$ was carried out. $SbCl_3$ (0.017 g, 0.07 mmol) in DCM (5 mL) was added dropwise to a solution of $[PdCl_2(Me_3Sb)_2]$ (0.037 g, 0.07 mmol) in DCM (10 mL). A yellow crystalline solid formed over the course of 10 minutes, after an additional 80 minutes some black precipitate formed. The solution was filtered and the residual powder was dried *in vacuo* to give a yellow powder (0.05 g). The filtered solution was stood at -18°C which yielded dark yellow crystals of *cis*-$[PdCl_2(Me_3Sb)_2]\cdot SbCl_3$ (**4-4**). 1H NMR (400 MHz, $CDCl_3$) δ ppm 1.45 (s, 2 H, $[PdCl_2(Me_3Sb)_2]$), 2.37 (s, 6 H, $[PdCl_2(Me_3Sb)_2]\cdot SbCl_3$). $^{13}C\{^1H\}$ NMR (101 MHz, $CDCl_3$) δ ppm 1.0 (s), 22.9 (s).

Reaction of $[PdCl_2(MeCN)_2]$ and MeLi

1.6 M MeLi in Et_2O (0.15 mL, 0.24 mmol) was added dropwise to $[PdCl_2(MeCN)_2]$ (0.030 g, 0.12 mmol) in THF (5 mL) at -78°C which caused no visual change to the orange suspension. The suspension was stirred at -78°C for 15 minutes then warmed to room temperature, yielding a fine black precipitate with no trace of the orange colour of $[PdCl_2(MeCN)_2]$. The suspension was stirred at room temperature for 2 days then filtered to yield a colourless solution which was dried *in vacuo* to a grey powder. Both the dried filtrate and residue were intractable and identified as likely being LiCl and Pd^0 respectively.

Reaction of $[PdCl_2(MeCN)_2]$ and Me_3Sb (4 eq)

1.6 M MeLi in Et_2O (0.75 mL, 1.20 mmol) was added dropwise to $SbCl_3$ (0.092 g, 0.40 mmol) in THF (5 mL) at -78°C which was stirred at -78°C for 15 minutes then warmed to room temperature and stirred at room temperature for 1 hour, yielding a colourless solution. This solution was added dropwise to a suspension of $[PdCl_2(MeCN)_2]$ (0.026 g, 0.10 mmol) in THF (5 mL) at -78°C which yielded a yellow solution and a yellow crystalline precipitate which was stirred at -78°C for 15 minutes then warmed to room temperature and stirred at room temperature for 1 hour, yielding a dark yellow solution with traces of yellow precipitate. The reaction solution was heated to 60°C for 40 minutes, darkening the solution. The reaction solution was cooled to room temperature and cooled overnight. The reaction solution was dried *in vacuo* to a red powder; a white precipitate formed in the

vacuum trap. ^{1}H NMR (400 MHz, $CDCl_3$) δ ppm 0.30 (s, minor) 1.14 (s, 1 H) 1.24 (s, 1 H) 1.82 - 1.93 (m, minor) 2.37 (s, minor).

Reaction of $[Pd_4(Me_3Sb)_8]$ (**4-1**) and Bromobenzene

A J-Young NMR tube was loaded with C_6H_5Br (0.003 g, 0.02 mmol), **4-1** (0.009 g, 0.005 mmol) and C_6D_6 (0.7 mL), the purple solution rapidly turned deep red over the course of 2 minutes. An initial ^{1}H NMR spectrum was taken. ^{1}H NMR (400 MHz,C_6D_6) δ ppm 0.64 (br s, 24 H, free Me_3Sb), 0.89 (s, 32 H, $[Pd_4(Me_3Sb)_8]$), 1.11 (s, 36 H, $[Pd_4(Me_3Sb)_8]$), 6.72 (br t, J= 7.32, 11 H, PhBr), 6.78 - 6.85 (m, 6 H, PhBr), 6.99 (t, J=7.55 Hz, 3 H), 7.25 (br d, J=8.46Hz, 11 H, PhBr).

The tube was stood at room temperature for 2 hours, then an ^{1}H NMR spectrum was taken. 1H NMR (400 MHz, C_6D_6) δ ppm 0.65 (br s, 13 H, free Me_3Sb), 0.89 (s, 1 H, $[Pd_4(Me_3Sb)_8]$), 1.11 (s, 1 H, $[Pd_4(Me_3Sb)_8]$), 1.16 (d, J=8.46 Hz, 1 H), 6.72 (br t, J= 7.32 Hz, 2 H, PhBr) 6.82 (t, J=6.86 Hz, 1 H, PhBr), 6.99 (t, J=7.55 Hz, 1 H), 7.25(br d, J=8.46Hz, 3 H, PhBr).

The tube was stood at room temperature for a further 4 hours, at which stage the reaction solution had turned deep yellow and NMR spectra were obtained. 1H NMR (400 MHz, C_6D_6) δ ppm 0.64 (s, 14 H, free Me_3Sb), 1.16 (d, J=8.69 Hz, 1 H), 6.72 (br t, J= 7.32, 1 H,), 6.79 - 6.84 (m, 1 H) 6.99 (t, J=7.55 Hz, 1 H, PhBr), 7.25(br d, J=8.46Hz, 3 H, PhBr). $^{13}C\{^{1}H\}$ NMR (101 MHz, C_6D_6) δ ppm -4.7 (s), 1.6 (s), 123.2 (s, PhBr), 123.5 (s), 127.2 (s, PhBr), 130.5 (s, PhBr), 132.1 (s, PhBr), 138.7 (s, 1 C), 143.3 (s).

Reaction of $[Pd_4(Me_3Sb)_8]$ (**4-1**) and PMe_3

PMe_3 (0.0365 g, 0.48 mmol) was added dropwise to added to a solution of **4-1** (0.015 g, 0.008 mmol) in n-hexane 5 mL) at room temperature, maintaining the purple colour. The reaction solution was stirred at room temperature; the purple solution started to lighten 1 hour after addition, becoming completely colourless after a further 30 minutes. A brown precipitate also developed. The reaction suspension was stirred for a further 30 mins then separated into a colourless solution and brown powder by filtration. The residue was analysed by ^{1}H NMR. The solution was stored at -18°C which yielded clear colourless plate crystals of $[PdMe(PMe_3)_3]$. ^{1}H NMR (400 MHz, C_6D_6) δ ppm 0.83 (dd, J=12.81, 0.91 Hz, 1 H, Pd-P*Me*$_3$). $^{13}C\{^{1}H\}$ NMR (101 MHz, C_6D_6) δ ppm 18.4 (d, J=68 Hz, Pd-P*Me*$_3$). ^{31}P NMR (162 MHz, C_6D_6) δ ppm 30.86 (s, Pd-*P*Me_3)

Reaction of $[Pd_4(Me_3Sb)_8]$ (**4-1**) and $P(OMe)_3$

$P(OMe)_3$ (0.1682 g, 1.35 mmol) was added dropwise to added to a solution of **4-1** (0.015 g, 0.008 mmol) in n-hexane (3 mL) at room temperature. The purple solution started to

lighten 5 minutes after addition, becoming completely colourless after a further 5 minutes. The reaction solution was stirred for 3 hours, at which point a very slight white precipitate formed. The solution was separated from the precipitate, reduced *in vacuo* to a 1 mL solution and stored at -18°C; a white precipitate formed in the vacuum trap. The reaction precipitate was dried *in vacuo* and analysis by ^{1}H NMR, which was devoid of any signals. The reaction solution did not produce any precipitate at -18°C and was dried to a white waxy solid *in vacuo*.

Reaction of $[Pd_4(Me_3Sb)_8]$ (**4-1**) and P^tBu_3

A J-Young NMR tube was loaded with $[Pd_4(Me_3Sb)_8]$ (**4-1**) (0.009 g, 0.005 mmol), P^tBu_3 (0.008 g, 0.04 mmol) and C_6D_6 (0.7 mL) yielding a purple solution. NMR spectra were obtained. ^{1}H NMR (400 MHz, C_6D_6) δ ppm 0.89 (s, 36 H, $[Pd_4(Me_3Sb)_8]$), 1.11 (s, 36 H,$[Pd_4(Me_3Sb)_8]$) 1.28 (d, J=9.61 Hz, 118 H, free P^tBu_3), 1.53 (br t, J=5.6 Hz ,16 H, $[Pd(P^tBu_3)_2]$). $^{31}P\{^{1}H\}$ NMR (162 MHz, C_6D_6) δ ppm 62.46 (s, free P^tBu_3), 85.37 (s, $[Pd(P^tBu_3)_2]$).

The solution was stood at room temperature for 1 hour and further NMR spectra were obtained. ^{1}H NMR (400 MHz, C_6D_6) δ ppm 0.61 (s, 8 H, free Me_3Sb), 0.89 (s, 37 H), 1.11 (s, 36 H), 1.28 (d, J=9.61 Hz, 118 H, , free P^tBu_3), 1.53 (br t, J=5.6 Hz, 32 H, $[Pd(P^tBu_3)_2]$). $^{31}P\{^{1}H\}$ NMR (162 MHz, C_6D_6) δ ppm 62.46 (s, free P^tBu_3), 85.37 (s, $[Pd(P^tBu_3)_2]$).

The solution was stood at room temperature for a further 90 minutes and further NMR spectra were obtained. ^{1}H NMR (400 MHz, C_6D_6) δ ppm 0.61 (s, 9 H, free Me_3Sb), 0.89 (s, 36 H), 1.11 (s, 36 H), 1.28 (d, J=9.83 Hz, 115 H, , free P^tBu_3), 1.53 (br t, J=5.6 Hz, 39 H, $[Pd(P^tBu_3)_2]$). $^{31}P\{^{1}H\}$ NMR (162 MHz, C_6D_6) δ ppm 62.46 (s, free P^tBu_3), 85.37 (s, $[Pd(P^tBu_3)_2]$).

A final set of NMR spectra were obtained after standing at room temperature for a total of 17.5 hours.^{1}H NMR (400 MHz, C_6D_6) δ ppm 0.65 (br s, 23 H, free Me_3Sb), 0.89 (s, 33 H), 1.11 (s, 36 H), 1.28 (d, J=9.61 Hz, 81 H, free P^tBu_3), 1.53(t, J=5.6 Hz, 93 H, $[Pd(P^tBu_3)_2]$). $^{13}C\{^{1}H\}$ NMR (101 MHz, C_6D_6) δ ppm 0.6 (s), 1.8 (s), 8.2 (s), 32.9 (d, J=13Hz), 33.7 (br s), 37.9 (s). $^{31}P\{^{1}H\}$ NMR (162 MHz, C_6D_6) δ ppm 62.46 (s, free P^tBu_3), 85.37 (s, $[Pd(P^tBu_3)_2]$).

$[Pd(P^tBu_3)_2]$ was identified by comparison to literature values.[607]

Reaction of $[Pd_4(Me_3Sb)_8]$ (**4-1**) and XantPhos

XantPhos (0.019 g, 0.032 mmol) in 1:1 n-hexane/toluene (5 mL) was added to a solution of **4-1** (0.015 g, 0.008 mmol) in n-hexane (3 mL) at room temperature, the reaction solution retained its purple colour however a golden precipitate instantly formed. The reaction

suspension was stirred for 2.5 hours then separated into a purple solution and yellow powder by filtration. Both were dried *in vacuo* to yield a waxy purple solid and yellow powder, respectively. NMR analyis of the purple solid suggesting that it consisted of **4-1** and free XantPhos. ^{1}H NMR (400 MHz, C_6D_6) δ ppm 0.59 (s, 1 H, free Me_3Sb) 0.89 (s, 12 H, $[Pd_4(Me_3Sb)_8]$) 1.11 (s, 12 H, $[Pd_4(Me_3Sb)_8]$) 1.36 (s, 6 H, Me-XantPhos) 6.73 - 6.80 (m, 2 H, Ar- XantPhos) 6.80 - 6.89 (m, 2 H, , Ar- XantPhos) 6.99 - 7.06 (m, 12 H, , Ar- XantPhos) 7.06 - 7.12 (m, 3 H, , Ar- XantPhos) 7.32 - 7.48 (m, 8 H, , Ar- XantPhos). ^{31}P{^{1}H} NMR (162 MHz, C_6D_6) δ ppm -17.29 (s, free XantPhos).

The yellow powder was identified as $[Pd(XantPhos)_2]$.[610]

Reaction of $[Pd_4(Me_3Sb)_8]$ (**4-1**) and $(Ph_2P)_2CH_2$ (dppm)

$(Ph_2P)_2CH_2$ (0.012 g, 0.032 mmol) in 1:1 n-hexane/toluene (5 mL) was added to a solution of **4-1** (0.015 g, 0.008 mmol) in n-hexane (3 mL) at room temperature to give a deep red/yellow solution. The reaction solution was stirred at room temperature for 4 hours then reduced *in vacuo* to a 1 mL solution which was stored at -18°C to yield a red/yellow oily solid. ^{1}H NMR (400 MHz, C_6D_6) δ ppm ,0.89 (s, 36 H, $[Pd_4(Me_3Sb)_8]$), 1.11 (s, 36 H, $[Pd_4(Me_3Sb)_8]$) *N.B.* A large amount of silicone grease was present. ^{13}C{^{1}H} NMR (101 MHz, C_6D_6) δ ppm) 0.6 (s, minor, $[Pd_4(Me_3Sb)_8]$), 1.8 (s), 8.2 (s, minor, $[Pd_4(Me_3Sb)_8]$). ^{31}P{^{1}H} NMR (162 MHz, C_6D_6) δ ppm 22.44 (br s).

Reaction of $[Pd_4(Me_3Sb)_8]$ (**4-1**) and 1,4-$(Ph_2P)_2(CH_2)_4$ (dppb)

1,4-$(Ph_2P)_2(CH_2)_4$ (0.014 g, 0.032 mmol) in 1:1 n-hexane/toluene (5 mL) was added to a solution of **4-1** (0.015 g, 0.008 mmol) in n-hexane (3 mL) at room temperature. The reaction solution was stirred at room temperature for 3 hours over which time no obvious visual change occurred. The solution was reduced *in vacuo* to a purple oil. ^{1}H NMR (400 MHz, C_6D_6) δ ppm 0.60 (s, 29 H, free Me_3Sb) 0.89 (s, 36 H, $[Pd_4(Me_3Sb)_8]$) 1.11 (s, 36 H, $[Pd_4(Me_3Sb)_8]$). *N.B.* A large amount of silicone grease was present. A ^{31}P{^{1}H} NMR was devoid of any signals.

Reaction of $[Pd_4(Me_3Sb)_8]$ (**4-1**) and $[Pd(PPh_3)_4]$

A J-Young NMR tube was loaded with $[Pd_4(Me_3Sb)_8]$ (**4-1**) (0.006 g, 0.003 mmol), $[Pd(PPh_3)_4]$ (0.004 g, 0.003 mmol) and C_6D_6 (0.7 mL) yielding a purple solution. A ^{1}H NMR spectrum was obtained. ^{1}H NMR (400 MHz, C_6D_6) δ ppm 0.68 (s, 6 H, free Me_3Sb), 0.89 (s, 36 H), 1.11 (s, 36 H), 6.89 - 7.07 (m, 19 H), 7.52 (br d, J=5.03 Hz, 11 H).

The solution was stood at room temperature for 1 hour and another ^{1}H NMR spectrum was obtained. ^{1}H NMR (400 MHz, C_6D_6) δ ppm 0.69 (br s, 8 H), 0.89 (s, 36 H), 0.94 (s, 13 H), 1.11 (s, 36 H), 6.90 - 7.13 (m, 24 H), 7.53 (br d, J=3.20 Hz, 9 H), 7.67 - 7.85 (m, 6 H).

The solution was stood at room temperature for a further 1 hour and another ^{1}H NMR spectrum was obtained. ^{1}H NMR (400 MHz, C_6D_6) δ ppm 0.69 (br s, 7 H), 0.89 (s, 36 H), 0.94 (s, 9 H) ,1.11 (s, 36 H), 6.92 - 7.14 (m, 23 H), 7.55 (br s, 8 H), 7.67 - 7.88 (m, 7 H).

The solution was stood at room temperature for a further 22 hour and a ^{1}H and $^{31}P\{^{1}H\}$ NMR spectrum was obtained. ^{1}H NMR (400 MHz, C_6D_6) δ ppm 0.73 (br s, 9 H, Me_3Sb ($[Pd(PPh_3)_2(SbMe_3)_2]$)), 0.89 (m, 36 H), 0.90 - 0.97 (m, 22 H), 1.11 (m, 36 H), 6.95 - 7.13 (m, 28 H Me_3Sb ($[Pd(PPh_3)_2(SbMe_3)_2]$)), 7.66 - 7.85 (m, 16 H, Me_3Sb ($[Pd(PPh_3)_2(SbMe_3)_2]$)).

6. Computational Modelling of Organo/Chloro Substituent Exchange in Organoantimony(III) Species

6.1 Introduction

6.1.1. Redistribution of Organoantimony Compounds

Organoantimony bonds are well known to be relatively labile in comparison to organophosphorous and organonitrogen bonds. Redistribution reactions are well established synthetic strategies for targeting heteroleptic organoantimony(III) halide species,[31,511,611] and have been observed serendipitously.[612] Mixtures of alkylstibine halides typically redistribute to a complex mixture of all possible compounds; the prototypical examples are methylchlorostibines ($Me_{3-n}SbCl_n$, n = 1, 2). Pure samples of both Me_2SbCl and $MeSbCl_2$ are thermally unstable; dismutation yields a mixture of Me_3Sb, $MeSbCl_2$, Me_2SbCl and $SbCl_3$ over the course of a few months.[612] A redox disproportionation reaction also occurs, which yields Me_3SbCl_2 and Sb^0. The formation of Me_2SbCl and $MeSbCl_2$ from Me_3Sb and $SbCl_3$ was the subject of a kinetic study (Scheme 6.1 a); the reaction was found to be second order overall and first order with respect to each reactant in DMF.[613] An activation enthalpy of 18 kcal/mol and entropy of -25 eu (cal/Kmol) is consistent with a four centred transition state with two points of attachment (Scheme 6.1 b).

a) $Me_3Sb + SbCl_3 \longrightarrow Me_2SbCl + MeSbCl_2$

b)

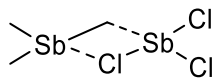

Scheme 6.1. a) formation of Me_2SbCl and $MeSbCl_2$ from Me_3Sb and $SbCl_3$. b) Proposed four centred transition state.

The scrambling of aryl/chloro substituents between aryl stibines (Ar_3Sb) and $SbCl_3$ is more reliable and typically yields the heteroleptic compound representing the total average stoichiometry of the system, *e.g.* 1 equivalent of Ph_3Sb and 2 equivalents of $SbCl_3$ produces $PhSbCl_2$ quantitatively.[31]

Similar reactivity has been observed in Sb(V) systems. The most commonly reported is the exchange of halides (X/X') between stiboranes R_3SbX_2 and $R_3SbX'_2$ (R = Me, Ph, Bn; X/X' = F, Cl, Br, I) to yield a mixture containing the mixed halide (R_3SbXX').[614,615] The mixed halide is typically favoured. Heating a solution of $(p\text{-Tol})_5Sb$ and $(4\text{-}CF_3C_6H_4)_5Sb$ yielded a mixture containing $(p\text{-Tol})_{5-n}(4\text{-}(CF_3)C_6H_4)_nSb$ (n = 0-5).[616] A computational investigation suggested that ligand exchange in Me_5Sb occurs *via* a concerted mechanism whereas the same reaction in Ph_5Sb is a stepwise process *via* a $[Ph_4Sb][Ph_6Sb]$ intermediate.[617]

6.1.2. Aims and Objectives

This body of work aims to elucidate a more detailed understanding of dismutation and substituent redistribution reactions of organoantimony(III) halide species based on a computational study. While this reactivity has been experimentally observed and probed, there have been no DFT based studies of it. This can be roughly categorised according to two approaches: computational chemistry will be utilised to determine the relative populations of different species in mixtures of stibines by calculating relative thermodynamic stabilities and computational methods will be used to propose an energetically reasonable mechanism for redistribution in organoantimony species.

The specific objectives of this body of work are:

a) By comparison of structural parameters of structures optimised with different functionals to experimental data, a suitable method for modelling heteroleptic chlorostibines will be elucidated (functional testing).
b) Obtain thermodynamic information on a library of chlorostibines from frequency calculations.
c) Use this thermodynamic information to predict the relative populations of different species in mixtures of stibines.
d) Ultilise relaxed PES scans and IRC to model mechanistic pathways for the organometallic/halide exchange in organoantimony(III) species.

6.2. Results and Discussions

6.2.1. Thermodynamic Modelling

Initially, a thermodynamic approach was taken to investigate the relative distribution of heteroleptic chlorostibines ($R_{3-n}SbCl_n$) on mixing a homoleptic stibine (R_3Sb) and $SbCl_3$ or a chlorostibine with either R_3Sb or $SbCl_3$ (Scheme 6.2). Two stibines were used for this model, $(p\text{-Tolyl})_3Sb$ and Me_3Sb to investigate both alkyl and aryl systems. This was modelled in the gas phase, diethyl ether, benzene, ethanol and water. To elucidate a suitable computational method, functional testing was undertaken. $(p\text{-Tol})SbCl_2$ was chosen as a model compound as it has been structurally characterised,[618] and contains both organoantimony(III) and haloantimony(III) bonds. Functional testing suggested that M062X/def2SVP with D3 empirical dispersion correction would be the most accurate functional/basis set for these compounds by comparison of calculated and experimental bond parameters. Frequency calculations on optimised structures in the gas phase yielded the Gibb's free energy of each component from which the Gibb's free energy of reaction and the equilibrium constant could be calculated (Equation 6.1). This is done by dividing the difference between the sum of the free energies of the products and sum of the free energies of the reactants, both in terms of J mol^{-1} K^{-1} , by -2477.57 J mol^{-1} K^{-1} (RT, R = universal gas constant 8.314 J mol^{-1} T = 298 K). This yields the natural log of the equilibrium constant, at standard conditions, which can be converted to the equilibrium constant with the exponential function. To account for solvent effects, a single point energy calculation for the gas phase optimised structure with the solvent modelled using the polarisable continuum model (PCM). This yields a single point energy which gives the Gibb's free energy of the compound when added to the thermal correction to free energy, which is in turn obtained in the output of the gas phase frequency calculation. The PCM models the solvent as a polarisable continuum field within the solute cavities.[619–621] In each case, equilibrium constants strongly favoured the heteroleptic stibines (Table 6.2 - Table 6.11), however no specific trends were apparent.

a) $R_3Sb + SbCl_3 \rightleftharpoons R_2SbCl + RSbCl_2$

b) $2R_3Sb + SbCl_3 \rightleftharpoons 3R_2SbCl$

c) $R_3Sb + 2SbCl_3 \rightleftharpoons 3RSbCl_2$

d) $R_2SbCl + SbCl_3 \rightleftharpoons 2RSbCl_2$

e) $RSbCl_2 + R_3Sb \rightleftharpoons 2R_2SbCl$

f) $A + B \rightleftharpoons C + D$

Scheme 6.2. a) - e) Reactions modelled here and f) genetic equilibrium (see Equation 6.1 a)

a) $$K = \frac{[C][D]}{[A][B]}$$ b) $$InK = -\frac{\Delta G^0}{RT}$$

Equation 6.1. a) Equlibrium constant (K) (see Scheme 6.2 f). b) Relationship between equilibrium constant(K) and reaction Gibb's free energy at standard conditions (ΔG^0). R = universal gas constant (8.314 kJ mol^{-1})

Table 6.2. Gibbs free energy and equilibrium constant(K) for the redistribution of $(p\text{-Tolyl})_3Sb$, $(p\text{-Tolyl})_2SbCl$, $(p\text{-Tolyl})SbCl_2$ and $SbCl_3$ in the gas phase.

Reactants	**Products**	**Gibbs Free Energy ΔG^0 (kcal mol^{-1})**	**InK**	**K**
$SbCl_3$ +$(p\text{-Tol})_3Sb$	$(p\text{-Tol})SbCl_2$ + $(p\text{-Tol})_2SbCl$	-6.089	10.28	$2.924x10^4$
$SbCl_3$ + $2(p\text{-Tol})_3Sb$	$3(p\text{-Tol})_2SbCl$	-9.256	15.63	$6.142X10^6$
$2SbCl_3$ + $(p\text{-Tol})_3Sb$	$3(p\text{-Tol})SbCl_2$	-9.012	15.22	$4.071X10^6$
$(p\text{-Tol})_2SbCl$ + $SbCl_3$	$2(p\text{-Tol})SbCl_2$	-2.923	4.936	$1.392X10^2$
$(p\text{-Tol})SbCl_2$ + $(p\text{-Tol})_3Sb$	$2(p\text{-Tol})_2SbCl$	-3.166	5.347	$2.100X10^2$

Table 6.8. Gibbs free energy and equilibrium constant(K) for the redistribution of $(p\text{-Tolyl})_3Sb$, $(p\text{-Tolyl})_2SbCl$, $(p\text{-Tolyl})SbCl_2$ and $SbCl_3$ in diethyl ether.

Reactants	**Products**	**Gibbs Free Energy (kcal mol^{-1})**	**InK**	**K**
$SbCl_3$ +$(p\text{-Tol})_3Sb$	$(p\text{-Tol})SbCl_2$ + $(p\text{-Tol})_2SbCl$	-6.683	11.29	$7.973X10^4$
$SbCl_3$ + $2(p\text{-Tol})_3Sb$	$3(p\text{-Tol})_2SbCl$	-9.908	16.73	$1.848X10^7$
$2SbCl_3$ + $(p\text{-Tol})_3Sb$	$3(p\text{-Tol})SbCl_2$	-10.142	17.13	$2.742X10^7$
$(p\text{-Tol})_2SbCl$ + $SbCl_3$	$2(p\text{-Tol})SbCl_2$	-3.458	5.840	$3.439X10^2$
$(p\text{-Tol})SbCl_2$ + $(p\text{-Tol})_3Sb$	$2(p\text{-Tol})_2SbCl$	-3.225	5.445	$2.318X10^2$

Table 6.9. Gibbs free energy and equilibrium constant(K) for the redistribution of (p-Tolyl)$_3$Sb, (p-Tolyl)$_2$SbCl, (p-Tolyl)SbCl$_2$ and SbCl$_3$ in benzene.

Reactants	Products	Gibbs Free Energy ΔG^0 (kcal mol^{-1})	InK	K
SbCl$_3$ +(p-Tol)$_3$Sb	(p-Tol)SbCl$_2$ + (p-Tol)$_2$SbCl	-6.480	10.94	5.657X10^4
SbCl$_3$ + 2(p-Tol)$_3$Sb	3(p-Tol)$_2$SbCl	-9.674	16.33	1.245X10^7
2SbCl$_3$ + (p-Tol)$_3$Sb	3(p-Tol)SbCl$_2$	-9.766	16.49	1.455X10^7
(p-Tol)$_2$SbCl + SbCl$_3$	2(p-Tol)SbCl$_2$	-3.286	5.549	2.571X10^2
(p-Tol)SbCl$_2$ + (p-Tol)$_3$Sb	2(p-Tol)$_2$SbCl	-3.194	5.393	2.200X10^2

Table 6.10. Gibbs free energy and equilibrium constant(K) for the redistribution of (p-Tolyl)$_3$Sb, (p-Tolyl)$_2$SbCl, (p-Tolyl)SbCl$_2$ and SbCl$_3$ in ethanol.

Reactants	Products	Gibbs Free Energy ΔG^0 (kcal mol^{-1})	InK	K
SbCl$_3$ +(p-Tol)$_3$Sb	(p-Tol)SbCl$_2$ + (p-Tol)$_2$SbCl	-75.23	127.0	1.500 X10^{55}
SbCl$_3$ + 2(p-Tol)$_3$Sb	3(p-Tol)$_2$SbCl	-215.04	363.1	5.170 X10^{157}
2SbCl$_3$ + (p-Tol)$_3$Sb	3(p-Tol)SbCl$_2$	-10.66	17.99	6.528 X10^{107}
(p-Tol)$_2$SbCl + SbCl$_3$	2(p-Tol)SbCl$_2$	64.58	-109.1	4.352X10^{-48}
(p-Tol)SbCl$_2$ + (p-Tol)$_3$Sb	2(p-Tol)$_2$SbCl	-139.8	236.1	3.447 X10^{102}

Table 6.11. Gibbs free energy and equilibrium constant(K) for the redistribution of (p-Tolyl)$_3$Sb, (p-Tolyl)$_2$SbCl, (p-Tolyl)SbCl$_2$ and SbCl$_3$ in water.

Reactants	Products	Gibbs Free Energy ΔG^0 (kcal mol^{-1})	InK	K
SbCl$_3$ +(p-Tol)$_3$Sb	(p-Tol)SbCl$_2$ + (p-Tol)$_2$SbCl	-7.046	11.90	1.470X10^5
SbCl$_3$ + 2(p-Tol)$_3$Sb	3(p-Tol)$_2$SbCl	-10.39	17.54	4.146X10^7
2SbCl$_3$ + (p-Tol)$_3$Sb	3(p-Tol)SbCl$_2$	-10.75	18.16	7.669X10^7
(p-Tol)$_2$SbCl + SbCl$_3$	2(p-Tol)SbCl$_2$	-3.705	6.257	5.215X10^2
(p-Tol)SbCl$_2$ + (p-Tol)$_3$Sb	2(p-Tol)$_2$SbCl	-3.341	5.642	2.819X10^2

Table 6.12. Gibbs free energy and equilibrium constant(K) for the redistribution of Me_3Sb, Me_2SbCl, $MeSbCl_2$ and $SbCl_3$ in the gas phase.

Reactants	Products	Gibbs Free Energy ΔG^0 (kcal mol^{-1})	InK	K
$SbCl_3$ +Me_3Sb	$MeSbCl_2$ + Me_2SbCl	-5.669	9.573	$1.438X10^4$
$SbCl_3$ + $2Me_3Sb$	$3Me_2SbCl$	-8.384	14.16	$1.408X10^6$
$2SbCl_3$ + Me_3Sb	$3MeSbCl_2$	-8.623	14.56	$2.111X10^6$
Me_2SbCl + $SbCl_3$	$2MeSbCl_2$	-2.954	4.989	$1.468X10^2$
$MeSbCl_2$ + Me_3Sb	$2Me_2SbCl$	-2.715	4.584	9.793

Table 6.13. Gibbs free energy and equilibrium constant(K) for the redistribution of Me_3Sb, Me_2SbCl, $MeSbCl_2$ and $SbCl_3$ in diethyl ether.

Reactants	Products	Gibbs Free Energy ΔG^0 (kcal mol^{-1})	InK	K
$SbCl_3$ +Me_3Sb	$MeSbCl_2$ + Me_2SbCl	-7.167	12.10	$1.805X10^5$
$SbCl_3$ + $2Me_3Sb$	$3Me_2SbCl$	-10.71	18.09	$7.190X10^7$
$2SbCl_3$ + Me_3Sb	$3MeSbCl_2$	-10.79	18.22	$8.181X10^7$
Me_2SbCl + $SbCl_3$	$2MeSbCl_2$	-3.622	6.116	$4.532X10^2$
$MeSbCl_2$ + Me_3Sb	$2Me_2SbCl$	-3.545	5.987	$3.983X10^2$

Table 6.14. Gibbs free energy and equilibrium constant(K) for the redistribution of Me_3Sb, Me_2SbCl, $MeSbCl_2$ and $SbCl_3$ in the benzene.

Reactants	Products	Gibbs Free Energy ΔG^0 (kcal mol^{-1})	InK	K
$SbCl_3$ +Me_3Sb	$MeSbCl_2$ + Me_2SbCl	-6.681	24.60	$4.803 X10^{10}$
$SbCl_3$ + $2Me_3Sb$	$3Me_2SbCl$	-9.960	36.66	$8.381 X10^{15}$
$2SbCl_3$ + Me_3Sb	$3MeSbCl_2$	-10.08	37.12	$1.322 X10^{16}$
Me_2SbCl + $SbCl_3$	$2MeSbCl_2$	-3.402	12.53	$2.752X10^5$
$MeSbCl_2$ + Me_3Sb	$2Me_2SbCl$	-3.279	12.07	$1.745X10^5$

Table 6.15. Gibbs free energy and equilibrium constant(K) for the redistribution of Me_3Sb, Me_2SbCl, $MeSbCl_2$ and $SbCl_3$ in ethanol.

Reactants	**Products**	**Gibbs Free Energy ΔG^0 (kcal mol^{-1})**	**InK**	**K**
$SbCl_3$ +Me_3Sb	$MeSbCl_2$ + Me_2SbCl	-7.741	13.07	$4.754X10^5$
$SbCl_3$ + $2Me_3Sb$	$3Me_2SbCl$	-11.59	19.58	$3.179X10^8$
$2SbCl_3$ + Me_3Sb	$3MeSbCl_2$	-11.63	19.64	$3.379X10^8$
Me_2SbCl + $SbCl_3$	$2MeSbCl_2$	-3.888	6.566	$7.109X10^2$
$MeSbCl_2$ + Me_3Sb	$2Me_2SbCl$	-3.852	6.505	$6.687X10^2$

Table 6.11. Gibbs free energy and equilibrium constant(K) for the redistribution of Me_3Sb, Me_2SbCl, $MeSbCl_2$ and $SbCl_3$ in water.

Reactants	**Products**	**Gibbs Free Energy ΔG^0 (kcal mol^{-1})**	**InK**	**K**
$SbCl_3$ +Me_3Sb	$MeSbCl_2$ + Me_2SbCl	-7.834	13.23	$5.568\ X10^5$
$SbCl_3$ + $2Me_3Sb$	$3Me_2SbCl$	-11.74	19.81	$4.042\ X10^8$
$2SbCl_3$ + Me_3Sb	$3MeSbCl_2$	-11.77	19.87	$4.271\ X10^8$
Me_2SbCl + $SbCl_3$	$2MeSbCl_2$	-3.933	6.64	$7.670\ X10^2$
$MeSbCl_2$ + Me_3Sb	$2Me_2SbCl$	-3.901	6.588	$7.260\ X10^2$

This contradicts the experimental observation that both pure Me_2SbCl and $MeSbCl_2$ form a mixture including Me_3Sb and $SbCl_3$ in each case;[612] there are a number of differences between the experimental observation and this computational study. In this computational study, the species have been modelled in both the gas phase and several solvents whereas the experimental observation was made in a pure sample of the compound. A redox disproportionation reaction was experimentally observed which is not accounted for in this computational study. This also does not account for any potential adducts or kinetic factors.

6.2.2. Transition States

To gain further insights into this reactivity and to account for kinetic effects, a mechanistic investigation was undertaken. The redistribution of Me_3Sb and $SbCl_3$ to Me_2SbCl and $MeSbCl_2$ was chosen as a model system. In accordance with the functional testing (*vide supra*), M062X/def2SVP with D3 empirical dispersion correction was used. While this

reactivity is often observed in the melt, this is complex to treat computationally so a solvent correction (diethyl ether) was used.

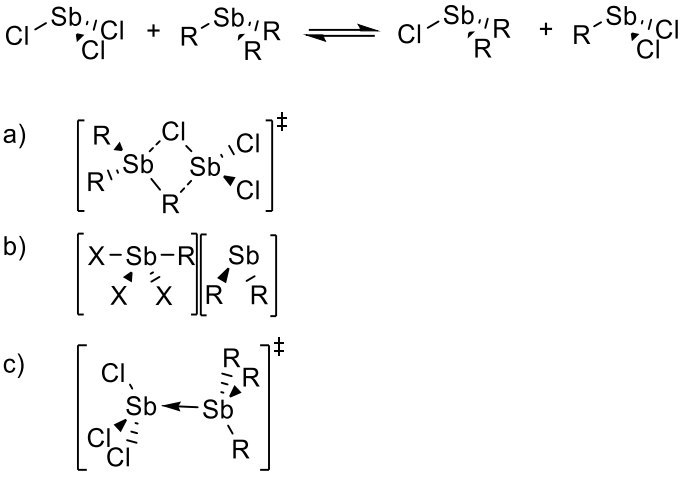

Figure 6.1. Hypothesised transition states for redistribution reactions of organoantimony(III) halides. a) Four membered cyclic transition state. b) Tight ion pair intermediate. c) Lewis acid/base adduct transition state.

Initially, a concerted cyclic mechanism, with a single transition state was considered (Figure 6.2 b). A relaxed potential energy scan (PES) along the Sb···Cl bond coordinate was performed; a local maximum on this coordinate was found. The Sb···Me was scanned while the Sb···Cl bond, corresponding to an energy maximum, was fixed. From this a transition state was found with transition state optimisation. Optimisation to a local minimum on both sides of the imaginary frequency yielded $Me_3Sb/SbCl_3$ and $Me_2SbCl/MeSbCl_2$ (Figure 6.2), however the barrier of 33.2 kcal mol^{-1} would preclude any reactivity at room temperature according to this mechanism (**Mechanism-A**). This corresponds to a reaction half-life of $3.6x10^{11}$ seconds at room temperature or $3.65x10^{6}$ s at 100°C,[622] assuming an initial concentration of 1 M of each reactant.

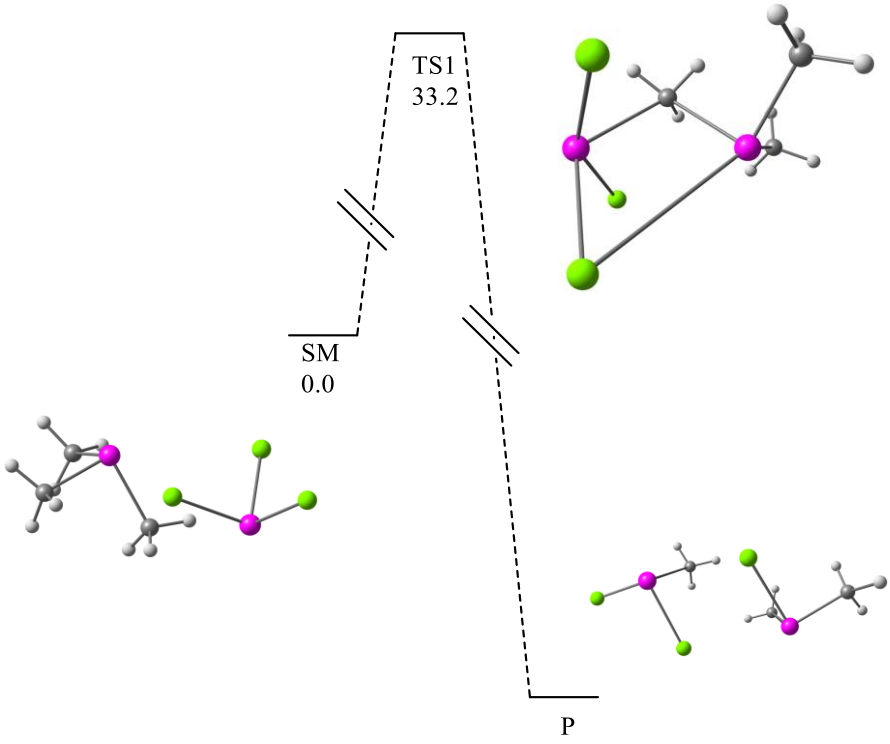

Figure 6.2. Free Energy diagram for the concerted cyclic redistribution between Me_3Sb and $SbCl_3$ to yield Me_2SbCl and $MeSbCl_2$ (**Mechanism-A**). All energies are free energies(1 atm, 298 K, kcal mol^{-1}) calculated at the M062X/Def2SVP(D3) smd=Diethylether level of theory.

The potential for a mechanism with an initial heterolytic bond fission to yield an ion pair intermediate was investigated. This could take the form of either a methyl transfer from Me_3Sb to $SbCl_3$, yielding $[Me_2Sb][MeSbCl_3]$ or a chloride transfer from $SbCl_3$ to Me_3Sb, yielding $[SbCl_2][Me_3SbCl]$. The former was considered as more feasible, as the electron donating nature of methyl groups would make the hypothetical dimethylstibenium ($[Me_2Sb]^+$) fragment more stable than the dichlorostibenium ($[SbCl_2]^+$). PES scan along the Sb···Cl and Sb···Me bond lengths were performed. This yielded a similar mechanism (**Mechanism-B**), in which $SbCl_3$ abstracts a Me from Me_3Sb (Figure 6.3-**TS1**) to yield $Me_2SbMeSbCl_3$ (Figure 6.3-**IM1**); which is best described as having a Sb-Me-Sb 3 centre 2 electron bond (3c–2e, Figure 6.4). While halides and hydrides are more commonly associated with 3c–2e bonds, alkyls are known, such as trimethylaluminium.[623] A chloride from the $MeSbCl_3$ fragment then transfers onto Me_2Sb (Figure 6.3-**TS2**) to yield the products, Me_2SbCl and $MeSbCl_2$. This corresponds to a reaction half-life of $3.3x10^7$ s at room temperature or 2188 s at 100°C,[622] assuming an initial concentration of 1 M of each reactant. While this is still a high barrier, it is lower than the barrier of **Mechanism-A,** and thus is more likely. This gives a rate constant of $4.57x10^{-4}$ $mol^{-1}s^{-1}$ at 100°C which is similar to the experimentally determined value of 5.3 ± 0.5 $x10^{-4}$ $mol^{-1}s^{-1}$.[613]

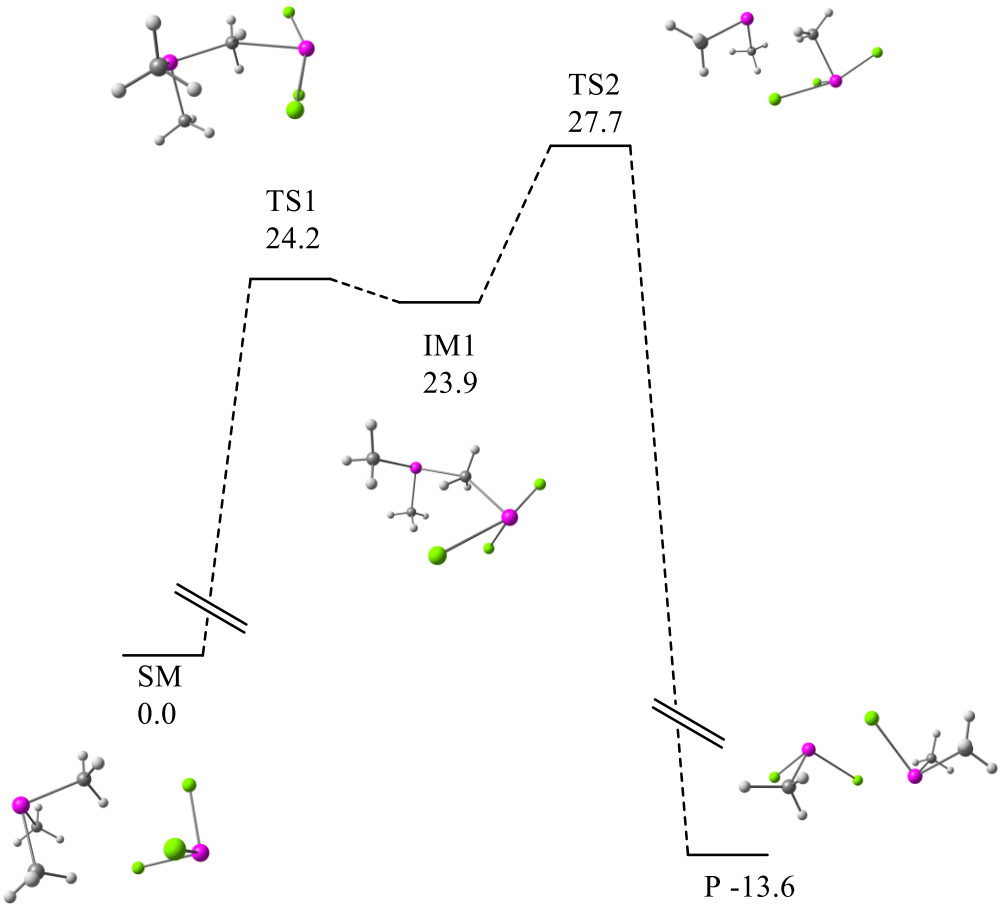

Figure 6.3. Free Energy diagram for the 3c–2e intermediate mechanism between Me_3Sb and $SbCl_3$ to yield Me_2SbCl and $MeSbCl_2$ (**Mechanism-B**). All energies are free energies(1 atm, 298 K, kcal mol^{-1}) calculated at the M062X/Def2SVP(D3) smd=Diethylether level of theory.

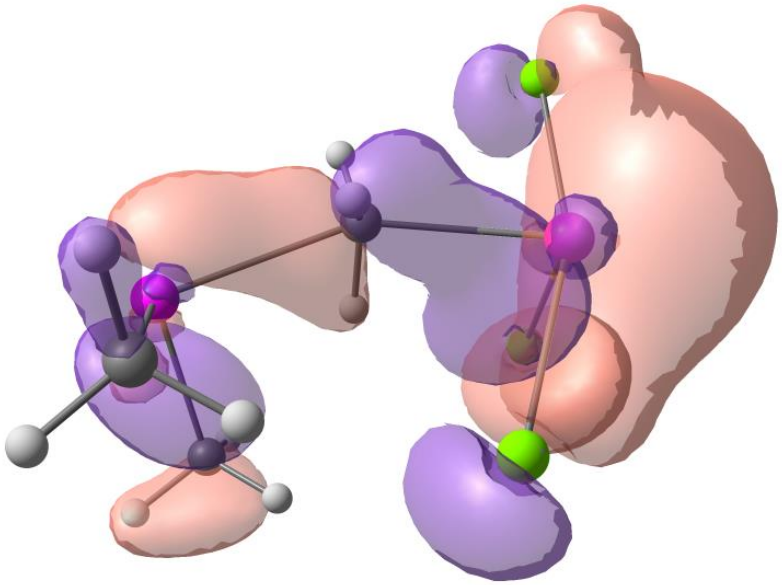

Figure 6.4. Visualisation of Kohn-Sham orbital corresponding to HOMO-8 of **IM1.**

A mechanism involving an initial adduct formation was probed by performing a PES scan on the Sb···Sb coordinate. From this, two different weak adducts, with mechanisms for their

formation, were found (Figure 6.5, **Mechanism-C** and **Mechanism-D**). While neither yielded methyl/chloride exchange, the small barrier suggests that in a solution of Me_3Sb and $SbCl_3$ the majority is the form of these adducts rather than the free species. Given the low barrier, the formation of these adducts would be expected to be instantaneous.

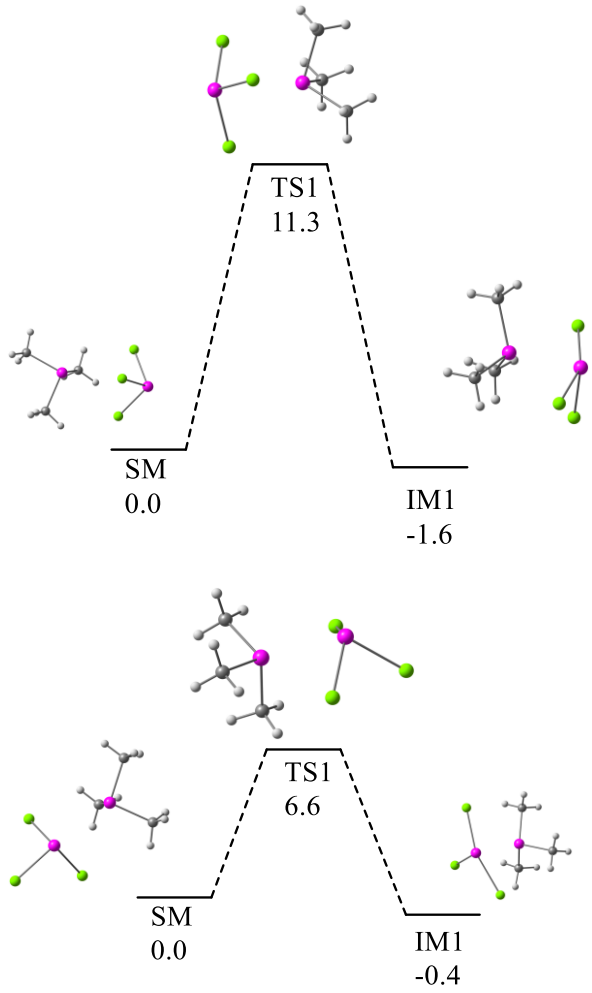

Figure 6.5. Free Energy diagram for the formation of an adduct between Me_3Sb and $SbCl_3$ two similar mechanisms were elucidated (**Mechanism-C** and **Mechanism-D**). All energies are free energies (1 atm, 298 K, kcal mol^{-1}) calculated at the M062X/Def2SVP(D3) smd=Diethylether level of theory.

The mechanism for the substituent exchange between Ph_3Sb and $SbCl_3$ was also probed. In this case, A PES scan, scanning the distance between the Sb atom on $SbCl_3$ and an *ipso* carbon on Ph_3Sb was performed. This yielded a mechanism (**Mechanism-E**) in which an *ipso* carbon forms a 3c-2e bond with the two Sb centres (Figure 6.6 **IM1**). One chloride in **IM1** is closer to the intermolecular Sb centre, the coordinate between these atoms were scanned to yield **TS2,** which corresponds to the breaking of the $PhCl_2Sb$-Cl bond and formation of the PhSb-Cl bond. This corresponds to a reaction half-life of $1.0x10^7$ s at room temperature or 831 s at 100°C,[622] assuming an initial concentration of 1 M of each reactant.

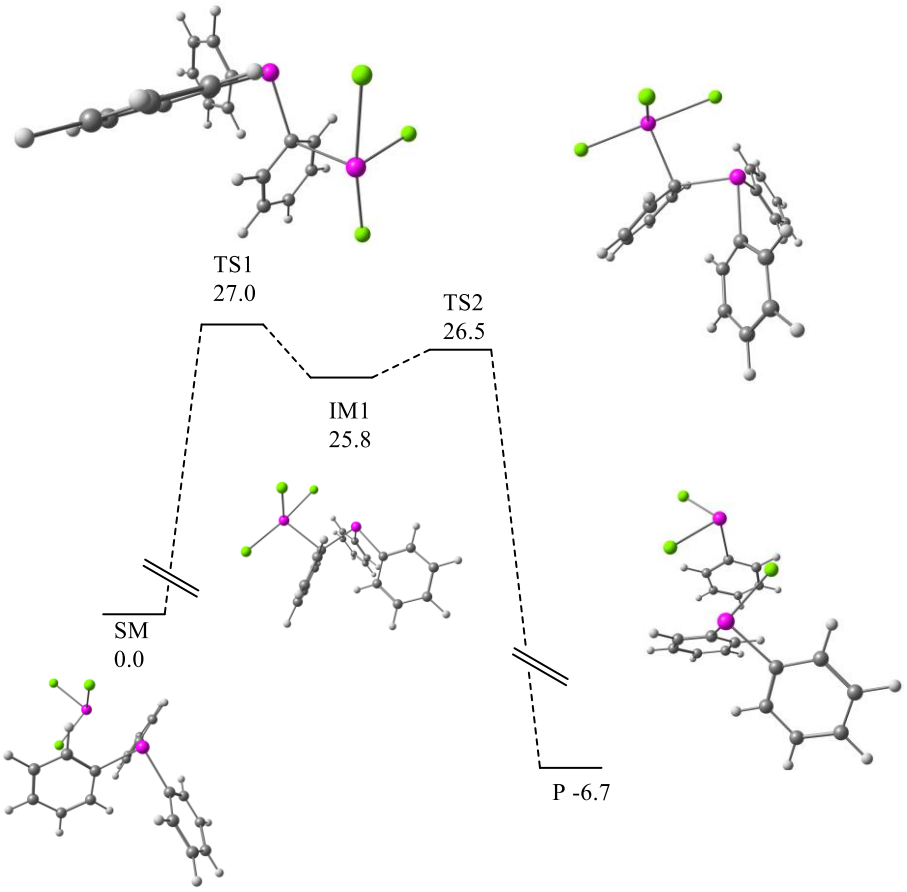

Figure 6.6. Free Energy diagram for the 3c–2e intermediate mechanism between Ph_3Sb and $SbCl_3$ to yield Ph_2SbCl and $PhSbCl_2$ (**Mechanism-E**). All energies are free energies(1 atm, 298 K, kcal mol^{-1}) at the M062X/Def2SVP(D3) smd=Diethylether level of theory.

6.3. Conclusions

An initial study of mixtures of stibines, $SbCl_3$ and chlorostibines will typically favour the formation of the heteroleptic chlorostibines thermodynamically. This body of work provides an initial understanding of the mechanisms by which substituent redistribution reactions between organoantimony(III) halides occurs. While some initial kinetic investigations have been carried out, [613] this represents the first computational investigation on such reactivity. This body of work suggests that methyl/chloro exchange between Me_3Sb and $SbCl_3$ occurs *via* a $Me_2SbMeSbCl_3$ intermediate containing a 3c-2e Sb-Me-Sb bond (Mechanism **B**). This is somewhat in disagreement with kinetic studies, which suggest a four centred transition state with two points of attachment however there is a close agreement in rate constants. Computational studies presented here suggest that the exchange between Ph_3Sb and $SbCl_3$ occurs *via* a somewhat similar mechanism in which an *ipso* carbon takes the place of the methyl group.

What is presented here could be furthered by higher levels of computational work and the interrogation of a greater variety of chemical system. Computations such as natural bond orbital (NBO), atom-in-molecules (AIM) and bond indices would give a better understanding of these mechanisms and a more precise understanding of the transition states and intermediates observed. This body of work has only investigated a limited number of systems and while a general model can be assumed from this work it would be pragmatic to investigate other organoantimony(III) halide systems. It would also be valuable to support this work with experimental studies, namely spectroscopic studies to observe predicted intermediates and further kinetic studies. The work discussed here, and any future work would be useful for targeting stibines that do not undergo this redistribution; this work suggests that sterically hindered stibines might be a potential route to this.

6.4. Computational Methods

All calculations were performed using Gaussian 09 Revision E0.01.[355] All geometries were optimised in vacuum without imposing symmetry constraints at the M062X/def2-SVP level of theory with the D3 empirical dispersion correction.[261,356,357] Subsequent analytical IR frequency calculations on optimised geometries were utilised to confirm the nature of stationary points (zero and exactly one imaginary mode for minima and transition states, respectively). Moreover, within the ideal gas/rigid rotor/harmonic approximation (RRHO)

these calculations also provided thermal and entropic corrections to the Gibbs Free Energy at 1 atm and 298.15 K. The Kohn-Sham orbitals were visualised using Chemcraft.[359]

7. Summary of Work and Global Conclusions

This body of work has advanced the understanding on the relationship between the structure and Lewis acidity of organoantimony cations. Salts of the form $[Ar_3SbCl][B(C_6F_5)_4]$ become more Lewis acidic with increased fluorination of the aryl substituent, this inference is not unexpected and is consistent with similar borane and phosphonium species. The value of this body of work is as a preliminary survey of the reactivity of these salts, which is currently lacking in the literature. The practical utility of these salts is severely limited by a tendency to reduce to the parent stibine (Ph_3Sb). A study into the structure and reactivity of cations of the form $[Cp_{2-n}SbX_n]^+$ (X = F, Cl; n = 0,1) has yielded similar conclusions, however the isolation of five novel salts firmly establishes the strategy of stabilisation of a rare stibenium ($Sb(III)^+$) ions with Cp* ligands. A preliminary survey into the potential of tetraarylstibonum/stibine ($[Ar_4Sb]^+/R_3Sb$) mixtures to act as 'frustrated Lewis Pair' (FLP) demonstrated that $[(3,5\text{-}F_2C_6H_3)_4Sb]^+/{}^tBu_3Sb$ can activate benzyl chloride, however side-reactions limit the potential to deploy this pair in a synthetically useful manner.

The prototypical phosphorous analogue of the triarylchlorostibonium salts reported here, $[(C_6F_5)_3PF][B(C_6F_5)_4]$, is extensively deployed with Et_3SiH to yield synthetically useful transformations whereas Et_3SiH decomposes the triarylchlorostibonium salts. Similarly, an extensive literature exists on Phosphorus containing FLPs whereas this body of work suggests that side reactions preclude extensive deployment of stibines in FLPs. An underlying trend is that while the chemistry of organoantimony is extensively rich, attempts to mimic the chemistry of organoPhosphorus is typically a futile route to synthetically useful reagents.

This body of work has revealed some advancement in the knowledge of the formation and reactivity of $[Pd_4\mu_3\text{-}(Me_3Sb)_4(Me_3Sb)_4]$ and thus a progression in the knowledge of the reactivity of complexes with rare bridging pnictine ligands. In the course of this work, another complex $[Pd_3\mu_3\text{-}(Me_3Sb)\mu_2\text{-}(Me_3Sb)_3(Me_3Sb)_3]$ was structurally characterised, adding to an extremely limited set of complexes with bridging pnictine ligands. A computational study revealed that the exchange of alkyl/aryl substituents in stibines with $SbCl_3$ likely occurs *via* a 3c-2e intermediate, which could have future implications for the design of more complex stibines.

References

1 J. D. Smith, in *Comprehensive Inorganic Chemistry*, Elsevier, New York, 1st Edn., 1973, pp. 547–683.

2 C. Y. Wang, *Antimony : its History, Chemistry, Mineralogy, Geology, Metallurgy, Uses, Preparations, Analysis, Production, and Valuation; with Complete Bibliographies*, Charles Griffin and Company, London, 2nd edn., 1919.

3 R. R. Seal II, K. J. Schulz and J. H. DeYoung Jr, in *Critical Mineral Resources of the United States—Economic and Environmental Geology and Prospects for Future Supply*, U.S. Geological Survey, Reston, Virginia, 2017, pp. C1–C13.

4 M. E. Weeks, *J. Chem. Educ.*, 1932, **9**, 11.

5 A. J. Shortland, *Archaeometry*, 2006, **48**, 657–669.

6 P. R. S. Moorey, in *Ancient Mesopotamian Materials and Industries: The Archaeological Evidence*, Eisenbrauns, Indiana, 1999, p. 241.

7 C. A. McAuliffe, in *Comprehensive Coordination Chemistry*, ed. G. Wilkinson, Pergamon, Oxford, 1st Edn., 1987, pp. 227–298.

8 W. Levason and G. Reid, in *Comprehensive Coordination Chemistry II*, eds. J. A. McCleverty and T. J. Meyer, Elsevier Inc., Amsterdam, 1st edn., 2003, pp. 465–544.

9 W. Levason and G. Reid, in *Comprehensive Coordination Chemistry II*, eds. J. A. McCleverty and T. J. Meyer, Elsevier Inc., Amsterdam, 1st edn., 2004, vol. 1, pp. 377–389.

10 L. C. Allen, *J. Am. Chem. Soc.*, 1989, **111**, 9003–9014.

11 J. Emsley, *The Elements*, Clarendon Pess, Oxford, 2nd edn., 1991.

12 P. Pyykko, *Chem. Rev.*, 1988, **88**, 563–594.

13 F. Jones, *J. Chem. Soc.*, 1876, **29**, 641–650.

14 E. Amberger, *Chem. Ber.*, 1961, **94**, 1447–1452.

15 J. M. Bellama and A. G. Macdiarmid, *Inorg. Chem.*, 1968, **7**, 2070–2072.

16 H. H. Nielsen, *J. Chem. Phys.*, 1952, **20**, 1955–1956.

17 W. Kutzelnigg, *Angew. Chem. Int. Ed. Engl.*, 1984, **23**, 272–295.

18 H. J. Breunig and R. Rösler, *Coord. Chem. Rev.*, 1997, **163**, 33–53.

19 A. J. Ashe, E. G. Ludwig, J. Oleksyszyn and J. C. Huffman, *Organometallics*, 1984, **3**, 337–338.

20 A. J. Ashe and E. G. Ludwig, *J. Organomet. Chem.*, 1986, **308**, 289–296.

21 F. A. Paneth, *Trans. Faraday Soc.*, 1934, **30**, 179–181.

22 N. Tokitoh, Y. Arai, T. Sasamori, R. Okazaki, S. Nagase, H. Uekusa and Y. Ohashi, *J. Am. Chem. Soc.*, 1998, **120**, 433–434.

23 R. J. Schwamm and M. P. Coles, *Chem. – A Eur. J.*, 2019, **25**, 14183–14191.

24 L. Tuscher, C. Helling, C. Ganesamoorthy, J. Krüger, C. Wölper, W. Frank, A. S. Nizovtsev and S. Schulz, *Chem. Eur. J.*, 2017, **23**, 12297–12304.

25 A. H. Cowley, N. C. Norman, M. Pakulski, D. L. Bricker and D. H. Russell, *J. Am. Chem. Soc.*, 1985, **107**, 8211–8218.

26 X. Zheng, X. Wang, Y. Qiu, Y. Li, C. Zhou, Y. Sui, Y. Li, J. Ma and X. Wang, *J. Am. Chem. Soc.*, 2013, **135**, 14912–14915.

27 T. Sasamori, E. Mieda, N. Nagahora, K. Sato, D. Shiomi, T. Takui, Y. Hosoi, Y. Furukawa, N. Takagi, S. Nagase and N. Tokitoh, *J. Am. Chem. Soc.*, 2006, **128**, 12582–12588.

28 T. Li, H. Wei, Y. Fang, L. Wang, S. Chen, Z. Zhang, Y. Zhao, G. Tan and X. Wang, *Angew. Chem. Int. Ed.*, 2017, **56**, 632–636.

29 R. Kretschmer, D. A. Ruiz, C. E. Moore, A. L. Rheingold and G. Bertrand, *Angew. Chem. Int. Ed.*, 2014, **53**, 8176–8179.

30 C. Ganesamoorthy, C. Helling, C. Wölper, W. Frank, E. Bill, G. E. Cutsail and S. Schulz, *Nat. Commun.*, 2018, **9**, 87.

31 S. Benz, A. I. Poblador-Bahamonde, N. Low-Ders and S. Matile, *Angew. Chem. Int. Ed.*, 2018, **57**, 5408–5412.

32 M. Á. García-Monforte, M. Baya, D. Joven-Sancho, I. Ara, A. Martín and B. Menjón, *J. Organomet. Chem.*, 2019, **897**, 185–191.

33 G. O. Doak and L. D. Freedman, *Synth.*, 1974, **1974**, 328–338.

34 H. A. Meinema, H. F. Martens and J. G. Noltes, *J. Organomet. Chem.*, 1973, **51**, 223–230.

35 S. Sato, Y. Matsumura and R. Okawara, *J. Organomet. Chem.*, 1972, **43**, 333–337.

36 Y. Matsumara and R. Okawara, *Inorg. Nucl. Chem. Lett.*, 1969, **5**, 449–452.

37 W. Hewertson and H. R. Watson, *J. Chem. Soc.*, 1962, 1490–1494.

38 E. Amberger and R. W. Salazar G, *J. Organomet. Chem.*, 1967, **8**, 111–114.

39 H. Schumann and M. Schmidt, *Inorg. Nucl. Chem. Lett.*, 1965, **1**, 1–5.

40 H. Schumann, T. Östermann and M. Schmidt, *J. Organomet. Chem.*, 1967, **8**, 105–110.

41 A. Steinicke, K.-H. Thiele, A. Haaland, V. I. Sokolov and H. V. Volden, *Z. Anorg. Allg. Chem.*, 1997, **623**, 1925–1930.

42 H. J. Breunig, R. Rösler and E. Lork, *Organometallics*, 1998, **17**, 5594–5595.

43 A. Sladek and H. Schmidbaur, *Chem. Ber.*, 1995, **128**, 565–567.

44 D. C. Mente, J. L. Mills and R. E. Mitchell, *Inorg. Chem.*, 1975, **14**, 123–126.

45 R. D. W. Kemmitt, D. I. Nichols and R. D. Peacock, *J. Chem Soc. (A)*, 1968, 2149.

46 G. S. Hiers, *Org. Synth.*, 1927, **7**, 80.

47 D. Tofan and F. P. Gabbaï, *Chem. Sci.*, 2016, **7**, 6768–6778.

48 D. G. Hendershot, J. C. Pazik, C. George and A. D. Berry, *Organometallics*, 1992, **11**, 2163–2168.

49 G. O. Doak, G. G. Long, M. E. Key, L. W. Bush, D. W. Thompson and A. L. Allred, in *Inorganic Syntheses: Volume IX*, ed. S. Y. Tyree Jr., McGraw-Hill, New York, 1967, pp. 92–97.

50 Y. Kitamura, M. Matsumura, Y. Murata, M. Yamada, N. Kakusawa, M. Tanaka, H. Okabe, H. Naka, T. Obata and S. Yasuike, *J. Fluor. Chem.*, 2017, **199**, 1–6.

51 R. E. Banks, R. N. Haszeldine and R. Hatton, *Tetrahedron Lett.*, 1967, **8**, 3993–3996.

52 M. Yang and F. P. Gabbaï, *Inorg. Chem.*, 2017, **56**, 8644–8650.

53 A. J. Banister and L. F. Moore, *J. Chem Soc. (A)*, 1968, 1137.

54 N. Bricklebank, S. M. Godfrey, H. P. Lane, C. A. McAuliffe and R. G. Pritchard, *J. Chem. Soc., Dalton Trans.*, 1994, 1759–1763.

55 G. E. Parris and F. E. Brinckman, *J. Org. Chem.*, 1975, **40**, 3801–3803.

56 H. von Landolt, *Ann. der Chemie und Pharm.*, 1851, **78**, 91–96.

57 J. Chatt and F. G. Mann, *J. Chem. Soc.*, 1940, 1192–1196.

58 B. Pan and F. P. Gabbaï, *J. Am. Chem. Soc.*, 2014, **136**, 9564–9567.

59 M. A. García-Monforte, P. J. Alonso, I. Ara, B. Menjón and P. Romero, *Angew. Chem. Int. Ed.*, 2012, **51**, 2754–2757.

60 A. J. Downs, R. Schmutzler and I. A. Steer, *Chem. Commun.*, 1966, 221–222.

61 E. L. Muetterties, W. Mahler, K. J. Packer and R. Schmutzler, *Inorg. Chem.*, 1964, **3**, 1298–1303.

62 G. E. Parris, G. G. Long, B. C. Andrews and R. M. Parris, *J. Org. Chem.*, 1976, 41, 1276–1277.

63 A. Schmidt, *Chem. Ber.*, 1968, **101**, 4015–4021.

64 A. L. Beauchamp, M. J. Bennett and F. A. Cotton, *J. Am. Chem. Soc.*, 1968, **90**, 6675–6680.

65 I. R. Beattie, K. M. S. Livingston, G. A. Ozin and R. Sabine, *J. Chem. Soc., Dalton Trans.*, 1972, 784–786.

66 M. Hall and D. B. Sowerby, *J. Chem. Soc., Dalton Trans.*, 1983, 1095–1099.

67 H. J. Breunig, M. Denker, K. H. Ebert and E. Lork, *Zeitschrift für Anorg. und Allg. Chemie*, 1997, **623**, 1151–1156.

68 J. F. Harrison, *J. Am. Chem. Soc.*, 1981, **103**, 7406–7413.

69 R. J. Boyd, N. Burford and C. L. B. Macdonald, *Organometallics*, 1998, **17**, 4014–4029.

70 F. Reiß, A. Schulz and A. Villinger, *Eur. J. Inorg. Chem.*, 2012, **2012**, 261–271.

71 A. H. Cowley, M. Lattman and J. C. Wilburn, *Inorg. Chem.*, 1981, **20**, 2916–2919.

72 F. Carré, C. Chuit, R. J. P. Corriu, A. Mehdi and C. Reyé, *J. Organomet. Chem.*, 1997, **529**, 59–68.

73 N. Burford, P. J. Ragogna, R. McDonald and M. J. Ferguson, *J. Am. Chem. Soc.*, 2003,

125, 14404–14410.

74 M. Olaru, D. Duvinage, E. Lork, S. Mebs and J. Beckmann, *Angew. Chem. Int. Ed.*, 2018, **57**, 10080–10084.

75 M. Olaru, D. Duvinage, E. Lork, S. Mebs and J. Beckmann, *Chem. Eur. J.*, 2019, **25**, 14758–14761.

76 Y. Mourad, Y. Mugnier, H. J. Breunig and M. Ateş, *J. Organomet. Chem.*, 1990, **388**, c9–c11.

77 J. T. Price, M. Lui, N. D. Jones and P. J. Ragogna, *Inorg. Chem.*, 2011, **50**, 12810–12817.

78 G. E. Coates and J. G. Livingstone, *Chem. Ind.*, 1958, 1366.

79 J. W. Wielandt, N. L. Kilah, A. C. Willis and S. B. Wild, *Chem. Commun.*, 2006, **1**, 3679–3680.

80 S. S. Chitnis, N. Burford, R. McDonald and M. J. Ferguson, *Inorg. Chem.*, 2014, **53**, 5359–5372.

81 N. L. Kilah, S. Petrie, R. Stranger, J. W. Wielandt, A. C. Willis and S. B. Wild, *Organometallics*, 2007, **26**, 6106–6113.

82 S. S. Chitnis, B. Peters, E. Conrad, N. Burford, R. McDonald and M. J. Ferguson, *Chem. Commun.*, 2011, **47**, 12331–12333.

83 N. L. Kilah, S. Petrie, R. Stranger, J. Wolfram Wielandt, A. C. Willis and S. Bruce Wild, *Organometallics*, 2007, **26**, 6106–6113.

84 K. G. Pearce, A. M. Borys, E. R. Clark and H. J. Shepherd, *Inorg. Chem.*, 2018, **57**, 11530–11536.

85 H. Althaus, H. J. Breunig and E. Lork, *Chem. Commun.*, 1999, **5**, 1971–1972.

86 C. Hering, M. Lehmann, A. Schulz and A. Villinger, *Inorg. Chem.*, 2012, **51**, 8212–8224.

87 W. Levason and G. Reid, *Coord. Chem. Rev.*, 2006, **250**, 2565–2594.

88 N. R. Champness and W. Levason, *Coord. Chem. Rev.*, 1994, **133**, 115–217.

89 V. K. Greenacre, W. Levason and G. Reid, *Coord. Chem. Rev.*, 2021, **432**, 213698.

90 G. Henrici-Olivé and S. Olivé, *J. Organomet. Chem.*, 1972, **46**, 101–104.

91 R. Talay and D. Rehder, *Chem. Ber.*, 1978, **111**, 1978–1988.

92 F. Näumann, D. Rehder and V. Pank, *Inorg. Chim. Acta.*, 1984, **84**, 117–123.

93 F. Näumann and R. Dieter, *Z. Naturforsch., B: Chem. Sci*, 1984, **39**, 1654.

94 I. Suzuki and Y. Yamamoto, *J. Org. Chem.*, 1993, **58**, 4783–4784.

95 J. E. Ellis, K. L. Fjare and G. F. Warnock, *Inorg. Chim. Acta.*, 1995, **240**, 379–384.

96 T. A. George, *J. Chem. Soc. D*, 1970, 1632–1632.

97 E. E. Isaacs and W. A. G. Graham, *J. Organomet. Chem.*, 1975, **90**, 319–328.

98 R. Schemm and W. Malisch, *J. Organomet. Chem.*, 1985, **288**, C9–C12.

99 C. L. Hyde and D. J. Darensbourg, *Inorg. Chem.*, 1973, **12**, 1286–1291.

100 H. Fischer and A. Ruhs, *J. Organomet. Chem.*, 1979, **170**, 181–194.

101 A. Ishiguro, M. Takahashi and M. Takeda, *J. Organomet. Chem.*, 2000, **611**, 558–565.

102 P. Umland and H. Vahrenkamp, *Chem. Ber.*, 1982, **115**, 3555–3564.

103 H. Joachim Breunig and W. Fichtner, *J. Organomet. Chem.*, 1981, **222**, 97–103.

104 H. Schumann, H. J. Breunig and U. Frank, *J. Organomet. Chem.*, 1973, **60**, 279–286.

105 H. Schumann and H. J. Breunig, *J. Organomet. Chem.*, 1971, **27**, C28–C30.

106 P. Jutzi and M. Kuhn, *J. Organomet. Chem.*, 1979, **177**, 349–356.

107 H. Schumann and H. J. Breunig, *J. Organomet. Chem.*, 1974, **76**, 225–233.

108 T. Bartik, T. Krümmling, C. Krüger, L. Markò, R. Boese, G. Schmid, P. Vivarelli and G. Pàlyi, *J. Organomet. Chem.*, 1991, **421**, 323–333.

109 G. Cetini, O. Gambino, R. Rossetti and P. L. Stanghellini, *Inorg. Chem.*, 1968, **7**, 609–610.

110 W. Hieber and V. Frey, *Chem. Ber.*, 1966, **99**, 2607–2613.

111 P. E. Garrou and G. E. Hartwell, *J. Organomet. Chem.*, 1974, **69**, 445–453.

112 W. Hieber and W. Freyer, *Chem. Ber.*, 1960, **93**, 462–467.

113 S. M. Godfrey, H. P. Lane, C. A. McAuliffe and R. G. Pritchard, *J. Chem. Soc., Dalton Trans.*, 1993, 1599.

114 G. M. Bodner, C. Gagnon and D. N. Whittern, *J. Organomet. Chem.*, 1983, **243**, 305–314.

115 G. M. Bodner, M. P. May and L. E. Mckinney, *Inorg. Chem.*, 1980, **19**, 1951–1958.

116 H. J. Breunig, T. Borrmann, E. Lork, O. Moldovan, C. I. Raţ and R. P. Wagner, *J. Organomet. Chem.*, 2009, **694**, 427–432.

117 P. K. Baker, M. Al-Jahdali and M. M. Meehan, *J. Organomet. Chem.*, 2002, **648**, 99–108.

118 P. K. Baker, M. B. Hursthouse, A. I. Karaulov, A. J. Lavery, K. M. A. Malik, D. J. Muldoon and A. Shawcross, *J. Chem. Soc., Dalton Trans.*, 1994, 3493–3498.

119 S. C. Tripathi, S. C. Srivastava and D. P. Pandey, *Transit. Met. Chem.*, 1977, **2**, 52–54.

120 R. Colton and C. Rix, *Aust. J. Chem.*, 1969, **22**, 305.

121 D. K. Gupta, A. N. Sahay, D. S. Pandey, N. K. Jha, P. Sharma, G. Espinosa, A. Cabrera, M. C. Puerta and P. Valerga, *J. Organomet. Chem.*, 1998, **568**, 13–20.

122 A. V. Malkov, I. R. Baxendale, M. Bella, V. Langer, J. Fawcett, D. R. Russell, D. J. Mansfield, M. Valko and P. Kočovský, *Organometallics*, 2001, **20**, 673–690.

123 D. Jan, L. Delaude, F. Simal, A. Demonceau and A. F. Noels, *J. Organomet. Chem.*, 2000, **606**, 55–64.

124 S. Wache, W. A. Herrmann, G. Artus, O. Nuyken and D. Wolf, *J. Organomet. Chem.*, 1995, **491**, 181–188.

125 P. K. Baker, S. G. Fraser and M. G. B. Drew, *J. Chem. Soc., Dalton Trans.*, 1988, 2729–2734.

126 M. Bruce, J. Matisons and R. Wallis, *Aust. J. Chem.*, 1982, **35**, 935.

127 B. F. G. Johnson, J. Lewis and A. J. Whitton, *J. Chem. Soc., Dalton Trans.*, 1990, 3129–3135.

128 Y. Liu, W. K. Leong and R. K. Pomeroy, *Organometallics*, 1998, **17**, 3387–3389.

129 B. F. G. Johnson, J. Lewis, M. A. Pearsall and L. G. Scott, *J. Organomet. Chem.*, 1991, **413**, 337–353.

130 G. Chen and K. L. Weng, *J. Clust. Sci.*, 2006, **17**, 111–118.

131 W. V. Taylor, U. H. Soto, V. M. Lynch and M. J. Rose, *Inorg. Chem.*, 2016, **55**, 3206–3208.

132 W. V. Taylor, C. X. Cammack, S. A. Shubert and M. J. Rose, *Inorg. Chem.*, 2019, **58**, 16330–16345.

133 J. R. Black, W. Levason, M. D. Spicer and M. Webster, *J. Chem. Soc., Dalton Trans.*, 1993, 3129–3136.

134 A. M. Hill, W. Levason and M. Webster, *Inorg. Chem.*, 1996, **35**, 3428–3430.

135 A. F. Chiffey, J. Evans, W. Levason and M. Webster, *Organometallics*, 1996, **15**, 1280–1283.

136 S. L. Benjamin, W. Levason and G. Reid, *Organometallics*, 2013, **32**, 2760–2767.

137 G. C. Welch, L. Cabrera, P. A. Chase, E. Hollink, J. D. Masuda, P. Wei and D. W. Stephan, *Dalton Trans.*, 2007, 3407.

138 U. Mayer, V. Gutmann and W. Gerger, *Monatshefte für Chemie*, 1975, **106**, 1235–1257.

139 H. Hirao, K. Omoto and H. Fujimoto, *J. Phys. Chem. A*, 1999, **103**, 5807–5811.

140 M. A. Beckett, G. C. Strickland, J. R. Holland and K. Sukumar Varma, *Polymer.*, 1996, **37**, 4629–4631.

141 M. A. Beckett, D. S. Brassington, S. J. Coles and M. B. Hursthouse, *Inorg. Chem. Commun.*, 2000, **3**, 530–533.

142 C. B. Caputo, L. J. Hounjet, R. Dobrovetsky and D. W. Stephan, *Science.*, 2013, **341**, 1374–1377.

143 R. F. Childs, D. L. Mulholland and A. Nixon, *Can. J. Chem.*, 1982, **60**, 801–808.

144 A. E. Ashley, T. J. Herrington, G. G. Wildgoose, H. Zaher, A. L. Thompson, N. H. Rees, T. Krämer and D. O'Hare, *J. Am. Chem. Soc.*, 2011, **133**, 14727–14740.

145 J. N. Bentley, S. A. Elgadi, J. R. Gaffen, P. Demay-Drouhard, T. Baumgartner and C. B. Caputo, *Organometallics*, 2020, **39**, 3645–3655.

146 J. R. Gaffen, J. N. Bentley, L. C. Torres, C. Chu, T. Baumgartner and C. B. Caputo, *Chem*, 2019, **5**, 1567–1583.

147 T. Baumgartner, T. Neumann and B. Wirges, *Angew. Chem. Int. Ed.*, 2004, **43**, 6197–

6201.

148 R. S. Drago, D. C. Ferris and N. Wong, *J. Am. Chem. Soc.*, 1990, **112**, 8953–8961.

149 R. S. Drago, N. Wong, C. Bilgrien and G. C. Vogel, *Inorg. Chem.*, 1987, **26**, 9–14.

150 R. S. Drago and B. B. Wayland, *J. Am. Chem. Soc.*, 1965, **87**, 3571–3577.

151 R. S. Drago, *Inorg. Chem.*, 1982, **21**, 1697–1698.

152 R. S. Drago and C. J. Bilgrien, *Polyhedron*, 1988, **7**, 1453–1468.

153 K. O. Christe, D. A. Dixon, D. McLemore, W. W. Wilson, J. A. Sheehy and J. A. Boatz, *J. Fluor. Chem.*, 2000, **101**, 151–153.

154 H. Böhrer, N. Trapp, D. Himmel, M. Schleep and I. Krossing, *Dalton Trans.*, 2015, **44**, 7489–7499.

155 M. Yang, D. Tofan, C. H. Chen, K. M. Jack and F. P. Gabbaï, *Angew. Chem. Int. Ed.*, 2018, **57**, 13868–13872.

156 P. Erdmann, J. Leitner, J. Schwarz and L. Greb, *ChemPhysChem*, 2020, **21**, 987–994.

157 H. Böhrer, N. Trapp, D. Himmel, M. Schleep and I. Krossing, *Dalton Trans.*, 2015, **44**, 7489–7499.

158 A. T. Maynard, M. Huang, W. G. Rice and D. G. Covell, *Proc. Natl. Acad. Sci.*, 1998, **95**, 11578–11583.

159 R. G. Parr, L. V. Szentpály and S. Liu, *J. Am. Chem. Soc.*, 1999, **121**, 1922–1924.

160 P. W. Ayers, W. Yang and J. Bartolotti, L., in *Chemical Reactivity Theory: A Density Functional View*, ed. P. K. Chatteraj, CRC Press, Boca Raton, FL, 1st Edn., 2009.

161 R. G. Parr and W. Yang, *J. Am. Chem. Soc.*, 1984, **106**, 4049–4050.

162 R. G. Parr, R. A. Donnelly, M. Levy and W. E. Palke, *J. Chem. Phys.*, 1978, **68**, 3801–3807.

163 A. R. Jupp, T. C. Johnstone and D. W. Stephan, *Dalton Trans.*, 2018, **47**, 7029–7035.

164 A. R. Jupp, T. C. Johnstone and D. W. Stephan, *Inorg. Chem.*, 2018, **57**, 14764–14771.

165 F. Grandinetti, G. Occhiucci, O. Ursini, G. de Petris and M. Speranza, *Int. J. Mass Spectrom. Ion Processes.*, 1993, **124**, 21–36.

166 Y. Hayashi, J. J. Rohde and E. J. Corey, *J. Am. Chem. Soc.*, 1996, **118**, 5502–5503.

167 S. Antoniotti, V. Dalla and E. Duñach, *Angew. Chem. Int. Ed.*, 2010, **49**, 7860–7888.

168 G. A. Olah, G. K. S. Prakash and J. Sommer, *Science.*, 1979, **206**, 13–20.

169 L. O. Müller, D. Himmel, J. Stauffer, G. Steinfeld, J. Slattery, G. Santiso-Quiñones, V. Brecht and I. Krossing, *Angew. Chem. Int. Ed.*, 2008, **47**, 7659–7663.

170 D. W. Stephan, *Org. Biomol. Chem.*, 2008, **6**, 1535–1539.

171 D. W. Stephan and G. Erker, *Angew. Chem. Int. Ed.*, 2015, **54**, 6400–6441.

172 J. M. Bayne and D. W. Stephan, *Chem. Soc. Rev.*, 2016, **45**, 765–774.

173 P. P. Power, *Nature*, 2010, **463**, 171–177.

174 D. W. Stephan, *Org. Biomol. Chem.*, 2012, **10**, 5740–5746.

175 A. R. Jupp and D. W. Stephan, *Trends Chem.*, 2019, **1**, 35–48.

176 D. W. Stephan, *Acc. Chem. Res.*, 2015, **48**, 306–316.

177 A. Moroz and R. L. Sweany, *Inorg. Chem.*, 1992, **31**, 5236–5242.

178 A. Moroz, R. L. Sweany and S. L. Whittenburg, *J. Phys. Chem.*, 1990, **94**, 1352–1357.

179 H. J. Himmel and J. Vollet, *Organometallics*, 2002, **21**, 5972–5977.

180 Z. L. Xiao, R. H. Hauge and J. L. Margrave, *Inorg. Chem.*, 1993, **32**, 642–646.

181 S. A. Kulkarni, *J. Phys. Chem. A*, 1998, **102**, 7704–7711.

182 S. A. Kulkarni and A. K. Srivastava, *J. Phys. Chem. A*, 1999, **103**, 2836–2842.

183 G. H. Spikes, J. C. Fettinger and P. P. Power, *J. Am. Chem. Soc.*, 2005, **127**, 12232–12233.

184 G. C. Welch, R. R. San Juan, J. D. Masuda and D. W. Stephan, *Science.*, 2006, **314**, 1124–1126.

185 K. Von Deuten and D. Rehder, *Cryst. Struct. Commun.*, 1980, **9**, 167.

186 G. C. Welch and D. W. Stephan, *J. Am. Chem. Soc.*, 2007, **129**, 1880–1881.

187 R. Roesler, W. E. Piers and M. Parvez, *J. Organomet. Chem.*, 2003, **680**, 218–222.

188 K. Chernichenko, M. Nieger, M. Leskelä and T. Repo, *Dalton Trans.*, 2012, **41**, 9029–9032.

189 V. Sumerin, K. Chernichenko, M. Nieger, M. Leskelä, B. Rieger and T. Repo, *Adv. Synth. Catal.*, 2011, **353**, 2093–2110.

190 Y. Guo and S. Li, *Inorg. Chem.*, 2008, **47**, 6212–6219.

191 A. Hamza, A. Stirling, T. A. Rokob and I. Pápai, *Int. J. Quantum Chem.*, 2009, **109**, 2416–2425.

192 T. A. Rokob, A. Hamza, A. Stirling, T. Soós and I. Pápai, *Angew. Chem. Int. Ed.*, 2008, **47**, 2435–2438.

193 S. Grimme, H. Kruse, L. Goerigk and G. Erker, *Angew. Chem. Int. Ed.*, 2010, **49**, 1402–1405.

194 J. Paradies, *Synlett*, 2013, **24**, 777–780.

195 D. W. Stephan and G. Erker, in *Frustrated Lewis Pairs I. Topics in Current Chemistry*, eds. D. W. Stephan and G. Erker, Springer Berlin Heidelberg, Berlin, Heidelberg, 2013, pp. 85–110.

196 J. Paradies, *Angew. Chem. Int. Ed.*, 2014, **53**, 3552–3557.

197 P. A. Chase, T. Jurca and D. W. Stephan, *Chem. Commun.*, 2008, 1701.

198 P. A. Chase, G. C. Welch, T. Jurca and D. W. Stephan, *Angew. Chem. Int. Ed.*, 2007, **46**, 8050–8053.

199 L. (Leo) Liu, L. L. Cao, Y. Shao, G. Ménard and D. W. Stephan, *Chem*, 2017, **3**, 259–267.

200 Z. Dong, H. H. Cramer, M. Schmidtmann, L. A. Paul, I. Siewert and T. Müller, *J. Am. Chem. Soc.*, 2018, **140**, 15419–15424.

201 A. Merk, H. Großekappenberg, M. Schmidtmann, M. Luecke, C. Lorent, M. Driess, M. Oestreich, H. F. T. Klare and T. Müller, *Angew. Chem. Int. Ed.*, 2018, **57**, 15267–15271.

202 Y. Soltani, A. Dasgupta, T. A. Gazis, D. M. C. Ould, E. Richards, B. Slater, K. Stefkova, V. Y. Vladimirov, L. C. Wilkins, D. Willcox and R. L. Melen, *Cell Reports Phys. Sci.*, 2020, **1**, 100016.

203 T. Mahdi, Z. M. Heiden, S. Grimme and D. W. Stephan, *J. Am. Chem. Soc.*, 2012, **134**, 4088–4091.

204 S. Schwendemann, T. A. Tumay, K. V. Axenov, I. Peuser, G. Kehr, R. Fröhlich and G. Erker, *Organometallics*, 2010, **29**, 1067–1069.

205 H. Wang, R. Fröhlich, G. Kehr and G. Erker, *Chem. Commun.*, 2008, 5966.

206 C. M. Mömming, E. Otten, G. Kehr, R. Fröhlich, S. Grimme, D. W. Stephan and G. Erker, *Angew. Chem. Int. Ed.*, 2009, **48**, 6643–6646.

207 A. Berkefeld, W. E. Piers and M. Parvez, *J. Am. Chem. Soc.*, 2010, **132**, 10660–10661.

208 A. E. Ashley, A. L. Thompson and D. O'Hare, *Angew. Chem. Int. Ed.*, 2009, **48**, 9839–9843.

209 M. Sajid, A. Klose, B. Birkmann, L. Liang, B. Schirmer, T. Wiegand, H. Eckert, A. J. Lough, R. Fröhlich, C. G. Daniliuc, S. Grimme, D. W. Stephan, G. Kehr and G. Erker, *Chem. Sci.*, 2013, **4**, 213–219.

210 G. Ménard, J. A. Hatnean, H. J. Cowley, A. J. Lough, J. M. Rawson and D. W. Stephan, *J. Am. Chem. Soc.*, 2013, **135**, 6446–6449.

211 A. J. P. Cardenas, B. J. Culotta, T. H. Warren, S. Grimme, A. Stute, R. Fröhlich, G. Kehr and G. Erker, *Angew. Chem. Int. Ed.*, 2011, **50**, 7567–7571.

212 M. Sajid, A. Stute, A. J. P. Cardenas, B. J. Culotta, J. A. M. Hepperle, T. H. Warren, B. Schirmer, S. Grimme, A. Studer, C. G. Daniliuc, R. Fröhlich, J. L. Petersen, G. Kehr and G. Erker, *J. Am. Chem. Soc.*, 2012, **134**, 10156–10168.

213 M. Rueping and B. J. Nachtsheim, *Beilstein J. Org. Chem.*, 2010, **6**, 1–24.

214 T. Mukaiyama and K. Narasaka, *Org. Synth.*, 1987, **65**, 6.

215 K. Maruoka, A. B. Concepcion and H. Yamamoto, *Bull. Chem. Soc. Jpn.*, 1992, **65**, 3501–3503.

216 G. J. Evans and E. D. Owen, *J. Chem. Soc.*, 1959, 4123–5125.

217 G. Sauvet, J. P. Vairon and P. Sigwalt, *J. Polym. Sci. Polym. Symp.*, 1975, **52**, 173–187.

218 L. J. Hounjet, C. Bannwarth, C. N. Garon, C. B. Caputo, S. Grimme and D. W. Stephan, *Angew. Chem. Int. Ed.*, 2013, **52**, 7492–7495.

219 H. Yamamoto, Ed., *Lewis Acids in Organic Synthesis: A Comprehensive Handbook*, Wiley-VCH Verlag, Weinheim, 1st edn., 2000.

220 D. Schinzer, Ed., *Selectivities in Lewis Acid Promoted Reactions*, Springer Netherlands, 1st edn., 1989.

221 L.-L. Gundersen, F. Rise, K. Undheim, E. Aguilar and P. García-García, in *Encyclopedia of Reagents for Organic Synthesis*, John Wiley & Sons, Ltd, Chichester, UK, 2007.

222 V. Cornel and C. J. Lovely, in *Encyclopedia of Reagents for Organic Synthesis*, John Wiley & Sons, Ltd, Chichester, UK, 2007.

223 W. E. Piers and T. Chivers, *Chem. Soc. Rev.*, 1997, **26**, 345–354.

224 S. Döring, G. Erker, R. Fröhlich, O. Meyer and K. Bergander, *Organometallics*, 1998, **17**, 2183–2187.

225 I. B. Sivaev and V. I. Bregadze, *Coord. Chem. Rev.*, 2014, **270**–**271**, 75–88.

226 G. Erker, *Dalton Trans.*, 2005, 1883.

227 D. W. Stephan, *Dalton Trans.*, 2009, 3129.

228 K. Ishihara, N. Hanaki, M. Funahashi, M. Miyata and H. Yamamoto, *Bull. Chem. Soc. Jpn.*, 1995, **68**, 1721–1730.

229 K. Ishihara and H. Yamamoto, *European J. Org. Chem.*, 1999, **1999**, 527–538.

230 C.-H. Chen and F. P. Gabbaï, *Angew. Chem. Int. Ed.*, 2017, **56**, 1799–1804.

231 T. J. Marks, *Acc. Chem. Res.*, 1992, **25**, 57–65.

232 X. Yang, C. L. Stern and T. J. Marks, *J. Am. Chem. Soc.*, 1994, **116**, 10015–10031.

233 P. Jutzi and T. Redeker, *Eur. J. Inorg. Chem.*, 1998, **1998**, 663–674.

234 U. Blaschke, G. Erker, M. Nissinen, E. Wegelius and R. Fröhlich, *Organometallics*, 1999, **18**, 1224–1234.

235 J. R. Lawson, L. C. Wilkins and R. L. Melen, *Chem. Eur. J.*, 2017, **23**, 10997–11000.

236 L. C. Wilkins, J. R. Lawson, P. Wieneke, F. Rominger, A. S. K. Hashmi, M. M. Hansmann and R. L. Melen, *Chem. Eur. J.*, 2016, **22**, 14618–14624.

237 J. R. Lawson and R. L. Melen, *Inorg. Chem.*, 2017, **56**, 8627–8643.

238 Q. Yin, Y. Soltani, R. L. Melen and M. Oestreich, *Organometallics*, 2017, **36**, 2381–2384.

239 J. Emsley, *The Elements*, Oxford University Press, Oxford, 3rd Edn., 1998.

240 N. LeBlond, P. Kolb, H. P. A. Mercier, W. J. Casteel and G. J. Schrobilgen, *Inorg. Chem.*, 2002, **35**, 929–942.

241 V. Y. Kavun, L. A. Zemnukhova, V. I. Sergienko, T. A. Kaidalova, R. L. Davidovich and N. I. Sorokin, *Russ. Chem. Bull.*, 2002, **51**, 1996–2002.

242 C. Leroy, R. Johannson and D. L. Bryce, *J. Phys. Chem. A*, 2019, **123**, 1030–1043.

243 H. Tou, M. Doi, M. Sera, M. Yogi, Y. Kitaoka, H. Kotegawa, G. -q. Zheng, H. Harima, H. Sugawara and H. Sato, *Phys. B Condens. Matter*, 2005, **359**–**361**, 892–894.

244 R. G. Kidd, in *Annual Reports on NMR Spectroscopy*, Academic Press, London, 1991, pp. 85–139.

245 R. G. Kidd, in *The Multinuclear Approach to NMR Spectroscopy*, Springer Netherlands, Dordrecht, 1983, pp. 445–456.

246 C. J. Jameson and J. Mason, in *Multinuclear NMR*, Springer US, Boston, MA, 1987, pp. 51–88.

247 C. J. Jameson and H. J. Osten, in *Annual Reports on NMR Spectroscopy*, Academic Press, London, 1986, vol. 17, pp. 1–78.

248 I. Morishima, K. Endo and T. Yonezawa, *J. Chem. Phys.*, 1973, **59**, 3356–3364.

249 Y. Nomura, Y. Takeuchi and N. Nakagawa, *Tetrahedron Lett.*, 1969, **10**, 639–642.

250 M. Kaupp, O. L. Malkina, V. G. Malkin and P. Pyykkö, *Chem. Eur. J.*, 1998, **4**, 118–126.

251 W. Tyrra and M. S. Wickleder, *J. Organomet. Chem.*, 2003, **677**, 28–34.

252 L. H. Thomas, *Math. Proc. Cambridge Philos. Soc.*, 1927, **23**, 542–548.

253 P. A. M. Dirac, *Math. Proc. Cambridge Philos. Soc.*, 1930, **26**, 376–385.

254 W. Kohn and L. J. Sham, *Phys. Rev.*, 1965, **140**, A1133.

255 P. Hohenberg and W. Kohn, *Phys. Rev.*, 1964, **136**, B864.

256 S. F. Sousa, P. A. Fernandes and M. J. Ramos, *J. Phys. Chem. A*, 2007, **111**, 10439–10452.

257 D. C. Langreth and M. J. Mehl, *Phys. Rev. B*, 1983, **28**, 1809–1834.

258 A. D. Becke, *Phys. Rev. A*, 1988, **38**, 3098–3100.

259 J. P. Perdew, J. A. Chevary, S. H. Vosko, K. A. Jackson, M. R. Pederson, D. J. Singh and C. Fiolhais, *Phys. Rev. B*, 1992, **46**, 6671–6687.

260 J. P. Perdew, K. Burke and M. Ernzerhof, *Phys. Rev. Lett.*, 1996, **77**, 3865–3868.

261 Y. Zhao and D. G. Truhlar, *Theor. Chem. Acc.*, 2008, **120**, 215–241.

262 R. Ditchfield, W. J. Hehre and J. A. Pople, *J. Chem. Phys.*, 1971, **54**, 724–728.

263 S. Kristyán and P. Pulay, *Chem. Phys. Lett.*, 1994, **229**, 175–180.

264 J. M. Pérez-Jordá and A. D. Becke, *Chem. Phys. Lett.*, 1995, **233**, 134–137.

265 A. Austin, G. A. Petersson, M. J. Frisch, F. J. Dobek, G. Scalmani and K. Throssell, *J. Chem. Theory Comput.*, 2012, **8**, 4989–5007.

266 J. Da Chai and M. Head-Gordon, *Phys. Chem. Chem. Phys.*, 2008, **10**, 6615–6620.

267 S. Grimme, S. Ehrlich and L. Goerigk, *J. Comput. Chem.*, 2011, **32**, 1456–1465.

268 S. Grimme, J. Antony, S. Ehrlich and H. Krieg, *J. Chem. Phys.*, 2010, **132**, 154104.

269 S. Grimme, *J. Comput. Chem.*, 2006, **27**, 1787–1799.

270 L. Goerigk, in *Non-Covalent Interactions in Quantum Chemistry and Physics*, eds. G. DiLabio and A. O. de la Roza, Elsevier, Amsterdam, 2017, pp. 195–219.

271 R. E. Skyner, J. L. McDonagh, C. R. Groom, T. Van Mourik and J. B. O. Mitchell, *Phys. Chem. Chem. Phys.*, 2015, 17, 6174–6191.

272 J. Tomasi, B. Mennucci and R. Cammi, *Chem. Rev.*, 2005, **105**, 2999–3094.

273 C. J. Cramer and D. G. Truhlar, *Chem. Rev.*, 1999, **99**, 2161–2200.

274 I. Mayer, *J. Comput. Chem.*, 2007, **28**, 204–221.

275 A. J. Bridgeman, G. Cavigliasso, L. R. Ireland and J. Rothery, *J. Chem. Soc., Dalton Trans.*, 2001, 2095–2108.

276 I. Mayer and P. Salvador, *Chem. Phys. Lett.*, 2004, **383**, 368–375.

277 J. B. Collins and A. Streitwieser, *J. Comput. Chem.*, 1980, **1**, 81–87.

278 H. P. Lüthi, J. H. Ammeter, J. Almlöf and K. Faegri, *J. Chem. Phys.*, 1982, **77**, 2002–2009.

279 A. E. Reed, R. B. Weinstock and F. Weinhold, *J. Chem. Phys.*, 1985, **83**, 735–746.

280 S. L. Benjamin, T. Krämer, W. Levason, M. E. Light, S. A. Macgregor and G. Reid, *J. Am. Chem. Soc.*, 2016, **138**, 6964–6967.

281 J. R. Lawson and R. L. Melen, in *Organometallic Chemistry Volume 41*, eds. I. Fairlamb, J. M. Lynam, N. J. Patmore and P. Elliott, Royal Society of Chemistry, London, 2017, pp. 1–27.

282 B. E. Maryanoff and A. B. Reitz, *Chem. Rev.*, 1989, **89**, 863–927.

283 Z. Lao and P. H. Toy, *Beilstein J. Org. Chem.*, 2016, **12**, 2577–2587.

284 P. A. Byrne and D. G. Gilheany, *Chem. Soc. Rev.*, 2013, **42**, 6670–6696.

285 M. M. Heravi, M. Ghanbarian, V. Zadsirjan and B. Alimadadi Jani, *Monatshefte fur Chemie*, 2019, **150**, 1365–1407.

286 K. I. Tanji, J. Koshio and O. Sugimoto, *Synth. Commun.*, 2005, **35**, 1983–1987.

287 J. B. Hendrickson and S. M. Schwartzman, *Tetrahedron Lett.*, 1975, **16**, 277–280.

288 G. A. Wiley, R. L. Hershkowitz, B. M. Rein and B. C. Chung, *J. Am. Chem. Soc.*, 1964, **86**, 964–965.

289 Y. Zhang, S. Zhang, X. Lu, Q. Zhou, W. Fan and X. P. Zhang, *Chem. Eur. J.*, 2009, **15**, 3003–3011.

290 K. Tsunashima and M. Sugiya, *Electrochem. Commun.*, 2007, **9**, 2353–2358.

291 C. J. Bradaric, A. Downard, C. Kennedy, A. J. Robertson and Y. Zhou, *Green Chem.*, 2003, **5**, 143–152.

292 R. He, X. Wang, T. Hashimoto and K. Maruoka, *Angew. Chem. Int. Ed.*, 2008, **47**, 9466–9468.

293 R. He, C. Ding and K. Maruoka, *Angew. Chem.*, 2009, **121**, 4629–4631.

294 C. M. Starks, *J. Am. Chem. Soc.*, 1971, **93**, 195–199.

295 S. Liu, Y. Kumatabara and S. Shirakawa, *Green Chem.*, 2016, **18**, 331–341.

296 T. Werner, *Adv. Synth. Catal.*, 2009, **351**, 1469–1481.

297 V. J. Scott, R. Çelenligil-Çetin and O. V. Ozerov, *J. Am. Chem. Soc.*, 2005, **127**, 2852–2853.

298 J. Zhu, M. Pérez and D. W. Stephan, *Angew. Chem. Int. Ed.*, 2016, **55**, 8448–8451.

299 M. Vogler, L. Süsse, J. H. W. Lafortune, D. W. Stephan and M. Oestreich,

Organometallics, 2018, **37**, 3303–3313.

300 M. Pérez, Z. W. Qu, C. B. Caputo, V. Podgorny, L. J. Hounjet, A. Hansen, R. Dobrovetsky, S. Grimme and D. W. Stephan, *Chem. Eur. J.*, 2015, **21**, 6491–6500.

301 M. Mehta, M. H. Holthausen, I. Mallov, M. Pérez, Z. W. Qu, S. Grimme and D. W. Stephan, *Angew. Chem. Int. Ed.*, 2015, **54**, 8250–8254.

302 M. Pérez, T. Mahdi, L. J. Hounjet and D. W. Stephan, *Chem. Commun.*, 2015, **51**, 11301–11304.

303 M. Perez, C. B. Caputo, R. Dobrovetsky and D. W. Stephan, *Proc. Natl. Acad. Sci.*, 2014, **111**, 10917–10921.

304 M. Mehta, I. Garcia de la Arada, M. Perez, D. Porwal, M. Oestreich and D. W. Stephan, *Organometallics*, 2016, **35**, 1030–1035.

305 J. H. W. LaFortune, T. C. Johnstone, M. Pérez, D. Winkelhaus, V. Podgorny and D. W. Stephan, *Dalton Trans.*, 2016, **45**, 18156–18162.

306 V. Fasano, J. H. W. LaFortune, J. M. Bayne, M. J. Ingleson and D. W. Stephan, *Chem. Commun.*, 2018, **54**, 662–665.

307 C. B. Caputo, D. Winkelhaus, R. Dobrovetsky, L. J. Hounjet and D. W. Stephan, *Dalton Trans.*, 2015, **44**, 12256–12264.

308 J. H. W. Lafortune, K. M. Szkop, F. E. Farinha, T. C. Johnstone, S. Postle and D. W. Stephan, *Dalton Trans.*, 2018, **47**, 11411–11419.

309 M. H. Holthausen, M. Mehta and D. W. Stephan, *Angew. Chem. Int. Ed.*, 2014, **53**, 6538–6541.

310 L. Süsse, J. H. W. Lafortune, D. W. Stephan and M. Oestreich, *Organometallics*, 2019, **38**, 712–721.

311 N. L. Dunn, M. Ha and A. T. Radosevich, *J. Am. Chem. Soc.*, 2012, **134**, 11330–11333.

312 G. Li, Z. Qin and A. T. Radosevich, *J. Am. Chem. Soc.*, 2020, **142**, 16205–16210.

313 G. Li, T. V. Nykaza, J. C. Cooper, A. Ramirez, M. R. Luzung and A. T. Radosevich, *J. Am. Chem. Soc.*, 2020, **142**, 6786–6799.

314 M. Lecomte, J. M. Lipshultz, S.-H. Kim-Lee, G. Li and A. T. Radosevich, *J. Am. Chem. Soc.*, 2019, **141**, 12507–12512.

315 C. Le Roux, H. Gaspard-Iloughmane, J. Dubac, J. Jaud and P. Vignaux, *J. Org. Chem.*, 1993, **58**, 1835–1839.

316 M. C. Singh and R. K. Peddinti, *Tetrahedron Lett.*, 2007, **48**, 7354–7357.

317 I. Cepanec, M. Litvić, M. Filipan-Litvić and I. Grüngold, *Tetrahedron*, 2007, **63**, 11822–11827.

318 Q. Wu, Y. Wang, W. Chen and H. Liu, *Synth. Commun.*, 2006, **36**, 1361–1366.

319 G. S. Lal, E. Lobach and A. Evans, *J. Org. Chem.*, 2000, **65**, 4830–4832.

320 S. Mazières, C. Le Roux, M. Peyronneau, H. Gornitzka and N. Roques, *Eur. J. Inorg. Chem.*, 2004, **2004**, 2823–2826.

321 A. K. Bhattacharya, M. A. Diallo and K. N. Ganesh, *Synth. Commun.*, 2008, **38**, 1518–1526.

322 S. Kobayashi, M. Tamura and T. Mukaiyama, *Chem. Lett.*, 1988, **17**, 91–94.

323 S. Uemura, A. Onoe and M. Okano, *Bull. Chem. Soc. Jpn.*, 1974, **47**, 147–150.

324 T. Mukaiyama, K. Suzuki, J. S. Han and S. Kobayashi, *Chem. Lett.*, 1992, **21**, 435–438.

325 S. Uemura, A. Onoe and M. Okano, *Bull. Chem. Soc. Jpn.*, 1974, **47**, 692–697.

326 A. Ninagawa, H. Matsuda and R. Nomura, *J. Org. Chem.*, 1980, **45**, 3735–3738.

327 A. Baba, H. Kashiwagi and H. Matsuda, *Tetrahedron Lett.*, 1985, **26**, 1323–1324.

328 G. G. Long, J. G. Stevens, R. J. Tullbane and L. H. Bowen, *J. Am. Chem. Soc.*, 1970, **92**, 4230–4235.

329 A. Baba, M. Fujiwara and H. Matsuda, *Tetrahedron Lett.*, 1986, **27**, 77–80.

330 M. Fujiwara, A. Baba and H. Matsuda, *J. Heterocycl. Chem.*, 1988, **25**, 1351–1357.

331 M. Fujiwara, A. Baba and H. Matsuda, *Bull. Chem. Soc. Jpn.*, 1990, **63**, 1069–1073.

332 M. Yang, N. Pati, G. Bélanger-Chabot, M. Hirai and F. P. Gabbaï, *Dalton Trans.*, 2018, **47**, 11843–11850.

333 G. Cavallo, P. Metrangolo, R. Milani, T. Pilati, A. Priimagi, G. Resnati and G. Terraneo, *Chem. Rev.*, 2016, **116**, 2478–2601.

334 L. Vogel, P. Wonner and S. M. Huber, *Angew. Chem. Int. Ed.*, 2019, **58**, 1880–1891.

335 L. Guan and Y. Mo, *J. Phys. Chem. A*, 2014, **118**, 8911–8921.

336 V. Angarov and S. Kozuch, *New J. Chem.*, 2018, **42**, 1413–1422.

337 N. Li, R. Qiu, X. Zhang, Y. Chen, S. F. Yin and X. Xu, *Tetrahedron*, 2015, **71**, 4275–4281.

338 I. Krossing and I. Raabe, *Angew. Chem. Int. Ed.*, 2004, **43**, 2066–2090.

339 D. M. Roe and A. G. Massey, *J. Organomet. Chem.*, 1970, **23**, 547–550.

340 S. Lin and J. M. Miller, *J. Fluor. Chem.*, 1977, **9**, 161–169.

341 A. F. M. M. Rahman, T. Murafuji, M. Ishibashi, Y. Miyoshi and Y. Sugihara, *J. Organomet. Chem.*, 2005, **690**, 4280–4284.

342 J. B. Lambert, S. Zhang and S. M. Ciro, *Organometallics*, 1994, **13**, 2430–2443.

343 S. Lancaster, Alkylation of boron trifluoride with pentafluorophenyl Grignard reagent; Tris(pentafluorophenyl)boron; borane, http://cssp.chemspider.com/215, (accessed 1 February 2018).

344 E. Martin, D. L. Hughes and S. J. Lancaster, *Inorg. Chim. Acta.*, 2010, **363**, 275–278.

345 D. J. MacDonald, M. C. Jennings and K. E. Preuss, *Acta Crystallogr. Sect. C Cryst. Struct. Commun.*, 2010, **66**, m137–m140.

346 S. J. Connelly, W. Kaminsky and D. M. Heinekey, *Organometallics*, 2013, **32**, 7478–7481.

347 M. Nava and C. A. Reed, *Organometallics*, 2011, **30**, 4798–4800.

348 L. Yang, D. R. Powell and R. P. Houser, *Dalton Trans.*, 2007, 955–964.

349 M. J. Begley and D. B. Sowerby, *Acta Crystallogr. Sect. C Cryst. Struct. Commun.*, 1993, **49**, 1044–1046.

350 Z. Han, F. Wang, J. Jiang, F. Wang, S. Cheng, M. Hong and H. Yin, *Dalton Trans.*, 2013, **42**, 8563.

351 G. Balázs, H. J. Breunig, E. Lork and W. Offermann, *Organometallics*, 2001, **20**, 2666–2668.

352 R. Arias Ugarte, D. Devarajan, R. M. Mushinski and T. W. Hudnall, *Dalton Trans.*, 2016, **45**, 11150–11161.

353 M. Hirai, J. Cho and F. P. Gabbaï, *Chem. Eur. J.*, 2016, **22**, 6537–6541.

354 A. Kostenko and R. Dobrovetsky, *European J. Org. Chem.*, 2019, **2019**, 318–322.

355 M. J. Frisch, G. W. Trucks, H. B. Schlegel, G. E. Scuseria, M. A. Robb, J. R. Cheeseman, G. Scalmani, V. Barone, B. Mennucci, G. A. Petersson, H. Nakatsuji, M. Caricato, X. Li, H. P. Hratchian, A. F. Izmaylov, J. Bloino, G. Zheng, J. L. Sonnenberg, M. Hada, M. Ehara, K. Toyota, R. Fukuda, J. Hasegawa, M. Ishida, T. Nakajima, Y. Honda, O. Kitao, H. Nakai, T. Vreven, J. Montgomery, J. A., J. E. Peralta, F. Ogliaro, M. Bearpark, J. J. Heyd, E. Brothers, K. N. Kudin, V. N. Staroverov, T. Keith, R. Kobayashi, J. Normand, K. Raghavachari, A. Rendell, J. C. Burant, S. S. Iyengar, J. Tomasi, M. Cossi, N. Rega, J. M. Millam, M. Klene, J. E. Knox, J. B. Cross, V. Bakken, C. Adamo, J. Jaramillo, R. Gomperts, R. E. Stratmann, O. Yazyev, A. J. Austin, R. Cammi, C. Pomelli, J. W. Ochterski, R. L. Martin, K. Morokuma, V. G. Zakrzewski, G. A. Voth, P. Salvador, J. J. Dannenberg, S. Dapprich, A. D. Daniels, O. Farkas, J. B. Foresman, J. V. Ortiz, J. Cioslowski and D. J. Fox, Gaussian 09 Revision E0.01, Gaussian, Inc., Wallingford, CT, 2016.

356 F. Weigend and R. Ahlrichs, *Phys. Chem. Chem. Phys.*, 2005, **7**, 3297–3305.

357 S. Grimme, J. Antony, S. Ehrlich and H. Krieg, *J. Chem. Phys.*, 2010, **132**, 154104.

358 A. V. Marenich, C. J. Cramer and D. G. Truhlar, *J. Phys. Chem. B*, 2009, **113**, 6378–6396.

359 G. A. Andrienko, Chemcraft - graphical software for visualization of quantum chemistry computations. https://www.chemcraftprog.com..

360 K. A. Peterson, *J. Chem. Phys.*, 2003, **119**, 11099–11112.

361 R. Krishnan, J. S. Binkley, R. Seeger and J. A. Pople, *J. Chem. Phys.*, 1980, **72**, 650–654.

362 T. J. Kealy and P. L. Pauson, *Nature*, 1951, **168**, 1039–1040.

363 R. C. J. Atkinson, V. C. Gibson and N. J. Long, *Chem. Soc. Rev.*, 2004, **33**, 313–328.

364 V. P. Sinditskii, A. N. Chernyi and D. A. Marchenkov, *Combust. Explos. Shock Waves*, 2014, **50**, 158–167.

365 L. A. Peña, A. J. Seidl, L. R. Cohen and P. E. Hoggard, *Transit. Met. Chem.*, 2009, **34**, 135–141.

366 A. Shafir and J. Arnold, *Organometallics*, 2003, **22**, 567–575.

367 K. Y. A. Lin, T. Y. Lin, Y. C. Chen and Y. F. Lin, *Catal. Commun.*, 2017, **95**, 40–45.

368 J. G. Lopez, A. Cabrera, E. Reyes, A. Toscano, C. Alvarez, C. Ortega, P. Sharma and N. Rosas, *Inorg. Chem. Commun.*, 2005, **9**, 82–85.

369 Y.-J. Shi, A. Laguna, M. D. Villacampa and M. C. Gimeno, *Eur. J. Inorg. Chem.*, 2017, **2017**, 247–255.

370 L. X. Dai, T. Tu, S. L. You, W. P. Deng and X. L. Hou, *Acc. Chem. Res.*, 2003, **36**, 659–667.

371 B. J. Marsh, L. Hampton, S. Goggins and C. G. Frost, *New J. Chem.*, 2014, **38**, 5260–5263.

372 A. Lewandowski, L. Waligora and M. Galinski, *Electroanalysis*, 2009, **21**, 2221–2227.

373 H. Yang and F. P. Gabbal, *J. Am. Chem. Soc.*, 2015, **137**, 13425–13432.

374 R. R. Gagne, C. A. Koval and G. C. Lisensky, *Inorg. Chem.*, 1980, **19**, 2854–2855.

375 G. P. Moss, P. A. S. Smith and D. Tavernier, *Pure Appl. Chem.*, 1995, **67**, 1307–1375.

376 H. Schnöckel, C. Dohmeier, E. Baum, R. Köppe and A. Ecker, *Organometallics*, 2002, **15**, 4702–4706.

377 B. M. Day and M. P. Coles, *Organometallics*, 2013, **32**, 4270–4278.

378 P. Jutzi, *Chem. Rev.*, 1986, **86**, 983–996.

379 M. J. Duer, N. A. Page, M. A. Paver, P. R. Raithby, M.-A. Rennie, C. A. Russell, C. Stourton, A. Steiner and D. S. Wright, *J. Chem. Soc., Chem. Commun.*, 1995, 1141–1142.

380 H. Sitzmann and G. Wolmershäuser, *Chem. Ber.*, 1994, **127**, 1335–1342.

381 R. B. Moffett, *Org. Synth.*, 1952, **32**, 41.

382 R. B. King, F. G. A. Stone, W. L. Jolly, G. Austin, W. Covey, D. Rabinovich, H. Steinberg and R. Tsugawa, in *Inorganic Syntheses*, John Wiley & Sons, Inc., 2007, vol. 7, pp. 99–115.

383 P. Jutzi, *Adv. Organomet. Chem.*, 1986, **26**, 217–295.

384 G. Wilkinson, F. A. Cotton and J. M. Birmingham, *J. Inorg. Nucl. Chem.*, 2003, **2**, 95–113.

385 H. O. House, R. A. Latham and G. M. Whitesides, *J. Org. Chem.*, 1967, **32**, 2481–2496.

386 R. S. Threlkel, J. E. Bercaw, P. F. Seidler, J. M. Stryker and R. G. Bergman, *Org. Synth.*, 1987, **65**, 42.

387 C. M. Fendrick, L. D. Schertz, E. A. Mintz, T. J. Marks, T. E. Bitterwolf, P. A. Horine, T. L. Hubler, J. A. Sheldon and D. D. Belin, John Wiley & Sons, Ltd, 2007, pp. 193–198.

388 L. De Vries, *J. Org. Chem.*, 1960, **25**, 1838.

389 P. Jutzi, A. Seufert and W. Buchner, *Chem. Ber.*, 2007, **112**, 2488–2493.

390 P. Jutzi and R. Dickbreder, *J. Organomet. Chem.*, 1989, **373**, 301–306.

391 R. J. Wiacek, J. N. Jones, C. L. Macdonald and A. H. Cowley, *Can. J. Chem.*, 2002, **80**, 1518–1523.

392 L. A. Paquette, M. R. Sivik, W. Bauer, M. Bühl, M. Feigel and P. von Ragué Schleyer, *J. Am. Chem. Soc.*, 1990, **112**, 8776–8789.

393 M. M. Exner, R. Waack and E. C. Steiner, *J. Am. Chem. Soc.*, 1973, **95**, 7009–7018.

394 B. Wrackmeyer, A. Sebald and L. H. Merwin, *Magn. Reson. Chem.*, 1991, **29**, 260–263.

395 P. Jutzi and A. Seufert, *J. Organomet. Chem.*, 1978, **161**, C5.

396 D. J. Burkey and T. P. Hanusa, *Comments Inorg. Chem.*, 1995, **17**, 41–77.

397 K. C. Waterman and A. Streitwieser, *J. Am. Chem. Soc.*, 1984, **106**, 3138–3140.

398 M. A. Beswick, J. S. Palmer and D. S. Wright, *Chem. Soc. Rev.*, 1998, **27**, 225.

399 M. A. Paver, C. A. Russell and D. S. Wright, *Angew. Chem. Int. Ed. Engl.*, 1995, **34**, 1545–1554.

400 E. D. Jemmis and P. von Ragué Schleyer, *J. Am. Chem. Soc.*, 1982, **104**, 4781–4788.

401 P. Jutzi, D. Kanne and C. Krüger, *Angew. Chem. Int. Ed. Engl.*, 1986, **25**, 164–164.

402 P. Jutzi, U. Holtmann, D. Kanne, C. Krüger, R. Blom, R. Gleiter and I. Hyla-Kryspin, *Chem. Ber.*, 1989, **122**, 1629–1639.

403 J. Vollet, E. Baum and H. Schnöckel, *Organometallics*, 2003, **22**, 2525–2527.

404 R. Allen Williams, T. P. Hanusa and J. C. Huffman, *Organometallics*, 1990, **9**, 1128–1134.

405 R. A. Andersen, R. Blom, J. M. Boncella, C. J. Burns and H. V. Volden, *Acta Chem. Scand.*, 1987, **41a**, 24–35.

406 T. V. Timofeeva, J. H. Lii and N. L. Allinger, *J. Am. Chem. Soc.*, 1995, **117**, 7452–7459.

407 T. K. Hollis, J. K. Burdett and B. Bosnich, *Organometallics*, 1993, **12**, 3385–3386.

408 C. Dohmeier, C. Robl, M. Tacke and H. Schnöckel, *Angew. Chem. Int. Ed. Engl.*, 1991, **30**, 564–565.

409 J. D. Gorden, A. Voigt, C. L. B. Macdonald, J. S. Silverman and A. H. Cowley, *J. Am. Chem. Soc.*, 2000, **122**, 950–951.

410 B. Buchin, T. Steinke, C. Gemel, T. Cadenbach and R. A. Fischer, *Z. Anorg. Allg. Chem.*, 2005, **631**, 2756–2762.

411 D. Weiss, T. Steinke, M. Winter, R. A. Fischer, N. Fröhlich, J. Uddin and G. Frenking, *Organometallics*, 2000, **19**, 4583–4588.

412 T. Cadenbach, C. Gemel, D. Zacher and R. A. Fischer, *Angew. Chem. Int. Ed.*, 2008, **47**, 3438–3441.

413 P. Jutzi, B. Neumann, L. O. Schebaum, A. Stammler and H. G. Stammler, *Organometallics*, 1999, **18**, 4462–4464.

414 P. Jutzi, B. Neumann, G. Reumann and H. G. Stammler, *Organometallics*, 1998, **17**, 1305–1314.

415 C. P. Sindlinger and P. N. Ruth, *Angew. Chem. Int. Ed.*, 2019, **58**, 15051–15056.

416 A. Hofmann, T. Tröster, T. Kupfer and H. Braunschweig, *Chem. Sci.*, 2019, **10**, 3421–3428.

417 H. Werner, H. Otto and H. J. Kraus, *J. Organomet. Chem.*, 1986, **315**, C57–C60.

418 O. T. Beachley, M. R. Churchill, J. C. Fettinger, J. C. Pazik and L. Victoriano, *J. Am. Chem. Soc.*, 1986, **108**, 4666–4668.

419 D. Loos, E. Baum, A. Ecker, H. Schnöckel and A. J. Downs, *Angew. Chem. Int. Ed. Engl.*, 1997, **36**, 860–862.

420 C. Dohmeier, H. Schnöckel, U. Schneider, R. Ahlrichs and C. Robl, *Angew. Chem. Int. Ed. Engl.*, 1993, **32**, 1655–1657.

421 A. Voigt, S. Filipponi, C. L. B. Macdonald, J. D. Gorden and A. H. Cowley, *Chem. Commun.*, 2000, 911–912.

422 C. L. B. Macdonald, J. D. Gorden, A. Voigt and A. H. Cowley, *J. Am. Chem. Soc.*, 2000, 122, 11725–11726.

423 C. T. Shen, Y. H. Liu, S. M. Peng and C. W. Chiu, *Angew. Chem. Int. Ed.*, 2013, **52**, 13293–13297.

424 C. H. Wang, Y. F. Lin, H. C. Tseng, G. S. Lee, S. M. Peng and C. W. Chiu, *Eur. J. Inorg. Chem.*, 2018, **2018**, 2232–2236.

425 O. T. Beachley, M. R. Churchill, K. Faegri, J. C. Fettinger, J. C. Pazik, L. Victoriano and R. Blom, *Organometallics*, 1989, **8**, 346–356.

426 H.-C. Tseng, C.-T. Shen, K. Matsumoto, D.-N. Shih, Y.-H. Liu, S.-M. Peng, S. Yamaguchi, Y.-F. Lin and C.-W. Chiu, *Organometallics*, 2019, **38**, 4516–4521.

427 E. . Fischer and H. Grubbert, *Z. Naturforsch.B*, 1956, **11**, 423.

428 E. O. Fischer and H. Grubert, *Z. Anorg. Allg. Chem.*, 1956, **286**, 237–242.

429 D. R. Armstrong, M. A. Beswick, N. L. Cromhout, C. N. Harmer, D. Moncrieff, C. A. Russell, P. R. Raithby, A. Steiner, A. E. H. Wheatley and D. S. Wright, *Organometallics*, 1998, **17**, 3176–3181.

430 M. A. Beswick, N. L. Cromhout, C. N. Harmer, P. R. Raithby, C. A. Russell, J. S. B. Smith, A. Steiner and D. S. Wright, *Chem. Commun.*, 1996, 1977–1978.

431 C. Müller, A. Stahlich, L. Wirtz, C. Gretsch, V. Huch and A. Schäfer, *Inorg. Chem.*, 2018, **57**, 8050–8053.

432 J. L. Atwood, W. E. Hunter, A. H. Cowley, R. A. Jones and C. A. Stewart, *J. Chem. Soc. Chem. Commun.*, 1981, 925–927.

433 B. Rhodes, J. C. W. Chien and M. D. Rausch, *Organometallics*, 1998, **17**, 1931–1933.

434 M. Schleep, C. Hettich, J. Velázquez Rojas, D. Kratzert, T. Ludwig, K. Lieberth and I. Krossing, *Angew. Chem. Int. Ed.*, 2017, **56**, 2880–2884.

435 M. Schleep, C. Hettich, D. Kratzert, H. Scherer and I. Krossing, *Chem. Commun.*,

2017, **53**, 10914–10917.

436 P. Jutzi, A. Mix, B. Rummel, W. W. Schoeller, B. Neumann and H. G. Stammler, *Science.*, 2004, **305**, 849–851.

437 P. Jutzi, F. Kohl and C. Krüger, *Angew. Chem. Int. Ed. Engl.*, 1979, **18**, 59–60.

438 M. Birkhahn, P. Krommes, W. Massa and J. Lorberth, *J. Organomet. Chem.*, 1981, **208**, 161–167.

439 W. Massa, J. Lorberth, S. Wocadlo, X.-W. Li, I. Sarraje and S.-H. Shin, *J. Organomet. Chem.*, 2003, **485**, 149–152.

440 R. J. Wiacek, J. N. Jones, C. L. Macdonald and A. H. Cowley, *Can. J. Chem.*, 2002, **80**, 1518–1523.

441 H. Sitzmann, Y. Ehleiter, G. Wolmershäuser, A. Ecker, C. Üffing and H. Schnöckel, *J. Organomet. Chem.*, 1997, **527**, 209–213.

442 J. Zhou, L. L. Liu, L. L. Cao and D. W. Stephan, *Angew. Chem. Int. Ed.*, 2019, **58**, 5407–5412.

443 J. Zhou, L. L. Liu, L. L. Cao and D. W. Stephan, *Chem*, 2018, **4**, 2699–2708.

444 M. R. Wolfson and T. H. Shaffer, *Paediatr. Respir. Rev.*, 2005, **6**, 117–127.

445 D. E. Yerien, S. Bonesi and A. Postigo, *Org. Biomol. Chem.*, 2016, **14**, 8398–8427.

446 S. Purser, P. R. Moore, S. Swallow and V. Gouverneur, *Chem. Soc. Rev.*, 2008, **37**, 1–200.

447 R. Ragni, A. Punzi, F. Babudri and G. M. Farinola, *European J. Org. Chem.*, 2018, 2018, 3500–3519.

448 M. A. McClinton and D. A. McClinton, *Tetrahedron*, 1992, **48**, 6555–6666.

449 Swarts Frédéric Jean Edmond, *Bull. Acad. Roy. Belgique.*, 1892, **3**, 474.

450 S. Liang, G. B. Hammond and B. Xu, *Chem. Eur.J*, 2017, **23**, 17850–17861.

451 J. Wu, *Tetrahedron Lett.*, 2014, 55, 4289–4294.

452 W. Frank, *J. Organomet. Chem.*, 1991, **406**, 331–341.

453 R. A. Bartlett, A. Cowley, P. Jutzi, M. M. Olmstead and H. Stammlerq, *Organometallics*, 1992, **11**, 2837–2840.

454 V. N. Sapunov, K. Kirchner and R. Schmid, *Coord. Chem. Rev.*, 2001, **214**, 143–185.

455 J. B. Lambert, L. Lin and V. Rassolov, *Angew. Chem. Int. Ed.*, 2002, **41**, 1429–1431.

456 M. Otto, D. Scheschkewitz, T. Kato, M. M. Midland, J. B. Lambert and G. Bertrand, *Angew. Chem. Int. Ed. Engl..*, 2002, **41**, 2275–2276.

457 J. N. Jones, A. H. Cowley and C. L. B. Macdonald, *Chem. Commun.*, 2002, 1520–1521.

458 J. B. Waters, Q. Chen, T. A. Everitt and J. M. Goicoechea, *Dalton Trans.*, 2017, **46**, 12053–12066.

459 D. A. Straus, C. Zhang and T. D. Tilley, *J. Organomet. Chem.*, 1989, **369**, C13–C17.

460 A. W. Addison, T. N. Rao, J. Reedijk, J. Van Rijn and G. C. Verschoor, *J. Chem. Soc.,*

Dalton Trans., 1984, 1349–1356.

461 T. K. Hollis and B. Bosnich, *J. Am. Chem. Soc.*, 1995, **117**, 4570–4581.

462 Y. X. Peng, L. F. Cun, H. S. Dai and J. L. Liu, *Polymer.*, 1996, **37**, 3979–3982.

463 J. Liu, J. Zhang, C. Wu, H. Liu, H. Liu, F. Sun, Y. Li, Y. Liu, Y. Dong and X. Li, *RSC Adv.*, 2019, **9**, 28409–28413.

464 S. C. Chmely, T. P. Hanusa and A. L. Rheingold, *Organometallics*, 2010, **29**, 5551–5557.

465 J. Zhou, H. Kim, L. L. Liu, L. L. Cao and D. W. Stephan, *Chem. Commun.*, 2020, **56**, 12953–12956.

466 R. A. Bartlett, M. M. Olmstead, A. Cowley, P. Jutzl and H. G. Stammler, *Organometallics*, 1992, **11**, 2837–2840.

467 S. Matsukawa, K. Fukazawa and J. Kimura, *RSC Adv.*, 2014, **4**, 27780–27786.

468 S. I. Gorelsky, AOMix: Program for Molecular Orbital Analysis ,*York Univ. Toronto*.

469 S. I. Gorelsky and A. B. P. Lever, *J. Organomet. Chem.*, 2001, **635**, 187–196.

470 T. Stahl, H. F. T. Klare and M. Oestreich, *ACS Catal.*, 2013, **3**, 1578–1587.

471 Q. Shen, Y.-G. Huang, C. Liu, J.-C. Xiao, Q.-Y. Chen and Y. Guo, *J. Fluor. Chem.*, 2015, **179**, 14–22.

472 C. B. Caputo and D. W. Stephan, *Organometallics*, 2012, **31**, 27–30.

473 S. B. Munoz, C. Ni, Z. Zhang, F. Wang, N. Shao, T. Mathew, G. A. Olah and G. K. S. Prakash, *European J. Org. Chem.*, 2017, **2017**, 2322–2326.

474 S. Yoshida, K. Shimomori, Y. Kim and T. Hosoya, *Angew. Chem. Int. Ed.*, 2016, **55**, 10406–10409.

475 M. Bergeron, D. Guyader and J. F. Paquin, *Org. Lett.*, 2012, **14**, 5888–5891.

476 J. Ichikawa, H. Fukui and Y. Ishibashi, *J. Org. Chem.*, 2003, **68**, 7800–7805.

477 D. S. Fadeev, I. P. Chuikov and V. I. Mamatyuk, *J. Fluor. Chem.*, 2016, **182**, 53–60.

478 D. Mandal, R. Gupta and R. D. Young, *J. Am. Chem. Soc.*, 2018, **140**, 10682–10686.

479 D. Mandal, R. Gupta, A. K. Jaiswal and R. D. Young, *J. Am. Chem. Soc.*, 2020, **142**, 2572–2578.

480 R. Gupta, A. K. Jaiswal, D. Mandal and R. D. Young, *Synlett*, 2020, **31**, 933–937.

481 P. Mehlmann, T. Witteler, L. F. B. Wilm and F. Dielmann, *Nat. Chem.*, 2019, **11**, 1139–1143.

482 I. Mallov, A. J. Ruddy, H. Zhu, S. Grimme and D. W. Stephan, *Chem. Eur. J.*, 2017, **23**, 17692–17696.

483 J. J. Cabrera-Trujillo and I. Fernández, *Chem. – A Eur. J.*, 2021, **27**, 3823–3831.

484 K. Samigullin, I. Georg, M. Bolte, H.-W. Lerner and M. Wagner, *Chem. Eur. J.*, 2016, **22**, 3478–3484.

485 T. W. Hudnall, Antimony(V) Cations as Lewis Acid Catalysts for C-F Activation,

https://acswebcontent.acs.org/prfar/2017/Paper15205.html, (accessed 14 January 2021).

486 V. K. Greenacre, W. Levason and G. Reid, *Organometallics*, 2018, **37**, 2123–2135.

487 H. A. Jenkins, S. S. Chitnis, N. Burford, R. McDonald, A. P. M. Robertson and M. J. Ferguson, *Chem. Eur. J.*, 2015, **21**, 7902–7913.

488 S. S. Chitnis, A. P. M. Robertson, N. Burford, B. O. Patrick, R. McDonald and M. J. Ferguson, *Chem. Sci.*, 2015, **6**, 6545–6555.

489 H. Großekappenberg, M. Reißmann, M. Schmidtmann and T. Müller, *Organometallics*, 2015, **34**, 4952–4958.

490 J. M. Dyke, J. W. Emsley, V. K. Greenacre, W. Levason, F. M. Monzittu, G. Reid and G. De Luca, *Inorg. Chem.*, 2020, **59**, 4517–4526.

491 J. S. Wenger and T. C. Johnstone, *Chem. Commun.*, 2021, **57**, 3484–3487.

492 C.-H. Chen and F. P. Gabbaï, *Dalton Trans.*, 2018, **47**, 12075–12078.

493 R. Kather, T. Svoboda, M. Wehrhahn, E. Rychagova, E. Lork, L. Dostál, S. Ketkov and J. Beckmann, *Chem. Commun.*, 2015, **51**, 5932–5935.

494 B. R. M. Lake and S. L. Benjamin, *Unpubl. Work*.

495 B. R. M. Lake, O. Coughlin, T. Bennett and S. L. Benjamin, *Manuscr. Prep.*

496 G. A. Olah, S. Kobayashi and M. Tashiro, *J. Am. Chem. Soc.*, 1972, **94**, 7448–7461.

497 G. Doleshall, N. A. Nesmeyanov and O. A. Reutov, *J. Organomet. Chem.*, 1971, **30**, 369–375.

498 C. A. Wamser, *J. Am. Chem. Soc.*, 1951, **73**, 409–416.

499 C. S. B. Gomes, S. I. Costa, L. F. Veiros and P. T. Gomes, *Polyhedron*, 2016, **116**, 162–169.

500 D. Sellmann, K. Hein and F. W. Heinemann, *Eur. J. Inorg. Chem.*, 2004, **2004**, 3136–3146.

501 J. Fawcett, D. A. J. Harding, E. G. Hope, K. Singh and G. A. Solan, *J. Chem. Soc., Dalton Trans.*, 2009, 6861–6870.

502 M. Watanabe, M. Sato, A. Nagasawa, K. Masahiro, I. Motoyama and T. Takayama, *Bull. Chem. Soc. Jpn.*, 1999, **72**, 715–723.

503 I. Ciabatti, C. Femoni, M. C. Iapalucci, G. Longoni and S. Zacchini, *Organometallics*, 2013, **32**, 5180–5189.

504 K. S. Coleman, J. Fawcett, D. A. J. Harding, E. G. Hope, K. Singh and G. A. Solan, *Eur. J. Inorg. Chem.*, 2010, **2010**, 4130–4138.

505 M. Yamashita, Y. Yamamoto, K. Y. Akiba, D. Hashizume, F. Iwasaki, N. Takagi and S. Nagase, *J. Am. Chem. Soc.*, 2005, **127**, 4354–4371.

506 K. Y. Akiba, M. Yamashita, Y. Yamamoto and S. Nagase, *J. Am. Chem. Soc.*, 1999, 121, 10644–10645.

507 J. Burt, J. W. Emsley, W. Levason, G. Reid and I. S. Tinkler, *Inorg. Chem.*, 2016, **55**,

8852–8864.

508 P. Braunstein, L. Douce, J. Fischer, N. C. Craig, G. Goetz-Grandmont and D. Matt, *Inorg. Chim. Acta.*, 1992, **194**, 151–156.

509 C. R. Groom, I. J. Bruno, M. P. Lightfoot and S. C. Ward, *Acta Crystallogr. Sect. B Struct. Sci. Cryst. Eng. Mater.*, 2016, **72**, 171–179.

510 H. J. Breunig, H. Althaus, R. Rösler and E. Lork, *Z. Anorg. Allg. Chem.*, 2000, **626**, 1137–1140.

511 M. Ateş, H. Joachim Breunig and S. Güleç, *J. Organomet. Chem.*, 1989, **364**, 67–71.

512 K. Izod, A. M. Madlool and P. G. Waddell, *Organometallics*, 2019, **38**, 2654–2663.

513 T. Naito, S. Nagase and H. Yamataka, *J. Am. Chem. Soc.*, 1994, **116**, 10080–10088.

514 B. A. Chalmers, M. Bühl, K. S. Athukorala Arachchige, A. M. Z. Slawin and P. Kilian, *Chem. Eur. J.*, 2015, **21**, 7520–7531.

515 Z. Benmaarouf, P. Riviere, M. Rivière-Baudet, A. Castel, A. Khallaayoun and M. Ahbala, *Phosphorus, Sulfur Silicon Relat. Elem.*, 1997, **128**, 19–29.

516 C. R. Witschonke and C. A. Kraus, *J. Am. Chem. Soc.*, 1947, **69**, 2472–2481.

517 P. P. Power, *Chem. Rev.*, 1999, **99**, 3463–3503.

518 P. Atkins, T. Overton, J. Rourke, M. Weller, F. Armstrong and M. Hagerman, *Inorganic Chemistry*, W.H. Freeman and Company, New York, 5th Edn., 2010.

519 M. J. Winter, *d-Block Chemisry*, Oxford University Press, Oxford, 1st Edn., 1994.

520 G. O. Spessard and G. L. Miessler, *Organometallic Chemistry*, Prentice-Hall, New Jersey, 1996.

521 M. Authors, *New Trends in Cross-Coupling*, Royal Society of Chemistry, Cambridge, 2014.

522 J. F. Hartwig, *Organotransition Metal Chemistry: From Bonding to Catalysis*, University Science Books, New York, 2010.

523 R. Bates, *Organic Synthesis Using Transition Metals*, John Wiley & Sons, Ltd, Chichester, UK, 2012.

524 C. C. C. Johansson Seechurn, M. O. Kitching, T. J. Colacot and V. Snieckus, *Angew. Chem. Int. Ed.*, 2012, **51**, 5062–5085.

525 A. O. King and N. Yasuda, Springer, Berlin, Heidelberg, 2017, pp. 205–245.

526 C. A. Ramsden, *Chem. Soc. Rev.*, 1994, 23, 111–118.

527 K. A. R. Mitchell, *Chem. Rev.*, 1969, **69**, 157–178.

528 D. G. Gilheany, *Chem. Rev.*, 2002, **94**, 1339–1374.

529 A. G. Orpen and N. G. Connelly, *Organometallics*, 1990, **9**, 1206–1210.

530 C. A. Tolman, *Chem. Rev.*, 1977, **77**, 313–348.

531 C. A. Tolman, *J. Am. Chem. Soc.*, 1970, **92**, 2956–2965.

532 C. A. Tolman, W. C. Seidel and L. W. Gosser, *J. Am. Chem. Soc.*, 1974, **96**, 53–60.

533 J. Jover and J. Cirera, *Dalton Trans.*, 2019, **48**, 15036–15048.

534 J. A. Bilbrey, A. H. Kazez, J. Locklin and W. D. Allen, *J. Comput. Chem.*, 2013, **34**, 1189–1197.

535 A. Immirzi and A. Musco, *Inorg. Chim. Acta.*, 1977, **25**, L41–L42.

536 T. L. Brown and K. J. Lee, *Coord. Chem. Rev.*, 1993, **128**, 89–116.

537 D. White, B. C. Taverner, P. G. L. Leach and N. J. Coville, *J. Comput. Chem.*, 1993, **14**, 1042–1049.

538 B. J. Dunne, R. B. Morris and A. G. Orpen, *J. Chem. Soc., Dalton Trans.*, 1991, 653–661.

539 A. M. Hill, N. J. Holmes, A. R. J. Genge, W. Levason, M. Webster and S. Rutschow, *J. Chem. Soc., Dalton Trans.*, 1998, 825–832.

540 N. J. Holmes, W. Levason and M. Webster, *J. Chem. Soc., Dalton Trans.*, 1998, 3457–3461.

541 M. Bouché, G. Dahm, A. Maisse-François, T. Achard and S. Bellemin-Laponnaz, *Eur. J. Inorg. Chem.*, 2016, **2016**, 2828–2836.

542 V. R. Bojan, E. J. Fernández, A. Laguna, J. M. López-de-Luzuriaga, M. Monge, M. E. Olmos, R. C. Puelles and C. Silvestru, *Inorg. Chem.*, 2010, **49**, 5530–5541.

543 M. Charton, in *The Chemistry of Organic Arsenic, Antimony, and Bismuth Compounds*, ed. S. Patai, John Wiley & Sons, Ltd., West Sussex, 1st Edn., 1994, pp. 367–439.

544 J. S. Jones and F. P. Gabbai, *Chem. Eur. J.*, 2017, **23**, 1136–1144.

545 R. Pastorek, J. Kameníček, Z. Trávníček, M. Pavlíček, B. Cvek, J. Husárek and Z. Sindelar, *Pol. J. Chem.*, 2005, **79**, 637–644.

546 N. Fey, *Dalton Trans.*, 2010, **39**, 296–310.

547 L. Perrin, E. Clot, O. Eisenstein, J. Loch and R. H. Crabtree, *Inorg. Chem.*, 2001, **40**, 5806–5811.

548 N. Fey, A. G. Orpen and J. N. Harvey, *Coord. Chem. Rev.*, 2009, **253**, 704–722.

549 W. V. Taylor, Z.-L. Xie, N. I. Cool, S. A. Shubert and M. J. Rose, *Inorg. Chem.*, 2018, **57**, 10364–10374.

550 S. L. Benjamin and G. Reid, *Coord. Chem. Rev.*, 2015, **297**–**298**, 168–180.

551 C. I. Raţ, C. Silvestru and H. J. Breunig, *Coord. Chem. Rev.*, 2013, **257**, 818–879.

552 A. Jolleys, B. R. M. Lake, T. Krämer and S. L. Benjamin, *Organometallics*, 2018, **37**, 3854–3862.

553 S. L. Benjamin, W. Levason, G. Reid and M. C. Rogers, *Dalton Trans.*, 2011, **40**, 6565.

554 M. D. Brown, W. Levason, G. Reid and M. Webster, *Dalton Trans.*, 2006, 5648.

555 M. Jiménez-Tenorio, M. Carmen Puerta, I. Salcedo, P. Valerga, I. de los Ríos and K. Mereiter, *Dalton Trans.*, 2009, 1842.

556 C. S. B. Gomes, P. Krishnamoorthy, L. C. Silva, S. I. Costa, P. T. Gomes, M. Jiménez-

Tenorio, P. Valerga and M. C. Puerta, *Dalton Trans.*, 2015, **44**, 17015–17019.

557 C. S. B. Gomes, S. I. Costa, L. C. Silva, M. Jiménez-Tenorio, P. Valerga, M. C. Puerta and P. T. Gomes, *Eur. J. Inorg. Chem.*, 2018, **2018**, 597–607.

558 B. Korthals, A. Berkefeid, M. Ahlmann and S. Mecking, *Macromolecules*, 2008, **41**, 8332–8338.

559 J. A. Casares, P. Espinet, J. M. Martín-Alvarez, J. M. Martínez-Ilarduya and G. Salas, *Eur. J. Inorg. Chem.*, 2005, **2005**, 3825–3831.

560 K. R. Gmernicki, E. Hong, C. R. Maroon, S. M. Mahurin, A. P. Sokolov, T. Saito and B. K. Long, *ACS Macro Lett.*, 2016, **5**, 879–883.

561 S. Martínez-Arranz, A. C. Alb́eniz and P. Espinet, *Macromolecules*, 2010, **43**, 7482–7487.

562 N. Carrera, E. Gutiérrez, R. Benavente, M. M. Villavieja, A. C. Albéniz and P. Espinet, *Chem. Eur. J.*, 2008, **14**, 10141–10148.

563 N. Belov, R. Nikiforov, L. Starannikova, K. R. Gmernicki, C. R. Maroon, B. K. Long, V. Shantarovich and Y. Yampolskii, *Eur. Polym. J.*, 2017, **93**, 602–611.

564 M. F. Ludmann-Obier, M. Dartiguenave and Y. Dartiguenave, *Inorg. Nucl. Chem. Lett.*, 1974, **10**, 147–149.

565 M. F. Ludmann, M. Dartiguenave and Y. Dartiguenave, *Inorg. Chem.*, 1977, **16**, 440–446.

566 J. S. Jones, C. R. Wade and F. P. Gabbaï, *Angew. Chem. Int. Ed.*, 2014, **53**, 8876–8879.

567 K. A. Jensen, P. H. Nielsen, S. Furberg, C. S. Petersen and J. Munch-Petersen, *Acta Chem. Scand.*, 1963, **17**, 1875–1885.

568 M. Mathew, G. J. Palenik and C. A. McAuliffe, *Acta Crystallogr. Sect. C Cryst. Struct. Commun.*, 1987, **43**, 21–24.

569 G. T. Morgan and V. E. Yarsley, *J. Chem. Soc. Trans.*, 1925, **127**, 184–190.

570 O. Hannebohn and W. Klemm, *Z. Anorg. Allg. Chem.*, 1936, **229**, 225–251.

571 J. Chatt and R. G. Wilkins, *J. Chem. Soc.*, 1956, 520–524.

572 J. Chatt and R. G. Wilkins, *J. Chem. Soc.*, 1953, 70–74.

573 J. Chatt and R. G. Wilkins, *J. Chem. Soc.*, 1952, 4259–4268.

574 J. Chatt and R. G. Wilkins, *J. Chem. Soc.*, 1951, 2532–2533.

575 D. M. Adams, J. Chatt, J. Gerratt and A. D. Westland, *J. Chem. Soc.*, 1964, 729–733.

576 P. J. D. Park and P. J. Hendra, *Spectrochim. Acta Part A Mol. Spectrosc.*, 1969, **25**, 227–235.

577 L. Maier, D. Seyferth, F. G. A. Stone and E. G. Rochow, *J. Am. Chem. Soc.*, 1957, **79**, 5884–5889.

578 P. L. Goggin, R. J. Goodfellow, S. R. Haddock, B. F. Taylor and I. R. H. Marshall, *J. Chem. Soc., Dalton Trans.*, 1976, 459–467.

579 C. A. McAuliffe, I. E. Niven and R. V. Parish, *Inorg. Chim. Acta.*, 1977, **22**, 239–248.

580 J. C. Bailar and H. Itatani, *J. Am. Chem. Soc.*, 1967, **89**, 1592–1599.

581 H. A. Tayim, A. Bouldoukian and F. Awad, *J. Inorg. Nucl. Chem.*, 1970, **32**, 3799–3803.

582 J. Yang, P. Li, Y. Zhang and L. Wang, *Dalton Trans.*, 2014, **43**, 14114–14122.

583 P. E. Garrou and G. E. Hartwell, *Inorg. Chem.*, 1976, **15**, 730–732.

584 S. Shigetoshi, TAKAHASHI Kenkichi and H. Nobue, *Nppon Kagaku Zosshi*, 1966, **87**, 610–613.

585 R. S. Barbiéri, S. I. Klein and A. C. Massabni, *J. Chem. Soc. Chem. Commun.*, 1987, 1617–1618.

586 D. H. Goldsworthy, F. R. Hartley, G. L. Marshall and S. G. Murray, *Inorg. Chem.*, 1985, **24**, 2849–2853.

587 P. Schwab, N. Mahr, J. Wolf and H. Werner, *Angew. Chem. Int. Ed. Engl.*, 1994, **33**, 97–99.

588 H. Werner, *Angew. Chem. Int. Ed.*, 2004, **43**, 938–954.

589 U. Herber, T. Pechmann, B. Weberndörfer, K. Ilg and H. Werner, *Chem. Eur. J.*, 2002, **8**, 309–319.

590 U. Herber, B. Weberndörfer and H. Werner, *Angew. Chem. Int. Ed.*, 1999, **38**, 1609–1613.

591 I.-S. Ke and F. P. Gabbaï, *Aust. J. Chem.*, 2013, **66**, 1281.

592 P. W. Frost, J. A. K. Howard, J. L. Spencer, D. G. Turner and D. Gregson, *J. Chem. Soc. Chem. Commun.*, 1981, 1104–1106.

593 E. G. Mednikov, N. K. Eremenko, S. P. Gubin, Y. L. Slovokhotov and Y. T. Struchkov, *J. Organomet. Chem.*, 1982, **239**, 401–416.

594 J. Dubrawski, J. C. Kriege-Simondsen and R. D. Feltham, *J. Am. Chem. Soc.*, 1980, 102, 2089–2091.

595 D. G. Evans and D. M. P. Mingos, *J. Organomet. Chem.*, 1982, **240**, 321–327.

596 A. Jolley and S. L. Benjamin, *Unpubl. Work*.

597 V. P. Ananikov, D. G. Musaev and K. Morokuma, *Eur. J. Inorg. Chem.*, 2007, **2007**, 5390–5399.

598 F. Fu, J. Xiang, H. Cheng, L. Cheng, H. Chong, S. Wang, P. Li, S. Wei, M. Zhu and Y. Li, *ACS Catal.*, 2017, **7**, 1860–1867.

599 C. E. Ellul, M. F. Mahon and M. K. Whittlesey, *J. Organomet. Chem.*, 2010, **695**, 6–10.

600 P. Leoni, E. Vichi, S. Lencioni, M. Pasquali, E. Chiarentin and A. Albinati, *Organometallics*, 2000, **19**, 3062–3068.

601 F. Lemaître, D. Lucas, K. Groison, P. Richard, Y. Mugnier and P. D. Harvey, *J. Am. Chem. Soc.*, 2003, **125**, 5511–5522.

602 M. T. Reetz, E. Bohres, R. Goddard, M. C. Holthausen and W. Thiel, *Chem. Eur. J.*, 1999, **5**, 2101–2108.

603 A. Hamieh, Y. Chen, S. Abdel-Azeim, E. Abou-hamad, S. Goh, M. Samantaray, R. Dey, L. Cavallo and J. M. Basset, *ACS Catal.*, 2015, **5**, 2164–2171.

604 S. M. Ivanov, L. M. Mironovich and M. E. Minyaev, *Phosphorus, Sulfur Silicon Relat. Elem.*, 2020, **195**, 666–676.

605 R. Tooze, K. W. Chiu and G. Wilkinson, *Polyhedron*, 1984, **3**, 1025–1028.

606 B. E. Mann and A. Musco, *J. Chem. Soc., Dalton Trans.*, 1975, 1673.

607 E. A. Mitchell and M. C. Baird, *Organometallics*, 2007, **26**, 5230–5238.

608 C. A. McAuliffe, G. Wilkinson, R. D. Gillard and J. A. McCleverty, *Comprehensive Coordination Chemistry*, Pergamon Press, Oxford, 1st Edn., 1987.

609 B. Lecachey, H. Oulyadi, P. Lameiras, A. Harrison-Marchand, H. Gérard and J. Maddaluno, *J. Org. Chem.*, 2010, **75**, 5976–5983.

610 M. De La Higuera Macias and B. A. Arndtsen, *J. Am. Chem. Soc.*, 2018, **140**, 10140–10144.

611 M. Wieber, D. Wirth and I. Fetzer, *Z. Anorg. Allg. Chem.*, 1983, **505**, 134–137.

612 J. G. Stevens, J. M. Trooster, H. A. Meinema and J. G. Noltes, *Inorg. Chem.*, 1981, **20**, 801–803.

613 H. Weingarten and J. R. V. Wazer, *J. Am. Chem. Soc.*, 1966, **88**, 2700–2702.

614 G. G. Long, C. G. Moreland, G. O. Doak and M. Miller, *Inorg. Chem.*, 1966, **5**, 1358–1361.

615 C. G. Moreland, M. H. O'Brien, C. E. Douthit and G. G. Long, *Inorg. Chem.*, 1968, **7**, 834–836.

616 G. Schröder, T. Okinaka, Y. Mimura, M. Watanabe, T. Matsuzaki, A. Hasuoka, Y. Yamamoto, S. Matsukawa and K. Y. Akiba, *Chem. Eur. J.*, 2007, **13**, 2517–2529.

617 M. Kobayashi and K. Y. Akiba, *Organometallics*, 2014, **33**, 1218–1226.

618 P. L. Millington and D. B. Sowerby, *J. Organomet. Chem.*, 1994, **480**, 227–234.

619 J. L. Pascual-ahuir, E. Silla and I. Tuñon, *J. Comput. Chem.*, 1994, **15**, 1127–1138.

620 S. Miertuš and J. Tomasi, *Chem. Phys.*, 1982, **65**, 239–245.

621 S. Miertuš, E. Scrocco and J. Tomasi, *Chem. Phys.*, 1981, **55**, 117–129.

622 M. G. Evans and M. Polanyi, *Trans. Faraday Soc.*, 1935, **31**, 875.

623 J. C. Green, M. L. H. Green and G. Parkin, *Chem. Commun.*, 2012, **48**, 11481.

624 R. John Errington, *Advanced Practical Inorganic and Metalorganic Chemistry*, CRC Press, Boca Raton, FL, 1st Edn., 1997.

625 D. F. Shriver and M. A. Drezdzon, *The manipulation of air-sensitive compounds*, Wiley, New York, 2nd Edn., 1986.

626 X. Bantreil and S. P. Nolan, *Nat. Protoc.*, 2011, **6**, 69–77.

627 P. W. Betteridge, J. R. Carruthers, R. I. Cooper, K. Prout and D. J. Watkin, *J. Appl. Crystallogr.*, 2003, **36**, 1487–1487.

628 J. Cosier and A. M. Glazer, *J. Appl. Crystallogr.*, 1986, **19**, 105–107.

629 2018.

630 R. C. Clark and J. S. Reid, *Acta Crystallogr. Sect. A*, 1995, **51**, 887–897.

631 O. V. Dolomanov, L. J. Bourhis, R. J. Gildea, J. A. K. Howard and H. Puschmann, *J. Appl. Crystallogr.*, 2009, **42**, 339–341.

632 G. M. Sheldrick, *Acta Crystallogr. Sect. A Found. Crystallogr.*, 2015, **71**, 3–8.

633 G. M. Sheldrick, *Acta Crystallogr. Sect. C Struct. Chem.*, 2015, **71**, 3–8.

Appendix I: General Experimental Methods

General Methods

Caution: All antimony containing compounds should be treated as toxic. Cp*Li and alkyl stibines are extremely pyrophoric. All manipulations were performed under an atmosphere of dry N_2 using standard Schlenk or glovebox (Mbraun Unilab 2000) techniques, [624,625] unless otherwise stated. All glassware was dried in an oven at 150°C and cooled under vacuum before use.

Solvents and Reagents

Diethyl ether, tetrahydrofuran (THF), dichloromethane, toluene, and n-hexane were dried using an Mbraun MB SPS5 and degassed if required. Acetonitrile (MeCN) was distilled over CaH_2 and stored over 3 Å /4 Å molecular sieves. All deuterated solvents were dried and stored over 4 Å molecular sieves. $SbCl_3$ was sublimed *in vacuo* at 40-65°C before use. Triethylsilane was distilled over CaH_2, degassed by freeze/pump/thaw and stored over 4 Å molecular sieves. ααα-trichlorotoluene, and 1,2-diflurorobenzene (DFB) were degassed by freeze/pump/thaw and dried over 4 Å molecular sieves. All other reagents were used as received unless otherwise stated. $[Et_3Si][B(C_6F_5)_4]$ was synthesised according to modified literature procedure,[342–344] and recrystalised in toluene at -10°C or by the addition of Et_3SiH to a solution of $[Ph_3C][B(B(C_6F_5)_4)]$ in toluene. IMes was synthesised using a modified literature procedure.[626] The synthesis of $Li[B(C_6F_5)_4)]$ requires the *in situ* generation of a potentially explosive nature of the $Li[B(C_6F_5)_4]$ intermediate.[344] Magnesium turnings were activated by the addition of a crystal of I_2, followed by the addition of ethylene bromide (0.5 mL). Activation was indicated by a slight effervescence and diminishing of the brown colour.

Spectroscopy

NMR spectra were recorded on a JEOL Eclipse 400 spectrometer or JEOL ECZ400 YH spectrometer at 298 K (399.60 MHz for ^1H, 96.251 for ^{11}B,376.01 MHz for ^{19}F, 161.76 MHz for ^{31}P and 100.48 MHz for $^{13}C\{^1H\}$).^1H and $^{13}C\{^1H\}$ spectra were referenced to residual solvent peaks and reported relative to tetramethylsilane. ^{11}B, ^{19}F and ^{31}P NMR are reported relative to external standards , $BF_3.OEt_2$, $CFCl_3$ and H_2PO_4 in H_2O (85% v/v) respectively.

Crystallography

All crystallographic measurements were performed using an Oxford Diffraction XcaliburS Single Crystal Diffractometer with a Sapphire CCD dectector (Enhance X-Ray source Mo Kα radiation, λ = 0.71073 Å or Cu Kα λ = 1.5406) with CrysAlisPro 1.171.39.46.[627–629] In each case, a specimen of suitable size and quality was selected, coated with Fomblin® Y oil, and mounted onto a nylon loop. The Analytical numeric absorption correction using a

multifaceted crystal model based on expressions derived by R.C. Clark & J.S. Reid.[630] Empirical absorption correction using spherical harmonics, implemented in SCALE3 ABSPACK scaling algorithm was applied for absorption correction. Using Olex2,[631] the structure was solved with the ShelXT structure solution program using Intrinsic Phasing and refined with the ShelXL refinement package using Least Squares minimisation, [632,633] unless otherwise stated. Hydrogen atoms were typically geometrically placed and refined using the riding model approximation

Appendix II: Summary of Crystallographic Data

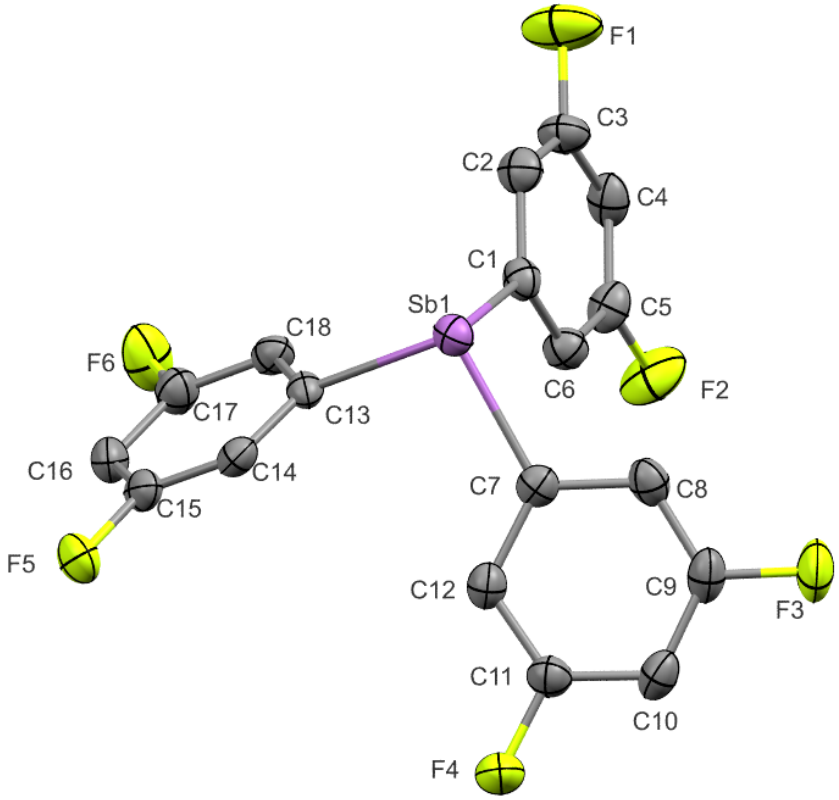

Figure 8.1. Solid state structure of **1-3**. Ellipsoids shown at 50% probability. Hydrogen atoms have been omitted. Selected structural parameters (bond lengths in angstroms and bond angles in degrees): Sb1-C13 2.159(4), Sb1-C7 2.156(4), Sb1-C1 2.159(4), C13-Sb1-C1 95.33(15), C7-Sb1-C13 97.76(15) C7-Sb1-C1 94.38(15).

Table 8.1. Crystal data and structure refinement for **1-3**.

Empirical formula	$C_{18}H_9F_6Sb$
Formula weight	461.00
Temperature/K	150.00(10)
Crystal system	monoclinic
Space group	$P2_1/c$
a/Å	5.2441(2)
b/Å	15.5747(4)
c/Å	19.4901(6)
α/°	90
β/°	96.736(4)
γ/°	90
Volume/Å^3	1580.87(9)
Z	4
ρ_{calc}g/cm^3	1.937
μ/mm^{-1}	1.807
F(000)	888.0
Crystal size/mm^3	0.157 × 0.126 × 0.099
Radiation	Mo Kα (λ = 0.71073)
2Θ range for data collection/°	6.716 to 61.688
Index ranges	$-6 \le h \le 7$, $-21 \le k \le 20$, $-27 \le l \le 27$
Reflections collected	24686
Independent reflections	4594 [R_{int} = 0.0844, R_{sigma} = 0.0865]
Data/restraints/parameters	4594/0/226
Goodness-of-fit on F^2	1.023
Final R indexes [I>=2σ (I)]	R_1 = 0.0499, wR_2 = 0.0739
Final R indexes [all data]	R_1 = 0.0937, wR_2 = 0.0886
Largest diff. peak/hole / e Å^{-3}	1.16/-0.79

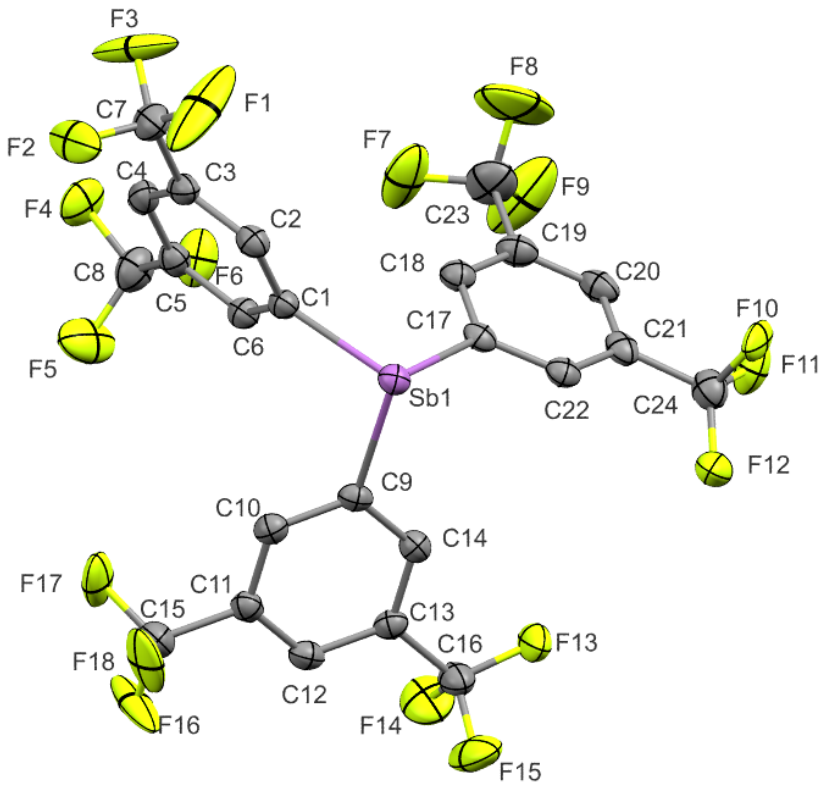

Figure 8.2. Solid state structure of **1**-**6**. Ellipsoids shown at 50% probability. Hydrogen atoms have been omitted. The trifluoromethyl groups are disordered and modelled over two positions, only one is shown. Selected structural parameters (bond lengths in angstroms and bond angles in degrees): Sb1-C17 2.155(2), Sb1-C1 2.144(2), Sb1-C9 2.160(2), C17-Sb1-C9 94.93(8), C1-Sb1-C17 97.05(8), C1-Sb1-C9 96.04(8).

Table 8.2. Crystal data and structure refinement for **1-6**.

Empirical formula	$C_{24}H_9F_{18}Sb$
Formula weight	761.06
Temperature/K	150.01(10)
Crystal system	triclinic
Space group	P-1
a/Å	10.0041(2)
b/Å	12.0201(3)
c/Å	12.6678(3)
α/°	113.030(2)
β/°	104.357(2)
γ/°	101.497(2)
Volume/Å^3	1280.91(6)
Z	2
ρ_{calc}g/cm^3	1.973
μ/mm^{-1}	1.222
F(000)	732.0
Crystal size/mm^3	0.435 × 0.403 × 0.211
Radiation	Mo Kα (λ = 0.71073)
2Θ range for data collection/°	6.654 to 54.968
Index ranges	-12 ≤ h ≤ 12, -15 ≤ k ≤ 15, -16 ≤ l ≤ 16
Reflections collected	43694
Independent reflections	5848 [R_{int} = 0.0396, R_{sigma} = 0.0245]
Data/restraints/parameters	5848/291/556
Goodness-of-fit on F^2	1.083
Final R indexes [I>=2σ (I)]	R_1 = 0.0261, wR_2 = 0.0542
Final R indexes [all data]	R_1 = 0.0294, wR_2 = 0.0556
Largest diff. peak/hole / e Å^{-3}	0.53/-0.37

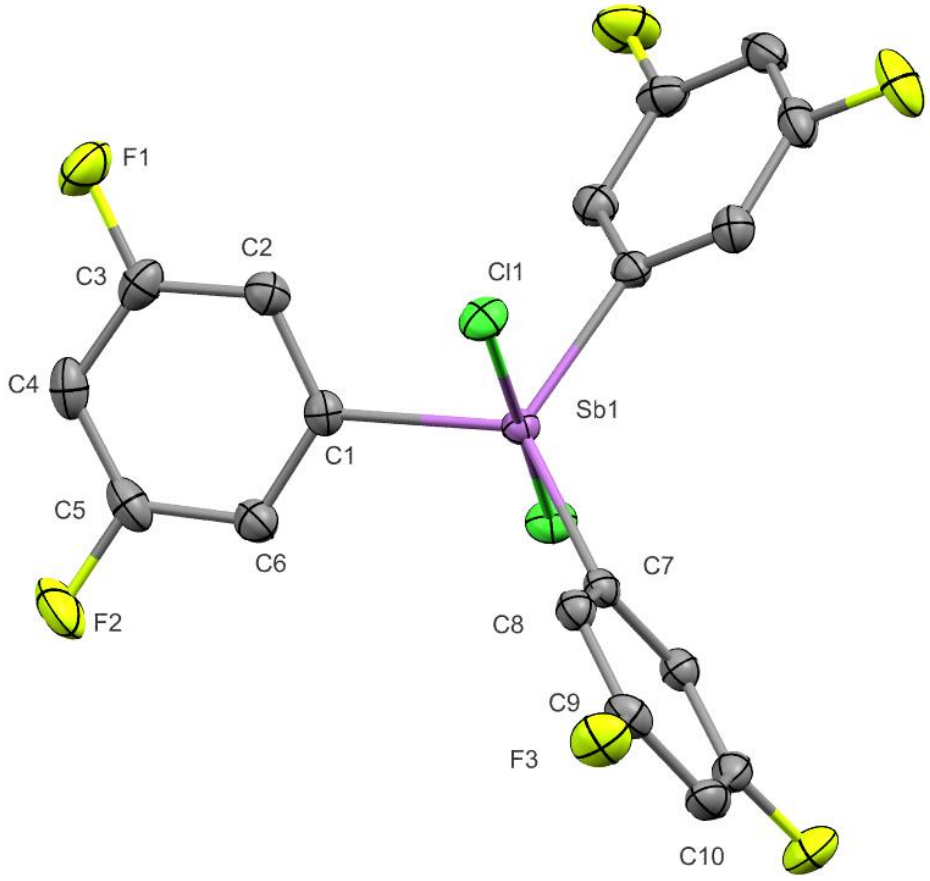

Figure 8.3. Solid state structure of **1-10**. Ellipsoids shown at 50% probability. Hydrogen atoms have been omitted. Selected structural parameters (bond lengths in angstroms and bond angles in degrees): Sb1-Cl1 2.4555(4), Sb1-C7 2.128(3), Sb1-C11 2.1089(18), Sb1-C1 2.1089(18), Cl1-Sb1-Cl11 176.02(2), C7-Sb1-Cl1[1] 91.991(12), C7-Sb1-Cl1 91.991(12),C1-Sb1-Cl1 89.01(5),C1-Sb1-Cl1[1] 88.86(5),C1[1]-Sb1-Cl1[1] 89.01(5),C1[1]-Sb1-Cl1 88.86(5),C1[1]-Sb1-C7 122.25(5),C1-Sb1-C7 122.25(5),C1-Sb1-C1[1] 115.51(10). [1]1-X,+Y,1/2-Z

Table 8.3. Crystal data and structure refinement for **1-10**.

Empirical formula	$C_{18}H_9Cl_2F_6Sb$
Formula weight	531.90
Temperature/K	150.01(10)
Crystal system	monoclinic
Space group	C2/c
a/Å	15.7714(3)
b/Å	10.8973(3)
c/Å	10.4367(2)
α/°	90
β/°	102.368(2)
γ/°	90
Volume/Å^3	1752.08(7)
Z	4
ρ_{calc}g/cm^3	2.016
μ/mm^{-1}	1.940
F(000)	1024.0
Crystal size/mm^3	? × ? × ?
Radiation	MoKα (λ = 0.71073)
2Θ range for data collection/°	6.44 to 54.966
Index ranges	-20 ≤ h ≤ 19, -13 ≤ k ≤ 14, -13 ≤ l ≤ 13
Reflections collected	7649
Independent reflections	1979 [R_{int} = 0.0209, R_{sigma} = 0.0205]
Data/restraints/parameters	1979/0/124
Goodness-of-fit on F^2	1.122
Final R indexes [I>=2σ (I)]	R_1 = 0.0185, wR_2 = 0.0410
Final R indexes [all data]	R_1 = 0.0198, wR_2 = 0.0414
Largest diff. peak/hole / e Å^{-3}	0.32/-0.63

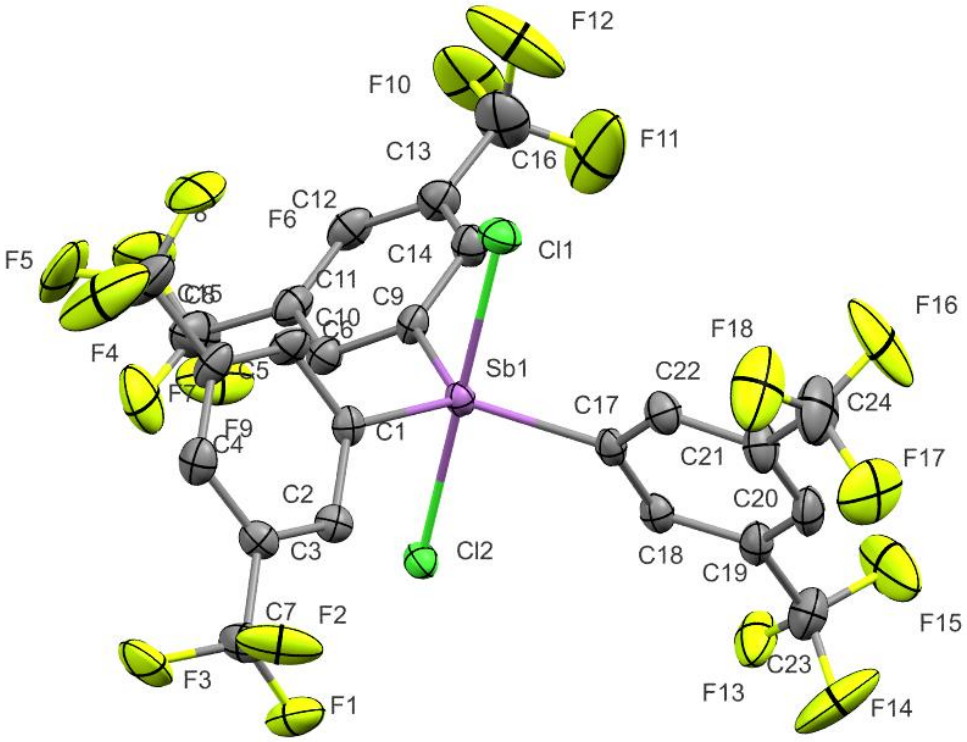

Figure 8.4. Solid state structure of **1-13**. Ellipsoids shown at 50% probability. Hydrogen atoms have been omitted. The trifluoromethyl groups are disordered and modelled over two positions, only one is shown. Selected structural parameters (bond lengths in angstroms and bond angles in degrees): Sb1-Cl2 2.4275(7), Sb1-Cl12.4330(7), Sb1-C1 2.117(3), Sb1-C17 2.120(2), Sb1-C9 2.117(3), Cl2-Sb1-Cl1 178.88(2), C1-Sb1-Cl2 90.25(8), C1-Sb1-Cl1 90.71(8), C1-Sb1-C17 120.21(10), C17-Sb1-Cl2 90.00(7), C17-Sb1-Cl1 90.02(7), C9-Sb1-Cl2 89.43(8), C9-Sb1-Cl1 89.62(8), C9-Sb1-C1 117.16(10), C9-Sb1-C17 122.63(10).

Table 8.4. Crystal data and structure refinement for **1-13**.

Empirical formula	$C_{24}H_9Cl_2F_{18}Sb$
Formula weight	831.96
Temperature/K	150.01(10)
Crystal system	monoclinic
Space group	C2/c
a/Å	16.284(2)
b/Å	22.8997(7)
c/Å	28.052(4)
α/°	90
β/°	145.53(4)
γ/°	90
Volume/Å^3	5920(3)
Z	8
ρ_{calc}g/cm^3	1.867
μ/mm^{-1}	1.241
F(000)	3200.0
Crystal size/mm^3	0.4 × 0.102 × 0.092
Radiation	MoKα (λ = 0.71073)
2Θ range for data collection/°	6.508 to 54.966
Index ranges	-20 ≤ h ≤ 20, -29 ≤ k ≤ 29, -36 ≤ l ≤ 36
Reflections collected	25543
Independent reflections	6597 [R_{int} = 0.0286, R_{sigma} = 0.0294]
Data/restraints/parameters	6597/1162/574
Goodness-of-fit on F^2	1.099
Final R indexes [I>=2σ (I)]	R_1 = 0.0324, wR_2 = 0.0655
Final R indexes [all data]	R_1 = 0.0403, wR_2 = 0.0682
Largest diff. peak/hole / e Å^{-3}	0.54/-0.35

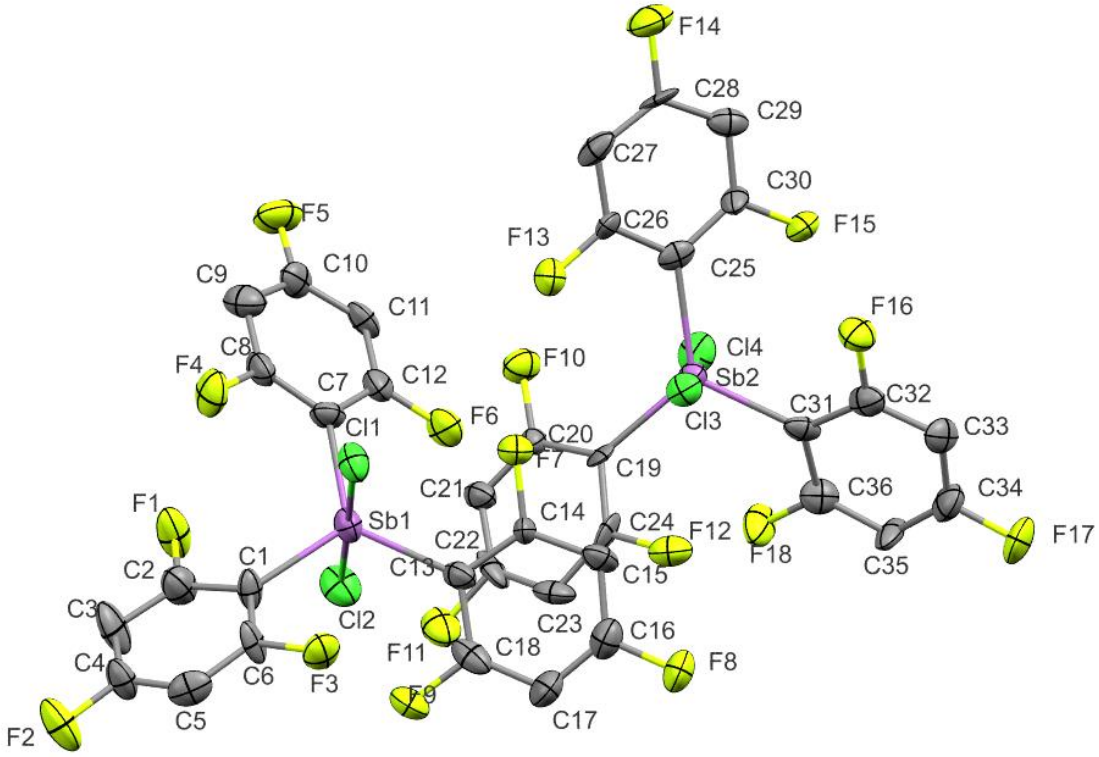

Figure 8.5. Solid state structure of **1-11.** Ellipsoids shown at 50% probability. Hydrogen atoms have been omitted. Selected structural parameters (bond lengths in angstroms and bond angles in degrees): Sb2-C25 2.092(10), Sb2-C19 2.086(11), Sb2-C31 2.061(12), Sb2-Cl3 2.395(3), Sb2-Cl4 2.422(3), Sb1-C13 2.094(12), Sb1-C1 2.082(11), Sb1-C7 2.091(10), Sb1-Cl2 2.408(3), Sb1-Cl1 2.433(3), C25-Sb2-Cl3 87.2(3), C25-Sb2-Cl4 88.5(3), C19-Sb2-C25 123.4(5), C19-Sb2-Cl3 93.3(3), C19-Sb2-Cl4 88.2(3), C31-Sb2-C25 123.1(5), C31-Sb2-C19 113.4(4), C31-Sb2-Cl3 92.5(3), C31-Sb2-Cl4 90.7(3), Cl3-Sb2-Cl4 175.58(10), C13-Sb1-Cl2 89.9(3), C13-Sb1-Cl1 91.1(3), C1-Sb1-C13 117.8(4), C1-Sb1-C7 117.3(5), C1-Sb1-Cl2 90.3(3), C1-Sb1-Cl1 89.4(3), C7-Sb1-C13 124.8(5), C7-Sb1-Cl2 89.8(3), C7-Sb1-Cl1 89.5(3), Cl2-Sb1-Cl1 178.99(13).

Table 8.5. Crystal data and structure refinement for **1-11.**

Empirical formula	$C_{36}H_{12}Cl_4F_{18}Sb_2$
Formula weight	1171.76
Temperature/K	150.01(10)
Crystal system	orthorhombic
Space group	Pbca
a/Å	20.9948(9)
b/Å	14.5992(8)
c/Å	24.9300(16)
α/°	90
β/°	90
γ/°	90
Volume/Å^3	7641.2(7)
Z	8
ρ_{calc}g/cm^3	2.037
μ/mm^{-1}	1.811
F(000)	4480.0
Crystal size/mm^3	0.275 × 0.19 × 0.043
Radiation	Mo Kα (λ = 0.71073)
2Θ range for data collection/°	6.66 to 58.836
Index ranges	-27 ≤ h ≤ 19, -16 ≤ k ≤ 20, -15 ≤ l ≤ 31
Reflections collected	20803
Independent reflections	8919 [R_{int} = 0.1223, R_{sigma} = 0.2279]
Data/restraints/parameters	8919/0/541
Goodness-of-fit on F^2	0.990
Final R indexes [I>=2σ (I)]	R_1 = 0.0835, wR_2 = 0.1030
Final R indexes [all data]	R_1 = 0.2050, wR_2 = 0.1593
Largest diff. peak/hole / e Å^{-3}	1.65/-1.15

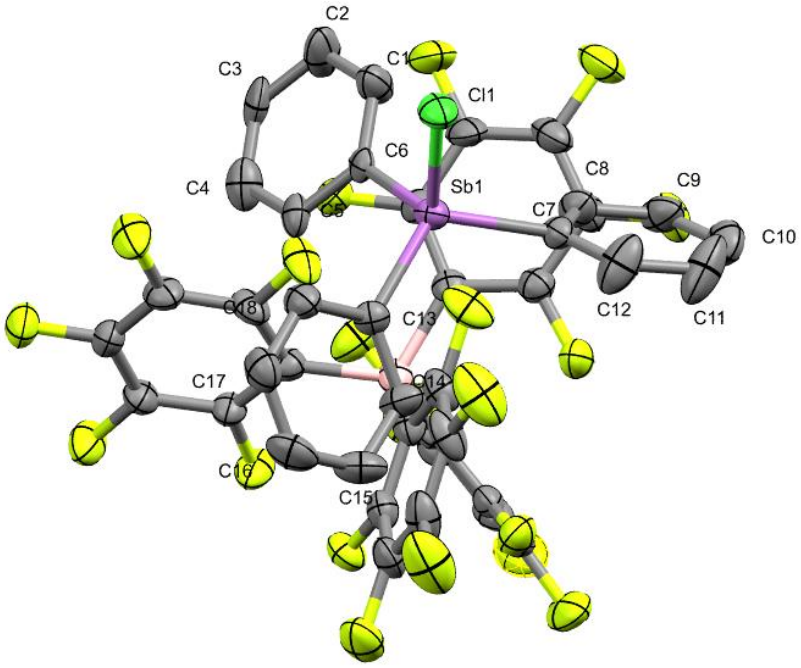

Figure 8.6. Solid state structure of **1-14.** Ellipsoids shown at 50% probability. Hydrogen atoms and labels for borate counteranion have been omitted. One aryl ring (C1-C6) is disordered over two positions, only one is shown. Selected structural parameters (bond lengths in angstroms and bond angles in degrees): Sb1-Cl1 2.2821(14), Sb1-C13 2.088(5), Sb1-C7 2.085(5), Sb1-C6 2.04(2),C13-Sb1-Cl1 104.10(14), C7-Sb1-Cl1 106.21(15), C7-Sb1-C13 116.9(2), C6-Sb1-Cl1 107.5(6), C6-Sb1-C13 112.6(5), C6-Sb1-C7 108.8(8).

Table 8.6. Crystal data and structure refinement for **1-14.**

Empirical formula	$C_{42}H_{15}BClF_{20}Sb$
Formula weight	1067.55
Temperature/K	150.00(10)
Crystal system	monoclinic
Space group	Ia
a/Å	18.2922(3)
b/Å	11.1990(2)
c/Å	19.0613(4)
α/°	90
β/°	92.763(2)
γ/°	90
Volume/Å^3	3900.25(13)
Z	4
ρ_{calc}g/cm^3	1.818
μ/mm^{-1}	0.905
F(000)	2080.0
Crystal size/mm^3	0.299 × 0.174 × 0.094
Radiation	Mo Kα (λ = 0.71073)
2Θ range for data collection/°	7.278 to 61.762
Index ranges	-25 ≤ h ≤ 25, -15 ≤ k ≤ 16, -26 ≤ l ≤ 27
Reflections collected	50560
Independent reflections	11251 [R_{int} = 0.0684, R_{sigma} = 0.0713]
Data/restraints/parameters	11251/118/641
Goodness-of-fit on F^2	1.044
Final R indexes [I>=2σ (I)]	R_1 = 0.0478, wR_2 = 0.0674
Final R indexes [all data]	R_1 = 0.0715, wR_2 = 0.0753
Largest diff. peak/hole / e Å^{-3}	0.55/-0.45
Flack parameter	-0.027(8)

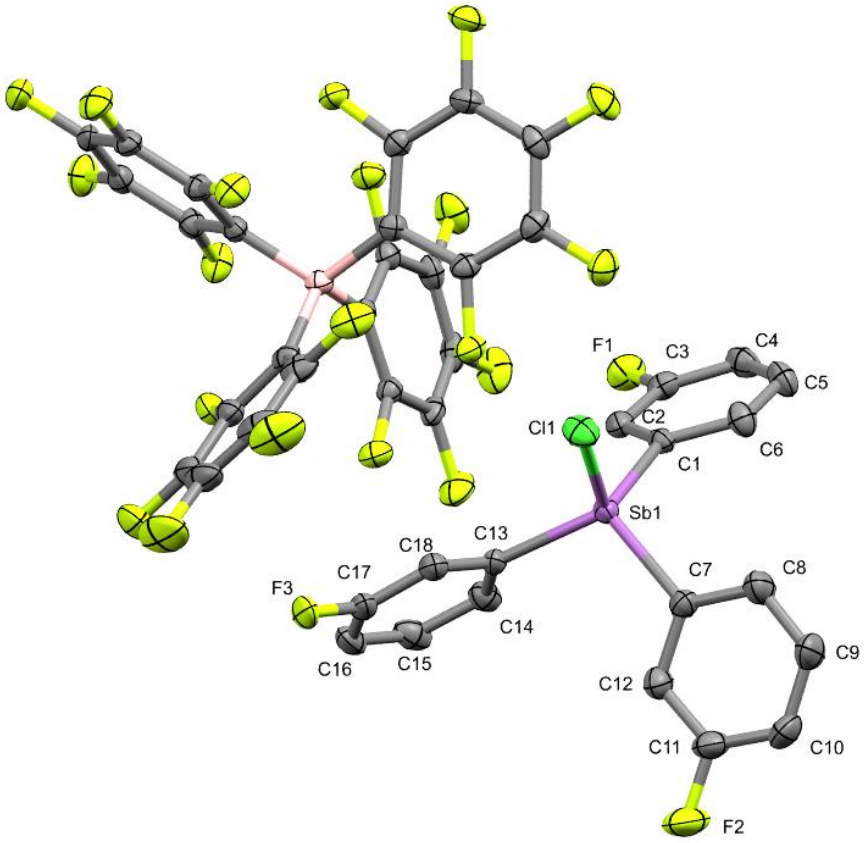

Figure 8.7. Solid state structure of **1-15**. Ellipsoids shown at 50% probability. Hydrogen atoms and labels for borate counteranion have been omitted. F3 is disordered over two positions, only one is shown. SHELXD (dual space) was used to provide an initial structure solution. Selected structural parameters (bond lengths in angstroms and bond angles in degrees): Sb1-Cl1 2.2762(9), Sb1-C1 2.087(3), Sb1-C13 2.084(3), Sb1-C7 2.088(4), C1-Sb1-Cl1 109.52(10), C1-Sb1-C7 110.06(14), C13-Sb1-Cl1 106.07(10), C13-Sb1-C1 115.28(13),C13-Sb1-C7 108.49(14),C7-Sb1-Cl1 107.05(10).

Table 8.7. Crystal data and structure refinement for **1-15.**

Empirical formula	$C_{42}H_{11}BClF_{23}Sb$
Formula weight	1120.52
Temperature/K	150.01(10)
Crystal system	monoclinic
Space group	$P2_1$
a/Å	8.92125(11)
b/Å	20.4543(3)
c/Å	10.90377(15)
α/°	90
β/°	100.5011(12)
γ/°	90
Volume/Å^3	1956.37(4)
Z	2
ρ_{calc}g/cm^3	1.902
μ/mm^{-1}	0.918
F(000)	1086.0
Crystal size/mm^3	0.456 × 0.393 × 0.181
Radiation	Mo Kα (λ = 0.71073)
2Θ range for data collection/°	6.516 to 61.784
Index ranges	-12 ≤ h ≤ 12, -29 ≤ k ≤ 29, -14 ≤ l ≤ 15
Reflections collected	43237
Independent reflections	11169 [R_{int} = 0.0408, R_{sigma} = 0.0428]
Data/restraints/parameters	11169/1/622
Goodness-of-fit on F^2	1.027
Final R indexes [I>=2σ (I)]	R_1 = 0.0311, wR_2 = 0.0548
Final R indexes [all data]	R_1 = 0.0384, wR_2 = 0.0578
Largest diff. peak/hole / e Å^{-3}	0.41/-0.33
Flack parameter	-0.036(5)

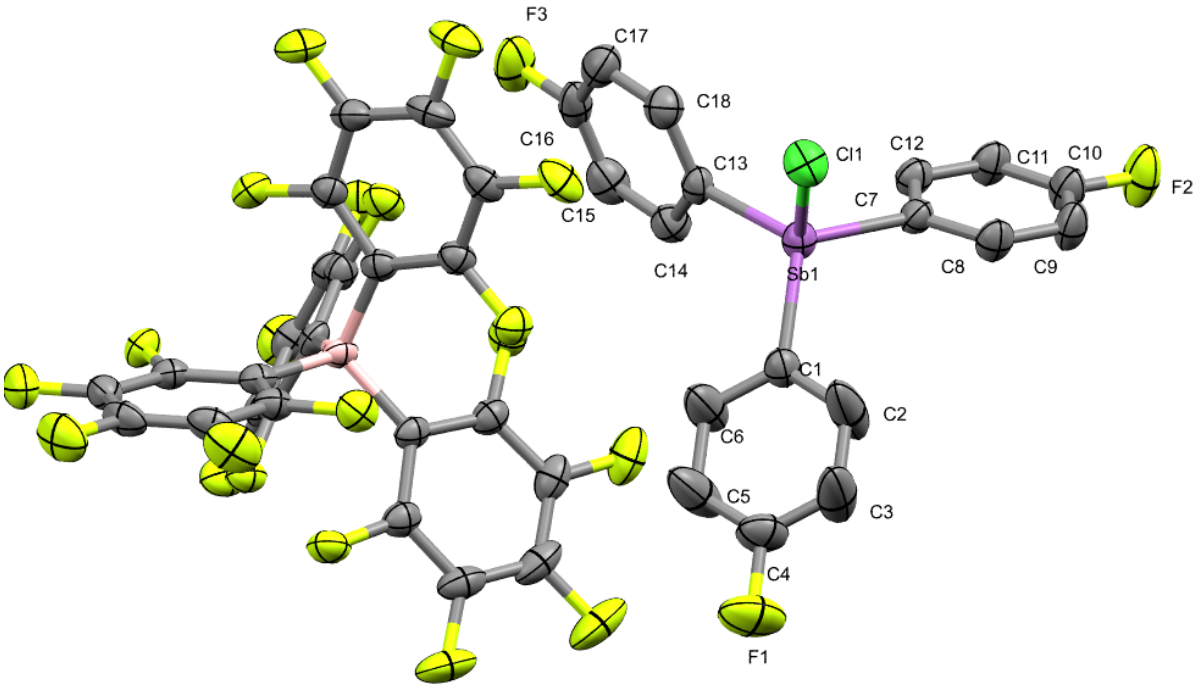

Figure 8.8. Solid state structure of **1-16.** Ellipsoids shown at 50% probability. Hydrogen atoms, disordered co-crystalised dichloromethane and labels for borate counteranion have been omitted. Selected structural parameters (bond lengths in angstroms and bond angles in degrees): Sb1-Cl1 2.2923(10), Sb1-C13 2.087(3), Sb1-C7 2.084(3), Sb1-C1 2.085(4), C13-Sb1-Cl1 105.58(10), C7-Sb1-Cl1 105.94(10), C7-Sb1-C13 109.66(13), C7-Sb1-C1 114.48(14),C1-Sb1-Cl1 103.77(10),C1-Sb1-C13 116.29(14).

Table 8.8. Crystal data and structure refinement for **1-16.**

Empirical formula	$C_{42.5}H_{13}BCl_2F_{23}Sb$
Formula weight	1163.99
Temperature/K	150.01(10)
Crystal system	monoclinic
Space group	$P2_1/n$
a/Å	15.4617(3)
b/Å	14.4843(4)
c/Å	18.3497(5)
α/°	90
β/°	97.825(2)
γ/°	90
Volume/Å^3	4071.19(18)
Z	4
ρ_{calc}g/cm^3	1.899
μ/mm^{-1}	0.949
F(000)	2260.0
Crystal size/mm^3	0.303 × 0.192 × 0.19
Radiation	Mo Kα (λ = 0.71073)
2Θ range for data collection/°	6.474 to 61.682
Index ranges	-21 ≤ h ≤ 21, -20 ≤ k ≤ 20, -26 ≤ l ≤ 24
Reflections collected	62976
Independent reflections	11917 [R_{int} = 0.0828, R_{sigma} = 0.0819]
Data/restraints/parameters	11917/556/640
Goodness-of-fit on F^2	1.022
Final R indexes [I>=2σ (I)]	R_1 = 0.0552, wR_2 = 0.0959
Final R indexes [all data]	R_1 = 0.1081, wR_2 = 0.1152
Largest diff. peak/hole / e Å^{-3}	0.57/-0.70

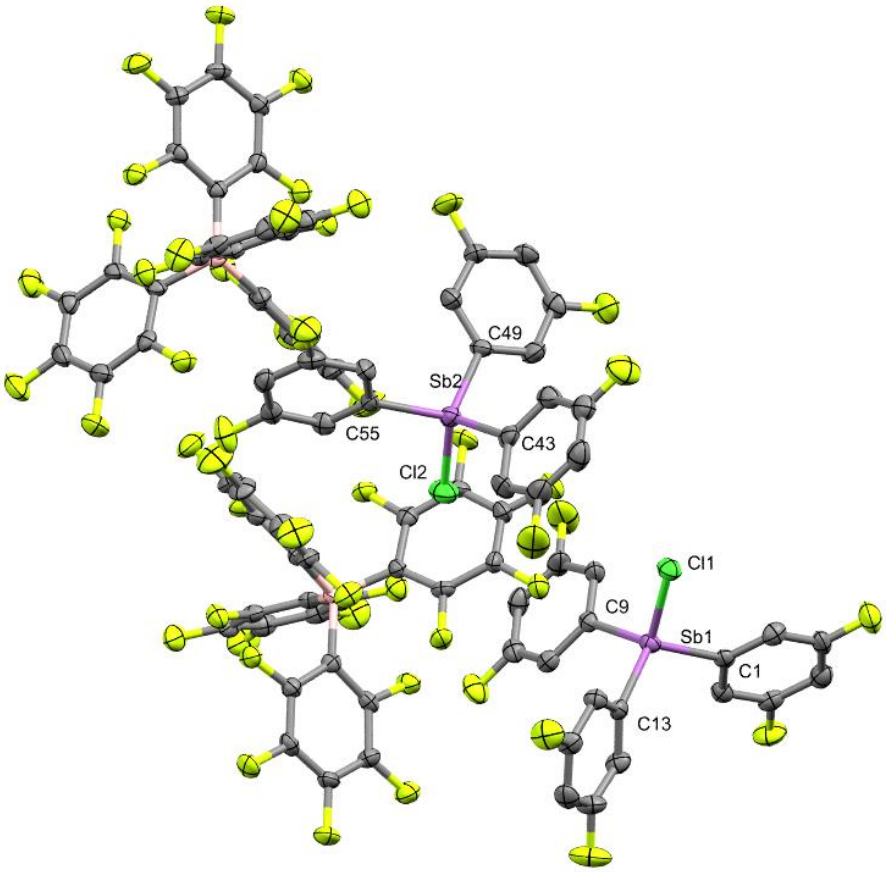

Figure 8.9. Solid state structure of **1-17.** Ellipsoids shown at 50% probability. Hydrogen atoms have been omitted and only selected labels are shown. The structure is racemically twinned (TWIN LAW (-1.0, 0.0, 0.0, 0.0, -1.0, 0.0, 0.0, 0.0, -1.0), BASF [0.480(12)]) Selected structural parameters (bond lengths in angstroms and bond angles in degrees): Sb1-Cl1 2.2608(16), Sb1-C13 2.096(7), Sb1-C9 2.096(6), Sb1-C1 2.088(7), Sb2-Cl2 2.2604(19), Sb2-C49 2.088(7), Sb2-C55 2.090(6), Sb2-C43 2.093(7), C13-Sb1-Cl1 109.11(19) C9-Sb1-Cl1 110.72(18), C9-Sb1-C13 107.9(3), C1-Sb1-Cl1 105.4(2), C1-Sb1-C13 116.4(2), C1-Sb1-C9 107.3(3), C49-Sb2-Cl2 108.9(2), C49-Sb2-C55 112.2(3), C49-Sb2-C43 108.1(3), C55-Sb2-Cl2 107.1(2), C55-Sb2-C43 112.9(3), C43-Sb2-Cl2 107.5(2).

Table 8.9. Crystal data and structure refinement for **1-17.**

Empirical formula	$C_{42}H_9BClF_{26}Sb$
Formula weight	1175.50
Temperature/K	150.01(10)
Crystal system	monoclinic
Space group	Pn
a/Å	13.6723(2)
b/Å	15.5501(3)
c/Å	19.0384(3)
α/°	90
β/°	94.8414(16)
γ/°	90
Volume/Å^3	4033.23(12)
Z	4
ρ_{calc}g/cm^3	1.936
μ/mm^{-1}	0.906
F(000)	2272.0
Crystal size/mm^3	0.164 × 0.151 × 0.086
Radiation	Mo Kα (λ = 0.71073)
2Θ range for data collection/°	6.488 to 54.968
Index ranges	-17 ≤ h ≤ 17, -20 ≤ k ≤ 19, -24 ≤ l ≤ 24
Reflections collected	48693
Independent reflections	17928 [R_{int} = 0.0576, R_{sigma} = 0.0801]
Data/restraints/parameters	17928/2/1280
Goodness-of-fit on F^2	1.000
Final R indexes [I>=2σ (I)]	R_1 = 0.0461, wR_2 = 0.0542
Final R indexes [all data]	R_1 = 0.0657, wR_2 = 0.0598
Largest diff. peak/hole / e Å^{-3}	1.08/-0.62
Flack parameter	0.480(12)

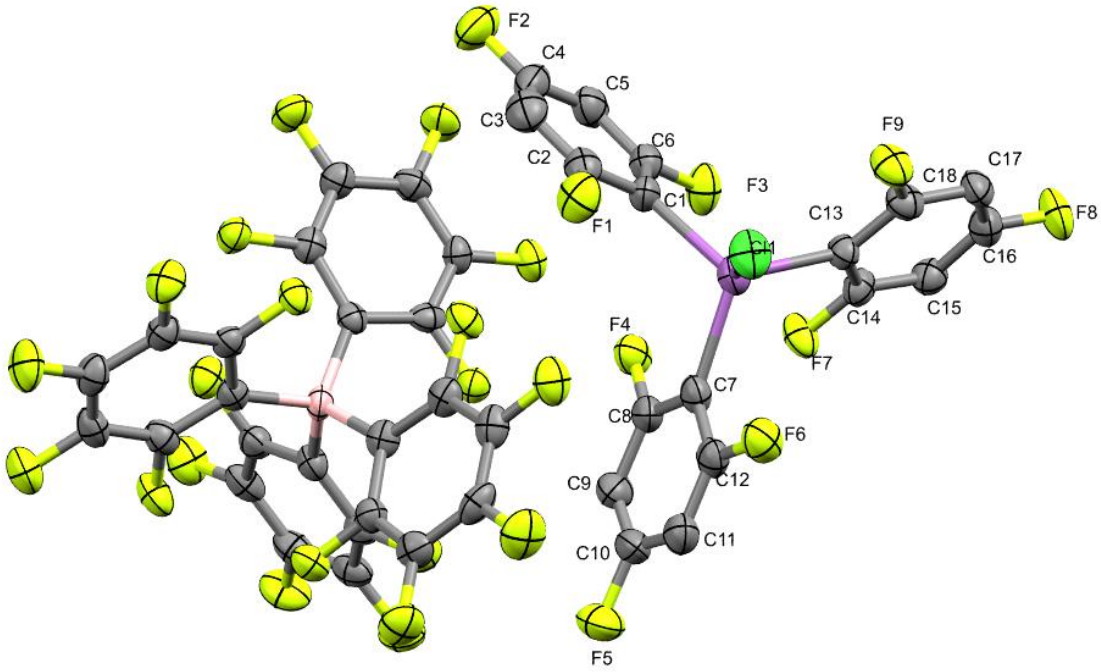

Figure 8.10. Solid state structure of **1-18.** Ellipsoids shown at 50% probability. Hydrogen atoms and labels for borate counteranion have been omitted. Selected structural parameters (bond lengths in angstroms and bond angles in degrees): Sb1-Cl12.2532(19), Sb1-C13 2.067(6), Sb1-C1 2.084(6), Sb1-C7 2.072(7), C13-Sb1-Cl1 108.2(2), C1-Sb1-C1 111.1(3), C13-Sb1-C7 112.7(3), C1-Sb1-Cl1 106.2(2), C7-Sb1-Cl1 107.2(2), C7-Sb1-C1 111.1(2).

Table 8.10. Crystal data and structure refinement for **1-18.**

Empirical formula	$C_{42}H_6BClF_{29}Sb$
Formula weight	1229.48
Temperature/K	150.01(10)
Crystal system	monoclinic
Space group	$P2_1/n$
a/Å	11.9508(4)
b/Å	16.2223(7)
c/Å	21.3075(7)
α/°	90
β/°	99.747(3)
γ/°	90
Volume/Å^3	4071.2(3)
Z	4
ρ_{calc}g/cm^3	2.006
μ/mm^{-1}	7.566
F(000)	2368.0
Crystal size/mm^3	0.159 × 0.089 × 0.073
Radiation	CuKα (λ = 1.54184)
2Θ range for data collection/°	13.254 to 133.202
Index ranges	-14 ≤ h ≤ 11, -19 ≤ k ≤ 17, -25 ≤ l ≤ 25
Reflections collected	17949
Independent reflections	7132 [R_{int} = 0.0723, R_{sigma} = 0.1006]
Data/restraints/parameters	7132/0/667
Goodness-of-fit on F^2	0.991
Final R indexes [I>=2σ (I)]	R_1 = 0.0573, wR_2 = 0.1183
Final R indexes [all data]	R_1 = 0.0907, wR_2 = 0.1375
Largest diff. peak/hole / e Å^{-3}	0.63/-1.27

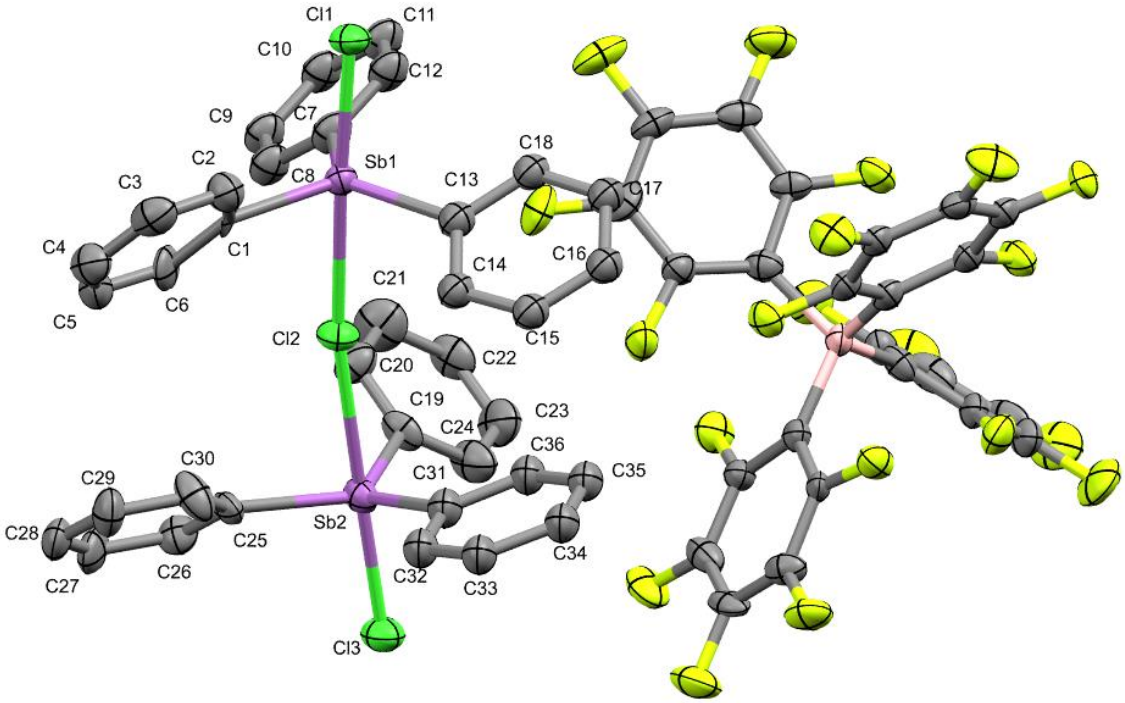

Figure 8.11. Solid state structure of **1-19.** Ellipsoids shown at 50% probability. Hydrogen atoms and labels for borate counteranion have been omitted. Selected structural parameters (bond lengths in angstroms and bond angles in degrees):Sb1-Cl2 2.679(3), Sb1-Cl1 2.388(3), Sb1-C7 2.123(11), Sb1-C13 2.104(12), Sb1-C1 2.120(9), Sb2-Cl2 2.782(3), Sb2-Cl3 2.372(3), Sb2-C25 2.105(10), Sb2-C19 2.109(9), Sb2-C31 2.087(12), Cl1-Sb1-Cl2 176.39(10), C7-Sb1-Cl2 84.4(4), C7-Sb1-Cl1 93.2(4), C13-Sb1-Cl2 86.1(3), C13-Sb1-Cl1 93.0(3), C13-Sb1-C7 123.4(4), C13-Sb1-C1 114.1(4), C1-Sb1-Cl2 87.2(3), C1-Sb1-Cl1 96.3(3), C1-Sb1-C7 121.0(4), Cl3-Sb2-Cl2 178.39(11), C25-Sb2-Cl2 83.7(3), C25-Sb2-Cl3 96.8(3), C25-Sb2-C19 118.3(5), C19-Sb2-Cl2 86.9(3), C19-Sb2-Cl3 94.2(3), C31-Sb2-Cl2 81.2(3), C31-Sb2-Cl3 97.2(4), C31-Sb2-C25 119.1(4), C31-Sb2-C19 119.2(4).

Table 8.11. Crystal data and structure refinement for **1-19.**

Empirical formula	$C_{60}H_{30}BCl_3F_{20}Sb_2$
Formula weight	1491.50
Temperature/K	150.01(10)
Crystal system	monoclinic
Space group	$P2_1/n$
a/Å	14.9294(4)
b/Å	20.3833(6)
c/Å	18.2449(5)
α/°	90
β/°	92.505(2)
γ/°	90
Volume/Å^3	5546.8(3)
Z	4
ρ_{calc}g/cm^3	1.786
μ/mm^{-1}	10.034
F(000)	2912.0
Crystal size/mm^3	0.089 × 0.067 × 0.03
Radiation	CuKα (λ = 1.54184)
2Θ range for data collection/°	7.344 to 143.912
Index ranges	-16 ≤ h ≤ 11, -24 ≤ k ≤ 24, -22 ≤ l ≤ 21
Reflections collected	29392
Independent reflections	10148 [R_{int} = 0.0845, R_{sigma} = 0.1467]
Data/restraints/parameters	10148/0/661
Goodness-of-fit on F^2	1.144
Final R indexes [I>=2σ (I)]	R_1 = 0.0734, wR_2 = 0.1546
Final R indexes [all data]	R_1 = 0.1190, wR_2 = 0.1786
Largest diff. peak/hole / e Å^{-3}	1.18/-1.04

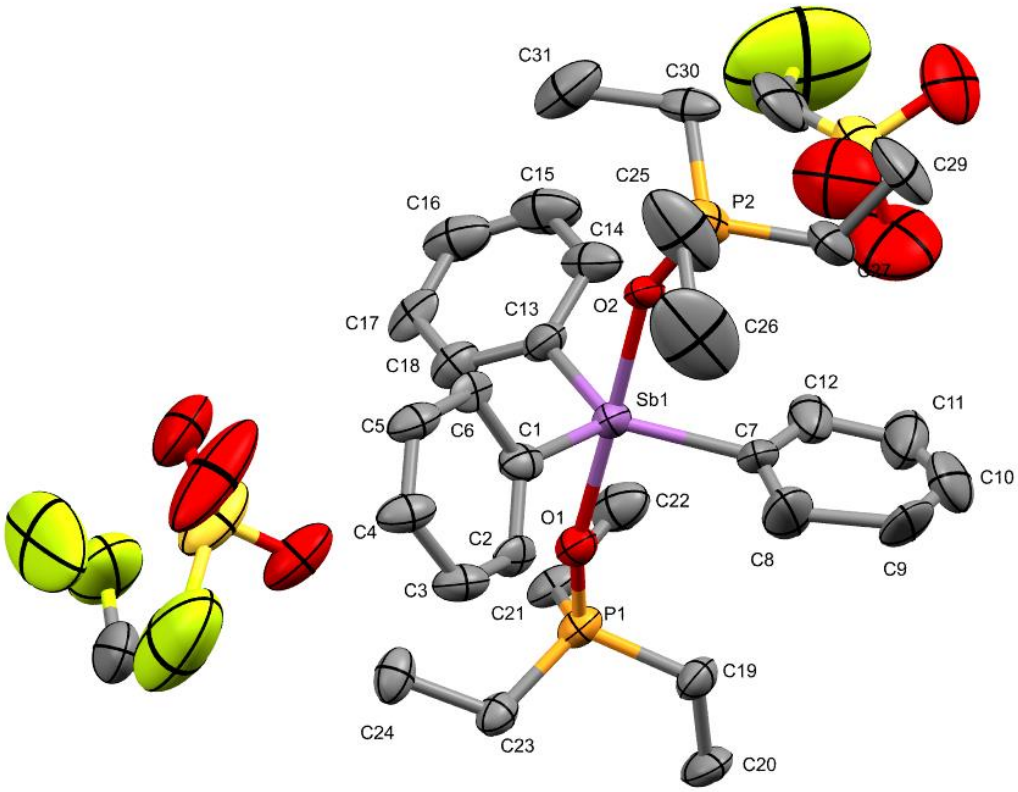

Figure 8.12. Solid state structure of **1**-**20**. Ellipsoids shown at 30% probability. Hydrogen atoms and labels for triflate counteranions have been omitted.Selected structural parameters aren't included two to the poor data quality and improper modelling of triflates.

Table 8.12. Crystal data and structure refinement for **1-20**.

Empirical formula	$C_{32}H_{42}F_4O_8P_2S_2Sb$
Formula weight	878.46
Temperature/K	150.00(10)
Crystal system	monoclinic
Space group	$P2_1/c$
a/Å	21.368(3)
b/Å	11.0048(10)
c/Å	20.551(4)
α/°	90
β/°	118.72(2)
γ/°	90
Volume/Å^3	4238.3(13)
Z	4
ρ_{calc}g/cm^3	1.377
μ/mm^{-1}	0.884
F(000)	1788.0
Crystal size/mm^3	0.232 × 0.158 × 0.067
Radiation	Mo Kα (λ = 0.71073)
2Θ range for data collection/°	6.868 to 58.844
Index ranges	-26 ≤ h ≤ 22, -14 ≤ k ≤ 13, -28 ≤ l ≤ 27
Reflections collected	31149
Independent reflections	10238 [R_{int} = 0.3323, R_{sigma} = 0.6375]
Data/restraints/parameters	10238/430/453
Goodness-of-fit on F^2	1.000
Final R indexes [I>=2σ (I)]	R_1 = 0.1739, wR_2 = 0.3781
Final R indexes [all data]	R_1 = 0.4662, wR_2 = 0.5232
Largest diff. peak/hole / e Å^{-3}	2.14/-0.60

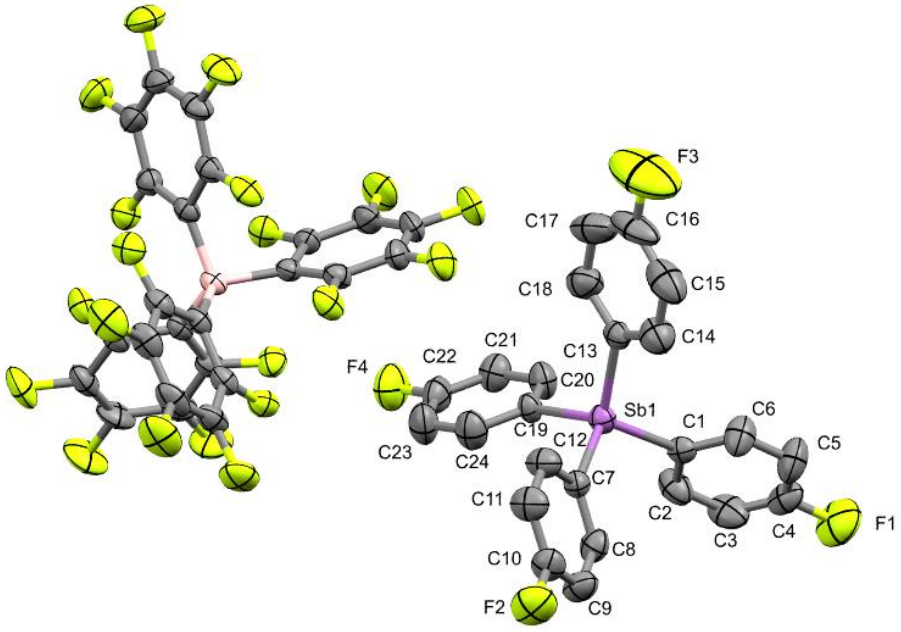

Figure 8.13. Solid state structure of $[(4\text{-}FC_6H_4)_4Sb][B(C_6F_5)_4]$. Ellipsoids shown at 50% probability. Hydrogen atoms and labels for borate counteranion have been omitted.Selected structural parameters (bond lengths in angstroms and bond angles in degrees): Sb1-C1 2.082(3), Sb1-C19 2.099(3), Sb1-C13 2.096(3), Sb1-C7 2.084(3), C1-Sb1-C19 108.34(13) C1-Sb1-C13 112.66(12), C1-Sb1-C7 109.90(12), C13-Sb1-C19 109.85(13), C7-Sb1-C19 110.43(12), C7-Sb1-C13 105.65(13).

Table 8.13. Crystal data and structure refinement for[(4-FC_6H_4)$_4$Sb][B(C_6F_5)$_4$].

Empirical formula	$C_{48}H_{16}BF_{24}Sb$
Formula weight	1181.17
Temperature/K	150.01(10)
Crystal system	triclinic
Space group	P-1
a/Å	11.2248(3)
b/Å	13.1814(3)
c/Å	15.2737(3)
α/°	84.529(2)
β/°	79.518(2)
γ/°	86.792(2)
Volume/Å^3	2210.32(9)
Z	2
ρ_{calc}g/cm^3	1.775
μ/mm^{-1}	0.762
F(000)	1152.0
Crystal size/mm^3	0.27 × 0.148 × 0.088
Radiation	Mo Kα (λ = 0.71073)
2Θ range for data collection/°	6.478 to 57.398
Index ranges	-15 ≤ h ≤ 15, -17 ≤ k ≤ 17, -20 ≤ l ≤ 20
Reflections collected	56571
Independent reflections	11387 [R_{int} = 0.0634, R_{sigma} = 0.0609]
Data/restraints/parameters	11387/0/667
Goodness-of-fit on F^2	1.032
Final R indexes [I>=2σ (I)]	R_1 = 0.0492, wR_2 = 0.0952
Final R indexes [all data]	R_1 = 0.0825, wR_2 = 0.1092
Largest diff. peak/hole / e Å^{-3}	0.51/-0.44

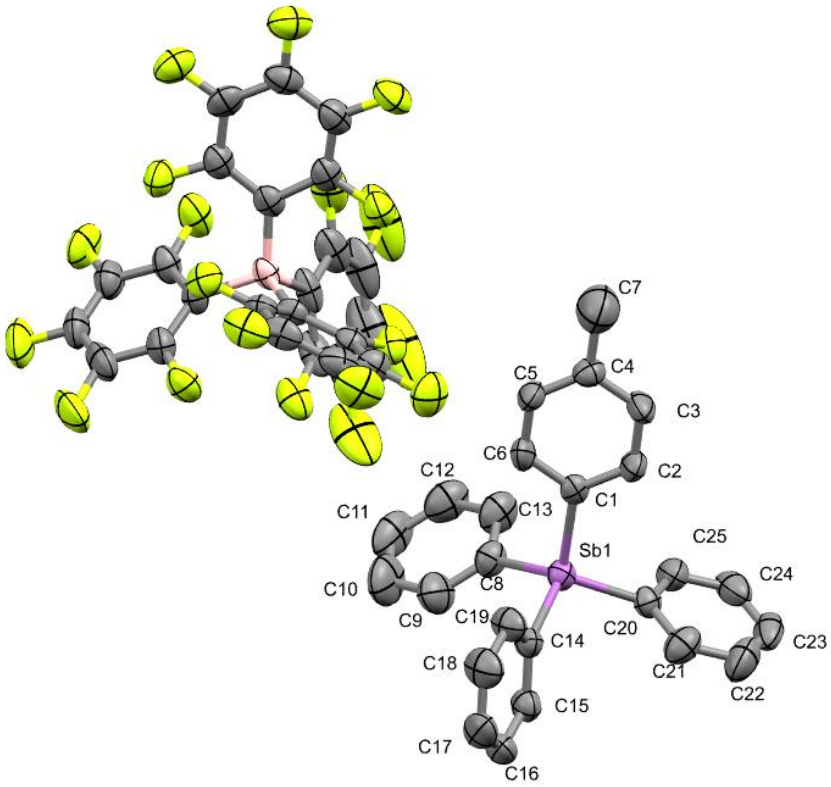

Figure 8.14. Solid state structure of $[Ph_3(p\text{-Tolyl})Sb][B(C_6F_5)_4]$. Ellipsoids shown at 50% probability. Hydrogen atoms and labels for borate counteranion have been omitted.Selected structural parameters (bond lengths in angstroms and bond angles in degrees): Sb1-C1 2.083(8), Sb1-C14 2.086(8), Sb1-C20 2.076(8), Sb1-C8 2.101(8), C1-Sb1-C14 111.2(3), C1-Sb1-C8 105.5(3), C14-Sb1-C8 107.5(3), C20-Sb1-C1 107.2(3), C20-Sb1-C14 109.7(3), C20-Sb1-C8 115.7(3).

Table 8.14. Crystal data and structure refinement for[[Ph_3(p-Tolyl)Sb][$B(C_6F_5)_4$.

Empirical formula	$C_{49}H_{22}BF_{20}Sb$
Formula weight	1123.22
Temperature/K	150.01(10)
Crystal system	triclinic
Space group	P-1
a/Å	11.1670(9)
b/Å	13.1448(10)
c/Å	15.0683(11)
α/°	84.179(6)
β/°	81.208(6)
γ/°	89.023(6)
Volume/Å^3	2174.6(3)
Z	2
ρ_{calc}g/cm^3	1.715
μ/mm^{-1}	0.757
F(000)	1104.0
Crystal size/mm^3	0.289 × 0.276 × 0.182
Radiation	Mo Kα (λ = 0.71073)
2Θ range for data collection/°	6.554 to 52.042
Index ranges	-13 ≤ h ≤ 13, -16 ≤ k ≤ 16, -18 ≤ l ≤ 18
Reflections collected	37165
Independent reflections	8560 [R_{int} = 0.0789, R_{sigma} = 0.0768]
Data/restraints/parameters	8560/0/641
Goodness-of-fit on F^2	1.175
Final R indexes [I>=2σ (I)]	R_1 = 0.0938, wR_2 = 0.1657
Final R indexes [all data]	R_1 = 0.1176, wR_2 = 0.1755
Largest diff. peak/hole / e Å^{-3}	0.84/-1.04

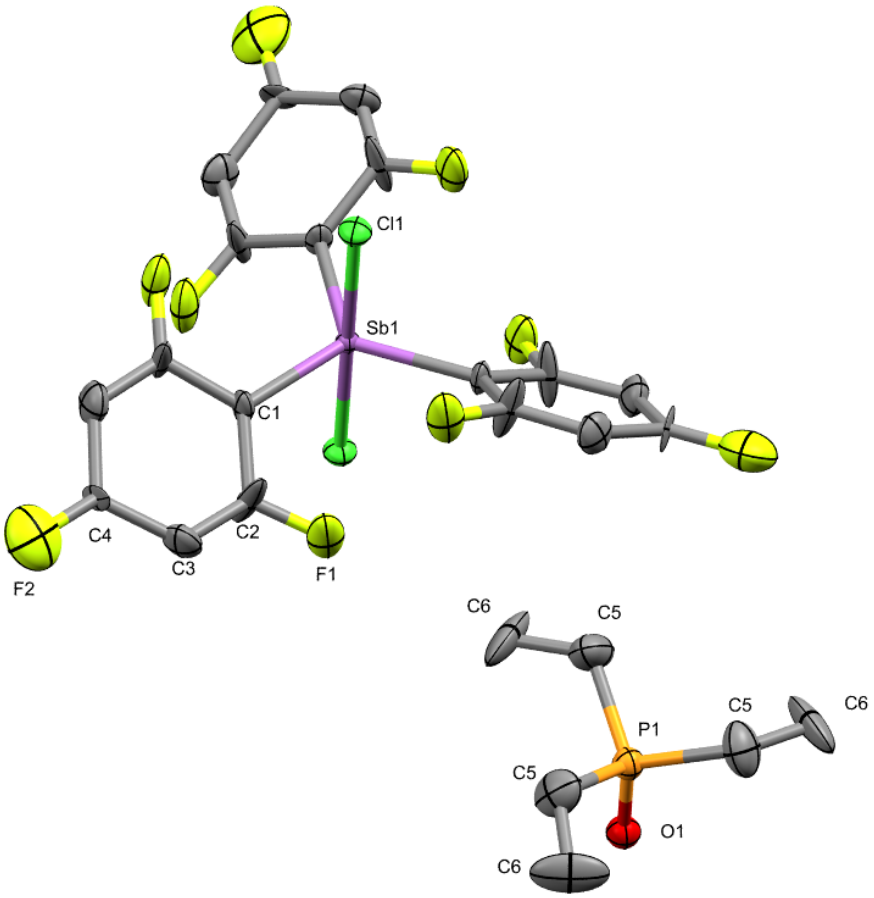

Figure 8.15. Solid state structure of **1-18/Et$_3$PO.** Ellipsoids shown at 50% probability. Hydrogen atoms and symetry eqiuvalent labels have been omitted. The structure is racemically twinned (TWIN LAW (-1.0, 0.0, 0.0, 0.0, -1.0, 0.0, 0.0, 0.0, -1.0), BASF [0.480(12)]). Selected structural parameters (bond lengths in angstroms and bond angles in degrees): Sb1-Cl1 2.404(3), Sb1-C1 2.085(12), P1-O1 1.496(9), Cl1-Sb1-Cl1^1 180.0, C1-Sb1-Cl1 90.0, C1^2-Sb1-Cl1 90.000(1), C1-Sb1-C1^3 120.000(2), C1-Sb1-C1^2 120.0.

Table 8.15. Crystal data and structure refinement for**1-18/Et$_3$PO.**

Empirical formula	$C_{15}H_{18}ClF_{4.5}OPSb_{0.5}$
Formula weight	427.09
Temperature/K	150.01(10)
Crystal system	trigonal
Space group	P321
a/Å	11.3249(3)
b/Å	11.3249(3)
c/Å	7.9259(2)
α/°	90
β/°	90
γ/°	120
Volume/Å^3	880.33(5)
Z	2
ρ_{calc}g/cm^3	1.611
μ/mm^{-1}	1.101
F(000)	428.0
Crystal size/mm^3	0.171 × 0.07 × 0.054
Radiation	Mo Kα (λ = 0.71073)
2Θ range for data collection/°	6.61 to 58.706
Index ranges	-15 ≤ h ≤ 15, -15 ≤ k ≤ 15, -10 ≤ l ≤ 10
Reflections collected	13627
Independent reflections	1507 [R_{int} = 0.0542, R_{sigma} = 0.0363]
Data/restraints/parameters	1507/24/74
Goodness-of-fit on F^2	1.147
Final R indexes [I>=2σ (I)]	R_1 = 0.0548, wR_2 = 0.1463
Final R indexes [all data]	R_1 = 0.0609, wR_2 = 0.1510
Largest diff. peak/hole / e Å^{-3}	1.72/-1.23
Flack parameter	0.39(9)

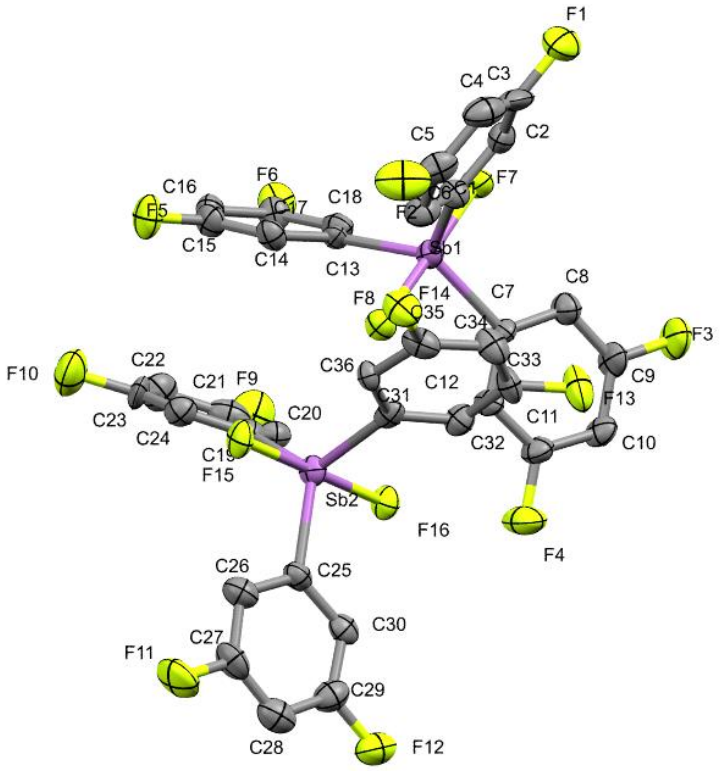

Figure 8.16. Solid state structure of **1-22.** Ellipsoids shown at 50% probability. Hydrogen atoms and labels for borate counteranion have been omitted.Selected structural parameters (bond lengths in angstroms and bond angles in degrees):Sb1-F8 1.974(4), Sb1-F7 1.979(4), Sb1-C13 2.093(8), Sb1-C1 2.087(8), Sb1-C7 2.105(7), Sb2-F16 1.966(4), Sb2-F15 1.974(4), Sb2-C31 2.100(8), Sb2-C25 2.106(7), Sb2-C19 2.103(8), F8-Sb1-F7 178.51(18) F8-Sb1-C13 89.3(2), F8-Sb1-C1 90.6(3), F8-Sb1-C7 90.6(2), F7-Sb1-C13 89.2(2), F7-Sb1-C1 90.4(3), F7-Sb1-C7 89.8(2), C13-Sb1-C7 121.2(3), C1-Sb1-C13 120.6(3), C1-Sb1-C7 118.2(3), F16-Sb2-F15 179.71(18), F16-Sb2-C31 91.1(2), F16-Sb2-C25 90.1(3), F16-Sb2-C19 90.3(3), F15-Sb2-C31 89.2(2), F15-Sb2-C25 90.0(3), F15-Sb2-C19 89.4(3), C31-Sb2-C25 114.5(3), C31-Sb2-C19 127.8(3), C19-Sb2-C25 117.6(3).

Table 8.16. Crystal data and structure refinement for**1-22.**

Empirical formula	$C_{18}H_9F_8Sb$
Formula weight	499.00
Temperature/K	150.01(10)
Crystal system	triclinic
Space group	P-1
a/Å	10.1157(7)
b/Å	11.7901(8)
c/Å	15.0686(10)
α/°	81.475(6)
β/°	73.071(6)
γ/°	85.529(6)
Volume/Å^3	1699.1(2)
Z	4
ρ_{calc}g/cm^3	1.951
μ/mm^{-1}	1.705
F(000)	960.0
Crystal size/mm^3	0.186 × 0.047 × 0.04
Radiation	Mo Kα (λ = 0.71073)
2Θ range for data collection/°	6.522 to 61.626
Index ranges	-13 ≤ h ≤ 14, -16 ≤ k ≤ 16, -21 ≤ l ≤ 20
Reflections collected	44978
Independent reflections	9801 [R_{int} = 0.1747, R_{sigma} = 0.2058]
Data/restraints/parameters	9801/0/487
Goodness-of-fit on F^2	0.998
Final R indexes [I>=2σ (I)]	R_1 = 0.0703, wR_2 = 0.1069
Final R indexes [all data]	R_1 = 0.1948, wR_2 = 0.1502
Largest diff. peak/hole / e Å^{-3}	1.28/-1.72

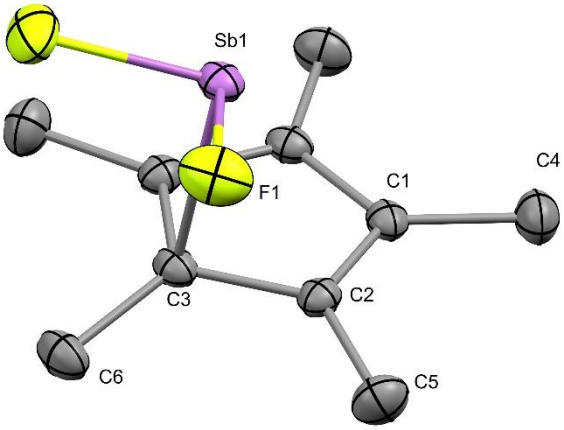

Figure 8.17. Solid state structure of **2-3**. Ellipsoids shown at 50% probability. Hydrogen atoms have been omitted. Selected structural parameters (bond lengths in angstroms and bond angles in degrees): Sb1-F1^{1} 1.9379(14) Sb1-F1 1.9379(14), Sb1-C21 2.6015(19), Sb1-C2 2.6015(19), Sb1-C3 2.254(3), C11-Sb1-F1 87.58(9), F1^{1}-Sb1-C2^{1} 128.55(6), F1-Sb1-C2^{1} 90.28(6), F1-Sb1-C2 128.55(6), F11-Sb1-C2 90.28(6), F1-Sb1-C3 95.12(6), F1^{1}-Sb1-C3 95.12(6), C2^{1}-Sb1-C2 53.07(8), C3-Sb1-C2^{1} 33.94(6), C3-Sb1-C2 33.94(6). 1+X,1/2-Y,+Z.

Table 8.17. Crystal data and structure refinement for **2-3**.

CCDC deposition number	1967957
Empirical formula	$C_{10}H_{15}F_2Sb$
Formula weight	294.97
Temperature/K	150.00(10)
Crystal system	orthorhombic
Space group	Pnma
a/Å	10.2120(2)
b/Å	13.0608(4)
c/Å	8.1901(2)
α/°	90
β/°	90
γ/°	90
Volume/Å^3	1092.37(5)
Z	4
ρ_{calc}g/cm^3	1.794
μ/mm^{-1}	2.507
F(000)	576.0
Crystal size/mm^3	0.238 × 0.138 × 0.088
Radiation	MoKα (λ = 0.71073)
2Θ range for data collection/°	7.1 to 61.53
Index ranges	-14 ≤ h ≤ 13, -18 ≤ k ≤ 16, -11 ≤ l ≤ 11
Reflections collected	7856
Independent reflections	1620 [R_{int} = 0.0326, R_{sigma} = 0.0283]
Data/restraints/parameters	1620/0/67
Goodness-of-fit on F^2	1.044
Final R indexes [I>=2σ (I)]	R_1 = 0.0222, wR_2 = 0.0403
Final R indexes [all data]	R_1 = 0.0321, wR_2 = 0.0428
Largest diff. peak/hole / e Å^{-3}	0.51/-0.48

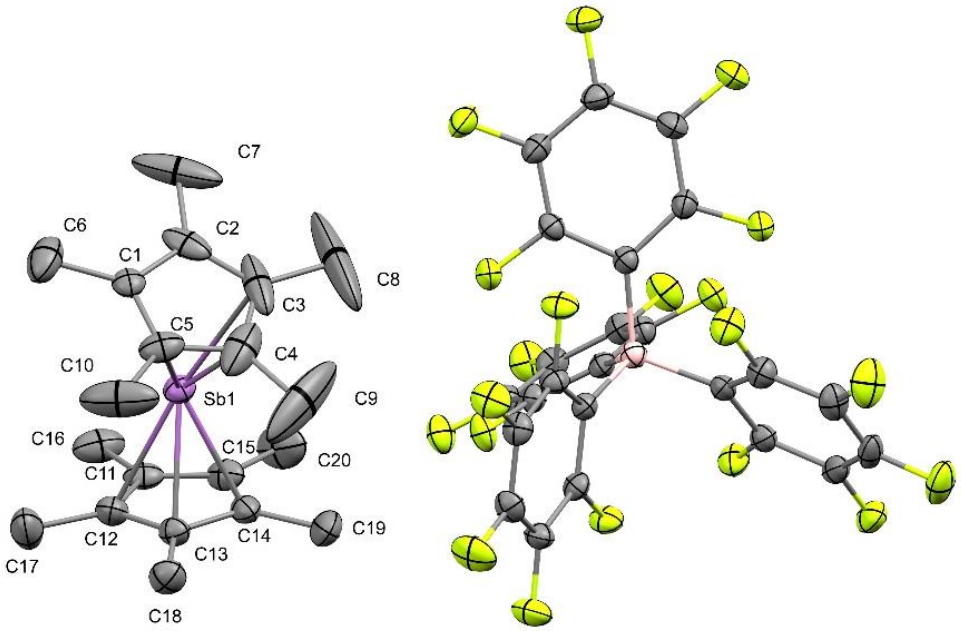

Figure 8.18. Solid state structure of **2-4**. Ellipsoids shown at 50% probability. Hydrogen atoms have been omitted. Selected structural parameters (bond lengths in angstroms and bond angles in degrees): Sb1-C1 2.674(3), Sb1-C14 2.487(3), Sb1-C13 2.458(3), Sb1-C12 2.601(3), Sb1-C15 2.635(3), Sb1-C5 2.522(3), Sb1-C4 2.454(3), Sb1-C3 2.573(3),C14-Sb1-C1 157.42(9),C14-Sb1-C12 53.93(9),C14-Sb1-C15 32.32(9),C14-Sb1-C5 126.20(10),C14-Sb1-C3 119.68(12),C13-Sb1-C1 135.11(9),C13-Sb1-C14 33.61(9),C13-Sb1-C12 32.71(9),C13-Sb1-C15 53.74(9),C13-Sb1-C5 109.51(10),C13-Sb1-C3 137.88(15),C12-Sb1-C1 131.21(9),C12-Sb1-C15 51.92(9),C15-Sb1-C1 169.91(9),C5-Sb1-C1 31.31(9),C5-Sb1-C12 123.03(10),C5-Sb1-C15 158.49(10),C5-Sb1-C3 53.09(12),C4-Sb1-C1 52.54(11),C4-Sb1-C14 107.63(12),C4-Sb1-C13 109.87(13)C4-Sb1-C12 138.57(14),C4-Sb1-C15 133.52(11),C4-Sb1-C5 32.54(12),C4-Sb1-C3 32.94(15),C3-Sb1-C1 51.31(10),C3-Sb1-C12 170.45(15),C3-Sb1-C15 127.65(10).

Table 8.18. Crystal data and structure refinement for **2-4**.

CCDC deposition number	1967954
Empirical formula	$C_{44}H_{30}BF_{20}Sb$
Formula weight	1071.24
Temperature/K	150.00(10)
Crystal system	triclinic
Space group	P-1
a/Å	12.4426(4)
b/Å	12.7883(4)
c/Å	15.2203(5)
α/°	108.476(3)
β/°	104.868(3)
γ/°	103.354(3)
Volume/Å3	2087.32(13)
Z	2
ρcalcg/cm3	1.704
μ/mm-1	0.784
F(000)	1060.0
Crystal size/mm3	0.267 × 0.141 × 0.125
Radiation	MoKα (λ = 0.71073)
2Θ range for data collection/°	6.552 to 61.594
Index ranges	-17 ≤ h ≤ 16, -18 ≤ k ≤ 18, -21 ≤ l ≤ 21
Reflections collected	43455
Independent reflections	11878 [Rint = 0.0554, Rsigma = 0.0633]
Data/restraints/parameters	11878/0/605
Goodness-of-fit on F2	1.039
Final R indexes [I>=2σ (I)]	R1 = 0.0452, wR2 = 0.0853
Final R indexes [all data]	R1 = 0.0714, wR2 = 0.0978
Largest diff. peak/hole / e Å-3	0.57/-0.57

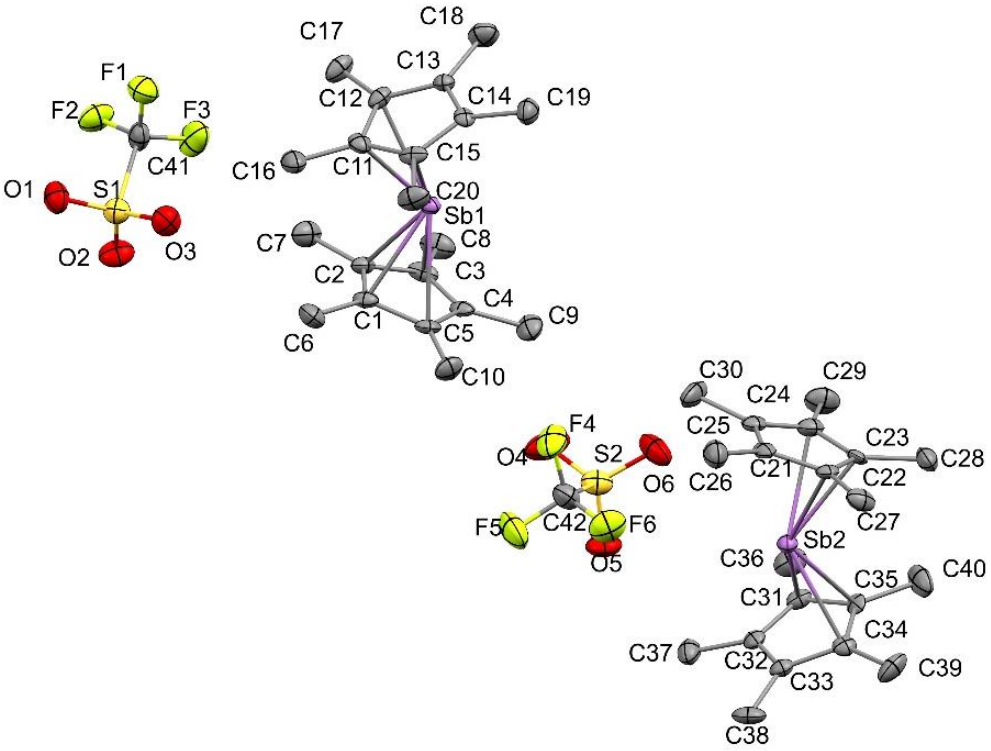

Figure 8.19. Solid state structure of **2-5**. Ellipsoids shown at 50% probability. Hydrogen atoms have been omitted. Selected (bond lengths in angstroms and bond angles in degrees): Sb1-C15 2.521(8), Sb1-C2 2.520(8), Sb1-C11 2.437(11), Sb1-C1 2.458(10), Sb1-C5 2.597(7), Sb1-C12 2.535(8), Sb2-C35 2.449(10), Sb2-C22 2.557(8), Sb2-C31 2.546(7), Sb2-C34 2.513(8), Sb2-C23 2.442(10), Sb2-C24 2.518(8), C15-Sb1-C5 121.2(3), C15-Sb1-C12 54.4(3), C2-Sb1-C15 136.0(3), C2-Sb1-C5 53.9(3), C2-Sb1-C12 109.1(3), C11-Sb1-C15 33.8(3), C11-Sb1-C2 107.9(3), C11-Sb1-C1 101.4(5), C11-Sb1-C5 126.2(4), C11-Sb1-C12 33.6(3), C1-Sb1-C15 114.7(4), C1-Sb1-C2 33.1(3), C1-Sb1-C5 33.1(3), C1-Sb1-C12 121.6(4), C12-Sb1-C5 154.0(3), C35-Sb2-C22 124.1(3), C35-Sb2-C31 33.0(3), C35-Sb2-C34 33.4(3), C35-Sb2-C24 110.2(3), C31-Sb2-C22 152.6(3), C34-Sb2-C22 118.3(3), C34-Sb2-C31 53.9(3), C34-Sb2-C24 137.5(3), C23-Sb2-C35 101.2(5), C23-Sb2-C22 32.8(3), C23-Sb2-C31 121.3(3), C23-Sb2-C34 113.7(3), C23-Sb2-C24 33.8(3), C24-Sb2-C22 54.0(3),C24-Sb2-C31 111.1(3).A TWIN and BASF correction was applied (-1.0, 0.0, 0.0, 0.0, 1.0, 0.0, 0.0, 0.0, -1.0), BASF [0.50(4)]

Table 8.19. Crystal data and structure refinement for **2-5**.

CCDC deposition number	**1967955**
Empirical formula	$C_{21}H_{30}F_3O_3SSb$
Formula weight	541.26
Temperature/K	150.01(10)
Crystal system	orthorhombic
Space group	$Pca2_1$
a/Å	17.1165(3)
b/Å	15.8699(3)
c/Å	16.6561(3)
α/°	90
β/°	90
γ/°	90
Volume/Å^3	4524.42(14)
Z	8
ρ_{calc}g/cm^3	1.589
μ/mm^{-1}	1.355
F(000)	2192.0
Crystal size/mm^3	0.223 × 0.214 × 0.148
Radiation	MoKα (λ = 0.71073)
2Θ range for data collection/°	6.826 to 61.852
Index ranges	-23 ≤ h ≤ 23, -22 ≤ k ≤ 21, -23 ≤ l ≤ 23
Reflections collected	45019
Independent reflections	12853 [R_{int} = 0.0591, R_{sigma} = 0.0765]
Data/restraints/parameters	12853/1/544
Goodness-of-fit on F^2	1.018
Final R indexes [I>=2σ (I)]	R_1 = 0.0490, wR_2 = 0.0674
Final R indexes [all data]	R_1 = 0.0869, wR_2 = 0.0807
Largest diff. peak/hole / e Å^{-3}	0.72/-0.50
Flack parameter	0.02(3)

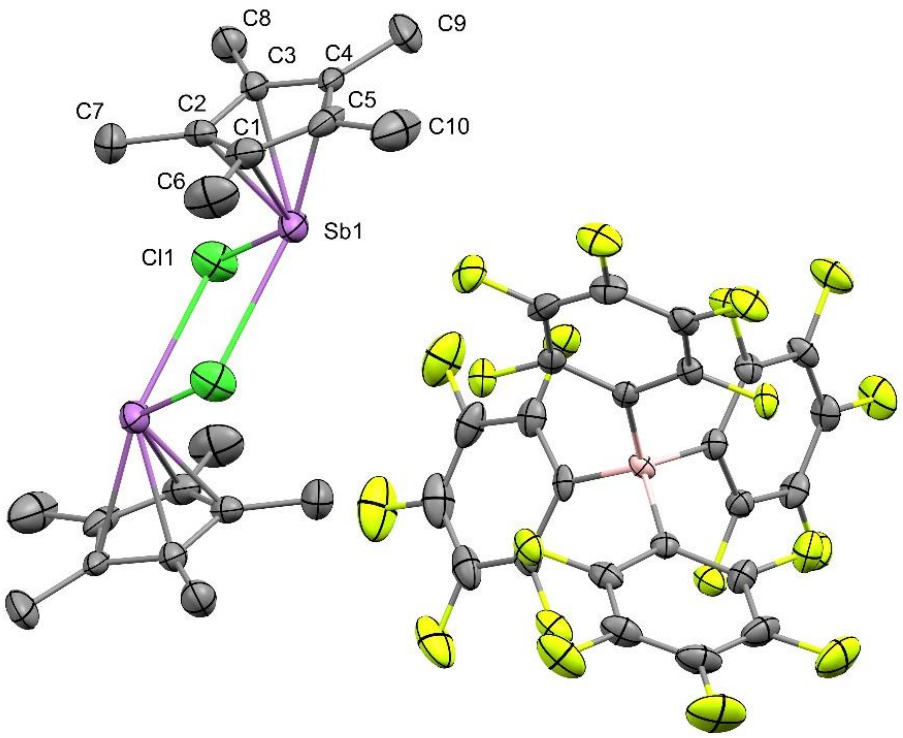

Figure 8.20. Solid state structure of **2-6** . Ellipsoids shown at 50% probability. Hydrogen atoms have been omitted. Selected structural parameters (bond lengths in angstroms and bond angles in degrees): Sb1-Cl1 2.5535(14), Sb1-C3 2.367(4), Sb1-C2 2.294(4), Sb1-C4 2.560(5), Sb1-C5 2.606(5),Sb1-C1 2.476(5), Cl1-Sb1-C4 123.62(11), Cl1-Sb1-C5 149.32(11), C3-Sb1-Cl1 94.75(12), C3-Sb1-C4 33.50(14), C3-Sb1-C5 55.05(15), C3-Sb1-C1 57.30(16), C2-Sb1-Cl1 97.02(13), C2-Sb1-C3 35.97(15), C2-Sb1-C4 56.68(16), C2-Sb1-C5 56.11(16), C2-Sb1-C1 35.06(16), C4-Sb1-C5 31.52(15), C1-Sb1-Cl1 129.56(13), C1-Sb1-C4 54.27(16), C1-Sb1-C5 32.46(16), Sb1-Cl1-Sb1[1] 102.53(4). 1. -x,-y,-z.

Table 8.20. Crystal data and structure refinement for **2-6**.

CCDC deposition number	1967956
Empirical formula	$C_{34}H_{15}BClF_{20}Sb$
Formula weight	971.47
Temperature/K	150.00(10)
Crystal system	triclinic
Space group	P-1
a/Å	10.5921(7)
b/Å	12.6396(8)
c/Å	12.8627(8)
α/°	90.679(5)
β/°	96.606(5)
γ/°	104.469(5)
Volume/Å^3	1654.89(19)
Z	2
ρ_{calc}g/cm^3	1.950
μ/mm^{-1}	1.056
F(000)	944.0
Crystal size/mm^3	0.354 × 0.203 × 0.161
Radiation	MoKα (λ = 0.71073)
2Θ range for data collection/°	6.664 to 59.148
Index ranges	-13 ≤ h ≤ 14, -17 ≤ k ≤ 17, -17 ≤ l ≤ 17
Reflections collected	17501
Independent reflections	8897 [R_{int} = 0.0655, R_{sigma} = 0.1266]
Data/restraints/parameters	8897/0/519
Goodness-of-fit on F^2	1.011
Final R indexes [I>=2σ (I)]	R_1 = 0.0683, wR_2 = 0.0966
Final R indexes [all data]	R_1 = 0.1196, wR_2 = 0.1178
Largest diff. peak/hole / e Å^{-3}	1.03/-0.70

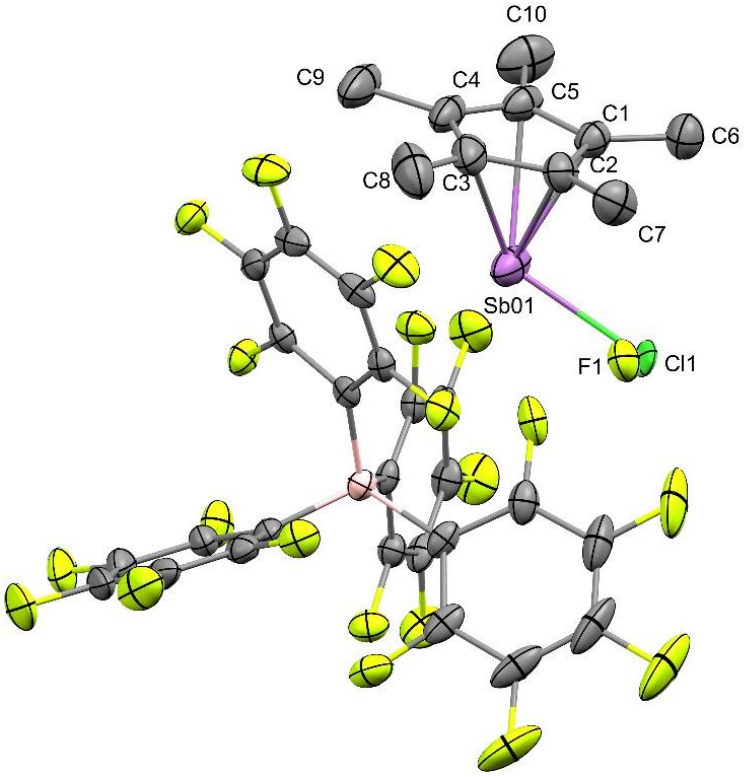

Figure 8.21. Solid state structure of **2-6**/[Cp*SbF][$B(C_6F_5)_4$]. Ellipsoids shown at 50% probability. Hydrogen atoms have been omitted. Selected structural parameters (bond lengths in angstroms and bond angles in degrees): Sb01-C1 2.384(5), Sb01-C2 2.292(5), Sb01-C5 2.574(5), Sb01-C3 2.463(6), Sb01-C4 2.608(5), Sb01-Cl1 2.548(8), Sb01-$Cl1^1$ 2.816(10), Sb01-F1 2.312(13), C1-Sb01-$Cl1^1$ 134.3(3), Cl1-Sb01-$Cl1^1$ 81.6(2), F1-Sb01-$Cl1^1$ 75.3(4).

Table 8.21. Crystal data and structure refinement for **2-6/[Cp*SbF][B(C_6F_5)$_4$].**

CCDC deposition number	1967958
Empirical formula	$C_{34}H_{15}BCl_{0.4}F_{20.6}Sb$
Formula weight	961.60
Temperature/K	150.01(10)
Crystal system	triclinic
Space group	P-1
a/Å	10.6582(3)
b/Å	12.6174(4)
c/Å	12.8229(3)
α/°	90.784(2)
β/°	95.717(2)
γ/°	105.278(3)
Volume/Å^3	1653.76(8)
Z	2
ρ_{calc}g/cm^3	1.931
μ/mm^{-1}	1.011
F(000)	934.0
Crystal size/mm^3	0.162 × 0.161 × 0.099
Radiation	MoKα (λ = 0.71073)
2Θ range for data collection/°	6.392 to 61.646
Index ranges	-14 ≤ h ≤ 15, -18 ≤ k ≤ 18, -18 ≤ l ≤ 18
Reflections collected	42866
Independent reflections	9520 [R_{int} = 0.0705, R_{sigma} = 0.0870]
Data/restraints/parameters	9520/0/528
Goodness-of-fit on F^2	1.158
Final R indexes [I>=2σ (I)]	R_1 = 0.0813, wR_2 = 0.1308
Final R indexes [all data]	R_1 = 0.1352, wR_2 = 0.1464
Largest diff. peak/hole / e Å^{-3}	0.95/-1.15

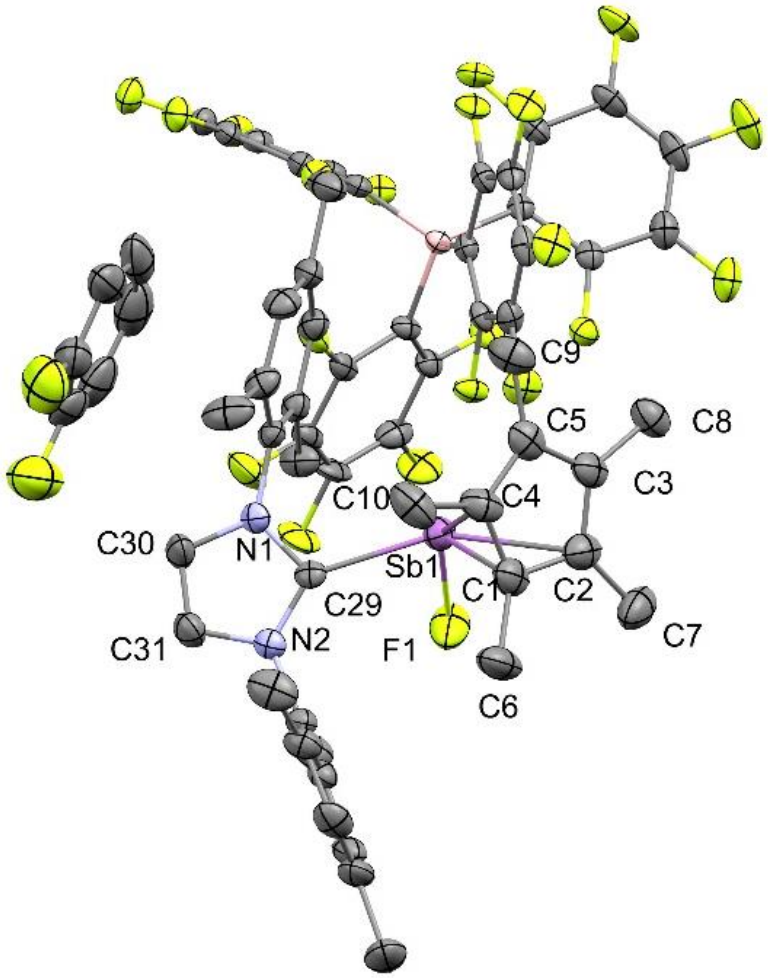

Figure 8.22. Solid state structure of **2-7**. Ellipsoids shown at 50% probability. Hydrogen atoms and labels on the counteranion, disordered solvent and mesityl groups have been omitted. Selected structural parameters (bond lengths in angstroms and bond angles in degrees): Sb1-F1 1.942(5), Sb1-C29 2.294(6), Sb1-C1 2.234(7), Sb1-C2 2.607(8), Sb1-C5 2.560(7), F1-Sb1-C29 87.0(2), F1-Sb1-C1 99.3(3), F1-Sb1-C2 93.5(2), F1-Sb1-C5 133.4(3), C29-Sb1-C2 139.2(3), C29-Sb1-C5 98.8(3), C1-Sb1-C29 105.8(3), C1-Sb1-C2 33.9(3), C1-Sb1-C5 34.6(3), C5-Sb1-C2 53.2(3).

Table 8.22. Crystal data and structure refinement for **2-7.**

CCDC deposition number	1967959
Empirical formula	$C_{58}H_{41}BF_{22.11}N_2Sb$
Formula weight	1318.58
Temperature/K	150.01(10)
Crystal system	monoclinic
Space group	$P2_1/c$
a/Å	18.2924(2)
b/Å	17.8036(2)
c/Å	17.4223(2)
α/°	90
β/°	113.5290(10)
γ/°	90
Volume/Å^3	5202.19(11)
Z	4
ρ_{calc}g/cm^3	1.684
μ/mm^{-1}	5.316
F(000)	2632.0
Crystal size/mm^3	0.248 × 0.147 × 0.101
Radiation	CuKα (λ = 1.54184)
2Θ range for data collection/°	7.242 to 143.982
Index ranges	$-22 \le h \le 21$, $-16 \le k \le 21$, $-21 \le l \le 21$
Reflections collected	38975
Independent reflections	10089 [R_{int} = 0.0326, R_{sigma} = 0.0314]
Data/restraints/parameters	10089/144/805
Goodness-of-fit on F2	1.096
Final R indexes [I>=2σ (I)]	R_1 = 0.0821, wR_2 = 0.2419
Final R indexes [all data]	R_1 = 0.0881, wR_2 = 0.2455
Largest diff. peak/hole / e Å-3	1.24/-2.60

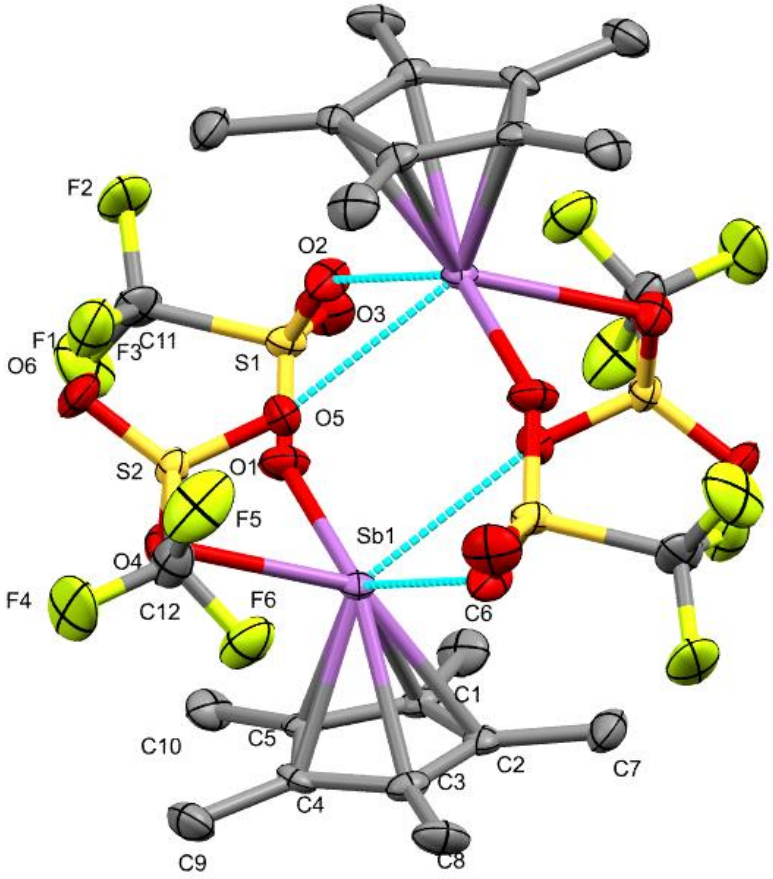

Figure 8.23. Solid state structure of **2-8**. Ellipsoids shown at 50% probability. Hydrogen atoms and labels on symmetry equivalent atoms have been omitted. Selected structural parameter (bond lengths in angstroms and bond angles in degrees): Sb1-O1 2.405(3), Sb1-O4 2.527(3), Sb1-C1 2.371(4), Sb1-C3 2.490(4), Sb1-C2 2.461(4), Sb1-C5 2.349(4), Sb1-C4 2.427(3) O1-Sb1-O4 79.14(10), O1-Sb1-C3 139.51(11), O1-Sb1-C2 119.52(12), O1-Sb1-C4 114.09(12), C1-Sb1-O1 86.84(12), C1-Sb1-O4 131.95(12), C1-Sb1-C3 56.70(13), C1-Sb1-C2 34.29(13), C1-Sb1-C4 57.86(13), C3-Sb1-O4 110.89(11), C2-Sb1-O4 142.16(11), C2-Sb1-C3 33.17(12), C5-Sb1-O1 82.97(12), C5-Sb1-O4 96.64(11), C5-Sb1-C1 35.69(13), C5-Sb1-C3 57.41(13), C5-Sb1-C2 57.68(13), C5-Sb1-C4 35.23(13), C4-Sb1-O4 86.62(11), C4-Sb1-C3 33.64(12), C4-Sb1-C2 56.12(13).

Table 8.23. Crystal data and structure refinement for **2-8.**

Identification code	**2-8**
Empirical formula	$C_{12}H_{15}F_6O_6S_2Sb$
Formula weight	555.11
Temperature/K	150.01(10)
Crystal system	monoclinic
Space group	$P2_1/n$
a/Å	11.1720(4)
b/Å	12.6147(4)
c/Å	13.0442(6)
α/°	90
β/°	91.620(4)
γ/°	90
Volume/Å^3	1837.60(12)
Z	4
ρ_{calc}g/cm^3	2.006
μ/mm^{-1}	1.814
F(000)	1088.0
Crystal size/mm^3	0.173 × 0.115 × 0.088
Radiation	Mo Kα (λ = 0.71073)
2Θ range for data collection/°	6.46 to 61.726
Index ranges	-15 ≤ h ≤ 14, -18 ≤ k ≤ 18, -17 ≤ l ≤ 18
Reflections collected	24868
Independent reflections	5297 [R_{int} = 0.0863, R_{sigma} = 0.0891]
Data/restraints/parameters	5297/0/249
Goodness-of-fit on F^2	1.046
Final R indexes [I>=2σ (I)]	R_1 = 0.0505, wR_2 = 0.0700
Final R indexes [all data]	R_1 = 0.0817, wR_2 = 0.0802
Largest diff. peak/hole / e Å^{-3}	0.76/-0.78

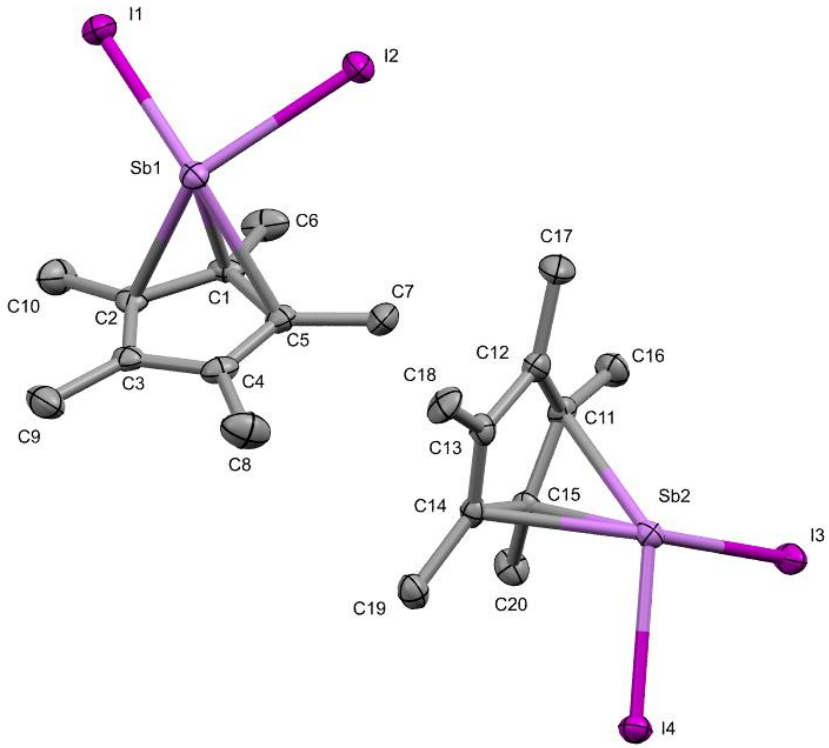

Figure 8.24. Solid state structure of Cp*SbI_2. Ellipsoids shown at 50% probability. Hydrogen atoms have been omitted. Selected structural parameter(bond lengths in angstroms and bond angles in degrees): Sb1-I2 2.8568(5), Sb1-I1 2.8667(5), Sb1-C1 2.294(5), Sb1-C2 2.589(5), Sb1-C5 2.561(5), I4-Sb2 2.8478(4), Sb2-I3 2.8608(5), Sb2-C11 2.592(4), Sb2-C15 2.269(5), Sb2-C14 2.594(4), I2-Sb1-I1 90.026(13), C1-Sb1-I2 99.62(12), C1-Sb1-I1 100.29(12), C1-Sb1-C2 33.87(16), C1-Sb1-C5 34.31(16), C2-Sb1-I2 133.07(11), C2-Sb1-I1 93.21(11), C5-Sb1-I2 92.50(11), C5-Sb1-I1 134.17(11), C5-Sb1-C2 53.82(16), I4-Sb2-I3 89.001(13), C11-Sb2-I4 133.73(11), C11-Sb2-I3 93.94(10), C11-Sb2-C14 53.62(14), C15-Sb2-I4 99.78(12), C15-Sb2-I3 100.38(12), C15-Sb2-C11 34.33(15), C15-Sb2-C14 34.32(15), C14-Sb2-I4 93.22(10), C14-Sb2-I3 134.27(11).

Table 8.24. Crystal data and structure refinement for Cp^*SbI_2.

Empirical formula	$C_{20}H_{30}I_4Sb_2$
Formula weight	1021.54
Temperature/K	150.00(10)
Crystal system	monoclinic
Space group	$P2_1/c$
a/Å	19.2370(5)
b/Å	8.48460(10)
c/Å	19.5769(5)
α/°	90
β/°	119.449(4)
γ/°	90
Volume/Å^3	2782.45(14)
Z	4
ρ_{calc}g/cm^3	2.439
μ/mm^{-1}	6.384
F(000)	1856.0
Crystal size/mm^3	0.176 × 0.118 × 0.114
Radiation	Mo Kα (λ = 0.71073)
2Θ range for data collection/°	6.404 to 61.588
Index ranges	-27 ≤ h ≤ 27, -10 ≤ k ≤ 12, -27 ≤ l ≤ 25
Reflections collected	20104
Independent reflections	7736 [R_{int} = 0.0415, R_{sigma} = 0.0572]
Data/restraints/parameters	7736/0/245
Goodness-of-fit on F^2	1.047
Final R indexes [I>=2σ (I)]	R_1 = 0.0387, wR_2 = 0.0670
Final R indexes [all data]	R_1 = 0.0549, wR_2 = 0.0726
Largest diff. peak/hole / e Å^{-3}	1.29/-1.12

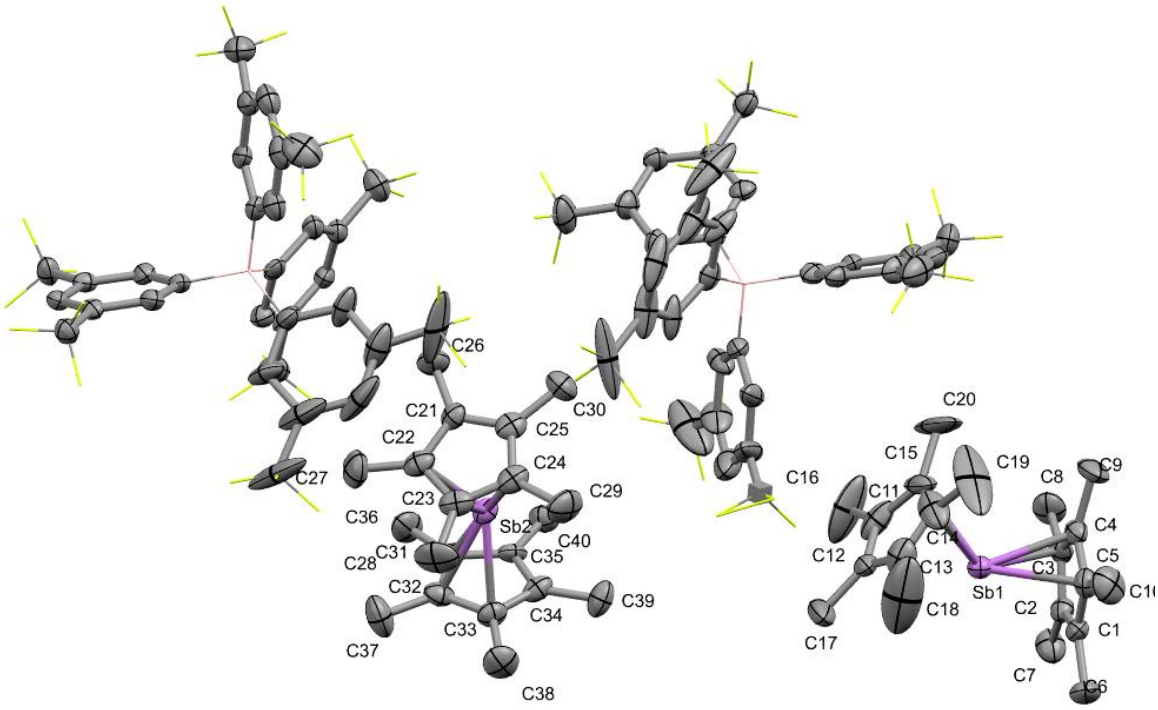

Figure 8.25. Solid state structure of [Cp*$_2$Sb][BArF]. Ellipsoids shown at 50% probability, fluorine atoms shown in wireframe. Hydrogen atoms have been omitted. Selected structural parameter (bond lengths in angstroms and bond angles in degrees): Sb1-C4 2.407(7), Sb1-C5 2.538(8),Sb1-C3 2.545(8),Sb1-C11 2.631(9),Sb1-C13 2.657(9),Sb1-C15 2.424(9),Sb1-C14 2.427(9),Sb2-C31 2.573(8),Sb2-C35 2.662(8),Sb2-C25 2.674(8),Sb2-C21 2.644(8),Sb2-C34 2.605(8),Sb2-C32 2.497(8),Sb2-C33 2.489(8),Sb2-C23 2.450(8),Sb2-C24 2.539(8),Sb2-C22 2.507(8),C4-Sb1-C5 33.6(3), C4-Sb1-C3 33.5(3), C4-Sb1-C11 134.2(3), C4-Sb1-C13 134.8(3), C4-Sb1-C15 106.6(3), C4-Sb1-C14 108.6(3), C5-Sb1-C3 54.1(3), C5-Sb1-C11 161.9(3), C5-Sb1-C13 123.7(3), C3-Sb1-C11 125.6(3), C31-Sb2-C35 31.3(2), C31-Sb2-C25 156.0(3), C31-Sb2-C21 131.6(2), C31-Sb2-C34 52.2(2), C35-Sb2-C25 142.3(2), C21-Sb2-C35 143.4(2), C21-Sb2-C25 31.0(2), C34-Sb2-C35 30.9(2), C34-Sb2-C25 139.4(3), C34-Sb2-C21 166.3(3), C32-Sb2-C31 32.7(2), C32-Sb2-C35 53.1(3), C32-Sb2-C25 164.4(3).

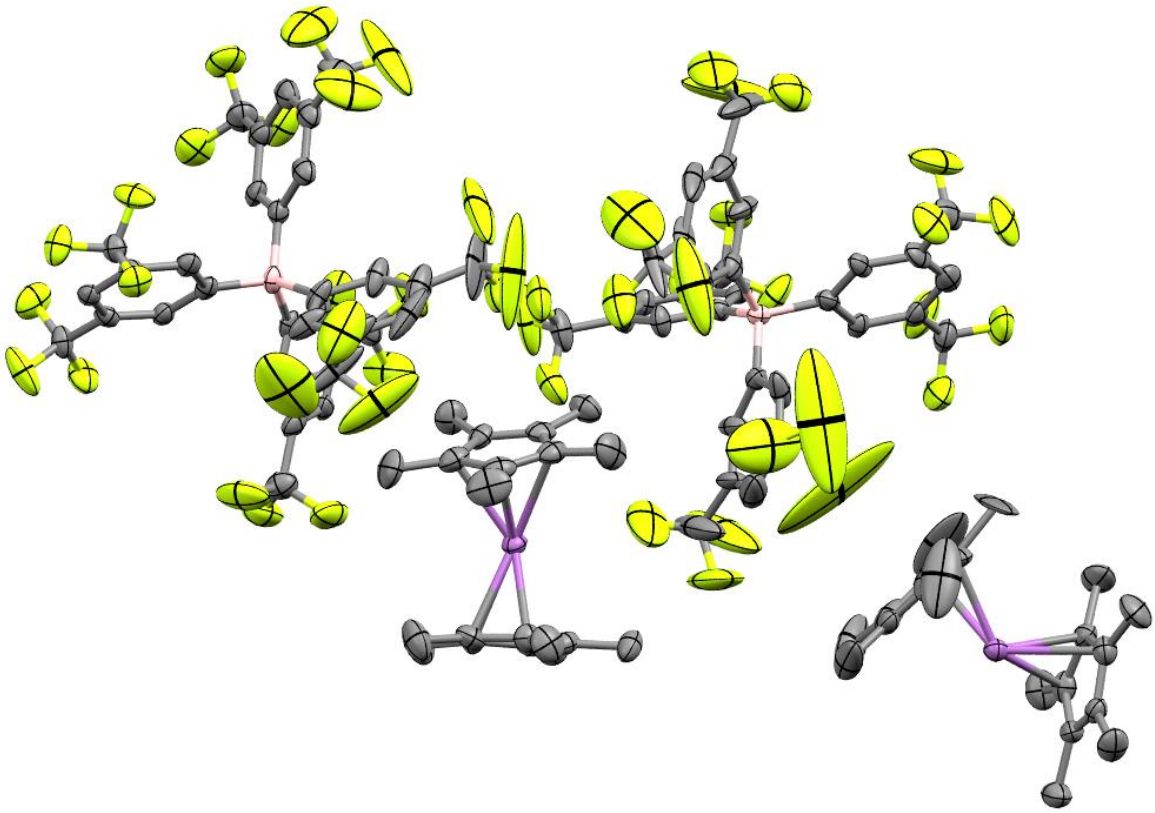

Figure 8.26. Solid state structure of [Cp*$_2$Sb][BArF]. Ellipsoids shown at 50% probability, Hydrogen atoms and labels have been omitted.

Table 8.25. Crystal data and structure refinement for [Cp*$_2$Sb][BArF].

Empirical formula	$BC_{52}F_{24}Sb$
Formula weight	1213.08
Temperature/K	150.01(10)
Crystal system	triclinic
Space group	P-1
a/Å	12.3990(5)
b/Å	21.4601(8)
c/Å	21.5097(9)
α/°	67.910(4)
β/°	89.140(3)
γ/°	88.653(3)
Volume/Å^3	5301.7(4)
Z	4
ρ_{calc}g/cm^3	1.520
μ/mm^{-1}	0.638
F(000)	2336.0
Crystal size/mm^3	0.184 × 0.139 × 0.125
Radiation	Mo Kα (λ = 0.71073)
2Θ range for data collection/°	6.53 to 61.908
Index ranges	-17 ≤ h ≤ 17, -30 ≤ k ≤ 30, -30 ≤ l ≤ 31
Reflections collected	139792
Independent reflections	30935 [R_{int} = 0.1802, R_{sigma} = 0.2405]
Data/restraints/parameters	30935/0/1405
Goodness-of-fit on F^2	1.006
Final R indexes [I>=2σ (I)]	R_1 = 0.1058, wR_2 = 0.2418
Final R indexes [all data]	R_1 = 0.2417, wR_2 = 0.3152
Largest diff. peak/hole / e Å^{-3}	1.96/-1.24

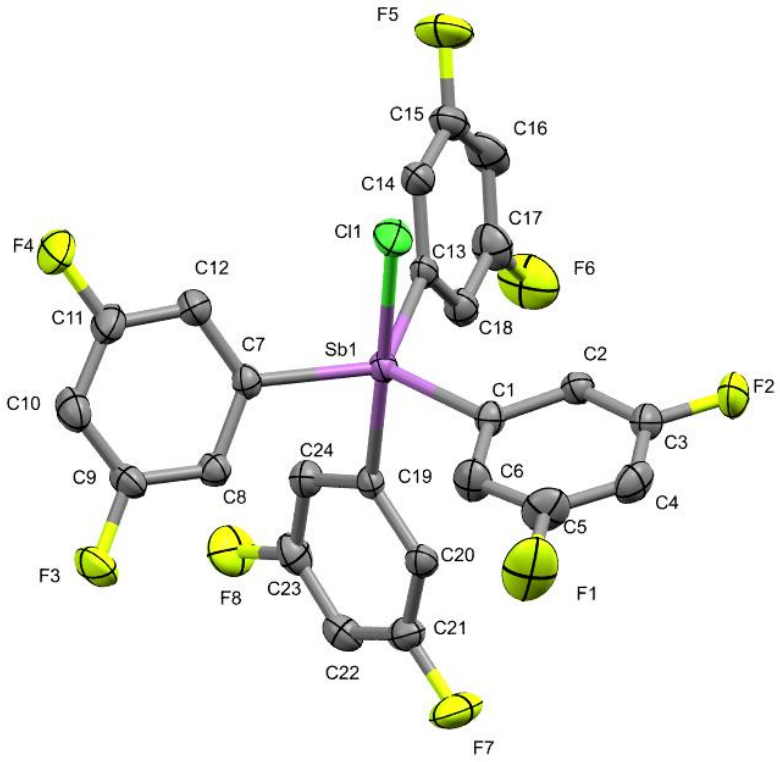

Figure 8.27. Solid state structure of **3-1**. Ellipsoids shown at 50% probability. Hydrogen atoms have been omitted. Selected structural parameters (bond lengths in angstroms and bond angles in degrees): Sb1-Cl1 2.5777(7), Sb1-C19 2.169(2), Sb1-C13 2.130(3), Sb1-C7 2.136(2), Sb1-C1 2.115(2) C19-Sb1-Cl1 175.37(7), C13-Sb1-Cl1 88.58(7), C13-Sb1-C19 96.05(10), C13-Sb1-C7 124.62(10), C7-Sb1-Cl1 84.16(7), C7-Sb1-C19 92.92(9), C1-Sb1-Cl1 80.91(7), C1-Sb1-C19 97.36(9), C1-Sb1-C13 114.88(9), C1-Sb1-C7 117.88(10).

Table 8.26. Crystal data and structure refinement for **3-1**.

Empirical formula	$C_{24}H_{12}ClF_8Sb$
Formula weight	609.54
Temperature/K	150.01(10)
Crystal system	monoclinic
Space group	$P2_1/c$
a/Å	10.1483(2)
b/Å	11.2917(2)
c/Å	19.4419(4)
α/°	90
β/°	94.001(2)
γ/°	90
Volume/Å^3	2222.45(7)
Z	4
ρ_{calc}g/cm^3	1.822
μ/mm^{-1}	1.439
F(000)	1184.0
Crystal size/mm^3	0.301 × 0.197 × 0.088
Radiation	Mo Kα (λ = 0.71073)
2Θ range for data collection/°	6.672 to 61.728
Index ranges	$-14 \le h \le 14$, $-16 \le k \le 16$, $-27 \le l \le 27$
Reflections collected	30619
Independent reflections	6476 [R_{int} = 0.0523, R_{sigma} = 0.0505]
Data/restraints/parameters	6476/0/307
Goodness-of-fit on F^2	1.039
Final R indexes [I>=2σ (I)]	R_1 = 0.0362, wR_2 = 0.0586
Final R indexes [all data]	R_1 = 0.0581, wR_2 = 0.0665
Largest diff. peak/hole / e Å^{-3}	0.54/-0.56

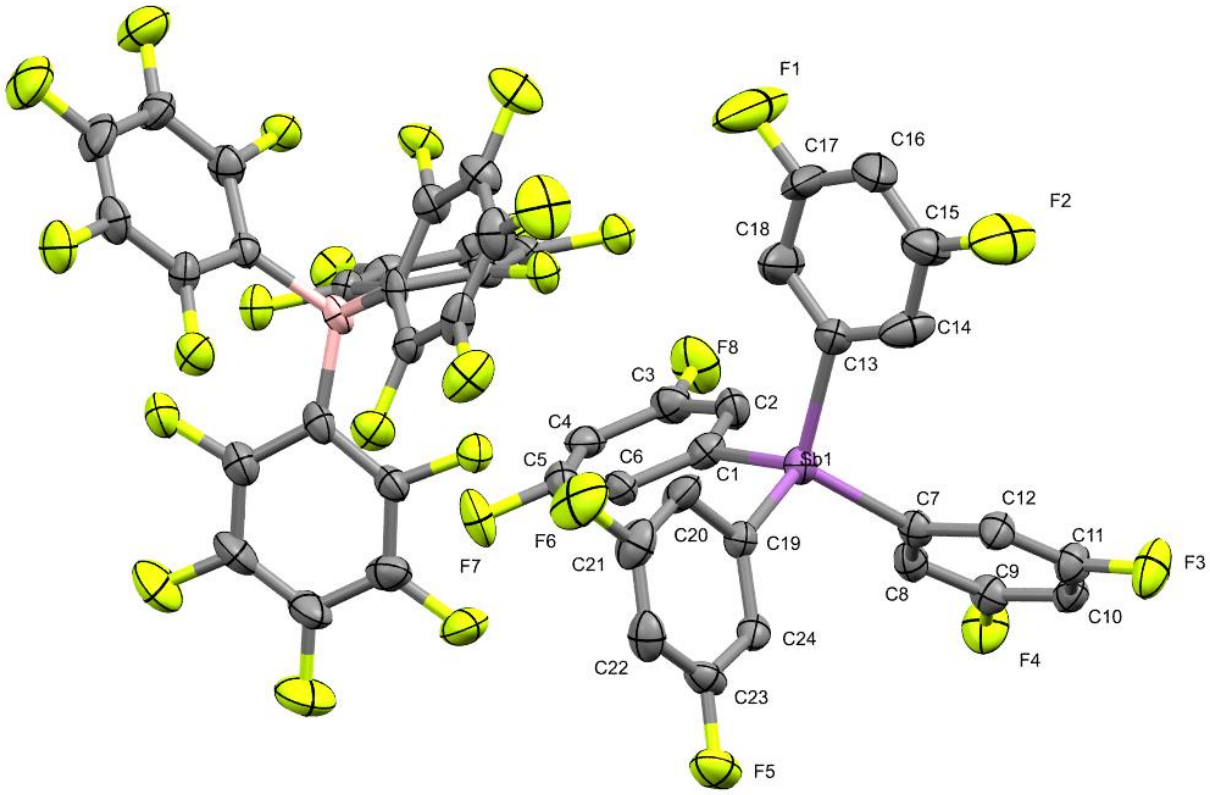

Figure 8.28. Solid state structure of **3-2**. Ellipsoids shown at 50% probability. Hydrogen atoms and labels on borate counteranion have been omitted. Selected structural parameters (bond lengths in angstroms and bond angles in degrees):Sb1-C13 2.107(6), Sb1-C19 2.086(6), Sb1-C7 2.089(5), Sb1-C1 2.089(5), C19-Sb1-C13 106.7(2), C19-Sb1-C7 113.2(2), C19-Sb1-C1 108.7(2), C7-Sb1-C13 111.0(2), C7-Sb1-C1 107.4(2), C1-Sb1-C13 109.9(2).

Table 8.27. Crystal data and structure refinement for **3-2**.

Empirical formula	$C_{48}H_{12}BF_{28}Sb$
Formula weight	1253.14
Temperature/K	150.00(10)
Crystal system	orthorhombic
Space group	Pbca
a/Å	20.2013(8)
b/Å	18.5698(6)
c/Å	23.7024(6)
α/°	90
β/°	90
γ/°	90
Volume/Å^3	8891.6(5)
Z	8
ρ_{calc}g/cm^3	1.872
μ/mm^{-1}	0.776
F(000)	4864.0
Crystal size/mm^3	0.195 × 0.134 × 0.1
Radiation	Mo Kα (λ = 0.71073)
2Θ range for data collection/°	6.662 to 61.882
Index ranges	-16 ≤ h ≤ 29, -26 ≤ k ≤ 25, -18 ≤ l ≤ 34
Reflections collected	62728
Independent reflections	12884 [R_{int} = 0.1679, R_{sigma} = 0.1927]
Data/restraints/parameters	12884/0/703
Goodness-of-fit on F^2	0.983
Final R indexes [I>=2σ (I)]	R_1 = 0.0713, wR_2 = 0.1008
Final R indexes [all data]	R_1 = 0.1987, wR_2 = 0.1404
Largest diff. peak/hole / e Å^{-3}	0.83/-0.84

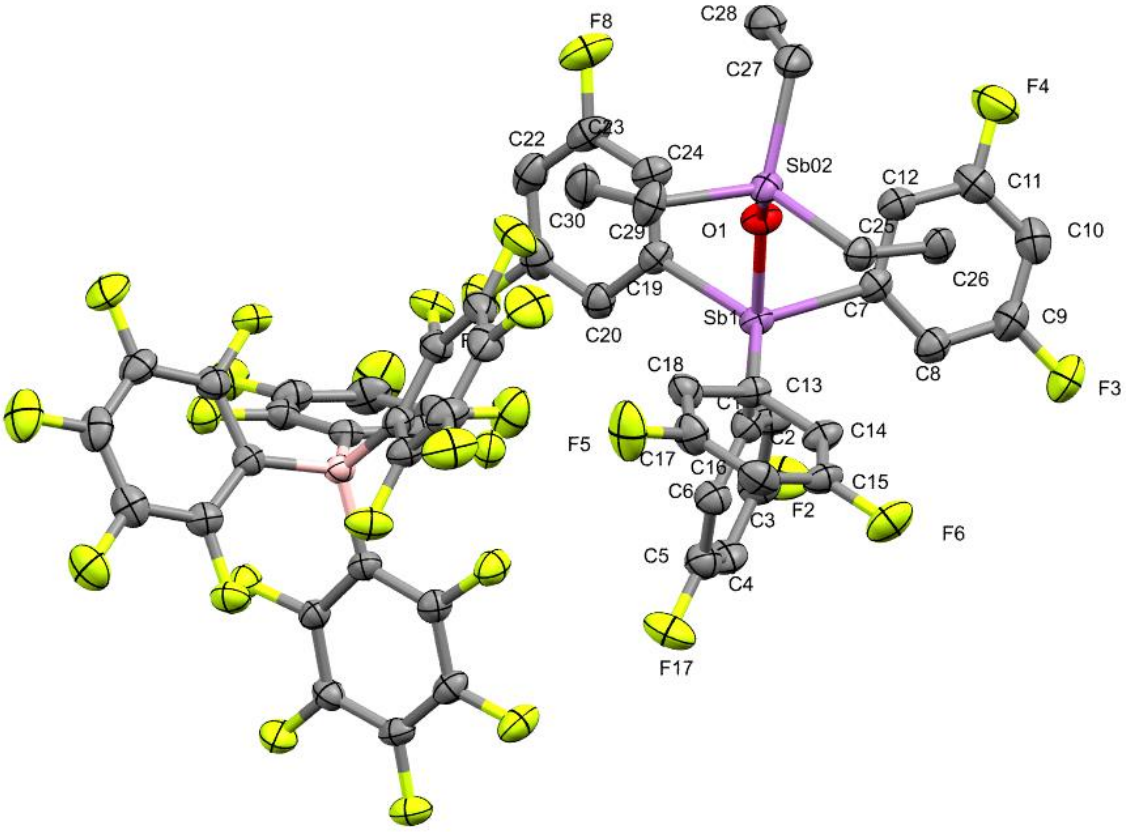

Figure 8.29. Solid state structure of $[(3,5\text{-}F_2C_6H_3)_4SbOSbEt_3][B(C_6F_5)_4]$. Ellipsoids shown at 50% probability. Hydrogen atoms and labels on borate counteranion have been omitted. Selected structural parameters (bond lengths in angstroms and bond angles in degrees): Sb1-O1 2.122(3), Sb1-C13 2.137(4), Sb1-C7 2.121(4), Sb1-C19 2.133(4), Sb1-C1 2.181(4), Sb02-O1 1.871(3), Sb02-C25 2.111(4), Sb02-C27 2.126(5), Sb02-C29 2.113(4), O1-Sb1-C13 85.70(13), O1-Sb1-C19 83.51(14), O1-Sb1-C1 178.07(14), C13-Sb1-C1 94.14(16), C7-Sb1-O1 85.36(14), C7-Sb1-C13 114.04(15), C7-Sb1-C19 118.39(16), C7-Sb1-C1 96.45(16), C19-Sb1-C13 125.14(15), C19-Sb1-C1 95.04(16), O1-Sb02-C25 107.62(15),O1-Sb02-C27 103.30(18), O1-Sb02-C29 108.60(17), C25-Sb02-C27 111.89(18), C25-Sb02-C29 115.09(19), C29-Sb02-C27 109.6(2).

Table 8.28. Crystal data and structure refinement for $[(3,5\text{-}F_2C_6H_3)_4SbOSbEt_3][B(C_6F_5)_4]$.

Empirical formula	$C_{54}H_{27}BF_{28}OSb_2$
Formula weight	1478.06
Temperature/K	150.01(10)
Crystal system	monoclinic
Space group	$P2_1/c$
a/Å	11.8913(2)
b/Å	14.4681(2)
c/Å	30.2782(5)
α/°	90
β/°	93.2960(10)
γ/°	90
Volume/Å^3	5200.58(14)
Z	4
ρ_{calc}g/cm^3	1.888
μ/mm^{-1}	9.550
F(000)	2872.0
Crystal size/mm^3	0.276 × 0.083 × 0.064
Radiation	Cu Kα (λ = 1.54184)
2Θ range for data collection/°	7.446 to 143.962
Index ranges	$-11 \le h \le 14$, $-17 \le k \le 17$, $-36 \le l \le 36$
Reflections collected	19875
Independent reflections	9962 [R_{int} = 0.0386, R_{sigma} = 0.0538]
Data/restraints/parameters	9962/0/778
Goodness-of-fit on F^2	1.024
Final R indexes [I>=2σ (I)]	R_1 = 0.0382, wR_2 = 0.0917
Final R indexes [all data]	R_1 = 0.0514, wR_2 = 0.0994
Largest diff. peak/hole / e Å^{-3}	0.79/-0.71

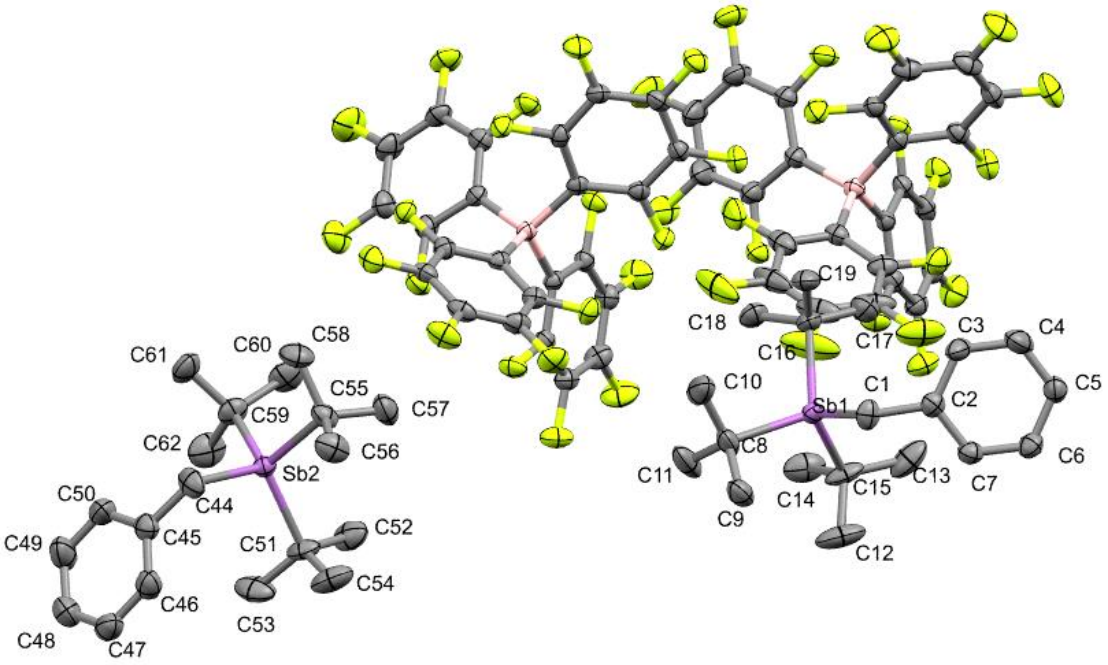

Figure 8.30. Solid state structure of [^{t}Bu$_3$BnSb][B(C$_6$F$_5$)$_4$]. Ellipsoids shown at 50% probability. Hydrogen atoms and labels on borate counteranion have been omitted. Selected structural parameters (bond lengths in angstroms and bond angles in degrees): Sb2-C44 2.154(5), Sb2-C59 2.188(5), Sb2-C55 2.186(4), Sb2-C51 2.191(5), Sb1-C16 2.186(4), Sb1-C1 2.150(4), Sb1-C8 2.195(5), Sb1-C15 2.187(5), C44-Sb2-C59 108.6(2), C44-Sb2-C55 101.81(19), C44-Sb2-C51 111.1(2), C59-Sb2-C51 112.5(2), C55-Sb2-C59 109.70(19), C55-Sb2-C51 112.6(2), C16-Sb1-C8 111.75(19), C16-Sb1-C15 111.85(19), C1-Sb1-C16 108.16(18), C1-Sb1-C8 100.91(19), C1-Sb1-C15 111.85(19), C15-Sb1-C8 111.8(2).

Table 8.29. Crystal data and structure refinement for [$^{t}Bu_3BnSb$][$B(C_6F_5)_4$].

Empirical formula	$C_{43}H_{34}BF_{20}Sb$
Formula weight	1063.26
Temperature/K	150.01(10)
Crystal system	triclinic
Space group	P-1
a/Å	16.0469(6)
b/Å	16.0934(8)
c/Å	17.8395(6)
α/°	66.160(4)
β/°	89.006(3)
γ/°	88.694(3)
Volume/Å^3	4212.7(3)
Z	4
ρ_{calc}g/cm^3	1.676
μ/mm^{-1}	6.304
F(000)	2112.0
Crystal size/mm^3	0.196 × 0.117 × 0.051
Radiation	Cu Kα (λ = 1.54184)
2Θ range for data collection/°	7.694 to 144.256
Index ranges	-19 ≤ h ≤ 17, -19 ≤ k ≤ 18, -21 ≤ l ≤ 17
Reflections collected	29917
Independent reflections	16179 [R_{int} = 0.0461, R_{sigma} = 0.0735]
Data/restraints/parameters	16179/0/1189
Goodness-of-fit on F^2	0.996
Final R indexes [I>=2σ (I)]	R_1 = 0.0470, wR_2 = 0.1068
Final R indexes [all data]	R_1 = 0.0679, wR_2 = 0.1192
Largest diff. peak/hole / e Å^{-3}	1.01/-0.63

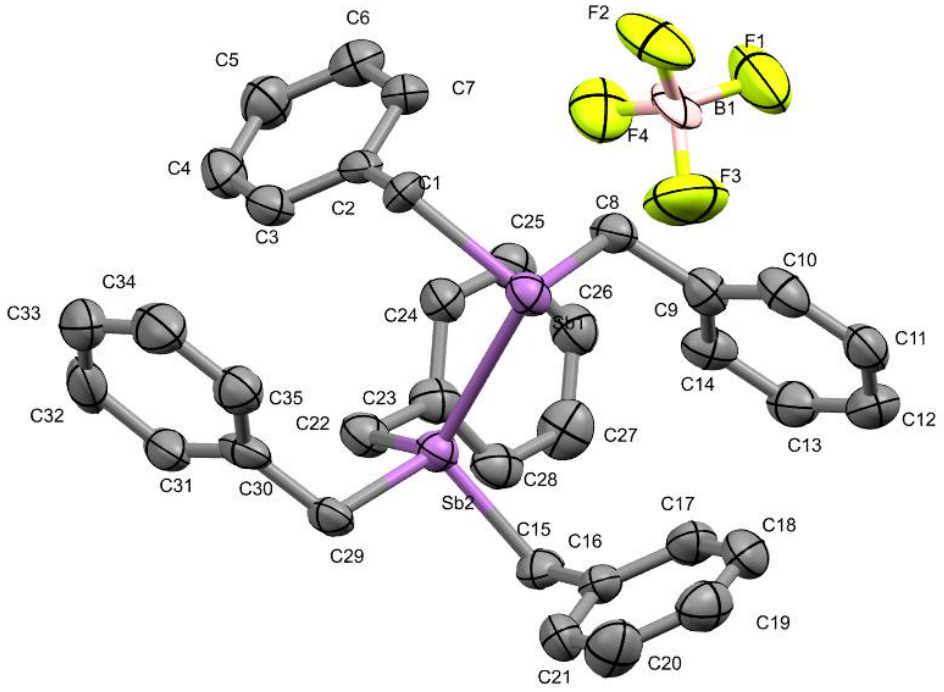

Figure 8.31. Solid state structure of $[Bn_2Sb(Bn_3Sb)][BF_4]$. Ellipsoids shown at 50% probability. Hydrogen atoms have been omitted. Selected structural parameters (bond lengths in angstroms and bond angles in degrees): Sb2-Sb1 2.8553(11), Sb2-C29 2.152(11), Sb2-C22 2.134(13), Sb2-C15 2.142(12), Sb1-C8 2.178(12), Sb1-C1 2.182(11), C29-Sb2-Sb1 106.7(3), C22-Sb2-Sb1 124.5(4), C22-Sb2-C29 106.4(5), C22-Sb2-C15 105.0(5), C15-Sb2-Sb1 109.8(3), C15-Sb2-C29 102.3(5), C8-Sb1-Sb2 97.7(3), C8-Sb1-C1 97.7(5), C1-Sb1-Sb2 96.3(3).

Table 8.30. Crystal data and structure refinement for $[Bn_2Sb(Bn_3Sb)][BF_4]$.

Empirical formula	$C_{35}H_{35}BF_4Sb_2$
Formula weight	785.94
Temperature/K	150.00(10)
Crystal system	triclinic
Space group	P-1
a/Å	9.6770(7)
b/Å	10.3100(8)
c/Å	17.2420(12)
α/°	84.926(6)
β/°	79.265(6)
γ/°	68.216(7)
Volume/Å^3	1569.1(2)
Z	2
ρ_{calc}g/cm^3	1.663
μ/mm^{-1}	14.047
F(000)	776.0
Crystal size/mm^3	0.096 × 0.053 × 0.028
Radiation	Cu Kα (λ = 1.54184)
2Θ range for data collection/°	9.24 to 144.478
Index ranges	$-11 \le h \le 11$, $-8 \le k \le 12$, $-20 \le l \le 21$
Reflections collected	17087
Independent reflections	6061 [R_{int} = 0.0916, R_{sigma} = 0.1110]
Data/restraints/parameters	6061/0/379
Goodness-of-fit on F^2	1.010
Final R indexes [I>=2σ (I)]	R_1 = 0.0755, wR_2 = 0.2082
Final R indexes [all data]	R_1 = 0.1120, wR_2 = 0.2358
Largest diff. peak/hole / e Å^{-3}	2.66/-1.24

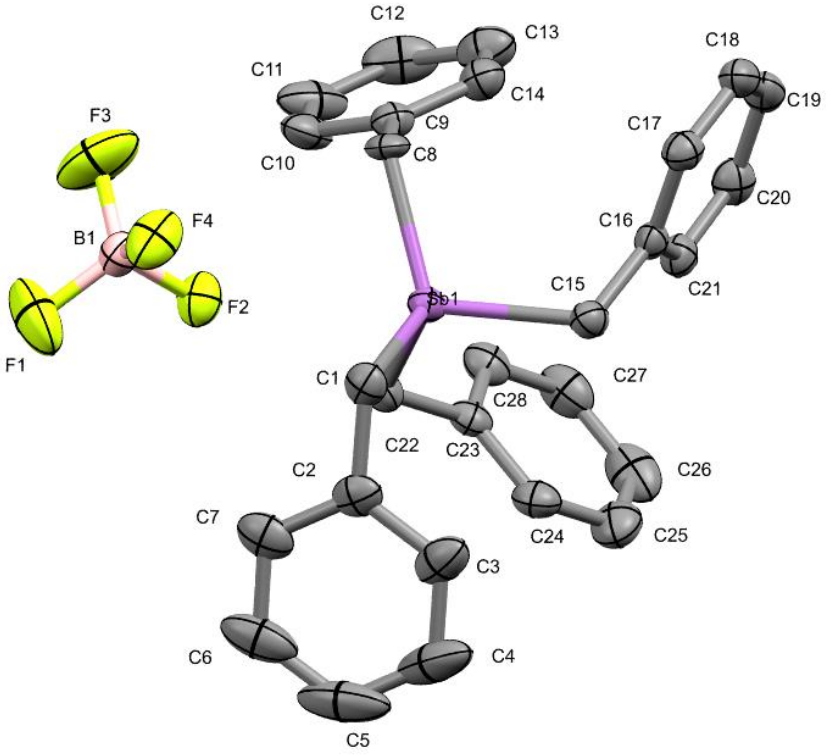

Figure 8.32. Solid state structure of **3-3**. Ellipsoids shown at 50% probability. Hydrogen atoms have been omitted. Selected structural parameters (bond lengths in angstroms and bond angles in degrees): Sb1-C15 2.140(4), Sb1-C22 2.138(4), Sb1-C1 2.145(4),Sb1-C8 2.149(3) C15-Sb1-C1 102.62(15), C15-Sb1-C8 110.10(15), C22-Sb1-C15 108.96(15), C22-Sb1-C1 106.73(15), C22-Sb1-C8 108.33(15), C1-Sb1-C8 119.65(15).

Table 8.31. Crystal data and structure refinement for **3-3**.

Empirical formula	$C_{28}H_{28}BF_4Sb$
Formula weight	573.06
Temperature/K	150.00(10)
Crystal system	triclinic
Space group	P-1
a/Å	10.9224(5)
b/Å	11.0630(5)
c/Å	12.7590(6)
α/°	94.110(4)
β/°	114.664(5)
γ/°	111.159(4)
Volume/Å^3	1260.87(12)
Z	2
ρ_{calc}g/cm^3	1.509
μ/mm^{-1}	9.052
F(000)	576.0
Crystal size/mm^3	0.174 × 0.106 × 0.084
Radiation	Cu Kα (λ = 1.54184)
2Θ range for data collection/°	7.902 to 143.818
Index ranges	-12 ≤ h ≤ 13, -13 ≤ k ≤ 12, -15 ≤ l ≤ 15
Reflections collected	10488
Independent reflections	4848 [R_{int} = 0.0400, R_{sigma} = 0.0576]
Data/restraints/parameters	4848/0/307
Goodness-of-fit on F^2	1.013
Final R indexes [I>=2σ (I)]	R_1 = 0.0357, wR_2 = 0.0880
Final R indexes [all data]	R_1 = 0.0423, wR_2 = 0.0926
Largest diff. peak/hole / e Å^{-3}	0.89/-0.88

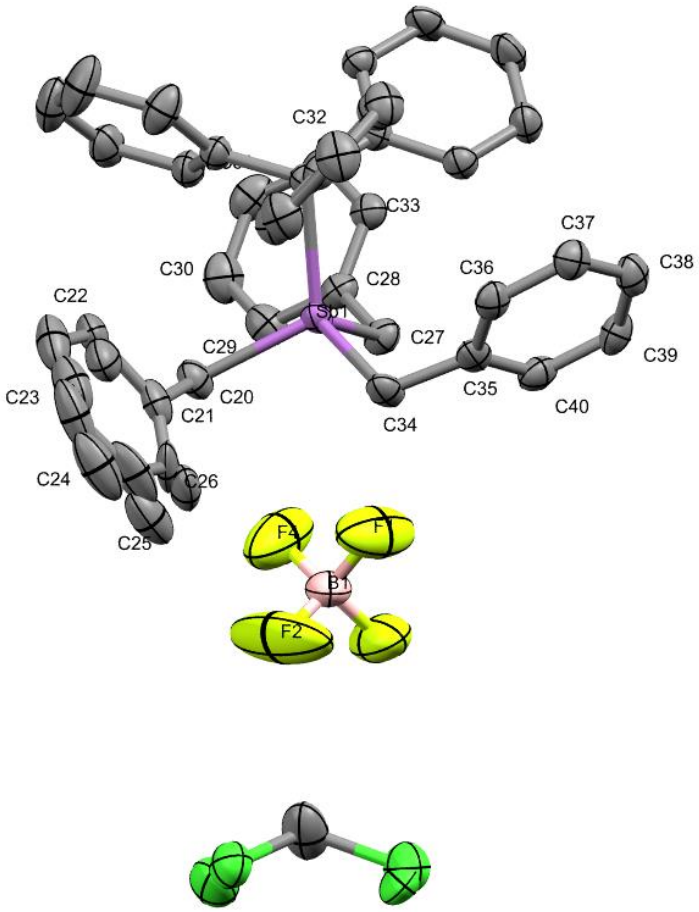

Figure 8.34. Solid state structure of **3-4**. Ellipsoids shown at 50% probability. Hydrogen atoms have been omitted. Selected structural parameters (bond lengths in angstroms and bond angles in degrees: Sb1-C1 2.238(3), Sb1-C34 2.155(3), Sb1-C27 2.149(3), Sb1-C20 2.146(3), C34-Sb1-C1 112.83(11), C27-Sb1-C1 111.95(11), C27-Sb1-C34 106.68(12), C20-Sb1-C1 113.27(12), C20-Sb1-C34 105.80(12), C20-Sb1-C27 105.74(12).

Table 8.32. Crystal data and structure refinement for **3-4**.

Empirical formula	$C_{41}H_{37.2}BCl_2F_4Sb$
Formula weight	809.37
Temperature/K	150.01(10)
Crystal system	triclinic
Space group	P-1
a/Å	9.7796(4)
b/Å	12.5723(5)
c/Å	14.8125(6)
α/°	90.976(3)
β/°	91.230(3)
γ/°	91.631(3)
Volume/Å^3	1819.79(13)
Z	2
ρ_{calc}g/cm^3	1.477
μ/mm^{-1}	7.773
F(000)	818.0
Crystal size/mm^3	0.132 × 0.103 × 0.07
Radiation	Cu Kα (λ = 1.54184)
2Θ range for data collection/°	7.034 to 144.094
Index ranges	-11 ≤ h ≤ 11, -15 ≤ k ≤ 15, -11 ≤ l ≤ 18
Reflections collected	11956
Independent reflections	6969 [R_{int} = 0.0337, R_{sigma} = 0.0520]
Data/restraints/parameters	6969/27/526
Goodness-of-fit on F^2	1.025
Final R indexes [I>=2σ (I)]	R_1 = 0.0328, wR_2 = 0.0797
Final R indexes [all data]	R_1 = 0.0376, wR_2 = 0.0831
Largest diff. peak/hole / e Å^{-3}	0.85/-0.44

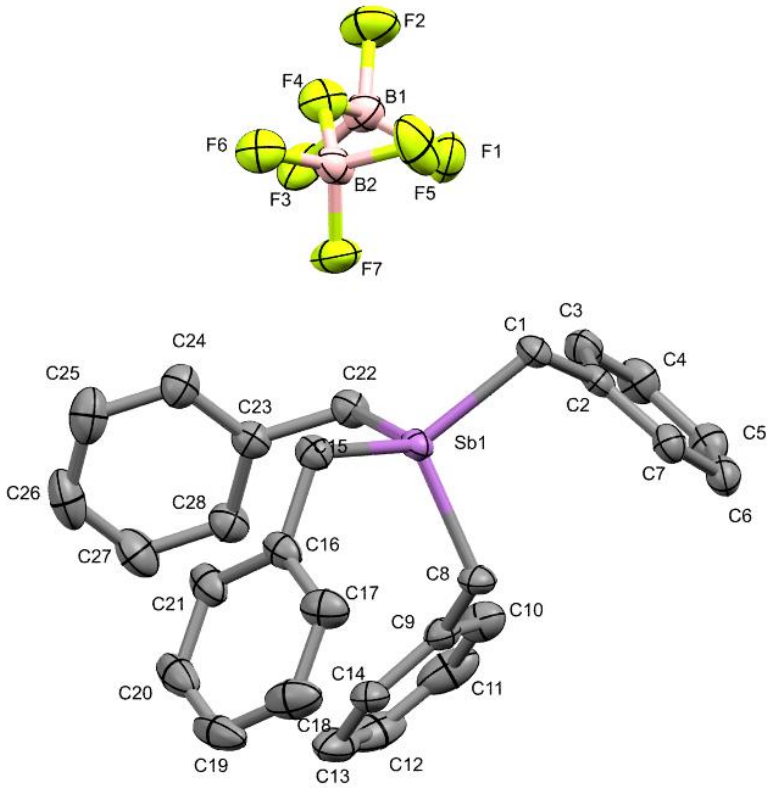

Figure 8.34. Solid state structure of **3-6**. Ellipsoids shown at 50% probability. Hydrogen atoms have been omitted. Selected structural parameters (bond lengths in angstroms and bond angles in degrees): Sb1-C15 2.140(4), Sb1-C22 2.138(4), Sb1-C1 2.145(4), Sb1-C8 2.149(3), C15-Sb1-C1 102.62(15), C15-Sb1-C8 110.10(15), C22-Sb1-C15 108.96(15), C22-Sb1-C1 106.73(15), C22-Sb1-C8 108.33(15), C1-Sb1-C8 119.65(15).

Table 8.33. Crystal data and structure refinement for **3-6**.

Empirical formula	$C_{28}H_{28}B_2F_7Sb$
Formula weight	640.87
Temperature/K	150.00(10)
Crystal system	triclinic
Space group	P-1
a/Å	10.6929(8)
b/Å	11.4665(7)
c/Å	13.1507(8)
α/°	67.701(6)
β/°	66.371(6)
γ/°	81.124(5)
Volume/Å^3	1366.75(18)
Z	2
ρ_{calc}g/cm^3	1.557
μ/mm^{-1}	8.576
F(000)	640.0
Crystal size/mm^3	0.123 × 0.065 × 0.042
Radiation	Cu Kα (λ = 1.54184)
2Θ range for data collection/°	7.836 to 144.028
Index ranges	-13 ≤ h ≤ 9, -14 ≤ k ≤ 13, -16 ≤ l ≤ 10
Reflections collected	10275
Independent reflections	5231 [R_{int} = 0.0362, R_{sigma} = 0.0499]
Data/restraints/parameters	5231/0/343
Goodness-of-fit on F^2	1.032
Final R indexes [I>=2σ (I)]	R_1 = 0.0309, wR_2 = 0.0786
Final R indexes [all data]	R_1 = 0.0356, wR_2 = 0.0814
Largest diff. peak/hole / e Å^{-3}	0.84/-0.71

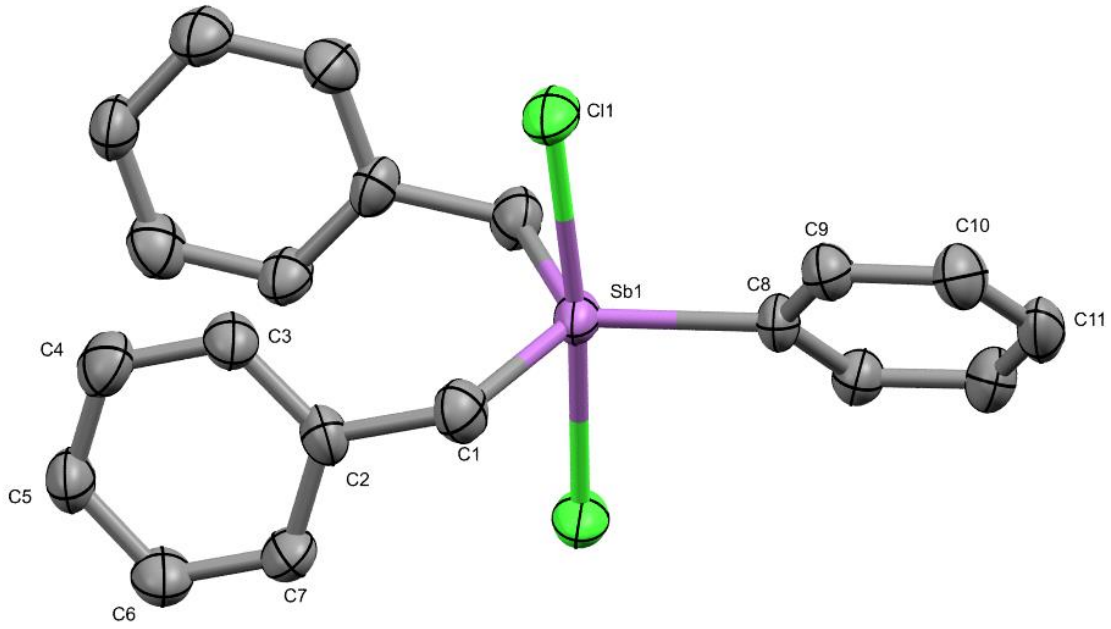

Figure 8.35. Solid state structure of **3-7**. Ellipsoids shown at 50% probability. Hydrogen atoms and labels on symmetry generated atoms have been omitted. Selected structural parameters (bond lengths in angstroms and bond angles in degrees): Sb1-Cl1 2.4732(16), Sb1-C8 2.123(8), Sb1-C1 2.128(7), Cl1^{1}-Sb1-Cl1 174.47(8), C8-Sb1-Cl1^{1} 92.76(4), C8-Sb1-Cl1 92.77(4), C8-Sb1-C1 116.06(18), C1-Sb1-Cl1 88.9(2), C11-Sb1-Cl1 88.7(2), C11-Sb1-C1 127.9(4).

Table 8.34. Crystal data and structure refinement for **3-7**.

Empirical formula	$C_{20}H_{20}Cl_2Sb$
Formula weight	453.01
Temperature/K	150.00(10)
Crystal system	monoclinic
Space group	C2/c
a/Å	12.145(2)
b/Å	13.2102(10)
c/Å	12.2442(17)
α/°	90
β/°	113.271(18)
γ/°	90
Volume/Å^3	1804.6(5)
Z	4
ρ_{calc}g/cm^3	1.667
μ/mm^{-1}	14.804
F(000)	900.0
Crystal size/mm^3	0.111 × 0.077 × 0.04
Radiation	Cu Kα (λ = 1.54184)
2Θ range for data collection/°	10.378 to 143.954
Index ranges	$-13 \leq h \leq 14$, $-9 \leq k \leq 16$, $-14 \leq l \leq 14$
Reflections collected	3358
Independent reflections	1728 [R_{int} = 0.0469, R_{sigma} = 0.0643]
Data/restraints/parameters	1728/0/106
Goodness-of-fit on F^2	1.043
Final R indexes [I>=2σ (I)]	R_1 = 0.0508, wR_2 = 0.1310
Final R indexes [all data]	R_1 = 0.0646, wR_2 = 0.1416
Largest diff. peak/hole / e Å^{-3}	2.06/-1.46

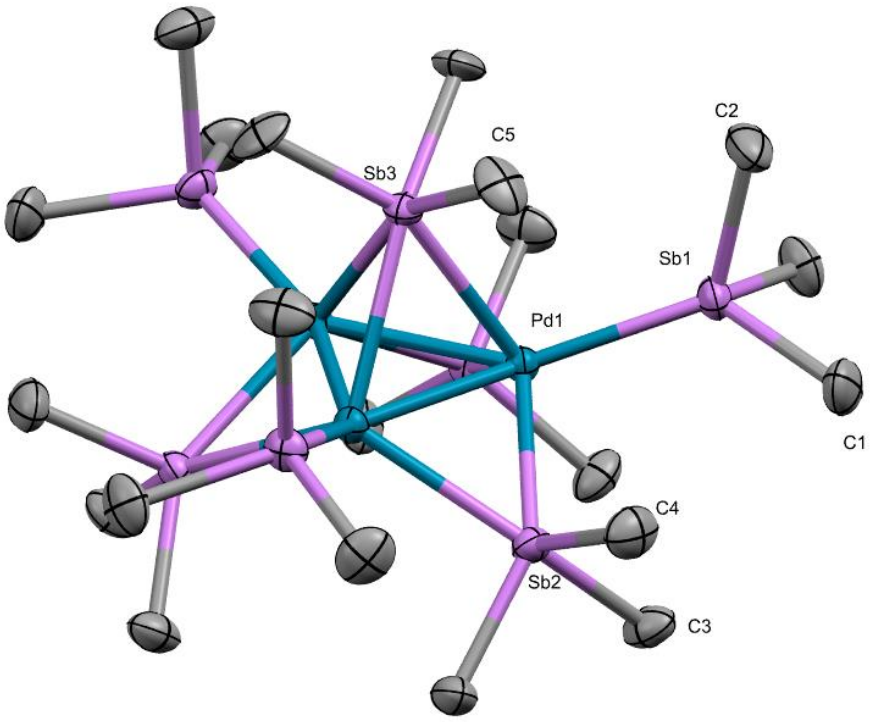

Figure 8.36. Solid state structure of **4-2**. Ellipsoids shown at 50% probability. Hydrogen atoms and labels for symmetry generated atoms have been omitted. Selected structural parameters (bond lengths in angstroms and bond angles in degrees): Sb2-Pd1 2.6935(10),Sb2-Pd1^{1} 2.6934(10), Sb2-C3 2.181(15), Sb1-Pd1 2.5255(14), Sb2-C4 2.14(2), Sb1-C1 2.153(14), Sb1-C2 2.13(2), Sb3-Pd1 2.7729(17), Pd1-Pd1^{1} 2.7534(17), Sb3-C5 2.159(19), Pd1-Sb2-Pd1^{1} 61.48(5), C3^{2}-Sb2-Pd1 95.8(4), C5^{3}-Sb3-C5 94.9(10), C1-Sb1-Pd1 122.2(5), C3^{2}-Sb2-Pd1^{1} 146.9(4), C1^{4}-Sb1-C1 95.2(10), C3^{2}-Sb2-C3 92.3(8), C2-Sb1-Pd1 118.5(7), C4-Sb2-Pd1^{1} 114.4(6), C2-Sb1-C1 96.2(7), C4-Sb2-C3 96.4(6), Sb2-Pd1-Sb2^{3} 122.63(6), Sb2-Pd1-Sb3 109.83(3), Sb2^{3}-Pd1-Pd1^{3} 59.26(2), Pd1^{3}-Sb3-Pd1^{1} 59.54(5), Sb2-Pd1-Pd1^{3} 111.48(2), C5^{1}-Sb3-Pd1 100.8(6), Sb2-Pd1-Pd^{1} 59.26(2), C5-Sb3-Pd1^{1} 156.7(8), Sb1-Pd1-Sb2 103.43(3), Sb1-Pd1-Sb3 106.08(5), Sb1-Pd1-Pd1^{1} 145.019(18), Sb1-Pd1-Pd1^{3} 145.020(18), C5-Sb3-Pd1 100.8(6), Pd1^{1}-Pd1-Sb3 60.23(2), C5-Sb3-C5^{1} 94.9(10),Pd11-Pd1-Pd1^{3} 60.0. 1)1-Y,1+X-Y,+Z; 2)1-Y,1-X,+Z; 3)+Y-X,1-X,+Z; 4)+Y-X,+Y,+Z. A TWIN and BASF correction was applied (0.0, 1.0, 0.0, 1.0, 1.0, 0.0, 0.0, 0.0, -1.0), BASF [0.44(4)]

Table 8.35. Crystal data and structure refinement for **4-2**.

Empirical formula	$C_7H_{21}PdSb_{2.33}$
Formula weight	495.72
Temperature/K	150.00(10)
Crystal system	trigonal
Space group	R3m
a/Å	19.2378(4)
b/Å	19.2378(4)
c/Å	9.5845(2)
α/°	90
β/°	90
γ/°	120
Volume/Å^3	3071.93(14)
Z	9
ρ_{calc}g/cm^3	2.404
μ/mm^{-1}	46.391
F(000)	2045.9
Crystal size/mm^3	0.111 × 0.061 × 0.043
Radiation	Cu Kα (λ = 1.54184)
2Θ range for data collection/°	9.194 to 143.546
Index ranges	-23 ≤ h ≤ 21, -17 ≤ k ≤ 23, -11 ≤ l ≤ 11
Reflections collected	5870
Independent reflections	1450 [R_{int} = 0.0506, R_{sigma} = 0.0407]
Data/restraints/parameters	1450/1/64
Goodness-of-fit on F^2	1.080
Final R indexes [I>=2σ (I)]	R_1 = 0.0386, wR_2 = 0.0916
Final R indexes [all data]	R_1 = 0.0387, wR_2 = 0.0918
Largest diff. peak/hole / e Å^{-3}	1.36/-0.81
Flack parameter	-0.01(4)

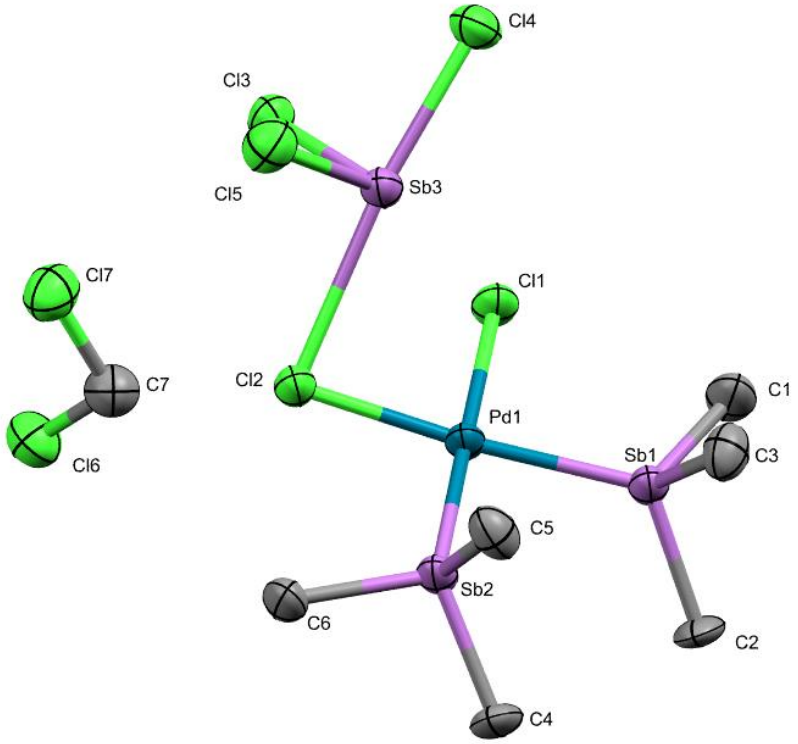

Figure 8.37. Solid state structure of cis-[$PdCl_2(Me_3Sb)$]·$SbCl_3(CH_2Cl_2)$. Ellipsoids shown at 50% probability. Hydrogen atoms have been omitted. Selected structural parameters (bond lengths in angstroms and bond angles in degrees): Sb2-Pd1 2.5076(7), Sb3-Cl2 2.895(2)Sb2-C4 2.111(9), Sb3-Cl3 2.382(2), Sb2-C6 2.105(9), Sb3-Cl4 2.480(2), Sb2-C5 2.115(10), Sb3-Cl5 2.400(3), Sb1-Pd1 2.5132(8), Pd1-Cl1 2.383(2),Sb1-C1 2.101(10). Pd1-Cl2 2.411(2), Sb1-C2 2.100(9), Sb1-C3 2.084(10), C4-Sb2-Pd1 122.5(3), Cl3-Sb3-Cl4 91.08(9) C4-Sb2-C5 100.8(5), Cl3-Sb3-Cl5 92.45(9), C6-Sb2-Pd1 114.7(3), Cl4-Sb3-Cl2 172.81(8), C6-Sb2-C4 103.3(4), Cl5-Sb3-Cl2 92.72(9), C6-Sb2-C5 100.1(4), Cl5-Sb3-Cl4 93.73(10), C5-Sb2-Pd1 112.4(3), Sb2-Pd1-Sb1 90.81(3), C1-Sb1-Pd1 114.1(3), Cl1-Pd1-Sb2 175.13(7), C2-Sb1-Pd1 122.4(3), Cl1-Pd1-Sb1 89.00(6), C2-Sb1-C1 103.2(5), Cl1-Pd1-Cl2 91.64(7),C3-Sb1-Pd1 112.8(3), Cl2-Pd1-Sb2 87.88(5),C3-Sb1-C1 99.8(5), Cl2-Pd1-Sb1 171.99(6),C3-Sb1-C2 101.4(5), Pd1-Cl2-Sb3 85.54(6),Cl3-Sb3-Cl2 91.80(7).

Table 8.36. Crystal data and structure refinement for cis-[$PdCl_2(Me_3Sb)$]·$SbCl_3(CH_2Cl_2)$.

Empirical formula	**$C_7H_{20}Cl_7PdSb_3$**
Formula weight	824.03
Temperature/K	150.00(10)
Crystal system	triclinic
Space group	P-1
a/Å	9.4614(5)
b/Å	11.1379(5)
c/Å	11.5911(6)
α/°	73.624(4)
β/°	68.548(5)
γ/°	81.704(4)
Volume/Å^3	1089.57(10)
Z	2
ρ_{calc}g/cm^3	2.512
μ/mm^{-1}	43.507
F(000)	760.0
Crystal size/mm^3	0.184 × 0.131 × 0.107
Radiation	Cu Kα (λ = 1.54184)
2Θ range for data collection/°	8.282 to 143.97
Index ranges	-11 ≤ h ≤ 11, -13 ≤ k ≤ 12, -14 ≤ l ≤ 14
Reflections collected	15003
Independent reflections	4228 [R_{int} = 0.0918, R_{sigma} = 0.0602]
Data/restraints/parameters	4228/0/169
Goodness-of-fit on F^2	1.053
Final R indexes [I>=2σ (I)]	R_1 = 0.0634, wR_2 = 0.1691
Final R indexes [all data]	R_1 = 0.0677, wR_2 = 0.1758
Largest diff. peak/hole / e Å^{-3}	2.58/-1.28

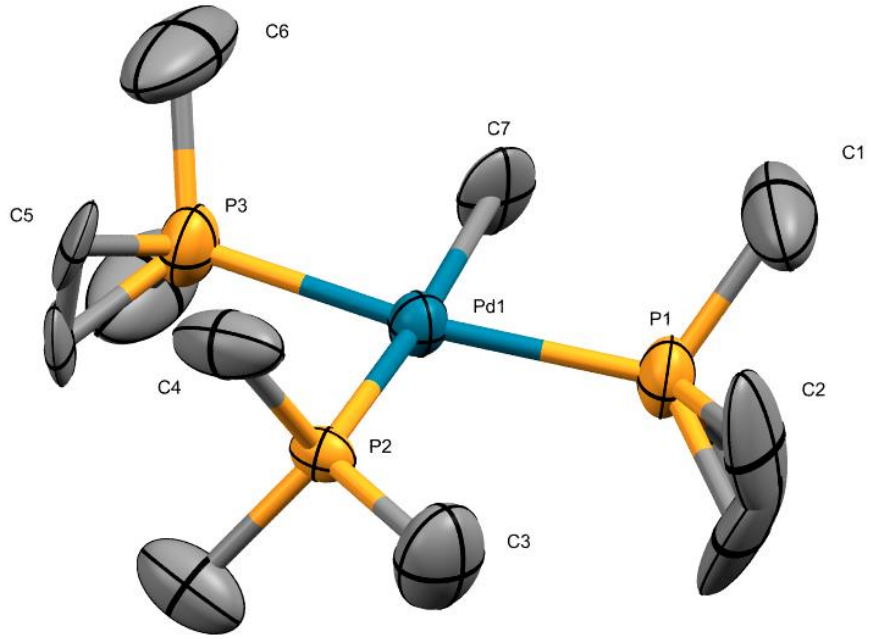

Figure 8.38. Solid state structure of **4-6**. Ellipsoids shown at 50% probability. Hydrogen atoms and labels for symmetry generated atoms have been omitted. Two methyl groups are disordered over two positions. Selected structural parameters (bond lengths in angstroms and bond angles in degrees):Pd1-P2 2.356(3), Pd1-P1 2.357(4), Pd1-P3 2.312(4),Pd1-C7 2.315(18), P2-C4 1.794(15), P2-C3 1.78(2),P2-Pd1-P1 101.41(15), C3-P2-C4^{1} 101.7(9),P3-Pd1-P2 89.64(15), P3-Pd1-P1 168.94(17), P3-Pd1-C7 86.5(4),C4^{1}-P2-C4 103.1(12). 1) +X,3/2-Y,+Z.

Table 8.37. Crystal data and structure refinement for **4-6.**

Empirical formula	$C_{10}H_{30}P_3Pd$
Formula weight	349.65
Temperature/K	150.00(10)
Crystal system	monoclinic
Space group	$P2_1/m$
a/Å	8.9524(9)
b/Å	10.2990(9)
c/Å	9.4486(12)
α/°	90
β/°	114.804(14)
γ/°	90
Volume/Å^3	790.80(17)
Z	2
ρ_{calc}g/cm^3	1.468
μ/mm^{-1}	12.079
F(000)	362.0
Crystal size/mm^3	0.187 × 0.112 × 0.079
Radiation	Cu Kα (λ = 1.54184)
2Θ range for data collection/°	10.314 to 143.7
Index ranges	$-10 \le h \le 9$, $0 \le k \le 12$, $0 \le l \le 11$
Reflections collected	1622
Independent reflections	1622 [R_{int} = ?, R_{sigma} = 0.0637]
Data/restraints/parameters	1622/0/89
Goodness-of-fit on F^2	1.042
Final R indexes [I>=2σ (I)]	R_1 = 0.0994, wR_2 = 0.2589
Final R indexes [all data]	R_1 = 0.1096, wR_2 = 0.2716
Largest diff. peak/hole / e Å^{-3}	3.85/-1.49

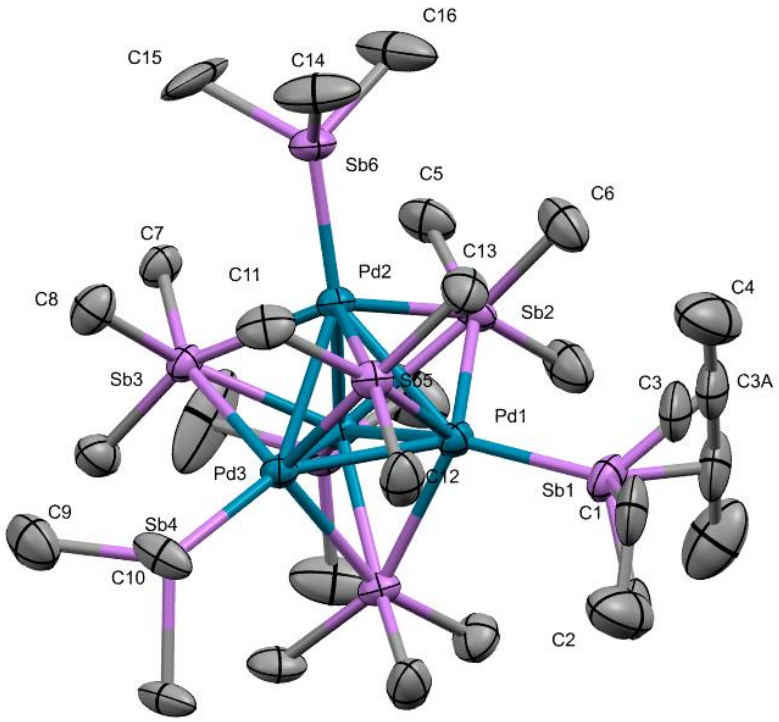

Figure 8.39. Solid state structure of **4-5**. Ellipsoids shown at 50% probability. Hydrogen atoms and labels for symmetry generated atoms have been omitted. The ethyl groups are disordered and modelled over two positions. Selected structural parameters (bond lengths in angstroms and bond angles in degrees): Sb5-Pd3 2.7730(13), Pd3-Pd2^{1} 2.8006(18),Sb5-Pd2 2.7843(16), Pd3-Sb4 2.518(2),Sb5-Pd1 2.7901(12), Pd3-Pd1 2.797(2), Pd2-Pd2^{1} 2.8034(19), Pd2-Sb6 2.5165(15), Pd2-Pd1 2.8033(19), Sb3-Pd3 2.786(2), Sb3-Pd2^{1} 2.7540(17), Sb3-Pd2 2.7540(17), Sb2-Pd2^{1} 2.7806(16), Pd1-Sb1 2.516(2), Sb2-Pd2 2.7805(16), Sb2-Pd1 2.737(2),Sb5-Pd3 2.7730(13), Pd3-Pd2^{1} 2.8006(18), Sb5-Pd2 2.7843(16), Pd3-Sb4 2.518(2), Sb5-Pd1 2.7901(12), Pd3-Pd1 2.797(2),Pd3-Sb5-Pd2 60.52(4), Pd1-Pd3-Pd2^{1} 60.11(5), Pd3-Sb5-Pd1 60.36(4), Pd1-Pd3-Pd2 60.11(5), Pd2-Sb5-Pd1 60.38(5), Sb5-Pd2-Pd3 59.54(4), Sb5-Pd2-Pd2^{1} 109.16(3), Sb5-Pd2-Pd1 59.91(4),Sb3-Pd2-Sb5 112.91(5), Sb3-Pd2-Sb2 112.59(5), Sb3-Pd2-Pd3 60.20(5), Sb3-Pd2-Pd2^{1} 59.40(3), Sb3-Pd2-Pd1 109.16(5), Sb2-Pd2-Sb5 111.79(6), Sb2-Pd2-Pd3 108.41(5), Sb2-Pd2-Pd2^{1} 59.73(3), Sb2-Pd2-Pd1 58.70(5), Pd3-Pd2-Pd2^{1} 59.97(3), Pd2^{1}-Sb3-Pd3 60.73(5), Pd3-Pd2-Pd1 59.88(5), Pd2-Sb3-Pd3 60.73(5), Pd2^{1}-Pd2-Pd1 60.00(3), Pd2-Sb3-Pd2^{1} 61.19(5), Sb6-Pd2-Sb5 107.05(5), Sb6-Pd2-Sb3 106.08(6), Sb6-Pd2-Sb2 105.82(5), Sb6-Pd2-Pd3 145.78(6), Sb6-Pd2-Pd2^{1} 143.78(4), Sb6-Pd2-Pd1 144.72(6), Pd2-Sb2-Pd2^{1} 60.55(5), Pd1-Sb2-Pd2 61.06(5), Pd1-Sb2-Pd2^{1} 61.06(5), Sb5-Pd1-Sb5^{1} 112.19(7), Sb5-Pd1-Pd3 59.52(3), Sb5-Pd1-Pd2 59.71(4), Sb5^{1}-Pd1-Pd2 109.00(6), Sb5^{1}-Pd1-Pd2^{1} 59.70(4), Sb5-Pd1-Pd2^{1} 109.00(6), Sb2-Pd1-Sb5 112.95(5), Sb2-Pd1-Pd3 109.77(8), Sb5-Pd3-Sb5^{1} 113.25(7), Sb2-Pd1-Pd2 60.23(5), Sb5-Pd3-Sb3 112.27(5), Pd3-Pd1-Pd2 60.02(5), Sb5-Pd3-Pd2^{1} 109.57(6), Pd2-Pd1-Pd21 60.00(6), Sb5-Pd3-Pd2 59.94(4), Sb1-Pd1-Sb5 106.84(5), Sb1-Pd1-Sb5^{1} 106.83(5), Pd1-Sb2 104.37(8), Sb5-Pd3-Pd1 60.12(4), Sb1-Pd1-Pd3 145.85(9), Pd1-Pd2 144.15(5), Sb3-Pd3-Pd2 59.07(5), Sb3-Pd3-Pd1 108.44(8), Pd2^{1}-Pd3-Pd2 60.07(5), Sb4-Pd3-Sb5 106.29(5), Sb4-Pd3-Sb5^{1} 106.29(5), Sb4-Pd3-Sb3 105.80(8), Sb4-Pd3-Pd2 144.13(5), Sb4-Pd3-Pd1 145.76(9). 1) -X,+Y,+Z

Table 8.38. Crystal data and structure refinement for **4-5**.

Empirical formula	$C_{26.39}H_{76.17}Pd_4Sb_8$
Formula weight	1793.25
Temperature/K	150.00(10)
Crystal system	orthorhombic
Space group	$Cmc2_1$
a/Å	18.4086(5)
b/Å	13.3785(4)
c/Å	20.2441(6)
α/°	90
β/°	90
γ/°	90
Volume/Å^3	4985.7(2)
Z	4
ρ_{calc}g/cm^3	2.389
μ/mm^{-1}	5.676
F(000)	3306.0
Crystal size/mm^3	0.127 × 0.064 × 0.056
Radiation	Mo Kα (λ = 0.71073)
2Θ range for data collection/°	7.116 to 54.962
Index ranges	-20 ≤ h ≤ 23, -17 ≤ k ≤ 17, -26 ≤ l ≤ 25
Reflections collected	18316
Independent reflections	5565 [R_{int} = 0.0698, R_{sigma} = 0.0793]
Data/restraints/parameters	5565/3/204
Goodness-of-fit on F^2	1.002
Final R indexes [I>=2σ (I)]	R_1 = 0.0479, wR_2 = 0.0775
Final R indexes [all data]	R_1 = 0.0689, wR_2 = 0.0849
Largest diff. peak/hole / e Å^{-3}	1.93/-1.61
Flack parameter	-0.09(4)

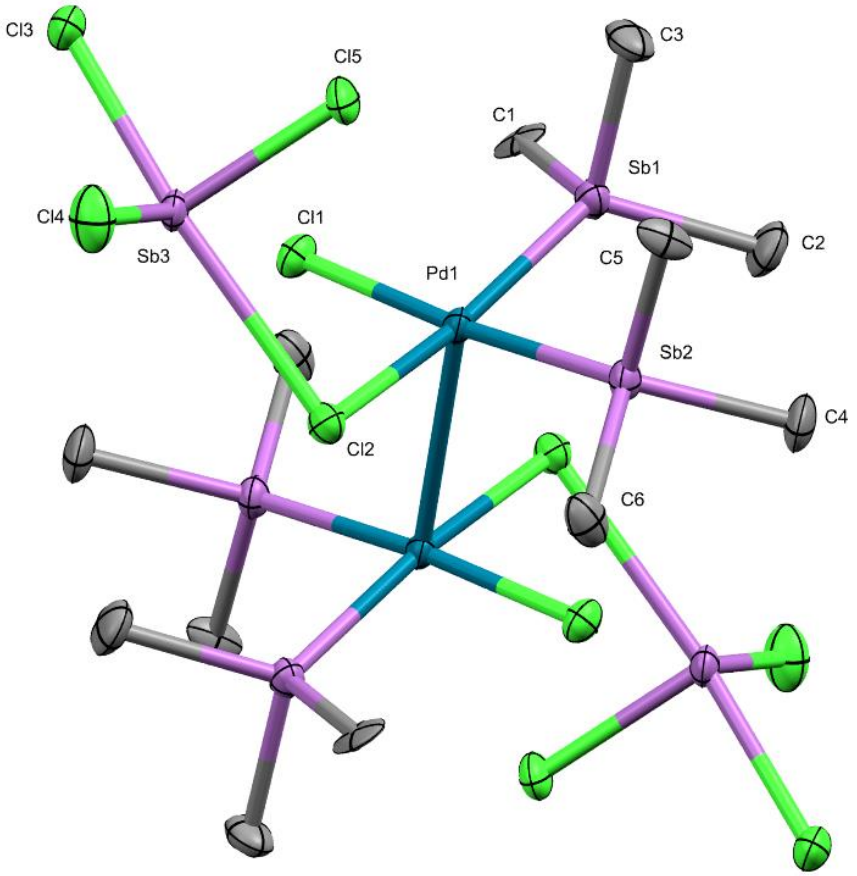

Figure 8.40. Solid state structure of **4-4**. Ellipsoids shown at 50% probability. Hydrogen atoms and labels for symmetry generated atoms have been omitted. Selected structural parameters (bond lengths in angstroms and bond angles in degrees):Sb3-Cl5 2.374(3), Sb1-Pd 12.5109(13), Sb3-Cl3 2.461(4), Sb1-C12.106(17), Sb3-Cl4 2.408(4), Sb1-C22.144(16), Sb2-Pd1 2.5128(13), Sb1-C3 2.108(14), Sb2-C5 2.101(14), Pd1 Pd11 3.1787(19), Sb2-C6 2.111(16), Pd1-Cl2 2.410(3), Sb2-C42.127(16), Pd1-Cl1 2.382(3),Cl5-Sb3-Cl3 91.35(13), C3-Sb1-Pd1 109.3(5), Cl5-Sb3-Cl4 93.95(14), C3-Sb1-C2 100.3(7), Cl4-Sb3-Cl3 93.25(15), Sb2-Pd1-Pd11 105.36(5), C5-Sb2-Pd 1110.8(4), Sb1-Pd1-Sb2 91.37(4), C5-Sb2-C6 102.9(6), Sb1-Pd1-Pd11 102.16(5), C5-Sb2-C4 99.0(7), Cl2-Pd1-Sb2 87.79(9), C6-Sb2-Pd1 114.2(4), Cl2-Pd1Sb1 171.88(9), C6-Sb2-C4 101.7(7), Cl2-Pd1-Pd11 85.84(9), C4-Sb2-Pd1 125.2(5), Cl1-Pd1-Sb2 173.74(9), C1-Sb1-Pd1 115.2(5), Cl1-Pd1-Sb1 88.19(10), C1-Sb1-C2 101.1(7), Cl1-Pd1-Pd11 80.83(9), C1-Sb1-C3 103.8(7), Cl1-Pd1-Cl2 91.76(13), C2-Sb1-Pd1 124.5(5).

Table 8.39. Crystal data and structure refinement for **4-4**.

Empirical formula	$C_6H_{18}Cl_5PdSb_3$
Formula weight	739.10
Temperature/K	150.01(10)
Crystal system	triclinic
Space group	P-1
a/Å	9.6021(5)
b/Å	9.8313(5)
c/Å	11.3497(7)
α/°	66.759(5)
β/°	68.354(5)
γ/°	76.490(4)
Volume/Å^3	910.18(10)
Z	2
ρ_{calc}g/cm^3	2.697
μ/mm^{-1}	49.320
F(000)	676.0
Crystal size/mm^3	? × ? × ?
Radiation	Cu Kα (λ = 1.54184)
2Θ range for data collection/°	8.918 to 144.822
Index ranges	-11 ≤ h ≤ 11, -9 ≤ k ≤ 12, -13 ≤ l ≤ 13
Reflections collected	9258
Independent reflections	3495 [R_{int} = 0.0729, R_{sigma} = 0.0854]
Data/restraints/parameters	3495/0/142
Goodness-of-fit on F^2	1.106
Final R indexes [I>=2σ (I)]	R_1 = 0.0574, wR_2 = 0.1668
Final R indexes [all data]	R_1 = 0.0827, wR_2 = 0.1821
Largest diff. peak/hole / e Å^{-3}	2.68/-1.61

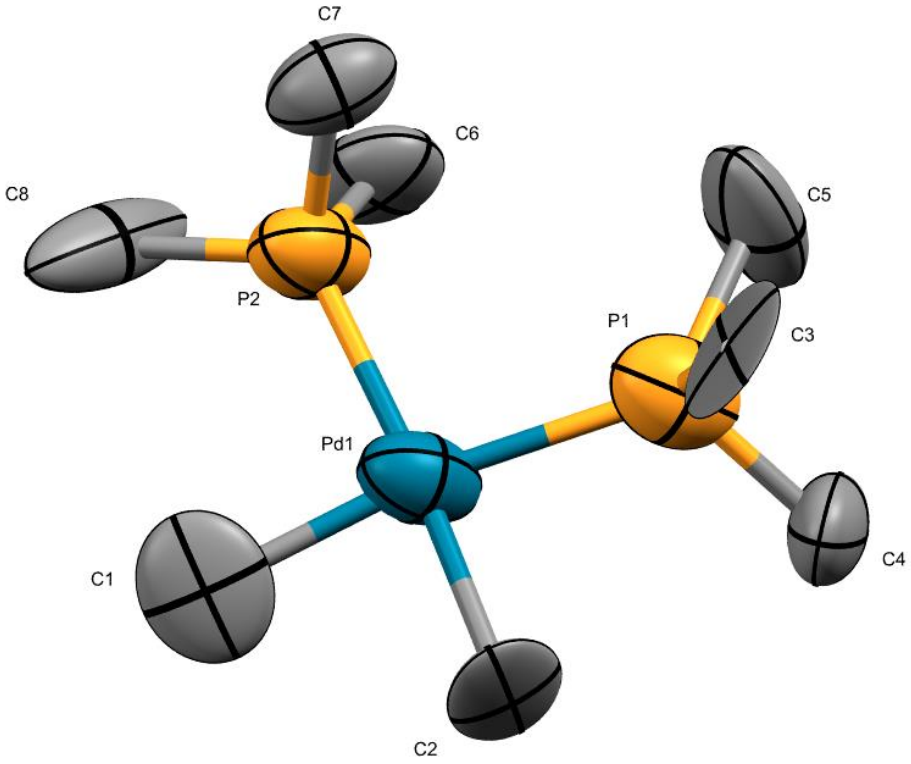

Figure 8.41. Solid state structure of **4-3**. Ellipsoids shown at 50% probability. Hydrogen atoms have been omitted. Pd1-P1 2.316(12), Pd1-P2 2.298(10), Pd1-C2 2.16(2), Pd1-C1 2.08(4), P2-Pd1-P1 97.4(4), C2-Pd1-P1 86.4(10), C2-Pd1-P2 174.5(11), C1-Pd1-P1 168.3(10), C1-Pd1-P2 93.4(11), C1-Pd1-C2 82.5(14).

Table 8.40. Crystal data and structure refinement for **4-3**.

Empirical formula	**$C_8H_{24}P_2Pd$**
Formula weight	288.61
Temperature/K	150.00(10)
Crystal system	orthorhombic
Space group	Pbca
a/Å	14.727(4)
b/Å	10.710(3)
c/Å	16.671(5)
α/°	90
β/°	90
γ/°	90
Volume/Å^3	2629.4(12)
Z	8
ρ_{calc}g/cm^3	1.458
μ/mm^{-1}	13.294
F(000)	1184.0
Crystal size/mm^3	0.084 × 0.053 × 0.037
Radiation	Cu Kα (λ = 1.54184)
2Θ range for data collection/°	10.614 to 145.234
Index ranges	-18 ≤ h ≤ 17, -11 ≤ k ≤ 12, -13 ≤ l ≤ 20
Reflections collected	7987
Independent reflections	2540 [R_{int} = 0.2603, R_{sigma} = 0.2355]
Data/restraints/parameters	2540/0/108
Goodness-of-fit on F^2	1.173
Final R indexes [I>=2σ (I)]	R_1 = 0.1995, wR_2 = 0.4687
Final R indexes [all data]	R_1 = 0.3101, wR_2 = 0.5819
Largest diff. peak/hole / e Å^{-3}	1.95/-1.85

Appendix III: Coordinates and Energies of Computational Structures

[Ph3SbCl]

Zero-point correction= 0.275563 (Hartree/Particle)

Thermal correction to Energy= 0.294215

Thermal correction to Enthalpy= 0.295159

Thermal correction to Gibbs Free Energy= 0.224303

Sum of electronic and zero-point Energies= -1393.844357

Sum of electronic and thermal Energies= -1393.825705

Sum of electronic and thermal Enthalpies= -1393.824760

Sum of electronic and thermal Free Energies= -1393.895616

35

Sb	-0.000002000	0.089299000	0.435321000
Cl	-0.000007000	0.534049000	2.719371000
C	-3.420841000	1.158431000	-1.998500000
H	-3.787667000	0.889729000	-2.989632000
C	-1.789549000	0.941860000	-0.241914000
C	-2.245627000	0.585079000	-1.517534000
H	-1.705856000	-0.135421000	-2.138513000
C	1.789532000	0.941889000	-0.241913000
C	0.000017000	-1.966726000	0.076310000
C	-3.664658000	2.414357000	0.060156000
H	-4.222541000	3.123368000	0.672658000
C	1.213076000	-4.013019000	-0.286592000
H	2.156258000	-4.552094000	-0.380670000
C	1.221836000	-2.641229000	-0.044328000
H	2.173281000	-2.111365000	0.049110000
C	-1.221787000	-2.641246000	-0.044370000
H	-2.173242000	-2.111394000	0.049035000
C	-2.489515000	1.851553000	0.555749000
H	-2.134672000	2.115903000	1.554117000
C	3.420853000	1.158451000	-1.998474000

H	3.787710000	0.889723000	-2.989587000
C	0.000044000	-4.693322000	-0.406540000
H	0.000055000	-5.767674000	-0.595360000
C	-4.125521000	2.069970000	-1.210791000
H	-5.046083000	2.514356000	-1.591249000
C	2.245649000	0.585075000	-1.517510000
H	1.705917000	-0.135469000	-2.138472000
C	-1.213000000	-4.013036000	-0.286634000
H	-2.156172000	-4.552123000	-0.380745000
C	2.489450000	1.851638000	0.555729000
H	2.134578000	2.116013000	1.554080000
C	4.125485000	2.070045000	-1.210785000
H	5.046039000	2.514449000	-1.591241000
C	3.664583000	2.414464000	0.060139000
H	4.222429000	3.123518000	0.672625000

$[(3\text{-}FC_6H_4)_3SbCl]$

Zero-point correction= 0.250941 (Hartree/Particle)

Thermal correction to Energy= 0.272068

Thermal correction to Enthalpy= 0.273012

Thermal correction to Gibbs Free Energy= 0.195502

Sum of electronic and zero-point Energies= -1691.252174

Sum of electronic and thermal Energies= -1691.231047

Sum of electronic and thermal Enthalpies= -1691.230103

Sum of electronic and thermal Free Energies= -1691.307613

35

Sb	0.025231000	-0.127771000	0.550295000
Cl	-0.324744000	-0.629680000	2.790306000
F	-2.053918000	4.669597000	-0.582743000
C	1.872271000	-1.013886000	0.110132000
C	-1.881623000	-0.569316000	-1.748865000

C	1.403779000	3.970622000	0.170110000
C	-0.960721000	3.998468000	-0.272678000
C	-1.049823000	2.625043000	-0.075473000
C	0.124265000	1.936830000	0.250837000
C	2.543547000	-0.586698000	-1.041567000
C	0.249108000	4.678726000	-0.154046000
C	2.387046000	-2.014963000	0.936545000
C	-1.661224000	-0.917474000	-0.411217000
C	3.605110000	-2.605020000	0.592857000
C	1.355092000	2.590990000	0.374898000
C	-2.516906000	-1.777255000	0.280138000
C	-2.989849000	-1.105254000	-2.406382000
F	4.404478000	-0.809517000	-2.431278000
C	-3.611397000	-2.290047000	-0.409225000
F	-4.436183000	-3.102617000	0.223445000
C	3.753111000	-1.199368000	-1.350648000
C	-3.858191000	-1.966866000	-1.740724000
C	4.291791000	-2.202799000	-0.549424000
H	-2.022642000	2.139132000	-0.180335000
H	0.264548000	5.756723000	-0.318651000
H	2.352751000	4.499352000	0.264476000
H	2.267129000	2.046090000	0.628550000
H	2.176140000	0.202041000	-1.702614000
H	1.862027000	-2.330406000	1.839856000
H	4.023994000	-3.386724000	1.227303000
H	5.244810000	-2.649676000	-0.834438000
H	-2.370377000	-2.053474000	1.326030000
H	-4.731500000	-2.395230000	-2.233648000
H	-3.179430000	-0.845695000	-3.448364000
H	-1.215286000	0.111204000	-2.284867000

[(4-$FC_6H_4)_3SbCl$]

Zero-point correction= 0.251124 (Hartree/Particle)

Thermal correction to Energy= 0.272206

Thermal correction to Enthalpy= 0.273150

Thermal correction to Gibbs Free Energy= 0.196066

Sum of electronic and zero-point Energies= -1691.256586

Sum of electronic and thermal Energies= -1691.235504

Sum of electronic and thermal Enthalpies= -1691.234559

Sum of electronic and thermal Free Energies= -1691.311643

35

Sb	-0.000002000	-0.088351000	0.581186000
Cl	-0.000017000	-0.434114000	2.881621000
F	5.222471000	-2.702660000	-1.375931000
F	-5.222551000	-2.702492000	-1.375955000
F	0.000087000	5.914497000	-0.756340000
C	1.788607000	-0.968249000	-0.049987000
C	-1.788632000	-0.968201000	-0.049993000
C	-2.251018000	-0.685258000	-1.343626000
H	-1.714825000	-0.001803000	-2.007866000
C	0.000031000	1.943171000	0.125456000
C	-3.423076000	-1.278389000	-1.797778000
H	-3.817193000	-1.085238000	-2.795580000
C	-2.492292000	-1.835050000	0.794537000
H	-2.139684000	-2.046622000	1.806170000
C	2.251143000	-0.685125000	-1.343527000
H	1.715084000	-0.001493000	-2.007693000
C	2.492101000	-1.835316000	0.794458000
H	2.139380000	-2.047025000	1.806024000
C	-3.665898000	-2.427335000	0.341707000
H	-4.245370000	-3.105085000	0.968787000
C	3.423182000	-1.278298000	-1.797673000

H	3.817415000	-1.085010000	-2.795403000
C	-4.111226000	-2.141775000	-0.946962000
C	4.111163000	-2.141904000	-0.946944000
C	3.665687000	-2.427643000	0.341634000
H	4.245032000	-3.105561000	0.968650000
C	0.000069000	4.630347000	-0.470349000
C	-1.221554000	3.974260000	-0.325199000
H	-2.147147000	4.536801000	-0.448179000
C	1.221673000	3.974262000	-0.325035000
H	2.147282000	4.536805000	-0.447890000
C	1.220947000	2.617941000	-0.024183000
H	2.174565000	2.096858000	0.093064000
C	-1.220865000	2.617939000	-0.024346000
H	-2.174498000	2.096853000	0.092773000

$[(3,5\text{-}F_2C_6H_3)_3SbCl]$

Zero-point correction= 0.226271 (Hartree/Particle)

Thermal correction to Energy= 0.249956

Thermal correction to Enthalpy= 0.250900

Thermal correction to Gibbs Free Energy= 0.166706

Sum of electronic and zero-point Energies= -1988.656708

Sum of electronic and thermal Energies= -1988.633023

Sum of electronic and thermal Enthalpies= -1988.632079

Sum of electronic and thermal Free Energies= -1988.716273

35

Sb	-0.006187000	-0.131188000	-0.639582000
Cl	-0.040822000	-0.615003000	-2.905052000
F	-3.679691000	-0.931374000	3.149519000
F	-4.592384000	-2.909969000	-0.976700000
F	4.057543000	-3.633623000	-0.815752000
F	-2.151847000	4.674675000	0.314166000

F	3.914912000	-0.836331000	2.916553000
F	2.497239000	4.566880000	-0.071143000
C	-1.122134000	2.622790000	-0.104275000
H	-2.104161000	2.145688000	-0.104549000
C	-2.147549000	-0.638477000	1.414496000
H	-1.535348000	-0.035860000	2.088949000
C	-1.813159000	-0.910091000	0.083839000
C	0.074255000	1.931183000	-0.312807000
C	2.334866000	-2.066720000	-0.672200000
H	1.953065000	-2.412233000	-1.634233000
C	-3.805675000	-2.183916000	-0.210549000
C	-4.180538000	-1.944190000	1.106014000
H	-5.110380000	-2.349161000	1.505882000
C	1.338799000	3.941360000	-0.083859000
C	-2.623435000	-1.678541000	-0.751325000
H	-2.380411000	-1.894055000	-1.792999000
C	-1.041026000	3.997083000	0.112850000
C	1.319959000	2.565713000	-0.304460000
H	2.265911000	2.044174000	-0.463096000
C	2.262648000	-0.597759000	1.286590000
H	1.830523000	0.214160000	1.875386000
C	4.027356000	-2.263034000	1.071504000
H	4.924061000	-2.742579000	1.464525000
C	-3.339749000	-1.171628000	1.899722000
C	0.174358000	4.672190000	0.126988000
H	0.213949000	5.748006000	0.299706000
C	3.406391000	-1.232522000	1.767758000
C	1.746315000	-1.038411000	0.064043000
C	3.478380000	-2.662498000	-0.141796000

[(2,4,6-$F_3C_6H_2)_3$SbCl]

Zero-point correction= 0.203131 (Hartree/Particle)

Thermal correction to Energy= 0.229068

Thermal correction to Enthalpy= 0.230013

Thermal correction to Gibbs Free Energy= 0.144725

Sum of electronic and zero-point Energies= -2286.089856

Sum of electronic and thermal Energies= -2286.063919

Sum of electronic and thermal Enthalpies= -2286.062975

Sum of electronic and thermal Free Energies= -2286.148262

35

symmetry c1

Sb	0.000476000	-0.004414000	0.506955000
Cl	-0.005067000	-0.015790000	2.817715000
F	-2.670514000	0.660450000	-1.207515000
F	-2.161425000	2.053503000	1.076212000
F	1.893087000	1.978423000	-1.225736000
F	-0.701641000	-2.909666000	1.054828000
F	-4.884159000	-3.438792000	-0.963108000
F	0.784590000	-2.634823000	-1.233882000
F	2.857832000	0.846238000	1.079729000
F	5.438398000	-2.473592000	-0.957969000
F	-0.554586000	5.940244000	-0.964215000
C	-2.731093000	-0.598666000	-0.799598000
C	-2.803629000	-3.259351000	0.062949000
H	-2.840111000	-4.296033000	0.396046000
C	-1.660149000	-1.111179000	-0.062303000
C	-3.846080000	-2.691987000	-0.672202000
C	1.795078000	-0.883071000	-0.054712000
C	0.715202000	4.000220000	-1.121896000
H	1.477888000	4.512278000	-1.707970000
C	-0.131020000	1.989906000	-0.054007000

C	1.896933000	-2.056074000	-0.808315000
C	-3.835663000	-1.369273000	-1.114996000
H	-4.662878000	-0.958956000	-1.693555000
C	3.123359000	-2.612219000	-1.126842000
H	3.192466000	-3.525884000	-1.716690000
C	-1.250920000	2.713120000	0.369147000
C	-1.425418000	4.050980000	0.078370000
H	-2.303523000	4.600185000	0.416701000
C	-0.420674000	4.669214000	-0.668897000
C	0.839521000	2.659390000	-0.801477000
C	-1.728199000	-2.444428000	0.353355000
C	2.977426000	-0.270951000	0.372143000
C	4.266961000	-1.959309000	-0.667195000
C	4.226094000	-0.783172000	0.082830000
H	5.137435000	-0.294804000	0.426392000

$[(F_5C_6)_3SbCl]$

Zero-point correction= 0.154017 (Hartree/Particle)

Thermal correction to Energy= 0.186393

Thermal correction to Enthalpy= 0.187337

Thermal correction to Gibbs Free Energy= 0.087156

Sum of electronic and zero-point Energies= -2880.800856

Sum of electronic and thermal Energies= -2880.768480

Sum of electronic and thermal Enthalpies= -2880.767535

Sum of electronic and thermal Free Energies= -2880.867717

35

Sb	-0.025261000	-0.007690000	-0.790997000
Cl	-0.087957000	-0.225494000	-3.075272000
F	-0.660887000	1.013078000	1.928072000
F	-1.979168000	-2.310888000	-1.183822000
F	1.963999000	-1.600771000	1.266481000

F	-2.890803000	0.939340000	-2.198823000
F	-4.955468000	2.864021000	1.525873000
F	0.572671000	2.949364000	0.436454000
F	2.903263000	-0.814224000	-1.130268000
F	5.248129000	2.908421000	0.485100000
F	-0.159889000	-5.762888000	1.413145000
C	-1.737015000	1.324414000	1.208707000
C	-3.953861000	1.918494000	-0.359021000
C	-1.741860000	0.982370000	-0.143095000
C	-3.927290000	2.261614000	0.995244000
C	1.714916000	1.038071000	-0.334162000
C	0.941222000	-3.705095000	1.352820000
C	0.005507000	-1.936625000	-0.001277000
C	1.713661000	2.325814000	0.200846000
C	-2.814497000	1.969765000	1.794516000
C	2.914715000	2.963972000	0.493901000
C	-1.041551000	-2.780114000	-0.372554000
C	-1.108903000	-4.086771000	0.092661000
C	-0.109419000	-4.540827000	0.960561000
C	0.987967000	-2.399778000	0.873848000
C	-2.857382000	1.271276000	-0.926963000
C	2.926533000	0.402076000	-0.604769000
C	4.120131000	2.309690000	0.221510000
C	4.136719000	1.019982000	-0.323182000
F	-2.807170000	2.294333000	3.063574000
F	-5.007557000	2.199083000	-1.084537000
F	1.859906000	-4.148522000	2.174735000
F	-2.089696000	-4.880466000	-0.257822000
F	5.275747000	0.422858000	-0.569276000
F	2.923144000	4.171222000	1.002545000

[(3,5-$(CF_3)_2C_6H_3)_3SbCl$]

Zero-point correction= 0.307177 (Hartree/Particle)

Thermal correction to Energy= 0.347706

Thermal correction to Enthalpy= 0.348650

Thermal correction to Gibbs Free Energy= 0.218649

Sum of electronic and zero-point Energies= -3413.903323

Sum of electronic and thermal Energies= -3413.862794

Sum of electronic and thermal Enthalpies= -3413.861849

Sum of electronic and thermal Free Energies= -3413.991851

53

Sb	-0.030248000	-0.305560000	-0.962542000
Cl	-0.082790000	-0.978173000	-3.176964000
C	-1.057975000	2.531492000	-0.664247000
H	-2.050246000	2.073447000	-0.661162000
C	-2.229741000	-0.521695000	1.096376000
H	-1.612374000	0.166206000	1.681412000
C	-1.860317000	-0.965341000	-0.176166000
C	0.111191000	1.774171000	-0.792468000
C	2.312407000	-2.262314000	-0.851125000
H	1.919069000	-2.657005000	-1.790506000
C	-3.882425000	-2.241783000	-0.356635000
C	-4.268839000	-1.811666000	0.913484000
H	-5.223248000	-2.133547000	1.337251000
C	1.455923000	3.758959000	-0.650393000
C	-2.677920000	-1.825697000	-0.914905000
H	-2.402475000	-2.167782000	-1.914851000
C	-0.949478000	3.912779000	-0.529194000
C	1.374409000	2.376452000	-0.786758000
H	2.296217000	1.796902000	-0.881106000
C	2.226772000	-0.685065000	1.006006000
H	1.767172000	0.153078000	1.538514000

C	3.982760000	-2.346784000	0.903865000
H	4.872065000	-2.808489000	1.339098000
C	-3.439005000	-0.958053000	1.635265000
C	0.300876000	4.529412000	-0.518245000
H	0.375983000	5.613597000	-0.398751000
C	3.372716000	-1.272522000	1.542748000
C	1.707919000	-1.188521000	-0.188515000
C	3.449844000	-2.833732000	-0.291920000
C	-2.192324000	4.771604000	-0.402304000
F	-2.358972000	5.510915000	-1.490311000
F	-3.275551000	4.016414000	-0.239545000
F	-2.087378000	5.587715000	0.637651000
C	2.803601000	4.453439000	-0.646433000
F	2.929113000	5.229087000	-1.714252000
F	2.928075000	5.215197000	0.432231000
F	3.794483000	3.566155000	-0.653073000
C	3.960109000	-0.690689000	2.812501000
F	4.682001000	0.390015000	2.536095000
F	2.987247000	-0.323414000	3.644463000
F	4.737553000	-1.567882000	3.427010000
C	4.144522000	-3.993995000	-0.977160000
F	5.356512000	-3.634598000	-1.379932000
F	4.276676000	-5.013449000	-0.138817000
F	3.454799000	-4.404479000	-2.036637000
C	-3.829064000	-0.521160000	3.033090000
F	-3.302163000	0.669884000	3.312078000
F	-5.145448000	-0.442163000	3.154594000
F	-3.378453000	-1.385663000	3.933891000
C	-4.803879000	-3.173188000	-1.119444000
F	-4.320381000	-3.437994000	-2.328805000
F	-4.947223000	-4.318339000	-0.464779000

F -6.004732000 -2.626348000 -1.255905000

Ph_3SbClF

Zero-point correction= 0.279093 (Hartree/Particle)

Thermal correction to Energy= 0.298565

Thermal correction to Enthalpy= 0.299509

Thermal correction to Gibbs Free Energy= 0.226766

Sum of electronic and zero-point Energies= -1493.839365

Sum of electronic and thermal Energies= -1493.819893

Sum of electronic and thermal Enthalpies= -1493.818949

Sum of electronic and thermal Free Energies= -1493.891691

36

Sb 0.000464000 -0.000112000 0.007322000

Cl 0.000302000 -0.000249000 2.488487000

F 0.000629000 0.000198000 -1.996896000

C -1.907150000 3.870331000 0.949741000

C -1.626101000 -2.431641000 1.068884000

C -0.939613000 1.913117000 -0.082141000

C -1.523672000 -2.264705000 -1.349202000

C 2.127142000 -0.142807000 -0.082130000

C 2.919302000 -0.192004000 1.069178000

C -1.186912000 -1.770486000 -0.082242000

C -2.298626000 -3.419175000 -1.455114000

C 2.723607000 -0.186723000 -1.349124000

C -2.737647000 -4.079932000 -0.309200000

C 4.110705000 -0.279928000 -1.454913000

C 4.305716000 -0.285001000 0.949717000

C -2.400707000 -3.585183000 0.949503000

C -1.199413000 2.451835000 -1.349068000

C -2.167208000 4.409462000 -0.308902000

C -1.812888000 3.699591000 -1.454832000

C	4.902527000	-0.329303000	-0.308940000
C	-1.293838000	2.623455000	1.069108000
H	4.572319000	-0.314088000	-2.442933000
H	4.920188000	-0.323084000	1.850379000
H	2.460434000	-0.158142000	2.056548000
H	2.102767000	-0.146940000	-2.242419000
H	-1.367359000	-2.050815000	2.055993000
H	-2.741192000	-4.098184000	1.850139000
H	-2.559254000	-3.801907000	-2.443059000
H	-1.179680000	-1.746254000	-2.242608000
H	-0.921717000	1.895455000	-2.242792000
H	-2.013491000	4.116809000	-2.442797000
H	-2.181933000	4.420962000	1.850626000
H	-1.093721000	2.208955000	2.056307000
H	-2.647129000	5.385503000	-0.396801000
H	-3.343719000	-4.983047000	-0.397209000
H	5.987686000	-0.402493000	-0.396940000

$(3\text{-}FC_6H_4)_3SbClF$

Zero-point correction= 0.254568 (Hartree/Particle)

Thermal correction to Energy= 0.276474

Thermal correction to Enthalpy= 0.277418

Thermal correction to Gibbs Free Energy= 0.198753

Sum of electronic and zero-point Energies= -1791.259427

Sum of electronic and thermal Energies= -1791.237521

Sum of electronic and thermal Enthalpies= -1791.236576

Sum of electronic and thermal Free Energies= -1791.315241

36

Sb	-0.015082000	0.000004000	0.129319000
Cl	-0.609799000	0.000027000	2.528392000
F	0.465432000	-0.000016000	-1.813109000
C	-4.407620000	0.000128000	0.003677000

C	1.164847000	-2.529310000	1.507007000
C	-2.062193000	0.000056000	-0.471071000
C	1.617561000	-2.357499000	-0.874535000
C	1.041952000	1.845797000	0.293789000
C	1.164977000	2.529266000	1.506989000
C	1.041845000	-1.845850000	0.293799000
C	2.311037000	-3.558497000	-0.797006000
C	1.617716000	2.357395000	-0.874544000
C	2.449021000	-4.258293000	0.395213000
C	2.311264000	3.558351000	-0.797022000
C	1.870043000	3.732850000	1.547200000
C	1.869841000	-3.732935000	1.547224000
C	-2.341496000	0.000048000	-1.843431000
C	-4.714571000	0.000120000	-1.351311000
C	-3.669564000	0.000080000	-2.271315000
C	2.449272000	4.258156000	0.395189000
C	-3.097815000	0.000096000	0.466310000
H	1.967539000	4.267700000	2.492765000
H	0.716379000	2.130637000	2.415291000
H	1.535411000	1.841242000	-1.829684000
H	0.716284000	-2.130642000	2.415309000
H	1.967320000	-4.267777000	2.492797000
H	1.535276000	-1.841354000	-1.829681000
H	-1.527130000	0.000018000	-2.565164000
H	-3.890736000	0.000073000	-3.339432000
H	-2.914734000	0.000102000	1.540234000
H	-5.760130000	0.000147000	-1.659998000
H	3.004035000	-5.196596000	0.400607000
H	3.004342000	5.196426000	0.400578000
F	2.861379000	4.053918000	-1.903614000
F	2.861105000	-4.054112000	-1.903599000

F -5.400673000 0.000167000 0.890487000

$(4\text{-}FC_6H_4)_3SbClF$

Zero-point correction= 0.254673 (Hartree/Particle)

Thermal correction to Energy= 0.276623

Thermal correction to Enthalpy= 0.277567

Thermal correction to Gibbs Free Energy= 0.198786

Sum of electronic and zero-point Energies= -1791.262741

Sum of electronic and thermal Energies= -1791.240791

Sum of electronic and thermal Enthalpies= -1791.239847

Sum of electronic and thermal Free Energies= -1791.318628

36

Sb -0.000724000 -0.000286000 0.053204000

Cl -0.001034000 -0.000851000 2.530676000

F -0.000822000 0.000078000 -1.950785000

F -6.162276000 -0.782434000 -0.370554000

C 1.673008000 3.973119000 1.002630000

C -2.901147000 -0.369024000 1.112934000

C 0.822342000 1.960393000 -0.036897000

C -2.706727000 -0.343224000 -1.304021000

C 1.286647000 -1.692890000 -0.037422000

C 1.767908000 -2.328746000 1.112519000

F 2.404928000 5.725665000 -0.369691000

C -2.110392000 -0.268102000 -0.037238000

C -4.083183000 -0.517857000 -1.418832000

F 3.762467000 -4.941169000 -0.371735000

C 1.652618000 -2.169219000 -1.304406000

C -4.848034000 -0.615545000 -0.262988000

C 2.493449000 -3.272880000 -1.419632000

C 2.609010000 -3.432869000 1.001323000

C -4.278145000 -0.543806000 1.002175000

C	1.051019000	2.516364000	-1.303662000
C	1.891376000	4.504487000	-0.262501000
C	1.588345000	3.795559000	-1.418401000
C	2.959064000	-3.887813000	-0.264017000
C	1.135182000	2.693519000	1.113325000
H	2.794017000	-3.664027000	-2.391679000
H	2.997807000	-3.946154000	1.880770000
H	1.489625000	-1.966448000	2.101454000
H	1.278249000	-1.674507000	-2.199163000
H	-2.447406000	-0.311899000	2.101621000
H	-4.916508000	-0.625117000	1.881913000
H	-4.572939000	-0.579673000	-2.390703000
H	-2.091736000	-0.265000000	-2.199093000
H	0.807767000	1.946065000	-2.198675000
H	1.776421000	4.252006000	-2.390241000
H	1.925553000	4.565015000	1.882372000
H	0.960937000	2.270726000	2.102053000

$(3,5\text{-}F_2C_6H_3)_3SbClF$

Zero-point correction= 0.230033 (Hartree/Particle)

Thermal correction to Energy= 0.254444

Thermal correction to Enthalpy= 0.255388

Thermal correction to Gibbs Free Energy= 0.171353

Sum of electronic and zero-point Energies= -2088.675979

Sum of electronic and thermal Energies= -2088.651568

Sum of electronic and thermal Enthalpies= -2088.650624

Sum of electronic and thermal Free Energies= -2088.734658

36

Sb	0.000701000	0.000136000	-0.074717000
F	0.000808000	-0.000898000	1.923869000
F	-2.256822000	4.087637000	2.580702000

F	5.056418000	-0.098771000	-2.078290000
F	4.671319000	-0.101906000	2.577349000
C	-1.027484000	1.866376000	0.023497000
C	2.131340000	-0.042577000	0.022032000
C	-2.372577000	4.307208000	0.257817000
H	-2.896400000	5.257827000	0.348358000
C	-1.310630000	2.374823000	1.295366000
H	-1.022813000	1.849323000	2.203821000
C	2.714147000	-0.057704000	1.293275000
H	2.115770000	-0.047216000	2.202237000
C	2.914958000	-0.055545000	-1.133567000
H	2.485801000	-0.043731000	-2.134188000
C	-1.980183000	3.590403000	1.380780000
C	4.101740000	-0.087423000	1.377681000
C	4.297514000	-0.085827000	-0.988357000
C	4.917841000	-0.102750000	0.254145000
H	6.002990000	-0.127494000	0.343505000
F	-2.436452000	4.432767000	-2.074072000
C	-1.404435000	2.554420000	-1.131416000
H	-1.196366000	2.180163000	-2.132503000
C	-2.071617000	3.765741000	-0.985038000
Cl	0.001488000	0.002433000	-2.537937000
F	-2.413099000	-3.999885000	2.575450000
F	-2.626487000	-4.321582000	-2.079259000
C	-1.102371000	-1.823610000	0.020005000
C	-1.512577000	-2.491621000	-1.135564000
H	-1.292079000	-2.123098000	-2.135989000
C	-1.400966000	-2.324167000	1.291464000
H	-1.088382000	-1.814487000	2.200616000
C	-2.229357000	-3.674225000	-0.989871000
C	-2.121258000	-3.510459000	1.376012000

C -2.547495000 -4.206577000 0.252682000

H -3.110280000 -5.134779000 0.342256000

$(2,4,6\text{-}F_3C_6H_2)_3SbClF$

Zero-point correction= 0.204845 (Hartree/Particle)

Thermal correction to Energy= 0.232369

Thermal correction to Enthalpy= 0.233314

Thermal correction to Gibbs Free Energy= 0.143692

Sum of electronic and zero-point Energies= -2386.084852

Sum of electronic and thermal Energies= -2386.057328

Sum of electronic and thermal Enthalpies= -2386.056384

Sum of electronic and thermal Free Energies= -2386.146005

36

Sb -0.007053000 -0.002534000 -0.015710000

Cl 0.008262000 -0.019015000 2.411338000

F -0.020617000 -0.000496000 -1.973666000

F 3.746733000 -4.916750000 -0.197940000

F -0.317601000 -2.970875000 1.060028000

F -2.428030000 1.771627000 1.062339000

F 2.870149000 -0.443087000 -1.217011000

F -1.824476000 -2.265918000 -1.203325000

F -1.080230000 2.754249000 -1.145467000

C 2.500842000 -1.598936000 -0.680839000

C 0.881521000 -2.884732000 0.494815000

F 2.749914000 1.184430000 1.020673000

C 2.940345000 -3.866410000 -0.156929000

F -6.141406000 -0.765120000 -0.218124000

C -2.949262000 0.689926000 0.492961000

C -2.085452000 -0.248553000 -0.058580000

C 1.256023000 -1.670120000 -0.066380000

C 2.073004000 2.186818000 0.472908000

C 1.702221000 -4.002636000 0.464248000

H	1.387210000	-4.948333000	0.899426000
C	-4.828101000	-0.600840000	-0.165440000
C	0.815604000	1.926342000	-0.060218000
C	-4.328405000	0.540281000	0.454379000
H	-4.993588000	1.286809000	0.883044000
C	2.649738000	3.448266000	0.438579000
H	3.637329000	3.631924000	0.855564000
C	-2.644731000	-1.363988000	-0.673884000
C	3.370629000	-2.677968000	-0.734406000
H	4.346241000	-2.596487000	-1.209029000
C	0.127899000	2.986238000	-0.643359000
C	-4.014497000	-1.572891000	-0.736085000
H	-4.433504000	-2.456699000	-1.212720000
C	0.650400000	4.270987000	-0.700863000
H	0.096845000	5.089896000	-1.155717000
F	2.443174000	5.681835000	-0.204241000
C	1.915596000	4.467601000	-0.157820000

$(F_5C_6)_3SbClF$

Zero-point correction= 0.155922 (Hartree/Particle)

Thermal correction to Energy= 0.189844

Thermal correction to Enthalpy= 0.190789

Thermal correction to Gibbs Free Energy= 0.086271

Sum of electronic and zero-point Energies= -2980.820908

Sum of electronic and thermal Energies= -2980.786986

Sum of electronic and thermal Enthalpies= -2980.786042

Sum of electronic and thermal Free Energies= -2980.890560

36

Sb	-0.000834000	-0.018259000	0.011828000
Cl	-0.001296000	-0.042419000	2.422239000
F	0.024361000	-0.011591000	-1.948124000
C	-4.252266000	-0.912288000	0.496025000

C	1.802064000	-2.437228000	0.521393000
C	-1.897870000	-0.925226000	-0.058582000
C	2.887159000	-0.650505000	-0.651270000
C	0.124130000	2.084029000	-0.019544000
C	1.219134000	2.734810000	0.522116000
C	1.755850000	-1.167252000	-0.033246000
C	4.071045000	-1.382168000	-0.701644000
C	-0.870046000	2.821288000	-0.645758000
C	4.098798000	-2.659023000	-0.140680000
C	-0.804824000	4.212441000	-0.690369000
C	1.312218000	4.121448000	0.484745000
C	2.970552000	-3.190571000	0.479406000
C	-2.057626000	-2.154734000	-0.684780000
C	-4.392671000	-2.153744000	-0.126441000
C	-3.297279000	-2.784504000	-0.716530000
C	0.301689000	4.852853000	-0.138593000
C	-2.999324000	-0.308553000	0.523373000
F	0.720927000	-2.939487000	1.087382000
F	3.018041000	-4.399319000	1.002885000
F	5.203875000	-3.367130000	-0.192521000
F	5.158506000	-0.898052000	-1.265698000
F	2.846124000	0.562189000	-1.179325000
F	-1.012330000	-2.760193000	-1.224704000
F	-3.448109000	-3.955765000	-1.301080000
F	-5.575174000	-2.729687000	-0.155184000
F	-5.300296000	-0.316947000	1.033535000
F	-2.871791000	0.875803000	1.100059000
F	2.192821000	2.026223000	1.079219000
F	2.352038000	4.746773000	0.998704000
F	0.398863000	6.164188000	-0.190089000
F	-1.760920000	4.911245000	-1.266498000

F -1.920252000 2.207958000 -1.167340000

$(3,5\text{-}(CF_3)_2C_6H_3)_3SbClF$

Zero-point correction= 0.310697 (Hartree/Particle)

Thermal correction to Energy= 0.349323

Thermal correction to Enthalpy= 0.350268

Thermal correction to Gibbs Free Energy= 0.228768

Sum of electronic and zero-point Energies= -3513.938184

Sum of electronic and thermal Energies= -3513.899558

Sum of electronic and thermal Enthalpies= -3513.898613

Sum of electronic and thermal Free Energies= -3514.020113

54

Sb 0.002667000 -0.004318000 -0.192132000

F -0.019184000 -0.008225000 1.807470000

Cl 0.028701000 0.000201000 -2.646255000

C 1.658896000 -1.342603000 -0.074076000

C -1.987324000 -0.767088000 -0.112470000

C -2.552317000 -0.981198000 1.145056000

H -1.985271000 -0.762429000 2.050637000

C 0.333154000 2.100404000 -0.082132000

C 2.109118000 -1.711117000 1.194897000

H 1.622657000 -1.320014000 2.089443000

C 0.405466000 2.684397000 1.189238000

H 0.304285000 2.073259000 2.085542000

C -2.719847000 -1.049939000 -1.271630000

H -2.292904000 -0.889666000 -2.261484000

C 3.366423000 -2.712983000 -1.078455000

C -3.854490000 -1.480065000 1.236719000

C 3.189307000 -2.588980000 1.310776000

C 0.472250000 2.887349000 -1.224725000

H 0.410614000 2.447613000 -2.221392000

C	3.823150000	-3.094050000	0.183458000
H	4.663973000	-3.781936000	0.284321000
C	2.287886000	-1.845666000	-1.218118000
H	1.944696000	-1.571703000	-2.215973000
C	0.690395000	4.259888000	-1.090241000
C	0.616285000	4.055831000	1.299180000
C	-4.013492000	-1.545518000	-1.156202000
C	-4.591294000	-1.764388000	0.095656000
H	-5.607552000	-2.153364000	0.177793000
C	0.763629000	4.852509000	0.164475000
H	0.934914000	5.925829000	0.259294000
C	-4.831565000	-1.859345000	-2.384759000
F	-4.163000000	-1.602177000	-3.504887000
F	-5.188282000	-3.144041000	-2.404532000
F	-5.954786000	-1.140897000	-2.404107000
C	-4.435387000	-1.703700000	2.611484000
F	-4.449335000	-0.571607000	3.313616000
F	-5.683623000	-2.161858000	2.550548000
F	-3.709342000	-2.584751000	3.298777000
C	0.884423000	5.084994000	-2.338724000
F	2.089642000	4.878729000	-2.867941000
F	-0.014365000	4.766535000	-3.268189000
F	0.773474000	6.387601000	-2.085816000
C	0.646684000	4.707114000	2.660443000
F	1.540436000	5.695056000	2.699467000
F	-0.537864000	5.236617000	2.966058000
F	0.954514000	3.833544000	3.615202000
C	3.638011000	-2.986970000	2.695618000
F	4.748089000	-3.720231000	2.660668000
F	3.878820000	-1.913146000	3.446377000
F	2.698138000	-3.698811000	3.316773000

C	4.087583000	-3.233236000	-2.298274000
F	5.246083000	-2.598297000	-2.476402000
F	4.365481000	-4.530713000	-2.171491000
F	3.364990000	-3.072730000	-3.403400000

Ph_3SbClH

Zero-point correction= 0.283662 (Hartree/Particle)

Thermal correction to Energy= 0.302348

Thermal correction to Enthalpy= 0.303292

Thermal correction to Gibbs Free Energy= 0.231146

Sum of electronic and zero-point Energies= -1394.637889

Sum of electronic and thermal Energies= -1394.619204

Sum of electronic and thermal Enthalpies= -1394.618259

Sum of electronic and thermal Free Energies= -1394.690406

36

Sb	-0.000329000	-0.000674000	-0.148641000
H	0.001917000	0.000958000	-1.896962000
Cl	-0.000607000	-0.002227000	2.397064000
C	0.371348000	4.132982000	-1.504292000
C	2.261419000	-1.580992000	-1.403753000
C	0.190430000	2.135981000	-0.144720000
C	2.394841000	-1.690257000	1.009858000
C	-1.945701000	-0.903525000	-0.147261000
C	-2.502880000	-1.160338000	-1.404714000
C	1.754875000	-1.233343000	-0.146417000
C	3.533227000	-2.488419000	0.900970000
C	-2.659269000	-1.235221000	1.008527000
C	4.037124000	-2.833724000	-0.352737000
C	-3.921187000	-1.818519000	0.898772000
C	-3.765374000	-1.743770000	-1.507996000
C	3.400410000	-2.379647000	-1.506065000
C	0.258717000	2.918984000	1.011779000

C	0.440316000	4.911772000	-0.350732000
C	0.383844000	4.303605000	0.902951000
C	-4.475388000	-2.073317000	-0.355253000
C	0.246814000	2.747505000	-1.401955000
H	0.213883000	2.445200000	1.991742000
H	0.538059000	5.995822000	-0.428388000
H	0.193726000	2.144720000	-2.311498000
H	1.769017000	-1.229974000	-2.313390000
H	2.002969000	-1.421819000	1.990466000
H	4.928384000	-3.458588000	-0.430734000
H	-2.228068000	-1.036607000	1.989144000
H	-1.954040000	-0.905349000	-2.313857000
H	-5.463242000	-2.530183000	-0.434132000
H	0.415302000	4.601982000	-2.488329000
H	0.437038000	4.910559000	1.808094000
H	3.788877000	-2.645708000	-2.490333000
H	4.029168000	-2.842287000	1.806082000
H	-4.474544000	-2.075040000	1.803396000
H	-4.192729000	-1.939993000	-2.492493000

$(3\text{-}FC_6H_4)_3SbClH$

Zero-point correction= 0.259263 (Hartree/Particle)

Thermal correction to Energy= 0.280358

Thermal correction to Enthalpy= 0.281302

Thermal correction to Gibbs Free Energy= 0.203367

Sum of electronic and zero-point Energies= -1692.058378

Sum of electronic and thermal Energies= -1692.037283

Sum of electronic and thermal Enthalpies= -1692.036339

Sum of electronic and thermal Free Energies= -1692.114274

36

Sb	0.021352000	0.000000000	-0.013738000

H	0.423162000	0.000001000	-1.714152000
Cl	-0.558480000	-0.000005000	2.451790000
C	-3.714065000	-0.000050000	-2.276031000
C	1.630600000	2.386555000	-0.932472000
C	-2.067188000	-0.000030000	-0.503253000
C	1.193411000	2.538124000	1.446803000
C	1.063149000	-1.860032000	0.231608000
C	1.630645000	-2.386527000	-0.932470000
C	1.063089000	1.860064000	0.231600000
C	1.894259000	3.744141000	1.489307000
C	1.193524000	-2.538065000	1.446820000
C	2.464560000	4.281099000	0.337034000
C	1.894411000	-3.744057000	1.489328000
C	2.321727000	-3.589691000	-0.858825000
C	2.321645000	3.589742000	-0.858831000
C	-3.084982000	-0.000044000	0.452690000
C	-4.738801000	-0.000065000	-1.334037000
C	-4.403320000	-0.000062000	0.015272000
C	2.464698000	-4.281020000	0.337049000
C	-2.379745000	-0.000034000	-1.866901000
H	-3.956351000	-0.000054000	-3.339572000
H	1.996917000	-4.273887000	2.437353000
H	1.996721000	4.273992000	2.437325000
H	-2.871592000	-0.000042000	1.521286000
H	-5.790591000	-0.000078000	-1.620685000
H	-1.586882000	-0.000023000	-2.617121000
H	1.552088000	1.887893000	-1.900528000
H	0.749808000	2.125935000	2.351755000
H	3.015873000	5.221545000	0.345851000
H	0.749932000	-2.125874000	2.351776000
H	1.552093000	-1.887886000	-1.900533000

H	3.016041000	-5.221450000	0.345870000
F	-5.380643000	-0.000075000	0.919168000
F	2.860970000	4.091454000	-1.968839000
F	2.861038000	-4.091407000	-1.968838000

$(4\text{-}FC_6H_4)_3SbClH$

Zero-point correction= 0.259332 (Hartree/Particle)

Thermal correction to Energy= 0.280456

Thermal correction to Enthalpy= 0.281400

Thermal correction to Gibbs Free Energy= 0.203593

Sum of electronic and zero-point Energies= -1692.060933

Sum of electronic and thermal Energies= -1692.039809

Sum of electronic and thermal Enthalpies= -1692.038864

Sum of electronic and thermal Free Energies= -1692.116672

36

Sb	-0.000480000	-0.000884000	-0.102311000
H	-0.001758000	-0.000876000	-1.850685000
Cl	0.000916000	-0.001228000	2.441113000
F	0.614363000	6.200893000	-0.390307000
C	-3.783140000	-1.704579000	-1.461490000
C	0.267747000	2.745809000	-1.352608000
C	-1.952175000	-0.879719000	-0.097279000
C	0.296886000	2.911577000	1.059538000
C	1.738872000	-1.249364000	-0.098969000
C	2.242552000	-1.608872000	-1.354464000
F	-5.680300000	-2.566818000	-0.391469000
C	0.212811000	2.128745000	-0.097550000
C	0.433574000	4.293979000	0.962425000
F	5.067266000	-3.629350000	-0.393366000
C	2.377777000	-1.710241000	1.058030000
C	0.485222000	4.881090000	-0.296683000

C	3.507091000	-2.518769000	0.959832000
C	3.372761000	-2.415735000	-1.463722000
C	0.404807000	4.127880000	-1.461079000
C	-2.668428000	-1.208115000	1.059689000
C	-4.472145000	-2.019685000	-0.297111000
C	-3.934478000	-1.779901000	0.962172000
C	3.988175000	-2.858491000	-0.299572000
C	-2.517664000	-1.132070000	-1.352959000
H	-2.235838000	-1.013377000	2.040523000
H	-4.513566000	-2.041802000	1.847761000
H	-4.242332000	-1.910665000	-2.428319000
H	-1.970921000	-0.883709000	-2.265405000
H	1.755761000	-1.255801000	-2.266344000
H	3.783867000	-2.705325000	-2.430749000
H	4.022209000	-2.891950000	1.845105000
H	1.990224000	-1.435555000	2.038670000
H	0.201693000	2.148574000	-2.264719000
H	0.448258000	4.629150000	-2.427911000
H	0.502849000	4.925544000	1.848321000
H	0.255022000	2.438007000	2.039799000

$(3,5\text{-}F_2C_6H_3)_3SbClH$

Zero-point correction= 0.234861 (Hartree/Particle)

Thermal correction to Energy= 0.258423

Thermal correction to Enthalpy= 0.259368

Thermal correction to Gibbs Free Energy= 0.176494

Sum of electronic and zero-point Energies= -1989.475589

Sum of electronic and thermal Energies= -1989.452026

Sum of electronic and thermal Enthalpies= -1989.451082

Sum of electronic and thermal Free Energies= -1989.533956

36

Sb	-0.001385000	-0.001815000	0.071443000
H	-0.000937000	0.001686000	1.816828000
Cl	-0.001951000	-0.007279000	-2.448924000
C	3.064169000	-2.772103000	1.420563000
C	0.584724000	2.682570000	1.329913000
C	1.584805000	-1.447901000	0.075401000
C	0.633455000	2.848219000	-1.093303000
C	-2.048092000	-0.648501000	0.074507000
C	-2.619843000	-0.822120000	1.337892000
C	0.460958000	2.094251000	0.068297000
C	0.931827000	4.199929000	-0.961323000
C	-2.786806000	-0.888734000	-1.084803000
C	1.062747000	4.821366000	0.275045000
C	-4.106329000	-1.305827000	-0.948859000
C	-3.943674000	-1.240340000	1.419111000
C	0.883835000	4.038538000	1.407162000
C	2.150414000	-1.981054000	-1.083604000
C	3.651783000	-3.324914000	0.291092000
C	3.174950000	-2.911313000	-0.947205000
C	-4.710421000	-1.489802000	0.289297000
C	2.036297000	-1.838881000	1.338936000
H	1.814365000	-1.690171000	-2.077934000
H	4.455921000	-4.055028000	0.371773000
H	1.615088000	-1.441433000	2.263609000
H	0.456483000	2.121029000	2.256539000
H	0.541522000	2.410194000	-2.086228000
H	1.296895000	5.882231000	0.352112000
H	-2.361495000	-0.759193000	-2.079052000
H	-2.069546000	-0.642854000	2.262783000
H	-5.746139000	-1.816987000	0.369590000
F	3.723551000	-3.428396000	-2.040362000

F 1.002761000 4.605035000 2.603212000

F -4.494600000 -1.406875000 2.616741000

F 3.499533000 -3.148313000 2.618304000

F 1.099704000 4.931390000 -2.056797000

F -4.822855000 -1.538781000 -2.042274000

$(2,4,6\text{-}F_3C_6H_2)_3SbClH$

Zero-point correction= 0.209996 (Hartree/Particle)

Thermal correction to Energy= 0.236591

Thermal correction to Enthalpy= 0.237535

Thermal correction to Gibbs Free Energy= 0.149044

Sum of electronic and zero-point Energies= -2286.891764

Sum of electronic and thermal Energies= -2286.865169

Sum of electronic and thermal Enthalpies= -2286.864225

Sum of electronic and thermal Free Energies= -2286.952716

36

Sb 0.000151000 -0.000833000 -0.335199000

H -0.000025000 -0.000702000 -2.064353000

Cl 0.001209000 -0.002185000 2.162987000

F -5.083674000 -3.549551000 0.122074000

C 4.292709000 -0.852453000 -0.630175000

C -1.783810000 -2.453504000 -0.722255000

C 1.892430000 -0.942957000 -0.201590000

C -2.915442000 -0.714176000 0.434867000

C -0.129374000 2.108795000 -0.200719000

C -1.233952000 2.769308000 -0.722575000

F 5.618973000 -2.621773000 0.120746000

C -1.763166000 -1.166465000 -0.200910000

C -4.054622000 -1.498026000 0.554563000

F -0.536160000 6.175716000 0.121335000

C 0.837495000 2.881192000 0.435601000

C -4.009217000 -2.780326000 0.017152000

C	0.727276000	4.259725000	0.554792000
C	-1.406238000	4.143151000	-0.630187000
C	-2.888004000	-3.288854000	-0.629436000
C	2.078572000	-2.166647000	0.434094000
C	4.414719000	-2.077758000	0.016051000
C	3.327876000	-2.759684000	0.553523000
C	-0.406056000	4.860726000	0.016683000
C	3.016488000	-0.315486000	-0.722612000
H	3.451783000	-3.720561000	1.049474000
H	5.158996000	-0.336706000	-1.039963000
H	-2.285505000	4.636126000	-1.040339000
H	1.497558000	4.847046000	1.051096000
H	-2.875940000	-4.297038000	-1.039055000
H	-4.948209000	-1.123591000	1.050446000
F	1.018704000	-2.795610000	0.923969000
F	2.848738000	0.858187000	-1.334003000
F	-0.684496000	-2.896232000	-1.334439000
F	-2.928411000	0.518323000	0.924329000
F	1.911355000	2.276890000	0.926004000
F	-2.166477000	2.038017000	-1.334920000

Silane Reduction Starting Point

Zero-point correction= 0.689496 (Hartree/Particle)

Thermal correction to Energy= 0.733592

Thermal correction to Enthalpy= 0.734537

Thermal correction to Gibbs Free Energy= 0.608210

Sum of electronic and zero-point Energies= -2448.275306

Sum of electronic and thermal Energies= -2448.231210

Sum of electronic and thermal Enthalpies= -2448.230265

Sum of electronic and thermal Free Energies= -2448.356592

81

Sb	2.390156000	-0.019876000	-1.068608000

H	0.930388000	-0.038616000	0.961111000
Cl	3.795083000	-0.008146000	-2.959276000
C	2.217306000	3.791757000	0.981238000
C	0.056980000	1.132394000	-2.641470000
C	2.912164000	1.740599000	-0.063960000
C	-0.405823000	-1.036781000	-1.621293000
C	2.888057000	-1.822187000	-0.123685000
C	3.268195000	-1.795881000	1.221703000
C	0.461077000	0.028550000	-1.883948000
C	-1.704809000	-0.989857000	-2.126465000
C	2.803673000	-3.021964000	-0.836421000
C	-2.122508000	0.110684000	-2.877798000
C	3.101875000	-4.216005000	-0.179922000
C	3.566965000	-2.997299000	1.862707000
C	-1.247057000	1.167863000	-3.134985000
C	4.243965000	1.980872000	0.283455000
C	3.542595000	4.037112000	1.346221000
C	4.552322000	3.138269000	0.998626000
C	3.481338000	-4.202324000	1.162992000
C	1.891758000	2.635862000	0.273632000
H	5.035535000	1.280037000	0.008390000
H	3.791651000	4.940050000	1.906037000
H	0.851740000	2.432216000	0.002429000
H	0.743171000	1.957397000	-2.849043000
H	-0.079281000	-1.895134000	-1.027838000
H	-3.140018000	0.143851000	-3.271165000
H	2.508090000	-3.039768000	-1.888087000
H	3.326416000	-0.852313000	1.772220000
H	3.713324000	-5.140350000	1.669885000
H	1.431850000	4.499295000	1.251259000
H	5.586437000	3.336716000	1.283552000

H	-1.578097000	2.023816000	-3.724793000
H	-2.390426000	-1.817359000	-1.935251000
H	3.036005000	-5.159920000	-0.722692000
H	3.867395000	-2.989620000	2.911487000
Si	-5.473595000	0.077433000	0.556934000
Si	0.024321000	-0.090480000	2.164967000
C	-5.162971000	1.306772000	-0.844824000
H	-4.078156000	1.357810000	-1.037237000
H	-5.617345000	0.900069000	-1.765203000
C	-0.986618000	-1.673107000	2.017590000
H	-1.382050000	-1.739139000	0.989790000
H	-0.303928000	-2.531861000	2.139040000
C	-2.138239000	-1.746693000	3.025178000
H	-2.864590000	-0.934862000	2.858985000
H	-1.778689000	-1.658900000	4.062382000
H	-2.684117000	-2.698866000	2.947389000
C	-5.720394000	2.703001000	-0.554683000
H	-5.540190000	3.399881000	-1.387471000
H	-5.260023000	3.139005000	0.345818000
H	-6.807816000	2.674529000	-0.381013000
C	1.142184000	-0.066815000	3.679001000
H	0.501905000	-0.077482000	4.577589000
H	1.709872000	-1.012613000	3.701619000
C	-4.609709000	-1.570934000	0.218136000
H	-3.526619000	-1.368367000	0.141392000
H	-4.733498000	-2.207132000	1.111207000
C	-5.093255000	-2.317686000	-1.028111000
H	-5.023768000	-1.693919000	-1.933725000
H	-6.144464000	-2.626892000	-0.925774000
H	-4.504749000	-3.230358000	-1.210600000
C	2.091532000	1.134694000	3.718949000

H	2.729853000	1.178384000	2.820120000
H	2.756568000	1.099225000	4.594781000
H	1.535995000	2.083862000	3.767566000
H	-4.894985000	0.638236000	1.821137000
C	-7.338405000	-0.138543000	0.806815000
H	-7.498044000	-1.046979000	1.412902000
H	-7.697903000	0.699602000	1.427154000
C	-8.153345000	-0.208996000	-0.488418000
H	-8.062062000	0.722581000	-1.067999000
H	-9.224005000	-0.364238000	-0.285557000
H	-7.821173000	-1.031000000	-1.140422000
C	-1.085263000	1.426017000	2.067038000
H	-1.736232000	1.421279000	2.958748000
H	-0.470060000	2.337435000	2.146953000
C	-1.932204000	1.450213000	0.792506000
H	-2.633285000	2.298878000	0.778292000
H	-2.528296000	0.528690000	0.698507000
H	-1.305177000	1.520137000	-0.112573000

Silane Reduction TS1

Zero-point correction= 0.687982 (Hartree/Particle)

Thermal correction to Energy= 0.731514

Thermal correction to Enthalpy= 0.732459

Thermal correction to Gibbs Free Energy= 0.606206

Sum of electronic and zero-point Energies= -2448.253376

Sum of electronic and thermal Energies= -2448.209843

Sum of electronic and thermal Enthalpies= -2448.208899

Sum of electronic and thermal Free Energies= -2448.335152

81

Sb	-2.235044000	0.071508000	-0.203992000
H	-0.728574000	-0.018749000	0.748458000
Cl	-4.277503000	0.265102000	-1.713745000

C	-3.412565000	-0.704255000	3.924406000
C	-1.712833000	-2.882854000	-0.619365000
C	-3.394940000	-0.239073000	1.550034000
C	-1.420030000	-1.624787000	-2.673749000
C	-1.771465000	2.076012000	-0.730534000
C	-1.393434000	2.918333000	0.318610000
C	-1.724211000	-1.667745000	-1.309816000
C	-1.085943000	-2.804127000	-3.340712000
C	-1.811987000	2.548906000	-2.044086000
C	-1.077073000	-4.020482000	-2.654875000
C	-1.441378000	3.868584000	-2.307082000
C	-1.053980000	4.246066000	0.051625000
C	-1.395908000	-4.061335000	-1.297757000
C	-4.792374000	-0.185670000	1.545001000
C	-4.806163000	-0.648197000	3.921251000
C	-5.492666000	-0.388948000	2.734310000
C	-1.066408000	4.715590000	-1.262217000
C	-2.703989000	-0.497849000	2.740171000
H	-5.330306000	0.013477000	0.617562000
H	-5.359978000	-0.807104000	4.848161000
H	-1.611914000	-0.539131000	2.752959000
H	-1.962134000	-2.924406000	0.444614000
H	-1.450750000	-0.681424000	-3.224301000
H	-0.826049000	-4.941510000	-3.183808000
H	-2.148556000	1.902301000	-2.856754000
H	-1.375124000	2.551365000	1.349354000
H	-0.790546000	5.750164000	-1.473349000
H	-2.871974000	-0.907321000	4.850312000
H	-6.583023000	-0.344282000	2.730666000
H	-1.399387000	-5.011961000	-0.761679000
H	-0.843401000	-2.772989000	-4.404277000

H	-1.458244000	4.239839000	-3.333170000
H	-0.777455000	4.911185000	0.871439000
Si	4.824511000	-0.123009000	0.143005000
Si	1.594348000	-0.108282000	0.470321000
C	5.524195000	-1.666210000	0.930151000
H	5.180105000	-2.539495000	0.352235000
H	6.616432000	-1.614297000	0.771947000
C	1.434584000	0.542317000	-1.277755000
H	2.080743000	-0.094623000	-1.905693000
H	0.414192000	0.366904000	-1.651638000
C	1.806682000	2.020301000	-1.420396000
H	2.815528000	2.232590000	-1.030926000
H	1.100952000	2.662502000	-0.872811000
H	1.791438000	2.326706000	-2.476224000
C	5.208187000	-1.827260000	2.418491000
H	5.702677000	-2.716846000	2.834083000
H	4.126762000	-1.940191000	2.589618000
H	5.547741000	-0.957538000	3.001688000
C	1.623760000	1.112895000	1.885982000
H	2.296933000	1.932345000	1.580534000
H	0.623131000	1.562033000	1.977778000
C	4.966249000	-0.084520000	-1.721408000
H	4.493750000	-0.998697000	-2.117523000
H	4.388094000	0.767931000	-2.112567000
C	6.426754000	0.003491000	-2.187395000
H	7.026362000	-0.838909000	-1.811200000
H	6.904003000	0.933919000	-1.846505000
H	6.485547000	-0.014552000	-3.284937000
C	2.071619000	0.502732000	3.215411000
H	1.383946000	-0.289025000	3.548205000
H	2.105456000	1.267653000	4.003976000

H	3.076693000	0.059096000	3.141725000
H	3.277505000	-0.277044000	0.413527000
C	5.241184000	1.457348000	1.055634000
H	4.869472000	2.311720000	0.466299000
H	4.679449000	1.462818000	2.004707000
C	6.744944000	1.598666000	1.329017000
H	7.119785000	0.770586000	1.949126000
H	6.958023000	2.535188000	1.863862000
H	7.330948000	1.608795000	0.398317000
C	1.377918000	-1.940504000	0.776913000
H	1.981302000	-2.195995000	1.663823000
H	0.329111000	-2.134254000	1.048274000
C	1.790671000	-2.784249000	-0.431566000
H	1.681323000	-3.856945000	-0.216735000
H	2.844041000	-2.610489000	-0.705935000
H	1.170360000	-2.555941000	-1.312297000

Silane Reduction IM1

Zero-point correction= 0.689656 (Hartree/Particle)

Thermal correction to Energy= 0.733473

Thermal correction to Enthalpy= 0.734417

Thermal correction to Gibbs Free Energy= 0.609524

Sum of electronic and zero-point Energies= -2448.254348

Sum of electronic and thermal Energies= -2448.210532

Sum of electronic and thermal Enthalpies= -2448.209587

Sum of electronic and thermal Free Energies= -2448.334480

36

Sb	-0.010799000	-0.007086000	-0.199906000
H	0.072532000	0.000045000	-1.932731000
Cl	-0.082155000	0.016534000	2.400764000
C	1.964047000	3.729145000	-1.272752000
C	2.028926000	-1.945407000	-1.304822000

C	0.732570000	1.997730000	-0.110512000
C	1.651765000	-2.380733000	1.046661000
C	-2.119590000	-0.374776000	-0.235479000
C	-2.711581000	-0.367232000	-1.504345000
C	1.381235000	-1.632948000	-0.103671000
C	2.566192000	-3.433108000	0.990227000
C	-2.903254000	-0.622722000	0.895862000
C	3.219229000	-3.737301000	-0.205038000
C	-4.270791000	-0.860758000	0.752934000
C	-4.080869000	-0.600462000	-1.640201000
C	2.951572000	-2.991759000	-1.352538000
C	0.512516000	2.871154000	0.958781000
C	1.739446000	4.601737000	-0.208269000
C	1.009865000	4.173617000	0.901875000
C	-4.861076000	-0.848568000	-0.511376000
C	1.451260000	2.431599000	-1.229980000
H	-0.038190000	2.532597000	1.836228000
H	2.132648000	5.619335000	-0.244091000
H	1.616127000	1.761133000	-2.077621000
H	1.816471000	-1.377013000	-2.213662000
H	1.152528000	-2.138658000	1.984394000
H	3.936793000	-4.559018000	-0.242095000
H	-2.446735000	-0.627228000	1.885182000
H	-2.109604000	-0.178921000	-2.396422000
H	-5.931635000	-1.033621000	-0.616724000
H	2.534386000	4.057894000	-2.143275000
H	0.828512000	4.856234000	1.734051000
H	3.457592000	-3.224836000	-2.291056000
H	2.770315000	-4.017092000	1.889490000
H	-4.877723000	-1.056429000	1.638766000
H	-4.535413000	-0.589351000	-2.632355000

Silane Reduction TS2

Zero-point correction= 0.282148 (Hartree/Particle)

Thermal correction to Energy= 0.300301

Thermal correction to Enthalpy= 0.301245

Thermal correction to Gibbs Free Energy= 0.233152

Sum of electronic and zero-point Energies= -1394.646894

Sum of electronic and thermal Energies= -1394.628741

Sum of electronic and thermal Enthalpies= -1394.627797

Sum of electronic and thermal Free Energies= -1394.695891

36

Sb	-0.002999000	-0.484287000	-0.417596000
H	-0.032542000	-0.642679000	-2.105282000
Cl	-0.068430000	-2.771207000	0.752553000
C	4.291203000	-0.140295000	-1.125161000
C	-2.953817000	-0.606491000	-1.239995000
C	2.134052000	-0.683502000	-0.169770000
C	-2.697204000	-0.666835000	1.166092000
C	0.029720000	1.649079000	0.010170000
C	1.152384000	2.263425000	0.578090000
C	-2.132017000	-0.627343000	-0.112461000
C	-4.083373000	-0.678793000	1.311274000
C	-1.101516000	2.428059000	-0.270468000
C	-4.908512000	-0.659071000	0.183009000
C	-1.100355000	3.799093000	-0.011338000
C	1.147683000	3.633262000	0.851865000
C	-4.345028000	-0.626263000	-1.090826000
C	2.764463000	-1.220789000	0.953772000
C	4.921605000	-0.671277000	0.000349000
C	4.158246000	-1.208104000	1.038464000
C	0.024350000	4.403266000	0.552579000
C	2.896912000	-0.139294000	-1.206716000

H	2.170687000	-1.662209000	1.755112000
H	6.011002000	-0.669134000	0.067946000
H	2.412965000	0.294723000	-2.087899000
H	-2.521072000	-0.572847000	-2.244302000
H	-2.059867000	-0.700217000	2.053054000
H	-5.993531000	-0.672547000	0.300595000
H	-1.998295000	1.970493000	-0.695514000
H	2.043985000	1.679325000	0.816642000
H	0.022741000	5.474428000	0.762659000
H	4.883300000	0.275879000	-1.942310000
H	4.649665000	-1.624717000	1.919763000
H	-4.985395000	-0.616369000	-1.974913000
H	-4.523453000	-0.707084000	2.309943000
H	-1.984061000	4.395352000	-0.246125000
H	2.027379000	4.097999000	1.301029000

Silane Reduction IM2

Zero-point correction= 0.282763 (Hartree/Particle)

Thermal correction to Energy= 0.301626

Thermal correction to Enthalpy= 0.302570

Thermal correction to Gibbs Free Energy= 0.232871

Sum of electronic and zero-point Energies= -1394.664262

Sum of electronic and thermal Energies= -1394.645398

Sum of electronic and thermal Enthalpies= -1394.644454

Sum of electronic and thermal Free Energies= -1394.714154

36

Sb	-0.023304000	-0.210798000	-0.837001000
H	0.005076000	0.131675000	-2.486685000
Cl	-0.227461000	-2.639661000	-1.794222000
C	3.922995000	-0.325791000	1.072829000
C	-2.276594000	-1.801034000	0.600666000

C	1.738450000	-0.862399000	0.180038000
C	-2.686664000	0.581265000	0.449325000
C	0.178975000	1.883568000	-0.302572000
C	0.246289000	2.300950000	1.035017000
C	-1.879024000	-0.529043000	0.175790000
C	-3.888252000	0.416477000	1.140675000
C	0.247211000	2.844213000	-1.315537000
C	-4.276113000	-0.849744000	1.577205000
C	0.380248000	4.201470000	-1.004058000
C	0.378132000	3.652691000	1.349956000
C	-3.468635000	-1.955702000	1.308788000
C	1.854556000	-2.163134000	0.680669000
C	4.031426000	-1.617912000	1.585637000
C	2.995921000	-2.533410000	1.392036000
C	0.445547000	4.604776000	0.328457000
C	2.773450000	0.058094000	0.379534000
H	1.065358000	-2.892734000	0.495952000
H	4.926843000	-1.913983000	2.135170000
H	2.695286000	1.078219000	-0.002172000
H	-1.668204000	-2.672611000	0.357814000
H	-2.390478000	1.580988000	0.125442000
H	-5.212115000	-0.976196000	2.124275000
H	0.197282000	2.539052000	-2.365781000
H	0.195110000	1.565329000	1.844215000
H	0.549371000	5.663151000	0.574912000
H	4.732783000	0.392097000	1.214076000
H	3.078181000	-3.546477000	1.789676000
H	-3.770108000	-2.949242000	1.645263000
H	-4.518952000	1.284541000	1.340037000
H	0.433157000	4.942172000	-1.804359000
H	0.429249000	3.966901000	2.394248000

Silane Reduction TS3

Zero-point correction= 0.280462 (Hartree/Particle)

Thermal correction to Energy= 0.299565

Thermal correction to Enthalpy= 0.300510

Thermal correction to Gibbs Free Energy= 0.228548

Sum of electronic and zero-point Energies= -1394.645431

Sum of electronic and thermal Energies= -1394.626328

Sum of electronic and thermal Enthalpies= -1394.625383

Sum of electronic and thermal Free Energies= -1394.697344

36

Sb	0.039751000	-0.000006000	0.661965000
H	-0.628328000	0.000088000	2.238262000
Cl	-2.651301000	0.000063000	2.624056000
C	4.367732000	0.000240000	1.306995000
C	0.114747000	2.479883000	-1.175332000
C	2.140402000	-0.000010000	0.359550000
C	-2.074433000	2.029782000	-0.227968000
C	-0.719805000	-1.699944000	-0.366444000
C	-2.074652000	-2.029354000	-0.228371000
C	-0.719755000	1.699893000	-0.366550000
C	-2.589200000	3.129199000	-0.916130000
C	0.114791000	-2.480407000	-1.174670000
C	-1.761081000	3.900025000	-1.732979000
C	-0.409601000	-3.578979000	-1.857419000
C	-2.589488000	-3.128756000	-0.916504000
C	-0.409576000	3.578469000	-1.858108000
C	2.691551000	-0.000207000	-0.930218000
C	4.913365000	0.000047000	0.023421000
C	4.076771000	-0.000177000	-1.094007000
C	-1.761270000	-3.900045000	-1.732817000

C	2.982588000	0.000213000	1.478216000
H	2.046370000	-0.000395000	-1.812877000
H	5.996747000	0.000068000	-0.108225000
H	2.565096000	0.000365000	2.487851000
H	1.176612000	2.246072000	-1.276763000
H	-2.715270000	1.446360000	0.439279000
H	-2.169006000	4.759107000	-2.268661000
H	1.176780000	-2.246974000	-1.275685000
H	-2.715580000	-1.445596000	0.438492000
H	-2.169250000	-4.759111000	-2.268483000
H	5.020763000	0.000410000	2.181314000
H	4.502647000	-0.000331000	-2.098721000
H	0.243870000	4.184983000	-2.487583000
H	-3.644329000	3.386291000	-0.807061000
H	0.243918000	-4.185862000	-2.486462000
H	-3.644749000	-3.385471000	-0.807834000

Silane Reduction Products

Zero-point correction= 0.280956 (Hartree/Particle)

Thermal correction to Energy= 0.301482

Thermal correction to Enthalpy= 0.302427

Thermal correction to Gibbs Free Energy= 0.223722

Sum of electronic and zero-point Energies= -1394.680059

Sum of electronic and thermal Energies= -1394.659533

Sum of electronic and thermal Enthalpies= -1394.658588

Sum of electronic and thermal Free Energies= -1394.737293

36

Sb	0.171699000	0.003390000	0.886815000
H	2.489454000	-0.048836000	2.645864000
Cl	3.758742000	0.192436000	2.550261000
C	-3.849389000	-1.750064000	1.352036000

C	-0.038162000	-1.962204000	-1.564316000
C	-1.943863000	-0.393795000	0.688432000
C	2.183861000	-1.762649000	-0.641391000
C	0.208551000	1.756703000	-0.375696000
C	0.563734000	1.715549000	-1.729505000
C	0.828498000	-1.406354000	-0.614052000
C	2.667307000	-2.648284000	-1.606882000
C	-0.144696000	2.987600000	0.195622000
C	1.796756000	-3.193502000	-2.551010000
C	-0.155597000	4.152467000	-0.573144000
C	0.559532000	2.882318000	-2.498197000
C	0.443706000	-2.850931000	-2.527582000
C	-2.779035000	0.328534000	-0.173149000
C	-4.673201000	-1.025150000	0.489648000
C	-4.136971000	0.014585000	-0.270772000
C	0.198176000	4.100642000	-1.922495000
C	-2.493991000	-1.431993000	1.453288000
H	-2.373938000	1.142846000	-0.779771000
H	-5.734192000	-1.269732000	0.411587000
H	-1.861857000	-2.005577000	2.137890000
H	-1.099971000	-1.701034000	-1.560226000
H	2.876839000	-1.348490000	0.097216000
H	2.172246000	-3.888160000	-3.304749000
H	-0.419904000	3.044564000	1.253209000
H	0.845449000	0.768577000	-2.197194000
H	0.194003000	5.010986000	-2.524864000
H	-4.263485000	-2.563651000	1.950891000
H	-4.777498000	0.585040000	-0.946366000
H	-0.241321000	-3.277087000	-3.263271000
H	3.725966000	-2.914764000	-1.618219000
H	-0.437134000	5.103260000	-0.116249000

H	0.838758000	2.836904000	-3.552751000

[Cp*SbFCl]

Zero-point correction= 0.225751 (Hartree/Particle)

Thermal correction to Energy= 0.242811

Thermal correction to Enthalpy= 0.243756

Thermal correction to Gibbs Free Energy= 0.181145

Sum of electronic and zero-point Energies= -1189.411952

Sum of electronic and thermal Energies= -1189.394892

Sum of electronic and thermal Enthalpies= -1189.393948

Sum of electronic and thermal Free Energies= -1189.456558

28

Sb	2.037192000	3.265200000	1.030724000
F	1.937727000	1.924117000	-0.364705000
C	4.146276000	4.427481000	2.014765000
C	4.288019000	3.265200000	1.149890000
C	3.851660000	3.980671000	3.301429000
C	3.600751000	4.834978000	4.505374000
H	2.832656000	4.483028000	5.001563000
H	3.412993000	5.753596000	4.220596000
H	4.393407000	4.827481000	5.082072000
C	4.356439000	5.849018000	1.572499000
H	3.948613000	5.980775000	0.691572000
H	5.316959000	6.035918000	1.519608000
H	3.940709000	6.456985000	2.219386000
C	4.973244000	3.265200000	-0.202295000
H	4.538305000	2.612382000	-0.789665000
C	4.146276000	2.102919000	2.014765000
C	3.851660000	2.549729000	3.301429000
C	3.600751000	1.695422000	4.505374000
H	2.832656000	2.047372000	5.001563000
H	3.412993000	0.776804000	4.220596000

H	4.393407000	1.702919000	5.082072000
C	4.356439000	0.681382000	1.572499000
H	3.948613000	0.549625000	0.691572000
H	5.316959000	0.494482000	1.519608000
H	3.940709000	0.073415000	2.219386000
H	5.917170000	3.505049000	-0.090189000
H	4.538305000	3.918018000	-0.789665000
Cl	2.157800802	5.003568952	-0.648539799

[Cp^*_2SbF]

Zero-point correction= 0.446490 (Hartree/Particle)

Thermal correction to Energy= 0.475175

Thermal correction to Enthalpy= 0.476119

Thermal correction to Gibbs Free Energy= 0.388985

Sum of electronic and zero-point Energies= -1118.720211

Sum of electronic and thermal Energies= -1118.691526

Sum of electronic and thermal Enthalpies= -1118.690582

Sum of electronic and thermal Free Energies= -1118.777715

52

Sb	0.037671000	-0.458970000	0.366884000
F	0.140419000	-2.442303000	0.216763000
C	-2.598753000	-0.899182000	0.472682000
C	2.798954000	2.695543000	1.210321000
H	2.292671000	2.648324000	2.187680000
H	2.420964000	3.582105000	0.684773000
H	3.870063000	2.851386000	1.412126000
C	1.804529000	-0.111630000	-1.106707000
C	-2.925571000	0.334076000	1.023749000
C	-1.951466000	-0.654682000	-0.819740000
C	-3.516768000	0.606229000	2.373387000
H	-3.712255000	-0.320403000	2.927644000

H	-4.469717000	1.151183000	2.284617000
H	-2.847552000	1.230789000	2.986340000
C	-2.045964000	0.788754000	-1.052055000
C	1.866800000	1.317884000	-0.764862000
C	-2.576741000	1.373265000	0.089614000
C	-1.792036000	1.420488000	-2.386313000
H	-1.743441000	2.515177000	-2.325651000
H	-2.608384000	1.160230000	-3.080614000
H	-0.858852000	1.067008000	-2.845413000
C	-1.904225000	-1.691212000	-1.914199000
H	-1.289156000	-1.354653000	-2.760988000
H	-2.917783000	-1.896506000	-2.295656000
H	-1.475629000	-2.630201000	-1.537432000
C	2.650059000	-0.793779000	-0.116337000
C	2.574770000	1.443783000	0.417131000
C	3.058250000	0.148051000	0.818813000
C	-2.864130000	-2.271221000	1.018282000
H	-1.974537000	-2.910525000	0.928008000
H	-3.679223000	-2.757717000	0.457825000
H	-3.161644000	-2.235926000	2.074470000
C	-2.791894000	2.833372000	0.354611000
H	-2.409620000	3.457004000	-0.464467000
H	-2.289173000	3.152001000	1.281020000
H	-3.862473000	3.062622000	0.476603000
C	1.240285000	2.438931000	-1.540272000
H	1.115952000	2.177213000	-2.600169000
H	1.874915000	3.334998000	-1.494979000
H	0.248838000	2.719771000	-1.148303000
C	1.634679000	-0.664416000	-2.501075000
H	1.325237000	-1.719312000	-2.470813000
H	2.585840000	-0.608752000	-3.054918000

H	0.881172000	-0.109645000	-3.077448000
C	3.881814000	-0.079546000	2.049599000
H	4.061125000	-1.146786000	2.230167000
H	3.389548000	0.336719000	2.941963000
H	4.862138000	0.416109000	1.964588000
C	3.065087000	-2.229906000	-0.223474000
H	3.539257000	-2.578044000	0.703385000
H	3.795846000	-2.355170000	-1.039493000
H	2.204818000	-2.879599000	-0.425746000

[Cp*SbF_2]

Zero-point correction= 0.226565 (Hartree/Particle)

Thermal correction to Energy= 0.243263

Thermal correction to Enthalpy= 0.244207

Thermal correction to Gibbs Free Energy= 0.182806

Sum of electronic and zero-point Energies= -829.082260

Sum of electronic and thermal Energies= -829.065562

Sum of electronic and thermal Enthalpies= -829.064618

Sum of electronic and thermal Free Energies= -829.126018

28

Sb	0.982764000	-0.000002000	-0.771047000
F	2.226349000	-1.383863000	-0.184883000
C	-0.877303000	1.175213000	0.718844000
C	-0.114569000	0.000006000	1.164138000
C	-1.964194000	0.719333000	-0.018718000
C	-2.990645000	1.543241000	-0.735864000
H	-3.037295000	1.288579000	-1.805898000
H	-2.782172000	2.617217000	-0.653150000
H	-3.994764000	1.364280000	-0.320682000
C	-0.491750000	2.581813000	1.066673000
H	0.580973000	2.748958000	0.889683000

H	-0.688229000	2.784899000	2.131534000
H	-1.057361000	3.313733000	0.476059000
C	0.843331000	0.000007000	2.329994000
H	1.492479000	-0.885866000	2.298673000
C	-0.877296000	-1.175210000	0.718843000
C	-1.964190000	-0.719337000	-0.018718000
C	-2.990639000	-1.543251000	-0.735859000
H	-3.037368000	-1.288513000	-1.805872000
H	-2.782100000	-2.617222000	-0.653236000
H	-3.994743000	-1.364378000	-0.320602000
C	-0.491744000	-2.581808000	1.066683000
H	0.580988000	-2.748943000	0.889740000
H	-0.688273000	-2.784903000	2.131532000
H	-1.057320000	-3.313729000	0.476037000
H	0.291507000	0.000003000	3.282771000
H	1.492474000	0.885885000	2.298677000
F	2.226342000	1.383870000	-0.184891000

[Cp*SbF]

Zero-point correction= 0.224021 (Hartree/Particle)

Thermal correction to Energy= 0.239674

Thermal correction to Enthalpy= 0.240619

Thermal correction to Gibbs Free Energy= 0.180619

Sum of electronic and zero-point Energies= -729.081495

Sum of electronic and thermal Energies= -729.065841

Sum of electronic and thermal Enthalpies= -729.064897

Sum of electronic and thermal Free Energies= -729.124897

27

F	-2.619683000	-0.070731000	-0.563292000
Sb	-0.697301000	-0.023491000	-0.964424000
C	0.916516000	-1.180576000	0.596748000

C	-0.193440000	-0.512851000	1.244119000
C	1.808770000	-0.183284000	0.081338000
C	1.264870000	1.085765000	0.351649000
C	-1.269878000	-1.135196000	2.075331000
H	-1.371361000	-2.206535000	1.863098000
H	-1.017956000	-1.016739000	3.140313000
H	-2.237002000	-0.647946000	1.895008000
C	1.163976000	-2.651256000	0.591729000
H	1.722335000	-2.958570000	-0.301443000
H	1.770682000	-2.914273000	1.473097000
H	0.229541000	-3.223477000	0.642833000
C	-0.002814000	0.907725000	1.054090000
C	3.077040000	-0.486658000	-0.651869000
H	3.458307000	0.397052000	-1.177782000
H	3.853835000	-0.824075000	0.051277000
H	2.930398000	-1.289976000	-1.387425000
C	1.855029000	2.418158000	0.030476000
H	1.090357000	3.120813000	-0.326706000
H	2.298879000	2.850299000	0.941239000
H	2.644887000	2.338842000	-0.725738000
C	-0.816059000	1.979754000	1.708945000
H	-1.880767000	1.712288000	1.731014000
H	-0.475421000	2.106523000	2.748306000
H	-0.701284000	2.940936000	1.192822000

[Cp*SbFCl]

Zero-point correction= 0.225751 (Hartree/Particle)

Thermal correction to Energy= 0.242811

Thermal correction to Enthalpy= 0.243756

Thermal correction to Gibbs Free Energy= 0.181145

Sum of electronic and zero-point Energies= -1189.411952

Sum of electronic and thermal Energies= -1189.394892

Sum of electronic and thermal Enthalpies= -1189.393948

Sum of electronic and thermal Free Energies= -1189.456558

C17SbH20Cl3F

Sb	-1.082528000	-0.687329000	-0.340375000
Cl	0.884676000	0.996062000	-1.023535000
F	0.123390000	-1.083995000	1.174412000
C	-2.918868000	-0.264735000	1.189645000
C	-2.245818000	0.944652000	0.716580000
C	-2.797615000	1.242331000	-0.602441000
C	-3.733618000	0.241002000	-0.920700000
C	-3.804386000	-0.685232000	0.161268000
C	-2.764682000	-0.834199000	2.566185000
C	-1.470717000	1.898083000	1.577179000
C	-2.437779000	2.456347000	-1.397345000
C	-4.516100000	0.102579000	-2.189594000
C	-4.688805000	-1.890441000	0.179786000
H	-3.151664000	-1.859609000	2.618625000
H	-3.323487000	-0.220840000	3.290194000
H	-1.710543000	-0.846231000	2.874469000
H	-0.970658000	1.367452000	2.398728000
H	-2.155930000	2.639058000	2.017980000
H	-0.711898000	2.438589000	0.993994000
H	-2.681979000	2.333437000	-2.459813000
H	-1.366417000	2.685788000	-1.312132000
H	-2.993628000	3.329194000	-1.018845000
H	-4.292648000	-0.846758000	-2.699678000
H	-4.306049000	0.922904000	-2.886855000
H	-5.596108000	0.108483000	-1.977576000
H	-4.434613000	-2.572539000	1.000626000
H	-4.628397000	-2.444596000	-0.767925000

H	-5.739282000	-1.585177000	0.309538000
C	2.836680000	0.985336000	0.393723000
Cl	3.491882000	2.448614000	-0.187486000
Cl	2.085592000	1.127525000	1.909951000
C	3.419187000	-0.275314000	-0.010009000
C	4.307681000	-0.326661000	-1.106697000
C	3.069655000	-1.460797000	0.673120000
C	4.854837000	-1.540039000	-1.489739000
C	3.626111000	-2.666828000	0.276992000
C	4.518068000	-2.708365000	-0.798691000
H	4.567581000	0.580236000	-1.652218000
H	2.349365000	-1.430813000	1.489613000
H	5.547816000	-1.579030000	-2.330340000
H	3.363697000	-3.582343000	0.807644000
H	4.953726000	-3.661220000	-1.104016000

$BnCl_3$ Exchange IM1

Zero-point correction= 0.325507 (Hartree/Particle)

Thermal correction to Energy= 0.352394

Thermal correction to Enthalpy= 0.353338

Thermal correction to Gibbs Free Energy= 0.265179

Sum of electronic and zero-point Energies= -2378.642752

Sum of electronic and thermal Energies= -2378.615865

Sum of electronic and thermal Enthalpies= -2378.614921

Sum of electronic and thermal Free Energies= -2378.703080

27

Cl	-2.929334000	-0.027308000	-0.331003000
Sb	-0.565351000	-0.010584000	-0.900236000
C	1.305177000	-1.148215000	0.440675000
C	0.163589000	-0.677910000	1.206228000
C	2.028252000	-0.020892000	-0.037484000

C	1.356828000	1.154986000	0.377689000
C	-0.730861000	-1.498025000	2.079192000
H	-0.799277000	-2.533839000	1.724110000
H	-0.317932000	-1.510153000	3.099832000
H	-1.741926000	-1.071910000	2.126191000
C	1.705967000	-2.573800000	0.269415000
H	2.277740000	-2.716839000	-0.656195000
H	2.352219000	-2.868358000	1.112119000
H	0.837721000	-3.244889000	0.264016000
C	0.186359000	0.769798000	1.156705000
C	3.259024000	-0.100439000	-0.884018000
H	3.589581000	0.895116000	-1.203695000
H	4.080706000	-0.564700000	-0.318562000
H	3.089904000	-0.714001000	-1.780904000
C	1.785054000	2.563514000	0.136923000
H	0.925669000	3.244769000	0.096970000
H	2.430681000	2.890972000	0.967570000
H	2.358901000	2.658421000	-0.792750000
C	-0.683883000	1.671143000	1.973522000
H	-1.717581000	1.301080000	2.008271000
H	-0.299129000	1.704433000	3.004527000
H	-0.688720000	2.692928000	1.574531000

$BnCl_3$

Zero-point correction= 0.101011 (Hartree/Particle)

Thermal correction to Energy= 0.110057

Thermal correction to Enthalpy= 0.111001

Thermal correction to Gibbs Free Energy= 0.064736

Sum of electronic and zero-point Energies= -1649.460192

Sum of electronic and thermal Energies= -1649.451146

Sum of electronic and thermal Enthalpies= -1649.450201

Sum of electronic and thermal Free Energies= -1649.496466

15

C	0.605835000	0.062739000	-0.000003000
C	1.287055000	-1.163237000	-0.000001000
C	1.327114000	1.255631000	-0.000004000
H	0.722438000	-2.097613000	0.000000000
H	0.812688000	2.215129000	-0.000005000
C	2.675669000	-1.189187000	0.000000000
C	2.724017000	1.222169000	-0.000002000
H	3.196834000	-2.147540000	0.000001000
H	3.280320000	2.160567000	-0.000002000
C	3.399777000	0.006504000	0.000000000
H	4.490728000	-0.014670000	0.000001000
C	-0.911976000	0.021535000	-0.000001000
Cl	-1.664600000	1.634392000	-0.000008000
Cl	-1.495585000	-0.858758000	-1.450775000
Cl	-1.495577000	-0.858740000	1.450787000

$BnCl_2F$

Zero-point correction= 0.102915 (Hartree/Particle)

Thermal correction to Energy= 0.111523

Thermal correction to Enthalpy= 0.112467

Thermal correction to Gibbs Free Energy= 0.067528

Sum of electronic and zero-point Energies= -1289.155619

Sum of electronic and thermal Energies= -1289.147011

Sum of electronic and thermal Enthalpies= -1289.146066

Sum of electronic and thermal Free Energies= -1289.191006

15

C	-0.472284000	-0.124289000	0.020861000
C	-1.306422000	-1.237253000	0.116875000
C	-1.010316000	1.161271000	-0.097229000

H	-0.880918000	-2.236416000	0.208012000
H	-0.347030000	2.025733000	-0.171428000
C	-2.691436000	-1.059630000	0.094867000
C	-2.389952000	1.328793000	-0.118417000
H	-3.346175000	-1.929086000	0.169687000
H	-2.811535000	2.330725000	-0.210203000
C	-3.232927000	0.217639000	-0.022317000
H	-4.315570000	0.352657000	-0.039301000
C	1.023010000	-0.314531000	0.036719000
Cl	1.775382000	0.582151000	1.391778000
F	1.347600000	-1.605037000	0.184946000
Cl	1.757253000	0.245480000	-1.498215000

$BnCl_3$ Exchange Product

Zero-point correction= 0.327364 (Hartree/Particle)

Thermal correction to Energy= 0.353482

Thermal correction to Enthalpy= 0.354426

Thermal correction to Gibbs Free Energy= 0.268792

Sum of electronic and zero-point Energies= -2378.673114

Sum of electronic and thermal Energies= -2378.646996

Sum of electronic and thermal Enthalpies= -2378.646052

Sum of electronic and thermal Free Energies= -2378.731686

42

C17SbH20Cl3F

Sb	1.458255000	-0.432515000	-0.923076000
Cl	0.500007000	-2.588160000	-0.349955000
F	-1.219015000	0.357421000	0.070509000
C	2.067759000	1.589913000	0.582573000
C	1.984111000	0.282303000	1.223377000
C	3.096071000	-0.507404000	0.731456000
C	3.803676000	0.310921000	-0.232443000

C	3.178188000	1.592312000	-0.290535000
C	1.134764000	2.715375000	0.879247000
C	1.101601000	-0.086811000	2.373384000
C	3.538110000	-1.822562000	1.286988000
C	5.050386000	-0.078605000	-0.951900000
C	3.623672000	2.702953000	-1.188103000
H	1.198259000	3.505960000	0.122466000
H	1.392215000	3.154851000	1.856145000
H	0.095667000	2.365184000	0.941272000
H	0.182524000	0.513195000	2.382848000
H	1.641087000	0.099251000	3.315324000
H	0.829414000	-1.151026000	2.341653000
H	4.141556000	-2.384696000	0.563208000
H	2.679798000	-2.437337000	1.587805000
H	4.155339000	-1.638754000	2.180393000
H	5.137829000	0.448065000	-1.910628000
H	5.100364000	-1.159737000	-1.131162000
H	5.921041000	0.200720000	-0.336770000
H	2.918768000	3.542497000	-1.169975000
H	3.724263000	2.358955000	-2.227890000
H	4.607910000	3.079062000	-0.870564000
C	-2.387971000	0.184260000	0.737646000
Cl	-2.253306000	-1.335494000	1.649996000
Cl	-2.512782000	1.548725000	1.892445000
C	-3.551785000	0.172350000	-0.217714000
C	-4.834290000	-0.119821000	0.257696000
C	-3.344151000	0.476411000	-1.563290000
C	-5.910003000	-0.111209000	-0.622864000
C	-4.430097000	0.479601000	-2.440175000
C	-5.708974000	0.187009000	-1.973243000
H	-4.987750000	-0.355282000	1.312931000

H	-2.344603000	0.710561000	-1.928980000
H	-6.910819000	-0.340465000	-0.254802000
H	-4.270503000	0.712466000	-3.493847000
H	-6.555233000	0.189798000	-2.661974000

$BnCl_3$ Exchange TS2

Zero-point correction= 0.324484 (Hartree/Particle)

Thermal correction to Energy= 0.350961

Thermal correction to Enthalpy= 0.351906

Thermal correction to Gibbs Free Energy= 0.264406

Sum of electronic and zero-point Energies= -2378.637306

Sum of electronic and thermal Energies= -2378.610828

Sum of electronic and thermal Enthalpies= -2378.609883

Sum of electronic and thermal Free Energies= -2378.697383

42

Sb	0.871489000	-0.610333000	-0.440635000
Cl	-0.303129000	-1.912803000	1.279985000
F	-0.715510000	0.749753000	-0.213457000
C	2.395335000	1.442048000	-0.266252000
C	2.145346000	0.646599000	0.933866000
C	3.012712000	-0.531768000	0.841898000
C	3.702264000	-0.455734000	-0.388258000
C	3.332113000	0.750637000	-1.056556000
C	1.772366000	2.778939000	-0.517793000
C	1.485755000	1.151980000	2.183391000
C	3.201787000	-1.523148000	1.946126000
C	4.669959000	-1.455422000	-0.937714000
C	3.849763000	1.148503000	-2.403205000
H	1.909506000	3.096604000	-1.558807000
H	2.230738000	3.539833000	0.133529000
H	0.695382000	2.757936000	-0.299857000

H	0.690533000	1.870521000	1.941349000
H	2.227370000	1.663462000	2.816868000
H	1.048644000	0.328580000	2.766622000
H	3.618960000	-2.468149000	1.575351000
H	2.254292000	-1.739991000	2.458285000
H	3.899610000	-1.114385000	2.694429000
H	4.460162000	-1.673769000	-1.994988000
H	4.645847000	-2.398631000	-0.377817000
H	5.697424000	-1.061355000	-0.887423000
H	3.371401000	2.065686000	-2.768695000
H	3.683159000	0.353780000	-3.146045000
H	4.935406000	1.326862000	-2.361489000
C	-2.524078000	1.081824000	0.509757000
Cl	-2.161610000	0.894904000	2.148343000
Cl	-2.575871000	2.692426000	-0.020149000
C	-3.228679000	0.053383000	-0.212145000
C	-3.532488000	-1.176244000	0.410730000
C	-3.567869000	0.263817000	-1.567969000
C	-4.183407000	-2.165887000	-0.310498000
C	-4.207997000	-0.737454000	-2.277300000
C	-4.518465000	-1.949299000	-1.649151000
H	-3.266000000	-1.351513000	1.452312000
H	-3.318695000	1.204303000	-2.059586000
H	-4.429506000	-3.111657000	0.172265000
H	-4.468876000	-0.578922000	-3.323737000
H	-5.027843000	-2.733581000	-2.211686000

$BnCl_3$ TS1

Zero-point correction= 0.325946 (Hartree/Particle)

Thermal correction to Energy= 0.351498

Thermal correction to Enthalpy= 0.352442

Thermal correction to Gibbs Free Energy= 0.268120

Sum of electronic and zero-point Energies= -2378.648774

Sum of electronic and thermal Energies= -2378.623222

Sum of electronic and thermal Enthalpies= -2378.622278

Sum of electronic and thermal Free Energies= -2378.706600

42

Sb	-0.895029000	0.658677000	-0.478376000
Cl	0.476858000	1.634610000	1.331343000
F	0.596233000	-0.638340000	-0.745178000
C	-2.503559000	-1.346663000	-0.463404000
C	-2.067772000	-0.751437000	0.807739000
C	-2.990033000	0.361644000	1.076731000
C	-3.859710000	0.467226000	-0.010761000
C	-3.564023000	-0.575737000	-0.951476000
C	-1.917310000	-2.600227000	-1.037397000
C	-1.271025000	-1.479828000	1.855250000
C	-2.989332000	1.149415000	2.349113000
C	-4.928282000	1.493854000	-0.225707000
C	-4.293600000	-0.749589000	-2.246725000
H	-2.244212000	-2.756995000	-2.073230000
H	-2.232643000	-3.475514000	-0.447029000
H	-0.818627000	-2.567660000	-1.023300000
H	-0.466533000	-2.071783000	1.395242000
H	-1.922909000	-2.168042000	2.416352000
H	-0.818950000	-0.776409000	2.569092000
H	-3.576801000	2.071465000	2.253119000
H	-1.968533000	1.421820000	2.653926000
H	-3.427175000	0.551928000	3.165159000
H	-4.771834000	2.045155000	-1.165648000
H	-4.964896000	2.221887000	0.594449000
H	-5.917590000	1.015490000	-0.296663000

H	-3.857911000	-1.550047000	-2.858040000
H	-4.284154000	0.178774000	-2.838022000
H	-5.350334000	-1.000942000	-2.064567000
C	2.841160000	-1.155400000	0.520977000
Cl	2.420519000	-1.085371000	2.140669000
Cl	2.648920000	-2.658765000	-0.199420000
C	3.355229000	-0.043471000	-0.170591000
C	3.624931000	1.171151000	0.523599000
C	3.567444000	-0.117907000	-1.578420000
C	4.100647000	2.264378000	-0.172564000
C	4.032283000	0.987657000	-2.256323000
C	4.300881000	2.174193000	-1.555234000
H	3.466455000	1.237470000	1.599113000
H	3.343823000	-1.036713000	-2.119890000
H	4.316299000	3.193397000	0.354446000
H	4.189707000	0.941490000	-3.333562000
H	4.672579000	3.044165000	-2.100084000

$BnCl_3$ Exchange Starting Point

Zero-point correction= 0.326167 (Hartree/Particle)

Thermal correction to Energy= 0.352511

Thermal correction to Enthalpy= 0.353455

Thermal correction to Gibbs Free Energy= 0.267318

Sum of electronic and zero-point Energies= -2378.649006

Sum of electronic and thermal Energies= -2378.622662

Sum of electronic and thermal Enthalpies= -2378.621718

Sum of electronic and thermal Free Energies= -2378.707855

42

Sb	-0.980733000	-0.635098000	0.178002000
Cl	1.840197000	1.788411000	-0.787629000
F	-0.592710000	-1.175974000	2.031901000

C	-2.841251000	0.495855000	0.984914000
C	-1.893581000	1.506603000	0.567267000
C	-1.960939000	1.585352000	-0.890394000
C	-2.848031000	0.603957000	-1.349151000
C	-3.381295000	-0.103626000	-0.213210000
C	-3.261419000	0.209448000	2.390500000
C	-1.195270000	2.466183000	1.480217000
C	-1.228172000	2.573801000	-1.740216000
C	-3.191244000	0.306283000	-2.773622000
C	-4.454829000	-1.138593000	-0.266520000
H	-3.642997000	-0.814276000	2.491052000
H	-4.066857000	0.904931000	2.672841000
H	-2.428662000	0.342762000	3.091054000
H	-1.005653000	2.009424000	2.460436000
H	-1.828624000	3.353655000	1.632756000
H	-0.236291000	2.796109000	1.061259000
H	-0.612192000	2.082326000	-2.507461000
H	-0.589727000	3.231472000	-1.137245000
H	-1.956085000	3.210346000	-2.266100000
H	-3.122192000	-0.770163000	-2.986556000
H	-2.524480000	0.839276000	-3.462811000
H	-4.224804000	0.616745000	-2.991401000
H	-4.436965000	-1.792782000	0.613948000
H	-4.372721000	-1.751156000	-1.173318000
H	-5.434036000	-0.634066000	-0.292184000
C	2.918048000	0.610560000	0.053092000
Cl	4.559154000	0.778895000	-0.628502000
Cl	2.961263000	1.062415000	1.770350000
C	2.397371000	-0.795388000	-0.190709000
C	2.185650000	-1.190708000	-1.522890000
C	2.127157000	-1.685026000	0.849642000

C	1.673258000	-2.450904000	-1.801056000
C	1.607781000	-2.952476000	0.560557000
C	1.372343000	-3.333810000	-0.756731000
H	2.414383000	-0.502760000	-2.339075000
H	2.286495000	-1.396870000	1.887181000
H	1.505813000	-2.747987000	-2.837156000
H	1.379962000	-3.632365000	1.382270000
H	0.963518000	-4.321186000	-0.976561000

[Bn_5Sb_2]

Zero-point correction= 0.598623 (Hartree/Particle)

Thermal correction to Energy= 0.634138

Thermal correction to Enthalpy= 0.635082

Thermal correction to Gibbs Free Energy= 0.525975

Sum of electronic and zero-point Energies= -1832.776929

Sum of electronic and thermal Energies= -1832.741413

Sum of electronic and thermal Enthalpies= -1832.740469

Sum of electronic and thermal Free Energies= -1832.849576

72

Sb	0.184353000	0.303408000	0.055451000
Sb	-0.909835000	-1.193013000	-2.111196000
C	-0.341027000	2.370404000	-0.285156000
H	0.169373000	2.950656000	0.497045000
H	0.123347000	2.632953000	-1.247318000
C	-2.967196000	-2.761556000	0.818929000
H	-2.748295000	-3.673036000	0.257814000
C	-0.345206000	-0.049126000	2.131824000
H	-1.188459000	0.632426000	2.308968000
H	-0.711613000	-1.080427000	2.228697000
C	-3.497204000	-0.411645000	0.879789000
H	-3.668665000	0.534027000	0.361387000
C	-0.129781000	-3.085051000	-1.322728000
H	-0.758702000	-3.380973000	-0.474445000
H	-0.276441000	-3.811588000	-2.136015000
C	1.687144000	-0.763586000	3.437023000
H	1.419244000	-1.804678000	3.243867000
C	1.311356000	-2.999615000	-0.919677000
C	-3.142126000	-2.835922000	2.201326000
H	-3.025130000	-3.794460000	2.709240000

C	-2.574378000	2.367948000	-1.448607000
H	-2.063959000	2.080879000	-2.373511000
C	-3.129865000	-1.544578000	0.139484000
C	-1.824458000	2.583757000	-0.283196000
C	2.330057000	-2.897784000	-1.878015000
H	2.074071000	-2.896480000	-2.941224000
C	-2.957660000	-1.437393000	-1.344203000
H	-3.528138000	-0.589854000	-1.747818000
H	-3.299423000	-2.349663000	-1.858389000
C	0.850271000	0.259819000	2.976409000
C	1.666368000	-3.011256000	0.436996000
H	0.881018000	-3.113576000	1.192479000
C	-3.499121000	-1.699224000	2.927713000
H	-3.652310000	-1.762506000	4.005608000
C	-2.490848000	2.993784000	0.878789000
H	-1.919155000	3.189314000	1.789936000
C	1.193396000	1.590027000	3.259158000
H	0.537077000	2.399982000	2.928478000
C	2.727067000	1.536662000	-0.939261000
C	3.032314000	2.783224000	-0.379453000
H	3.049739000	2.893395000	0.708485000
C	-3.687356000	-0.489886000	2.258266000
H	-3.994620000	0.401733000	2.808786000
C	2.344617000	0.380275000	-0.067669000
H	2.701569000	0.482877000	0.967754000
H	2.680221000	-0.582771000	-0.470039000
C	2.846216000	-0.464792000	4.151684000
H	3.483703000	-1.272979000	4.513477000
C	4.010386000	-2.852068000	-0.137364000
H	5.057145000	-2.805434000	0.164222000
C	2.353171000	1.889871000	3.971064000

H	2.602074000	2.929058000	4.190615000
C	3.187391000	0.862202000	4.412974000
H	4.094218000	1.095087000	4.971894000
C	-3.872445000	3.185990000	0.876654000
H	-4.374256000	3.520611000	1.785750000
C	2.721365000	1.401399000	-2.334115000
H	2.502853000	0.426215000	-2.780070000
C	3.301791000	3.733419000	-2.585699000
H	3.526846000	4.587458000	-3.225351000
C	3.005246000	-2.941115000	0.825345000
H	3.266816000	-2.968374000	1.884336000
C	3.668071000	-2.828754000	-1.490607000
H	4.448733000	-2.764614000	-2.249931000
C	3.320298000	3.874092000	-1.197868000
H	3.564583000	4.838412000	-0.750329000
C	-4.609326000	2.964839000	-0.286843000
H	-5.688534000	3.120624000	-0.290476000
C	-3.955543000	2.557399000	-1.451234000
H	-4.523313000	2.402297000	-2.370030000
C	3.005889000	2.493099000	-3.152422000
H	3.004719000	2.374059000	-4.236739000

Chapter 6

Me_2SbCl

Zero-point correction= 0.073532 (Hartree/Particle)

Thermal correction to Energy= 0.080861

Thermal correction to Enthalpy= 0.081805

Thermal correction to Gibbs Free Energy= 0.040560

Sum of electronic and zero-point Energies= -779.883213

Sum of electronic and thermal Energies= -779.875884

Sum of electronic and thermal Enthalpies= -779.874940

Sum of electronic and thermal Free Energies= -779.916185

10

Sb	-0.322704000	0.000000000	-0.440254000
C	-0.913684000	-1.578204000	0.912003000
H	-0.461562000	-1.393327000	1.894902000
H	-2.009174000	-1.592259000	1.005140000
H	-0.574556000	-2.550264000	0.532599000
C	-0.913694000	1.578198000	0.912005000
H	-2.009184000	1.592230000	1.005159000
H	-0.461554000	1.393333000	1.894897000
H	-0.574593000	2.550265000	0.532594000
Cl	1.971341000	0.000003000	0.273152000

Me_3Sb

Zero-point correction= 0.108577 (Hartree/Particle)

Thermal correction to Energy= 0.116571

Thermal correction to Enthalpy= 0.117515

Thermal correction to Gibbs Free Energy= 0.075783

Sum of electronic and zero-point Energies= -359.615028

Sum of electronic and thermal Energies= -359.607035

Sum of electronic and thermal Enthalpies= -359.606090

Sum of electronic and thermal Free Energies= -359.647823

13

Sb	-0.000018000	-0.000114000	-0.422142000
C	-1.732853000	-0.624355000	0.731788000
H	-1.518287000	-0.546996000	1.806611000
H	-2.595024000	0.011762000	0.490057000
H	-1.991364000	-1.664118000	0.490157000
C	0.325477000	1.812941000	0.731381000
H	-0.445447000	2.556908000	0.489388000
H	0.284629000	1.588587000	1.806181000
H	1.307730000	2.241331000	0.490157000
C	1.407468000	-1.188009000	0.731792000
H	1.233902000	-1.039922000	1.806584000
H	1.287059000	-2.252911000	0.491048000
H	2.437150000	-0.892315000	0.489294000

$MeSbCl_2$

Zero-point correction= 0.038501 (Hartree/Particle)

Thermal correction to Energy= 0.045110

Thermal correction to Enthalpy= 0.046054

Thermal correction to Gibbs Free Energy= 0.005591

Sum of electronic and zero-point Energies= -1200.147312

Sum of electronic and thermal Energies= -1200.140702

Sum of electronic and thermal Enthalpies= -1200.139758

Sum of electronic and thermal Free Energies= -1200.180221

7

Sb	0.000002000	0.338942000	-0.472219000
C	-0.000042000	1.653013000	1.227704000
H	0.000046000	1.035024000	2.134139000
H	0.898753000	2.283829000	1.207922000
H	-0.898966000	2.283648000	1.207979000
Cl	1.812501000	-0.964884000	0.357857000

Cl -1.812482000 -0.964916000 0.357843000

$SbCl_3$

Zero-point correction= 0.003493 (Hartree/Particle)

Thermal correction to Energy= 0.009353

Thermal correction to Enthalpy= 0.010298

Thermal correction to Gibbs Free Energy= -0.029221

Sum of electronic and zero-point Energies= -1620.406835

Sum of electronic and thermal Energies= -1620.400974

Sum of electronic and thermal Enthalpies= -1620.400030

Sum of electronic and thermal Free Energies= -1620.439549

4

Cl 0.587126000 -1.025448000 1.775447000

Sb -0.587126000 0.000199000 0.000000000

Cl 0.587126000 2.050299000 0.000000000

Cl 0.587126000 -1.025448000 -1.775447000

$(p\text{-tol})_2SbCl$

Zero-point correction= 0.237745 (Hartree/Particle)

Thermal correction to Energy= 0.254889

Thermal correction to Enthalpy= 0.255833

Thermal correction to Gibbs Free Energy= 0.186709

Sum of electronic and zero-point Energies= -1241.296399

Sum of electronic and thermal Energies= -1241.279255

Sum of electronic and thermal Enthalpies= -1241.278311

Sum of electronic and thermal Free Energies= -1241.347435

30

Sb 0.015390000 -1.511420000 -0.617889000

C 1.590301000 -0.114037000 -0.191895000

C 1.529276000 0.738003000 0.919760000

C 2.553633000 1.644585000 1.165083000

C 3.663717000 1.733302000 0.310679000

C	3.718104000	0.882863000	-0.795230000
C	2.695434000	-0.036432000	-1.042195000
C	4.766992000	2.716502000	0.599066000
H	2.495766000	2.301928000	2.036248000
H	4.573885000	0.935199000	-1.472100000
H	2.774388000	-0.694890000	-1.912084000
H	5.295165000	2.448087000	1.526309000
H	4.364980000	3.730960000	0.733934000
H	5.502688000	2.743011000	-0.214907000
C	-1.557493000	-0.076044000	-0.286127000
C	-1.558063000	1.105374000	-1.035928000
C	-2.603244000	-0.304993000	0.612707000
C	-2.584621000	2.036623000	-0.889942000
C	-3.626169000	0.631574000	0.754668000
H	-2.612157000	-1.212629000	1.220761000
C	-3.634371000	1.815478000	0.008584000
H	-2.568182000	2.954989000	-1.481590000
H	-4.435709000	0.439230000	1.463076000
C	-4.726462000	2.835911000	0.193682000
H	-4.834639000	3.470833000	-0.695573000
H	-4.503216000	3.493893000	1.047874000
H	-5.692238000	2.352491000	0.394177000
Cl	-0.143327000	-2.443550000	1.592147000
H	0.674153000	0.686358000	1.599207000
H	-0.745402000	1.321031000	-1.736940000

(p-tol)$SbCl_2$

Zero-point correction= 0.120611 (Hartree/Particle)

Thermal correction to Energy= 0.132130

Thermal correction to Enthalpy= 0.133074

Thermal correction to Gibbs Free Energy= 0.077952

Sum of electronic and zero-point Energies= -1430.853162

Sum of electronic and thermal Energies= -1430.841643

Sum of electronic and thermal Enthalpies= -1430.840699

Sum of electronic and thermal Free Energies= -1430.895821

17

Sb	1.361429000	-0.320306000	-0.537751000
Cl	1.831062000	1.978903000	-0.125148000
Cl	1.825696000	-1.074433000	1.674174000
C	-0.744293000	-0.127496000	-0.234975000
C	-1.620161000	-0.777941000	-1.106193000
C	-3.000957000	-0.674135000	-0.923543000
C	-3.528279000	0.078109000	0.128064000
C	-2.637757000	0.728249000	0.997432000
C	-1.263380000	0.630565000	0.822704000
C	-5.014006000	0.199909000	0.336628000
H	-1.241103000	-1.375345000	-1.941002000
H	-3.677598000	-1.186387000	-1.610896000
H	-3.035564000	1.321239000	1.824523000
H	-0.585896000	1.147509000	1.506919000
H	-5.300831000	-0.175713000	1.329724000
H	-5.572796000	-0.366876000	-0.418759000
H	-5.330969000	1.251634000	0.280631000

$(p\text{-tol})_3Sb$

Zero-point correction= 0.355028 (Hartree/Particle)

Thermal correction to Energy= 0.377702

Thermal correction to Enthalpy= 0.378647

Thermal correction to Gibbs Free Energy= 0.297346

Sum of electronic and zero-point Energies= -1051.736321

Sum of electronic and thermal Energies= -1051.713646

Sum of electronic and thermal Enthalpies= -1051.712702

Sum of electronic and thermal Free Energies= -1051.794003

43

Sb	0.000000000	0.000000000	1.581051000
C	-0.400698000	1.803597000	0.457535000
C	-1.199519000	1.823331000	-0.691458000
C	-1.393167000	3.008364000	-1.401413000
C	-0.798807000	4.206075000	-0.989522000
C	0.000000000	4.182827000	0.159206000
C	0.190931000	3.002208000	0.875192000
C	-1.035741000	5.488997000	-1.742249000
H	-2.017157000	3.001133000	-2.298629000
H	0.478861000	5.104464000	0.499092000
H	0.819416000	3.024891000	1.770517000
H	-1.231526000	5.296579000	-2.805654000
H	-0.171293000	6.162180000	-1.665007000
H	-1.908683000	6.023387000	-1.336026000
C	-1.361612000	-1.248813000	0.457535000
C	1.762310000	-0.554784000	0.457535000
C	-0.979292000	-1.950480000	-0.691458000
C	-2.695454000	-1.335753000	0.875192000
C	2.178811000	0.127148000	-0.691458000
C	2.504523000	-1.666455000	0.875192000
C	-1.908736000	-2.710700000	-1.401413000
C	-3.622435000	-2.091414000	0.159206000
H	-3.029340000	-0.802811000	1.770517000
C	3.301903000	-0.297664000	-1.401413000
C	3.622435000	-2.091414000	0.159206000
H	2.209925000	-2.222080000	1.770517000
C	-3.243164000	-2.794824000	-0.989522000
H	-1.590479000	-3.247475000	-2.298629000
H	-4.660026000	-2.137526000	0.499092000

C	4.041971000	-1.411250000	-0.989522000
H	3.607636000	0.246343000	-2.298629000
H	4.181165000	-2.966938000	0.499092000
C	-4.235741000	-3.641476000	-1.742249000
C	5.271481000	-1.847521000	-1.742249000
H	-3.971209000	-3.714823000	-2.805654000
H	-5.250958000	-3.229434000	-1.665007000
H	-4.262065000	-4.664662000	-1.336026000
H	5.202735000	-1.581756000	-2.805654000
H	5.422251000	-2.932746000	-1.665007000
H	6.170748000	-1.358726000	-1.336026000
H	1.620508000	0.997549000	-1.045912000
H	-1.674157000	0.904626000	-1.045912000
H	0.053649000	-1.902176000	-1.045912000

Adduct 1 Starting Point

Zero-point correction= 0.112375 (Hartree/Particle)

Thermal correction to Energy= 0.128376

Thermal correction to Enthalpy= 0.129320

Thermal correction to Gibbs Free Energy= 0.063846

Sum of electronic and zero-point Energies= -1980.043497

Sum of electronic and thermal Energies= -1980.027497

Sum of electronic and thermal Enthalpies= -1980.026552

Sum of electronic and thermal Free Energies= -1980.092026

17

Sb	2.124403000	0.015879000	0.301341000
C	2.798716000	1.793038000	-0.747861000
H	3.558017000	1.529273000	-1.498241000
H	1.950847000	2.282384000	-1.247338000
H	3.235274000	2.500975000	-0.028551000
C	1.987829000	-1.220613000	-1.475839000

H	1.099367000	-0.940286000	-2.057974000
H	2.887435000	-1.092138000	-2.095416000
H	1.896597000	-2.277210000	-1.185445000
C	4.138078000	-0.645220000	0.790509000
H	4.786502000	-0.597943000	-0.096462000
H	4.562130000	-0.007309000	1.579349000
H	4.111513000	-1.680481000	1.160248000
Cl	-0.860861000	1.205485000	-1.463605000
Sb	-2.453274000	-0.014210000	-0.164529000
Cl	-1.182950000	-2.022861000	-0.057058000
Cl	-1.771659000	0.854694000	1.937815000

Adduct 1 TS1

Zero-point correction= 0.111941 (Hartree/Particle)

Thermal correction to Energy= 0.127494

Thermal correction to Enthalpy= 0.128438

Thermal correction to Gibbs Free Energy= 0.063141

Sum of electronic and zero-point Energies= -1980.025174

Sum of electronic and thermal Energies= -1980.009621

Sum of electronic and thermal Enthalpies= -1980.008677

Sum of electronic and thermal Free Energies= -1980.073975

17

Sb	-1.568604000	-0.000210000	-0.115167000
C	-2.798719000	1.635022000	-0.800712000
H	-3.834308000	1.500771000	-0.457577000
H	-2.399749000	2.577399000	-0.400274000
H	-2.779919000	1.680981000	-1.898262000
C	-2.209538000	-0.000564000	1.942273000
H	-1.812768000	0.892246000	2.444942000
H	-3.307051000	0.000099000	2.003625000
H	-1.813888000	-0.894237000	2.444291000

C	-2.800181000	-1.633977000	-0.801611000
H	-3.835672000	-1.498905000	-0.458499000
H	-2.781332000	-1.679425000	-1.899180000
H	-2.402152000	-2.576932000	-0.401594000
Cl	0.955789000	2.004563000	1.130560000
Sb	1.882304000	0.000168000	0.064846000
Cl	0.956770000	-2.004231000	1.131234000
Cl	1.370898000	-0.000492000	-2.311843000

Adduct 1 Product

Zero-point correction= 0.113775 (Hartree/Particle)

Thermal correction to Energy= 0.129506

Thermal correction to Enthalpy= 0.130451

Thermal correction to Gibbs Free Energy= 0.067725

Sum of electronic and zero-point Energies= -1980.048519

Sum of electronic and thermal Energies= -1980.032787

Sum of electronic and thermal Enthalpies= -1980.031843

Sum of electronic and thermal Free Energies= -1980.094569

17

Sb	1.385125000	-0.165474000	0.060630000
C	2.645412000	0.690444000	-1.416812000
H	3.664375000	0.772389000	-1.016120000
H	2.643616000	0.053996000	-2.310760000
H	2.247602000	1.684275000	-1.656757000
C	2.041869000	-2.162712000	0.358539000
H	1.935876000	-2.720267000	-0.580141000
H	3.091799000	-2.151038000	0.680676000
H	1.409391000	-2.625522000	1.126213000
C	1.771136000	0.867604000	1.870988000
H	2.856112000	0.915054000	2.033842000
H	1.347101000	1.874319000	1.771359000

H	1.283612000	0.334459000	2.696323000
Cl	-1.369183000	-2.418708000	-0.422380000
Sb	-1.355285000	0.129486000	-0.527031000
Cl	-1.797239000	0.267630000	1.840485000
Cl	-0.407215000	2.582001000	-0.467191000

Adduct 2 Starting Point

Zero-point correction= 0.112619 (Hartree/Particle)

Thermal correction to Energy= 0.128704

Thermal correction to Enthalpy= 0.129648

Thermal correction to Gibbs Free Energy= 0.063471

Sum of electronic and zero-point Energies= -1980.049116

Sum of electronic and thermal Energies= -1980.033031

Sum of electronic and thermal Enthalpies= -1980.032087

Sum of electronic and thermal Free Energies= -1980.098265

17

Sb	1.936693000	-0.026583000	-0.204274000
C	2.105531000	-0.519566000	1.885854000
H	1.919320000	-1.593233000	2.025482000
H	3.110763000	-0.269764000	2.253632000
H	1.353366000	0.045194000	2.453441000
C	2.903034000	1.899266000	-0.123548000
H	2.230945000	2.620241000	0.361712000
H	3.837866000	1.827608000	0.449819000
H	3.125497000	2.249778000	-1.140820000
C	3.633668000	-1.167370000	-0.894252000
H	3.852930000	-0.919315000	-1.941792000
H	4.511737000	-0.937354000	-0.274410000
H	3.410789000	-2.240894000	-0.823793000
Cl	-1.157920000	-1.858468000	0.899566000
Sb	-1.496701000	-0.002515000	-0.572138000

Cl	-0.958712000	1.700899000	1.036110000
Cl	-3.862558000	0.123908000	-0.110652000

Adduct 2 TS1

Zero-point correction= 0.112868 (Hartree/Particle)

Thermal correction to Energy= 0.128114

Thermal correction to Enthalpy= 0.129058

Thermal correction to Gibbs Free Energy= 0.064551

Sum of electronic and zero-point Energies= -1980.038337

Sum of electronic and thermal Energies= -1980.023092

Sum of electronic and thermal Enthalpies= -1980.022147

Sum of electronic and thermal Free Energies= -1980.086654

17

Sb	1.599085000	-0.000496000	-0.014497000
C	1.705549000	0.010045000	-2.142858000
H	1.194851000	0.907740000	-2.514659000
H	2.756838000	0.012995000	-2.460879000
H	1.197418000	-0.885285000	-2.523824000
C	2.799564000	-1.684369000	0.522641000
H	2.242003000	-2.598210000	0.281381000
H	3.741351000	-1.656869000	-0.042287000
H	3.011734000	-1.656372000	1.599423000
C	2.803592000	1.675080000	0.539719000
H	3.013860000	1.636734000	1.616545000
H	3.746214000	1.649706000	-0.023919000
H	2.249423000	2.592863000	0.305726000
Cl	-0.833379000	2.264476000	-0.308925000
Sb	-1.281534000	-0.000040000	0.684497000
Cl	-0.836963000	-2.264913000	-0.308876000
Cl	-3.223835000	0.001584000	-0.789524000

Adduct 2 Product

Zero-point correction= 0.113775 (Hartree/Particle)

Thermal correction to Energy= 0.129506

Thermal correction to Enthalpy= 0.130451

Thermal correction to Gibbs Free Energy= 0.067725

Sum of electronic and zero-point Energies= -1980.048519

Sum of electronic and thermal Energies= -1980.032787

Sum of electronic and thermal Enthalpies= -1980.031843

Sum of electronic and thermal Free Energies= -1980.094569

17

Sb	1.385127000	-0.165478000	0.060631000
C	1.771139000	0.867602000	1.870988000
H	1.283599000	0.334466000	2.696319000
H	2.856113000	0.915039000	2.033852000
H	1.347116000	1.874322000	1.771350000
C	2.645407000	0.690440000	-1.416818000
H	2.247584000	1.684266000	-1.656767000
H	3.664370000	0.772399000	-1.016128000
H	2.643616000	0.053987000	-2.310762000
C	2.041862000	-2.162719000	0.358542000
H	1.935904000	-2.720264000	-0.580147000
H	3.091781000	-2.151049000	0.680717000
H	1.409356000	-2.625537000	1.126188000
Cl	-1.369197000	-2.418705000	-0.422388000
Sb	-1.355283000	0.129490000	-0.527029000
Cl	-0.407207000	2.582003000	-0.467193000
Cl	-1.797239000	0.267632000	1.840487000

Cyclic Mechanism Starting Point

Zero-point correction= 0.112897 (Hartree/Particle)

Thermal correction to Energy= 0.128533

Thermal correction to Enthalpy= 0.129477

Thermal correction to Gibbs Free Energy= 0.065116

Sum of electronic and zero-point Energies= -1980.042615

Sum of electronic and thermal Energies= -1980.026979

Sum of electronic and thermal Enthalpies= -1980.026035

Sum of electronic and thermal Free Energies= -1980.090396

17

Sb	-2.427818000	0.084486000	0.351977000
C	-3.077847000	-1.919440000	-0.165010000
H	-3.468128000	-1.941751000	-1.192806000
H	-2.229686000	-2.614162000	-0.084922000
H	-3.865940000	-2.248128000	0.527268000
C	-1.389179000	0.375576000	-1.544112000
H	-0.757347000	-0.502885000	-1.747625000
H	-2.119356000	0.459106000	-2.362557000
H	-0.779543000	1.291237000	-1.526663000
C	-4.263353000	1.037766000	-0.311856000
H	-4.586713000	0.625884000	-1.278662000
H	-5.056422000	0.873743000	0.431769000
H	-4.105498000	2.120909000	-0.415394000
Cl	1.144512000	1.821794000	0.742990000
Sb	2.001634000	0.051804000	-0.596756000
Cl	0.794845000	-1.690678000	0.507195000
Cl	4.006897000	-0.247478000	0.647416000

Cyclic Mechanism TS1

Zero-point correction= 0.111882 (Hartree/Particle)

Thermal correction to Energy= 0.126785

Thermal correction to Enthalpy= 0.127729

Thermal correction to Gibbs Free Energy= 0.067128

Sum of electronic and zero-point Energies= -1979.992684

Sum of electronic and thermal Energies= -1979.977781

Sum of electronic and thermal Enthalpies= -1979.976837

Sum of electronic and thermal Free Energies= -1980.037438

17

Sb	1.723918000	0.151732000	-0.407601000
C	3.094426000	-1.223168000	0.515069000
H	3.473962000	-0.845383000	1.473970000
H	2.587284000	-2.187365000	0.650118000
H	3.936607000	-1.354684000	-0.181715000
C	0.306190000	0.347391000	1.631890000
H	-0.347664000	-0.044883000	2.434642000
H	1.220875000	-0.201524000	1.924656000
H	0.398073000	1.427362000	1.787371000
C	2.692643000	1.928616000	0.321240000
H	3.004539000	1.819713000	1.368772000
H	3.582588000	2.099359000	-0.304601000
H	2.015482000	2.786850000	0.212969000
Cl	-1.711382000	2.305070000	0.226907000
Sb	-1.649524000	-0.213851000	0.406695000
Cl	-0.377461000	-2.459498000	0.353039000
Cl	-1.453827000	-0.236658000	-1.999309000

Cyclic Mechanism Product

Zero-point correction= 0.112863 (Hartree/Particle)

Thermal correction to Energy= 0.128660

Thermal correction to Enthalpy= 0.129604

Thermal correction to Gibbs Free Energy= 0.065333

Sum of electronic and zero-point Energies= -1980.064595

Sum of electronic and thermal Energies= -1980.048799

Sum of electronic and thermal Enthalpies= -1980.047855

Sum of electronic and thermal Free Energies= -1980.112125

17

Sb	2.503823000	0.387101000	-0.257479000
C	4.187835000	-0.842076000	0.292929000
H	3.912054000	-1.522774000	1.109305000
H	4.532381000	-1.422832000	-0.573108000
H	5.003173000	-0.181880000	0.625898000
C	-1.627305000	-0.649000000	1.843497000
H	-2.355590000	-1.359141000	2.261402000
H	-0.607899000	-1.021758000	2.004496000
H	-1.764525000	0.333381000	2.314286000
C	1.987949000	0.867788000	1.774785000
H	2.006906000	-0.038581000	2.394987000
H	2.733810000	1.582181000	2.155628000
H	0.995124000	1.334606000	1.806095000
Cl	-4.156453000	0.565965000	0.158463000
Sb	-2.004200000	-0.473425000	-0.257839000
Cl	1.001386000	-1.574419000	-0.350355000
Cl	-0.799467000	1.622518000	-0.471934000

3c-2e Intermediatory Mechanism Starting Point

Zero-point correction= 0.112721 (Hartree/Particle)

Thermal correction to Energy= 0.128579

Thermal correction to Enthalpy= 0.129523

Thermal correction to Gibbs Free Energy= 0.063920

Sum of electronic and zero-point Energies= -1980.042054

Sum of electronic and thermal Energies= -1980.026195

Sum of electronic and thermal Enthalpies= -1980.025251

Sum of electronic and thermal Free Energies= -1980.090854

17

Sb	-3.106884000	0.077844000	-0.303002000
C	-2.058879000	1.546261000	0.901955000
H	-1.144874000	1.107182000	1.326192000

H	-1.788103000	2.418966000	0.291589000
H	-2.716872000	1.879908000	1.717753000
C	-1.329533000	-0.782498000	-1.196685000
H	-1.594519000	-1.699956000	-1.742106000
H	-0.871406000	-0.074788000	-1.901089000
H	-0.603391000	-1.030371000	-0.410041000
C	-3.225284000	-1.395502000	1.286105000
H	-2.245370000	-1.504848000	1.772690000
H	-3.967574000	-1.084994000	2.035155000
H	-3.532226000	-2.367154000	0.873392000
Cl	1.156302000	-0.618870000	1.845918000
Sb	2.699429000	0.168660000	0.202851000
Cl	2.250863000	-1.545128000	-1.382704000
Cl	1.235580000	1.786046000	-0.745808000

3c-2e Intermediatory Mechanism TS1

Zero-point correction= 0.112870 (Hartree/Particle)

Thermal correction to Energy= 0.127782

Thermal correction to Enthalpy= 0.128726

Thermal correction to Gibbs Free Energy= 0.066619

Sum of electronic and zero-point Energies= -1980.006053

Sum of electronic and thermal Energies= -1979.991141

Sum of electronic and thermal Enthalpies= -1979.990197

Sum of electronic and thermal Free Energies= -1980.052303

17

Sb	-2.670476000	-0.597546000	0.117389000
C	-3.009697000	0.874774000	-1.423080000
H	-2.251897000	1.667460000	-1.352464000
H	-2.971192000	0.404612000	-2.415336000
H	-4.009591000	1.308711000	-1.277837000
C	-0.421135000	-0.765345000	-0.285423000

H	-0.160818000	-1.817881000	-0.400196000
H	-0.459033000	-0.158446000	-1.196876000
H	-0.152748000	-0.303167000	0.674998000
C	-2.435491000	0.853997000	1.695041000
H	-1.718212000	1.625286000	1.381081000
H	-3.411927000	1.317879000	1.895678000
H	-2.080852000	0.363580000	2.611963000
Cl	2.340037000	0.598718000	1.808410000
Sb	1.922111000	0.177999000	-0.503670000
Cl	2.537186000	-2.225688000	-0.138162000
Cl	0.451061000	2.286284000	-0.502007000

3c-2e Intermediatory Mechanism IM1

Zero-point correction= 0.113206 (Hartree/Particle)

Thermal correction to Energy= 0.128629

Thermal correction to Enthalpy= 0.129573

Thermal correction to Gibbs Free Energy= 0.067315

Sum of electronic and zero-point Energies= -1980.006803

Sum of electronic and thermal Energies= -1979.991380

Sum of electronic and thermal Enthalpies= -1979.990435

Sum of electronic and thermal Free Energies= -1980.052694

17

Sb	-2.579888000	-0.662015000	0.038249000
C	-3.048533000	0.964923000	-1.285450000
H	-2.335189000	1.789912000	-1.149465000
H	-3.047281000	0.623840000	-2.328833000
H	-4.061490000	1.308369000	-1.024746000
C	-0.149647000	-0.720476000	-0.517915000
H	-0.162288000	-1.405897000	-1.370434000
H	-0.601054000	0.276931000	-0.650424000
H	-0.094341000	-1.197559000	0.467506000

C	-2.161003000	0.594439000	1.725893000
H	-1.426350000	1.358251000	1.430952000
H	-3.100041000	1.084132000	2.023995000
H	-1.776444000	0.000920000	2.565130000
Cl	1.827646000	0.356501000	1.976608000
Sb	1.890164000	0.257118000	-0.426089000
Cl	2.715455000	-2.128497000	-0.336878000
Cl	0.394280000	2.464791000	-0.446728000

3c-2e Intermediatory Mechanism TS2

Zero-point correction= 0.113006 (Hartree/Particle)

Thermal correction to Energy= 0.127643

Thermal correction to Enthalpy= 0.128587

Thermal correction to Gibbs Free Energy= 0.067675

Sum of electronic and zero-point Energies= -1980.001303

Sum of electronic and thermal Energies= -1979.986666

Sum of electronic and thermal Enthalpies= -1979.985722

Sum of electronic and thermal Free Energies= -1980.046634

17

Sb	-2.560126000	-0.710448000	-0.041748000
C	-3.353917000	1.015300000	-1.020757000
H	-3.086525000	1.931238000	-0.483419000
H	-2.990881000	1.062999000	-2.055613000
H	-4.446401000	0.863834000	-1.037272000
C	0.243876000	-1.017247000	-0.636235000
H	0.532129000	-2.048431000	-0.872060000
H	-0.375594000	-0.569703000	-1.427659000
H	-0.153021000	-0.963521000	0.391672000
C	-2.243384000	0.189709000	1.868874000
H	-1.565373000	1.044268000	1.738773000
H	-3.226509000	0.542877000	2.218646000

H	-1.829372000	-0.534983000	2.580679000
Cl	1.703925000	0.431970000	2.003805000
Sb	1.902992000	0.394293000	-0.410699000
Cl	3.438510000	-1.604139000	-0.307313000
Cl	-0.273263000	1.976215000	-0.475919000

3c-2e Intermediatory Mechanism Product

Zero-point correction= 0.112714 (Hartree/Particle)

Thermal correction to Energy= 0.128678

Thermal correction to Enthalpy= 0.129622

Thermal correction to Gibbs Free Energy= 0.064451

Sum of electronic and zero-point Energies= -1980.064256

Sum of electronic and thermal Energies= -1980.048292

Sum of electronic and thermal Enthalpies= -1980.047348

Sum of electronic and thermal Free Energies= -1980.112518

17

Sb	-2.354564000	0.184879000	0.471313000
C	-4.138073000	-0.962475000	0.081546000
H	-4.244632000	-1.146177000	-0.995914000
H	-4.095786000	-1.919673000	0.618123000
H	-5.005431000	-0.389539000	0.442901000
C	1.515175000	-1.168295000	1.541978000
H	2.324411000	-1.847746000	1.844600000
H	0.566457000	-1.716936000	1.484531000
H	1.441968000	-0.341448000	2.260796000
C	-2.707196000	1.583425000	-1.121837000
H	-2.935600000	1.038191000	-2.047380000
H	-3.564768000	2.215413000	-0.846737000
H	-1.820252000	2.212753000	-1.267118000
Cl	0.809188000	1.708904000	-0.024179000
Sb	2.006733000	-0.371985000	-0.386389000

Cl	4.124678000	0.472530000	0.445350000
Cl	-0.989539000	-1.315453000	-0.940882000

$Ph_3Sb/SbCl_3$ Exchange Mechanism Starting Point

Zero-point correction= 0.277452 (Hartree/Particle)

Thermal correction to Energy= 0.302108

Thermal correction to Enthalpy= 0.303052

Thermal correction to Gibbs Free Energy= 0.217886

Sum of electronic and zero-point Energies= -2554.473744

Sum of electronic and thermal Energies= -2554.449088

Sum of electronic and thermal Enthalpies= -2554.448144

Sum of electronic and thermal Free Energies= -2554.533310

38

Sb	-1.555142000	0.024110000	-1.286006000
Cl	2.078757000	-1.347026000	1.483437000
Sb	2.741488000	0.522036000	0.167791000
Cl	5.007064000	-0.204335000	-0.099398000
Cl	2.012837000	-0.357966000	-1.944030000
C	-3.439146000	0.392684000	-0.273892000
C	-3.707268000	1.579506000	0.418913000
C	-4.450282000	-0.575057000	-0.366145000
C	-4.954055000	1.790665000	1.013741000
C	-5.694057000	-0.367978000	0.230631000
C	-5.948230000	0.817480000	0.922487000
H	-2.940001000	2.353498000	0.506353000
H	-4.268182000	-1.511843000	-0.902059000
H	-5.146343000	2.720557000	1.552825000
H	-6.467540000	-1.134857000	0.154689000
H	-6.921001000	0.981575000	1.389773000
C	-0.444319000	1.452328000	-0.072869000
C	-0.293702000	1.321906000	1.316529000

C	0.081125000	2.593737000	-0.699200000
C	0.359130000	2.309899000	2.060577000
C	0.733175000	3.583061000	0.042602000
C	0.869841000	3.443122000	1.424583000
H	-0.681539000	0.439419000	1.831117000
H	-0.014826000	2.716600000	-1.781889000
H	0.467390000	2.190725000	3.140425000
H	1.132848000	4.465410000	-0.460925000
H	1.376672000	4.215532000	2.005851000
C	-1.092328000	-1.766767000	-0.163815000
C	-0.278971000	-2.739136000	-0.759860000
C	-1.580953000	-1.996751000	1.129800000
C	0.061345000	-3.903746000	-0.070342000
C	-1.233554000	-3.156383000	1.824185000
C	-0.408963000	-4.109849000	1.225749000
H	0.107254000	-2.588521000	-1.771082000
H	-2.245506000	-1.269730000	1.605170000
H	0.700092000	-4.649921000	-0.546998000
H	-1.614077000	-3.317946000	2.834810000
H	-0.138800000	-5.017669000	1.768692000

$Ph_3Sb/SbCl_3$ Exchange Mechanism TS1

Zero-point correction= 0.277165 (Hartree/Particle)

Thermal correction to Energy= 0.301056

Thermal correction to Enthalpy= 0.302000

Thermal correction to Gibbs Free Energy= 0.219997

Sum of electronic and zero-point Energies= -2554.433125

Sum of electronic and thermal Energies= -2554.409234

Sum of electronic and thermal Enthalpies= -2554.408290

Sum of electronic and thermal Free Energies= -2554.490293

Sb	1.090624000	0.312892000	1.126670000
Cl	-3.640933000	-1.237924000	-1.607366000
Sb	-2.539538000	0.425293000	-0.088209000
Cl	-3.393736000	-0.816337000	1.762004000
Cl	-1.671383000	2.075091000	1.724809000
C	2.760732000	-1.001919000	0.666797000
C	3.932886000	-0.747984000	1.394076000
C	2.761741000	-2.055204000	-0.256576000
C	5.083075000	-1.512387000	1.193076000
C	3.908810000	-2.827657000	-0.453324000
C	5.071542000	-2.556014000	0.267679000
H	3.960303000	0.060612000	2.132201000
H	1.868072000	-2.285354000	-0.841386000
H	5.987539000	-1.294798000	1.764432000
H	3.892540000	-3.645339000	-1.176633000
H	5.967563000	-3.159180000	0.110336000
C	1.635102000	1.801562000	-0.360316000
C	2.667130000	1.565727000	-1.280700000
C	0.965176000	3.033297000	-0.398629000
C	3.014733000	2.535374000	-2.222492000
C	1.312396000	4.000835000	-1.344768000
C	2.336865000	3.754346000	-2.257580000
H	3.210047000	0.617558000	-1.272332000
H	0.160067000	3.242319000	0.308712000
H	3.820756000	2.335718000	-2.931271000
H	0.779536000	4.953541000	-1.362335000
H	2.609677000	4.512334000	-2.994194000
C	-0.294071000	-0.806531000	-0.247997000
C	-0.703597000	-2.079010000	0.234512000
C	-0.127617000	-0.658821000	-1.655053000
C	-0.967198000	-3.129086000	-0.636689000

C	-0.393757000	-1.707340000	-2.522693000
C	-0.820305000	-2.939145000	-2.012603000
H	-0.824751000	-2.234212000	1.310434000
H	0.211583000	0.300118000	-2.058042000
H	-1.293658000	-4.093772000	-0.246572000
H	-0.275753000	-1.570404000	-3.598361000
H	-1.037908000	-3.760904000	-2.697445000

$Ph_3Sb/SbCl_3$ Exchange Mechanism IM1

Zero-point correction= 0.276972 (Hartree/Particle)

Thermal correction to Energy= 0.301841

Thermal correction to Enthalpy= 0.302785

Thermal correction to Gibbs Free Energy= 0.217229

Sum of electronic and zero-point Energies= -2554.433546

Sum of electronic and thermal Energies= -2554.408677

Sum of electronic and thermal Enthalpies= -2554.407732

Sum of electronic and thermal Free Energies= -2554.493289

38

Sb	-1.027400000	0.316751000	-1.112894000
Cl	3.701502000	-1.366990000	1.460162000
Sb	2.606480000	0.392239000	0.042067000
Cl	3.028700000	-0.928647000	-1.900982000
Cl	1.673523000	2.179187000	-1.617398000
C	-2.600538000	-1.119309000	-0.670429000
C	-3.542984000	-1.331384000	-1.685518000
C	-2.735928000	-1.833963000	0.528929000
C	-4.601275000	-2.226177000	-1.507526000
C	-3.787723000	-2.732829000	0.707395000
C	-4.723511000	-2.928943000	-0.310326000
H	-3.457507000	-0.797490000	-2.637134000
H	-2.020461000	-1.690717000	1.343475000

H	-5.326984000	-2.376646000	-2.309072000
H	-3.878087000	-3.281964000	1.646701000
H	-5.546036000	-3.632545000	-0.169258000
C	-1.755122000	1.837108000	0.260241000
C	-2.945855000	1.654648000	0.978007000
C	-1.050907000	3.040566000	0.418685000
C	-3.413810000	2.645395000	1.843409000
C	-1.517154000	4.026612000	1.290729000
C	-2.698437000	3.831455000	2.005561000
H	-3.523809000	0.734693000	0.868839000
H	-0.128910000	3.215646000	-0.139215000
H	-4.343902000	2.486348000	2.392570000
H	-0.954344000	4.955199000	1.404512000
H	-3.064252000	4.604585000	2.683806000
C	0.337765000	-0.649097000	0.410078000
C	0.598711000	-2.015754000	0.120488000
C	0.226654000	-0.278367000	1.781590000
C	0.764483000	-2.949140000	1.133763000
C	0.422250000	-1.206574000	2.794565000
C	0.691175000	-2.540281000	2.467882000
H	0.680021000	-2.337353000	-0.921957000
H	-0.007087000	0.759189000	2.040184000
H	0.966254000	-3.992569000	0.889213000
H	0.359264000	-0.898532000	3.838915000
H	0.842665000	-3.270490000	3.265156000

$Ph_3Sb/SbCl_3$ Exchange Mechanism TS2

Zero-point correction= 0.276919 (Hartree/Particle)

Thermal correction to Energy= 0.300893

Thermal correction to Enthalpy= 0.301837

Thermal correction to Gibbs Free Energy= 0.219413

Sum of electronic and zero-point Energies= -2554.433566

Sum of electronic and thermal Energies= -2554.409592

Sum of electronic and thermal Enthalpies= -2554.408648

Sum of electronic and thermal Free Energies= -2554.491072

38

Sb	-0.913981000	0.298938000	-1.103079000
Cl	3.765115000	-1.426306000	1.266685000
Sb	2.657811000	0.479205000	0.043101000
Cl	2.711249000	-0.717492000	-2.030924000
Cl	1.501319000	2.459804000	-1.237035000
C	-2.281798000	-1.342280000	-0.684071000
C	-2.809888000	-2.035640000	-1.778967000
C	-2.639438000	-1.752910000	0.609515000
C	-3.680537000	-3.114304000	-1.591204000
C	-3.501127000	-2.830951000	0.800669000
C	-4.024590000	-3.512848000	-0.301887000
H	-2.541782000	-1.741126000	-2.798322000
H	-2.241444000	-1.224991000	1.482536000
H	-4.085268000	-3.643921000	-2.455779000
H	-3.768265000	-3.141490000	1.812778000
H	-4.700788000	-4.356521000	-0.151622000
C	-2.001849000	1.726751000	0.122426000
C	-3.365404000	1.517244000	0.376924000
C	-1.406860000	2.909547000	0.587695000
C	-4.110201000	2.456660000	1.093058000
C	-2.150048000	3.840932000	1.314580000
C	-3.502914000	3.617052000	1.569944000
H	-3.865119000	0.615229000	0.017852000
H	-0.356454000	3.115792000	0.374195000
H	-5.170672000	2.275535000	1.278652000
H	-1.667670000	4.751804000	1.674501000

H	-4.084021000	4.349200000	2.133705000
C	0.482476000	-0.453482000	0.560738000
C	0.654352000	-1.859973000	0.437511000
C	0.311062000	0.070623000	1.877653000
C	0.670285000	-2.689712000	1.548133000
C	0.367598000	-0.752841000	2.991779000
C	0.544047000	-2.132260000	2.822067000
H	0.794175000	-2.295201000	-0.557209000
H	0.150191000	1.145331000	2.009784000
H	0.803496000	-3.765171000	1.427683000
H	0.263716000	-0.331420000	3.992221000
H	0.582985000	-2.780129000	3.700162000

$Ph_3Sb/SbCl_3$ Exchange Mechanism Product

Zero-point correction= 0.277109 (Hartree/Particle)

Thermal correction to Energy= 0.302043

Thermal correction to Enthalpy= 0.302988

Thermal correction to Gibbs Free Energy= 0.216059

Sum of electronic and zero-point Energies= -2554.483014

Sum of electronic and thermal Energies= -2554.458080

Sum of electronic and thermal Enthalpies= -2554.457136

Sum of electronic and thermal Free Energies= -2554.544064

38

Sb	-1.694250000	1.017054000	-0.927028000
Cl	4.826083000	0.741152000	-0.349361000
Sb	2.599374000	1.268463000	0.443756000
Cl	1.662217000	1.145641000	-1.786994000
Cl	-0.501747000	1.554288000	1.162919000
C	-1.107196000	-1.046529000	-1.025339000
C	-0.601552000	-1.540085000	-2.233250000
C	-1.296021000	-1.920614000	0.053781000

C	-0.314955000	-2.900231000	-2.372860000
C	-1.006833000	-3.276377000	-0.086906000
C	-0.524737000	-3.767581000	-1.302545000
H	-0.427032000	-0.867095000	-3.077353000
H	-1.682287000	-1.545307000	1.005686000
H	0.071229000	-3.280046000	-3.320556000
H	-1.157601000	-3.953428000	0.756122000
H	-0.303860000	-4.831397000	-1.411041000
C	-3.528246000	0.606912000	0.142992000
C	-4.384758000	-0.388730000	-0.346217000
C	-3.923190000	1.361042000	1.254139000
C	-5.614644000	-0.628359000	0.268337000
C	-5.150894000	1.116707000	1.871814000
C	-5.997931000	0.123534000	1.379177000
H	-4.092856000	-0.997410000	-1.207473000
H	-3.264981000	2.135260000	1.656402000
H	-6.271542000	-1.409844000	-0.118298000
H	-5.445159000	1.704318000	2.743566000
H	-6.957165000	-0.066940000	1.864006000
C	2.185780000	-0.773713000	0.952673000
C	2.527552000	-1.823643000	0.092525000
C	1.661869000	-1.052090000	2.219662000
C	2.361548000	-3.143177000	0.508554000
C	1.497733000	-2.376027000	2.633055000
C	1.853915000	-3.419176000	1.780135000
H	2.938570000	-1.613096000	-0.898263000
H	1.379357000	-0.241714000	2.897868000
H	2.629893000	-3.960660000	-0.163343000
H	1.095169000	-2.589101000	3.625029000
H	1.730889000	-4.454414000	2.104584000

Appendix IV: Calculation of Equilibrium Constants (Chapter 6)

Table 9.1. Gas phase Gibbs free energy of of P-$Tol_{3-n}SbCl_n$.

Gas Phase		
Compound	Gibbs (Hartree)	Gibbs (Kcal mol^{-1})
PTol2SbCl	-1241.347435	-778956.6876
PTol3Sb	-1051.794003	-660010.203
PTolSbCl2	-1430.895821	-897900.0057
SbCl3	-1620.439549	-1016840.401

Table 9.2. Equilibrium constants for the redistribution of P-$Tol_{3-n}SbCl_n$ in the gas phase.

		Uncorrected Gibbs Energy (kcal mol^{-1})	**Difference in Gibbs Free Energy (kcal mol^{-1})**	**InK**	**K**
Reactants	SbCl3 +PTol3Sb	-1676850.604	-6.089347336	10.28338601	29242.72
Products	PTolSbCl2 +PTol2SbCl	-1676856.693			
Reactants	SbCl3 + 2PTol3Sb	-2336860.807	-9.25575775	15.63066197	6142006
Products	3PTol2SbCl	-2336870.063			
Reactants	2SbCl3 + PTol3Sb	-2693691.005	-9.012284258	15.21949608	4071394
Products	3PTolSbCl2	-2693700.017			
Reactants	PTol2SbCl + SbCl3	-1795797.089	-2.922936922	4.936110064	139.2276
Products	2PTolSbCl2	-1795800.011			
Reactants	PTolSbCl2 + PTol3Sb	-1557910.209	-3.166410414	5.347275951	210.0354
Products	2PTol2SbCl	-1557913.375			

Table 9.2. Calculation of the Gibbs Free energy of P-$Tol_{3-n}SbCl_n$ in solution.

Diethyl Ether				
Compound	**Single point energy**	**Thermal Correction to free energy**	**Gibbs free energy (Hartree)**	**Gibbs (kcal mol^{-1})**
PTol2SbCl	-1241.539671	0.186709	-1241.352962	-778960.156

PTol3Sb	-1052.096037	0.297346	-1051.798691	-660013.145
PTolSbCl2	-1430.980047	0.077952	-1430.902095	-897903.943
SbCl3	-1620.416495	-0.029221	-1620.445716	-1016844.27
Benzene				
Compound	**Single point energy**	**Thermal Correction to free energy**	**Gibbs free energy (Hartree)**	**Gibbs (kcal mol^{-1})**
PTol2SbCl	-1241.53766	0.186709	-1241.350951	-778958.894
PTol3Sb	-1052.094326	0.297346	-1051.79698	-660012.071
PTolSbCl2	-1430.977784	0.077952	-1430.899832	-897902.523
SbCl3	-1620.414256	-0.029221	-1620.443477	-1016842.87
Ethanol				
Compound	**Single point energy**	**Thermal Correction to free energy**	**Gibbs free energy (Hartree)**	**Gibbs (kcal mol^{-1})**
PTol2SbCl	-1241.542339	0.077952	-1241.464387	-779030.076
PTol3Sb	-1052.098273	0.297346	-1051.800927	-660014.548
PTolSbCl2	-1430.983	0.077952	-1430.905048	-897905.796
SbCl3	-1620.419398	-0.029221	-1620.448619	-1016846.09
Water				
Compound	**Single point energy**	**Thermal Correction to free energy**	**Gibbs free energy (Hartree)**	**Gibbs (kcal mol^{-1})**
PTol2SbCl	-1241.542803	0.186709	-1241.356094	-778962.121
PTol3Sb	-1052.098655	0.297346	-1051.801309	-660014.787
PTolSbCl2	-1430.983507	0.077952	-1430.905555	-897906.114
SbCl3	-1620.419891	-0.029221	-1620.449112	-1016846.4

Table 9.3. Equilibrium constants for the redistribution of P-$Tol_{3-n}SbCl_n$ in solution.

Diethyl Ether		**Uncorrected Gibbs Energy (kcal mol^{-1})**	**Difference in Gibbs Free Energy (kcal mol^{-1})**	**InK**	**K**
Reactants	SbCl3 +PTol3Sb	-1676857.415	-6.683259504	11.28635526	79726.34
Products	PTolSbCl2 +PTol2SbCl	-1676864.099			
Reactants	SbCl3 + 2PTol3Sb	-2336870.56	-9.908116106	16.73233221	18482450
Products	3PTol2SbCl	-2336880.468			
Reactants	2SbCl3 + PTol3Sb	-2693701.686	-10.14166241	17.12673355	27418638
Products	3PTolSbCl2	-2693711.828			
Reactants	PTol2SbCl + SbCl3	-1795804.427	-3.458402902	5.840378298	343.9094
Products	2PTolSbCl2	-1795807.885			
Reactants	PTolSbCl2 + PTol3Sb	-1557917.087	-3.224856602	5.445976958	231.8237
Products	2PTol2SbCl	-1557920.312			
Benzene		**Uncorrected Gibbs Energy (kcal mol^{-1})**	**Difference in Gibbs Free Energy (kcal mol^{-1})**	**InK**	**K**
Reactants	SbCl3 +PTol3Sb	-1676854.937	-6.48009719	10.94326488	56571.74
Products	PTolSbCl2	-			

	+PTol2SbCl	1676861.417			
Reactants	SbCl3 + 2PTol3Sb	-2336867.008	-9.674023874	16.33700893	12447233
Products	3PTol2SbCl	-2336876.682			
Reactants	2SbCl3 + PTol3Sb	-2693697.802	-9.766267696	16.4927857	14545405
Products	3PTolSbCl2	-2693707.569			
Reactants	PTol2SbCl + SbCl3	-1795801.76	-3.286170506	5.549520821	257.1143
Products	2PTolSbCl2	-1795805.046			
Reactants	PTolSbCl2 + PTol3Sb	-1557914.594	-3.193926684	5.393744054	220.0256
Products	2PTol2SbCl	-1557917.788			
Ethanol		**Uncorrected Gibbs Energy (kcal mol^{-1})**	**Difference in Gibbs Free Energy (kcal mol^{-1})**	**InK**	**K**
Reactants	SbCl3 +PTol3Sb	-1676860.64	-75.23177163	127.047663	1.5E+55
Products	PTolSbCl2 +PTol2SbCl	-1676935.872			
Reactants	SbCl3 + 2PTol3Sb	-2336875.188	-215.0399548	363.1487484	5.2E+157
Products	3PTol2SbCl	-2337090.228			

Reactants	2SbCl3 + PTol3Sb	-2693706.733	-10.6553601	17.99424059	65282893
Products	3PTolSbCl2	-2693717.388			
Reactants	PTol2SbCl + SbCl3	-1795876.168	64.57641153	-109.0534224	4.35E-48
Products	2PTolSbCl2	-1795811.592			
Reactants	PTolSbCl2 + PTol3Sb	-1557920.344	-139.8081832	236.1010854	3.4E+102
Products	2PTol2SbCl	-1558060.152			
Water		**Uncorrected Gibbs Energy (kcal mol^{-1})**	**Difference in Gibbs Free Energy (kcal mol^{-1})**	**InK**	**K**
Reactants	SbCl3 +PTol3Sb	-1676861.189	-7.045721252	11.89846258	147040.4
Products	PTolSbCl2 +PTol2SbCl	-1676868.235			
Reactants	SbCl3 + 2PTol3Sb	-2336875.977	-10.38645994	17.54013542	41455678
Products	3PTol2SbCl	-2336886.363			
Reactants	2SbCl3 + PTol3Sb	-2693707.591	-10.75070382	18.15525231	76687732
Products	3PTolSbCl2	-2693718.341			
Reactants	PTol2SbCl + SbCl3	-1795808.52	-3.70498256	6.25678973	521.542

		3	3		
Products	2PTolSbCl2	-1795812.228			
Reactants	PTolSbCl2 + PTol3Sb	-1557920.901	-3.340738689	5.641672846	281.934
Products	2PTol2SbCl	-1557924.242			

Table 9.4. Gas phase Gibbs free energy of of $Me_{3-n}SbCl_n$.

Compound	**Gibbs (Hartree)**	**Gibbs (Kcal/mol)**
Me2SbCl	-779.916185	-489404.4253
Me3Sb	-359.647823	-225682.2458
MeSbCl2	-1200.180221	-753123.8903
SbCl3	-1620.439549	-1016840.401

Table 9.5. Equilibrium constants for the redistribution of $Me_{3-n}SbCl_n$ in the gas phase.

		Uncorrected Gibbs Energy (kcal mol^{-1})	**Difference in Gibbs Free Energy (kcal mol^{-1})**	**lnK**	**K**
Reactants	SbCl3 +Me3Sb	-1242522.647	-5.668916306	9.573383064	14376.97
Products	MeSbCl2 +Me2SbCl	-1242528.316			
Reactants	SbCl3 + 2Me3Sb	-1468204.892	-8.38352024	14.15767077	1407986
Products	3Me2SbCl	-1468213.276			

Reactants	2SbCl3 + Me3Sb	-2259363.048	-8.623228678	14.56247842	2110591
Products	3MeSbCl2	-2259371.671			
Reactants	Me2SbCl + SbCl3	-1506244.826	-2.954312372	4.989095358	146.8036
Products	2MeSbCl2	-1506247.781			
Reactants	MeSbCl2 + Me3Sb	-978806.1361	-2.714603934	4.584287706	97.9334
Products	2Me2SbCl	-978808.8507			

Diethyl Ether				
Compound	**Single point energy**	**Thermal Correction to free energy**	**Gibbs free energy (Hartree)**	**Gibbs (kcal mol^{-1})**
Me2SbCl	-779.9607615	0.04056	-779.9202015	-489406.946
Me3Sb	-359.7246916	0.075783	-359.6489086	-225682.927
MeSbCl2	-1200.191436	0.005591	-1200.185845	-753127.419
SbCl3	-1620.416495	-0.029221	-1620.445716	-1016844.27
Benzene				
Compound	**Single point energy**	**Thermal Correction to free energy**	**Gibbs free energy (Hartree)**	**Gibbs (kcal mol^{-1})**
Me2SbCl	-779.9593518	0.04056	-779.9187918	-489406.061
Me3Sb	-359.7242963	0.075783	-359.6485133	-225682.679
MeSbCl2	-1200.189436	0.005591	-1200.183845	-753126.165
SbCl3	-1620.414256	-0.029221	-1620.443477	-1016842.87

Ethanol				
Compound	**Single point energy**	**Thermal Correction to free energy**	**Gibbs free energy (Hartree)**	**Gibbs (kcal mol^{-1})**
Me2SbCl	-779.9625397	0.04056	-779.9219797	-489408.062
Me3Sb	-359.725206	0.075783	-359.649423	-225683.25
MeSbCl2	-1200.193989	0.005591	-1200.188398	-753129.021
SbCl3	-1620.419398	-0.029221	-1620.448619	-1016846.09
Water				
Compound	**Single point energy**	**Thermal Correction to free energy**	**Gibbs free energy (Hartree)**	**Gibbs (kcal mol^{-1})**
Me2SbCl	-779.9628379	0.04056	-779.9222779	-489408.249
Me3Sb	-359.7252936	0.075783	-359.6495106	-225683.305
MeSbCl2	-1200.19442	0.005591	-1200.188829	-753129.292
SbCl3	-1620.419891	-0.029221	-1620.449112	-1016846.4

Table 9.6. Equilibrium constants for the redistribution of P-Tol$_{3-n}$SbCl$_n$ in solution.

Diethyl Ether		**Uncorrected Gibbs Energy (kcal mol^{-1})**	**Difference in Gibbs Free Energy (kcal mol^{-1})**	**InK**	**K**
Reactants	SbCl3 +Me3Sb	-1242527.198	-7.16718817	12.10358985	180518.7349
Products	MeSbCl2 +Me2SbCl	-1242534.365			
Reactants	SbCl3 + 2Me3Sb	-1468210.125	-10.71253872	18.09080099	71901018.89
Products	3Me2SbCl	-1468220.837			
Reactants	2SbCl3 + Me3Sb	-2259371.468	-10.78902579	18.21996855	81814786.2
Products	3MeSbCl2	-2259382.25			

		7			
Reactants	Me2SbCl + SbCl3	-1506251.216	-3.622	6.116	453.220
Products	2MeSbCl2	-1506254.838			
Reactants	MeSbCl2 + Me3Sb	-978810.3461	-3.545	5.987	398.302
Products	2Me2SbCl	-978813.8915			
Benzene		**Uncorrected Gibbs Energy (kcal mol^{-1})**	**Difference in Gibbs Free Energy (kcal mol^{-1})**	**InK**	**K**
Reactants	SbCl3 +Me3Sb	-1242525.545	-6.681	11.283	79447.176
Products	MeSbCl2 +Me2SbCl	-1242532.226			
Reactants	SbCl3 + 2Me3Sb	-1468208.223	-9.960	16.820	20170602.0
Products	3Me2SbCl	-1468218.183			
Reactants	2SbCl3 + Me3Sb	-2259368.41	-10.084	17.029	24860882.2
Products	3MeSbCl2	-2259378.494			
Reactants	Me2SbCl + SbCl3	-1506248.927	-3.402	5.746	312.923
Products	2MeSbCl2	-1506252.329			
Reactants	MeSbCl2 +	-	-	5.537	253.887

	Me3Sb	978808.8435	3.278690599	7	6
Products	2Me2SbCl	-978812.1222			
Ethanol		**Uncorrected Gibbs Energy (kcal mol^{-1})**	**Difference in Gibbs Free Energy (kcal mol^{-1})**	**lnK**	**K**
Reactants	SbCl3 +Me3Sb	-1242529.342	-7.740536868	13.07183253	475362.2985
Products	MeSbCl2 +Me2SbCl	-1242537.083			
Reactants	SbCl3 + 2Me3Sb	-1468212.592	-11.59270167	19.57717627	317877381.8
Products	3Me2SbCl	-1468224.185			
Reactants	2SbCl3 + Me3Sb	-2259375.435	-11.62890894	19.6383213	337920528.8
Products	3MeSbCl2	-2259387.063			
Reactants	Me2SbCl + SbCl3	-1506254.154	-3.888372068	6.566488778	710.8694353
Products	2MeSbCl2	-1506258.042			
Reactants	MeSbCl2 + Me3Sb	-978812.2709	-3.852164799	6.505343748	668.7054962
Products	2Me2SbCl	-978816.1231			

Water		Uncorrected Gibbs Energy (kcal mol^{-1})	Difference in Gibbs Free Energy (kcal mol^{-1})	InK	K
Reactants	SbCl3 +Me3Sb	-1242529.706	-7.834192586	13.22999363	556817.9532
Products	MeSbCl2 +Me2SbCl	-1242537.541			
Reactants	SbCl3 + 2Me3Sb	-1468213.011	-11.73502698	19.81752817	4.0424E+08
Products	3Me2SbCl	-1468224.746			
Reactants	2SbCl3 + Me3Sb	-2259376.108	-11.76755077	19.87245272	427067536.9
Products	3MeSbCl2	-2259387.876			
Reactants	Me2SbCl + SbCl3	-1506254.65	-3.933358189	6.642459094	766.9787488
Products	2MeSbCl2	-1506258.584			
Reactants	MeSbCl2 + Me3Sb	-978812.5966	-3.900834397	6.587534537	725.9887634
Products	2Me2SbCl	-978816.4974			